Applied Optics

July
1962

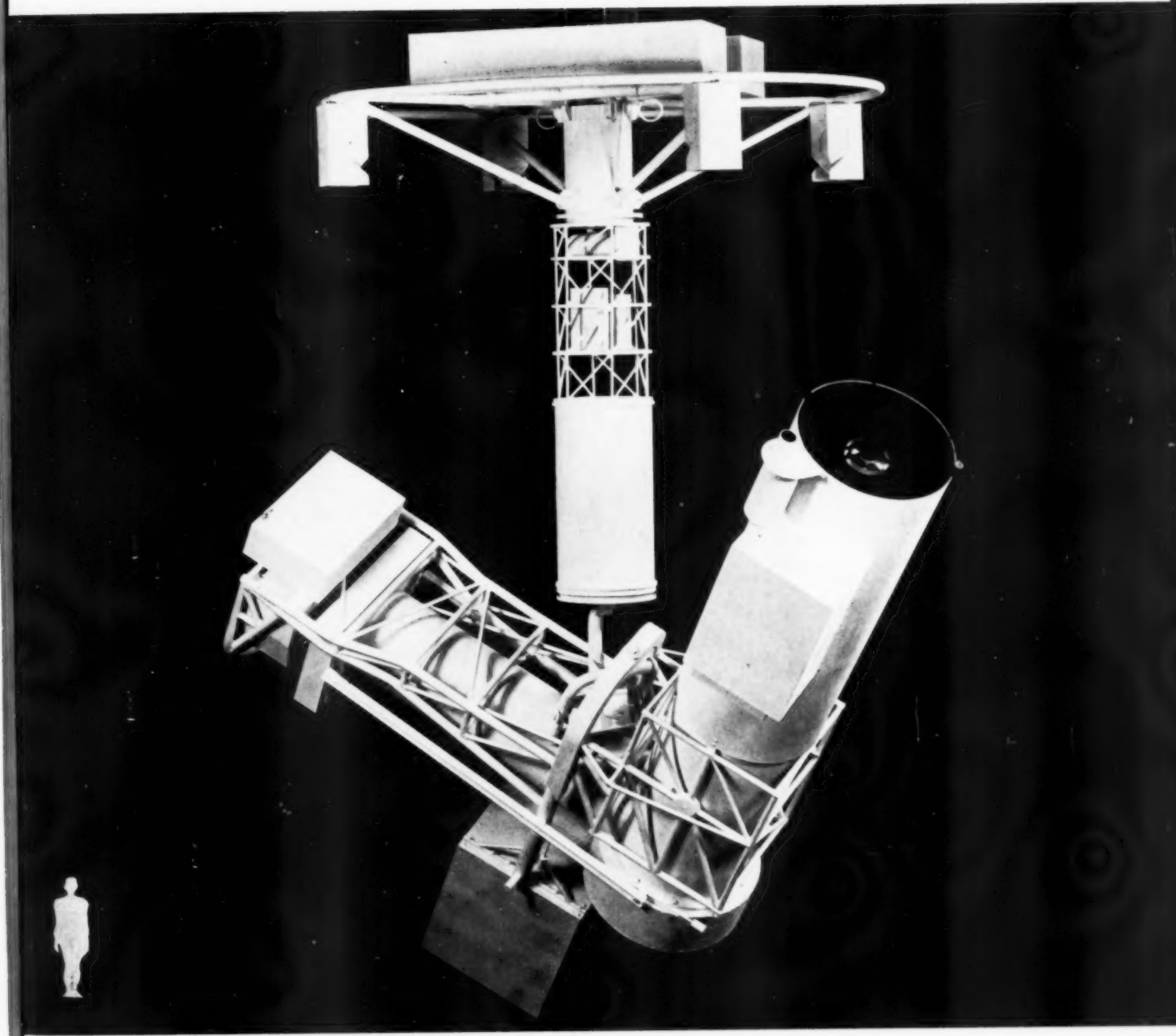

OPTICAL ENGINEERING

Effective Jan. 1, 1965. All back issues and single copies are sold at $3.00 per copy.

ENGINEERS

ELECTRO-OPTICAL SYSTEMS

explore your Future in

SATELLITE AND SPACE VEHICLE DEVELOPMENT

at RCA's new Space Center in Princeton, N. J.

Here is an opportunity to let your imagination soar with the team that created Tiros. Now at this rapidly growing division of RCA, a number of challenging opportunities are available for electronic engineers.

To qualify Supervisory Engineers must have 5 to 10 years experience . . . Engineers, 3 to 5 years experience in the following fields:

TELEVISION CAMERA DESIGN and EVALUATION
SOLID STATE CIRCUIT DESIGN EXPERIENCE
KNOWLEDGE OF ELECTRO-OPTICAL SYSTEMS and OPTICAL SYSTEMS

Work to be performed must conform to stringent operational and environmental specifications.

FOR A CONFIDENTIAL INTERVIEW call collect:

MR. D. D. BRODHEAD
609-448-3400 or write:

MR. D. D. BRODHEAD, DEPT. #NY-1
ASTRO-ELECTRONICS DIVISION
PRINCETON, NEW JERSEY

An Equal Opportunity Employer

The Most Trusted Name in Electronics

RADIO CORPORATION OF AMERICA

Applied Optics

VOLUME 1
NUMBER 4

July
1962

A bimonthly publication of the Optical Society of America

John N. Howard, Editor

Roderic M. Scott, Feature Editor

Patricia R. Wakeling, Managing Editor

COVER: A photograph of a scale model of Stratoscope II. This instrument weighs 6300 lb (286 kg) and has a 36-in. (91 cm) diameter primary mirror capable of resolving celestial objects separated by 0.1 sec of arc. It contains an internal, automatic guidance system, two television cameras, and extensive command and telemetry equipment. Scientific data will be recorded on 70-mm film at an effective focal length of 300 ft (91.4 m). The Stratoscope telescope system is being built for Princeton University with support from the National Science Foundation, the Office of Naval Research, and the National Aeronautics and Space Administration.

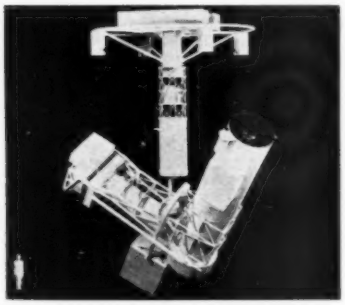

Published bimonthly by the Optical Society of America, Inc., in cooperation with the American institute of Physics, at 20th and Northampton Streets, Easton, Pa. Editorial offices: 1155 16th St. N.W., Washington 6, D.C. Supported in part by a grant from the National Science Foundation. Advertising Office: 55 West 16th Street, New York 11, N.Y. A. P. Oppenheim—Chelsea 2-1311. Subscription rates: $6.00 to OSA members, $8.00 other AIP Soceities' members; nonmembers and libraries: $10.00 per year. Single copies $2.00. Second class postage paid at Easton, Pa.

©Copyright 1962 by the Optical Society of America.

387 **Optical Engineering**—Roderic M. Scott

399 **Overlapping-Monoculars—An Ultrawide-Field Viewing System**—Martin Shenker, Joseph LaRussa, Paul R. Yoder, Jr., and Wright H. Scidmore

403 **High-Precision, Strain-Free Mounting of Large Lens Elements**—Leo G. Deterding

407 **A High-Speed Rotating-Mirror Framing Camera**—W. C. Davis

411 **A Rapid-Scanning Fabry-Perot Interferometer with Automatic Parallelism Control**—J. V. Ramsay

415 **Control of a Ruling Engine by a Modulated Interferometer**—Horace W. Babcock

421 **Diffraction Anomalies in Grating Spectrophotometers**—James E. Stewart and William S. Gallaway

431 **A High-Resolution Grating-Prism Spectrometer for the Infrared**—T. K. McCubbin, Jr., R. P. Grosso, and J. D. Mangus

437 **Infrared Filter Grating Spectrophotometers—Design and Properties**—Nelson L. Alpert

443 **Performance of the Beckman IR-7 Infrared Spectrophotometer I. Frequency Reproducibility and Accuracy (630–4000 cm^{-1})**—Peter J. Krueger

455 **Fundamental Principles and Methods for the Calibration of Radiometers for Photometric Use**—A. K. Ångström and A. J. Drummond

465 **Spectral Irradiance from Stars and Planets, above the Atmosphere, from 0.1 to 100 μ**—R. C. Ramsey

473 **Total Absorptance by Nitrous Oxide Bands in the Infrared**—Darrell E. Burch and Dudley Williams

483 **Inspecting Infrared Optical Materials and Systems by Means of the Evaporograph**—Gene W. McDaniel and Arthur P. DiMattia

493 **A Very High Temperature Infrared Cell for Pure Liquids or Solutions**—E. Fishman

497 **Astronomical Refraction—Some History and Theories**—A. I. Mahan

513 **Continuous Optically Pumped Cs Laser**—P. Rabinowitz, S. Jacobs, and G. Gould

517 **Observations Relating to the Transverse and Longitudinal Modes of a Ruby Laser**—V. Evtuhov and J. K. Neeland

521 **Influence of Scattering on Fluorescence Spectra of Dilute Solutions Obtained with the Aminco–Bowman Spectrophotofluorometer**—J. M. Price, M. Kaihara, and H. K. Howerton

DEPARTMENTS

533 **Letters to the Editor**

Crossed Roof Prism Interferometer—G. Gould, S. Jacobs, P. Rabinowitz, and T. Shultz

Stimulated Emission of Infrared Radiation from Ytterbium Activated Silicate Glass—H. W. Etzel, H. W. Gandy, and R. J. Ginther

Measurement of Microcurrent by the Michelson Interferometer—I-Hsiun Chen

Emission Pattern of Ruby Laser Output—R. L. Aagard, D. L. Hardwick, and J. F. Ready

Use of an Oxyacetylene Flame to Calibrate a Prism Spectrometer in the 10–30 μ Region—Fred P. Dickey and W. H. Rogge

A Distortionless Interferometer Plate Mount—J. V. Ramsay and E. G. V. Mugridge

409 **Meetings Calendar**

414 **Optical Activities in the Universities**

420 **From the Editor**

471 **Books**

512 **Patents**

539 **Meeting Reports**

545 **Of Optics and Opticists**

New Light Pumps for EXPANDING PARAMETERS IN OPTICAL LASER RESEARCH

IN THE RAPIDLY EXPANDING PARAMETERS of Optical Laser Research, it is not enough to have equipment suitable only for the present state of the art. New pumping devices and methods require increased power, increased efficiency and shorter peaks. Only Electro Powerpacs Light Pumps are designed with the versatility and flexibility to meet these needs as they arise.

POWER —
Up to 10,000 Volts; up to 20,000 Joules; up to 2,000 Watts.

VERSATILITY —
Continuously variable voltages 0-10,000. Variable peak power and pulse length. Operates with all size rods. One mount for airblast or cryogenic cooling.

FLEXIBILITY —
100 to 20,000 joules, achieved by varying the voltage, the number of capacitor banks or the number of capacitors. Capacitors can be eliminated from circuit by merely removing a fuse.

SPECIAL FEATURES —
Higher peaks and shorter pulses require lower average powers, permit faster re-cycling, reduce heat build-up • Separate 500 volt D.C. supply energizes trigger pulse • Pulse can simultaneously lock in an oscilloscope sweep for laser beam or flash examination • Safety interlocks and automatic capacitor discharge for personnel protection • Over-voltage meter switch for equipment protection.

MODELS FOR YOUR EVERY NEED —
Almost any combination of volts, joules and watts, up to the limits listed above, is available in standard models. In addition, our engineers are well qualified to develop equipment to suit special requirements.

PARTIAL LIST OF LABORATORIES USING ELECTRO POWERPAC LASER EQUIPMENT:

American Optical Company
Bell Telephone Laboratories
General Telephone & Electronics
Lincoln Laboratory of M.I.T.
National Aeronautics & Space Adm.
Perkin-Elmer Corporation
Westinghouse Air Arm Division
International Business Machines
Radio Corporation of America
Avco Corporation
Harvard University
McMasters University
University of Dayton
University of Virginia

Be sure you get full information on Electro Powerpacs Light Pumps before you make your final selection.

ELECTRO POWERPACS, INC.
A Subsidiary of Hydra-Power Corporation
6 HADLEY STREET, CAMBRIDGE 40, MASS.

✻ Mountainous region southeast of the crater Albategnius

Raytheon laser hits moon

On Wednesday, May 9th, a team of Massachusetts Institute of Technology scientists illuminated the moon's surface and detected and recorded the reflection. The new first was accomplished with 13 bursts of 6934-angstrom light from a 50-joule, 4-barreled Raytheon ruby laser. The new Raytheon laser is the most powerful yet reported. Raytheon is currently investigating laser systems in the areas of communications, ranging, detection, space vehicle guidance, weapon systems, and medicine.* Write for further information to Martin B. Curran, Raytheon Company, Lexington, Massachusetts.

*For those interested in pursuing basic laboratory investigations, Raytheon is now offering a complete laser head for $975.

RAYTHEON

For new laser fact folio, fill out and mail coupon on page A25

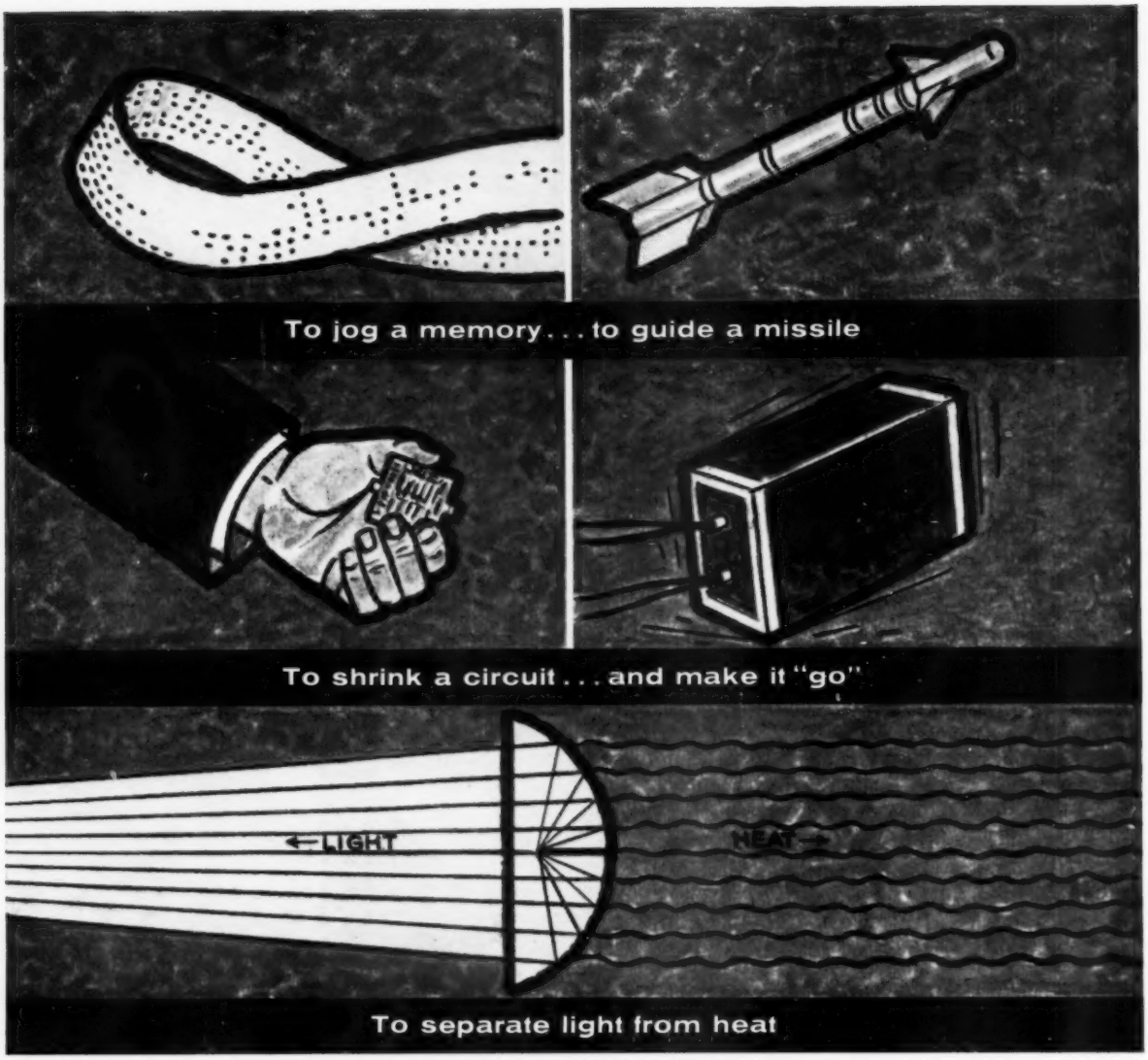

. . . rely on Bausch & Lomb MULTI-FILMS

First it was thin films, pioneered by Bausch & Lomb a generation ago. Now multi-films — perfected by Bausch & Lomb — usher in the "miracle" state of the art. From enhancing the speed and accuracy of computer memories . . . to protecting solar cells from harmful radiation . . . B&L Multi-Films control heat, light and wavelength to meet your most sophisticated design specifications.

We're now designing, producing and delivering multi-film components in five major classes: color filters, color separating filters, heat control filters, neutral beam dividers, first surface mirrors. And you can be sure of the precision and efficiency essential to end-product success . . . because you're dealing with the world's prime source, equipped with the world's most comprehensive facilities, staffed with the world's leaders in multi-film technology.

BAUSCH & LOMB

BAUSCH & LOMB INCORPORATED
77131 Bausch Street, Rochester 2, N. Y.

☐ Please send me B&L Multi-Film Handbook E-306.

Name.....

Professional Address.....

.....

.....

NEW HORIZONS IN OPTICAL TECHNOLOGY

To keep pace with our fast-moving world, any field of science or technology that isn't progressing like a runaway snowball is standing still. This holds true particularly to the field of Applied Optics with its intimate ties to the defense industry and various aerospace programs. Optical Coating Laboratory, Inc., specialists in vacuum deposited coatings (ultraviolet, visual and infrared applications), has recently introduced several "New Horizon" products, including a unique Solar Simulator. Other advanced products and services from OCLI are: **FILTERS AND COATINGS**– All-dielectric ultraviolet filters for the 2500-4000 angstrom range. All-interference infrared bandpass filters for the region beyond 8 microns. Metal-dielectric and all-dielectric reflective coatings for use with laser systems in ultraviolet, visual and infrared regions. **RESEARCH AND PRODUCTION**– Continuing and expanding research is carried out in basic phenomena of optical interference, in basic studies of optical properties of various new materials, and in theoretical design of optical interference systems. □ Thirty-two vacuum chambers provide production capacity for large volume and specialty items. Products range from simple aluminum front surface mirrors to sophisticated multilayer infrared filters. Complete substrate fabrication is carried out. A new building, providing double the former laboratory space has recently been added to the OCLI facility. This extra capacity, with its new production and test equipment, plus additional engineering and research personnel ensures continued complete services to the Optical Engineer.

New Solar Simulator reproduces sun's spectral distribution at zero air mass. Uses only all-dielectric beam splitters and trimming filters designed by OCLI especially for this instrument. Spectral match certified. 1 KW input.

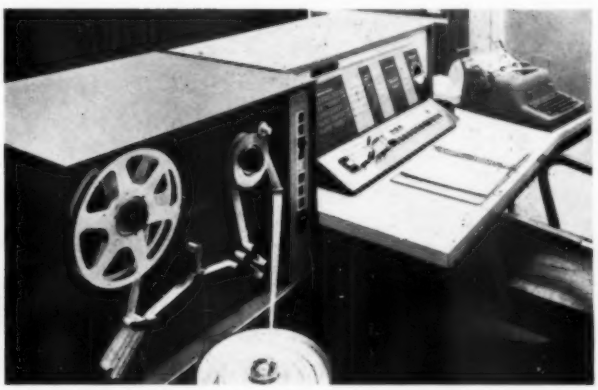

OCLI's computer facilities and exclusive programming are constantly employed to assist filter design, test data presentation, and systems evaluation.

for further information contact:

OPTICAL COATING LABORATORY, INC.

2789 GIFFEN AVENUE, SANTA ROSA, CALIFORNIA • TELEPHONE 707 LI 5-6440 • TELETYPE ZR 33

optical engineer

to design novel and ingenious optical devices for spacecraft

We have a need for someone who knows his theory (graduate work) and has also designed hardware. He must have made enough mistakes to learn what is practical and what isn't. He must be a guy who likes hardware and isn't happy until the gadget is working properly.

If this description fits you, there is a good job waiting in Colorado. Send a resume to D. S. Stacey, Technical Director.

BALL BROTHERS RESEARCH CORPORATION
BOULDER 30, COLORADO
AN EQUAL OPPORTUNITY EMPLOYER

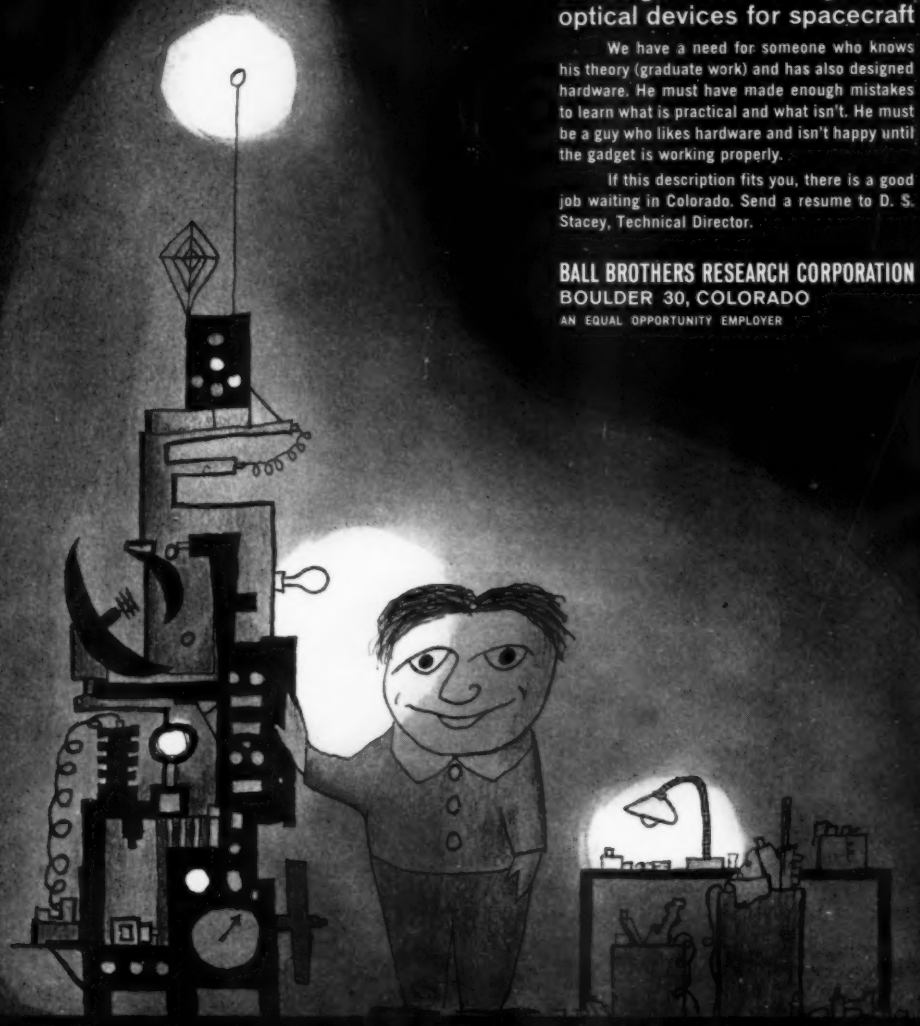

OSO-I Designed and built by BBRC and launched March 7, 1962. All systems worked perfectly.

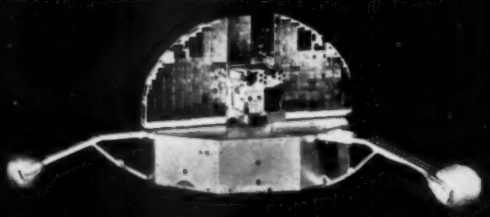

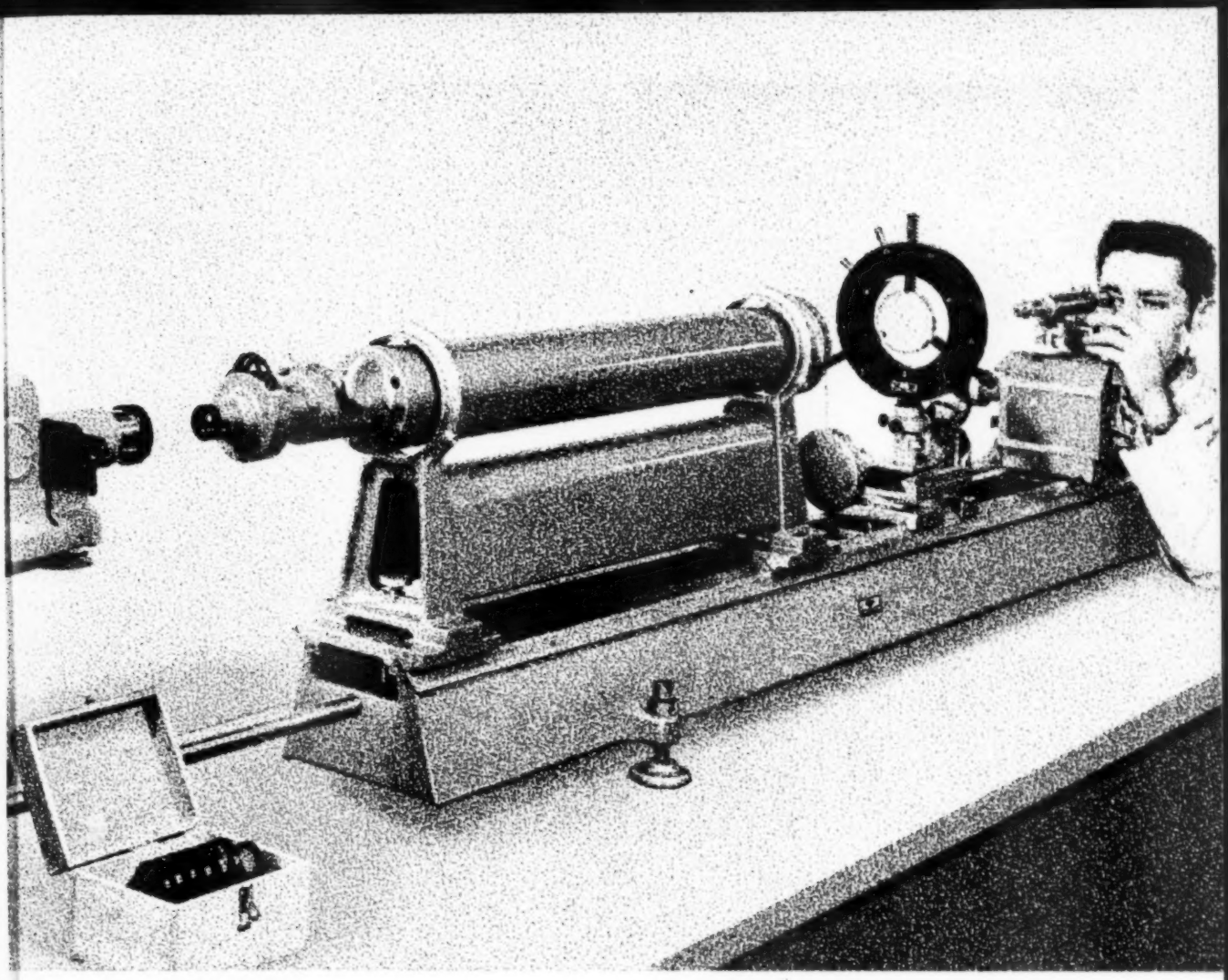

You owe it to your work . . .

You owe it to your work to avoid compromise in the selection of optical instruments. Equipment must be equal to your abilities and to the challenge of your work. Gaertner provides such instruments. For example, the lathe-bed-type optical bench owes its acceptence to its dependably permanent straightness, achieved by precision grinding of V and flat ways directly on a substantial casting of normalized meehanite. The complete assembly is widely used for measuring the focal lengths and aberrations of lenses and lens systems. The precision bed and carriages with rotary and three-way motions are available separately. These, together with a large selection of holders, diaphragms, slits and other accessories, provide versatile equipment for experimental setups where alignment and stability are important. Further, a number of beds can be bolted together end-to-end to provide a bench of any desired length. To meet unusual needs, Gaertner offers modifications of its wide range of precision optical and measuring instruments as well as special systems from your drawing or sketches. (Gaertner people have been doing this in Chicago since 1896.) For complete information on Gaertner optical and instrument benches, send for Bulletin 156-59. Find out why Gaertner instruments are the equipment of choice for the serious investigator. GSC-2-210

Gaertner

Gaertner Scientific Corporation 1294 Wrightwood Avenue Chicago 14, Illinois, U.S.A. Area Code 312, BUckingham 1-5335

A FLY'S EYE—150X MAGNIFICATION

like to hire a new kind of private eye?

Looking for a new kind of eye? Impressed by the long distance vision of TIROS and NIMBUS? Those were ELGEET lens systems specifically engineered to prove that "pie-in-the-sky" could become actual "eye-in-the-sky" concepts. At ELGEET we have the optical know-how and the design imagination you may be seeking for your own project. We'll send our Design Section to meet with you in your office and take that optical problem off your desk. We feed it into experienced minds and high-speed computers to break-through to your possible solutions. Let ELGEET be your Private Eye. Take your choice of a deep look, a quick look, a dim look, a bright look, a wide look, a forward look, a top-side look or an underbelly look. But first: *write to* ELGEET OPTICAL COMPANY, *838 Smith Street, Rochester 6, New York for a fully illustrated information file on our optical capabilities and performance.*

CREATIVE OPTICS
Elgeet
FOR EARTH AND SPACE

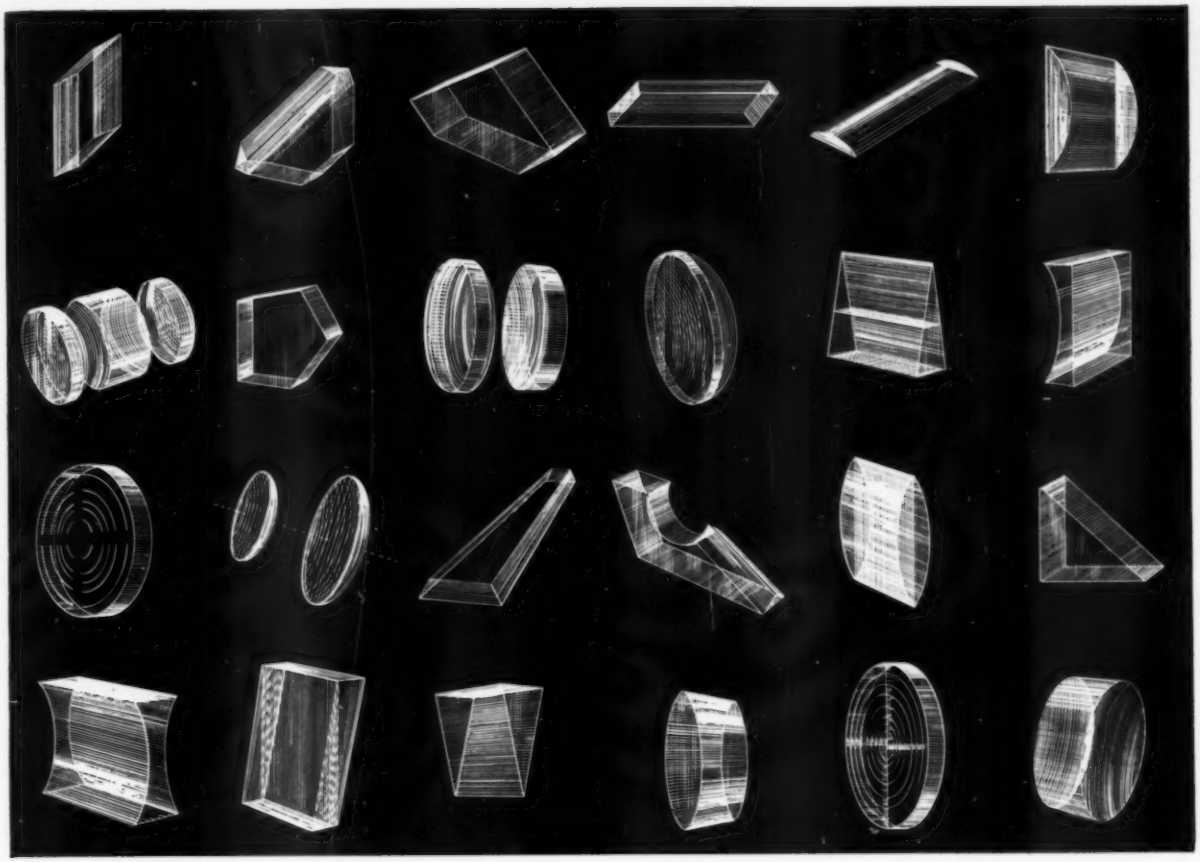

OPTICS FOR ELECTRONICS . . .

Components and systems for visible, ultraviolet, and infrared radiation. GEC's Astron-Optics Division specializes in design, development, and manufacturing of optical components and systems for the ultraviolet through infrared spectrum.

Here are a few of the optical components you can order from Astron-Optics: prisms, flats, spherical, aspherical and parabolic surfaces, reticles, information choppers, encoders, precision vacuum coating, and optically polished synthetic crystals.

Also available from Astron-Optics are infrared and optical-electronic systems.

For complete information regarding your precision optical requirements, write today to:

ASTRON OPTICS DIVISION

. . . precision optics at work

GENERAL ELECTRODYNAMICS CORPORATION

4430 FOREST LANE • GARLAND, TEXAS • BROADWAY 6-1161

ONLY JARRELL-ASH MAKES 11 TYPES OF SPECTROMETERS...

because no one spectrometer is versatile enough for all analytical and research problems

WADSWORTH STIGMATIC SPECTROGRAPH

HIGH APERTURE SPECTROGRAPHS

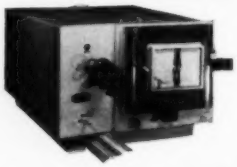

F/6.3 plane grating instruments for analysis of faint or short duration light sources as encountered in combustion studies, shock tube investigations, high temperature and free radical studies; time resolved spectroscopy. Photoelectric attachment available.

1M & 2M NORMAL INCIDENCE VACUUM SPECTROGRAPHS

1M & 0.5M SEYA-NAMIOKA VACUUM SPECTROMETERS

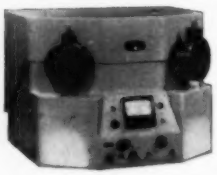

Vacuum Scanning Spectrometers, Seya-Namioka Model available in 1.0 or 0.5 meter models with optional camera and light sources and detectors for absorption and emission studies. Virtually universal monochromators, they offer a complete scanning range from 0 to 10,000A.

6.65M VACUUM EAGLE SPECTROGRAPH

1.8M EVACUABLE EBERT SCANNING SPECTROMETER

0.5M EBERT SCANNING SPECTROMETER

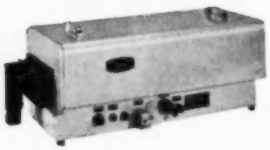

0.5 meter Ebert-type plane grating instrument is available with a variety of photomultiplier receivers and electronics systems. Also available as a flame spectrometer with full accessories. Applications include combustion and reaction studies, flame temperature measurement and atomic absorption spectroscopy.

5.0M VACUUM SPECTROGRAPH

1.0M EVACUABLE EBERT SCANNING SPECTROMETER

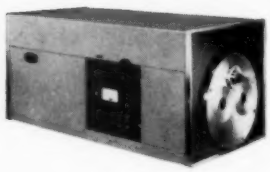

For direct measurement of relative line intensities . . . ultra high resolutions. Equipped with 12-speed precision linear wavelength scanning drive. High aperature (F/8.6). Very high photoelectric speed. Similar to 1.83M ultra high resolution spectrometer.

1.0M VACUUM GRAZING INCIDENCE SPECTROGRAPHS

3.4 and 2.25M EBERT SPECTROGRAPHS

These instruments may be fitted with multiple photomultipliers or adapted for precise scanning work. The Ebert, with order sorter, permits high resolution studies to be made with ease. Plasma sources, laser, crystal studies, high temperature measurements, combustion studies only hint at the spectrometer's full range of applications.

Let us bring your files up to date with complete information about all eleven. Write for literature or ask to have our analytical methods engineer visit your laboratory.

Jarrell—Ash **JARRELL-ASH COMPANY**

26 Farwell Street
Newtonville 60, Massachusetts

OPTOVAC

HIGH QUALITY STANDARDS

. . . in Optical Crystal Blanks

CALCIUM FLUORIDE
BARIUM FLUORIDE
SODIUM CHLORIDE
POTASSIUM CHLORIDE
POTASSIUM BROMIDE

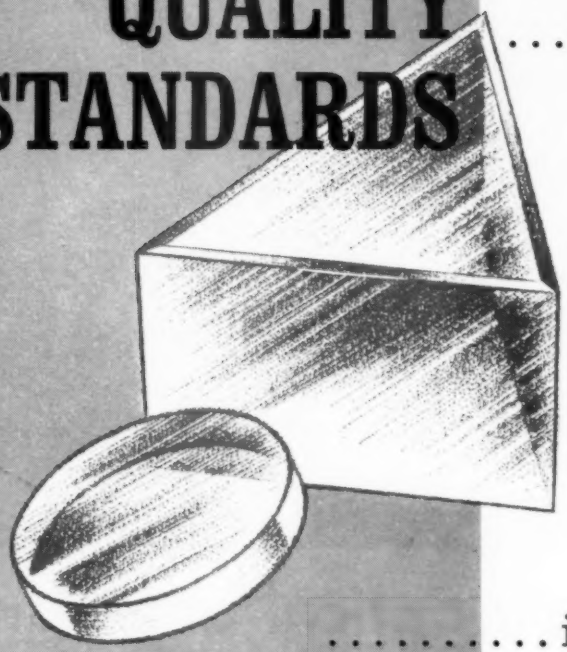

Prompt Delivery • Large Size Availability • Precision Cutting • Scattering Free • Impurity-absorption Free • Strain Free

. . . . . in Optical Maser Crystals

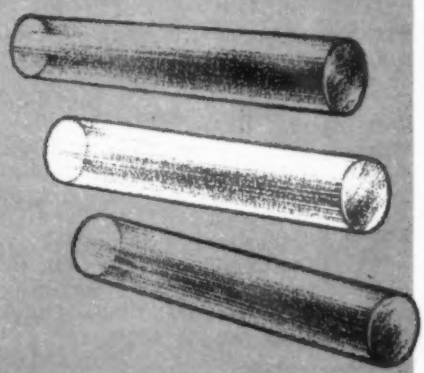

Quality is essential in optical masers — for the development of new maser materials and to attain CW operation. Optical scattering, for example, can be the main obstacle to the successful masing of new materials. Optovac has been working with many of the research laboratories in the field with utmost emphasis on quality. Our particular interest is in the melt grown halides with rare earth and uranium dopings.

Optovac "firsts" in maser materials:

U^{+3} in CaF_2 grown for and first masedby Stevenson and Sorokin of IBM.

U^{+3} in BaF_2 first masedby Dr. Perry Miles of MIT.

Nd^{+3} in CaF_2 first masedby Bell Laboratories.

First CW operation of U^{+3} in CaF_2 by Bell Laboratories, as reported at the Phys. Soc., New York, January 24, 1962.

OPTOVAC, INC.

NORTH BROOKFIELD, MASSACHUSETTS

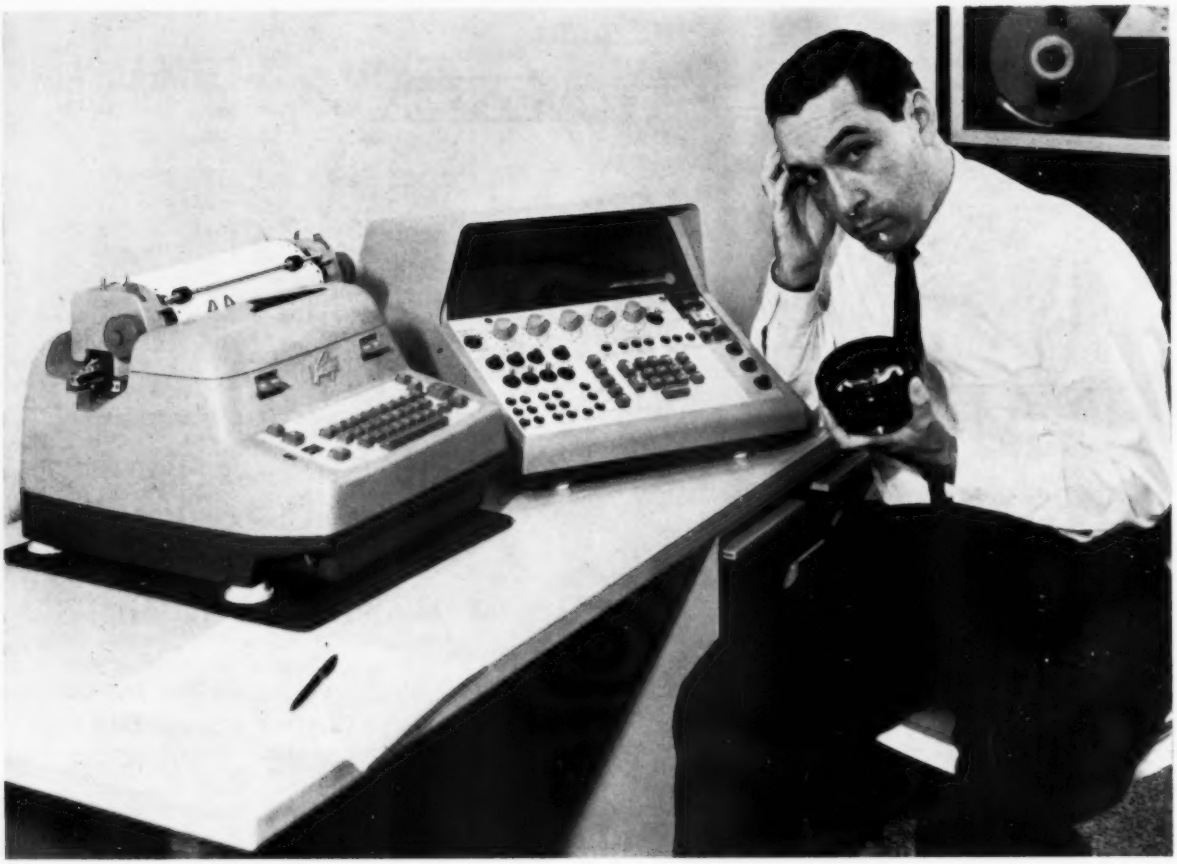

How to save 10% on optical glass and spend more on lens design changes

A fable specially designed for Design Engineers who think the lowest-priced optical glass is best

Once upon a time there was an optical engineer who loved his battery of computers better than anything else in the entire world. He spent all of his days and many of his nights while his computers clicked their relays and flashed their five watt bulbs just like a movie marquee.

Every so often he would feed his favorite computers with a mixture of formulas and problems and stand back to wait for the results he expected to be correct every time.

And correct they were! For the computer had a wonderful brain, and as fast as new lens designs were completed they were rushed into Production where talented craftsmen slowly worked the designs into optical perfection.

When all of the lenses were polished and finished everyone stood back and admired the work. Everyone, that is, except the customer. "The products are beautiful, the computers are brilliant, the craftsmen are skilled," he said, "but the lenses aren't uniform. They're worthless and must be re-worked, every one."

Glass not uniform? "It's that bonehead purchasing agent," thought the designer. But when he confronted the purchasing agent he found the P.A. had followed the specs to the tenth place and bought the lowest-priced glass—as the designer had suggested.

And that's the story of how quality optical glass, the kind Ohara produces, came to be the only glass allowed near the designer's favorite computers. The results have been rewarding. Glass now costs a bit more to start, but lens designs are guaranteed.

Moral: The best of computers and men are helpless when optical glass lacks uniformity through multiple melts.

Ohara Optical Glass not only provides .0008n_D on the first melt, but Ohara's ability to maintain melt uniformity guarantees the same high quality melt after melt.

If you require the very finest quality glass then specify Ohara.

For your copy of Ohara's reference catalog just write or call today.

OHARA OPTICAL GLASS

Exclusive distributors:
Pacific Optical Corporation
120 South Glasgow
Inglewood, California

AS LASER SPECIALISTS

Semi-Elements has the most complete line of highest quality LASER Single Crystals . . .

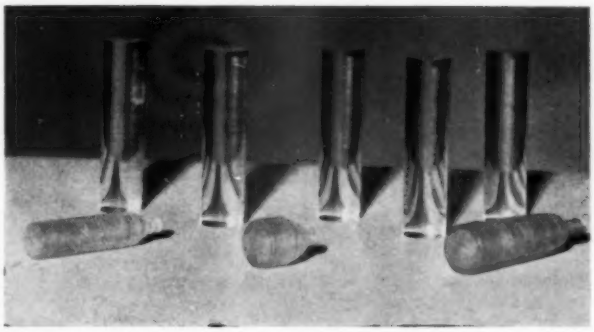

CaF_2, BaF_2, CdF_2, SrF_2, CaO_2,
$CaWO_4$, MgO, MnF_2, Al_2O_3, TiO_2,
$KMnF_2$, $RbMnF_2$, $SrMoO_4 \cdot SrWO_4$
$SrF_2 : BaF_2$, $SrF_2 \cdot CaF_2$
$SrF_2 \cdot BaF_2 \cdot CaF_2$

Due to the vast research and development effort of Semi-Elements during the past months, our LASER Crystals have been increasing rapidly. We have received many inquiries asking how it is possible to have so many new single crystals available over such a short period of time. Our progressive organization, highly specialized facilities, and ranking technical personnel having specific capabilities and experience with LASERS, account for our continuing strides in the LASER field. Semi-Elements will consider all your LASER Single Crystal problems. Tell us about your requirements.

We are currently in
FULL SCALE PRODUCTION OF
$CaWO_4$ single Crystal
GLASS LASERS
doped with rare earths and
transition elements

Some new Crystals now in development which show promise are:

CESIUM MOLYBDATE
BARIUM MOLYBDATE
LEAD MOLYBDATE
CESIUM TUNGSTATE
ZINC TUNGSTATE

—ANNOUNCING—
PLASTIC LASERS
LIQUID LASERS
DOPED WITH RARE EARTHS AND TRANSITION ELEMENTS

Write for Complete Information—or Phone

SINGLE CRYSTAL DIVISION Dial 412 - 352 - 1548

SEMI-ELEMENTS, INC.

SAXONBURG BOULEVARD, SAXONBURG, PA., U.S.A.

HARSHAW MANUFACTURES A COMPLETE LINE OF SCINTILLATION AND OPTICAL CRYSTALS

SCINTILLATION *Mounted* NaI(T1) *Crystals*

Crystal detectors designed for the most sophisticated counting problems. Our physics and engineering group are available to assist you in your special detector problems.

More detailed information is contained in our 32-page book, "Harshaw Scintillation Phosphors". We invite you to write for your free copy!

STANDARD LINE

(Hermetically Sealed Crystal Assemblies)

- The accepted standard of the industry
- Proven through years of service in research, medical and industrial applications
- unparalleled performance
- dependability
- consistent good quality

INTEGRAL LINE

(Crystal photo multiplier tube combination assembly)

- Improved resolution
- Ready to use plug-in unit
- Permanently light sealed
- Capsule design facilitates decontamination
- Close dimensional tolerances
- Harshaw guaranteed

Large Crystal MATCHED WINDOW LINE

(Designed primarily for crystals 4" dia. and larger)

- "Small crystal" performance achieved through improved optical design
- Low mass containers
- Available in standard aluminum or complete low background assemblies
- Convenient mounting flange
- Ready to use

Every Harshaw crystal is a product of our experience in crystal growing technology since 1936

Other Phosphors Available from The Harshaw Chemical Company

ROUGH CUT THALLIUM ACTIVATED SODIUM IODIDE CRYSTAL BLANKS • EUROPIUM ACTIVATED-LITHIUM IODIDE (NORMAL) • EUROPIUM ACTIVATED LITHIUM IODIDE (96% Li^6 ENRICHED) • THALLIUM ACTIVATED CESIUM IODIDE • THALLIUM ACTIVATED POTASSIUM IODIDE • ANTHRACENE • PLASTIC PHOSPHORS

OPTICAL *Crystals*

For Infrared and Ultra Violet Transmitting Optics

"HARSHAW QUALITY" INHERENT IN EACH HARSHAW-GROWN CRYSTAL GUARANTEES THE MOST EFFICIENT OPTICAL TRANSMISSION POSSIBLE THROUGH:

1) Negligible light scattering in crystals, permitting higher sensitivity and improved resolution
2) Freedom from absorptions caused by trace impurities in crystal optics
3) Minimum strain

"HARSHAW QUALITY" meets the demand for uniformity of optical properties such as dispersion and refractive index.

Prices, specifications, or other information will be sent in answer to your inquiry.

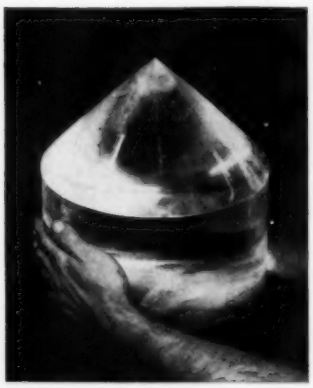

The following infrared and ultra violet transmitting crystals are available; others are in the process of development:

SODIUM CHLORIDE • SODIUM CHLORIDE MONOCHROMATOR PLATES • POTASSIUM BROMIDE • POTASSIUM BROMIDE PELLET POWDER (through 200 on 325 mesh) • POTASSIUM CHLORIDE • OPTICAL SILVER CHLORIDE • THALLIUM BROMIDE IODIDE • LITHIUM FLUORIDE • LITHIUM FLUORIDE MONOCHROMATOR PLATES • CALCIUM FLUORIDE • BARIUM FLUORIDE • CESIUM BROMIDE • CESIUM IODIDE

Additional information on the physical and optical properties of the above crystals is available in our 36-page booklet "Synthetic Optical Crystals". Send for your free copy.

HARSHAW

THE HARSHAW CHEMICAL CO.

Crystal Division • Cleveland 6, Ohio

Optical Engineering

Roderic M. Scott

The optical design itself is very often a small portion of the engineering effort on an optical instrument The optical engineer, when he sets about to design an optical system, must concern himself with problems in the fields of structures, associated electronic systems, materials, specifications, and test methods. This paper describes some examples of current activities in each of these fields. In addition, this paper considers the influences on design of temperature and mechanical shape, and presents pertinent examples of solutions to specific problems. Various methods are described for supporting refractive and reflective optical elements, both large and small, and the influence of the need for reduced weight is discussed. Requirements for satellite systems are also considered. Furthermore, the importance of electronic subsystems, as well as their interrelation with optical and structural design, is treated. Several examples of guidance systems are discussed as well as some problems of focusing. Sections are also included on performance specifications and quality control by the use of modulation transfer functions.

Introduction

Webster defines engineering, first, as "the art of managing engines" and second, as "the applied science concerned with the utilization of properties of matter, sources of power, and physical forces for supplying human needs in the form of structures, precision instruments, communication, public safety, and other productive work."

In optical engineering, we need not concern ourselves very much with the first definition. We should, however, point out that astronomers, particularly the classical sort as differentiated from the radio astronomer, and on occasion many others who utilize optical instruments and manage optical systems, might be considered as optical engineers. We may look forward to a period during which unmanned optical systems in space will become common. These systems will be utilized both in the interests of public safety and in other productive work as optical engines under human control, and thus requiring the services of optical engineers.

Of more immediate concern, however, is the second part of the definition. This point involves the application of science in combining many disciplines to surround and support the specific optical components and hence to provide the various functions stated above in the definition. It would be quite impossible in any article of reasonable length to provide a complete coverage of all aspects of optical engineering. This article will, therefore, concentrate on certain aspects of current interest.

The selection and definition of optical materials is part of the problem of the optical designer whenever the physical properties of the materials enter directly into the optical characteristics of the system. In many cases, however, these materials have both optical properties and "engineering" properties. This is quite obviously true of materials which are used to support reflecting surfaces of mirrors. It is also true, if not obviously so, for the materials of the refracting elements of the system as well.

Surrounding the optics must be a structure to hold them in their proper positions. The design and analysis of this structure, like any mechanical structure, is a basic engineering activity. The performance of a microscope, and certainly the convenience of its use, depends directly on the skill and creativity of the designer who conceived its mechanism and structure. The performance of a large telescope is as much determined by the characteristics of its structure and mounting as in the quality and execution of its optical design. Thus this paper will also include a section on structures.

Many modern optical instruments are combined with various electronic devices. In some instruments these devices measure or compare intensities. In other instances, electronics may be the mechanism by which the guiding or pointing of the instrument is achieved. In addition, an electronic mechanism may record or transmit the information which the instrument was designed to provide. We shall discuss some aspects of the

The author is with The Perkin-Elmer Corporation, Norwalk, Connecticut.

Received 9 March 1962.

interrelationship between electronics and optics in a few instruments.

In order for a machine to operate properly, the engineer must not only design it to perform its function, but must also provide specifications for its components. Thus, quality control and determination of optical elements and systems becomes an important aspect of optical engineering. In this connection, an engineer, as he proceeds with the design of the system, must be able to predict its performance with some accuracy. This engineering function is of great importance for two basic reasons: First, it permits the eventual user of the system to decide whether the expected performance is worth the investment and man-hours of effort required for its manufacture. Second, it permits an accurate evaluation of the relative importance of various factors which influence performance. It is the basis of sound engineering to apportion the design effort among the many aspects of a system so as to deal most forcefully with those aspects which have the greatest influence on the performance of the device. Thus, this review of optical engineering will discuss some modern methods of performance prediction and appraisal.

Engineering Structures

In times past, only astronomers were interested in optical systems of very large size. Today, however, missile and satellite tracking, high-resolution reconnaissance, high-speed wind tunnels, and shock tubes all call for larger and more massive optics. Not only must the elements be of larger size and, therefore, greater weight than have been required in the past, but some must survive accelerations and vibrations of large magnitude. Even astronomers, who had turned to their advantage the most advanced engineering methods in the construction of the largest optical systems in existence today, are developing requirements for systems which, although of more modest size, require even more advanced engineering considerations. Current undertakings in astronomical instruments pose a wide variety of new problems not faced before by designers of optical instruments. A good example of such an undertaking is the Orbiting Astronomical Observatory, presently under construction for NASA.

Before discussing some of the particular problems of space optics, we should consider problems associated with terrestrial instruments. The current design and construction of such instruments is not aimed at the largest possible size, but at higher performance.

Some recent instruments which represent the current state of the art in the optical engineering of devices of astronomical type are the ROTI and IGOR for missile tracking, the 305-cm (120-in.) reflector at Lick Observatory, the 91-cm (36-in.) and 213-cm (84-in.) telescopes for the Kitt Peak National Observatory, the 50-cm (20-in.) Satrack satellite tracking telescopes, and the 91-cm (36-in.) Balloon-Borne Telescope for Project Stratoscope II.* For some time it has been the general practice, as part of the optical design effort, to compute the effect of misalignments of the various optical components on system performance. Such computations furnish a good indication of the required accuracies in construction and adjustment. They do not, however, necessarily point the way to an optimum original choice of optical form.

Cassegrain and Cassegrain-like catadioptric systems are enjoying considerable popularity at the moment because of their ability to provide long focal lengths in short and, therefore, light packages. Meinel[1] has suggested that the mechanical deflections and optical effects should be analyzed together. Since this approach offers a good example of the problems of the optical engineer, it will be presented here.

Decollimation of the secondary mirror in a Cassegrain system results in an image error resembling coma. The total length of such a comatic image in an otherwise perfect system is given by

$$\epsilon = \frac{3m}{16F_c}(m^2 - 1)\delta. \tag{1}$$

Here F_c is the f ratio of the Cassegrain system, m is the magnification of the secondary, and δ is the lateral displacement of the secondary from the axis of the primary.

The length l of the structure from primary to secondary is related to the focal length f_p of the primary by

$$l = \frac{mf_p}{m + 1}. \tag{2}$$

Upon the assumption that the principal weight supported is the secondary mirror itself, the deflection of the structure δ is

$$\delta = \frac{Pl^3}{8EI}. \tag{3}$$

Equation (3) is the normal beam deflection formula. It is a great simplification over the actual deflection relation for any particular structure, and should represent a good approximation. Thus it will serve for the initial stage of engineering selection. The Young's modulus of elasticity and the moment of inertia of the cross section are E and I, respectively. The load P is the weight of the secondary mirror and is given by

$$P = \rho_m ka^3 = \rho_m k \frac{A^3}{(m + 1)^3}. \tag{4}$$

In this expression, ρ_m is the effective density of the mirror material, whether it is solid or a lightened structure, k is the thickness-to-diameter ratio, and a and A are the apertures of the secondary and of the system.

* The Stratoscope II Telescope System is being built for Princeton University with support from the National Science Foundation, the Office of Naval Research, and NASA.

The moment of inertia of the cross section of the support structure may be considered to be the product of the square of an effective radius R^2 and a cross section area α. If, however, the weight of the structure is to be minimized to some value W, then

$$I = R^2 \alpha, \quad W = \rho_s \alpha l \tag{5}$$

and

$$I = \frac{R^2 W}{\rho_s l}$$

where ρ_s is the density of the material of the structure.

By a combination of all of the above, it follows that

$$\epsilon = \frac{3}{128} \frac{\rho_m \rho_s k}{E W} \cdot \frac{A^4 l^2}{R^2} \cdot \frac{m(m^2 - 1)}{(m + 1)^4}. \tag{6}$$

Since the radius of the structure is closely related to the aperture, $R \simeq 2A$, and $m > 1$, this expression becomes in effect

$$\epsilon = K \frac{A^2 l^2}{m} = K \frac{A^2 f_p^4}{f_t}. \tag{7}$$

In the second expression the effective focal length of the telescope has been substituted for the magnification ratio. It is then apparent that the effect of the deflection of the structure can be greatly reduced by making the focal length of the primary as short as possible. A similar analysis could be used for the case where the weight of the structure itself represents the major deflection producing force.

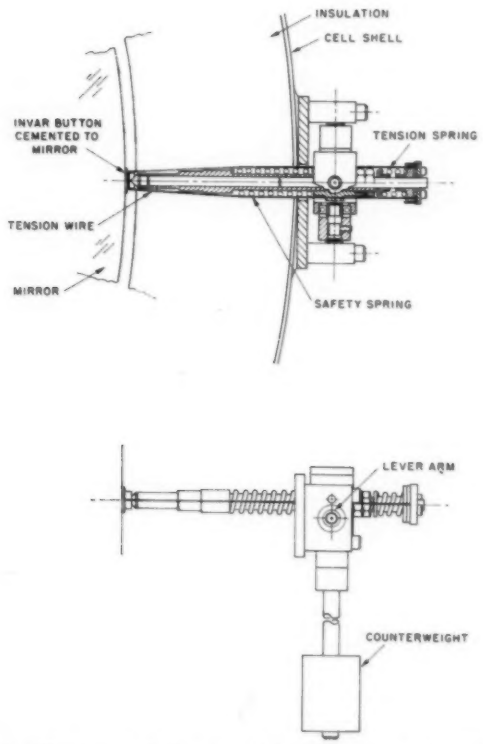

Fig. 1. The design of edge support for a 91-cm (36-in.) mirror for Stratoscope II.

This problem of the selection of the focal ratio of the primary mirror in Cassegrain-like systems is influenced strongly by the difficulty of making accurate optical surfaces on deep curves. There are currently under development several types of catadioptric systems which combine the basic Cassegrain two-mirror system with other optics to achieve better field performance.[2] Some of these systems have the advantage that the primary mirrors are spherical and thus quite straightforward in manufacture, even for deep curves, and especially when used off-axis. Paraboloids, however, present a more difficult task. The 500-cm (200-in.) telescope has a relative aperture of $f/3.3$ and the Kitt Peak 213-cm (84-in.) telescope is to have a relative aperture of $f/2.75$. These values represent the present best compromise between difficulty in optical manufacture and shortness of tube. This difficulty comes about partially in working the surface and partially in testing it. The 91-cm (36-in.) Stratoscope II telescope mirror has a speed of $f/4$. This value was chosen because of the extreme requirements on surface accuracy resulting from a desire to utilize, to the maximum, the conditions of nearly perfect "seeing" occurring at the balloon altitude of 25 km (80,000 ft). In spite of the desirability of a short instrument, it was believed that $f/4$ represented the fastest system which could be made to the required accuracy.

The support of large reflecting optics has been the subject of considerable engineering attention throughout the development of telescopes. Large mirrors tend to deform under their own weight if not properly supported. Since most mirrors must perform in various positions with respect to the direction of gravity, a variety of counterbalanced support systems have been developed.

The support system of the 500-cm (200-in.) Hale telescope, the 305-cm (120-in.) Lick telescope, and the 213-cm (84-in.) and 91-cm (36-in.) Kitt Peak telescopes are well described in a recent book.[1] The back supports for such large mirrors are well developed. On the other hand, designs for mirror edge supports, which become more and more important as the telescope moves away from the zenith, are still in a fluid state. Since the back supports are never required to supply a tension force, their design is simplified. When the mirror is nearly vertical, however, much of the support for its weight comes from the edge. Figure 1 depicts the edge support for the 91-cm (36-in.) mirror of the Stratoscope II telescope. The attachments are cemented* to the edge

* Cement EC-1472 and/or 1473, manufactured by Minnesota Mining and Manufacturing Company.

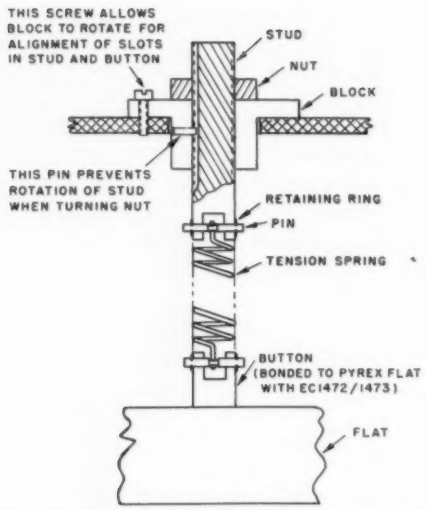

Fig. 2. A support for a 94-cm (37-in.) flat operated face downward. The support is completely in tension from the back of the mirror.

of the mirror and provide forces of either sign as required. This type of mount has been successfully applied to a 94-cm (37-in.) flat supported with its reflecting face downward. The fifteen tension supports are springs attached to buttons cemented to the back, as shown in Fig. 2. This mirror is always used in a horizontal position. No errors produced by the support system are detectable. The success of this design, in which the attachment is by cement, encourages the use of such bidirectional supports in those systems in which the mirrors must operate on edge or inverted.

Turning now to optical systems for satellite use, we find that the engineering problems are significantly different. First, the optical system is expected to perform in use under conditions of nearly zero gravitational field. On the other hand, the range of operating temperatures can be very large indeed. The satellite capsule itself is sometimes exposed to the direct rays of the sun on one side and to the cold of space on the other. At other times it may be shielded from the sun when in the shadow of the earth. The expected temperature history of such a satellite is a complex problem indeed, for it involves radiative interaction with the earth as well. It is beyond the scope of this paper to consider these expected variations, but it might be well to point out some of the measures which have been taken to reduce their effect on the optics. In a later section we will discuss some of the characteristics of optical materials for this application.

Temperature variations have three important effects on optical systems. The first of these is the misalignment of the optics due to differential expansion or contraction of various portions of the structure. This may be caused either by inclusion of materials of different coefficients of expansion, or by temperatures differing from point to point, or by both effects together. One obvious course is to build the structure of invar and rely on its small temperature coefficient of expansion. It must be remembered, however, that this coefficient is small only at low temperatures. In applications where temperatures may become very high, invar behaves much like normal iron alloys.

The second important effect of temperatures on optical systems is the distortion of the optical elements. This effect becomes particularly important for mirrors, due to difference in expansion of the mountings and optics.

It has been seriously proposed to build the entire positioning structure of quartz or alternately of beryllium, depending upon whether the mirrors are of quartz or beryllium. Whether it is practical or not to build the entire structure of a single material, it is still important to be sure that the variation of temperature from point to point does not disturb the structure or the optics. Thus, an important segment of the thermal analysis involves the consideration of the thermal paths connecting an optical structure to the rest of the satellite. Some discussion of this problem is included in a paper by Spitzer.[3]

For satellites carrying optical systems in low orbits, the interaction of any magnetic material in the satellite (including the structure of the optical system) with the magnetic field of the earth, is an important consideration. Since any such satellites for astronomical work will have a requirement limiting the total magnetization of the satellite to a low value, care must be exercised in the employment of materials such as invar.

The third important effect of temperature change on optical systems is variation of focus. Short-focal-length optical systems can generally be focused on the ground with sufficient accuracy so that focus need not be corrected in orbit—provided proper corrections are made for the effect of expected operating temperatures and the index of refraction of the air. There seems little chance of applying this principle to either large optical systems or ones of high resolution. Therefore on these systems some form of focusing mechanism will be necessary.

In the Stratoscope II telescope system, a method of focusing has been explored which could also be used in satellite optical systems. In this telescope, the guidance system utilizes an image in the focal plane of the principal optics. If the image departs from its desired position, correction signals, developed by photocells, move a small relay lens to bring the image back to its nominal position. The gain around this loop depends on the sharpness of the image. On command, a small ac signal is introduced into the loop. The resulting amplitude of motion of the relay lens is a measure of the sharpness of the image. Sharper images require smaller

motions to produce signals which just balance the injected ac voltage. The amplitude of motion of the relay lens is telemetered to the ground and the operator may drive the focusing element to reduce the motion to a minimum. Minimum motion of the relay lens indicates a minimum size of image and, therefore, the best focus. The amplitude and frequency of the injected signals are not important, as long as they lie within the linear performance range of the servo loop. In Stratoscope II, which is always under an operator's command, it was not felt worthwhile to make this focusing automatic. The automation of this feature, if desirable for a satellite application, would not seem to be difficult.

Other automatic focus devices have been developed over the past few years. Some of these are completely contained within the instrument and determine a condition of focus for infinity. One such system utilizes a pair of pentaprisms at the opposite ends of a diameter of the aperture. These prisms redirect rays emanating from a point source near the focal plane back to a point image, also near the focal plane. A beam from the source located outside the useful field of the instrument passes through the optical system, is reflected by one of the prisms across the aperture, and is then reflected by the second prism back into the system. A second beam from the source traces the same loop in the opposite direction. Since the beams are returned parallel to themselves by the pentaprisms, they intersect at the source only if the source is in the focal plane for objects at infinity. A variety of beamsplitter and photocell arrangements have been used to detect this condition.

In systems of moderate size, an optically flat, dichroic filter on the object side of the system may be used as an autocollimating reflector for the determination of proper focus. The focus detector works in a wavelength region reflected by the filter. Provision for the offset of focus, due to any chromatic error of the system, must be included.

A variety of other systems developed for aerial photography depends on the principle that the highest spatial frequencies are observed at the proper focal plane. Devices which scan the focal plane and analyze the resulting signal for its high-frequency components provide information which is utilized to bring the optics into proper focus.

There are several other structural featuers of satellite optical systems which must be considered by the engineer. One of these concerns the question of asymmetry of the instrument with respect to its center of gravity. The various optical components and auxiliaries must be designed and laid out with due consideration for perturbing torques, such as residual air drag, solar radiation pressure, and tidal and magnetic forces. These all produce torques which, if large enough, must be counteracted in some way. Hence, they impose additional loads on the guidance mechanisms. Many such guidance mechanisms have been suggested. Among these are jets of various sorts, magnetically supported spheres for producing torque through inertial reaction, and a variety of flywheel configurations. Although these devices are not directly a part of the optical system, their design is conditioned by the weight distribution and moment of inertia of the optics and its structure.

A particularly interesting example of the inertial problem arises in the Stratoscope II system. Because of the shape of this system, as established by the optical configuration, the three principal moments of inertia of the system are not equal, nor do they correspond to the available axes in the support. To further complicate the problem, the coordinates in which the errors in guidance are detected could not conveniently be made to correspond with the principal axes of inertia. Torques to provide motions for acquisition or to correct pointing can be applied to the instrument only through its support axes. The equivalent limitation in satellites concerns the fact that torques can only be brought to bear on the satellite about axes associated with torque-producing mechanisms. In some optical satellites, great efforts are made to make the moments of inertia equal, and thus to alleviate this problem.

The solution in the former case was to resolve the error signals from the coordinate system of the detectors into errors in the coordinate system of the principal axes of inertia. This resolution is fixed, since the detector coordinates and the inertia axes are both fixed in the structure. At this point, the filter networks for the servo systems are inserted to compensate for the variation in the magnitude of the moments of inertia. The result is then further resolved into the coordinates of the axis of the support system. At this point the resolution is dependent on the relative angles between the axis and must, therefore, be done in an active manner with resolvers. The block diagram of Fig. 3 shows the system just described.

Optical Materials

A problem of growing significance to the optical instrument designer is the selection of optical materials as influenced by their physical properties. In the past,

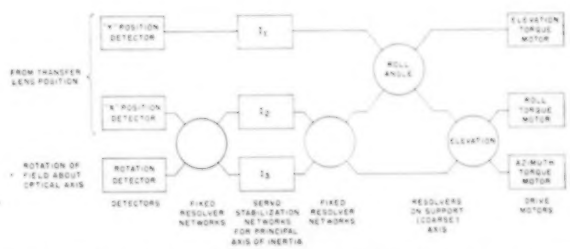

Fig. 3. Block diagram of the guidance system for Stratoscope II showing the axes transformations.

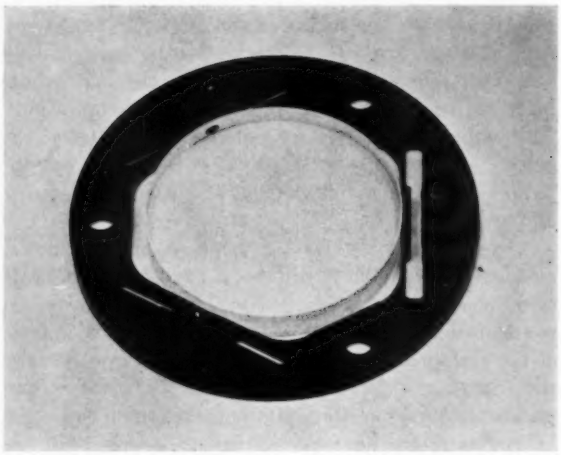

Fig. 4. A lens mount to provide for large differential expansion.

the lens designer has had quite a free hand in the selection of the specific materials which he wished to employ. His selection was based almost exclusively on index of refraction, dispersion, and transparency. Some materials, of course, were known to be attacked by moisture and were often avoided for this reason. Optical systems, however, have grown rapidly in size and this has introduced new requirements for selection. Perhaps even more importantly, optical engineers are being required to consider systems in which the environmental conditions of temperature and vibration are increasingly important.

In one recently designed lens system, the designer, together with the optical engineer, succeeded in choosing materials for the lens elements and mounting to produce an optical system whose focal length and focal position are quite independent of temperature over a considerable range.

An important lack in glass catalogues is information concerning the physical properties of the large variety of optical glasses now available. While there is some information on density and coefficient of expansion, this variation and the change of index of refraction with temperature over wide temperature ranges are lacking for most glasses. Such data as are available at all are spread widely in the literature.[4]

In the Stratoscope II telescope, an optical element called the transfer lens is composed of quartz-fluorite triplets. These two materials have very different coefficients of expansion, and the lens must operate at the extremely low temperatures of the higher levels of the stratosphere. Unfortunately, the requirements for centering and spacing are extreme in this design. Consequently, the design engineer is faced with the difficult problem of holding the elements in proper alignment over the entire temperature range from room temperature, the conditions under which the lens will be assembled and tested, down to −51°C (−60°F). The type of mounting selected for this particular application is shown in Fig. 4. The thin, flexible springs are positioned to allow a large differential expansion between the optics and the cell. It is interesting to note that the only material with a temperature coefficient of expansion close to quartz—invar—could not be used. This lens is located in a strong magnetic field required by the servo mechanism which positions it. Invar is sufficiently magnetic to bring undesired forces into action on the lens.

The temperature problem becomes an extremely important consideration in the mounting of large elements when the weight becomes great enough to make spring mountings impractical. Figure 5 presents the engineering solution to a problem of this type. The differential expansion between the elements of a very large triplet and its mounting would produce unacceptable strain at low temperature if the clearances were sufficiently small properly to position the elements at high temperature. In this case, dissimilar metals are used to provide temperature compensation and maintain centering over a wide range of temperature. A further complication is the fact that the central element is kept dry. In this case, a seal is provided by the injection of Thiokol around the edges of the outer elements. This material provides no mechanical support, but simply insures that the flow of air in and out of the separation space is through the desiccator. There is an article in this issue by Leo J. Deterding which treats another aspect of the mounting of large lenses. In this case the necessary flexibility is provided by a plastic support.

Nonuniform temperature distributions within the glass itself have profound effects on the quality of the image because of the variation of index of refraction with temperature. A normal method of handling such a situation has been to set a tolerance for the image quality degradation from this cause; to compute

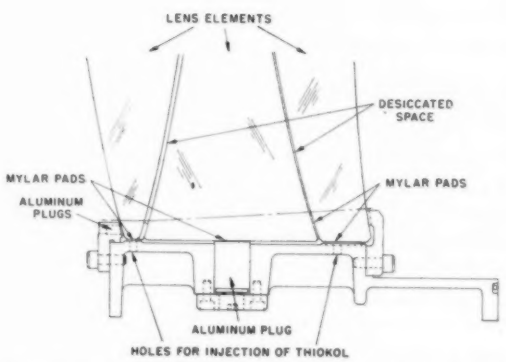

Fig. 5. The mounting for a large triplet whose optical components have widely different coefficients of expansion.

Table I. Physical Constants of Materials for Mirror Structures

	DENSITY (ρ)		MODULUS OF ELASTICITY (E)		E/ρ	$(E/\rho)'$	THERMAL CONDUCTIVITY (K)		SPECIFIC HEAT (C)		COEFFICIENT OF EXPANSION (α)		$K/C\alpha$	$(K/C\alpha)'$
	GRAMS / CM^3	LBS / IN^3	NEWTONS / CM^2	LBS / IN^2			CAL. / CM. -SEC. -°C	BTU / FT. -HR. -°F	CAL. / GM. -°C	BTU / LB. -°F	$°C^{-1}$	$°F^{-1}$		
FUSED QUARTZ	2.20	.080	7.0×10^6	10.1×10^6	3.18×10^6	1.00	.0033	.80	.188	.188	$.55 \times 10^{-6}$	$.31 \times 10^{-6}$	31.9×10^3	1.00
PYREX (7740)	2.35	.085	6.8×10^6	9.8×10^6	2.89×10^6	.91	.0027	.65	.25	.25	3.2×10^{-6}	1.8×10^{-6}	3.38×10^3	.106
VYCOR (7900)	2.18	.079	6.7×10^6	9.7×10^6	3.07×10^6	.97	.0022	.53	.19	.19	$.80 \times 10^{-6}$	$.44 \times 10^{-6}$	14.5×10^3	.45
INVAR (36%Ni)	8.0	.292	14.8×10^6	21.4×10^6	1.85×10^6	.58	.026	6.3	.095	.095	1.3×10^{-6}	$.70 \times 10^{-6}$	190×10^3	5.95
TITANIUM	4.54	.164	11.6×10^6	16.8×10^6	2.55×10^6	.80	.042	10.1	.126	.126	8.5×10^{-6}	4.7×10^{-6}	39.1×10^3	1.22
MAGNESIUM	1.74	.063	4.5×10^6	6.5×10^6	2.59×10^6	.81	.38	92	.25	.25	26×10^{-6}	14×10^{-6}	58.5×10^3	1.83
BERYLLIUM	1.82	.066	28×10^6	40×10^6	15.4×10^6	4.84	.38	92	.516	.516	12.4×10^{-6}	6.9×10^{-6}	59.5×10^3	1.86
PYROCERAM (9608)	2.50	.090	8.7×10^6	12.5×10^6	3.48×10^6	1.10	.0047	1.14	.19	.19	$.40 \times 10^{-6}$	$.22 \times 10^{-6}$	62.0×10^3	1.95
"FOAMGLASS"	.143	.0052	$.12 \times 10^6$	$.18 \times 10^6$	$.84 \times 10^6$	.26	.00014	.033	.20	.20	8.3×10^{-6}	4.6×10^{-6}	$.085 \times 10^3$	.0027
SILICA-SLIP CAST	1.9	.069					.00078	.188	.22	.22	$.54 \times 10^{-6}$	$.30 \times 10^{-6}$	6.5×10^3	.206
ALUMINUM	2.70	.097	6.9×10^6	10.0×10^6	2.56×10^6	.80	.53	128	.215	.215	23.9×10^{-6}	13.3×10^{-6}	100 x 1	3.14
ALLOY LA-685 (SUPER INVAR)	8.13	.294	13.8×10^6	20×10^6	1.70×10^6	.53	.026	6.3	.12	.12	0.1×10^{-6}	$.06 \times 10^{-6}$	2165×10^3	68.0

by normal optical methods the effect on the image due to a small variation of index; and then to attempt to maintain the temperature uniformity within the limits set by the tolerance. Almost all large optical systems are investigated in this fashion today. It is interesting to note that a rather complete paper by Sliusarev[5] in Russian has appeared on this subject. This paper provides a theoretical treatment of nonuniform temperature distribution in various optical components. Both the variations of the shape of the lens and variation of refractive index are discussed, and some rather general formulas are presented.

The selection of materials for mirrors in large optical systems is a problem receiving more and more attention. Table I is a tabulation of the important physical factors for a considerable number of materials which have been considered for potential use in mirrors. Some of these materials do not permit a satisfactory optical polish. However, the technique of coating such materials, either by chemical deposition of Kanigen (a nickel phosphide) or by vacuum deposition of silicon monoxide or quartz, has reached a sufficient state of development to permit the serious consideration of any otherwise desirable material.

For applications to large optics in environments with wide temperature variations, there are five important physical properties. The density and modulus of elasticity are significant because they influence the structural design of the mirror. The optical engineer no longer need confine himself to solid disks for blanks but, for nearly all of the materials listed, can consider fabricated structures which provide high rigidity and reduced weight. Figure 6 is an example of such a fabricated structure in fused quartz. The important relationship between the density and the modulus of elasticity is their ratio, since this is the factor which enters all equations for the analysis of deformation produced by the direct weight of the mirror. It can be seen from an examination of Table I that, of the materials listed, beryllium has the most favorable ratio. This material is nearly 5 times as rigid, for a given weight and structure, as fused quartz. There are many difficulties associated with the fabrication of mirrors of beryllium. The advantages of the material are so attractive, however, that there is little doubt that a great many large optical mirrors will be fabricated from this material in the future.

The distortion of a mirror under transient conditions in its thermal environment is related to the thermal conductivity, specific heat, and coefficient of expansion. These three quantities are related in the figure of merit shown in the 13th column of Table I. The variations

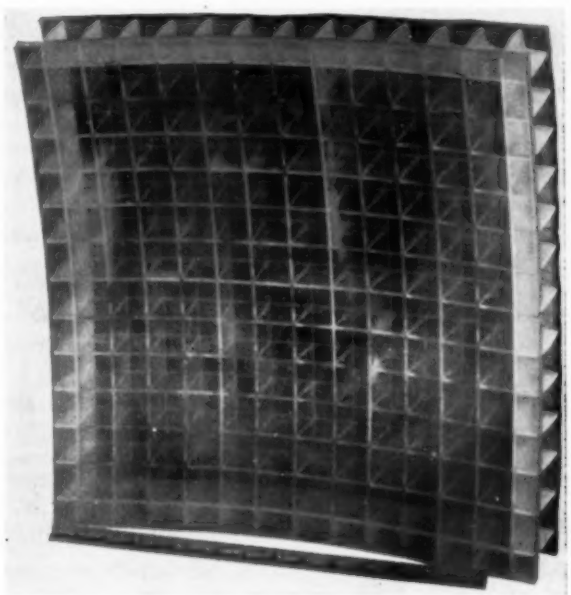

Fig. 6. A large lightweight mirror of fused quartz.

of this figure of merit appear in the 14th column. It would appear that the last entry, alloy 685, is so much better with regard to its thermal time constant for expansion that it would be chosen for most applications where temperature variations are important. The figure of merit is so large for this material because of the very low coefficient of expansion. It must be remembered that invar-type materials have very low coefficients of expansion only over small temperature ranges. If they are operated outside of this range, the coefficients become large and resemble more normal metals. In many engineering applications, temperature variations may be made small and centered about some nominal value. In such cases this material would be of great advantage. However, in other applications the ranges are large or the nominal value cannot be well controlled. In these applications this material loses most of its attractiveness. Among the more normal metals, aluminum offers an advantage. In spite of its large coefficient of expansion, its thermal conductivity and specific heat combine to yield a very short thermal time constant; thus it would stabilize very quickly.

A profitable area for the application of engineering skill and creativity lies in the choice of structure for mirrors of various shapes. Many optical systems, because of their intended use, permit advantage to be taken of noncircular optical components. Large mirrors may be fabricated in any shape and may be webbed or otherwise stiffened to provide the required rigidity. Optical manufacturing techniques now permit the polishing and figuring to high accuracies of large mirrors in shapes other than circular. But it is the engineer's job to provide the structural design which furnishes the rigidity required during optical working. Often the forces which distort mirrors are greatest during the polishing process. Mounting systems may be designed which will support the mirror sufficiently well, during its use, to reduce its distortion to an acceptable value. This is true even though the mirror is extremely flexible. Optical systems designed for satellite use are peculiar in that their mirrors will be required to perform under conditions of very nearly zero gravitational force. Consequently there exists a great opportunity for engineering development in the techniques of manufacturing large reflecting surfaces in which the support required for optical working may be subsequently removed from the finished optics. Some important steps are being made in this direction and, in fact, some large aluminum mirrors have been figured to astronomical quality by supporting them in plaster molds.

Performance Specification and Quality Control

A very important aspect of engineering is the setting of specifications for quality control. In recent years methods for specifying the performance of optical systems and for inspection of optical components have undergone considerable evolution. Since the 1951 Symposium at the National Bureau of Standards on optical image evaluation the whole field of performance, definition, and specification has been under intensive investigation along the lines outlined by Schade.[6] The literature in this field is now very extensive, and a good historical review has been given by Perrin in two papers, "Methods of Appraising Photographic Systems"[7] and "Manipulation and Significance of Sine Wave Response Functions."[8]

The general approach to the performance definition of optical systems by the use of the modulation transfer function[9] provides an extremely important and valuable tool to the optical engineer. It permits the incorporation of many nonoptical effects in the analysis of optical system performance. The effect of the atmosphere, of vibration, of image motion, of improper focus, and of certain varieties of imperfections in the optical components themselves may be handled conveniently by this approach.[10] The power of this tool permits the engineer to evaluate the effects of the many degrading factors, and thus allows him to concentrate engineering design effort on those factors which have important effects. As a corollary, when the inevitable compromise must be made, various alternatives may be compared and system performance optimized without the time consuming and costly procedure of setting up the various alternatives in model or prototype form. In addition, it is now possible to predict the over-all performance of the optical device, and thus to face the crucial decision whether this performance would justify the cost and effort.

Today, when space and weight are often extremely important considerations, transfer-function methods provide a good insight into the effect of these limitations on performance. While these methods have received their principal application to photographic systems, they are also directly applicable to many other types of optical instruments such as telescopes[11] and astronomical spectrographs.[12] A paper by Lohman, "Contrast Transfer in the Grating Spectrograph,"[13] is a particularly valuable reference. It contains a complete bibliography of the literature on the application of modulation transfer functions as applied to the engineering of many forms of optical instruments.

Many papers have appeared describing instruments for the measurement of the modulation transfer functions of detectors. A recent paper by Kelley[14] describes equipment and an experimental procedure for evaluating films. He places particular emphasis on the effects of processing upon the modulation transfer function of the films commonly in use by the movie industry. Publications by Lamberts[15] and by Higgins *et al.*[16] report the methods employed at the Research

Laboratories of the Eastman Kodak Company and the results on a variety of Eastman Kodak materials.

While the literature on the performance of photographic materials[17] is extensive, the understanding of the action of the eye in terms of its modulation transfer function is not on such a firm foundation. A paper by M. M. Benarie[18] discusses the problem of the informational capacity of the human eye and its dependence on brightness and angular subtense. A series of experiments conducted in the Optical Laboratory of Boston University[19] has shown the relationship between the detectability and recognition of objects and the resolution of the optical instruments and the photographic materials upon which the images were recorded. Since the performance of the eye is an important factor in detecting and recognizing the images on the photographic material, some information about its performance can be deduced from these experiments.[20]

Except for satellite-borne astronomical telescopes, almost all optical instruments are affected by the earth's atmosphere. Since this imposes a limitation of performance beyond the control of the engineer, he must be prepared to understand it and to include its effect in the predictions of the performance of his instrument.

Experimental investigations of the earth's atmosphere are being carried forward by many investigators. A classic paper by Keller,[21] and another by Keller *et al.*[22] are examples. Ramsey[23] has given a discussion of the effect of atmosphere on telescope performance and has deduced transfer functions for stationary and uniformly moving disturbances. Currently, the Institute of Optical Research in Stockholm is carrying on an extensive series of investigations on the effect of air turbulence on photographic images, and some measurements have been published by Djurle and Bäck.[24]

When an optical instrument is to be designed to provide images of a certain quality, it is important that the physical constants of the optical elements be specified by the engineer. The effects on performance due to variations in spacing, radii of curvature, and index of refraction are generally part of the optical design itself. However, tolerances on surface imperfection and variation of index within a single element generally fall in the province of the optical engineer.

For optical systems in which the image quality does not approach that of the diffraction limit, small variations of path length from those anticipated by the design do not produce serious optical defects. The tolerances may be deduced from the expected image sizes as predicted by ray trace data and point scatter diagrams. On the other hand, when the systems are expected to produce images strongly influenced by diffraction, analysis by the use of the modulation transfer function method provides a method of setting tolerances which may be brought into play.

Maréchal[25] has shown that, for the case of nearly perfect images, the intensity in the center of the diffraction maximum as a percentage of the intensity in a perfect image is given by

$$I_{\max} = 1 - \frac{4\pi^2}{\lambda^2}\Delta^2, \tag{8}$$

where Δ is the rms deviation of the wave front from a sphere centered on the image. That reference sphere is selected which makes the average deviation zero.

The transfer function for an optical system may be computed by the designer in the process of the ray trace computations.[26] The optical system as manufactured will have an actual transfer function which differs from the computed transfer function. This is because of distortions of the various optical surfaces and variations in the index of refraction of the material of the lenses as well as minor manufacturing errors. These effects produce optical path lengths different from those predicted by the designer. It can be shown that the ratio of these two transfer functions is related to the autocorrelation function of the wave-front distortions in the pupil. It must be borne in mind that the distortions referred to are the ones which are introduced by the surface inaccuracies and index variations not included in the lens computation. The relation given below

$$M(k) = \exp - \left(\frac{2\pi}{\lambda}\right)^2 [C(0) - C(F\lambda k)] \tag{9}$$

in which $M(k)$ is the ratio of the computed system transfer function to the transfer function resulting from the system containing distortions, and $C(F\lambda k)$ is the autocorrelation function of the wave-front distortions in the pupil expressed in terms of the spatial frequency k in the image, the focal length F, and the wavelength λ. $C(0)$ is the value of the autocorrelation function at zero frequency, the mean squared distortion.

The above relation is of value to the engineer. If he has some indication of the nature of the wave-front distortion to be expected from such effects as uncorrected zones in the optical surface, random fluctuations of index of refraction, or any other characteristics whose spatial spectrum may be approximated, he may estimate the autocorrelation function. Then he can set limitations on the amplitude of the error corresponding to his accepted performance degradation.

The nature of this relation[27] indicates that, for very low spatial frequencies, the ratio approaches unity. For the higher frequencies the ratio decreases and approaches some limiting value asymptotically. For a random deviation (rms) of $\lambda/20$ in the wave front, the asymptote is 0.1; for $\lambda/10$ the asymptote is 0.7.

Among the new techniques available for the investigation of the quality of optical surfaces is one which is

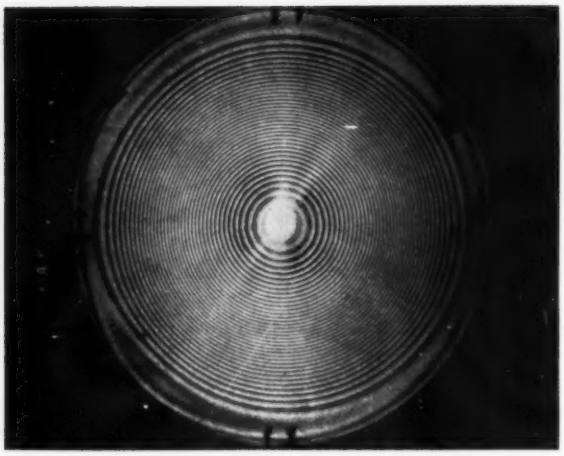

Fig. 7. A scatter plate interferogram of a 91-cm (36-in.) aperture parabolic mirror from the center of curvature.

proving to be exceedingly useful and powerful. This method is based on the scatter plate interferometer suggested by Burch.[28] His device permits the examination of optical systems in terms of path length differences between a selected ray in the aperture and all other rays. Figure 7 is a photograph of a scatter plate interferogram of a 91-cm (36-in.) parabolic mirror taken at the center of curvature. The central bright spot shows the location of the comparison beam in the aperture. Each maximum indicates the position of a ray which differs in length from that of the comparison beam by an integral number of wavelengths. It is a straightforward matter to measure the position of each maximum and compare these with the computed positions that the maxima should have for a perfect parabola. Thus one can find the departure of the surface from its desired form. It is believed that the probable error of the determination of the departure of a point on the surface from a selected parabola is of the order of $\lambda/50$, and is dependent primarily on the accuracy of measurement of the location of the maxima. This technique may be applied to any component of a system which produces an approximate focus or which can be combined with known elements to produce such a focus.

Another useful application of the same technique has been to combine the scatter plate interferometer with the more normal Fizeau type of interference. This permits the separation of the effects of a variation of the index from a variation of the surface figure in large pieces of glass to be used as windows. It is important that such pieces be accepted or rejected before the effort is expended to bring their surfaces to acceptable optical quality.

Figure 8 shows the two types of interference. The normal Fizeau pattern is on the left, and the scatter plate interferometer pattern is on the right. The formulas included in the picture permit separation of the thickness effect and the index effect. Two contour plots show the two variations. It is interesting to note that, in preparing this sample, the optician made an attempt to compensate for variations of index by polishing in a variation of thickness. His test method indicated to him only optical thickness and he was unaware of the index variation but believed that all the errors were in the surface. This particular sample was brought to a much better surface figure (more uniform path length) than would be required for this inspection method to permit acceptance or rejection of the glass. Considerable cost can be saved by the employment of such methods to inspect optical materials before large investments of polishing and figuring time are committed.

Conclusion

In recent years, the field of optics has entered into a veritable renaissance. Not only are new lens and optical-system designs being rapidly created to do the older and familiar tasks better, but many new and exceptionally demanding applications are appearing. Furthermore, the creative role of the optical engineer in designing the over-all instrument or system has been made even more challenging by the requirements imposed by a large number of new conditions. Fortunately, the technology to provide materials, structures, and analytical methods has kept pace with the growing requirements. There is little doubt that these developments will continue in this direction for a considerable period of time. Clearly, the optical engineer will be required correspondingly to broaden and refine his growing dexterity in the design of structures, in the utilization of electronic systems, and in methods of analysis and performance evaluation.

It is probably unlikely that we shall experience another large step forward in improving the resolution of optical microscopes, like that afforded by the recently developed method of phase contrast. On the other hand, it would seem that some of the techniques now employed to improve the resolution of radio telescopes might have an optical application. To design the optical equivalent of the Mills cross,[29] for example, is an exceedingly interesting problem, and a practical solution may appear in the near future.

Even in the interim, there is much to occupy the full skill and attention of the optical designer, and many opportunities for worthwhile contributions, both theoretical and practical. Demands are on the increase for more and better industrial controls, laboratory equipment, military and space systems, and products for the consuming public. Manifestly, satisfying these demands through optics by solving engineering problems in the design, manufacture, assembly, adjustment, pointing, and control of a great variety of optics—

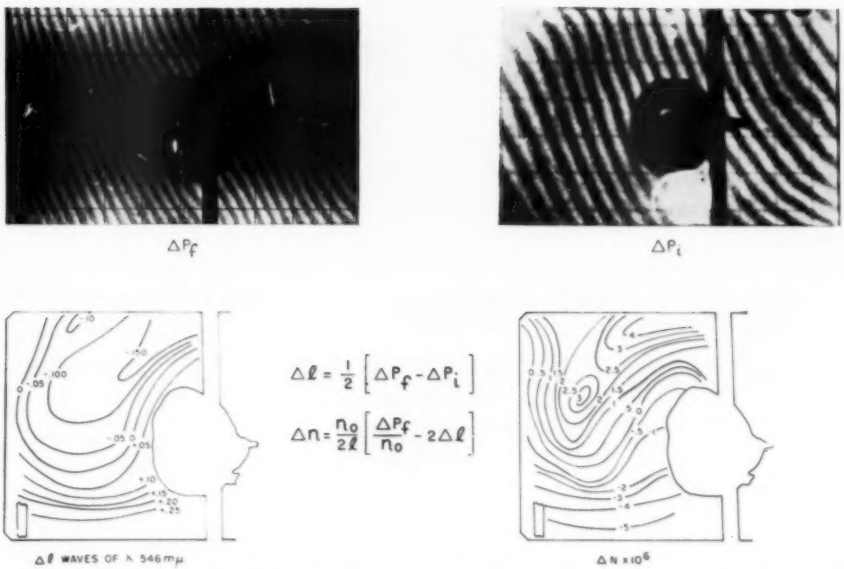

Fig. 8. The use of Fizeau and scatter plate interferometry to separate variations of index from variations of mechanical thickness

large and small—will provide a continual challenge to the optical engineer.

The assistance of Harold Hemstreet, Project Engineer on Stratoscope II, who provided material and illustrations; Grace Schroeder and John Restivo for the preparation of figures; Leon Flanders, Jr., for reading the manuscript; and Sherry Augat for the preparation of the manuscript and the many details of the references is gratefully acknowledged.

References

1. A. B. Meinel, *Telescopes*, edited by G. P. Kuiper and B. M. Middlehurst (Univ. of Chicago Press, 1960), Vol. I, Chap. 2, p. 25.
2. J. G. Baker, Proc. Am. Phil. Soc. **82,** 339 (1940). See also, C. K. Seyfert, Sky and Telescope **13,** 72 (1954); E. H. Linfoot, Proc. Phys. Soc. (London) **57,** 209 (1945); F. Whipple, Sky and Telescope **8,** 90 (1945); A. Offner, "Diffraction Limited Study," ASTIA Document 246, 268, WADD Tech. Rept. 60-140 (1960).
3. L. Spitzer, Jr., Astron. J. **65,** 242 (1960).
4. J. E. Stanworth, *Physical Properties of Glass* (Clarendon Press, Oxford, 1950); G. W. Morey, *The Properties of Glass* (Reinhold, New York, 1938); F. A. Molby, J. Opt. Soc. Am. **39,** 600 (1949); R. J. Spindler, J. Opt. Soc. Am. **44,** 677 (1954).
5. S. G. Sliusarev, Optics and Spectroscopy **6,** 211 (1959).
6. O. H. Schade, RCA Rev. **9,** 527 (1948).
7. F. H. Perrin, J. Soc. Motion Picture Television Engrs. **69,** 151 (1960).
8. F. H. Perrin, J. Soc. Motion Picture Television Engrs. **69,** 239 (1960).
9. E. Ingelstam, J. Opt. Soc. Am. **51,** 1441 (1961).
10. R. M. Scott, Phot. Sci. Eng. **3,** 201 (1959).
11. R. M. Scott and R. V. Shack, "Predictions of Performance by Modulation Transfer Technique," Stockholm meeting, ICO (1959).
12. E. H. Linfoot, Monthly Notices Roy. Astron. Soc. **121,** 115 (1960).
13. A. Lohman, Optica Acta **6,** 175 (1959).
14. D. H. Kelley, J. Opt. Soc. Am. **51,** 319 (1961).
15. R. L. Lamberts, J. Opt. Soc. Am. **49,** 425 (1959).
16. G. C. Higgins, R. C. Lamberts, and R. N. Wolfe, Optica Acta **6,** 272 (1959).
17. D. P. Paris, J. Opt. Soc. Am. **51,** 988 (1961).
18. M. M. Benarie, J. Opt. Soc. Am. **51,** 371 (1961).
19. D. E. Macdonald, J. Opt. Soc. Am. **46,** 715 (1956).
20. R. E. Hufnagel, "Visual Detection and Recognition of Blurred Images on Grainy Film," to be published (1962).
21. G. Keller, Astron. J. **58,** 113 (1953).
22. G. Keller, W. M. Protheroe, P. E. Barnhart, and J. Galli, "Investigations of Stellar Scintillations and the Behavior of Telescopic Images," ASTIA Document AFCRC TR 57-186, AD 117279 (1956).
23. J. V. Ramsey, Optica Acta **6,** 344 (1959).
24. E. Djurle and A. Bäck, J. Opt. Soc. Am. **51,** 1029 (1961).
25. A. Maréchal, *Optical Image Evaluation* (Natl. Bur. Standards, Washington D.C., 1956), Circ. 526, Chap. 2, p. 9.
26. A. Offner, J. L. Rayces, and R. H. Bernard, in preparation.
27. R. B. Mallinson and M. D. Rosenau, in preparation.
28. J. M. Burch, Nature **17,** 889 (1953).
29. B. Y. Mills and A. G. Little, Australian J. Phys. **6,** 272 (1953).

The Optical Society of America

Officers of the Society

President	DAVID L. MACADAM, Research Laboratories, Eastman Kodak Company, Rochester 4, N.Y.
President-Elect	STANLEY S. BALLARD, Department of Physics, University of Florida, Gainesville, Fla.
Past President	WALLACE R. BRODE, 3900 Connecticut Avenue N.W., Washington 8, D.C.
Executive Secretary	MARY E. WARGA, OSA, 1155 16th Street N.W., Washington 6, D.C.
Treasurer	ARCHIE I. MAHAN, Applied Physics Laboratory, 8621 Georgia Avenue, Silver Spring, Md.
Editor of the Journal of the Optical Society of America	DEANE B. JUDD, National Bureau of Standards, Washington 25, D.C.
Editor of Applied Optics	JOHN N. HOWARD, Geophysics Research Directorate, AFCRL, Bedford, Mass.

Directors-at-Large

* *Term expires December 31 of the indicated year.*

BRUCE BILLINGS (62)* Baird Atomic, 33 University Rd., Cambridge, Mass.
JOHN A. SANDERSON (62)* Naval Research Laboratory, Washington 25, D.C.
VAN ZANDT WILLIAMS (62)* Perkin-Elmer Corporation, Norwalk, Conn.
RUDOLF KINGSLAKE (63)* Eastman Kodak Company, Rochester 4, N.Y.
EARLE K. PLYLER (63)* National Bureau of Standards, Washington 25, D.C.
DAVID RICHARDSON (63)* Bausch & Lomb, Inc., Rochester 2, N.Y.
GEORG H. HASS (64)* ERDL, Fort Belvoir, Va.
R. CLARK JONES (64)* Polaroid Corp., Cambridge, Mass.
E. D. MCALISTER (64)* Scripps Institution of Oceanography, La Jolla, Calif.

Local Sections

Rochester
DONALD P. FEDER, *President*
JOHN L. TUPPER, *President-Elect*
JOSEPH L. ROOD, *Secretary*
Bausch and Lomb, Inc.,
Rochester 2, N.Y.
FRANK MOSER, *Treasurer*

Detroit
MARY E. BERGER, *President*
RICHARD MAJKOWSKI, *President-Elect*
DANIEL L. HARMON, *Secretary*
16152 Parkside, Detroit 21, Mich.
SAMUEL COHEN, *Treasurer*

Niagara Frontier
HERMAN A. SZYMANSKI, *President*
ERNEST W. SCHUSTIK, *President-Elect*
J. F. HIGGINS, *Secretary*
Higgins Analytical Laboratories,
707 Seventh St., Niagara Falls, N.Y.
THOMAS FROST, *Treasurer*

New England
STEPHEN M. MACNEILLE, *President*
DAVID S. GREY, *Vice-President*
W. ALEXANDER PATTERSON, *Secretary*
Cryovac Company,
Cambridge, Mass.
WILLIAM J. DAVIS, *Treasurer*

Texas
CHARLES S. WILLIAMS, *President*
P. O'B. MONTGOMERY, *Vice-President*
HARRY J. AUVERMANN, *Secretary-Treasurer*
LTV Research Center
P.O. Box 5003,
Dallas 22, Tex.

Chicago
PAUL F. FENLON, *President*
HAROLD F. BENNETT, *Vice-President*
C. ROBERT ANDERSON, *Secretary*
2421 North Luna Avenue,
Chicago 39, Ill.
JOHANN F. MOHLER, *Treasurer*

Southwestern Connecticut
WALTER SLAVIN, *President*
LEONARD EISNER, *Vice-President*
FRANK WONG, *Secretary*
Farrand Optical Co., 4401 Bronx Blvd.
New York 70, N.Y.
RICHARD W. HAMILTON, *Treasurer*

Southern California
WILBUR I. KAYE, *President*
R. HENRY FRELS, *Vice-President*
ERNEST DAVIDSON, *Secretary*
Applied Research Laboratories, Inc.,
3717 Park Place, Glendale 8, Calif.
RUSSELL A. TEMPLE, *Treasurer*

Northern California
SUMNER P. DAVIS, *President*
ROBERT E. LEWIS, *Vice-President*
ELDRED F. TUBBS, *Secretary-Treasurer*
General Telephone and Electronics
Laboratories, Inc., 1015 Corporation
Way, Palo Alto, Calif.

National Capital
RICHARD TOUSEY, *President*
FREDERICK W. PAUL, *First Vice-President*
HARRY K. HAMMOND, III, *Secretary*
National Bureau of Standards
Washington 25, D.C.
RICHARD S. HUNTER, *Treasurer*

The Optical Society of America was organized in 1916 "*to increase and diffuse the knowledge of optics in all its branches, pure and applied, to promote the mutual interests of investigators of optical problems, of designers, manufacturers and users of optical instruments and apparatus of all kinds and to encourage cooperation among them.*" The Society invites to membership all who are interested in any branch of optics, either in research, in instruction, in optical or illuminating engineering, in the manufacture and distribution of optical goods of all kinds, or in physiological and medical optics. Further information may be obtained from the Executive Secretary of the Society. **Annual Dues:** Regular members and Fellows, $17.00; Associate members, $13.00; Corporate members, $125.00. These dues include subscription to the Society's official journal, the *Journal of the Optical Society of America*, but not to its other publications.

Overlapping-Monoculars—An Ultrawide-Field Viewing System

Martin Shenker, Joseph LaRussa, Paul R. Yoder, Jr., and Wright H. Scidmore

The overlapping-monoculars instrument was developed as a result of a study program concerned with wide angle viewing devices for tanks. The instrument is a binocular eyepiece device supplying to the user an undistorted horizontal field of view of 140° and an undistorted vertical field of 90°, thus providing what is believed to be the closest approach yet achieved to the fixated field of unaided human vision. The discussion includes fundamental theory of the device, optical design criteria, and a description of the performance of the system.

The basic idea of the overlapping-monoculars was conceived several years ago during a study on wide-field viewing devices for armored vehicles conducted under contract by the Farrand Optical Co., Inc., for Frankford Arsenal. The device uses two wide-field, unity-power monocular telescopes mounted not with their axes parallel as in a normal pair of binoculars, but with their axes convergent toward the observer. This gross decollimation between two telescopes is permissible because an erecting telescope of exactly unity-power is a constant deviation device. This principle is illustrated in Fig. 1.

When a one-power telescope is rotated through different viewing positions only the field stop moves. Objects in the field remain stationary.

With an instrument consisting of two 90° unity-power telescopes we achieve an unusually large field of view 140° wide by 90° high with a central 40° overlap. This field of view projected to infinity would appear as shown in Fig. 2(a). Figure 2(b) illustrates a view of the arrangement from above.

The concept of the instrument imposes certain unique requirements on the optical design correction to be achieved for the telescopes. These requirements arise as a result of two characteristics of the instrument:

First, in the overlap region an object in the outside world, while appearing at the same angle to the user as seen through both telescopes, is actually being observed at a different field angle relative to the axis of each telescope. This requires that prime consideration be given to the correction of distortion in the instruments. For instance, in a 40° overlap system if 10% distortion is allowed at the edge of the 90° field of each telescope (normally quite acceptable) then a point at the edge of the field of one telescope and 5° off-axis for the other telescope would have a difference in apparent direction to the eyes (in binocular terms—convergence or divergence) of approximately $4\frac{1}{2}°$ as seen through both telescopes. This would certainly be visually intolerable. In order to correct distortion as well as other lateral aberrations, namely, coma, lateral chromatic aberration, and chromatic variation in magnification, the individual telescopes were designed as purely symmetrical instruments. This required that only longitudinal aberrations be corrected in the separate halves of a given monocular telescope.

The second factor imposing stringent requirements on the detail design of this instrument is that the central, and therefore the most important, portion of its field of view lies at the center of the overlap region which is composed of the outer portions of the individual fields of view of the separate telescopes. This required that every effort be made to achieve a smooth correction over the whole field of view, not permitting any of the usual degradation in performance normally tolerated in even moderately wide-field instruments.

The primary purpose of the design and construction of this first overlapping-monoculars system was as a research instrument to be used in an evaluation by the U.S. Army. The instruments which were designed and constructed did not have to fit into any particular armor configuration but were to have maximum values of field of view, exit pupil diameter, eye relief, and image quality with minimum vignetting across the entire field of view. The intent was to explore the usefulness of a vision system having extreme optical parameters and to observe their individual effects on the performance of tank personnel engaged in various missions caused by reducing the values of these parameters. The telescopes

The first two authors are with the Farrand Optical Co., Inc., New York, N.Y. and the remaining authors are at the Frankford Arsenal, Philadelphia, Pa.

The paper was presented at the Spring meeting of the Optical Society of America, Pittsburgh, Pennsylvania (March 1961).

Received 5 October 1961.

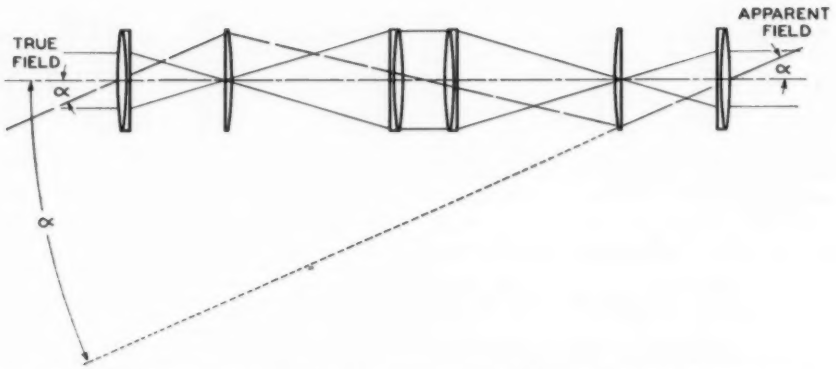

Fig. 1. Illustration of the manner in which a unity-power erecting telescope acts as a constant deviation system.

were, for simplicity, constructed as straight tubes, each providing a 90° circular field of view and a 15-mm diam exit pupil located 25 mm from the last lens surface. Vignetting is practically nonexistent.

The image quality achieved in the device is depicted in various ways by Figs. 3, 4, and 5.

Figure 3 shows the sagittal and tangential image curves indicating a maximum astigmatic difference of the order of one diopter.

In an instrument having an exit pupil as large as this one it is necessary to evaluate the dioptral errors and their variations for the whole pupil. The entrance pupil of the observer would never cover more than 50% of the diameter of the exit pupil of the instrument at any one time; however, the eye can be located anywhere within the exit pupil. Therefore in Fig. 4 these dioptral variations are shown across the pupil for seven different semifield angles for the meridional and sagittal bundles.

In an evaluation performed in this manner, a pure defocusing (caused by astigmatism and/or field curvature) would be represented by a vertical line displaced from the origin. Pure coma would be represented by a slanted, straight line passing through the origin in the meridional graphs and would have no effect on the sagittal graphs. Pure spherical aberration would be represented by a horizontal axis parabola having its vertex at the origin.

Thus it can be seen that the residual aberrations of the instrument are the astigmatism and oblique spherical aberration occurring at the more extreme field angles.

Figure 5 displays the effect of the residual aberrations in terms of angular deviations at the exit pupil. Here again the ordinates represent heights in the exit pupil while the abscissae are angular mils of deviation relative to the principal ray. The upper curves show deviations in the meridional plane of the exit pupil, and the lower

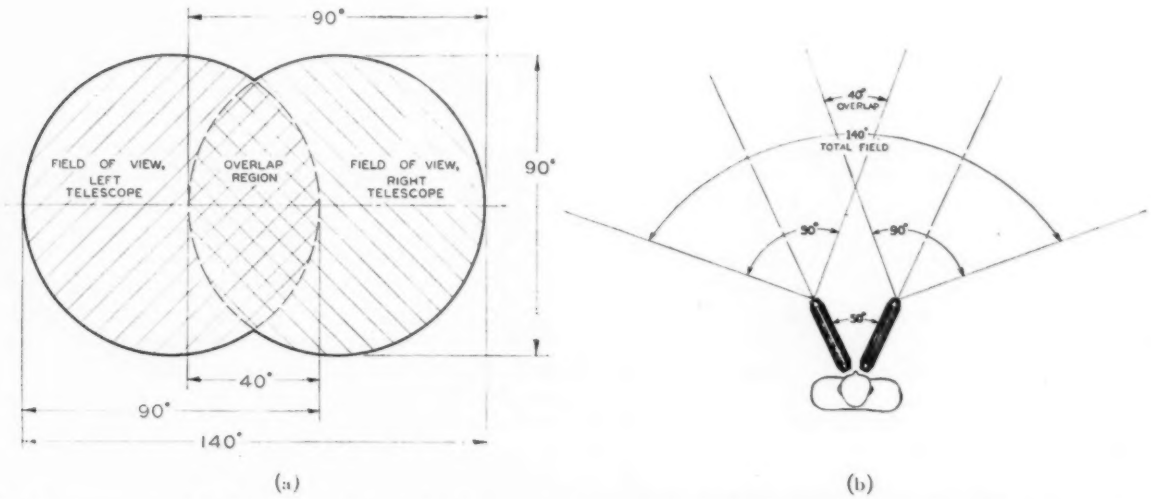

(a) (b)

Fig. 2. Appearance of the field of view of an overlapping-monoculars system. The dimensions pertain to the research model discussed in the text. (a) View through the instrument. (b) View of system arrangement from above.

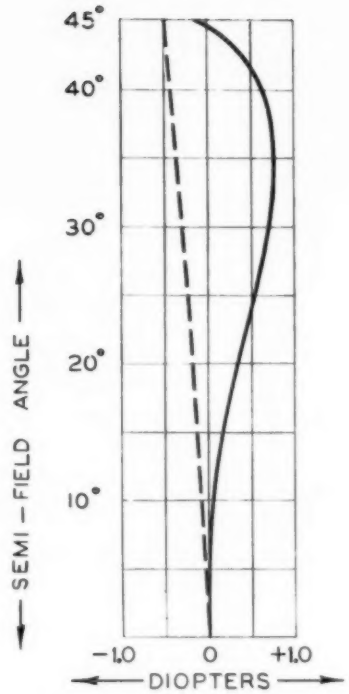

Fig. 3. Graphs of ray trace data for tangential (solid curve) and sagittal (dotted curve) fields of the research model.

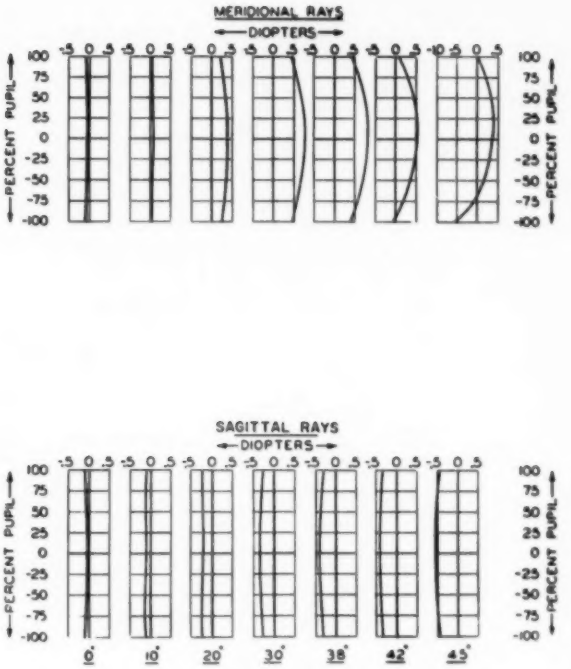

Fig. 4. Graphs of ray trace data for dioptral variations in focus across the exit pupil for various semifield angles in the research model.

graphs show sagittal deviations in the sagittal plane of the exit pupil. Meridional deviations in the sagittal portions of the pupil are not reported since they are negligible.

Figure 6 illustrates the optical system used in one of the 90° telescopes. The eyepiece with the field lens has a small Petzval sum and introduces very strongly overcorrected astigmatism. Half of the erector system also contributes very little to the Petzval sum and compensates for the astigmatism of the eyepiece. An aspheric surface on the field lens compensates for the spherical aberration of the pupil introduced by all other parts of each of the duplicate halves of the system. The system functions, therefore, in truly symmetrical fashion at all field angles.

Figures 7 and 8 show the overlapping-monoculars system in the laboratory and as mounted on a typical armored vehicle for field use in connection with the research program mentioned previously.

Figures 6, 7, and 8 overleaf

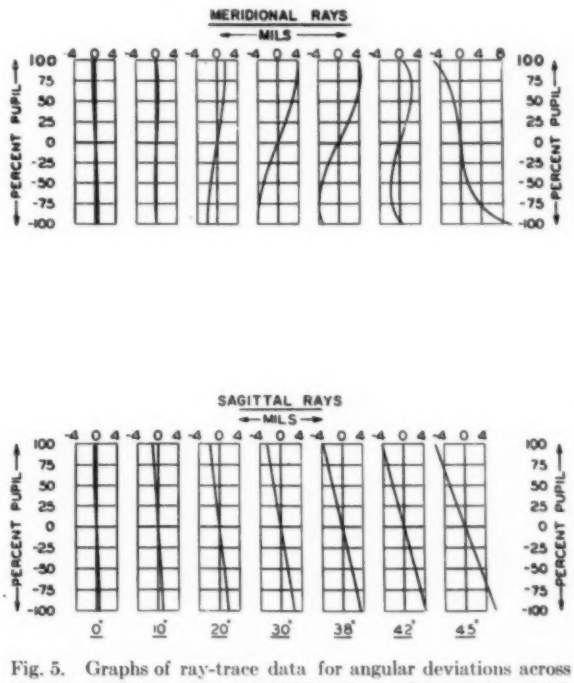

Fig. 5. Graphs of ray-trace data for angular deviations across the exit pupil for various semifield angles in the research model.

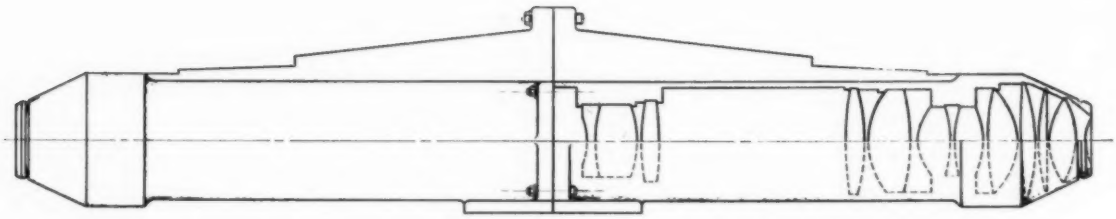

Fig. 6. Illustration of one telescope used in the research model of the overlapping-monoculars system.

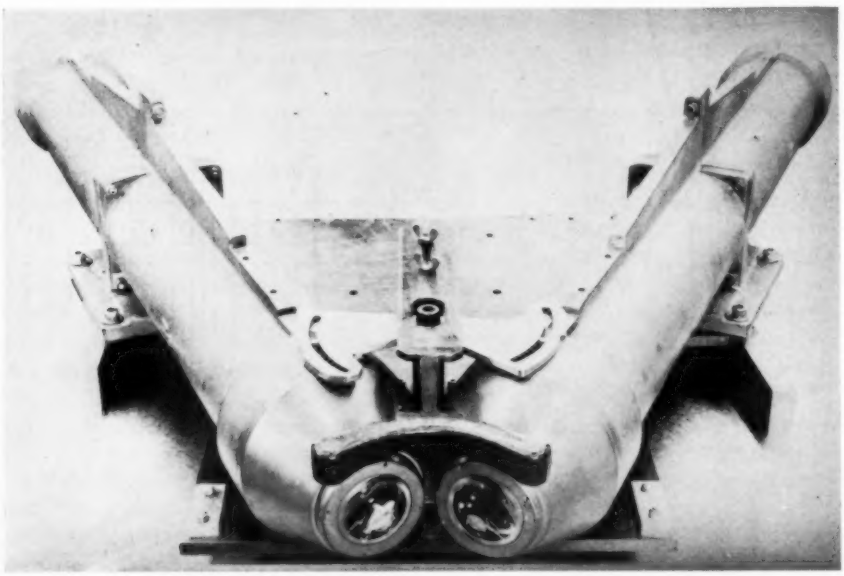

Fig. 7. Rear view photograph of the overlapping-monoculars system showing the adjustable headrest and the cam used to vary the eyepiece interpupillary setting.

Fig. 8. Photograph of the research model mounted in the commander's position on a typical armored vehicle.

High-Precision, Strain-Free Mounting of Large Lens Elements

Leo G. Deterding

This paper explains how the eight lens elements of a 600 mm, $f/2.0$ ballistic camera are mounted and retained in almost perfect alignment. The total weight of the glass in this lens is 107 kg, the largest element weighing 21.1 kg. The lens is aligned to less than 3 μ of tangential distortion and the elements are supported in the mount in such a way that they are completely free of any strains. The near perfect alignment of the lens is maintained by soldering the lens elements into the supporting cells.

One of the most critical tasks in the design and fabrication of large optical systems is the process by which large lens elements are mounted.

A unique method of accomplishing this has been developed at Nortronics, a Division of the Northrop Corporation, at Anaheim, California. It was developed as part of the total optical engineering effort in the design and development of a 600-mm, $f/2.0$ Ballistic Camera (Fig. 1) which Nortronics is building for the Air Force Missile Test Center, Patrick Air Force Base, Florida. This camera features extreme accuracy, photographing missile trajectories against a star background. The photographic data thus derived are used to calibrate electronic tracking gear.

The method of mounting and alignment which forms the subject of this paper was developed and first used for the 600-mm lens of this ballistic camera. The lens consists of 8 elements arranged in 3 cells (Fig. 2). The forward lens cell assembly consists of two elements; the main lens cell has 5 elements; and the last element is mounted alone. These lenses are assembled without difficulty and are aligned to less than 3 μ of tangential distortion. Although the eight elements of this lens weigh 107 kg, with the heaviest single element weighing 21.1 kg, they are mounted in such a way as to be completely free of strain.

In this paper the discussion will be limited to spherical surfaces, although the method can be applied to aspheric surfaces as well. First, the definition of the term optical axis must be stated. Any lens element which is made from a single piece of glass has two and only two surfaces. They may be plano, concave, or convex. Any spherical concave or convex surface has a single point in space which is the center of its curvature. The optical axis of any lens element is a line in space which connects the two centers of curvature (Fig. 3). Since the optical axis is not a physical body, it is impossible to see, touch, measure, or locate it directly, but it can be located by certain procedures.

It is the locating and positioning of this elusive but vitally important optical axis which will determine whether the final physical lens will perform in a manner which theory and mathematics have predicted for the lens (provided other tolerances are maintained), since optical design is always based upon a perfect alignment.

There have been many methods used for the alignment of the various elements of a lens system but, unfortunately, a large number of them can be placed in the category of trial and error. The method about to be presented is a positive foolproof method, which uses only the two spherical surfaces of the individual elements to align all of the optical axes of all of the elements into coincidence with each other. Assuming the lens elements are figured correctly, only two mistakes can be made in mounting. Both are usually made. Lens elements can only be decentered and tilted with respect to each other (Fig. 4).

Simple Tools Required

The tools which are necessary to achieve a near perfect optical alignment are surprisingly simple. The most important tool is a good precision rotary table, one which can be rotated either by hand or power and will run true within 0.0002 total indicator reading. It will be necessary to make a holding fixture and mount it on the rotary table (Fig. 5). The size of the holding fixture and rotary table will be determined by the size

The author is with Nortronics, a Division of the Northrop Corporation, Anaheim, California.

Received 29 January 1962.

Fig. 1. Principal features of the Nortronics 600-mm, f/2.0 ballistic camera.

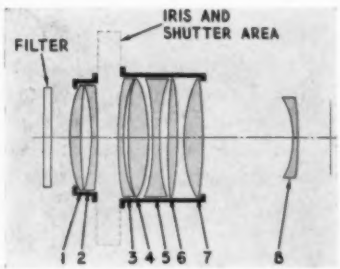

Fig. 2. Lens system of 600-mm ballistic camera.

of the lens elements which are to be aligned. The holding fixture is simply a plate which can be fastened to the rotary table upon which three precision steel balls are located. The holding fixture must be securely mounted on the rotary table so that the top and outside surface of each of the three balls is true to the axis of the rotary table within 2.5 μ. The other tools which are needed are a good dial indicator, accurate to 2.5 μ, a good microscope with a reticle in the eyepiece, and a small very fine reticle on a small glass disk.

The first step in locating the optical axis is to set the lens element on the ball fixture.

Because the balls are centered with respect to the rotating axis, the center of curvature of the surface in contact with the balls must fall somewhere on the rotating axis. The center of curvature will always remain fixed in space on the rotating axis regardless of how the lens is shifted about. The upper surface must now be located so that its center of curvature will also fall on the rotating axis. This will occur when the lens element can be rotated by means of the rotary table and the upper surface runs true with respect to some fixed point as shown by a dial indicator. When this has been achieved the lens element is centered and squared on the fixture and the optical axis is coincident with the rotating axis (Fig. 6).

A reticle is now fastened to the center of the upper surface with red wax. The lens is again rotated by means of the rotary table and with the aid of the reticle in the microscope, the waxed-on reticle is centered on the lens element within 5 μ T.I.R. Care must be taken during this centering operation that the lens element is not moved on the fixture. This is easily checked by observing the indicator on the top surface. When this has been done, the lens element can be removed from the optical-axis-locating fixture and installed in the lens mount.

Lens Element Must Be Free of Strain

All the aforementioned procedures which have been carried out in locating the optical axis of the lens elements can be in vain if the mount is not properly designed to hold the various lens elements in their proper alignment in a strain-free condition. Strain in a lens element not only may cause breakage but it causes

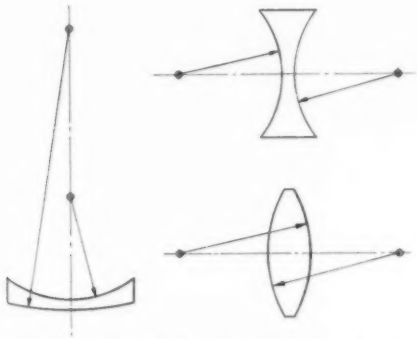

Fig. 3. The optical axis of any lens element is a line in space which connects the two centers of curvature.

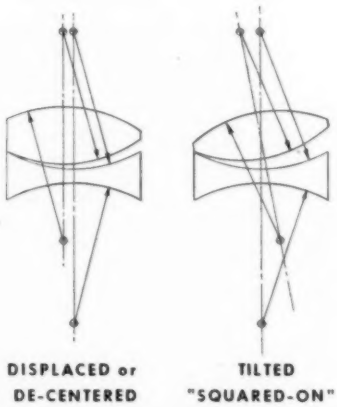

Fig. 4. Faulty mounting results from two common errors, the decentering and/or tilting of one lens with respect to the other.

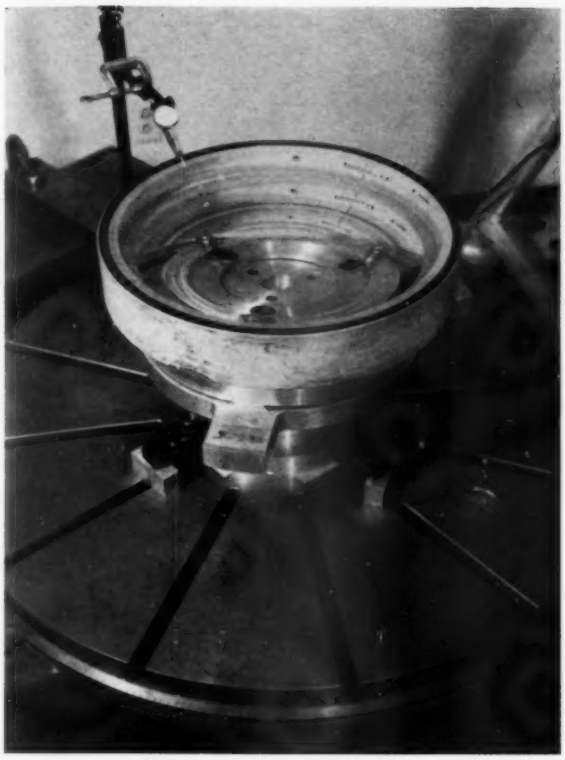

Fig. 5. A holding fixture is mounted on the rotary table. Also included is a dial indicator accurate to within 2.5 μ.

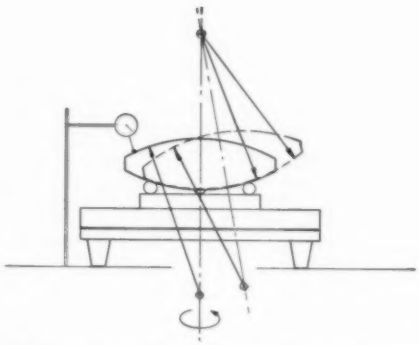

Fig. 6. The lens element is centered and squared on the fixture and the optical axis is coincident with the rotary axis.

a refractive index change wherever the strain is present. This means that the lens will not perform according to the theoretical design since the refractive index is assumed to be constant.

Assuming a lens element is made from a strain-free, fine annealed blank, strain in the finished lens can only be caused by introducing excessive pressure by improper mounting. Figure 7 shows a double convex lens element of 38 cm diameter and weighing 14.5 kg. The picture was taken with plane-polarized light. The large blurred cross through the center of the lens is characteristic of a positive lens but the concentrated dark pattern at the bottom is strain which is caused only by the weight of the element resting on edge.

In Fig. 8 the same element is shown in the same position but mounted in a strain-free mount. This was accomplished by distributing the weight of the lens element over the full lower periphery of the lens element.

This strain-free mount is simply two interlocking steel rings with a rubbery potting compound* between the rings and the glass as shown. Once a lens element has been mounted in this manner, considerable concentrated loads and pressures can be applied to the steel rim without causing strain in the glass (Fig. 9). There are probably many commercial compounds available which will serve the purpose of potting the lens element in the steel rings. The compound used should have a shore hardness of 20 to 30, it should cure from a liquid to a solid at room temperature, it should

* PR 1201-Q potting compound, manufactured by Products Research Co., Los Angeles, Calif., or #727 Sealing Compound manufactured by Coast Pro-Seal and Manufacturing Co., Los Angeles, Calif.

Fig. 7. A double-convex lens, 38 cm in diameter and weighing 14.5 kg, is photographed with plane-polarized light. The large blurred cross through the center of the lens is normal, but the concentrated dark pattern at the bottom is strain which is caused only by the weight of the element resting on edge.

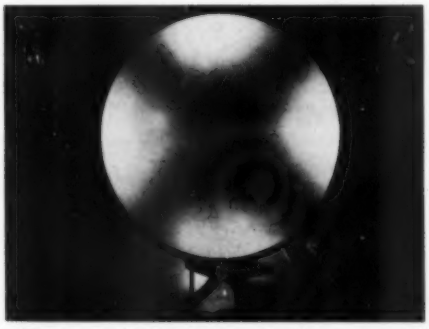

Fig. 8. The same element is shown in the same position but mounted in a strain-free mount.

not shrink during cure, and it should contain no volatile substance which will contaminate a sealed nitrogen-filled optical system. Two satisfactory compounds are listed in the footnote.

The flange of the steel rings is spaced away from the glass surfaces before potting by 50 to 125 μ with spacers cut from teflon sheet so that the steel does not touch the glass at any point. The potting compound fills the space between the flange and the glass during potting. The potting compound does not adhere to the glass but it does adhere to the metal; therefore, the lens element receives support only in compression. Since the metal rings completely enclose the potting compound on 3 sides, the glass element cannot shift.

After the lens elements have been potted in their steel rims and the optical axis has been located, the elements are ready to be assembled into the main lens cell. Figure 10 shows this being done. The main lens cell is clamped to a rotary table and centered on the rotating axis. The mounted lens elements are then installed one at a time and centered by means of viewing the reticle with the microscope and squared on by means of the indicator on the top surface. The lens elements are positioned and temporarily held in place by four screws which push against the metal edge of the potted lens element. After the elements are centered and squared on they are permanently fastened in place by soldering with 50-50 solder. During the soldering operation, the reticle and "squaring on" indication are periodically observed to insure that the lens element does not shift.

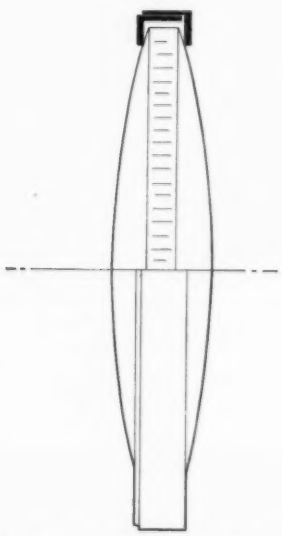

Fig. 9. Cross section of strain-free mount.

Fig. 10. Elements are assembled into the main lens cell.

The air spacing between the various elements must also be controlled during this assembly phase. This is done by carefully measuring and making proper spacers as assembly progresses.

After all the lens elements are installed in their respective cells, the cell assemblies are mounted in the camera housing which is fine-grain cast iron in this instrument. The completed lens assembly is checked for alignment by measuring tangential distortion. For this particular lens, the requirement was that tangential distortion shall not be greater than 3 μ over a total field of 24°. By using the alignment procedure described in this paper, this requirement was easily accomplished. The alignment problem is, of course, one of the many encountered in the process of manufacturing. The importance of its precise solution lies in the fact that, with all other factors under control, the optimum performance of a lens can be attained only when various elements are placed and held where they belong.

A High-Speed Rotating-Mirror Framing Camera

W. C. Davis

A new arrangement for a high-speed rotating-mirror framing camera using mirror strips instead of lens strips as framing stops is described. The design is especially simple when a few frames close together in time are required. A camera which takes 14 frames resolving about 150 line pairs across the frame at a rate of 10,000,000 frames per second, or 14 frames resolving 250 line pairs at a rate of 5,000,000 frames per second is also described. The effective exposure time is 80% of the time between frames, and the camera operates at effective aperture of $f/20$.

The Miller-Bowen type of framing camera has been in use for many years, and has proven very useful. A number of papers[1,2] have been published describing various particular cameras. This paper describes a new arrangement which allows simple construction, and which gives nearly theoretical resolution even at the highest framing rates. It is particularly simple when a few frames close together in time are required, and the alignment is simpler than that for the Miller-Bowen type, but it can be used for any exposure time to frame interval ratio. Much of the development of this camera was done by Holland.[3]

The system is shown schematically in Fig. 1. The object, or a real image of it, is at the focus of L1, so the light from each object point goes through the framing stop as a parallel bundle. The framing stop is located at one focal point of L2, and the rotating mirror at the other (not conjugate foci). Therefore, the parallel light from an object point is focused on the rotating mirror, and light from each point of the framing aperture reflects from the rotating mirror as a parallel bundle. The rotating mirror is located at one focal point of L3, and the framing mirrors in the other focal plane. The framing stop is therefore imaged on a framing mirror when the rotating mirror is in the proper position. The parallel bundle from an object point reflects from the framing mirror into the center of L4, and is finally brought to a focus on the film by L4. There are, of course, many other possible arrangements of lenses which will accomplish the same things, but the one described uses the fewest possible lenses, giving good imagery. L2, L3, and L4 must be large-diameter lenses to avoid vignetting. The height of the framing aperture is the dimension that must be considered to calculate how large the lenses must be. If the focal length of L1 is small compared with that of L2, the tendency to vignetting will be reduced. The effective f number can be computed by dividing the focal length of L4 by the diameter of the circle with area equal to that of the illuminated area of a framing mirror. The writing arm to be used for calculating exposure time is the focal length of L3, written in what follows as f. If w is the width of the framing mirror (and also of the image of the framing aperture), and n the rotation speed of the rotating mirror, then the effective exposure time will be approximately $w/4\pi nf$. The dimensions of the image on the film will be projected dimensions of the rotating mirror multiplied by the ratio of the focal lengths of L4 and L3.

The framing mirrors should be arranged so the optical path from L3 to L4 is about the same length whichever mirror is used, so that all frames will be in focus even though the light rays are not perfectly parallel. The framing aperture should be moved toward the rotating mirror the proper distance[4] to be in focus on the framing mirrors when the rotating mirror is distorted by centrifugal force in operation. A capping shutter can conveniently be placed near the framing aperture. A microscope in focus on the film plane and remote control of the position of L1 from the microscope position will help in focusing. The microscope should be focused on the film; then L4 should be moved to focus the rotating mirror in the film plane; finally L1 should be moved until the object is in focus.

A camera of this type which has been in use for several years is shown in Fig. 2. The table-top construc-

The author is at the University of California, Los Alamos Scientific Laboratory, Los Alamos, New Mexico.

Received 18 October 1961.

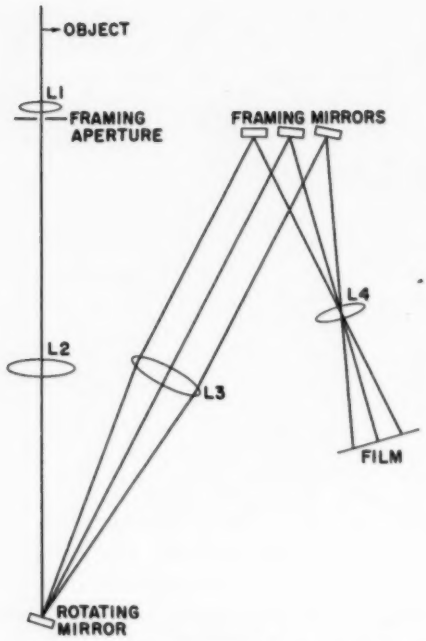

Fig. 1. Optical diagram of the camera.

tion is possible because of the simple alignment which results when only one lens is used as L3. (For long time coverage this lens would have to be impractically large, and several lenses would be necessary.) The object is placed outside the building and imaged at the focus of L1 by an objective lens, which can be easily changed to vary the magnification. Ordinary two-element achromats have been found satisfactory as objectives. L1 is a 7.6-cm diameter, 38-cm focal-length achromat. L2 is an 18-cm diameter, 89-cm focal-length achromat. L3 is a 20-cm diameter, 1-meter focal-length telephoto lens made by Perkin-Elmer as an aerial-photography objective. An achromat is satisfactory for L2, but L3 is used at its periphery for the first and last frames, and must be a high quality objective. It is apparent in the photograph that L3 is not at the center of the line from the rotating mirror to the framing mirrors, but it is optically centered. This lens is a telephoto type, and has its principal planes far outside its front element. The framing mirrors are pieces cut from optical flats. They are mounted individually, so that the light can be directed to L4, which it could not if their planes were parallel. L4 is a 10-cm diameter, 61-cm photographic objective. The

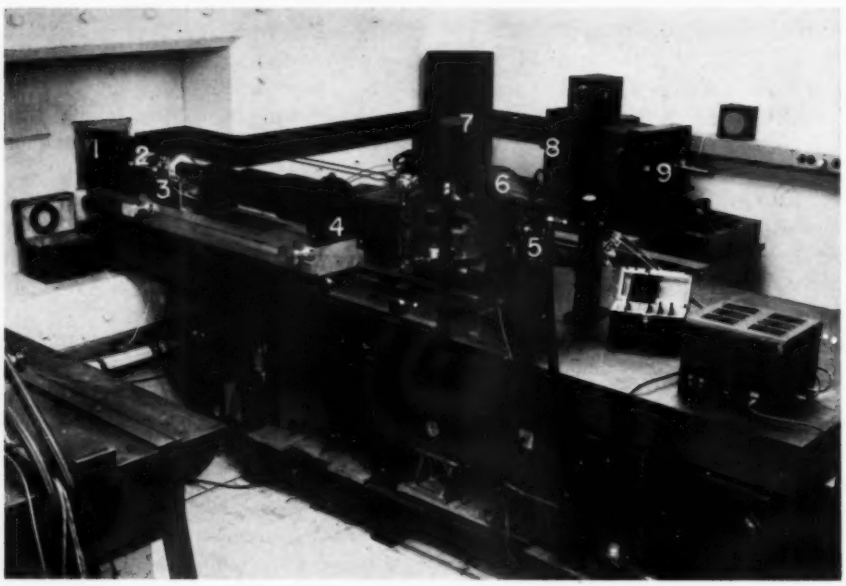

Fig. 2. Photograph of an example of the camera: (1) position of real image; (2) L1; (3) framing aperture; (4) L2; (5) rotating mirror; (6) L3; (7) framing mirrors; (8) lens board for L4; (9) film track.

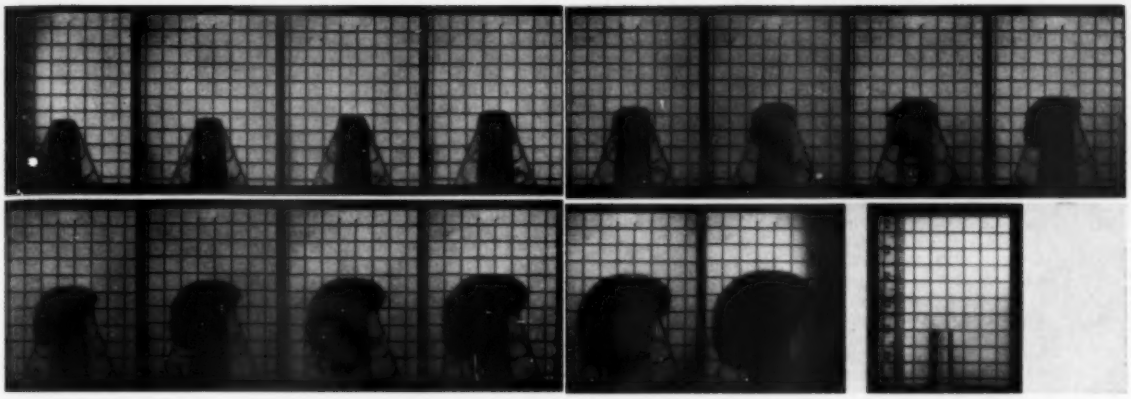

Fig. 3. Framing camera photograph of an explosion in Dithekite 13. The detonation propagates up to the glass tube at bottom center, and then expands irregularly as it enters a box full of the explosive. The shock wave from the glass tube moving out into the box of liquid explosive can be seen, with the superimposed grid lines distorted by refraction. The silhouette back-light is so bright that the light of detonation seems dim. The still picture at bottom right shows a millimeter scale, removed before firing. The framing time is 0.25 μsec, and the exposure time 0.20 μsec.

film is 35 mm strip film; the large box camera is not necessary. The effective f number is about $f/20$.

Figure 3 shows an example of the sequence of photographs which can be obtained with this camera. Vignetting of the 14th frame is clearly visible.

It is a pleasure to acknowledge the support of the U.S. Atomic Energy Commission for this work.

References

1. Bibliography on High-Speed Photography, through December 1955, compiled by Elsie L. Garvin, Eastman Kodak Company, Rochester, New York, available from the company.
2. B. Brixner, J. Opt. Soc. Am. **45**, 876 (1955).
3. T. E. Holland, Los Alamos Scientific Laboratory reports, 1950 to 1952.
4. T. E. Holland and W. C. Davis, J. Opt. Soc. Am. **48**, 365 (1958).

Meetings Calendar

1962

July

— Symp. on Cosmic Rays, La Paz *G. W. Clark, c/o Lab. de Física Cósmica de Chacaltaya, La Paz, Bolivia*

— Crystallographic Computing Symp., Munich *D. W. Smits, IUCr, c/o Mathematisch Institut., U. of Groningen, Reitdiepskade 4, Groningen, Netherlands*

— Zaporozh'ye Conf. on Spectroscopy and its Uses *V. S. Rossikhin, DGU, Shevchenkovskaya Ul., 59, Dnepropetrovsk, USSR*

2–4 High-Resolution NMR Spectroscopy Symp., U. of Colo., Boulder *M. T. Rogers, Mich. State U., E. Lansing, Mich.*

2–6 Inst. of Phys. and The Phys. Soc. Conf. on the Ionosphere, London *IPPS, 47 Belgrave Sq., London, S.W. 1, England*

2–7 Magnetic and Electric Resonance and Relaxation, internatl. conf., Eindhoven *D. J. Kroon, Philips Research Labs, Eindhoven, Netherlands*

8–14 6th Internatl. Cong. on Glass, Sheraton-Park Hotel, Washington, D.C. *Am. Ceramic Soc., 4055 N. High St., Columbus 14, Ohio*

9–11 11th Internatl. Astrophysics Symp., Liège *P. Swings, Inst. of Astrophysics, Sclessin, Belgium*

9–20 Summer Course in Optics *Inst. of Optics, River Campus Station, Rochester 20, N.Y.*

9–20 Optical Physics Summer Course, UCLA *H. L. Tallman, Rm. 6532, Engin. Bldg., UCLA, Los Angeles 24, Calif.*

10–20 Infrared Spectroscopy Summer Course, U. of Minn. *Director, Center for Continuation Study, U. of Minn., Minneapolis 14, Minn.*

16–19 Novae, Novoids, and Supernovae, internatl. colloq., Lyons *J. Dufay, U. de Lyons, rue de Cavenne, Lyons, France*

16–20 Paramagnetic Resonance, IUPAP conf., Jerusalem *W. Low, Hebrew U., Jerusalem, Israel*

16–20 Physics of Semiconductors, internatl. conf., Exeter *IPPS, 47 Belgrave Sq., London, S.W.1, England*

16–21 Fundamentals of Infrared Tech. Summer Conf., U. of Mich. *R. E. Carroll, 126 W. Engin. Bldg., Ann Arbor, Mich.*

25–31 Symp. in Commemoration of 50th Anniversary of the Discovery of X-ray Diffraction and of Crystal-structure Analysis, Munich *F. Bopp, Inst. für Theoretische Physik, Schellingstr. 4-8, Munich, Germany*

August

5–11 Radiation Research, 2nd internatl. congress, Harrogate *A. Howard, Mt. Vernon Hospital, Northwood, Mx., England*

6–10 Soc. of Photo-Optical Instrumentation Engrs., Statler Hilton Hotel, NYC *A. J. Carr, 205 Ave. I, Suite 23, P.O. Box 288, Redondo Beach, Calif.*

6–11 Fundamentals of Infrared Tech. Summer Conf., U. of Mich. *R. E. Carroll, 126 W. Engin. Bldg., Ann Arbor, Mich.*

6–17 MIT Infrared Summer Course *J. M. Austin, 7-103, MIT, Cambridge 39, Mass.*

13–15 Interdisciplinary Conf. on Electromagnetic Scattering, Potsdam, N.Y. *M. Kerker, Clarkson Col. of Tech., Potsdam, N.Y.*

13–17 Special Topics of Infrared Tech. Summer Conf., U. of Mich. *R. E. Carroll, 126 W. Engin. Bldg., Ann Arbor, Mich.*

14–16 Precision Electromagnetic Measurements, internatl. conf., Boulder, Colo. *G. Birnbaum, Hughes Research Labs, Malibu, Calif.*

14–18 Fisk U. Infrared Summer Course *Director, Fisk Infrared Inst., Fisk U., Nashville, Tenn.*

19–26 6th Gen. Assembly of Internatl. Commission for Optics and Congress on Image Formation, Munich *H. Schober, Inst. for Medical Optics, Arnulfstr. 205, Munich 19, Germany*

21–24 Far Infrared Spectroscopy, internatl. symp., Sheraton-Gibson Hotel, Cincinnati *F. F. Bentley, ASD, Wright-Patterson AFB, Ohio*

22–24 X-ray Optics and X-ray Microanalysis, 3rd internatl. IUPAP symp., Stanford *L. Zeitz, Biophysics Lab, Stanford U., Stanford, Calif.*

27–29 Ballistic Missile and Space Technology, 7th symp., Statler Hilton Hotel, Los Angeles *Aerospace Corp., P.O. Box 95085, Los Angeles 45, Calif.*

27–29 APS West Coast Summer Mtg., U. of Wash. *R. Geballe, U. of Wash., Seattle, Wash.*

27–30 Am. Astronomical Soc. Mtg., Yale U. *H. Smith, Yale U. Observatory, New Haven, Conn.*

27–31 Infrared Spectroscopy Gordon Conf., Kimball Union Acad., Meriden, N.H. *M. K. Wilson, Tufts U., Medford 55, Mass.*

27–Sept. 1 Information Processing, 2nd internatl. conf., Munich *IFIPS, 1634 Arch St., Philadelphia 3, Pa.*

29–Sept. 5 Internatl. Cong. of Electron Microscopy, 5th, Philadelphia *7701 Burholme Ave., Philadelphia 11, Pa.*

30–Sept. 5 Symp. on Photo Interpretation, Delft *Commission VII, Internatl. Training Centre for Aerial Survey, Kanaalweg 3, Delft, Netherlands*

September

— Relativity and Gravitation, internatl. IUPAP conf., Poland *P. Fleury, 3, blvd. Pasteur, Paris 15, France*

— Tashkent Conf. on Spectral Analysis *B. M. Gandel'sman, St. Comm. on the Coordination of Scientific Research, Bratskaya Ul., 29, Tashkent, USSR*

— Volograd Conf. on Spectral Analysis *B. G. Voronov, 11, VNIITMASH, Volgograd, USSR*

— Conf. on Plasma Spectroscopy, USSR *N. A. Prilezhaeva, TGU, pl. Revolyutsii, 1, Tomsk, USSR*

— British Assoc. Advancement Science Internatl. Mtg., Manchester *G. Allen, Burlington House, London W.1, England*

3–7 Internatl. Symp. on Information Theory, Brussels *M. Selleslags, U. Libré, 50, av. Franklin D. Roosevelt, Brussels, Belgium*

7–12 Internatl. Conf. on Crystal Lattice Defects, Kyoto *R. R. Hasiguti, U. of Tokyo, Bunkyo-ku, Tokyo, Japan*

9–14 Illuminating Engr. Soc. Technical Conf., Statler Hilton Hotel, Dallas *H. M. Walne, Dallas Power and Light Co., Dallas, Tex.*

9–14 Am. Soc. of Photogrammetry, semi-ann. mtg., Chase and Park Plaza Hotels, St. Louis, Mo. *C. E. Palmer, 1515 Mass. Ave., N.W., Washington 5, D.C.*

10–15 Molecular Structure and Spectroscopy, internatl. IUPAC symp., Tokyo *Science Council of Japan, Ueno Park, Tokyo, Japan*

10–15 Technical Forum on Forming Bonds in and with Fibers, Berkhamsted *Gen. Secy., Soc. of Dyers and Colourists, Dean House, 19 Piccadilly, Bradford, Yorkshire, England*

16–20 Electrochemical Soc. Mtg., Statler Hilton Hotel, Boston, Mass. *Electrochem. Soc., 30 E. 42 St., New York 17, N.Y.*

16–22 Low Temperature Physics, 8th internatl. conf., Queen Mary Col. *G. O. Jones, Queen Mary Col., U. of London, Mile End Rd., London, E.1, England*

17–19 9th Ottawa Symp. on Applied Spectroscopy *B. Farrar, J. T. Donald & Co. Ltd., 1181 Guy St., Montreal 25, Que., Canada*

17–22 6th Internatl. Congress on High Speed Photography, Scheveningen *J. G. A. de Graaf, 14, Burgemeester de Monchyplein, The Hague, Netherlands*

24–28 Union of German Physical Societies, Stuttgart *H. Franke, Verband Deutscher Physik. Gell., Gänseheide 15A, Stuttgart, Germany*

30–Oct. 5 ASTM Pacific Area Mtg., Statler Hilton Hotel, Los Angeles *ASTM, 1916 Race St., Philadelphia 3, Pa.*

October

— Symp. on the Question of Introducing Molecular Spectroscopy, USSR *V. M. Chulanovskii, Comm. on Spectroscopy Akad. Nauk USSR, proezd Sapunova, 13/15, Moscow, USSR*

— Belorussian Conf. on Spectral Analysis *B. I. Stepanov, Inst. Fiz. Akad. Nauk BSSR, Leninskii Prospekt, 70, Minsk, USSR*

— Infrared Information Symp., Eastern States Fall Mtg.

— URSI Mtg., Montreal *M. G. George, Thayer School of Engr., Dartmouth Col., Hanover, N.H.*

4–6 **Optical Society of America Annual Meeting, Manger Hotel, Rochester** *Hilda Kingslake, 56 Westland Ave., Rochester, N.Y.*

10–12 The Fiber Soc. Fall Mtg., Boston, Mass. *J. S. Jacobs, P.O. Box 405, Athens, Ga.*

12–13 SPSE Symp. on Photography of Electronic Display, Shoreham Hotel, Washington, D.C. *E. S. Cobb, P.O. Box 1609, Main P.O., Washington, D.C.*

15–19 ISA 17th Ann. Instrument-Automation Conf. and Exhibit *W. H. Kushnick, 313 6th Ave., Pittsburgh 22, Pa.*

22–24 10th Detroit ANACHEM Conf., McGregor Memorial Conf. Center, Wayne State U. *D. F. Boltz, Wayne State U., Detroit 2, Mich.*

22–26 SMPTE Semi-Ann. Convention, Chicago, Ill. *C. S. Stodter, 55 W. 42 St., New York 35, N.Y.*

November

14–16 4th Ann. Eastern Analytical Symp., Statler Hilton Hotel, NYC *P. Lublin, Gen. Telephone & Electronics Labs, Bayside, N.Y.*

December

— Am. Astronomical Soc. Mtg., U. of Ariz. and Kitt Peak Natl. Observatory, Tucson *H. Smith, Yale U. Observatory, New Haven, Conn.*

3–7 19th Internatl. Ophthalmological Cong., New Delhi *Y. K. C. Pandit, Bombay Mutual Bldg., Sir Pherozeshah Metha Rd., Bombay 1, India*

FUTURE MEETINGS

OPTICAL SOCIETY OF AMERICA

1962 4–6 October
Rochester, N.Y.
Manger Hotel

Details to be announced

1963 24–28 March
Spring Meeting
Jacksonville, Fla.

1963 22–26 October
Fall Meeting
Chicago, Ill.

1964 Spring Meeting
Washington, D.C.

1965 Spring Meeting
Dallas, Tex.

Executive Office
1155 16th Street, N.W. Washington 6, D.C.

A Rapid-Scanning Fabry-Perot Interferometer with Automatic Parallelism Control

J. V. Ramsay

A description is given of a Fabry-Perot interferometer whose plates are maintained automatically parallel independently of their separation.* Errors in the spacing of the plates due to lack of parallelism nowhere exceed the errors in the flatness of the plates themselves. The mounting of piezoelectric barium titanate ceramics to achieve rapid scanning rates is discussed.

Introduction

The available flatness and reflectance of Fabry-Perot interferometer plates is not fully exploited unless the errors due to lack of parallelism do not exceed the errors in flatness of the plates themselves. This paper describes an automatic method of maintaining precise control of the parallelism independently of the plate separation.

Barium titanate ceramics, whose length can be varied in response to an electrical signal, are used to obtain the correcting movements necessary to maintain precise control of the parallelism of the plates. Detailed information on the manufacture and properties of these ceramic supports will be provided elsewhere.[1]

When effective control of the parallelism of the interferometer plates is established, several methods of varying the order of interference are available.[2] In the present instrument three identical barium titanate ceramic supports, electrically connected in parallel, give an approximately parallel displacement of one plate over 12 orders at low scanning frequencies, or over 1 order at high scanning frequencies, the ultimate frequency obtainable being limited by the inertia of the interferometer plate and the stiffness of the mount.

Testing for Parallelism

The test for the parallelism of the two optically flat surfaces is a comparison of the separation of the surfaces at two pairs of corresponding points by use of superposition fringes. Figure 1 shows the scheme adopted for one pair of corresponding points.

White light from a source S is collimated by a lens L, after which it passes through the interferometer plates P_1 and P_2 whose optically flat surfaces F_1 and F_2 have the usual high reflectance coatings. After passage through F_2, the beam is caused, by means of a truncated square pyramid on the back of P_2, to return through the opposite side of the interferometer, and is received by a photomultiplier M. The light emerging from the interferometer AB is in the form of channel spectra, i.e., some wavelengths, depending on the distance AB, are transmitted freely while others are largely suppressed. A maximum transmission (i.e., a white light superposition fringe) from the two interferometers AB and CD in series occurs when AB = CD, the total amount transmitted, as indicated by the photomultiplier output, decreasing rapidly as AB becomes greater or less than CD.

A second system operates in a plane normal to that of the first; a simultaneous occurrence of a maximum response from each of the two photomultipliers denotes parallelism of the surfaces F_1 and F_2.

The accurate assessment of parallelism by this method demands that the individual ray should make the same angle with the normal to F_1 on its forward and return passage. For a permissible error of 5 nm (1 nm = 10^{-9} meters) and a separation 1 meter, the tolerance on the 90° angle between the internally reflecting surfaces is ± 10 sec of arc.

The system ABCD comprises essentially three interferometers (AB, BC, CD) in series. An achromatic white light fringe is produced only when the separations of two interferometers are equal independently of the wavelength. Consequently, due to the dispersion in

The author is at the C.S.I.R.O. Division of Physics, National Standards Laboratory, Sydney, Australia.

Received 9 February 1962.

* The method of automatic parallelism control is the subject of Australian Provisional Patent Application No. 7311, 1961.

BC (in this case fused silica), no white light fringe occurs when AB or CD is equal to BC.

The *finesse* (the ratio of the half-width of the fringe to the fringe spacing) of the white light fringe is approximately the same as that of the fringes produced by a single Fabry-Perot interferometer, and thus allows precise control of parallelism.

Automatic Parallelism Control

The maintenance of a signal at its maximum value is difficult; it is much easier to maintain the mean value of an oscillating signal at its maximum. This latter procedure is used for the automatic control of the parallelism of the two interferometer plates.

One interferometer plate is oscillated about its center by applying oscillatory voltages of identical amplitudes and frequencies to each of the three barium titanate supports on which the interferometer plate is mounted, the phase of the voltage on each support being 120° in advance of that applied to the previous one. This introduces a wedge of constant angle between the two plates, the apex of the wedge rotating at the driving frequency. The amplitude of oscillation necessary to produce a sufficient signal is small (of the order of 5 nm), and is less than the errors in flatness of the plates. The output of each photomultiplier then contains an oscillatory component. When the oscillation is symmetrical about the position giving maximum response (i.e., the central white light fringe), the signal contains no component at the driving frequency. Any error in the mean position produces a component at the driving frequency, the phase of which relative to the driving frequency indicates the direction of the error. A phase sensitive detector, driven by the photomultiplier output, is used to apply a dc correcting voltage to the ceramics, thus adjusting the mean position of the plates for equality of separation near the extremities of a diameter. Another system operating about a plane normal to that of the above ensures parallelism of the plates.

A Servo-Controlled Interferometer

A rapid-scanning Fabry-Perot interferometer incorporating the above principles is shown in Fig. 2.

In the parallelism control the two light sources used

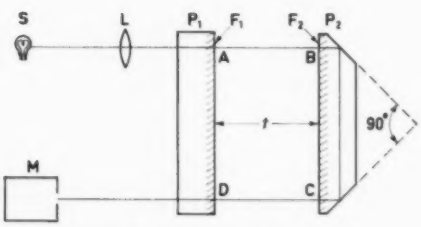

Fig. 1. Test for parallelism. For details see text.

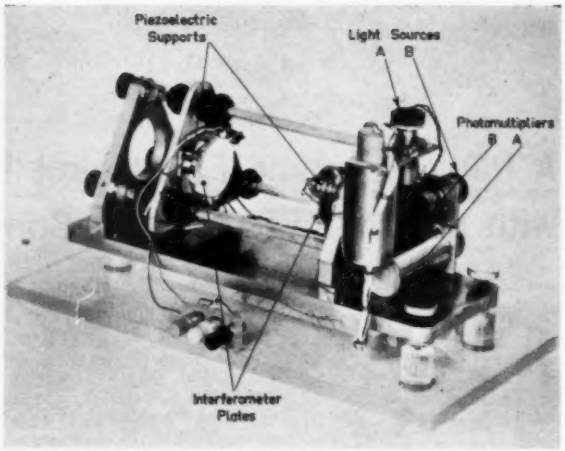

Fig. 2. A rapid-scanning Fabry-Perot interferometer with automatic parallelism control.

are 2.5-volt, 0.3-amp tungsten lamps, which are usually operated at 1.5 volts maximum. The interferometer plate incorporating the prism is oscillated at a frequency of 9 kc/s. Four areas in each of the interferometer plates (which are 50 mm in diameter by 11 mm thick), of approximately 6 mm by 6 mm, are used for parallelism control, leaving a clear working aperture of 38 mm diameter. The photomultipliers are Philips type 931A. While the automatic parallelism control will lock on with an oscillation having an amplitude of approximately 2 nm at the edge of the plates, it operates more reliably with an amplitude of 4–5 nm. (The amount of movement is derived from the known voltage–displacement characteristics of the ceramics.) The interferometer plates are mounted with a novel form of mounting which is basically kinematic and introduces distortions less than $\lambda/80$ in the plates. Details of this mounting are available elsewhere.[3]

In the present instrument a displacement of the edge of the plate of approximately 4 μ is available for parallelism control, and a further 5 μ for order control, enabling approximately 20 orders to be scanned for a wavelength of 500 nm. The response time of the servomechanism is approximately 5 msec, with the result that vibrations with frequencies less than 200 cps and amplitudes less than 4 μ have no significant effect on the parallelism of the interferometer plates, provided that the maximum rate of movement does not exceed 2 μ/sec.

The automatic parallelism control will move the plate to the position of the white light fringe if it is within approximately 50 nm of its correct position. If the plates are outside this range the control may lock on to a subsidiary maximum due to colored fringes on either side of the central white light fringe. Bringing the plates to within this range is easily accomplished in setting up

by manual control of the dc voltage applied to the ceramics, after which the servocontrol is switched on and remains locked on. The control operates satisfactorily for plate separations up to at least 15 cm, which is the limit of the present interferometer.

Rapid scanning is achieved by application of a variable voltage to the three ceramic supports which are electrically connected in parallel. A rate of scan of 1000 orders per second ($\lambda = 500$ nm), with a maximum amplitude of 10 orders at 100 cps, is possible. This rate of scan can be considerably increased by choosing a frequency of scan which is a natural resonant frequency of the assembly, this being determined by the mass of the interferometer plate and the stiffness of the supports (27 kc/s in the present arrangement).

Discussion

The automatic control of the parallelism of Fabry-Perot interferometer plates, as discussed above, is a particular application of a more general method of the automatic maintenance of a fixed integral ratio between the separation of corresponding points on two pairs of optically flat surfaces; in the case of parallelism control the fixed integral ratio is unity and the two pairs of surfaces coalesce into one pair. These principles have also been successfully applied to maintain the separation of one Fabry-Perot interferometer automatically and precisely 10 times that of another. Another application has been to the automatic maintenance of a fixed separation of two interferometer plates using a monochromatic source. Indeed the general principles have many other applications in the field of automatic control in optics.

I wish to thank H. Kobler and E. G. V. Mugridge for their assistance in this project.

References

1. J. V. Ramsay and E. G. V. Mugridge. Submitted to J. Sci. Instr.
2. See, for example, various papers in "Le colloque internationale sur les progrès récents en spectroscopie interferentielle," J. Phys. Radium **19**, No. 3 (1958).
3. J. V. Ramsay and E. G. V. Mugridge, Appl. Optics **1**, 538 (1962).

Continued from page 414

engaged in lens design but had not been fortunate enough to be taught this scientific technique as undergraduates. Significantly, the demand for this course comes mostly from people who have some specialty other than optics. I hope that other readers who may be engaged in similarly interesting activities will tell me about them.

Finally, I would like to mention the growing realization that optics may be drifting from the parent field of physics into the neighboring field of engineering. Being a physicist myself, by training and professional experience, I always regard optics as one of the five basic fields of physics, and this in fact is the way optics is still taught in the general physics course that is taken by so many students in their freshman or sophomore year. The teaching of optics on an advanced level is in a decline, as I have mentioned previously in this column, and this drop-off is taken by most of us to indicate that the profession of physics no longer regards optics as one of its more exciting divisions—nuclear physics, solid-state physics, and some theoretical areas win the popularity polls these days. This effect is seen strongly on the undergraduate level and accounts largely for the fact that there are not more Institutes of Optics functioning in the country—the old law of demand vs supply. Engineering, on the other hand, seems to have awakened to the fact that it has many things in common with optics, chiefly in the field of electrical engineering. Many of the techniques developed by the electrical engineer are now being used in modern optical analysis, and optics in turn can feed some new life and spirit into facets of electrical engineering (see my March column, page 96). Therefore it seems to some of us that optics may soon be popularly regarded as a new and exciting phase of engineering instead of an old-fashioned and dull part of physics. This trend is already seen in some universities, where men acknowledged as optical scientists are being given appointments as professors of electrical engineering, apparently without disturbing the serenity of the physics departments located nearby. At first blush this trend or dislocation seems to us professional physicists to be a bad thing, but I believe that the more we see of it the more we begin to feel that the renaissance of optics, which is already under way, may work toward its realization best in engineering schools rather than in the traditional physics departments. There will still be optical physicists—people especially interested in the theory and the "why" of phenomena—but more of the training will be on the engineering side which will deal both with the fundamentals and the applications thereof. Any persons whose feelings I may have ruffled by these remarks are invited to submit their complaints.

Applied Optics

Optical Activities in the Universities

reported by STANLEY S. BALLARD, Department of Physics, University of Florida, Gainesville, Florida. Professor Ballard hopes to receive news and comments for this column, which should be sent to him at the above address

Since the featured subject of this issue is Optical Engineering, it seems appropriate to say a few words about the training of optical engineers as it exists in the U.S.A. today. Any question as to what constitutes optical engineering is readily answered if one peruses the excellent lead article by Roderic M. Scott, which article is herewith assigned as required reading. There are several levels of competence in which optical engineers or optical physicists perform, and the training needed in each category varies according to the extensiveness of technique and knowledge required. One could start by considering the training of optical technicians who are employed as machinists, handy men, and/or technicians in optical shops, both those that manufacture large precision optical instruments and those that surface and shape ophthalmic lenses. I do not believe that any special training ground is provided for people at this level, so that most of them learn their techniques on the job. This situation may be at least partially satisfactory, since most of the big optical shops have their own specialized practices, the knowledge of which must be acquired by participation and training on the spot. However, the ophthalmic lens industry uses sufficiently standardized techniques so that centralized training should be feasible. I do not know whether there is any considerable program along these lines in the country—I do *not* of course refer to the schools of optometry which train people in refraction and which give the student a knowledge of physiological optics as well as geometrical optics and its application to spectacle lenses.

For training in optics at the college bachelor's level we naturally think first of the Institute of Optics of the University of Rochester. A recent issue of the *Institute of Optics Newsletter* has as its lead article "What Is an Optical Engineer?" a most timely question for this issue of *Applied Optics*. The article states that there seems to be no definitive answer to this question, and that the answer you get depends on the person of whom you ask it. The (anonymous) authors then go on to give their particular answer to the question, and I will quote and paraphrase liberally from their statements. To begin with, they assume that their embryonic optical engineer will receive the liberal college instruction necessary to transform him into a reasonably cultured and literate citizen. In addition to the usual so-called cultural courses he will take during his freshman and sophomore years, he takes 4 terms of mathematics, 4 terms of physics, and 2 terms of an elective science such as chemistry or biology. This curriculum differs not at all from that of any other budding scientist or engineer. His professional specialization begins in the junior year. He takes 2 terms of geometrical optics which include an analysis of optical systems, and of typical optical instruments in the laboratory; 2 terms of electromagnetic theory, with emphasis on physical optics in the second of these terms; one term of physiological optics. Then he has 3 terms of electives in the sciences and engineering, and here is where the optical engineer begins to deviate from the optical physicist in the choices made. In the senior year he must take 4 courses chosen from the following: physical optics (2 terms); radiometry and spectrophotometry (2 terms); optical testing (2 terms); modern physics and introductory solid-state physics (1 term each); scientific or engineering electives (2 terms). Thus a man receiving a B.S. degree in optics from the University of Rochester should have basic competence in at least two of the three "core" areas: geometrical optics, physical optics, and radiometry. Also he has added to his basic foundation, via elective courses, either a further concentration in one area or a broader capability extending across the entire realm of optics and perhaps invading other fields of science and engineering. The *Newsletter* goes on to say that the above constitutes their present operational definition of an optical engineer (or an optical physicist) at the B.S. level. He has been exposed to less physics than a B.S. physics major and has had more specialized training in optics.

Our optical engineer or optical physicist can go on further, to the M.S. and perhaps to the Ph.D. I will not go into detail on the curriculum he would follow in this event but suggest reference to the graduate catalog of the University of Rochester, which is one of the few schools at which he could pursue graduate study with a specialty in optics. As noted in my January column [*Applied Optics*, **1**, 84 (1962)], however, there are some other universities in the country where students can train at the graduate level and take a research specialty in optics. The number of these opportunities is unhappily very small, but this is another story. It is this situation, in fact, which encourages OSA to carry out a survey in order to establish just how much need there is for people trained in optics at the various educational levels, and then be able to compare these data with the known facilities for such training. This would give a quantitative answer which would be most important in deciding how hard to push for the enhancement of the facilities for training optical physicists and engineers in the U.S.A.

At the masthead of my column it states that I would be glad to receive news and comments. This invitation has been heeded by a few readers, and I was especially interested to receive a letter from Walter Wallin, a west-coast optical engineer of note. He described a course on "Design of Optical Systems" that he has been giving for several years at the University of California at Los Angeles. This one-semester course is available both to resident students and to extension students and gives either upper division or graduate credit. The enrollment gradually increased to where it now runs between 15 and 25 students each semester. Then some of the students who had finished the semester course petitioned for a more advanced course, so after teaching the regular course for three semesters he teaches an advanced course for one semester. Mr. Wallin says that the majority of his students are extension-graduate engineers and physicists who are trying to fill a gap in what has been taught them as undergraduates. They are principally people who are working in industry and who feel a growing need for a knowledge of optics in their work. A number of them are actually

Continued on previous page

Control of a Ruling Engine by a Modulated Interferometer

Horace W. Babcock

This paper describes a system of interferometric control as applied to the smaller ruling engine of the Mount Wilson Observatory. The usual mechanism intermittently advances the grating carriage with a spacing closely approximating an integral number of fringes of green Hg^{198} light. A Michelson interferometer monitors this motion. The interferometer is modulated by deflecting the compensating plate electromagnetically, thus correcting for barometric pressure changes and also causing the fringe pattern to oscillate with a small amplitude at 60 cps. The oscillating fringe pattern is scanned by a phototube and is reproduced on a monitoring cathode-ray tube; any decentering of the nth fringe is detected by synchronous demodulation and is converted to a stored electrical charge. During each spacing operation, a differential correction proportional to the stored error signal is introduced into the mechanism. Corrections average about 1 centifringe (2.5×10^{-7} cm). The system is relatively simple and ensures a very high order of precision in spacing, with extremely straight grooves.

Introduction

The practicability of interferometric control of a ruling engine for diffraction gratings has been demonstrated by Harrison and his associates at the Massachusetts Institute of Technology.[1] The system developed by Harrison requires continuous advance of the grating blank. In order to provide for essentially straight grooves to be produced by the ruling diamond, it was necessary to employ a rather elaborate mechanical linkage designed to yield nearly uniform speed of the diamond over the greater part of its travel; even so, about 5% of the resulting groove length is sacrificed because of curvature. To ensure parallelism of the grooves, the M.I.T. engine also requires a secondary interferometer and servo system for continuously adjusting the azimuth of the grating carriage as it moves along its ways under the control of the primary interferometer.

The purpose of this paper is to describe a different system of interferometric control recently applied to the 25-cm ruling engine of the Mount Wilson Observatory.[2] This engine, which has been successfully operated in a purely mechanical mode for many years, has a demonstrated capacity in the production of gratings up to 15×25 cm. Tests of the performance of one of these gratings have been described by Pierce.[3] The addition of interferometric control was undertaken with the double aim of still further reducing residual errors of spacing and of minimizing the nonproductive time spent in critical adjustments of mechanical parts.

In order to ensure straightness of the grooves, to avoid extensive mechanical alterations to the machine, to achieve maximum simplicity, and to permit operating either with or without interferometric control, it was decided to retain intermittent advance of the grating carriage, together with simple, crank-driven, reciprocating motion of the ruling diamond. By appropriate choice of the spur gears used in the intermittent drive for the worm that advances the 900-tooth gear and the main screw, it is a simple matter to advance the grating carriage an integral number of fringes in each spacing operation. The spacing most in demand is approximately 600 grooves per millimeter, or 15,000 per inch. If gearing is chosen to make the spacing 610.3 grooves per millimeter, the grating constant will be three wavelengths of green mercury light (λ 5460.7531); thus almost exactly six fringes will pass in the field of the interferometer for each spacing cycle.

The control system employs an electrooptic "fringe-clamp" device. After each incremental advance of the grating carriage, while the diamond is ruling a groove, a phototube senses any deviation from exact centering of the stationary $6n$th fringe. The resulting electrical error signal is stored, and during the next spacing operation it is converted to a shaft rotation which, after a large reduction through gearing, is introduced as a differential correction into the spacing mechanism of the machine. In the present instance, the differential

The author is at the Mount Wilson and Palomar Observatories, (Carnegie Institution of Washington, California Institute of Technology), Pasadena, Calif.

Received 7 November 1961 (Received by *J. Opt. Soc. Am.* 26 September 1961).

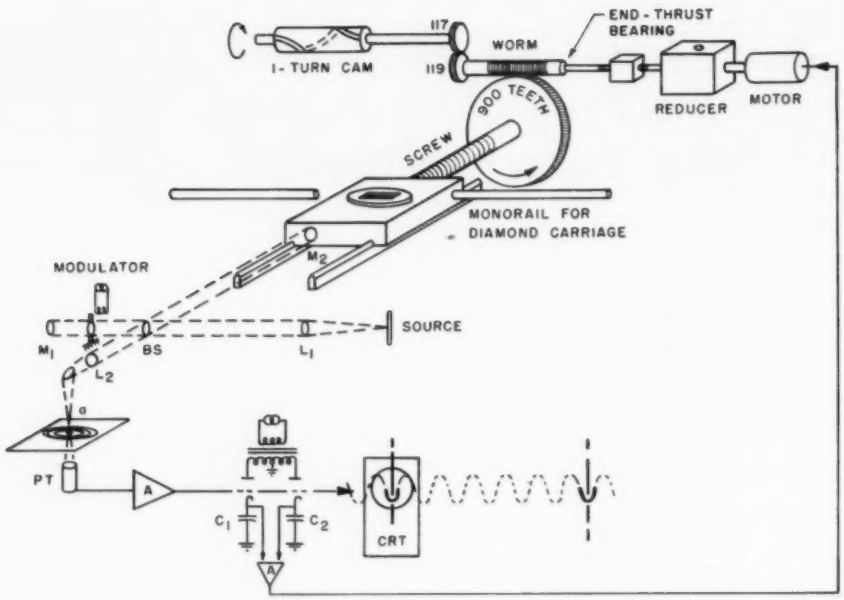

Fig. 1. Schematic diagram of ruling engine with intermittent control system. The moving mirror, M_2, of the Michelson interferometer is on the grating carriage. The circular fringe system, which is imaged at a, is modulated by oscillation of the tilted compensating plate. Any displacement of the chosen fringe is measured by the phototube–amplifier–demodulator section, and during the next subsequent spacing operation the appropriate differential correction is applied by the motor.

correction is applied through a rotation of the screw-mounted end-thrust bearing of the worm that advances the main spacing gear (Fig. 1).

The Modulated Interferometer

The interferometer is of the Michelson type, with the moving mirror carried on one end of the grating carriage. The beam splitter, fixed mirror, and compensating plate are mounted on a substantial bench attached to the base of the machine. The source, a water-cooled Meggers Hg^{198} isotope lamp excited at 2500 Mc/s, together with its collimating lens, is mounted outside the enclosure that houses the ruling engine. An interference filter isolates the green line. Light emergent from the interferometer is focused by a projection lens to form a system of concentric rings on a screen, also outside the enclosure. A small aperture in the center of the screen admits light from the center of the fringe pattern to a 10-stage electron-multiplier phototube. The radius of the aperture is only a fraction of the width of the narrowest fringes, which occur for maximum path difference. To provide for sensitive detection of the position of the $6n$th fringe, which is just appearing or disappearing at the center of the concentric pattern, as well as to compensate for changes in barometric pressure, the interferometer is modulated.

Modulation is accomplished by giving a slight angular displacement to the tilted compensating plate of the interferometer, which is supported on a flat steel spring, or Cardan hinge. The voice coil and magnet from a loudspeaker are so mounted (the voice coil being attached to the plate holder) that a small alternating current applied to the coil provides an angular vibration of the compensating plate, such that the optical fringe pattern sweeps back and forth with an adjustable range at a frequency of 60 cps. At the same time, a direct current applied to the same coil from a simple analog computer deflects the plate in order to compensate for changes in barometric pressure.

Fringe Clamp Circuit

With the interferometer modulated at 60 cps, the amplified output of the phototube is conveniently applied to the vertical deflecting plates of a monitoring oscilloscope while a 60 cps sine wave is applied to the horizontal plates. The resulting trace reproduces the portion of the fringe system that is being scanned. If the amplitude of modulation is sufficient, two or more complete fringes can easily be displayed, although in actual operation the amplitude is set at about $^1/_5$ fringe. If a dark fringe is centered on the aperture, the scanning will result in a U-shaped pattern appearing on the oscilloscope. Any slight decentering of the fringe will cause the U to become asymmetric. For control purposes the phototube signal is further amplified and then demodulated by a balanced synchronous rectifier. Any error in the centering of the $6n$th fringe results in a proportional imbalance in the charge de-

veloped on the capacitors C_1 and C_2. At the conclusion of the scan phase, which occupies about 40% of each cycle, the error-correcting motor (Fig. 1) is caused to turn in the direction and by an amount determined by the stored signal. Switching of the signal circuit and of the correcting motor at the appropriate phases is accomplished through mercury switches operated by cams on the main crankshaft of the ruling engine.

When the machine is operating under interferometric control, the clamping of the fringes is readily monitored by observation of the oscilloscope, which also displays the intermittent advance of the fringe pattern during the spacing part of each cycle. An indication of error amplitude is also given by a sensitive voltmeter connected across C_1 and C_2.

Feedback for Error Correction

Error correction appears in the form of intermittent rotation of the shaft of a small reversible motor. After passing through a miniature variable-speed transmission and further gear reducers, the shaft rotation is introduced as a differential correction into the spacing mechanism of the ruling engine. The mechanical differential for this purpose might take any one of several forms; in the present case the simplest method was to control the position of the end-thrust bearing of the spacing worm that advances the 900-tooth gear on the main screw. The end-thrust bearing is mounted on a fine-pitch screw that is rotated by the correcting motor. The range of longitudinal travel of the worm is 25 mm corresponding to an accumulated correction of some 100 fringes in the ruling of a single grating. The intermittent driving device, which rotates the worm through spur gears, is a cylindrical cam that is given exactly one turn for each spacing operation. A 1:1 spur gear ratio yields a spacing of 600 grooves per millimeter. It was found by trial ruling under interferometric control that multiplying the grating space by the factor 0.983151 would, at a temperature of 23.9°C and at a fixed barometric pressure, result in a cumulative correction of zero for a large ruling. This factor was closely approximated by spur gears for driving the worm in the ratio 117:119 or 0.983193.

By providing additional sets of spur gears in appropriate ratios, or otherwise altering the mechanical spacing, it is readily possible to rule under interferometric control at other grating constants corresponding to integral numbers of fringes other than six. Table I shows the spacing in grooves per millimeter that results from the use of various integral numbers of fringes per cycle, the appropriate ratios for zero cumulative correction, and the tooth-numbers for gear pairs approximating these ratios. A greater variety of spacings can be made available by employing the blue mercury line as a supplement to the green line.

Table I. Groove Spacing Related to Number of Fringes

Number of fringes	Spacing (grooves/mm)	Ratio	Gear teeth	Residual
18	203.4	2.949453	233:79	+0.000096
9	406.9	1.474726	146:99	−0.000021
8	457.7	1.310868	97:74	+0.000057
6	610.3	0.983151	117:119	−0.000042
5	732.4	0.8192925	68:83	+0.000015
4	915.4	0.655434	78:119	−0.000028
3	1220.7	0.491575	58:118	+0.000050

During ruling operations, a continuous record of the corrections applied by the control system is recorded on a strip chart, along with a record of barometric pressure and an indication of the performance of the temperature control for the machine. Temperature variations are held to ±0.01°C.

Automatic Correction for Barometric Pressure Variation

The index of refraction for air at 20°C and 760 mm pressure is approximately 1.00027 for green light. In ruling a 25-cm grating the optical path difference reaches 25 cm if it is assumed that the two arms of the interferometer are made equal when the grating carriage is in mid-position. If a change of atmospheric pressure corresponding to 2.5 cm of mercury occurs, the fringe pattern can be expected to swell or shrink by about one part in 100,000. The equation for phase shift as derived is $\Delta m = 3.27 \Delta p \Delta s$, where Δm is the phase shift in centifringes needed to offset a change of Δp inches of mercury in the barometric pressure since the beginning of the ruling, and Δs is the interferometer–mirror separation on the engine, in millimeters, at the time of correction. Thus, the largest correction required, if the barometer changes by 2.5 cm will be 4.09 fringes at the end of a 25-cm ruling, and the correction will be proportional to the distance from the middle of the ruling.

For sensing the pressure changes, we have employed a modified aircraft altimeter equipped with a photoelectric sensor and a motor-driven follower, rather similar to that described by Harrison. The motor turns a low-resistance, center-tapped potentiometer, P_1, that is supplied from a regulated dc source. Thus, the current output is proportional to any change occurring in the barometric pressure. This current is applied in turn to the terminals of P_2, a center-tapped potentiometer of considerably higher resistance than P_1. The second potentiometer is rotated through a rack and gear by the grating carriage, so that the displacement of the wiper from the mid-position is proportional to the optical path difference in the interferometer. This

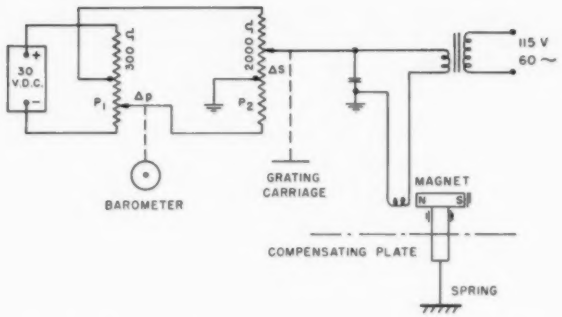

Fig. 2. Computer for automatic barometric correction. With inputs from a barometer and from the grating carriage, the analogue computer delivers to the deflecting coil of the compensating plate a direct current proportional to $\Delta p \Delta s$. The transformer introduces a 60 cps component for oscillating the fringe system with small amplitude.

simple analog computer (Fig. 2) provides a current, representing the product $3.27\ \Delta p \Delta s$, that is applied to the deflecting coil of the compensating plate of the interferometer, thereby imparting the required phase correction.

Performance of Grating Carriage

As described in an earlier paper,[2] the grating carriage of our 25-cm machine is equipped with Graphitar bearing shoes at the four corners, and these slide on hardened Nitralloy steel ways. (It was earlier found to be imperative to eliminate all ball bearings and steel balls in order to avoid accidental and cyclic errors.) The ways are symmetric, 23 cm apart, and have 90° roof tops. They were carefully finished by lapping with a rigid, full-length, reversible cast-iron lapping tool fitting both ways. With this method, a very high degree of parallelism and straightness was achieved. As a result, the rulings, even with grooves 15 cm in length, show no effect of "fanning" or lack of parallelism, nor has there been any evidence of varying friction as the carriage proceeds along the ways. The coefficient of friction is satisfactorily low, so that the sapphire end-thrust bearing of the lead screw is conservatively loaded.

The interferometer showed in tests that, because of elastic stresses built up in the machine, the grating carriage exhibits a tendency to creep forward gradually by a small fraction of a fringe during the interval between spacing operations when it should remain stationary. It was found that this undesirable effect could be eliminated by reducing the forward stress transmitted to the carriage during the stationary phase of each ruling cycle. At this point it should be recalled that an equalizing yoke, attached to the grating carriage, receives the forward thrust of the two halves of the main driving nut. The anticreep device consists essentially of a small solenoid mounted on the end of the grating carriage, which, in "bootstrap" fashion, applies an increased bending moment to the yoke during the appropriate phase and thus decreases the forward thrust. The solenoid is energized through a cam-operated switch; it dissipates only about $^1/_2$ watt, and thermal insulation prevents local heating.

Diamond Carriage

With a spacing system capable of positioning the grating blank to a precision of 1 centifringe, or 2.5×10^{-7} cm, enormous demands are placed on the reciprocating diamond carriage if equivalent precision is to be achieved in reproducibility of the line of motion of the ruling edge. These demands are met, as described ten years ago,[2] by the cylindrical monorail that guides and supports the diamond carriage. It is an essential feature that the diamond moves on the axis of the interrupted rail. Inverted V-blocks of Graphitar on the two ends of the lightweight carriage ride on coaxial sections of a hardened steel cylinder that has been lapped to a high degree of straightness and roundness. Rotation of the carriage about the axis of the rail is constrained by a simple outrigger, yet even such rotation would not displace the diamond.

Capability of the Control System

It will be noted that the interferometric control system with intermittent spacing, as described here, senses the error, ϵ, in the position of a given groove of the grating and uses this information to correct the placing of the next succeeding groove. The correction that is fed back into the mechanism is $-\beta\epsilon$, where the feedback coefficient, β, is an adjustable positive constant. It will be shown from a consideration of the response to different types of error that the best value of β is a little less than 1.

Occasional single-groove errors. These errors may arise randomly or as the result of a single defective gear-tooth. If $\beta = 1$, such an error will initiate a continuing train of errors alternating between $+\epsilon$ and $-\epsilon$. If $\beta > 1$, the amplitude of the alternating errors will increase exponentially to a limit set by the capacity of the mechanism. But if $\beta < 1$, the amplitude of the error in groove position will decrease exponentially according to the series ϵ, $\epsilon(1 - \beta)$, $\epsilon(1 - \beta)^2$, $\epsilon(1 - \beta)^3, \ldots$.

Abrupt continuing error. A mechanical error of this kind would affect the positions of all the succeeding grooves by the amount ϵ. If, with the control system, $\beta = 1$, only one groove will be ruled out of position. If $\beta < 1$, the error will decrease exponentially.

Error of run. A very gradual change in pitch along the length of the screw, which under mechanical operation would result in a slight progressive change in the grating constant, will be compensated for by the interferometric control system. Any residuals will, in

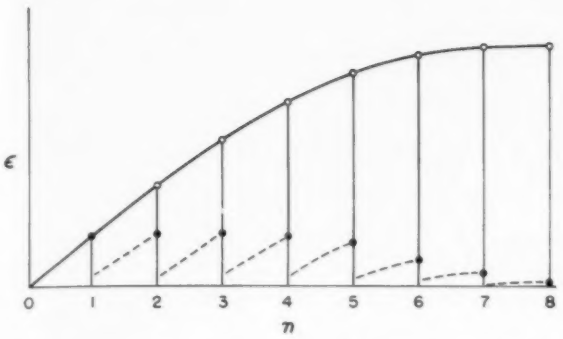

Fig. 3. The sine curve of amplitude b represents an inherent mechanical error, where the ordinates correspond to errors in the positions of numbered grooves. The filled circles indicate groove positions as corrected by the intermittent interferometric control system. The phase is shifted 90°. If there are N grooves per turn, and if the feedback coefficient is 0.7, the amplitude of the error is reduced by the factor $2.8\pi/N$.

general, be far below the slight random errors which are of the order of one centifringe.

Periodic error. The response of the control system in correcting for periodic errors is interesting and effective. Let the mechanical error be represented by $b \sin \theta$, where b, the amplitude, is small compared to the grating constant, a. The angular position of the screw is represented by θ and the number of grooves per turn is N. For a well-adjusted mechanical ruling engine without interferometric control, b will be no greater than about 5 centifringes. This follows from application of the formula for the intensity of Rowland ghosts: $I_g/I = (\pi mb/a)^2$, where m is the order number. One assumes here that the Rowland-ghost intensity in the fifth order of a 600 groove/millimeter grating will be about 1%.

In Fig. 3, the error in position of each groove is represented by the ordinate. As before, the correction applied through feedback is $-\beta\epsilon$. For successive grooves, the errors in position will be:

$$\begin{aligned}
\epsilon_1 &= b \sin \theta_1, \\
\epsilon_2 &= b(\sin \theta_2 - \sin \theta_1) + (1 - \beta)\epsilon_1, \\
\epsilon_3 &= b(\sin \theta_3 - \sin \theta_2) + (1 - \beta)\epsilon_2, \\
\epsilon_n &= b(\sin \theta_n - \sin \theta_{n-1}) + (1 - \beta)\epsilon_{n-1}.
\end{aligned}$$

Expanding the expression for ϵ_n we have:

$$\begin{aligned}
\epsilon_n = b(\sin \theta_n - \sin \theta_{n-1}) &+ (1 - \beta)b(\sin \theta_{n-1} - \sin \theta_{n-2}) \\
&+ (1 - \beta)^2 b(\sin \theta_{n-2} - \sin \theta_{n-3}) \\
&+ (1 - \beta)^3 b(\sin \theta_{n-3} - \sin \theta_{n-4}) + \ldots .
\end{aligned}$$

As we expect to make $^1/_2 < \beta < 1$, terms involving $(1 - \beta)$ to powers higher than 2 can be neglected. Also, since N is large,

$$\begin{aligned}
\sin \theta_n - \sin \theta_{n-1} &\approx \sin \theta_{n-1} - \sin \theta_{n-2} \\
&\approx 2 \sin {}^1/_2 (\theta_n - \theta_{n-1}) \cos {}^1/_2 (\theta_n - \theta_{n-1}) = \frac{2\pi}{N} \cos \theta_n.
\end{aligned}$$

Hence

$$\epsilon_n = \frac{2\pi b}{N} (3 - 3\beta + \beta^2) \cos \theta_n.$$

One concludes that the maximum practicable degree of compensation for periodic error will be obtained when $\beta = 1$, and that the residual error "leaking through" the correcting system will be shifted 90° in phase with respect to the inherent error. The amplitude of the periodic error will be reduced by the factor $2\pi/N$ if $\beta = 1$. For the 25-cm Mount Wilson machine, where $N = 900$, this corresponds to 0.00698. But we have shown that β must be less than 1 if random errors are to be controlled. It therefore appears that a suitable compromise will be to place $\beta \approx 0.7$. It follows that

$$\epsilon_n = 2.8 \frac{\pi b}{N} \cos \theta_n,$$

so that when $N = 900$,

$$\epsilon_n = 0.01\, b \cos \theta_n.$$

The interferometric control, with $\beta = 0.7$, should therefore reduce the primary periodic error to 1% of its uncontrolled value, with a consequent reduction in Rowland ghost intensity by the factor 10^{-4}. The ghost intensity should then be so low as to be of little practical interest. At the same time, accidental errors, which are generally no greater than 2 or 3 centifringes, will rapidly be brought under control.

The 25-cm ruling engine with interferometric control has proved to be reliable in operation and in the past few months has produced several gratings of high quality in sizes up to 13 × 20 cm. These are blazed plane gratings ruled on aluminized blanks that are flat to one-fortieth wavelength. There is no bar to the employment of the control system for larger gratings up to the limit set by the dimensions of the machine. It may be emphasized again, however, that several characteristics, in addition to adequate precision in spacing of the grooves, must be combined in any really satisfactory grating, especially if it is to be used in spectrophotometry of absorption lines arising in faint astronomical sources.

The mechanical design required in the modification of the ruling engine as described here is due to R. R. Van Devender. Mechanical construction and technical operation are the responsibility of Stuart Roberts. L. E. Blakée constructed and installed the electronic equipment. I am indebted to Sylvia Burd for numerical computations. All grating blanks have been figured and aluminized by Messrs. Hendrix, Day, and Johnson of the Optical Shop.

References

1. G. R. Harrison, N. Sturgis, S. C. Baker, and G. W. Stroke, J. Opt. Soc. Am. **47**, 15 (1957). See also G. R. Harrison and G. W. Stroke, J. Opt. Soc. Am. **45**, 112 (1955).
2. H. D. Babcock and H. W. Babcock, J. Opt. Soc. Am. **41**, 776 (1951). For an account of certain developments in the ruling of gratings, see Annual Report of the Director, Mount Wilson Observatory, in the Yearbook, Carnegie Institution of Washington, No. 11 (1912) to No. 60 (1961), inclusive.
3. A. K. Pierce, J. Opt. Soc. Am. **47**, 6 (1957).

From the Editor

Perhaps it is appropriate in an issue featuring Optical Engineering to discuss terminology: symbols, units, and nomenclature. In the May issue of this journal, Prof. Ingelstam has already discussed some aspects of the interplay between scientists and engineers. All of us who went to colleges which trained engineers remember the jocular distinctions between physicists and engineers; such as the engineer knows how but he doesn't know why and vice versa for the physicist. This philosophical distinction is also reflected in their attitudes toward terminology. In pondering a problem the physicist supposedly reasons his way to the solution. The effect is proportional to the fourth power of the temperature, say, or inversely proportional to the area. Being interested chiefly in dimensions he neglects the constants of proportionality and therefore tends to be indifferent about units. It is precisely this indifference that makes him more willing to change his symbols and units and accept new definitions.

The engineer in general has much stronger feelings about terminology. When pondering a question he reaches for a handbook to seek an analogous problem he has solved before, and he desires a numerical answer. It is disconcerting, when trained to think in terms of Btu or foot-pounds, to find quantities expressed in joules or kilowatt hours. The engineer relies chiefly on his memory rather than his reason, and there is something sacred to him about the way things were first learned. Generalizations such as the above are exceedingly dangerous and oversimplified; we all know engineers with poor memories as well as unreasoning physicists, but fortunately few of these are in optics.

When this journal began to take shape, long before the first issue appeared, we were asked by Deane Judd, the Editor of *J. Opt. Soc. Am.*, what were our opinions concerning terminology. At that time we indicated we would go slow in formulating editorial policies on terminology until we had a better feeling for the problem. As we saw it, we were attempting to lure into *Applied Optics* authors from many other disciplines on the fringes of conventional optics (such as electronics, solid-state physics, and space physics); to impose a common terminology on them might prove more difficult than on the *J. Opt. Soc. Am.* audience. So we were initially disposed to defer such matters as uniform terminology until a year or so had gone by and we had a better feeling for what changes might be required. However, as the papers came in for the first issue on optical pumping, our editorial sensitivity was deeply disturbed by statements such as "We used a 5-in. ruby rod and it made a 2-cm spot on the wall"; "The spot was 5 mm in diameter and was imaged on the spectrometer slit, which was $^1/_4$ in. long." This mixing of units demonstrates the hybrid nature of optical engineering: the physical properties of the radiation are expressed in metric units, and the engineering dimensions of the apparatus are expressed in "homely" units. (Your Editor has himself sinned in this manner; he once wrote a paper on atmospheric transmission expressing the water vapor concentration as "precipitable cm H_2O per 1000 yards.")

We thereupon decided to see if we could not use the metric system throughout *Applied Optics*. By and large the authors consented quite readily to the proposed changes. When we inserted into the "Information for Contributors" a request that "in general, the metric system of units is preferred," we were somewhat embarrassed to see that the very next sentence was "Manuscripts should be submitted on $8^1/_2$ by 11 inch paper!" We are aware that there is nothing magical in the metric system—a distance is just as far in feet as it is in meters—but surely our communication with each other is improved when we use a common nomenclature. The metric system is slowly but surely winning general acceptance: for example, it was recently adopted by India and China, and even Great Britain is considering decimal currency and has adopted Celsius temperature.

Let us consider some more specific matters of terminology: In the past year, Dr. Judd has devoted two or three Editorials in *J. Opt. Scc. Am.* to optical terminology. In his April 1962 issue there is a detailed report on the SUN (symbols, units, and nomenclature) Committee of IUPAP and IUPAC, and the IAU is also participating in this effort to draw up a common list of preferred units, symbols, and definitions. This was discussed at the March meetings of the *J. Opt. Soc. Am.* Associate Editors and the *Applied Optics* Editors and Reporters. Both journals decided to adopt these recommendations after they are approved by the AIP Publications Board. Some of these changes will begin in this issue (for example, Angstrom becomes Ångstrom again). There will be a report on some of the proposed changes in the June *Physics Today*, and as soon as a revised AIP Style Manual is issued we shall expect authors to conform. We shall devote future columns to a discussion of the proposed changes in optics terminology, and we invite your comments. Some of the recommendations will probably excite controversy: for example, the recommended prefix for 10^{-9} is nano- and 10^9 is giga-. The old familiar $m\mu$ for millimicrons might give way to nm for nanometers (as used now by the Royal Society), and kMc for kilomegacycles becomes Gc, gigacycles. The recommended nomenclature for photometry is new to most of us.

The publications of the Optical Society represent a powerful segment of the optics literature, and if we adopt this proposed terminology we can make a real contribution to the clarity and precision of our scientific literature.

J. N. Howard

Diffraction Anomalies in Grating Spectrophotometers

James E. Stewart and William S. Gallaway

The Wood anomalies are dark or bright bands in the spectrum produced by a diffraction grating. They occur at observed wavelengths for which light of the same wavelength is diffracted in another order so as to graze the surface of the grating. The equations describing the position of the anomalies are discussed for a variety of grating arrangements. Some experimental observations of Wood anomalies are described, including a new finding concerning the reluctance of two anomalies to coincide. Finally, a discussion is given of spectrophotometric errors introduced by Wood anomalies.

I. Introduction

The diffraction grating is both beautiful in its simplicity and powerful in its utility. Since its invention by Fraunhofer in 1819, the art of ruling the grating has been brought to a state of near perfection. With the development of effective replication processes in the past decade good gratings have become comparable with prisms in cost. The availability of these replicas has generated a revolution in the design of general purpose spectrophotometers and there is at present a concerted demand for the replacement of prisms with gratings.

There are obvious advantages to be had by using gratings. Aside from the primary objective of greater resolving power, the superior dispersion of gratings in some spectral regions carries with it the dividend of increased radiant power available at the detector.

Unfortunately, there are also problems peculiar to diffraction gratings. Certain forms of anomalous behavior are associated with imperfections in gratings. For example, there are the celebrated ghosts of Rowland and of Lyman which appear when periodic errors exist in the rulings. Improved ruling engines and techniques have virtually exorcised these. There remains, however, another kind of "anomaly," found even in perfect gratings. This is the Wood anomaly. The purpose of this article is to review the equations which describe the wavelengths where these anomalies occur, to present illustrations of anomalies found with gratings used in typical spectrophotometers, and to discuss certain experimental difficulties which these anomalies can introduce. It is largely addressed to the new user of grating spectrophotometers who in all probability is unaware of the existence of Wood anomalies. In addition, a previously unreported property of Wood anomalies is disclosed as a challenge to our theoretical colleagues who may wish to explain it.

The Wood anomalies were described by Wood[1] in 1902 and later[2,3] as bands of abnormally high or low intensity in the light diffracted by reflection gratings. These bands are sometimes exceedingly narrow, and Wood was probably amused when he found he could make one or the other of the sodium D lines disappear by causing a dark band to fall on it. Wood established that light missing from dark bands in the diffracted beam can be found as an excess in the reflected zero-order beam, and conversely that bright bands in the diffracted light correspond to energy missing from the zero order. He found that sometimes, but by no means always, the anomalies could be weakened by lightly rubbing the grating to remove ridges from the tops of the grooves. He also established that the anomalies are highly sensitive to the state of polarization of the incident light, being much more pronounced when the electric vector of incident radiation is perpendicular to the rulings of the grating. These are the *S*-anomalies. More recently, Palmer[4,5] has studied the *P*-anomalies with light polarized parallel to the rulings and found them to be strongest with deeply grooved gratings, weakening and disappearing for wavelengths greater than the groove depth. The *S*-anomalies, on the other hand, are generally stronger at longer wavelengths.

In 1907, Lord Rayleigh,[6] in developing his "dynamical theory of the grating," called attention to mathematical singularities which occur in his theory at wavelengths for which light of the same wavelength is diffracted in another order so as to graze the surface of the grating.

The authors are with Beckman Instruments, Inc., Fullerton, California.

Received 5 December 1961.

This paper was presented at the Molecular Structure and Spectroscopy Symposium, Ohio State University, June 12–16, 1961.

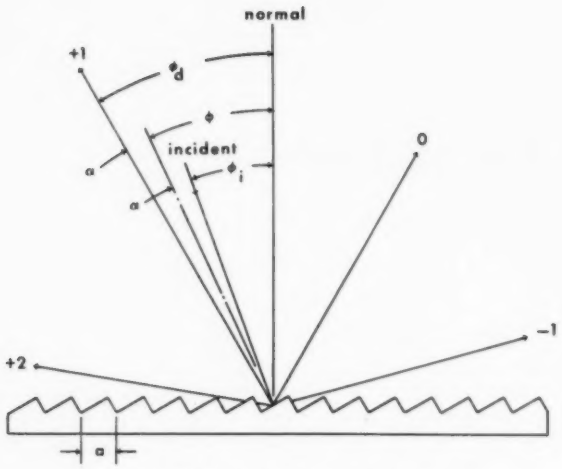

Fig. 1. Diffraction grating nomenclature.

He found that these wavelengths, which have come to be called the Rayleigh wavelengths, correspond to the Wood anomalies. Rayleigh's singularities occur only for polarization of the electric vector perpendicular to the rulings, and can only account for the *S*-anomalies.

More sophisticated theories have been published by Voight,[7] Fano,[8] and Artmann.[9] In the past decade, evidently inspired by the needs of workers in microwave propagation, even more elegant theories have been advanced by Twersky,[10] Wait,[11] Karp and Radlow,[12] Lippmann and Oppenheim,[13] Meecham,[14] and Millar.[15] Unfortunately, the mathematics associated with these theories is formidable. Solutions have been found for transmission as well as reflection gratings; for gratings of sine wave cross section; for semicircular cylindrical bosses on a plane; and for semielliptical cylinders on a plane; and indeed the intensity distributions calculated for these special cases resemble the Wood anomalies of actual gratings. The theories have not been extended to the case of the real echelette grating. Consequently, although the wavelength region where a Wood anomaly might be found can be calculated with certainty, no prediction can be made about its intensity, or even whether it will be dark or light.

II. The Rayleigh Wavelengths

The nomenclature to be used in deriving the Rayleigh wavelengths is illustrated in Fig. 1, showing a cross section of an echelette grating with ruled facets oriented to maximize the diffracted radiation in a preferred direction—the blaze direction. Radiant energy is incident at an angle ϕ_i from the normal and is diffracted at an angle ϕ_d, differing from the incident angle by 2α. The grating equation relating wavelength λ, order n, grating spacing a, and the angles can be written in the alternative forms

$$n\lambda = a\,(\sin\phi_i + \sin\phi_d) \tag{1}$$

or

$$n\lambda = 2a\sin\phi\cos\alpha \tag{2}$$

where

$$\phi = \phi_i \pm \alpha = \phi_d \mp \alpha.$$

The positive side of the normal is the side containing the incident beam. Negative diffracted orders lie in the quadrant containing the reflected or zero-order beam. We proceed to calculate the Rayleigh wavelengths, λ_R, for a number of cases.

A. The Zero-Order

Gratings are often used as reflection filters because the zero-order radiation is rich in long wavelengths but

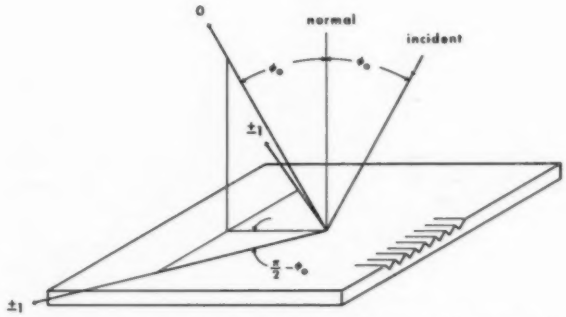

Fig. 2. Wood anomalies in the zero order of a grating with its rulings perpendicular to the monochromator slit.

not short wavelengths. The Rayleigh wavelengths in the zero-order radiation are found by setting $\phi_d = \pi/2$ for positive grazing orders m_+, or $-\pi/2$ for negative grazing orders m_-

$$\lambda_R = \frac{a}{m_\pm}(\sin\phi_i \pm 1). \tag{3}$$

As ϕ_i is increased, the Rayleigh wavelengths for grazing positive orders become longer while the Rayleigh wavelengths for grazing negative orders become shorter. Two Rayleigh wavelengths coincide for

$$\lambda_R = 2a/(m_+ - m_-). \tag{4}$$

B. The Zero-Order for a Grating with Rulings Perpendicular to the Slit

This arrangement is often found to be advantageous when using a grating as a filter. In cross section, as in Fig. 1, ϕ_i is seen to be zero. However, the grazing wavelets sweep across the grating at an angle to the rulings (see Fig. 2), and the Rayleigh wavelengths are given, not by $\pm a/m_\pm$, but by

$$\lambda_R = \pm a\cos\phi_0/m_\pm. \tag{5}$$

C. Spectrograph Arrangement: The Grating Illuminated from a Fixed Direction

When the angle of incidence on the grating is fixed and the various wavelengths are observed at different angles, as in a photographically recording spectrograph, the Rayleigh wavelengths are also given by (3). In the special case of a fixed angle of incidence normal to the grating the Rayleigh wavelengths are $\lambda_R = \pm a/m$.

D. Ideal Littrow Arrangement

In this case the direction of incidence and observation are the same, i.e., $\phi_i = \phi_d$ or $\alpha = 0$. The Rayleigh wavelengths are found by solving

$$n\lambda = 2a \sin\phi \tag{6}$$

and

$$(n + k)\lambda = a(\sin\phi + \sin\pi/2) \tag{7}$$

for grazing positive orders or

$$-k'\lambda = a(\sin\phi - \sin\pi/2) \tag{8}$$

for grazing negative orders, with $k,k' = 1,2,3,\ldots$. It is seen from (1) and Fig. 1 that, as the direction of the incident radiation is rotated counterclockwise from the normal, the diffracted rays move clockwise and longer wavelengths appear in the direction of observation, wavelengths in negative orders approach grazing from in front of the grating surface, and positive orders approach grazing from "behind"* the grating. Solution of (6), (7), and (8) shows that the Rayleigh wavelengths for positive and negative grazing orders occur simultaneously and

$$\lambda_R = 2a/(n + 2k). \tag{9}$$

For spectra observed in the first order, Wood anomalies should occur at $\lambda_R = 2a/3, 2a/5, \ldots$ for grazing $+2$ and -1 orders, $+3$ and -2 orders, etc. Spectra observed in second order will have $\lambda_R = 2a/4, 2a/6, \ldots$ for grazing $+3$ and -1 orders, $+4$ and -2 orders, etc.

E. The General Littrow Arrangement

This applies also, of course, to Ebert, Czerny-Turner, or any grating arrangement having a fixed, nonvanishing value of 2α—the angle between the incident and observed beams. In this case the equations to be solved are Eq. (1) and

$$(n + k)\lambda = a(\sin\phi_i + 1) \tag{10}$$

or

$$-k'\lambda = a(\sin\phi_i - 1). \tag{11}$$

The solutions are

$$\lambda_R = \frac{2a}{n + 2k}\left\{\frac{1 \pm [2\sqrt{nk + k^2}/(n + 2k)]\sin\alpha}{1 + [n\tan\alpha/(n + 2k)]^2}\right\} \tag{12}$$

and an identical equation in k' instead of k. The double root expresses the separation of the Rayleigh wavelengths which were coincident in the case of the ideal Littrow. If $\phi_i > \phi_d$, that is, if the beam from the entrance slit of the monochromator makes a *larger* angle with the grating normal than the ray to the exit slit, the *longer* Rayleigh wavelength of the separated pair corresponds to grazing diffraction on the same side of the normal as the incident ray (i.e., a grazing positive order). For $\phi_i < \phi_d$ the shorter Rayleigh wavelength corresponds to grazing in a positive order.

Because of the term in $\tan\alpha$ in (12) the splitting of the λ_R's is not symmetric. However, for small α,

$$1 + \left(\frac{n\tan\alpha}{n + 2k}\right)^2 \approx 1$$

and the separation between Rayleigh wavelengths is given by

$$\frac{\Delta\lambda}{\lambda_R{}^0} \approx \frac{4\sqrt{nk + k^2}}{n + 2k}\sin\alpha, \tag{13}$$

where $\lambda_R{}^0$ is given by (9). Equation (13) is in error by no more than 1% for $\alpha \leq 5.7°$, and 10% for $\alpha \leq 17°$. The separation of wavelength amounts to roughly $1^3/_4$% of $\lambda_R{}^0$ per degree of angle 2α.

F. The Grating Viewed at a Fixed Angle to the Normal

This case is treated by solving Eqs. (1) and (10) for positive grazing orders and (1) and (11) for negative grazing orders. The solutions are

$$\lambda_R = \frac{a(1 - \sin\phi_d)}{k}, \quad k = 1,2,3,\ldots \tag{14}$$

and

$$\lambda_R = \frac{a(1 + \sin\phi_d)}{n + k'}, \quad k' = 1,2,3,\ldots. \tag{15}$$

In the special case where the fixed direction of viewing is normal to the grating, (14) and (15) reduce to

$$\lambda_R = \frac{a}{k} \tag{14'}$$

and

$$\lambda_R = \frac{a}{n + k'}. \tag{15'}$$

Rayleigh wavelengths corresponding to positive and negative grazing orders thus occur in pairs. For example, when viewing the first-order spectrum, the $+2$ and -1 anomalies should be at $a/2$, the $+3$ and -2 at $a/3$, and so on. The $+1$ anomaly is not attainable in practice, because it requires grazing incident light.

* This is a conveniently descriptive fiction, as diffraction "behind" the grating requires $\sin\phi_d > 1$.

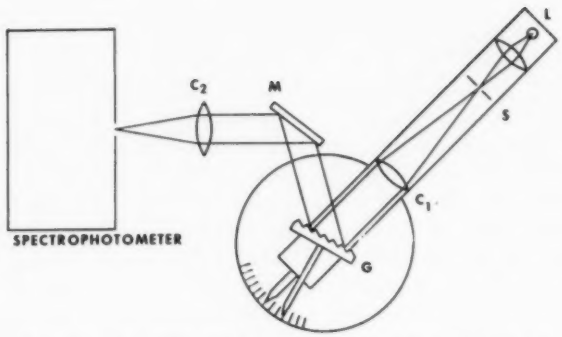

Fig. 3. Apparatus for the study of Wood anomalies. L, source; S, slit; C_1 and C_2, collimating lenses; G, grating; M, Newtonian mirror. The spectrophotometer is a Beckman DK-2.

G. Transmission Gratings

The foregoing discussion is phrased in terms of reflection gratings, the most important type of grating used in modern optical instruments. Transmission gratings are of interest in the propagation of microwaves. The equations given above are valid for transmission gratings with the same sign convention—that orders and angles on the same side of the normal as the incident beam are positive.

III. Experimental Observations

Gratings were studied in the visible and near infrared with some auxiliary apparatus used in conjunction with a Beckman DK-2 spectrophotometer (see Fig. 3). An image of a tungsten lamp L is focused on a 0.25 mm wide slit S. The light from S, collimated by a lens C_1 of 29-cm focal length and 25-mm square aperture, falls on the grating G. The diffracted light is reflected by a plane mirror M through a second lens C_2 of 25-cm focal length and 50-mm diameter, which focuses it on the entrance slit of the DK-2. The source, slit, first collimator, and grating are placed on an arm which is mounted on an Ellis dividing head. The arm can be rotated about an axis through the grating in order to control the angle between incident and observed light. The grating can be rotated independently about the same axis to select the angle of incidence. Both angles are read from a scale on the dividing head to 0.1 deg. In some experiments the grating is used in an ideal Littrow arrangement, with incident and diffracted beams coincident, by replacing M with a semireflecting mirror. A pile-of-plates polarizer consisting of fourteen glass microscope slides mounted at the Brewster's angle in a Makas-Shurcliff[16] arrangement was used to study the polarization properties of the anomalies. All of the anomalies observed were *S*-type.

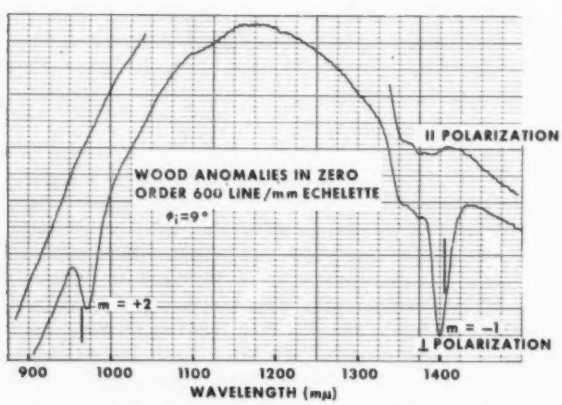

Fig. 4. Typical zero-order anomalies. The order of diffraction of the grazing light is designated by $m = -1$ and $+2$. The calculated Rayleigh wavelengths are shown by vertical lines.

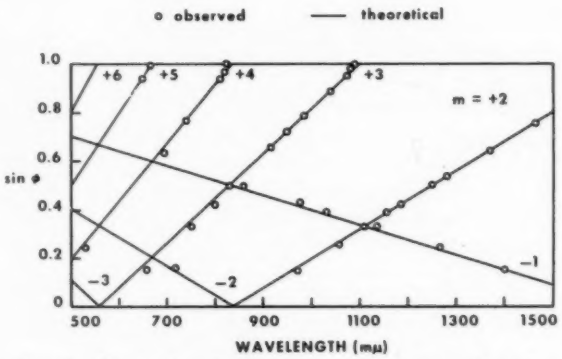

Fig. 5. Observed and calculated zero-order anomalies of a 600 line/mm grating. The m values are the diffraction orders of grazing light.

A. The Anomalies in the Zero Order

The Wood anomalies appearing in the zero-order light were studied by first adjusting the grating on the arm for the desired incident angle and then rotating the arm and grating until the beam fell on the slit of the monochromator. The radiant energy was recorded by scanning the DK-2. A typical pair of anomalies is shown in Fig. 4 for a 600 line/mm echelette, blazed in the red. The recording is uncorrected for such effects as spectral characteristics of source and detector, dispersion of the prism and grating, and transmission of the spectrophotometer and auxiliary apparatus. The vertical lines are drawn at the calculated Rayleigh wavelengths and the designations $+2$ and -1 are the spectral orders in which light of those wavelengths grazes the grating surface [$m_+ = +2$ and $m_- = -1$ in Eq. (3)]. The Rayleigh wavelengths do not coincide with the maxima of the effect but seem to fall at the wavelength where the slope is greatest, as pointed out by Palmer.[4] The anomalies begin to appear before the

grazing beam emerges from the surface of the grating ($\lambda > \lambda_R$) and to persist until the grazing beam is as much as ten degrees above the horizon ($\lambda < \lambda_R$).

The positions of the peaks of the anomalies are plotted for the 600 line/mm grating as a function of angle of incidence in Fig. 5. The experimental points are seen to follow closely the loci of the calculated Rayleigh wavelengths, except in the areas where two anomalies should coincide [Eq. (4)]. One of these areas, that of the $m_+ = 2$ and $m_- = -1$ anomalies, is shown in greater detail in Fig. 6. Instead of crossing, the anomalies appear to repel each other, exchange identities, and then separate, never approaching closer than 25 mμ.

Similar noncrossing behavior is shown by an 1800 line/mm grating (Fig. 7), for which the +2 and −1 anomalies remain separated by 70 mμ. The long wavelength anomaly of the +2, −1 pair is a *bright* band, not outstanding in intensity for small angles of incidence. However, between 20 and 28° it increases abruptly in intensity by a factor of ten, but begins to fade again at greater angles until at 60° it has all but vanished. It

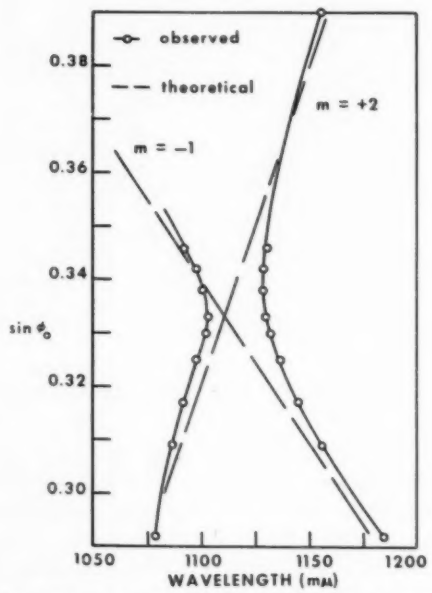

Fig. 6. Detailed study of the zero-order anomalies in the vicinity of coincident Rayleigh wavelengths.

may be significant that the change in intensity occurs near the blaze angle of 27°. The short wavelength anomaly at 368 mμ is a weak *dark* band. The +1 anomalies are fairly weak *bright* bands.

The 600 line/mm grating was also studied with its rulings perpendicular to the slit of the monochromator. Equation (5) tells us that m_+, m_- pairs of anomalies have coincident Rayleigh wavelengths, but in the case

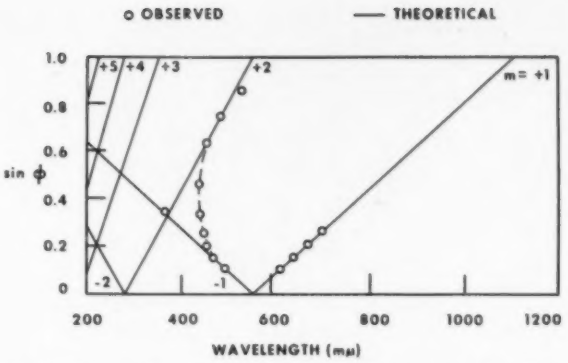

Fig. 7. Observed and calculated zero-order anomalies of an 1800 line/mm grating.

of the +2, −2 anomaly two peaks were observed separated by about 25 mμ. The positions of these peaks are plotted with the calculated Rayleigh wavelengths in Fig. 8. Peaks on the short wavelength side of the theoretical line correspond to the grazing beam above the horizon, while peaks on the long wavelength side of the line are associated with grazing light "below" the horizon.

The zero-order anomalies of a 75 line/mm grating were observed in the infrared by rotating the grating of a Beckman IR-7 until zero-order radiation fell on the exit slit. The grating was then held fixed while the wavelength was scanned with the sodium chloride foreprism. Two strong bright bands were observed at about 12.9 and 13.9 μ in good agreement with Rayleigh wavelengths calculated for 4° between incident and emergent beams and grazing −1 and +1 orders, respectively. The grating was then rotated, making

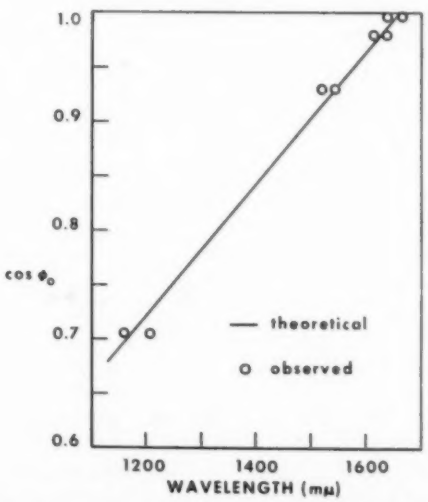

Fig. 8. Zero-order Wood anomalies ($m = \pm 1$) of a 600 line/mm grating with rulings perpendicular to the slit.

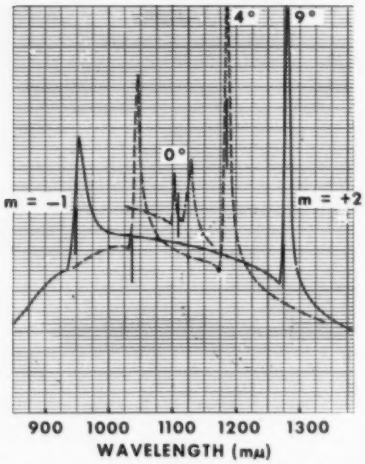

Fig. 9. Wood anomalies in the first-order diffracted spectrum of a 600 line/mm grating for 0°, 4°, and 9° half-angle between incident and diffracted beam. The Rayleigh wavelengths are shown by vertical lines.

its rulings perpendicular to the slit. A *single* bright band was observed at 13.5 μ. This is not necessarily in conflict with the noncrossing behavior observed with the other gratings, as the resolving power of the foreprism is only about 60 mμ at this wavelength.

B. The Anomalies in Diffracted Orders

The Wood anomalies appearing in the diffracted light were studied using the equipment shown in Fig. 3 by first setting the arm relative to the dividing head and mirror to obtain the desired angle between the incident and diffracted radiation. The grating was then adjusted on the arm for a selected angle of incidence and the wavelength and intensity of maximum diffracted radiation were recorded by scanning with the DK-2. This procedure was repeated for other values of the angle of incidence. Finally, a smooth curve of intensity vs wavelength was drawn.

Anomalies appearing in the first-order spectrum of the 600 line/mm grating are shown in Fig. 9. These anomalies correspond to grazing light in the -1 and $+2$ orders. They are extremely strong when the angle between incident and diffracted beams is 18° and 8°, but are somewhat weaker for 0°. In the zero-degree case, observed with the semitransparent mirror, the Rayleigh wavelengths coincide. However, the anomalies remain separated and the noncrossing phenomenon is thus observed in diffracted radiation as well as in the zero-order radiation. Other anomalies, observed in the recorded first-order energy spectrum of a Cary 14 Spectrophotometer using a similar 600 line/mm grating, are seen in Fig. 10. (Compare Fig. 9.) In this case the angle between incidence and diffraction is 16°. Notice

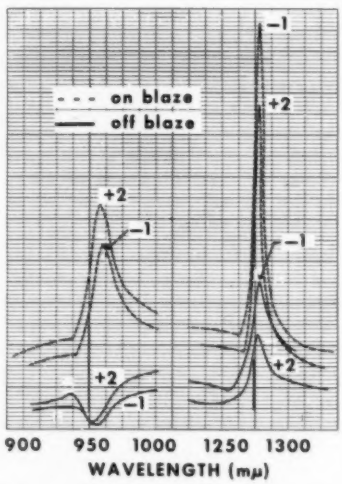

Fig. 11. Effect on the Wood anomalies of reversing the blaze direction and of reversing the incidence and diffraction angles for a 600 line/mm grating.

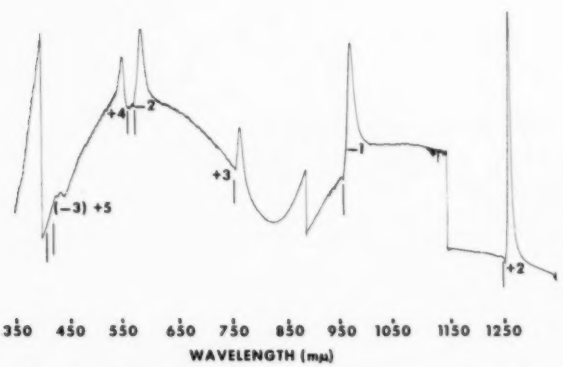

Fig. 10. Wood anomalies in the first-order spectrum of the Cary Model 14 Spectrophotometer. The Rayleigh wavelengths are shown by vertical lines. The abrupt changes in intensity near 1150, 880, and 400 mμ are due to changes in slit width.

that the $+4$ and -2 anomalies, whose Rayleigh wavelengths nearly coincide, show evidence of repelling each other.

The influence of the grating blaze on the appearance of the $+2$ and -1 anomalies of the 600 line/mm grating is illustrated in Fig. 11. In the upper pair of curves, made on the blaze side of the grating, the directions of incidence and diffraction have been interchanged. In one case the incident beam is closer to the normal than the diffracted beam and the reverse is true in the other case. The effect on the anomalies is negligible. The lower pair of curves were made in the same way on the off-blaze side of the grating. Again, exchange of the directions of incidence and diffraction does not materially affect the appearance of the anomalies. However, the anomalies observed on the blaze

side of the grating are markedly different from those on the off-blaze side. The peak near 950 mμ has changed from bright to dark and the 1275 mμ peak is materially weaker in the off-blaze orientation.

The observation that reversing the blaze direction of a grating frequently inverts the appearance of an anomaly suggests an interesting grating arrangement. If the grating is mounted so that it is always viewed in the direction of its normal then the radiation usually lost in the zero order can be intercepted with a plane mirror and returned to the grating at the same angle of incidence as the original incident beam. Both beams, the original incident beam and the returned zero-order, will have radiation of the same wavelength diffracted in the direction of the grating normal. An arrangement of this sort might serve two purposes. First, it offers a means of recovering some lost light; and second, as the anomalies corresponding to the two incident beams are in opposite directions relative to the blaze, we might find bright anomalies occurring simultaneously with dark ones, thus reducing the energy contrast at the anomalies. An experimental arrangement was set up using the 600 line/mm grating. Figure 12 shows the effect on the first-order spectrum. An increase in available energy of 50% is attained at 1000 mμ, but virtually no increase is observed closer to the blaze. Furthermore, the anomalies at about 850 and 500 mμ are reduced in intensity. Figure 13, the second-order spectrum, shows similar results. The Rayleigh wavelengths for this grating arrangement are degenerate, according to Eqs. (14′) and (15′). The anomalies seen in Figs. 13 and 14, however, are evidently adjoining dark and light bands which nearly, but not completely, overlap. This is doubtless another illustration of the noncrossing effect.

For the 1800 line/mm grating in an ideal Littrow arrangement the Wood anomaly of longest wavelength in the first-order spectrum is expected at about 370 mμ. However, the considerable thickness of glass used in the auxiliary apparatus limited observations to wavelengths longer than 375 mμ. With the angle between the incident and emergent beams set at 12° and 30° strong anomalies were seen in the neighborhood of the Rayleigh wavelengths, 406 and 460 mμ, respectively. The former is bright and the latter is a dark band.

The Wood anomalies in the spectrum of the 75 line/mm grating in the Beckman IR-7 are shown in Fig. 14. All anomalies are weak with the exception of the strong dark band in the first order near 1057 cm^{-1}. The +2 anomaly of the grating used to prepare Fig. 14 is unusually strong. Several other 75 line/mm gratings displayed weaker anomalies at somewhat higher frequencies approaching the Rayleigh frequency of 1089 cm^{-1}. These differences, with gratings of the same spacing and blaze angle, must be due to variation in the contour of the ruled facets or differences in the aluminum coating or underlying material. It was ob-

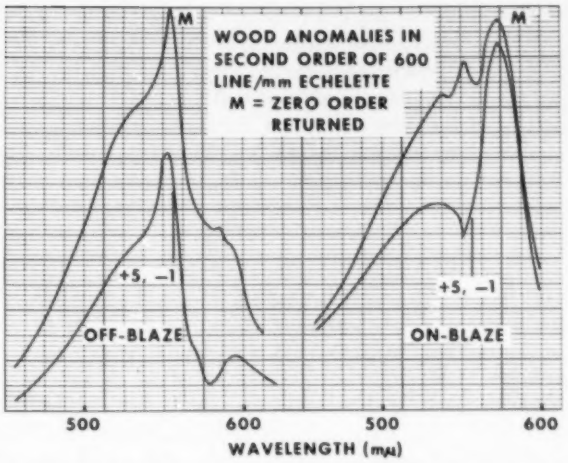

Fig. 13. Wood anomalies in the second-order spectrum of a 600 line/mm grating viewed in the direction of its normal. The curve marked M was made with the zero-order beam returned to the grating. Rayleigh wavelengths are shown by vertical lines.

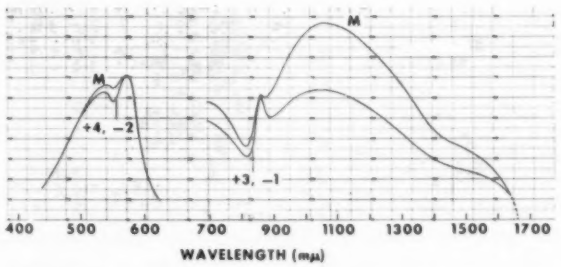

Fig. 12. Wood anomalies in the first-order spectrum of a 600 line/mm grating viewed in the direction of its normal. The curve marked M was made with the zero-order beam returned to the grating. Rayleigh wavelengths are shown by vertical lines.

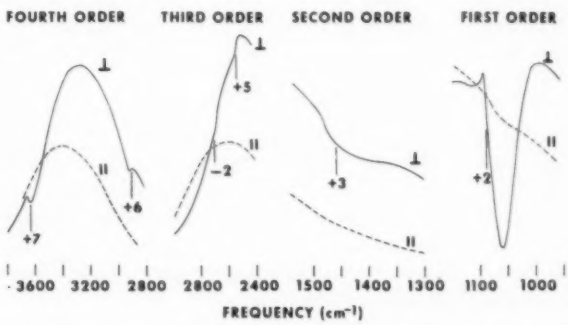

Fig. 14. Wood anomalies in the spectrum of the Beckman IR-7 spectrophotometer. Rayleigh wavelengths are shown by vertical lines.

served some time ago by Strong[17] that the nature of the metallic coating evaporated on the grating greatly influences the appearance of the Wood anomalies and the wavelength of the greatest disturbance. Strong, and later Palmer[4], also noted that the Rayleigh wavelength is shifted by coating the grating with a dielectric, the equation for the grazing wave becoming

$$n\lambda_{\text{vacuum}} = a(\sin\phi_i \pm \mu)$$

where μ is the refractive index of the dielectric. Meltzer and Keller[18] have very recently proposed a method of aluminization of gratings which seems to control anomalies by insulating the reflecting facets from one another.

A strong dark anomaly is observed at 23.2 μ in the first-order spectrum of a 30 line/mm grating in the IR-7 with, possibly, a very weak bright anomaly at 21.7 μ. An 8 line/mm grating has been installed in an IR-7 for use in the very far infrared. The Rayleigh wavelengths for this grating are 86.2 and 80.4 μ in the first order and 64.7 and 60.3 μ in the second-order spectrum. No anomalies are observed near these wavelengths. This is possibly because the necessarily deep grooves of this coarse grating are made by a rolling rather than a plowing action of the diamond tool, which results in smoother facet edges. Wood's early experiments demonstrated that the nature of the ruling edges often played a role in determining the intensity of the anomalies.

IV. Spectrographic Errors Caused by Wood's Anomalies

The two important characteristics of Wood anomalies —intensity and polarization—each lead to complications in spectrophotometry. Moderate attenuation of light intensity of certain wavelengths is not in itself serious in absorption spectrophotometers if proper precautions are taken and if both beams of double-beam instruments are affected equally. The spectroscopist should be aware that the response period of a double-beam instrument is determined not only by the amplifier response, but also by the radiant power available at the detector and that the tracking error in the recorded spectrum depends on the ratio of observed bandwidth to response period.[19] Care must be taken to insure that tracking errors do not become excessive in regions of strong dark Wood's anomalies. In some instruments the slit width or gain are automatically adjusted to maintain constant electrooptical energy in the reference beam, either as an inherent feature or as an ad hoc attachment. This eliminates tracking error, but reduces either resolving power or signal-to-noise ratio in the affected region.

Because of the polarization property of Wood's anomalies, spectroscopy with polarized radiation requires special precautions. If only the sample beam is

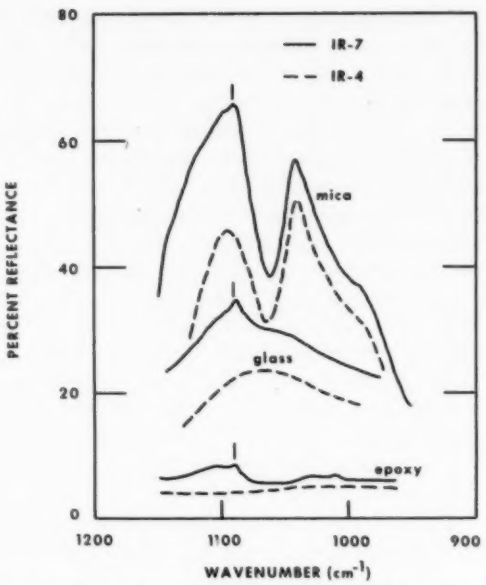

Fig. 15. Comparison of reflection spectra of mica, glass, and epoxy resin made with a Beckman IR-7 prism-grating spectrophotometer and a Beckman IR-4 double-prism spectrophotomer. The Rayleigh wavelength is marked with a vertical line.

polarized the anomalies will appear in the spectrum for one direction of polarization (perpendicular to the rulings for *S*-anomalies) but not the other. Therefore, the polarizer should be located at a position where the sample and reference beams are common, for example, immediately before the entrance slit. Studies of samples which are themselves polarizers are particularly troublesome. This includes not only transmission spectra of certain oriented samples but also reflection spectra which are always at least partially polarized for other than normal incidence. As an example, Fig. 15 contains infrared spectra of several materials in the vicinity of the +1 anomaly of the 75 line/mm echelette. Spectra from the prism-grating IR-7 are compared with spectra of the same samples recorded with a double-prism IR-4 spectrophotometer. Notice, first of all, that the IR-4 curves seem to indicate generally lower reflectivity. This is because radiation reflected from the sample is richer in the component which is preferentially reflected from the prism faces. Furthermore, in the IR-7 spectra a bump appears at the frequency of the Wood anomaly near 1090 cm^{-1}. The anomaly appears inverted because the reference beam is richer in perpendicularly polarized radiation than is the sample beam after its encounter with the reflecting sample. Figure 16 is an example of the absorption spectrum of an oriented material, in this case a sheet of Polaroid film, studied in the 350 to 700 mμ spectral region with a double-beam grating spectro-

photometer. Spectra were recorded with the sample in both orientations. Notice the extreme effects of polarization on the appearance of the Wood anomalies near the calculated Rayleigh wavelengths at 395, 455, and 655 mμ. For comparison, spectra were also recorded with a quartz prism spectrophotometer. Polarization by the prism instrument is slight and, of course, there are no Wood anomalies. The curves recorded with the grating instrument are particularly exaggerated because the monochromator utilizes two 1200 line/mm gratings in tandem.

The presence of unsuspected Wood anomalies in emission spectrometers can be especially serious because there is usually no background energy trace to reveal them. Wood's experiments with the mutilated sodium doublet is an appropriate example. Raman and fluorescence spectrophotometers are also vulnerable and the polarization property of the anomalies adds an additional hazard.

If the spectroscopist is aware of the existence and properties of Wood's anomalies and has determined their wavelengths and relative intensities for his particular instrument, he is unlikely to be misled by their instrusion in his spectra. It is for this reason that we have written this article.

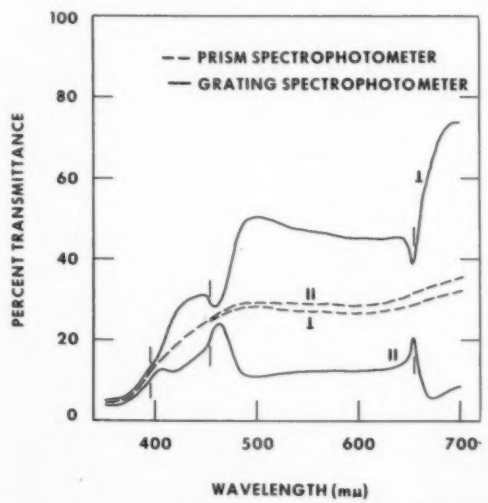

Fig. 16. Comparison of absorption spectra of a Polaroid film in two orientations recorded on a double-grating spectrophotometer and a Beckman DK-2 prism spectrophotometer. Rayleigh wavelengths are shown by vertical lines.

We wish to express our special thanks to R. Hawes of the Applied Physics Corporation, manufacturers of the Cary Model 14, for very graciously providing the material for Fig. 10. We also would like to thank D. Richardson of Bausch & Lomb for providing the probable explanation for the lack of Wood anomalies in the 8 line/mm grating.

References

1. R. W. Wood, Phil. Mag. **4**, 396 (1902).
2. R. W. Wood, Phil. Mag. **23**, 310 (1912).
3. R. W. Wood, Phys. Rev. **48**, 928 (1935).
4. C. H. Palmer, Jr., J. Opt. Soc. Am. **42**, 269 (1952).
5. C. H. Palmer, Jr., J. Opt. Soc. Am. **46**, 50 (1956); ibid. **51**, 1438 (1961).
6. Lord Rayleigh, Proc. Roy. Soc. (London) **A79**, 399 (1907); Phil. Mag. **14**, 60 (1907).
7. W. Voigt, Nachr. Ges. Wiss. Göttingen **K1**, 545 (1910); 71 (1911).
8. U. Fano, Ann. Physik. **32**, 393 (1938); Phys. Rev. **50**, 573 (1936); ibid. **51**, 288 (1937); J. Opt. Soc. Am. **31**, 213 (1941).
9. K. Artmann, Z. Physik **119**, 529 (1942).
10. V. Twersky, J. Appl. Phys. **23**, 407, 1099 (1952); J. Opt. Soc. Am. **42**, 855 (1952); ibid. **50**, 1134 (1960); ibid. **52**, 145 (1962); J. Acoust. Soc. Am. **22**, 539 (1950); ibid. **24**, 42 (1962); IRE Trans. on Antennas and Propagation **AP-4**, 330 (1956); ibid. **AP-7**, S307 (1959); J. Research. Natl. Bur. Standards **64D**, 715 (1960); Sylvania Electronic Defense Labs, "Notes on Scattering by Gratings," Report EDL-M105 (1957); "On Scattering of Waves by the Infinite Grating of Circular Cylinders," Report EDL-E28 (1958); "Multiple Scattering of Waves and Optical Phenomena," Report EDL-L20 (1961).
11. J. R. Wait, Appl. Sci. Research **B4**, 393 (1955).
12. S. N. Karp and J. Radlow, IRE Trans. on Antennas and Propagation **AP-4**, 654 (1956); S. N. Karp, New York University, Inst. of Mathematical Sciences, Division of Electromagnetic Research, "Diffraction by an Infinite Grating of Arbitrary Cylinders," Research Report No. EM-85 (1955).
13. B. A. Lippmann, J. Opt. Soc. Am. **43**, 408 (1953); B. A. Lippmann and A. Oppenheim, "Towards a Theory of Wood's Anomalies," Contract No. OSR-TR-54-25 (June 30, 1954).
14. W. C. Meecham, J. Appl. Phys. **27**, 361 (1956). Wood anomalies have been observed with 3.2-cm microwaves by W. C. Meecham and C. W. Peters, J. Appl. Phys. **28**, 216 (1957).
15. R. F. Millar, Can. J. Phys. **38**, 272 (1960); ibid. **39**, 81, 104 (1961).
16. A. S. Makas and W. S. Shurcliff, J. Opt. Soc. Am. **45**, 998 (1955).
17. J. Strong, Phys. Rev. **46**, 326 (1943); ibid. **48**, 480 (1935); ibid. **49**, 291 (1936).
18. R. J. Meltzer and J. D. Keller, Symposium on Molecular Structure and Spectroscopy, Ohio State University, June 12–16, 1961.
19. S. Broderson, J. Opt. Soc. Am. **43**, 1216 (1953).

These shots were taken by OSA President D. L. MacAdam during the Luncheon for the Local Sections Officers, Los Angeles, October 1961 meeting.

C. S. Williams *Texas*, W. Brouwer *New England*, and Stanley S. Ballard *President Elect OSA*.

D. A. Pontarelli *Chicago*, R. E. Lewis *Northern California*, and S. P. Davis *Northern California*.

R. Clark Jones *New England*, R. Kingslake *Rochester*, and E. Bickel *Chicago*.

E. Davidson *Southern California*, G. C. Higgins *Rochester*, and Hilda Kingslake *Program Chairman for the OSA-Rochester October 1962 meeting*.

A High-Resolution Grating-Prism Spectrometer for the Infrared

T. K. McCubbin, Jr., R. P. Grosso, and J. D. Mangus

A high-resolution infrared spectroscopic system consisting of a large Littrow-type grating monochromator followed by a prism order-sorting system is described. The system has been designed to provide sufficient radiant energy per spectral pass band so that a spectral resolution of about 0.08 cm^{-1} can be achieved at wavelengths beyond 7 μ. An order-sorting system permits simultaneous recording of the spectrum being measured and a higher-order calibration spectrum. Wavelengths of the lines in absorption spectra can be measured to within 0.005 cm^{-1}.

Introduction

The relationship between the spectral band-pass of an infrared spectrometer when its resolution is limited by the wide slits that are necessary to provide sufficient radiant power for the detector and design parameters such as the dispersive power of the grating, the sizes of apertures and focal lengths in the optical system, and the source and detector properties has been explained by John Strong.[1] This paper describes an application of Strong's precepts to the design of an infrared spectrometer that will be used for the resolution of details in absorption spectra and the measurement of wavelengths in the infrared beyond about 5 μ.

Different design problems are encountered at shorter infrared wavelengths because of the superior detectors that can be used at those wavelengths. Consideration has been given to the possibility of using a cooled photoconductive detector at long waves, but the principal advantage of such detectors over the heat receiving Golay cell seems to be speed of response. Photoconductive and photovoltaic detectors at long wavelengths can enable spectroscopists to investigate transient phenomena that could not be observed with slower detectors, but at wavelengths beyond the 6.3-μ water band, the photoelectric detectors are not significantly better than the Golay cell for the observation of time-independent phenomena.

Another detector, the bolometer at liquid helium temperature,[2,3] shows promise, and it is hoped that the use of such a detector will in the future result in a substantial improvement in energy-limited spectral resolution.

An infrared spectroscopic optical train consists of two sets of conjugate optical surfaces. The slits (entrance, intermediate, and exit) together with the source and detector make up one of the sets of conjugate surfaces. The other set consists of the aperture stop (which is the edge of the diffraction grating) and images of the aperture stop. For example, the order-sorting prism in the optical system shown in Fig. 1 is at the image of the grating formed by m_1 and m_4. The germanium lens is at the exit pupil which is the prism face image formed by m_6 and m_7.

The design of the optical system for the spectrometer started with the assumption that a Golay detector having a circular sensitive area 4.5 mm in diameter would be used and that the numerical aperture of the optical system for illuminating the detector would be 0.55. It was known from past experience that a 20 by 12.6 cm diffraction grating used at incidence angles greater than 45 degrees can be fully illuminated by means of an autocollimating optical system of 2.5-m focal length with sufficient optical definition for the infrared region of the spectrum. The grating when turned to the echelle incidence angles can be illuminated with a beam 15 cm in diameter. The instrument thus will have an f number of approximately 16 or a numerical aperture of $^1/_{32}$. Application of the optical sine theorem yields the result that the product of the detector height times the numerical aperture of the optical system which illuminates it must equal the product of the slit height times the numerical aperture of the spectrometer. The slit height may thus be as great as 7.9 cm. A 7.5-cm slit height was chosen. An objective mirror of 26-cm diameter is ample for these grating and slit dimensions.

The authors are in the Department of Physics, The Pennsylvania State University, University Park, Pa.

Received 18 January 1962.

This research received support from the Air Force Cambridge Research Laboratories, Office of Aerospace Research.

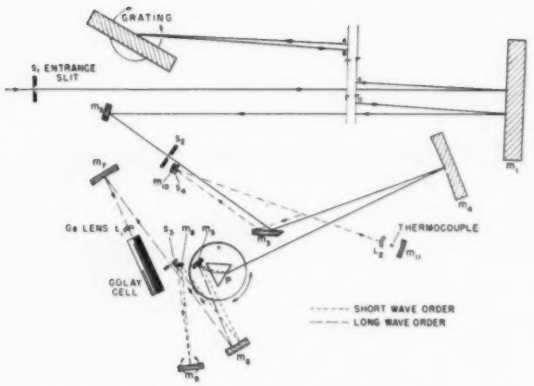

Fig. 1. The 2.5-m grating spectrometer and the optical system for simultaneous observation of two spectral orders. The optical path of the shortwave order from m_8 to m_6, through the prism, and from m_4 to m_3 has not been shown for clarity.

From Strong's[1] article the following proportionality for the signal to noise ratio of energy limited spectroscopy may be derived:

$$\frac{S}{N} \propto \left(\frac{l}{F}\right)\left(\frac{1}{W_0}\right) A,$$

where

l = slit length,
F = spectrometer focal length,
W_0 = minimum detectable power,
A = area of the grating or echelle aperture. If an echelle of height a is used at an incidence angle of 63°, $A = a^2$.

If one introduces detectivity, $D = (1/W_0)$ and uses the previously derived relation $h_d N_d = lN_s$ and the fact that $N_s = (a/2F)$, one obtains the proportionality

$$\frac{S}{N} \propto a h_d N_d D.$$

Thus the best detector for an infrared spectrometer will be the one having the largest product $D \cdot h_d \cdot N_d$. The product instead of detectivity alone must be examined because detectivity often depends upon the size of the sensitive area[4] of a detector and upon the angular size of the cone[5] of radiant energy that is permitted to fall upon it.

Description of the Apparatus

The Optical System

The grating spectrometer has a Littrow optical system of 2.5 m focal length as shown in Fig. 1. It employs a spherical mirror having a diameter of 26 cm to illuminate a 12.6 by 20.3 cm plane 40-line-per-mm blazed grating. The grating is used as an echelle over a range of incidence angles from 50 to 75 degrees. Under these circumstances the f number of the system is slightly higher than 16.

The straight entrance slit, S_1, is 7.5 cm long. S_2, the exit slit of the grating monochromator, is equipped with several sets of curved jaws that can be changed to match the curvature of the spectral lines at different incidence angles. An estimate of the effect upon spectral resolution can be made by using the relationship for the sagitta, σ of the curved spectral lines of length l produced by a grating spectrometer of focal length F when the grating incidence angle is θ. That relationship is

$$\sigma = \frac{l^2}{4F} \tan\theta.$$

When a slit having the correct curvature for some incidence angle, θ_0, is used at some other incidence angle the wave-number error, $\Delta\nu$, calculated from the sagitta error and the dispersion, is given by

$$\Delta\nu = \frac{1}{8\lambda}\left(\frac{l}{F}\right)^2\left(1 - \frac{\tan\theta_0}{\tan\theta}\right).$$

Computations made with that formula show that when the 40-line-per-mm grating is used from 6.5 to 16 μ in the 6th through 3rd orders, the wave-number error along the slit will be smaller than about one-third of the energy-limited spectral resolution if slits having values of θ_0 of 55°, 62.5°, and 70° are used over appropriate ranges of incidence angles. Radii of these slits are 89, 66, and 46 cm. These three slits will in fact reduce the wave-number error to below the diffraction limited spectral resolution except for a restricted range of angles in the third order. If a coarser grating had been used to cover this same spectral range in the sixth and higher orders, one exit slit, suitably curved, could have been used without spoiling the spectral resolution because the grating would be used over a more restricted range of incidence angles in the higher orders.

The slit jaws were easily and precisely made by hand on a grinding wheel of 18 by 3 mm flat ground tool steel. After rough grinding they were finished to a circular shape by lapping the edges of mating jaws against one another using oil and fine emery. This method generates mating circles in a manner analogous to the generation of spherical optical surfaces.

The order-selecting prism system that follows the curved grating exit slit S_2 is arranged so that the prism uses the curved slit to advantage and produces almost straight spectral lines.

The purpose of the order-sorting prism and associated optical trains is to select two orders of the grating spectrum for observation. The spectrum to be measured, observed in a low order, is sent to the Golay detector and a spectrum with near infrared absorption standards, observed in a higher order, is sent to a thermocouple detector. The output of each detector goes to

its own breaker point rectified amplifying system and to a separate pen recorder. The two sets of single-pole double-throw breaker points run in synchronism with the light chopper. Marker pips are common to the two systems. When the system is in operation two spectra are simultaneously drawn on separate strip recorders.

The double-order selecting system which receives the flux from grating exit slit S_2 begins (except for beam folding mirrors) with m_4, a spherical mirror which has a 74-cm focal length and a 15-cm diameter. This mirror receives the fan-shaped bundle of rays which upon reaching the mirror surfaces has spread to a width of 4.5 cm and a height of 12 cm.

Collimated light from m_4 falls upon the surface of a 60° prism which has a 7.5-cm-wide face and a 6.0-cm height. The prism and its mounting table are for a Perkin-Elmer infrared monochromator, model 99, 12 etc. and thus can easily be changed. The beam of radiant energy falling upon the prism is of small cross section because the prism is placed close to the exit pupil. Dispersed radiation from the prism, after reflection from m_8, the Wadsworth mirror, falls upon m_6, a concave mirror of 5-cm diameter and 22-cm focal length. This mirror is also near the pupil, and therefore its surface is large enough to collect both the long-wave order to be measured and the shortwave calibrating order. The various grating orders each form a line in the spectrum which is imaged upon the plane of the slit S_3.

The desired long-wave order passes through the slit S_3, selection having been made by turning the Wadsworth prism plane mirror assembly. The long-wave radiant energy falls upon a concave mirror m_7 of 10-cm diameter and 25-cm radius of curvature. This mirror is positioned a distance equal to its radius behind S_3. Therefore, if the Golay cell and lens were removed, it would reimage the slit at one-to-one magnification. The mirror m_7 forms a small exit pupil at a distance from its surface of approximately one-half of its radius. A germanium meniscus lens L_1 of diameter 2.8 cm and radii + 2.5 and + 3.25 cm, placed at this pupil causes a reduced image of S_3 to be formed upon the 4.5-mm entrance aperture of the Golay cell. Both surfaces of this lens are coated with ZnS layers having an optical thickness of a quarter wave for 10 μ.

The more easily refracted shortwave orders converge toward a focus upon one of the jaws of S_3 as shown in Fig. 1. The prism (NaCl or KBr depending upon the wavelength to be studied in the low-order spectrum) provides insufficient dispersion to separate the shortwave orders. Additional dispersion is gained by sending the high-order radiation back through the prism a second time. Double passing is accomplished by means of the field mirror m_8 and the reimaging mirror m_9 as has been described by one of us.[6]

Radiant energy returned to the system by the m_8 and m_9 combination is recollimated by m_6, further dispersed by the prism and refocused by m_4 to form a spectrum at S_4 sufficiently dispersed to permit separation of shortwave orders.

Selection of the shortwave order is made by turning the double pass reimaging mirror m_9 which is mounted upon the prism table of a student-type spectrometer. The wavelength passing through S_4 also depends upon the rotational position of the prism Wadsworth mirror assembly. This feature is not convenient because accurate adjustment of the prism spectrometer is essential to accurate wavelength measurements as will be discussed below. A system for independent adjustment of the low and high orders of the spectra has been devised and will be incorporated in a future modification of the instrument.

S_4, a curved slit constructed of black paper, is mounted in contact with the surface of a field mirror m_{10}. This field mirror provides an exit pupil in which is placed the corrector lens of a Bouwer-Makzutov optical system. This optical system, consisting of a negative corrector lens of NaCl and a concave spherical mirror, forms an image of the slit S_4 upon the 4 by 0.2 mm sensitive area of a two-junction vacuum thermopile.*

The 40 line per mm 12.6 by 20 cm transfer grating was manufactured by Bausch & Lomb for low-order infrared use. Additional information about this grating has been published elsewhere.[6] Astigmatism, which is the result of the convex curvature of the aluminum coating upon which the grating is ruled, requires the position of the objective mirror to be translated 2 cm for refocusing when the grating is turned from the 65th to the 87th order of the mercury green line. David Richardson of Bausch & Lomb informed us that it is not possible to deposit a flat aluminum coating of the thickness required for a coarse echelle.

The spectroscopic optical system was built upon masonry piers in a 3-meter-square room that adjoins the main working area of The Pennsylvania State University Physics Department Spectroscopic Laboratory.

The Grating Drive

The spectrometer first was assembled using a 180-tooth worm wheel of 15-cm pitch diameter to drive the grating. Qualitative examination of the spectra revealed no "jumping" or other evidence of improper behavior of the drive. However, measurements from the spectra were not reproducible. Calculations showed that an unreasonable degree of perfection in the worm and wheel would be necessary before wavelengths could be measured to a degree of accuracy limited by spectral resolution and the signal-to-noise ratio.

* Manufactured by Charles M. Reeder Co., Chicago, Ill.

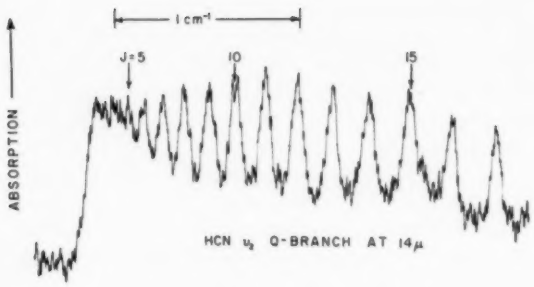

Fig. 2. The Q branch of the HCN ν_2 band near 14 μ observed in the third order of a 40-line-per-mm grating singly passed. Path length 30 cm. Pressure less than 1 mm Hg. The maximum absorption is about 50%. Slit width 0.65 mm.

The scanning of the visible and near infrared spectrum by turning the grating imposes such severe requirements upon the precision of the rotational motion of the grating that several other scanning systems have been developed for high precision work.[7–10]

It is very doubtful whether any system for grating rotation can operate well enough so as not to limit the precision of wavelength measurement obtainable with large modern gratings in the near infrared. However, at longer wavelengths requirements become relaxed because of the increased wave-number dispersion and the fact that the signal-to-noise ratio of the detector limits the spectral resolution.

The wavelength scan is accomplished by turning the grating by means of an arm and a tangent screw. The arm, 40 cm long, is moved by a micrometer head which provides 2.6 cm of motion. The micrometer motion is imparted to the crank by means of a short pushrod. A 5-cm spur gear mounted on the large knurled part of the micrometer turns the micrometer and at the same time translates along its axis. This gear is turned by a pinion about 3 cm long. Marker pips originate from a switch actuated by a cam on the pinion shaft. The crank, constructed of 6-mm aluminum alloy plate, tapers from a width of 12 cm at the bearing end to 3 cm at the driven end. The crank, which is moderately compliant for bending in response to forces at right angles to its driving force, is steadied at the end by means of a teflon bearing running upon a steel guide. Provision has been made to loosen the crank at the bearing to allow coarse manual setting of the grating angle. A 750-gram weight with a string and a pulley keep the arm, pushrod, and micrometer in contact.

The bearing which supports the grating and its mount and provides the rotation axis is a pair of cast iron cones of 5.5 cm diameter, 10 cm length, and 3° angle between the axis and an element of the cone. Much of the weight of the inner cone and the grating and its mounting is borne by a shoulder on the top (large) end of the inner cone. The shoulder bears upon the top surface of the outer cone casting. Adjustment was accomplished by lapping the cones together with fine emery and oil until the proper degree of contact was established.

The Electronic System

The small signals and slow scan rates that were encountered when the spectrometer was operated with narrow slits made it necessary to increase the gain of the Perkin-Elmer Models 81 and 107 13-cycle amplifiers and to provide filter circuits having longer time constants.

Performance of the Spectrometer

Resolution of Spectral Details

Figure 2 shows several examples of the resolution obtainable with this spectrometer. The HCN $\nu_2 Q$ branch was measured singly passed in the third order. This spectrum provides a very excellent resolution test in that it consists of a series of close absorption lines of known frequency. An incorrect method of measuring resolution would be to search the spectrum for a pair of just resolvable lines, measure their separation on the record, and compute resolution from the known dispersion, for such a determination would be subject to a shrinkage error[11] that will lead to too favorable an estimate of resolution.

Figure 2, the Q branch of the HCN band at 14 μ, shows lines 5 and 6 clearly resolved and lines 4 and 5 barely resolved. These spacings were calculated according to a well-known formula of molecular spectroscopy[12] using Rank's[13] value for $(B' - B'')$ and found to be 0.088 and 0.074 cm^{-1} respectively.* Another example of the spectral resolution was published earlier.[6] The spectra in the illustration and others that are routinely observed exhibit a spectral resolution of at least 0.08 cm^{-1}.

Measurement of Wavelength

It has been the authors' experience that development of a system for the measurements of wavelength to an accuracy limited by noise on the trace and the width of the lines is more difficult than the achievement of maximum resolution. The optical system for simultaneously recording the standard spectrum in a high order and the unknown spectrum in a lower order along with the mechanical system for scanning have already

* We suggest that the spectrum of the 14 μ HCN Q branch shown in Fig. 2 can provide a useful test of infrared spectral resolution, for it is in a region of atmospheric transparency, the sample can easily be prepared from common chemicals, and the band is so strong that it can be observed at fractional mm pressures in a cell several cm long. Spacings between successive lines beginning with the closest pair are: 0.029, 0.044, 0.059, 0.074, 0.088, 0.103, 0.117, and 0.133 cm^{-1}.

been described. Simultaneous recording of the unknown and standard spectra results in an economy of observing time which is important when slow scan rates are used. Furthermore, errors caused by a drift of the calibration in the time interval between when the standard and unknown spectra are observed are eliminated if the two spectra are observed at the same time.

A further unsuspected source of error has been discovered and corrected. The near infrared dispersion of the prism is small even when it is doubly passed. This means that adjustment of m_9 to cause the desired order to pass through S_4 is very critical, for S_4 can only be widened to the point where neighboring orders are no longer resolved. Images of S_2, each formed with radiant energy of a wavelength corresponding to a grating order, are projected upon the S_4 plane. If part of the radiant energy in the desired order falls upon a jaw of S_4 instead of passing accurately through that slit, the calibration spectrum will be displaced (and some of its energy will be lost). The displacement takes place because when radiant energy from one side of S_2 does not reach the detector the effective center of this slit is displaced. Assuming that the long-wave order passes accurately through S_3 and to the Golay detector, the grating spectrometer will behave as if its exit slit S_2 were in different positions for the two observed orders. Careful adjustment for maximum energy to thermocouple completely eliminates this source of error. A future modification to the system will be to obtain further dispersion for the calibrating spectrum by means of an LiF prism. This prism will have such high dispersion that spectral orders will be resolvable with a wide S_4.

An example of the accuracy of wavelength measurements is provided by the study of the spectrum of ordinary and isotopic N_2O in the region from 7.6 to 8 μ that is currently in progress. The 100 band and the $11^1O\text{-}01^1O$ band in ordinary N_2O have been measured in the 6th order of a 40-line-per-mm Bausch & Lomb grating. CO lines observed in the 10th order served as wavelength standards. Edlén's Formula as tabulated by Penndorf[14] shows that the dispersion of air between 4.7 and 8 μ is so small that no significant error will result if the CO vacuum wave numbers are multiplied by the order ratio, $6 \div 10$, to obtain standards with which to measure the N_2O lines. The CO fundamental wavelengths are very well known both from direct measurements and by calculation from molecular constants.[13,15] The CO lines $R(30)$ through $P(30)$ occurring from 4.3 to 5.0 μ can provide calibration for the entire long-wave spectrum when a grating is used that is coarse enough to permit these lines to be observed in the 9th or higher order.

Several graphical and numerical procedures (all of which give identical results from a given set of data) have proved convenient for interpolation between the standards which for the 6th order N_2O measurement occur about 2.3 cm^{-1} apart with an occasional double gap at the band center or where a CO line is spoiled by a N_2O near infrared line. One method has been to compute the wave-number dispersion by dividing the wave-number interval between CO lines by the distance between the lines as measured on the chart. (The CO spectrum for $R(30)$ to $P(30)$ is 13.9 m long and the dispersion is about 0.04 cm^{-1} per cm. The chart moved 15 cm per hour.) The dispersion as a function of position on the spectra can be expressed as the sum of a linear function that can be set up on a desk calculator plus a correction term that is obtained from a curve. The frequency of an unknown line is obtained by adding to (or subtracting from) the frequency of a nearby standard line the product of the distance between the standard and unknown lines as measured on the charts and the dispersion for a point midway between the standard and unknown lines. The frequency of an unknown line can be measured from each of the CO lines that are nearest to it as well as the two next nearest CO lines. The agreement of these four determinations is limited only by the observer's ability to pick line centers.

Several checks have been applied to estimate the accuracy of the measured wavelengths. A check that was used to test the grating drive was to measure the spacings of CO lines on the chart. The functional relationship between the position of these lines on the recorder chart and the distance measured along the chart should very closely approximate a second-degree polynomial. Thus a table of differences constructed from the measured positions of the lines should show second differences which very slowly undergo a systematic increase or decrease. The tables of second differences constructed from spectra obtained with the instrument being described behaved erratically with variations corresponding to several hundredths of wave numbers until the tangent screw grating drive mechanism was installed at which time a tenfold improvement was noted.

A second check of the accuracy of wavelength measurements is to compare the observed values of certain wave-number intervals which are called values of $\Delta_2F(J)$[16] with the very precisely known values of the same wave-number intervals that have been determined by Rank *et al.*[17] from near infrared measurements. When such a comparison was made for 15 Δ_2F'' values from the 100 band of N_2O, the mean deviation was 0.005 cm^{-1}. It was by a comparison of known and observed values of Δ_2F'' computed for several assumed numberings of the lines in the 110-010 "hot" band that the correct assignment of values of J to the lines could be unmistakably made. It would have been meaningless to have applied that test if the uncertainty in the wave-number values

for the lines had been hundredths instead of thousandths of wave numbers.

Conclusions

The Advantages of Using Gratings as Echelles in the Infrared

If one compares the performance of a grating used in the first order at low angles of incidence with the performance of a suitably ruled and blazed grating of the same ruled area used as an echelle, the echelle, i.e., the grating used at an angle of incidence near 60° in the third or higher order with the spectrum produced by the small facets of the grooves, will prove superior because it will provide more radiant power per spectral pass band and because it can provide better measurement of wavelength. A further advantage will be that the smaller optical aperture of an echelle having a given ruled width will permit the use of a compact spectrometer. These advantages should, in the authors' opinion, compel infrared spectroscopists who seek high resolution and accurate wavelength measurements to use diffraction gratings as echelles.

The energy advantage of an echelle arises from the fact that the angular dispersion of a grating or an echelle is proportional to the tangent of the incidence and diffraction angle and the area of its effective aperture is proportional to the cosine of this angle. Strong[1] has shown radiant power per width of pass band to be proportional to the product of angular dispersive power, aperture area, and efficiency. Therefore radiant power per band width should increase with incidence angle provided the efficiency does not diminish. Some measurements made by comparing the intensity of the spectrum singly and doubly passed for the 40 l/mm grating used in the spectrograph reveal that its echelle efficiency varies from 40 to 65% over its blaze in the fourth through sixth orders. Some further discussion of high-order and first-order high-angle grating performance appears in an article by one of the authors.[18] In that article it was shown that a grating can perform successfully at nearly grazing incidence even in the first order.

Echelle gratings are well suited for infrared wavelength measurements because when the calibration spectrum is observed in a high order only one or two accurately known bands of absorption lines will be needed to provide standards over the entire blaze.[19] A further advantage is that the high angular dispersion resulting from the use of a large incidence angle decreases the errors caused by irregularities of the grating drive.

Future Work

A vacuum spectrometer is being constructed like the instrument described in this paper but with a redesigned prism system that will permit independent adjustment of the two observed spectral orders. This new instrument, when equipped with a coarse grating, will be used to wavelengths out to the limit of a cesium bromide prism. Experiments using bolometers at liquid helium temperature are being planned.

The most pressing future work in this laboratory will be that of using the 2.5-m spectrometer and the vacuum spectrometer that is under construction to solve problems in high-resolution molecular spectroscopy, for it is the authors' opinion that a new instrument is scientifically significant only if it is used to make measurements. It seems reasonable, however, to speculate about how the spectrometer would perform with a detector having a minimum detectable power an order of magnitude smaller than that of the Golay cell, for it is not unreasonable that such a detector may become available. With such an improved detector, the instrument described in this paper could be used under conditions of diffraction limited resolution with a spectral pass band approaching the Doppler widths of absorption lines.

References

1. John Strong, J. Opt. Soc. Am. **39,** 320 (1949); see also John Strong, *Concepts of Classical Optics* (W. H. Freeman and Co., San Francisco, 1958), p. 270.
2. F. J. Low, J. Opt. Soc. Am. **51,** 1300 (1961).
3. W. S. Boyle and K. F. Rodgers, J. Opt. Soc. Am. **49,** 66 (1959).
4. R. C. Jones, J. Opt. Soc. Am. **37,** 879 (1947).
5. P. Bratt, W. Engeler, H. Levinstein, A. MacRae, and J. Pehek, Infrared Physics **1,** 27 (1961).
6. T. K. McCubbin, Jr., J. Opt. Soc. Am. **51,** 887 (1961).
7. G. H. Dieke and H. M. Crosswhite, J. Opt. Soc. Am. **35,** 471 (1945).
8. D. H. Rank, E. Shull, H. Bennett, and T. A. Wiggins, J. Opt. Soc. Am. **43,** 952 (1953).
9. J. N. Shearer and T. A. Wiggins, J. Opt. Soc. Am. **45,** 133 (1955).
10. G. A. Ameer and W. M. Benesch, J. Opt. Soc. Am. **51,** 303 (1961).
11. D. H. Rank, J. Opt. Soc. Am. **47,** 671 (1957).
12. G. Herzberg, *Infrared and Raman Spectra* (D. Van Nostrand, New York, 1945), p. 384.
13. D. H. Rank, G. Skorinko, D. P. Eastman, and T. A. Wiggins, J. Mol. Spec. **4,** 518 (1960).
14. R. Penndorf, J. Opt. Soc. Am. **47,** 176 (1957).
15. E. K. Plyler, L. R. Blaine, and W. S. Connor, J. Opt. Soc. Am. **45,** 102 (1955).
16. G. Herzberg, *op. cit.*, p. 390.
17. D. H. Rank, D. P. Eastman, B. S. Rao, and T. A. Wiggins, J. Opt. Soc. Am. **51,** 929 (1961).
18. R. C. Lord and T. K. McCubbin, Jr., J. Opt. Soc. Am. **47,** 689 (1957).
19. D. H. Rank, D. P. Eastman, W. B. Birtley, G. Skorinko, and T. A. Wiggins, J. Opt. Soc. Am. **50,** 821 (1960).

THE FIRST CALIBRATED INFRARED SIGNAL GENERATOR!

MODEL 501 1 to 14 microns

Here, for the first time, is a standard calibrated Infrared Signal Generator that operates with the ease and efficiency you expect from standard electronic test equipment... eliminates the drawbacks of improvised setups. Developed with the cooperation of some of the country's leading infrared physicists, the Model 501 Generator provides advanced features found in no other single instrument.

INFRARED TELEWAVE INSTRUMENTATION

FEATURES

- Wide Wave Length Range: 1-14 microns
- Calibrated Output Power
- Choice of Point Source or Collimated Beam Output
- Calibrated Step Attenuator
- Precision Servo Controlled Modulation
- Clean Spectral Profile
- Negligible Stray Light—Exclusive Prefiltering Monochromator
- Rapid Power Setting

APPLICATIONS

- System Sensitivity Measurements
- System Responsivity Measurements
- Detectivity Measurements
- Detector Responsivity Measurements
- Detector and System Frequency Response Measurements
- Jamming Susceptibility Measurements
- Resolution Measurements
- Standardization and Calibration
- Pattern Plotting

A B C D E F G H I
1 2 3 4 5 6 7 8 9 10 11 12

TELEWAVE LABORATORIES, INC.
43-20 34th St., Long Island City 1, N. Y.

We're interested in your needs. Tell us about them below—we'll rush complete information on the Model 501 and how it can help solve your problems._____

_____

_____

_____

_____

Name_____

Title_____ Dept._____

Company_____

Address_____

City_____ Zone_____ State_____

HOW THE MODEL 501 INFRARED SIGNAL GENERATOR WORKS

The instrument consists of a source, chopper, attenuator, monochromator and a power monitor.

The source produces a broadband radiated noise spectrum in the band of wavelengths from 1 to 14 microns, which is then filtered to produce the desired output signal.

Selection of desired wave length is accomplished by a monochromator (optical bandpass filter). The spectral profile of the output is governed by the entrance and exit apertures of the monochromator, which are cam-programmed to provide the bandwidth specified.

A choice of two specific output signals is provided: (a) a point source that radiates into a 5° cone; (b) a collimated beam one inch in diameter.

To distinguish output radiation from background radiation, the signal can be modulated by means of a chopper – a rotating shutter device located between the light source and the lens system focusing into monochromator.

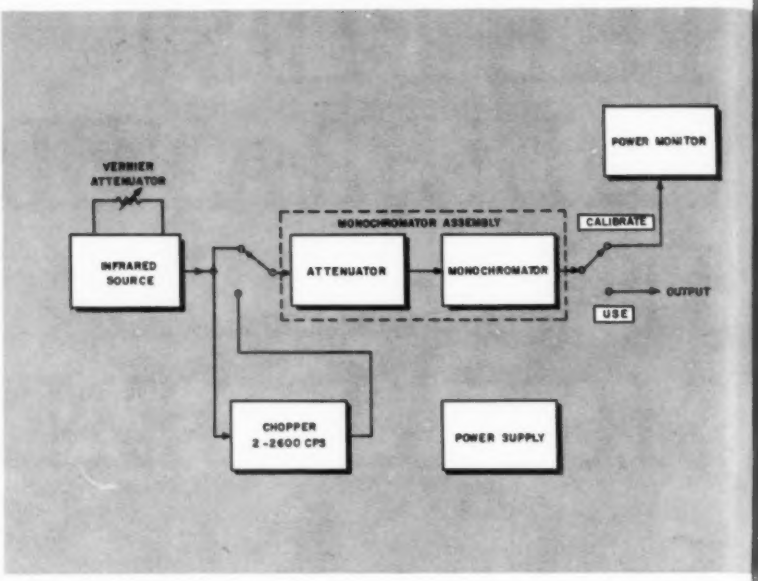

Power is monitored by means of a factory-adjusted thermistor bolometer and preamplifier, and a synchronous voltmeter.

Stepwise attenuation of the output signal is obtained by means of neutral attenuator grids placed within the monochromator.

SPECIFICATIONS

- Wave Length Range – 1-14 microns
- Dial Calibration – 0.2 microns
- Output Format – Switch selection of (a) Point Source 5.4° Cone of Radiation or (b) Collimated Beam 1-inch Diameter.
- Bandwidth – .35 micron Typical at 3 db points (at 5 microns)
- Power Output – 1 microwatt Typical (at 5 microns)
- Power Output Accuracy – ± 15%
- Step Attenuator – 10^7:1 in seven 10:1 steps
- Step Attenuator Accuracy – ± 10% per step
- Vernier Attenuator – 100:1 in two 10:1 ranges
- Vernier Attenuator Accuracy – ± 5%
- Modulation Frequency – 2-2600 cps in 2 ranges
- Modulation Frequency Accuracy – ± 2%
- Modulation Waveshape – 100% square wave

Postage Will be Paid by Addressee

No Postage Stamp Necessary If Mailed in the United States

BUSINESS REPLY CARD
First Class Permit No. 18, Long Island City 1, N. Y.

TELEWAVE LABORATORIES, INC.
43-20 34th ST., LONG ISLAND CITY 1, N.Y.

This card will bring you new information on latest developments in infrared generators

INFRARED TELEWAVE INSTRUMENTATION

TELEWAVE LABORATORIES INC.
43-20 34th St., Long Island City 1, N. Y.
EXeter 2-3288

Infrared Filter Grating Spectrophotometers—Design and Properties

Nelson L. Alpert

Advances in multilayer interference filter technology have enabled the development of filter grating spectrophotometers out to 250 cm^{-1} (40 μ). Properties of the filters are described. Factors which determine the rejection and transmission requirements for the filters are discussed and special design problems in filter grating systems are elaborated. Unwanted radiation measurements in the resulting system are reported. The features of filter grating spectrophotometers compared to foreprism grating instruments are listed.

Introduction

With the growing interest in high-resolution infrared spectrophotometers, significant attention has been given to methods of solving the inherent problem of overlapping grating orders. Technological progress in interference filters has enabled the development of filter grating spectrophotometers covering the most commonly applied regions of the infrared, out to 250 cm^{-1} (40 μ).

These instruments have design aspects and properties which differ significantly from those of the foreprism grating systems which have previously been the only type of grating spectrophotometer available in this spectral region. It is the objective of this paper to record the pertinent experience in the development of two different filter grating spectrophotometer systems at Perkin-Elmer.

One of these is a versatile instrument utilizing gratings with ruled areas of 64 mm × 64 mm. This scans the range from 4000 to 550 cm^{-1} with no breaks in the chart presentation. It has demonstrated resolution better than 0.3 cm^{-1}. A filter grating interchange which operates from 2000 to 250 cm^{-1} has been developed for this instrument. The second type of system from which experience has been derived is a low cost less versatile instrument which has been developed in two versions covering different spectral ranges. In this case the gratings employed have a ruled area of 52 mm × 52 mm. One of these instruments covers the region from 12,000 to 1300 cm^{-1} and the other from 4000 to 625 cm^{-1}. These instruments provide survey scans with a resolution of better than 4 cm^{-1} for all frequencies beyond roughly 3000 cm^{-1} and better than 2 cm^{-1} beyond 1900 cm^{-1}. Some of the design aspects, which will be discussed, are unique to one or the other type of instrument although most are common to both.

It would be neglect not to note that the concept of the use of filters with gratings has been in use for many years. A germanium plate with an antireflection coating was utilized by Lord and McCubbin[1] to operate a small grating spectrometer in the 3–5 μ region of the spectrum. The same workers operated a filter grating spectrometer in the 5–200 μ range employing several means of filtering including germanium, AgS coated AgCl, sooted quartz, residual ray (reststrahlen) reflection filters, and crystal chopper filters.[2] In the far infrared, beyond about 200 cm^{-1} (50 μ), filter grating techniques of some sort have always been essential because of a lack of suitable foreprism materials.

Interference Filters

The key element in the new filter grating systems is the multilayer interference filters. The phenomenon of constructive and destructive interference of light incident on thin films has been dealt with analytically since the days of Newton. The application of vacuum coating techniques to control the deposition of alternating high and low index of refraction dielectrics on a suitable substrate, in order to control transmission and rejection characteristics, has occurred within the past 15 years or so.[3] The extension of this technology to the infrared region has occurred only over the past few years, mostly inspired by the military applications of

The author is with The Perkin-Elmer Corporation, Norwalk, Conn.

Received 8 March 1962.

the infrared. However, the utilization of these filters in spectrophotometers has also contributed significantly to the advancement of the frontier.

A. Properties

Filters fall into four categories:

1. Spike filters which transmit only a narrow spectral band. With a resolving power of up to 100:1, these may be used for fixed wavelength applications such as filter photometers.

2. Broad band filters which transmit a relatively broad band of energy with sharp cutoffs on both sides of this band. These are potentially useful in grating instrumentation which takes advantage of higher than first-order diffraction. Thus, these provide rejection of both longer and shorter wavelength than the desired order.

3. Short-wave pass filters which reject energy of wavelengths longer than the characteristic cutoff. These have not found application in the instrument systems described here.

4. Long-wave pass filters which reject energy of wavelengths shorter than the characteristic cutoff. Because design considerations have led us to work only in the first grating order, the instruments to which we have referred have utilized only this type of filter.

Figure 1 shows the transmission curve of a typical long-wave pass interference filter with a germanium substrate. The transmission efficiency of these interference filters averages from 75% to 90% with some of the recently developed long wavelength versions averaging closer to 60%. Recently developed at Perkin-Elmer are filters with KRS-5 substrates which are opaque below 22 μ, and are efficient transmitters from 25 μ to about 40 μ. These are currently being incorporated in the long wavelength ("mid-infrared") interchange described in the Introduction. Direct measurements show the transmission in the "dead" band of typical filters to be less than 5 parts in 10^4. Indirect measurements indicate that these filters can be made sufficiently opaque as to transmit only 1 in 10^6. This is based on the spectral purity attainable with the mid-infrared interchange at 30 μ, the blaze

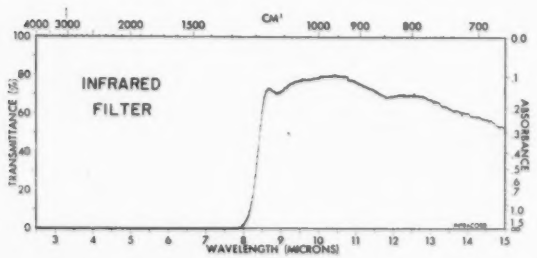

Fig. 1. Transmittance curve of a long-wave pass interference filter.

of the long wavelength grating. It is pertinent to note that almost all of the energy rejected by interference filters is reflected, not absorbed.

With proper choice of substrate, high and low index materials, and in some cases an overcoating material, the filters so far utilized proved to be durable and insensitive to temperature, moisture, and most vapors experienced in laboratory environments. This is in spite of the fact that each filter consists of as many as 40 or more layers coated on the substrate. However, scratches must be avoided, particularly in cases where the higher rejection ratios are required.

B. Determination of Filter Specifications

The function of the filter is to reduce the energy of the unwanted overlapping grating orders to a level which will not interfere with the accuracy of the spectrum being recorded. This implies two fundamental conditions which the filter must satisfy. First, the relative energy of an unwanted order must be small enough so that a totally absorbing band at the wavelength of the unwanted order will not appear as a spurious band on a spectrum. The second condition, far more stringent, is that at any grating angle the energy summed over all unwanted orders must be significantly less than the total scattered light level that can be tolerated for quantitative measurements.

Three factors influence the relative energy of the various orders of gratings: the relative energy radiated by the source at the various wavelengths involved; the relative efficiency of the grating for the various orders; and effects of the different angular dispersions in the different orders. This assumes utilization of a nonselective detector whose response is very nearly constant with wavelength.

The angular dispersion factor is the most straightforward to consider. The radiation of all grating orders passes through the same physical slit opening. Taking into account the well-known fact that the angular dispersion, $d\theta/d\lambda$, is proportional to the order number n for a given grating angle, it follows directly that the higher-order wavelength interval which passes through the slit is $1/n$ as wide as in the first order. Therefore, whatever source radiation factor may be determined must be multiplied by the $1/n$ angular dispersion factor.

By far the most significant factor is the relative energy radiated by the source in the unwanted orders as compared to the desired order. Although precise data concerning the variation of emissivity with wavelength are rarely available, it is generally adequate to assume a blackbody energy distribution utilizing for computation either Planck's distribution law or, beyond about 5 μ with common source temperatures, the Rayleigh-Jeans approximation.

The latter states that $E_\lambda d\lambda$ is proportional to $d\lambda/\lambda^4$. Taking into account the angular dispersion factor

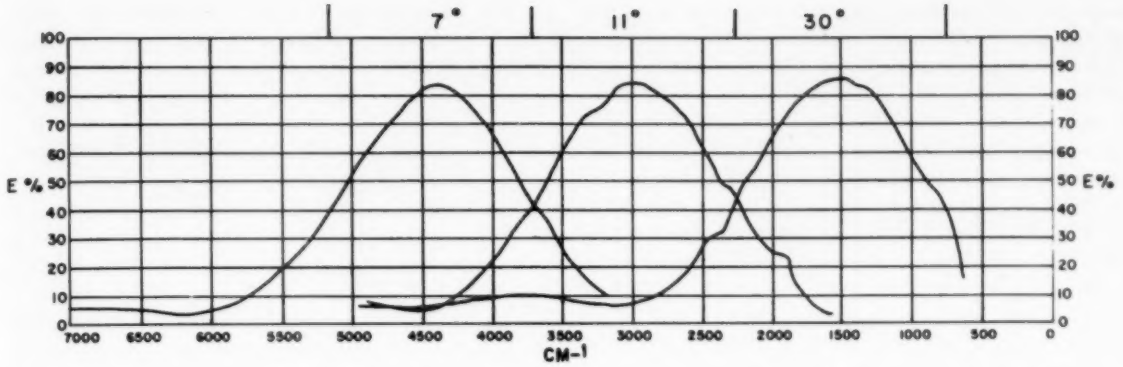

Fig. 2. Efficiency measurements made in the first three orders of a 100 l/mm grating blazed at 22°7′, using unpolarized incident radiation.

mentioned above, the ratio of nth order to first-order radiated power is given by:

$$\frac{E_n}{E_1} = \frac{1}{n}\cdot\left(\frac{\lambda_1}{\lambda_n}\right)^4 = n^3 \text{ for } \lambda > \sim 5\ \mu. \qquad (1)$$

This expression shows the rapid growth of the filtering requirement when operating at longer wavelengths. For example, if one is working in first order at 30 μ with a 30 μ blazed grating, the following table roughly describes the relative energy in the first six orders*:

n	1	2	3	4	5	6
λ (μ)	30	15	10	7.5	6.0	5.0
E_n/E_1	1	8	27	64	125	216

With successively higher orders, beyond the sixth in this case, the problem gets worse more slowly because we are nearing the peak of the source radiation curve. Also there remains the third factor mentioned above, the relative efficiency of the grating in higher orders, which rapidly ameliorates the requirement at angles away from the blaze. When one is working with gratings blazed below 10 μ as is more commonly the case, the requirements on filter rejection are far less severe. As one approaches wavelengths on the short-wavelength side of the source radiation peak, the rejection requirements approach the trivial. For example, the shorter-wavelength version of the lower-cost instrument described in the Introduction uses no rejection filter in scanning from 0.83 μ to 1.3 μ with a grating blazed at 1.25 μ. At these wavelengths the source itself serves as the order rejection filter by virtue of its inherent characteristics.

The remaining factor which influences the filter rejection requirements is the relative grating efficiency in different orders. Figure 2 is a plot of efficiency measurements[4] made on the first three orders of a 100 l/mm grating blazed at 22°7′, a nominal blaze frequency of 1333 cm^{-1}. It is usual for the actual efficiency peak to occur on the short-wavelength side of the nominal blaze. The shape of this curve is general in that it is very nearly the same for all gratings of the same quality. A useful rule of thumb is that the efficiency is better than 50% of the peak efficiency between $\nu_1/2$ and $3\nu_1/2$, or from $2\lambda_1/3$ to $2\lambda_1$. That is, a grating may be utilized within this range of variation of efficiency over a spectral region whose high- and low-frequency limits are in a ratio of 3:1. We shall call this the *half-width*.

Within the context of this rough approximation the efficiency function in higher orders is very simply related to the first-order curve. It may be inferred from the measurements shown that it has the same height, width, and shape as the first-order curve but it centers around the pertinent blaze frequency ν_2, ν_3, etc. Since the frequency half-width is the same in higher orders as it is in first order, it follows that:

1. The wavelength half-width decreases in higher orders from $4\lambda_1/3$ in first order to $4\lambda_1/15$ in second order, $4\lambda_1/35$ in third order, $4\lambda_1/63$ in fourth order, and $4\lambda_1/(4n^2-1)$ in nth order.

2. The angular range of the half-width around the blaze angle thereby also decreases in higher orders, as is indicated in Fig. 2.

The latter indicates how the higher-order grating efficiency aids the filtering process everywhere except in the vicinity of the blaze angle. This factor combined with the wider useful wavelength range in first order contributed to the decision to utilize two gratings each in first order, rather than one grating in four or more orders to cover the desired spectral range of the filter grating instruments developed at Perkin-Elmer.

Even after the factors of order efficiency, relative source intensity, and angular dispersion have been accounted for, and the allowable leakage is determined by summing over all pertinent higher orders, experience

* These ratios are consistently higher than, but compare closely with, exact E_n/E_1 ratios for a source temperature of 2000°K published on p. 692 of ref. 2.

has shown that the result may be taken only as a first approximation. In many cases the derived rejection factors have proved to be more stringent, and in some cases less stringent, than actually required. In other words, the final determination of optimized filter specifications has generally been based on measurements in actual application to the instruments concerned.

C. Special Transmission Specifications

In the above we have been concerned only with the rejection characteristics of the filters. Although this deserves the greater attention, the transmission characteristics of the filter cannot be ignored. First of all, the transmission curves of many filters exhibit a phenomenon called *banding*, which looks like a damped oscillation superimposed on the general energy characteristic. The sharper the cutoff the more severe the banding tends to be. If the peak-to-peak oscillation exceeds roughly 10%, the resulting variations in energy reaching the detector may tax the servo system of the instrument. Banding may be kept within reasonable bounds in good filter designs.

A related consideration is a reasonable matching of filter characteristics at the filter switch points. Here again the requirement is to control the characteristics adequately to avoid a deleterious variation of energy in the system.

Filter Grating Instrument Design and Performance

A. Basic Considerations

Since our concern in this paper is primarily with the dispersing system of the instrument, the basic considerations of instrument design which we shall consider relate to this alone. Thus, the basic factors are the spectral range to be covered and the abscissa readout. These determine the specification of gratings and filters and the characteristics of the scanning drive mechanism.

The consideration of spectral range points to one of the inherent advantages of filter grating systems compared to foreprism grating systems. That is, the spectral range of the grating system is no longer defined by the properties of the prism, whose absorption edge limits the long-wavelength end and decreased dispersion limits the short-wavelength utility. For example, as described in the Introduction, two filter grating interchanges have so far been designed for the versatile instrument, one covering the range from 4000 to 550 cm^{-1} (2.5 to 18.2 μ) and the other from 2000 to 250 cm^{-1} (5 to 40 μ). Both extensive regions show approximately the same high resolution throughout. Elimination of the prism also avoids the environmental effects of moisture and temperature sensitivity which plague most infrared prism materials.

The instruments we have developed have utilized two gratings mounted back to back, both operated in only first order. This design appears to represent a practical balance between a wide spectral range, concomitant filter specifications, minimum number of grating change points, and mechanical requirements for precision and reproducibility of the grating drive.

Operation of a filter grating system in higher orders is certainly not impossible. The type of filter required for operation in orders higher than the first is a bandpass rather than a long wave pass. With the requirement for reasonably sharp cutoffs and high rejection on both sides of the pass band, these are significantly more difficult to make. This approach may lead to a design requiring a larger number of more expensive filters. Analysis has shown that under some unique circumstances, mostly in the region below 5 μ, it may be feasible to use second order, but under no conditions does it appear practical to consider use of third or higher orders.

The reference above to the number of grating change points deserves elaboration. Taking into account the efficiency characteristics of a blazed grating, as discussed previously, the grating may be used in first order over a factor of at least three in wavelength or frequency. Thus, the use of two gratings each in first order enables the instrument to reach a wavelength or frequency roughly nine times the selected minimum, depending on other imposed limitations. To cover a comparable range with one grating would require four or more orders.

In addition, at each point where either the order or the grating is changed, there is necessarily a discontinuity in angular dispersion and, therefore, in spectral slit width and resolution. This may be seen from the following expression for the angular dispersion which is a close approximation in the case where the angles of incidence and diffraction are nearly equal, as in the Littrow configuration:

$$\frac{d\theta}{d\lambda} = \frac{2 \tan \theta}{\lambda}. \qquad (2)$$

From this we may note that the angular dispersion depends only on the wavelength λ and the grating angle θ. It is independent of the order number as well as the number of grooves per unit width, except in so far as these determine the angle θ at which the wavelength λ is observed. At a grating or order change-over wavelength, this particular wavelength is observed at two different grating angles and, therefore, with correspondingly different angular dispersions proportional to $\tan \theta$.

Each of the dual grating systems designed here requires four filters. This number depends on the sharpness of cutoff that is attainable under practical conditions.

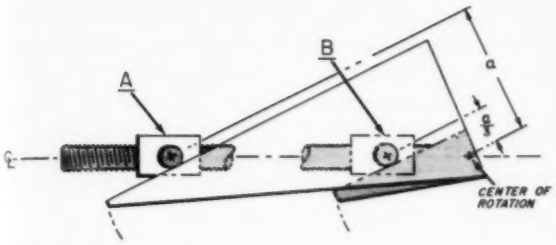

Fig. 3. Schematic diagram of double cosecant arm mechanism.

The grating scan consideration points out another advantage of filter grating systems in that there is nothing equivalent to the tracking requirement of prism grating systems. The only associated mechanism is the filter wheel and the actuator for position change of this wheel.

B. Scan Mechanisms

With the grating as the only dispersing element in the system it is particularly attractive to take advantage of the inherently simple trigonometric functions to produce linear wavelength or linear frequency abscissas. In fact, in cases where the alternative of a cam drive was considered the large angular range required for the grating drive led us to choose mechanical linkages which generate the appropriate trigonometric function. For a specified precision of readout the function generators permitted less tight mechanical tolerances.

The high versatility instrument, with its high accuracy and precision specifications and its requirement for a continuous abscissa presentation over the grating change point, presented a challenging design problem. This was aggravated by the selection of two gratings whose groove spacings were in a 3:1 ratio. The grating change point of 2000 cm^{-1} was chosen as the most innocuous, but the 3:1 ratio was deemed unacceptable as a scale change factor. This combination of requirements and circumstances appeared to necessitate an uncomfortably complex mechanism whose long-term reliability was questionable.

The solution was a double cosecant arm mechanism whose principle is shown in Fig. 3. The two constant legs of the cosecant function generator are dimensioned in the same ratio as the number of grooves per unit width of the two gratings. The linearly driven member in this case is an outer ball-bearing race attached to a nonrotating-nut riding on a precision lead screw. As this member reaches the grating change point, the constant legs are interchanged without changing the position of the nut on the lead screw during the change. In the schematic diagram, when the nut is in position A, it drives the arm associated with the 300 l/mm grating. After grating change, with this arm out of the way, the nut shown in position B drives the second arm associated with the 100 l/mm grating. An important consequence of this arrangement is the equality of the cm^{-1} per unit rotation of the lead screw both sides of the change point. Thus the change point can, in fact, be shifted from the nominal 2000 cm^{-1} without changing the calibration.

The principle of the double cosecant arm appears to be general in that it could be applied to the use of more than two gratings and it is equally applicable to multigrating systems with sine generating linkages for linear wavelength readout.

C. Double Diffraction

One phenomenon which requires close attention in filter grating systems is double diffraction. This can cause a type of unwanted radiation which is difficult to detect but which would interact seriously with the accurate determination of band depths.

The effect which may occur in a foreprism grating system in regions of poor prism dispersion arises from the fact that a relatively broad spectrum of diffracted light is spread across the focal plane of the collimator. Some of this spectrum may impinge on the grating a second time, near the edge closest to the slits. It is then possible that a wavelength different from the primary wavelength which passes through the exit slit will, after this second diffraction, satisfy the angular relationship so that the collimator will also send a portion of this doubly diffracted energy through the exit slit.

Since the filter allows a wide band of spectral energy to enter the grating monochromator, the likelihood that the effect will occur is not negligible. This is true in Littrow monochromators. In other monochromator systems, the effect either cannot occur or is unlikely. The magnitude of the effect depends on a number of geometric factors, most important of which relate to the off-axis angle of the collimator.

One effective way to verify the absence of double diffraction is to check the band bottoms of samples whose thickness is great enough to cause the bottoms of many bands to transmit significantly less than 1%. If the effect is found to be present, it may easily be eliminated by effective baffling either at the edge of the grating nearest the exit slit or at either side of the collimator mirror. The baffle position should be chosen to minimize the loss in primary radiation.

D. Unwanted Radiation

The greatest single concern in the development of filter grating systems was the degree of spectral purity that could be attained. The results have dissipated this concern.

The key factor is the ability to reproduce the high rejection characteristics of the filters in production, which has proved to be feasible. Taking advantage of

the 20:1 ordinate scale expansion in the versatile filter grating instrument, extensive measurements were taken of the spectral purity in an average production instrument with a standard interchange. Measurements were made on the absorption edges of several optical materials. Unwanted radiation, which includes scatter and unwanted orders, did not exceed 0.05% throughout the region from 4000 to 550 cm^{-1}. The measurements were made under the least favorable conditions of the widest available slit program. It should be noted that in a filter grating system, as contrasted to a foreprism grating system, the band of radiation entering the grating monochromator is unaffected by the slit width.

We have not found reference to measurements of unwanted radiation in foreprism grating systems made down to this level. In order to pursue the comparison of filter grating and prism grating systems, we are in the process of obtaining these data on a large foreprism grating instrument, recently developed by Bodenseewerk, Perkin-Elmer's West German subsidiary.

Summary

The growth of filter grating systems has been outstanding, spurred on by the obvious advantages and features which are inherent in the systems. Among the advantages which have come to our attention are:

1. The interference filters employed are physically small, thin, and durable and are therefore easy to maneuver in an instrument.

2. The optical path length of the instrument is shorter. This decreases the effect of atmospheric absorption bands within the instrument which minimizes or forestalls the need for purging the spectrophotometer. Another related advantage is the more compact size of such instruments.

3. The elimination of the prism material avoids the environmental problems of moisture sensitivity and the requirement for temperature compensation.

4. The artificial wavelength restrictions imposed by prism materials are lifted.

5. Slit curvature mismatch problems which plague double monochromators are eliminated. This is particularly important under narrow-slit, high-resolution conditions.

These advantages and the general utility of filter grating systems have been verified in both a versatile, high-performance instrument and in a more limited purpose, low-cost instrument.

Many at Perkin-Elmer have contributed significantly to the development of filter grating systems. In particular, I wish to acknowledge the specific contributions made by Roy Bastien, whose filter designs have been the backbone of the filter grating systems developed; C. F. deMey II, who conceived and developed the concept of the double cosecant arm; and Hamilton W. Marshall, who has made many helpful suggestions.

References

1. R. C. Lord and T. K. McCubbin, Jr., J. Opt. Soc. Am. **45**, 441 (1955).
2. R. C. Lord and T. K. McCubbin, Jr., J. Opt. Soc. Am. **47**, 689 (1957).
3. L. I. Epstein, J. Opt. Soc. Am. **42**, 806 (1952).
4. H. W. Marshall, "Efficiencies for Infrared Gratings," Molecular Structure and Spectroscopy Symposium, Ohio State University (1961).

REFEREES

The following people referee papers submitted to APPLIED OPTICS from time to time, and the Editors wish to acknowledge with gratitude this service:

H. H. Allen, Jr., G. F. Aroyan, J. G. Atwood, A. V. Baez, J. G. Baker, S. S. Ballard, R. Barakat, R. B. Barnes, E. Barr, E. S. Barr, A. M. Bass, J. R. Benford, L. E. Bergstein, B. H. Billings, L. S. Birks, H. H. Blau, W. S. Boyle, F. F. Byrne, H. Cary, R. M. Chapman, L. H. Chasson, C. B. Childs, C. H. Church, K. C. Clark, G. W. Cleek, V. J. Coates, R. J. Collins, W. A. Craven, Jr., A. Danti, H. A. Daw, E. S. Dayhoff, J. A. Dobrowolski, K. Dressler, M. Dreyfus, W. G. Driscoll, S. Q. Duntley, D. Dutton, H. Edgerton, D. F. Eggers, Jr., R. S. Estey, E. Evtuhov, W. Fastie, D. P. Feder, P. A. Franken, J. S. Garing, N. Ginsburg, G. E. Gross, F. F. Hall, Jr., G. B. Harrison, L. W. Herscher, M. Herzberger, I. C. Hisatsune, R. E. Hopkins, G. A. Hornbeck, E. O. Hulburt, R. S. Hunter, W. L. Hyde, J. A. Hynek, S. S. Impiombato, R. C. Jones, R. N. Jones, K. Innes, J. A. Jamieson, L. D. Kaplan, S. Katz, J. W. Kemp, K. G. Kessler, J. I. F. King, R. Kingslake, W. F. Koehler, N. Kriedl, E. W. Kutzscher, J. Lambe, E. Leith, E. V. Lowenstein, D. J. Lovell, C. F. Luck, T. K. McCubbin, R. K. McDonald, R. H. McFee, J. R. McNally, Jr., R. P. Madden, A. D. May, A. B. Meinel, P. E. Mengers, L. H. Meuser, D. F. Nelson, P. Nolan, R. A. Oetjen, J. Parsons, F. H. Perrin, G. N. Plass, E. K. Plyler, H. D. Polster, R. Potter, R. W. Powell, D. Richardson, D. W. Robinson, D. Z. Robinson, N. Rosenberg, J. A. Sanderson, J. B. Saunders, A. L. Schawlow, B. F. Scribner, J. H. Shaw, W. Sinton, F. S. Smith, E. Snitzer, I. Spiro, V. J. Stakutis, O. N. Stavroudis, S. Sternberg, H. S. Stewart, B. Stoicheff, G. W. Stroke, R. E. Stroup, R. Tabeling, R. M. Talley, Y. Tanaka, R. Tousey, A. F. Turner, G. A. Vanasse, M. E. Warga, J. U. White, B. W. Wild, P. G. Wilkinson, P. A. Wilks, Jr., V. Z. Williams, D. E. Williamson, M. K. Wilson, W. Wolfe, E. M. Wormser, N. Wright, H. W. Yates, M. Zelikoff, and G. J. Zissis.

Performance of the Beckman IR-7 Infrared Spectrophotometer I. Frequency Reproducibility and Accuracy (630–4000 cm^{-1})

Peter J. Krueger

A modified Beckman IR-7 prism/grating infrared spectrophotometer has been calibrated with an absolute accuracy of up to ± 0.05 cm^{-1} from 630 cm^{-1} to 2050 cm^{-1}, and with an absolute accuracy of the order of ± 0.10 cm^{-1} from 2000 cm^{-1} to 4000 cm^{-1}. This represents an improvement over the manufacturer's specifications by factors ranging between 10 for the longer wavelengths and 50 for the shorter wavelengths. The frequency reproducibility of the modified instrument and the linearity of the frequency (wave number) presentation have been critically examined.

I. Introduction

Small infrared grating spectrophotometers which are capable of a resolution of about 0.3 cm^{-1}, without sacrificing many of the automatic features found on the more inexpensive double-beam low-resolution prism instruments currently used by chemists as auxiliary tools, are now readily available. These are of two basic types, as far as the rotation of the grating is concerned. Instruments modeled essentially on the design of specialized high-resolution research spectrophotometers depend on a precision lead screw,[1] whereas those approaching the medium-resolution field from the basic design for simple spectrophotometers employ a complex cam system[2] or a cosecant bar mechanism.[3] The first category demands calibration using primary emission line standards in different grating orders, or secondary absorption line standards, since the frequency (wave number) presentation is nonlinear with respect to the rotation of the lead screw. Instruments using a cam system, like the Beckman IR-7, usually present spectra linearly in cm^{-1}, these frequency units being directly proportional to the energy changes involved in the vibrational transitions and thus very convenient. The absolute frequency accuracy in this case is a function of the original production of the cams (or the "masters" from which they are derived).

Since increasing emphasis is now being placed on small frequency differences in problems in chemical spectroscopy, it is imperative that small prism and grating spectrophotometers, which contribute the bulk of the spectroscopic results of chemical interest published at the present, be calibrated as accurately as possible.[4] Only in this way can results from different laboratories be integrated.

The feasibility of accurately calibrating a Beckman IR-7 spectrophotometer has now been examined in this laboratory. This commercial instrument is capable of a resolution of 0.3–0.4 cm^{-1} throughout most of the NaCl foreprism region, and its specifications assure the user of frequency reproducibility of 0.25 cm^{-1} in the first and second grating orders (650–2050 cm^{-1}) and 1.0 cm^{-1} in the third and fourth orders (2000–4000 cm^{-1}).[2] The absolute frequency accuracy specified is ± 0.5 cm^{-1} at 650 cm^{-1}, ± 2.0 cm^{-1} at 1404.96 cm^{-1}, ± 2.5 cm^{-1} at 2016.7 cm^{-1}, and ± 5 cm^{-1} at 4000 cm^{-1}.[2,5]

At least part of the large reproducibility tolerances, especially at the shorter wavelengths, were thought to be due to the difficulty of indexing the recorder pen and the monochromator setting, without any backlash, to a major chart-paper grid line at some specified starting wave-number value as given by the indicator dial. This wave-number read-out dial has a linear distance of 4 mm per cm^{-1} in the first and second orders, but only 1 mm per cm^{-1} in the third and fourth orders, since the cam system is designed to compress the last two orders (2000–4000 cm^{-1}) automatically by a factor of four in a continuous scan. This abscissa compression introduces another difficulty for high precision work above 2000 cm^{-1}, since although a maximum abscissa expansion of 2.5 cm^{-1}/in. can be achieved in the first and second orders, this automatically changes to 10 cm^{-1}/in. in the

The author is in the Department of Chemistry, University of Alberta, Calgary, Alberta, Canada.

Received 19 October 1961.

This paper was presented in part at the Eighth Ottawa Symposium of the Canadian Association for Applied Spectroscopy, September 18–20, 1961.

third and fourth orders. To overcome these difficulties, the instrument was modified to provide a fiducial marking system locked in with the cam system, a variable scanning speed control which would conveniently permit scanning speeds of 0.4 cm^{-1}/minute (or lower) in all orders for both directions of grating rotation, and abscissa expansion of 2.5 cm^{-1}/in. in the third and fourth orders. These modifications have been described in detail.[6-8]

This publication describes the method of calibration employed, and the rigorous reproducibility and accuracy tests to which the modified instrument was subjected.

II. Calibration Scheme

Since the use of emission lines for calibration purposes lends itself only with great difficulty to a commercial instrument like this, the vibration-rotation lines in absorption bands of simple gases at fairly low pressures were used, following established procedures. The calibration scheme used is given in Table I, and is essentially that recommended by the IUPAC Commission on Molecular Structure and Spectroscopy.[9] The spectra illustrated in this report were found to be invaluable in band correlation, and in matching the resolution of the IR-7 to that shown in the report for certain absorption lines whose positions are strongly resolution-dependent. In general, the more precise data in Part I of the Commission Tables provided the basis for the calibration, supplemented by less suitable calibration lines from Part II to fill in any gaps. Since some of this work was completed before the Commission report was published, reference was also made to the work of Pickworth and Thompson[10] on DCl; Plyler *et al.*[11] on HBr, C_2H_2, and water vapor; and to some unpublished data compiled in the laboratory of R. N. Jones, National Research Council, Ottawa.

All calibration runs were performed at a scanning speed of 0.4 cm^{-1}/min in the direction of increasing frequency. The amplifier gain settings were between 15 and 30% and a pen response (filter period) of 32 sec was used. From the observed bandwidths, the single beam/double beam energy ratios, and graphs provided by the manufacturer,[5] the "tracking error" in most of this work was estimated to be less than 0.02 or 0.01 cm^{-1}.

Double-beam operation was employed throughout, except for the atmospheric water vapor bands, and for certain reproducibility tests mentioned later. Slit widths were programmed for constant energy using a regular "Select" setting that would give the resolution required and maintain a high signal to noise ratio. The approximate spectral slit widths used in the different regions are given in Table I. Figure 1 shows some typical examples of resolution employed in this work, but does not necessarily represent the best resolution that can be obtained with this instrument.

Work of the highest precision requires that both calibrants and runs to be measured be recorded for both directions of grating rotation, and the results averaged if slightly different.[11] Duplicate runs are often used as well. Except for the reproducibility tests discussed later, the calibration described here was based on a single series of spectra with an acceptable signal-to-noise ratio, using the conventional direction of grating rotation. Thus all the required spectra could be recorded in less than 150 hr of instrument time.

The spectra were recorded on ruled chart paper, and the centers of the lines to be measured determined with a pair of dividers at several places between the $^2/_3$ and $^3/_4$ maximum absorption points, and the average taken in the case of noisy traces. Fractional distances of line centers between reference marks were then measured with a machine-divided steel rule graduated in hundredths of an inch.

Preliminary adjustment of the microswitch in the fiducial marking system had brought the reference "pips" almost in exact coincidence with successive whole wave-number units in the first order as indicated on the frequency dial. This coincidence was not as exact in the higher orders, but it was found to be close enough to the whole wave number unit in question to avoid confusion. Since these reference marks occurred at 4 cm^{-1} intervals in the third and fourth orders, this had to be taken into consideration in establishing a convenient "fiducial scale" (in cm^{-1}) in step with the nominal frequency.

The final complete calibration of the instrument was then established by plotting the fiducial scale values of the calibrant lines as abscissa against the true frequencies of the corresponding lines as ordinate. This was done on meter width graph paper subdivided in millimeters, using a scale of 1.00 cm^{-1} = 2.00 cm on both axes. Including the overlap between the orders, this should require a set of some 70 calibration lines which would be straight diagonals for a perfect cam system. In practice, the data for substantial regions could be fitted with straight lines, whereas other sections exhibited slight curvature as was expected. In no case were sharp changes observed in the calibration lines.

Since a calibration graph of this size is rather inconvenient to use, the data were reduced to numerical tables, the format of which is illustrated in Table II.

III. Frequency Reproducibility

As a test of the reproducibility of the method employed, a calibrant with sharp lines was selected in each of the four orders, and a region of about 100 cm^{-1} was scanned three times under the same instrumental

Table I. Calibration Scheme

Grating order	Calibrant	Region (cm^{-1})	Pressure (mm) in 10-cm cell	Slit width[a] (cm^{-1})	Number of calibration points
I.	1. Carbon dioxide,[b] ν_2 fund.	635–705	70	0.6–0.4	43
	2. Hydrogen cyanide,[c] ν_2 fund.	640–790	30	0.9–0.5	44
	3. Acetylene,[d] ν_5 fund.	690–790	15	0.6–0.3	39
	4. Ammonia,[e] ν_2 fund.	770–1155	50	0.2–0.4	114
		820–830	15	0.2	
		840–895	15	0.3	
		920–950	15	0.3	
		955–975	15	0.3	
		990–1000	15	0.3	
		1030–1050	15	0.3	
II.	5. Ammonia,[e] ν_2 fund.	1090–1215	50	0.4	26
	6. Methane,[f] ν_4 fund.	1210–1260	250	0.4	51
		1260–1370	60	0.4	
	7. Water vapor,[g] ν_2 fund.	1355–1890	[h]	0.3–0.4	94
	8. Ammonia,[e] ν_4 fund.	1545–1635	75	0.2–0.3	24
	9. Deuterium bromide[i,j]	1725–1950	125	0.3–0.5	54
	10. Deuterium chloride[k,l]	1890–2050	250	0.4–0.5	26
III.	11. Deuterium chloride[k,l]	2000–2235	250	0.5–0.4	48
	12. Carbon monoxide[m]	2050–2245	150	0.4–0.3	50
	13. Carbon dioxide,[b] ν_3 fund. of $C^{13}O_2$ and $C^{13}O_2$	2235–2290	250	0.4	87
		2260–2310	50	0.5	
		2300–2390	20	0.4	
	14. Hydrogen bromide[n,o]	2390–2725	140	0.4–0.5	21
	15. Hydrogen chloride[p,q]	2620–3005	120	0.4–0.8	33
	16. Methane,[f] ν_3 fund.	2895–3000	60	0.7–0.8	10
IV.	17. Hydrogen chloride[p,q]	2740–3055	120	1.3–0.6	30
	18. Methane,[f] ν_2 fund.	2895–3185	60	0.7–0.5	30
		3150–3195	300	0.5	
	19. Ammonia[e]	3190–3500	75	0.4–0.5	42
		3490–3570	300	0.5–0.6	
	20. Acetylene,[d] $\nu_1 + \nu_5$ comb.	3215–3350	30	0.7–0.8	34
	21. Hydrogen cyanide,[c] ν_3 fund.	3240–3380	20	0.5	52
		3380–3395	250	0.5	
	22. Water vapor[g]	3445–3995	[h]	0.6–1.3	39
	23. Carbon dioxide[b]	3565–3660	400	0.6–0.7	78
		3620–3730	200	0.6–0.7	
					Total = 1069

[a] Approximate values (programmed slit used).
[b] Matheson, bone dry grade, 99.8% min.
[c] Prepared by action of dilute H_2SO_4 on KCN.
[d] Welder's grade.
[e] Matheson, anhydrous, 99.99% min.
[f] Matheson, C.P. grade, 99.0% min.
[g] Single-beam spectrum.
[h] Entire optical path at 30% relative humidity, 27°C.
[i] Prepared from D_2O and PBr_3.
[j] DBr^{79} and DBr^{81} lines resolved.
[k] Prepared from D_2O and PCl_5.
[l] DCl^{35} and DCl^{37} lines well resolved.
[m] Matheson, C.P. grade, 99.5% min.
[n] Matheson, anhydrous, 99.8% min.
[o] HBr^{79} and HBr^{81} lines not resolved.
[p] Matheson, anhydrous, 99.0% min.
[q] HCl^{35} and HCl^{37} lines well resolved.

conditions. These tests were spread out over a period of a month, and the instrument was used by several other operators in the intervening periods. Except when in use for precise measurements, the fiducial microswitch arm was always disengaged from the actuating gear to prevent unnecessary wear on the switch. No special temperature or humidity control was employed for the instrument room.

Tables III, IV, V, and VI give the results of these reproducibility tests, using acetylene (ν_5), and methane (ν_4), carbon monoxide, and hydrogen cyanide respectively in the four orders. It should be noted that the measured mean value reported in these tables is a fiducial scale value only, as compared with the true frequencies listed in adjacent columns, but these are sufficient for examining the reproducibility. The difference between the fiducial values and the true frequencies indicates the magnitude of the correction to be applied to the fiducial scale in these regions.

Table VII summarizes these reproducibility tests. The surprisingly good precision (standard deviation of ± 0.02 cm^{-1}) in the first two orders speaks very highly

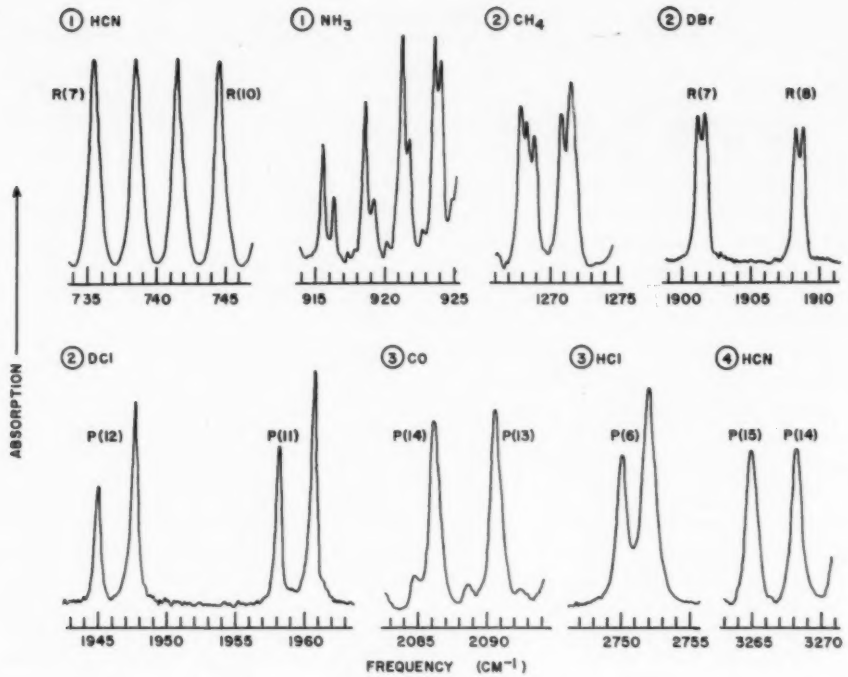

Fig. 1. Examples of resolution used in calibration. Numbers in circles refer to grating order.

Table II. Example of Beckman IR-7 Calibration Table[a]

Fiducial scale (cm^{-1})	0	1	2	3	4	5	6	7	8	9
630	—	—	—	—	634.54	635.53	636.52	637.51	638.50	639.49
640	640.48	641.47	642.46	643.45	644.45	645.44	646.43	647.43	648.42	649.41
650	650.40	651.37	652.35	653.34	654.33	655.31	656.30	657.28	658.27	659.25
660	660.25	661.24	662.23	663.21	664.20	665.19	666.18	667.16	668.15	669.14
670	670.13	671.12	672.10	673.09	674.08	675.07	676.06	677.05	678.04	679.03
680	680.01	681.00	681.98	682.97	683.96	684.95	685.95	686.94	687.93	688.92
690	689.91	690.90	691.89	692.89	693.88	694.87	695.86	696.86	697.85	698.85
700	699.85	700.82	701.81	702.81	703.81	704.81	705.82	706.82	707.83	708.83
710	709.83	710.83	711.83	712.84	713.84	714.84	715.83	716.82	717.82	718.81
720	719.81	720.81	721.80	722.79	723.78	724.77	725.76	726.75	727.75	728.74
730	729.71	730.72	731.71	732.70	733.69	734.68	735.68	736.67	737.66	738.65
740	739.64	740.64	741.63	742.62	743.61	744.60	745.59	746.58	747.57	748.56
750	749.55	750.55	751.55	752.55	753.55	754.56	755.56	756.56	757.57	758.57
760	759.57	760.58	761.58	762.58	763.59	764.59	765.59	766.60	767.60	768.60
770	769.60	770.60	771.61	772.61	773.61	774.61	775.61	776.62	777.62	778.62
780	779.62	780.62	781.62	782.62	783.62	784.62	785.62	786.62	787.61	788.61
790	789.61	790.61	791.61	792.60	793.60	794.60	795.60	796.60	797.60	798.60
etc.										
	Proportional Parts:									
		0.1	0.2	0.3	0.4	0.5	0.6	0.7	0.8	0.9
		0.10	0.20	0.30	0.40	0.50	0.60	0.70	0.80	0.89

[a] Part of first order. Vacuum corrected absolute frequencies (cm^{-1}) are in the body of the table.

Table III. First-Order Reproducibility Test (Acetylene, ν_5 fund.)

J	Jones *et al.*[a] (cm^{-1})	Fiducial values (cm^{-1}) Mean[b]	Max. deviation from mean
P-16	691.45	691.43	±0.03
P-15	693.80	693.89	±0.01
P-14	696.15	696.21	±0.02
P-13	698.55	698.67	±0.04
P-12	700.90	701.01	±0.02
P-11	703.25	703.38	±0.03
P-10	705.60	705.77	±0.03
P-9	707.95	708.10	±0.03
P-8	710.30	710.48	±0.00
P-7	712.65	712.81	±0.04
P-6	715.10	715.22	±0.02
P-5	717.35	717.53	±0.00
P-4	719.90	720.03	±0.05
P-3	722.05	722.31	±0.04
P-2	724.35	724.63	±0.03
R-1	733.85	734.08	±0.00
R-2	736.15	736.47	±0.02
R-3	738.55	738.88	±0.03
R-4	740.85	741.21	±0.04
R-5	743.25	743.56	±0.02
R-6	745.65	746.00	+0.05
R-7	748.00	748.40	±0.03
R-8	750.35	750.69	±0.01
R-9	752.70	753.11	±0.02
R-10	755.10	755.49	±0.01
R-11	757.45	757.79	±0.04
R-12	759.85	760.16	±0.02
R-13	762.10	762.50	±0.03
R-14	764.50	764.79	±0.01
R-15	766.75	767.14	±0.04
R-16	769.10	769.48	±0.03
R-17	771.45	771.78	±0.03
R-18	773.80	774.18	±0.04
R-19	776.10	776.52	±0.02
R-20	778.45	778.89	±0.01
R-21	780.75	781.23	±0.00
R-22	783.05	783.57	±0.02
R-23	785.40	785.94	±0.01

[a] Unpublished data compiled in the laboratory of R. N. Jones.

[b] Average of three independent experimental determinations.

of the long-term mechanical stability of the cam wavelength drive system. Although these measurements were all made using double-beam operation of the instrument, some further single-beam measurements on carbon dioxide in the first order indicated that the mode of operation did not affect the precision.

The IUPAC Commission on Molecular Structure and Spectroscopy reports that a spectrophotometer whose best resolution is about 0.3 cm^{-1} will be capable of a wave-number precision of about ±0.03 to ±0.06 cm^{-1}.[9] The present results show that this is also valid for an instrument employing cams, provided

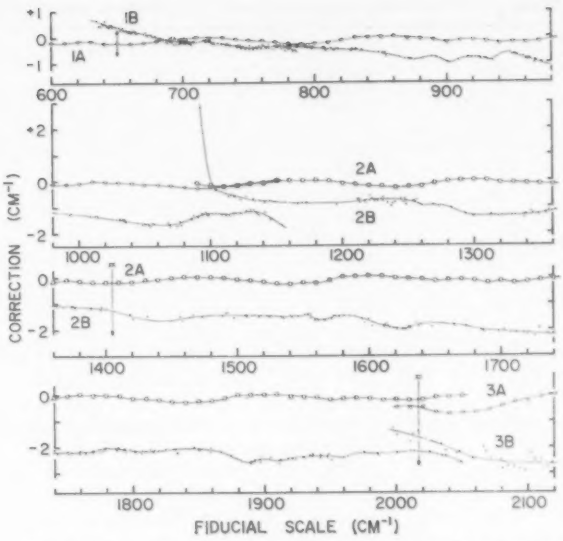

Fig. 2. Correction to be applied to dial wave-number read-out (B − A) and fiducial scale values (B) to give absolute frequency (cm^{-1}) for the range 600–2120 cm^{-1}.

Table IV. Second-Order Reproducibility Test (Methane, ν_4 fund.)

IUPAC Tables[a] (cm^{-1})	Fiducial values (cm^{-1}) Mean[b]	Max. deviation from mean
1265.50	1266.44	±0.01
1267.9	1268.81	±0.04
1271.5	1272.49	±0.01
1275.20	1276.16	±0.03
1281.65	1282.70	±0.00
1287.8	1289.02	±0.03
1292.65	1293.95	±0.00
1297.65	1299.02	±0.02
1311.45	1312.75	±0.03
1316.8	1318.16	±0.03
1322.10	1323.44	±0.01
1327.25	1328.53	±0.04
1332.45	1333.79	±0.04
1336.85	1338.29	±0.04
1337.65	1338.94	±0.04
1341.8	1342.99	±0.01
1342.8	1344.03	±0.03
1347.9	1349.24	±0.01
1353.10	1354.36	±0.03
1355.55	1356.69	±0.01
1358.1	1359.28	±0.03
1366.05	1367.16	±0.03
1368.55	1369.60	±0.05

[a] Supplemented by unpublished data compiled in the laboratory of R. N. Jones.

[b] Average of three independent experimental determinations.

Table V. Third-Order Reproducibility Test (Carbon Monoxide)

J	IUPAC Tables (cm^{-1})	Fiducial values (cm^{-1}) Mean[a]	Max. deviation from mean
P-11	2099.09	2101.34	±0.08
P-10	2103.27	2105.71	±0.09
P-9	2107.43	2109.98	±0.04
P-8	2111.55	2114.25	±0.03
P-7	2115.63	2118.25	±0.07
P-6	2119.68	2122.27	±0.11
P-5	2123.70	2126.39	±0.05
P-4	2127.69	2130.27	±0.03
P-3	2131.64	2134.11	±0.09
P-2	2135.55	2138.12	±0.04
P-1	2139.43	2142.06	±0.04
R-0	2147.09	2149.83	±0.05
R-1	2150.86	2153.73	±0.09
R-2	2154.60	2157.53	±0.07
R-3	2158.30	2161.10	±0.06
R-4	2161.97	2164.70	±0.02
R-5	2165.60	2168.41	±0.03
R-6	2169.20	2171.96	±0.04
R-7	2172.76	2175.71	±0.03
R-8	2176.29	2179.23	±0.05
R-9	2179.77	2182.67	±0.03
R-10	2183.23	2186.10	±0.08
R-11	2186.64	2189.51	±0.05
R-12	2190.02	2192.85	±0.03
R-13	2193.36	2196.13	±0.03
R-14	2196.66	2199.38	±0.06
R-15	2199.93	2202.65	±0.11

[a] Average of three independent experimental determinations.

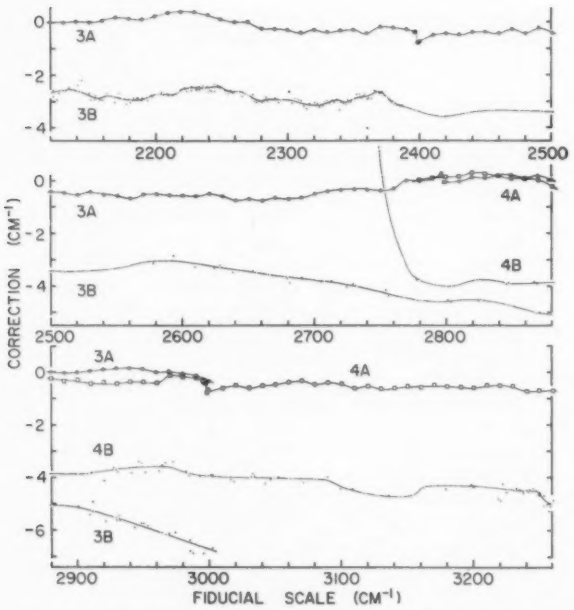

Fig. 3. Correction to be applied to dial wave-number read-out (B − A) and fiducial scale values (B) to give absolute frequency (cm^{-1}) for the range 2120–3260 cm^{-1}.

Table VI. Fourth-Order Reproducibility Test (Hydrogen Cyanide)

J	IUPAC Tables (cm^{-1})	Fiducial Values (cm^{-1}) Mean[a]	Max. deviation from mean
P-21	3245.1	3249.72	±0.10
P-20	3248.5	3253.56	±0.12
P-19	3251.8	3257.07	±0.09
P-18	3255.15	3260.27	±0.09
P-17	3258.45	3263.53	±0.09
P-16	3261.7	3266.75	±0.23
P-15	3265.0	3269.96	±0.20
P-14	3268.2	3273.22	±0.12
P-13	3271.45	3276.46	±0.18
P-12	3274.65	3279.67	±0.21
P-11	3277.8	3282.83	±0.15
P-10	3281.0	3286.07	±0.19
P-9	3284.1	3289.29	±0.11
P-8	3287.25	3292.33	±0.13
P-7	3290.35	3295.51	±0.07
P-6	3293.4	3298.47	±0.13
P-5	3296.5	3301.39	±0.25
P-4	3299.5	3304.48	±0.08
P-3	3302.55	3307.59	±0.15
P-2	3305.55	3310.57	±0.07
P-1	3308.5	3313.68	±0.04
R-0	3314.4	3319.75	±0.17
R-1	3317.3	3322.78	±0.12
R-2	3320.2	3325.47	±0.09
R-3	3323.1	3328.16	±0.08
R-4	3325.95	3330.76	±0.24
R-5	3328.8	3333.80	±0.18
R-6	3331.6	3336.67	±0.25
R-7	3334.35	3339.54	±0.12
R-8	3337.15	3342.35	±0.11
R-9	3339.9	3345.21	±0.15
R-10	3342.6	3347.81	±0.09
R-11	3345.3	3350.60	±0.06
R-12	3348.0	3353.29	±0.01
R-13	3350.65	3355.96	±0.04
R-14	3353.3	3358.59	±0.19
R-15	3355.9	3361.15	±0.05
R-16	3358.5	3363.84	±0.10
R-17	3361.05	3366.52	±0.06
R-18	3363.6	3369.07	±0.25
R-19	3366.15	3371.55	±0.11
R-20	3368.65	3374.16	±0.04
R-21	3371.1	3376.61	±0.07
R-22	3373.6	3379.07	±0.03
R-23	3376.0	3381.47	±0.11
R-24	3378.45	3383.90	±0.10

[a] Average of three independent experimental determinations.

the linear distance the cam follower moves on the cam for a given frequency interval is sufficiently large. The IR-7 grating cams correspond to approximately 5, 5, 16.7, and 18.5 cm^{-1} per mm of cam follower movement in the first, second, third, and fourth orders, respectively. It is obvious that a small mechanical discrepancy would produce poorer precision in the

Table VII. Beckman IR-7 Reproducibility

Order	Calibrant	Region (cm $^{-1}$)	No. of lines measured	Average max. deviation (cm^{-1}) from mean	Standard deviation from mean (cm^{-1})[a]	Percentage within standard deviation
1	C_2H_2	691–786	38	±0.02	±0.02	77
2	CH_4	1265–1368	23	±0.02	±0.02	70
3	CO	2099–2200	27	±0.06	±0.05	78
4	HCN	3245–3379	46	±0.12	±0.10	62

[a] Based on three independent measurements of each line.

Table VIII. First-Order Accuracy Test (Ammonia, 75 mm, 10 cm cell)

Garing *et al.*[17a]			
Line no.	Frequency (cm^{-1})	This work (cm^{-1})	Δ (cm^{-1})[b]
91	670.19	670.13	+0.06
108	690.16	690.18	−0.02
111	692.29	692.28	+0.01
115	700.95	700.90	+0.05
117	702.94	702.95	−0.01
122	707.04	707.06	−0.02
126	709.65	709.61	+0.04
133	712.31	712.28	+0.03
134	713.99	714.03	−0.04
136	716.23	716.27	−0.04
137	719.65	719.70	−0.05
141	723.28	723.26	+0.02
145	726.11	726.13	−0.02
151	728.57	728.58	−0.01
155	732.30	732.30	0.00
156	732.95	732.89	+0.06
157	735.14	735.09	+0.05
158	736.51	736.55	−0.04
160	737.51	737.47	+0.05
161	739.37	739.39	−0.02
162	741.62	741.61	+0.01
165	743.30	743.25	+0.05
166	743.96	743.90	+0.06
167	744.48	744.50	−0.02
170	745.41	745.35	+0.06
178	748.80	748.75	+0.05
180	749.86	749.85	+0.01
181	751.61	751.65	−0.04
182	753.59	753.62	−0.03
183	755.63	755.66	−0.03
184	756.59	756.60	−0.01
186	758.93	758.87	+0.06
188	760.69	760.73	+0.04
189	761.91	761.92	−0.01
190	762.64	762.62	+0.02
191	764.07	764.13	−0.06
193	764.82	764.75	+0.07
194	765.55	765.59	−0.04
195	766.23	766.29	−0.06
197	767.03	767.07	−0.04

[a] Accuracy within ±0.03 cm^{-1}.
[b] Δ = literature value − present value.

Table IX. Second-Order Accuracy Test (Acetylene, 140 mm, 10 cm cell)

	Frequency (cm^{-1})			
J	Bell and Nielsen[12]	This work	Δ_1 (cm^{-1})[a]	Δ_2 (cm^{-1})[b]
P-20	1282.3	1282.36	−0.06	+0.12
P-19	1284.6	1284.55	+0.05	+0.17
P-18	1286.8	1286.72	+0.08	+0.14
P-17	1289.0	1288.99	+0.01	+0.11
P-16	1291.2	1291.27	−0.07	+0.05
P-15	1293.5	1293.47	+0.03	+0.10
P-14	1295.8	1295.78	+0.02	+0.13
P-13	1298.0	1298.08	−0.08	+0.17
P-12	1300.3	1300.41	−0.11	+0.06
P-11	1302.7	1302.64	+0.06	+0.20
P-10	1304.9	1304.94	−0.04	+0.12
P-9	1307.2	1307.23	−0.03	+0.15
P-8	1309.5	1309.60	−0.10	+0.16
P-7	1311.8	1311.87	−0.07	+0.15
P-6	1314.2	1314.19	+0.01	+0.23
P-5	1316.4	1316.48	−0.08	+0.09
P-4	1318.7	1318.78	−0.08	+0.01
P-3	1321.1	1321.12	−0.02	+0.17
P-2	1323.5	1323.47	+0.03	+0.18
P-1	1325.8	1325.77	+0.03	+0.20
R-0	1330.6	1330.48	+0.12	+0.25
R-1	1333.0	1332.77	+0.23	+0.23
R-2	1335.3	1335.15	+0.15	+0.11
R-3	1337.7	1337.53	+0.17	+0.12
R-4	1340.1	1340.03	+0.07	+0.20
R-5	1342.4	1342.38	+0.02	+0.06
R-6	1344.9	1344.85	+0.05	+0.12
R-7	1347.1	1347.21	−0.11	−0.07
R-8	1349.7	1349.64	+0.06	+0.08
R-9	1352.1	1352.05	+0.05	+0.08
R-10	1354.4	1354.45	−0.05	−0.13
R-11	1356.9	1356.90	0.00	+0.06
R-12	1359.3	1359.33	−0.03	+0.03
R-13	1361.8	1361.74	+0.06	+0.19
R-14	1364.2	1364.20	0.00	+0.21
R-15	1366.6	1366.60	0.00	−0.02
R-16	1369.1	1369.06	+0.04	+0.20
		Algebraic mean =	+0.01	+0.14

[a] Δ_1 = Bell and Nielsen value − present value.
[b] Δ_2 = Bell and Nielsen value − Thompson *et al.* value.[13]

Table X. Third-Order Accuracy Test (Nitrous oxide, 20 mm, 10 cm cell)

	Frequency (cm^{-1})		
J	Thompson and Williams[15]	This work	$\Delta(cm^{-1})$[a]
P-47	2177.01	2177.16	−0.15
P-46	2178.15	2178.26	−0.11
P-45	2179.25	2179.39	−0.14
P-44	2180.36	2180.56	−0.20
P-43	2181.52	2181.52	0
P-42	2182.64	2182.58	+0.06
P-41	2183.78	2183.71	+0.07
P-40	2184.89	2184.86	+0.03
P-38	2187.11	2187.25	−0.14
P-37	2188.18	2188.34	−0.16
P-36	2189.32	2189.38	−0.06
P-35	2190.38	2190.42	−0.04
P-34	2191.44	2191.50	−0.06
P-33	2192.45	2192.53	−0.08
P-32	2193.50	2193.55	−0.05
P-31	2194.59	2194.55	+0.04
P-30	2195.66	2195.64	−0.02
P-29	2196.69	2196.65	−0.04
P-28	2197.73	2197.90	−0.17
P-25	2200.79	2200.81	−0.02
P-24	2201.76	2201.90	+0.14
P-16	2209.51	2209.57	−0.06
P-15	2210.44	2210.45	−0.01
P-14	2211.40	2211.43	−0.03
P-13	2212.30	2212.44	−0.14
P-12	2213.23	2213.44	−0.21
P-11	2214.14	2214.38	−0.24
P-10	2215.08	2215.18	−0.10
P-9	2215.93	2216.15	−0.22
P-8	2216.82	2216.92	−0.10
P-7	2217.71	2217.87	−0.16
P-6	2218.61	2218.70	−0.09
P-5	2219.49	2219.65	−0.16
P-4	2220.38	2220.41	−0.03
P-3	2221.22	2221.26	−0.04
P-2	2222.03	2222.07	−0.04
P-1	2222.90	2222.87	+0.03
R-29	2245.64	2245.75	−0.11
R-30	2246.28	2246.36	−0.08
R-32	2247.52	2247.50	+0.02
R-33	2248.10	2248.14	−0.04
R-34	2248.68	2248.70	−0.02
R-35	2249.29	2249.18	+0.11
R-36	2249.84	2249.81	+0.03
R-37	2250.44	2250.36	+0.08
R-38	2251.00	2250.91	+0.09
R-39	2251.59	2251.55	+0.04
R-40	2252.10	2252.03	+0.07
R-41	2252.65	2253.57	+0.08

[a] Δ = literature value − present value.

third and fourth orders. Slight variations in reference mark intervals in the third and fourth orders[6] would also contribute to a lower precision.

IV. Absolute Frequency Accuracy

As an independent test of this modified and calibrated instrument, some measurements were made on absorption bands not employed in the calibration, and the absolute frequencies obtained compared with published values from different laboratories. Tables VIII, IX, X, and XI give these comparative results for ammonia, acetylene, nitrous oxide, and cyclopropane in the four orders respectively. The instrumental conditions were kept as close as possible to those used in the calibration.

Table XI. Fourth-Order Accuracy Test (Cyclopropane, 80 mm, 10 cm cell)

	Frequency (cm^{-1})		
J	Günthard *et al.*[16]	Present work	$\Delta(cm^{-1})$[a]
P-27	3064.70	3064.53	+0.17
P-26	3066.16	3066.10	+0.06
P-25	3067.62	3067.49	+0.13
P-24	3069.04	3068.85	+0.19
P-23	3070.38	3070.36	+0.02
P-22	3071.71	3071.89	−0.18
P-21	3073.10	3073.22	−0.12
P-20	3074.49	3074.62	−0.13
P-19	3075.89	3075.94	−0.05
P-18	3077.26	3077.30	−0.04
P-17	3078.58	3078.48	+0.10
P-16	3079.90	3079.99	−0.09
P-15	3081.29	3080.92	+0.37
P-14	3082.73	3082.33	+0.40
P-13	3084.15	3083.93	+0.21
P-12	3085.57	3085.70	+0.13
P-11	3086.45	3086.47	−0.02
P-10	3087.81	3087.96	−0.15
P-9	3089.29	3089.50	−0.21
P-8	3090.78	3090.90	−0.12
P-7	3092.17	3092.22	−0.05
P-6	3093.65	3093.58	+0.07
P-5	3095.10	3095.05	+0.05
P-4	3096.47	3096.50	−0.03
R-2	3105.40	3105.35	+0.05
R-3	3106.70	3106.88	−0.18
R-4	3108.10	3108.19	−0.09
R-5	3109.47	3109.40	+0.07
R-6	3110.53	3110.60	−0.07
R-7	3111.98	3111.90	−0.01
R-8	3113.25	3113.23	+0.02
R-9	3114.59	3114.55	+0.04
R-10	3116.33	3116.27	+0.06
R-11	3117.68	3117.65	+0.03
R-12	3118.87	3118.81	+0.06
R-13	3120.17	3120.06	+0.11
R-14	3121.51	3121.33	+0.18
R-15	3122.72	3122.71	+0.01
R-16	3124.07	3123.98	+0.09
R-17	3125.38	3125.22	+0.16
R-18	3126.73	3126.57	+0.16

[a] Δ = literature value − present value.

Table XII. Beckman IR-7 Accuracy

Order	Gas	Region (cm^{-1})	No. of lines measured	Literature reference	Average deviation from literature values (cm^{-1})	Algebraic mean of deviations (cm^{-1})	Standard deviation (cm^{-1})	Percentage with standard deviation
1	NH_3	670–767	40	17	$\pm 0.03_5$	$+0.00_5$	$\pm 0.04_0$	65
2	C_2H_2	1282–1369	37	12	$\pm 0.06_1$	$+0.01$	$\pm 0.07_9$	81
3	N_2O	2177–2253	49	15	$\pm 0.08_6$	-0.05	$\pm 0.10_6$	73
4	cyclo-C_3H_6	3064–3126	41	16	$\pm 0.10_9$	$+0.03_9$	$\pm 0.14_9$	73

Since a long path cell was not available, the ammonia measurements were made with 75 mm of gas in a standard 10-cm cell. Thus only the most intense lines in this region could be measured, which accounts for the many serial numbers missing in Table VIII.

The second-order acetylene band was compared with the values of Bell and Nielsen,[12] leading to a standard deviation of $\pm 0.07_9$ cm^{-1} with 81% confidence. Christensen *et al.*[13] report that their measurements on this band were uniformly 0.1 cm^{-1} lower than the values given by Bell and Nielsen, and 0.5 cm^{-1} lower than the earlier measurements of Levin and Meyer.[14] Since the algebraic mean of the deviations of the present measurements from those of Bell and Nielsen was only + 0.01 cm^{-1}, confirmatory evidence is provided for their work.

The nitrous oxide band (ν_3) selected for a third-order accuracy test was only incompletely resolved, which accounts for lines missing in Table X. Thompson and Williams[15] have previously measured this band with a resolving power of 0.15 cm^{-1}, and have analyzed it and the overlying hot band $\nu_3 + \nu_2 - \nu_2$.

In the fourth order the parallel cyclopropane band at 3101 cm^{-1} was measured with resolution comparable to that of Günthard *et al.*[16]

Table XII summarizes these accuracy tests. The results indicate that an absolute accuracy of up to ± 0.05 cm^{-1} can be obtained in the first two orders (630–2050 cm^{-1}), and an absolute accuracy of the order of ± 0.10 cm^{-1} in the third and fourth orders (2000–4000 cm^{-1}).

V. Frequency Linearity

The fiducial marking system incorporated into this instrument lends itself ideally to the examination of the linearity of the cam frequency drive system. To examine this aspect all of the 1069 gas phase calibrant lines were plotted so that the absolute frequencies could be obtained at any point by applying a correction to the fiducial scale value. Examination of the "B" curves in Figs. 2, 3, and 4 reveals the exact nature of the cam linearity, since the fiducial scale is linear by its very nature.

The precise relationship of the wave-number read-out dial relative to the uniform rotation of the main monochromator shaft (i.e., relative to the fiducial scale) was also established at 10 cm^{-1} intervals. This information is shown in the "A" curves in Figs. 2, 3, and 4. Slight nonlinearity here must be ascribed to one or more periodic errors in the wave-number dial mechanism itself. No obvious periodicity related directly to the rotation of any one mechanical part could be found. Since the difference between the fiducial scale and the dial wave-number scale is within 0.25 cm^{-1} in the first two orders, and almost within 1 cm^{-1} in the third and fourth orders, the vertical distance between the "A" and "B" lines at any given fiducial scale value corresponds very nearly to the correction to be applied to the dial wave-number values at that point.

The manufacturers' absolute frequency specifications are also indicated in Figs. 2, 3, and 4 by means of vertical arrows originating from the "A" curves.

Several sharp discontinuities of about 0.4 cm^{-1} at 400 cm^{-1} intervals in the third and fourth order "A" curves are due to a defect in the printed scale of the wave-number dial. The ends of the conical scale band do not meet to give a perfectly continuous wave number scale. This defect is not noticeable in the first two orders.

VI. Condensed Phase Measurement

In the vibrational spectra of pure liquids or solutions, the band half-widths are seldom narrower than 5 cm^{-1}. The determination of the band center for a symmetrical band, or the point of maximum absorption for an asymmetrical band, is now the factor that limits precise absolute frequency measurements. Pure liquid indene, with camphor and cyclohexanone as additives, has recently been proposed as a suitable and convenient liquid calibrant for low resolution spectrophotometers,[18] and Jones *et al.*[19] have remeasured the 80 absorption bands in this spectrum (600–4000 cm^{-1}) under high resolution, determining the band centers with uncertainties ranging from ± 0.2 cm^{-1} for relatively sharp bands at long wavelengths to ± 3 cm^{-1} for very broad bands at shorter wavelengths.

As a first step in examining the question of absolute frequency accuracy in the spectra of condensed phases without the use of the fiducial system, the reproducibility limit of manual indexing of the wave number dial to the chart paper grid was investigated. For ten independent spectra begun at 600 cm^{-1} according to the dial, the fiducial system showed a precision of ± 0.04 cm^{-1} (maximum deviation from the mean) in the initial setting. In the fourth order, ten independent settings to 3399 cm^{-1} gave a precision of only ± 0.11 cm^{-1} (maximum deviation from the mean) for the initial setting. This order of precision can only be obtained if backlash is carefully eliminated in both monochromator and recorder drive mechanisms.

The double-beam indene–camphor–cyclohexanone spectrum was examined without the fiducial marking system at a scanning speed of 8 cm^{-1}/min, an amplifier gain of 5%, a filter period of 8 sec, and abscissa expansions of 20 and 25 cm^{-1}/in. The recorder pen and wave-number dial were carefully indexed at the beginning of each grating order. Measurements based on the inch-calibrated chart paper grid were corrected according to Figs. 2, 3, and 4 and as already described. The results are presented graphically in Fig. 5. Most of the present measurements fall within the uncertainty limits proposed by Jones *et al.*[19] No doubt the agreement could be improved still further by averaging the results of several independent determinations.

Some measurements on polystyrene film, using the data of Plyler *et al.*[11] and the above procedure, except that the chart paper was carefully indexed at 600 cm^{-1} according to the wave-number dial and the four orders scanned automatically, corroborated the indene results. The repositioning of the optical elements and the recorder pen relative to the chart grid lines in a higher order following an automatic order change is sufficiently precise to permit measurements with an accuracy of 0.5–1.0 cm^{-1}, provided the measured values are corrected as described.

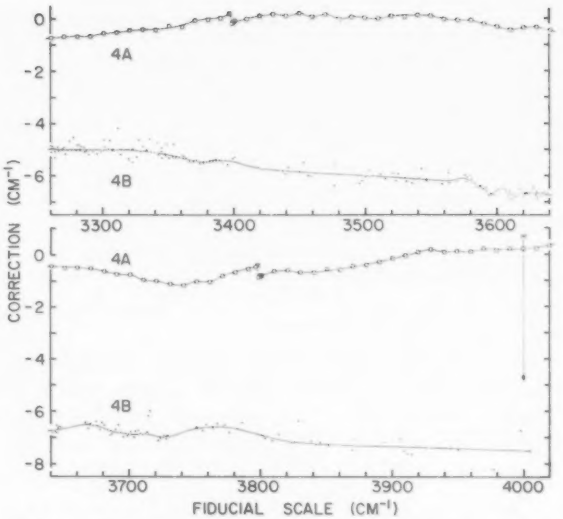

Fig. 4. Correction to be applied to dial wave-number read out (B − A) and fiducial scale values (B) to give absolute frequency (cm^{-1}) for the range 3260–4000 cm^{-1}.

VII. Conclusion

This investigation has demonstrated:

(a) the high-frequency reproducibility inherent in the design of the Beckman IR-7 infrared spectrophotometer,

(b) the operation of a fiducial marking system to overcome the difficulty of accurately reading out frequencies,

(c) that an infrared spectrophotometer nominally linear in frequency, and using a cam system, is capable of accurate frequency measurements by the conventional calibration curve, interpolation, or superposition methods,[9]

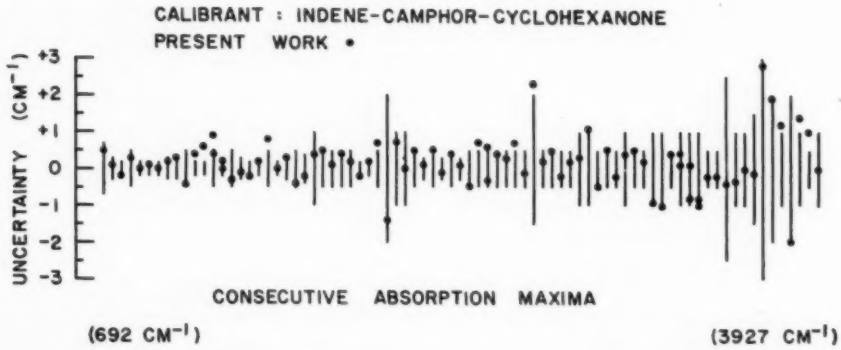

Fig. 5. Comparative presentation of liquid calibrant measurements with uncertainties in absolute frequencies as determined by Jones *et al.*[19]

(d) that for less exacting measurements on relatively broad bands, the correction curves for the wave number dial obtained with the fiducial system produce satisfactory results without it, and

(e) that more routine use of a spectrophotometer like this is compatible with maintenance of a reliable calibration.

The author gratefully acknowledges the assistance of R. N. Jones in providing the indene samples and some calibration data in the early stages of this work.

References

1. S. Mizushima and colleagues, "A report on the Perkin-Elmer grating spectrophotometer model 112 G," Tokyo University, Hongo, Tokyo, Japan. English translation by Perkin-Elmer Corp., Norwalk, Conn. (1959).
2. Bulletin 439-B, "IR-7 prism-grating infrared spectrophotometer." Beckman Instruments, Inc. (1960).
3. Bulletin on Model 421 Infrared Spectrophotometer, Perkin-Elmer Corporation (1961).
4. R. N. Jones, "Spectroscopic calibration standards," in Perkin-Elmer Instrument News **2**, No. 1a, 1 (1960).
5. "IR-7 infrared spectrophotometer instruction manual," Beckman Instruments, Inc. (1960).
6. P. J. Krueger and G. H. Schulze, to be published.
7. P. J. Krueger and G. H. Schulze, to be published.
8. P. J. Krueger, to be published.
9. International Union of Pure and Applied Chemistry Commission on Molecular Structure and Spectroscopy, *Tables of Wavenumbers for the Calibration of Infra-Red Spectrometers* (Butterworths, London, 1961). Reprinted from Pure and Appl. Chem. **1**, 537–699 (1961).
10. J. Pickworth and H. W. Thompson, Proc. Roy. Soc. (London) **A218**, 37 (1953).
11. E. K. Plyler, A. Danti, L. R. Blaine, and E. D. Tidwell, J. Research Natl. Bur. Standards **64**, 29 (1960).
12. E. E. Bell and H. H. Nielsen, J. Chem. Phys. **18**, 1382 (1950).
13. M. T. Christensen, D. R. Eaton, B. A. Green, and H. W. Thompson, Proc. Roy. Soc. (London) **A237**, 15 (1956).
14. A. Levin and C. F. Meyer, J. Opt. Soc. Am. **16**, 137 (1928).
15. H. W. Thompson and R. L. Williams, Proc. Roy. Soc. (London) **A220**, 435 (1953).
16. Hs. H. Günthard, R. C. Lord, and T. K. McCubbin, Jr., J. Chem. Phys. **25**, 768 (1956).
17. J. S. Garing, H. H. Nielsen, and K. N. Rao, J. Mol. Spectroscopy **3**, 496 (1959).
18. R. N. Jones, P. K. Faure, and W. Zaharias, Rev. universelle mines **15**, 417 (1959).
19. R. N. Jones, N. B. W. Jonathan, M. A. MacKenzie, and A. Nadeau, Spectrochim. Acta **17**, 77 (1961).

Information for Contributors

Scope: Papers are welcomed in the broad areas of applied optics, in disciplines related to optics and employing optical techniques. Papers should be sent to *The Editor, APPLIED OPTICS, 1155 Sixteenth St., N.W., Washington 6, D.C.* Manuscripts may be submitted in English, French, German, or Russian, and the presentation should be as succinct as comprehension will permit. In general, the metric system of units is preferred. One original and one carbon of the manuscript, with two sets of all illustrations, must be sent. Manuscripts should be typed double or triple spaced on one side of 22 × 28 cm (8½ × 11 in.) paper, leaving a 3.8 cm (1½ in.) margin all round.

An **abstract,** adequate as an index and summary, of not more than 100 words should appear at the beginning of the paper after the *title, author's name, affiliation, and address.* In the case of papers in a non-English language, they must be accompanied by an abstract in English as well as an abstract in the language of the paper.

Figures suitable for printer's use should be sent. Bear in mind that illustrations will normally be reduced to column width (8.4 cm—3⅜ in.—20 picas). *Halftones:* two sets of glossy prints are needed, which should be mailed flat, with any proportion or framing indicated on a working copy. *Line drawings* should be suitable for reproduction and be not larger than 22 × 28 cm (8½ × 11 in.). *Captions* should be listed on a separate sheet in addition to each caption appearing on each illustration.

Tables should be typed on separate sheets and the data therein be intelligible, by title, without reference to the text. Tables should include a minimum of vertical ruling.

References must be typed on a separate sheet, be numbered consecutively in the order of their appearance in the text, and follow this form:

1. F. C. Brown, Phys. Rev. **12**, 345 (1821).
2. J. Culpeper, *Space Optics* (Georgetown Institute of Technology Press, Washington, D.C., 1861) pp. 012, 345.

A list of abbreviations for the names of journals is published in the American Institute of Physics *Style Manual.* To make for uniformity of presentation generally, the *Style Manual,* second edition, should be used.

No **galley proofs** will be sent to authors; all proofreading will be done in the house. Therefore, an author will not see his paper from the time it is accepted and any alterations agreed between Editor and author, until it appears in print.

Letters to the Editor should follow the above suggestions, but no abstract is required.

ICO SIXTH CONGRESS
MUNICH AUGUST 19–26 1962
IMAGE FORMATION AND VISION
INTERNATIONAL COMMISSION OF OPTICS

The International Commission of Optics will hold its 6th Congress in Munich August 19–26. An invitation is extended, by the German Optical Committee, the German Association for Applied Physics and the German Physical Society, to all scientists and research workers working in optics and its related fields, to take part. The theme of the 6th Congress is **IMAGE FORMATION AND VISION**, and in view of the current progress and development of research in these fields, particular emphasis will be given to:

Image structure and image receivers
Behavior of the visual organ in relation to perception

There will be some ten general papers, including:

Image formation without silver (Eggert, Switzerland)
Fiber optics (Snitzer, USA)
Theoretical and experimental bases of lasers (Haken, Germany)
Photochemistry of the retina and its significance for the visual process (Rushton, Gt. Britain)
Light receptors in the animal kingdom (Autrum, Germany)
Psychological problems of optical perception (Metzger, Germany)

Shorter papers will include those on

Nonlinear systems (Ingelstam, Sweden)
Photometry of optical instruments (Hansen, Germany)
Magnetic image formation (Oosterkamp, Netherlands)
Electrophysiological studies on eye movements (Bouman, Netherlands)
Fiber optics (Van Heel, Netherlands)
Stimuli in vision (Kelly, USA)
Definition of the optical image (Ronchi, Italy)
Power of the eye in relation to vision and thermal hazards (Weale, Gt. Britain)

Since physical as well as physiological, biological, and psychological problems will be discussed, a large number of participants is expected. Papers may be presented in English, French, or German. No plans have been made for publication of the proceedings; individual papers will be published in the usual way in the journals.

Notification of attendance should be sent to and full information obtained from Prof. Dr. Dr. H. Schober, 6. ICO-Kongress, Arnulfstr. 205(AEG-Haus), Munchen 19, Germany.

The OPTICAL SOCIETY OF AMERICA has no other information than this.

Fundamental Principles and Methods for the Calibration of Radiometers for Photometric Use

A. K. Ångström and A. J. Drummond

If a photocell is calibrated by means of a source of known spectral energy distribution, employment of the cell for the measurement of the illumination produced by another source of different energy distribution will entail correction of the initial calibration constant. The basic principles for obtaining such a correction factor, applicable for the general case, of wavelength selective receivers, are set out in this paper. As an example, the case is discussed in detail of deriving the natural illumination flux from radiometric measurements of solar shortwave radiation with the aid of current standard meteorological filters. Equations are presented from which the illumination can be computed from known values of the air mass (i.e., optical path length) and the atmospheric turbidity. These equations have been applied to a comprehensive series of measurements of illumination and shortwave radiation assembled in South Africa. It is shown that the equations are valid over very wide ranges of air mass and turbidity.

Introduction

With regard to many investigations within radiometry the technical problem is that of measuring the energy, effective in some special respect, emitted by a given source. As an example, let us consider here the case of illumination.

The curve representing the responsivity of the human eye has, as is well known, a maximum at about 555 mμ, around which there is a rather symmetrical fall off on both sides to zero values at practically 400 and 700 mμ. Putting the responsivity arbitrarily equal to 100 at the maximum, we get the distribution curve $\varphi(\lambda)$ shown in Fig. 1. Here every ordinate corresponds to equal amounts of energy. We denote the responsivity, as a function of wavelength, by $\varphi(\lambda)$. For a given source of light, the illumination through an elementary surface (E), expressed, for example, in lux, is defined by the integral

$$E = c \int_0^\infty \varphi(\lambda) F(\lambda) d\lambda, \tag{1}$$

where $F(\lambda)$ is the energy flux at the illuminated plane (in watts or calories) with respect to wavelength λ. The constant c is independent of the source, i.e., it is independent of $F(\lambda)$. Let us denote the area representing the integral by A. We then have

$$E = c \cdot A. \tag{2}$$

Let us now suppose that an instrument, the responsivity of which varies exactly in proportion to that of the human eye, is exposed to a known luminous flux. At the location of the receiving instrument, the output parameter of the latter, δ, may be found to be proportional to E, which implies

$$E = k \cdot \delta, \tag{3}$$

where k is a constant. With these assumptions, the instrument, after calibration in the named way, may be used for determining the illumination through any plane from any source of light.

Suppose now that the responsivity of the instrument is a wavelength function which is not proportional for various wavelengths to the responsivity of the eye. The former characteristic may be expressed by the function $f(\lambda)$, and what the instrument actually responds to is now the integral

$$\int_0^\infty f(\lambda) F(\lambda) d\lambda = B. \tag{4}$$

We have

$$h \cdot \delta = B, \tag{5}$$

where δ, as before, is the instrument output parameter and h is a constant, *independent of the energy distribution within the spectrum of the source*. Also, for this case, after appropriate instrument calibration, we may write

$$E = k_0 \cdot \delta = c \cdot A, \tag{6}$$

where k_0 is a constant only as long as the relative energy distribution within the spectrum of the source remains constant.

A. K. Ångström is at the Eppley Foundation for Research, and A. J. Drummond is at the Eppley Laboratory, Inc., Newport, R.I.
Received 11 January 1962.

Now let the instrument be directed toward another source whose energy distribution is different from that of the source used for calibration. We have

$$E_1 = k_1 \cdot \delta_1 = c \int_0^\infty \varphi(\lambda) F_1(\lambda) d\lambda = c \cdot A_1 \tag{7}$$

and

$$h \cdot \delta_1 = B_1, \tag{8}$$

where

$$B_1 = \int_0^\infty f(\lambda) F_1(\lambda) d\lambda. \tag{9}$$

From (5) and (6), combined with (8) and (9), we derive

$$\begin{aligned} E &= k_0 \cdot \frac{B}{h} = c \cdot A, \\ E_1 &= k_1 \cdot \frac{B_1}{h} = c \cdot A_1, \end{aligned} \tag{10}$$

which gives:

$$k_1 = \frac{B}{A} \cdot \frac{A_1}{B_1} \cdot k_0. \tag{11}$$

These results may be summarized as follows: If a photometric receiver, whose responsivity is $f(\lambda)$, is calibrated by means of a source of given energy distribution $F(\lambda)$, then, where it is desired to determine the illumination of a surface irradiated by another source of different energy distribution $F_1(\lambda)$, the calibration constant of the photometer requires multiplication by the factor $(B/A) \cdot (A_1/B_1)$. In this instance,

$$\begin{aligned} A &= \int_0^\infty \varphi(\lambda) F(\lambda) d\lambda, \\ B &= \int_0^\infty f(\lambda) F(\lambda) d\lambda, \\ A_1 &= \int_0^\infty \varphi(\lambda) F_1(\lambda) d\lambda, \\ B_1 &= \int_0^\infty f(\lambda) F_1(\lambda) d\lambda. \end{aligned} \tag{12}$$

From a knowledge of the functions enumerated above, the values of the integrals may, in general, be conveniently evaluated graphically.

From (11) and (12) it is evident that it is the relative values of the functions $\varphi(\lambda)$, $f(\lambda)$, $F(\lambda)$, and $F_1(\lambda)$ which determine the correction to the calibration constant k_0 and that the absolute values at various wavelengths are immaterial. We may multiply all of these functions by a constant without changing the value of the correction factor.

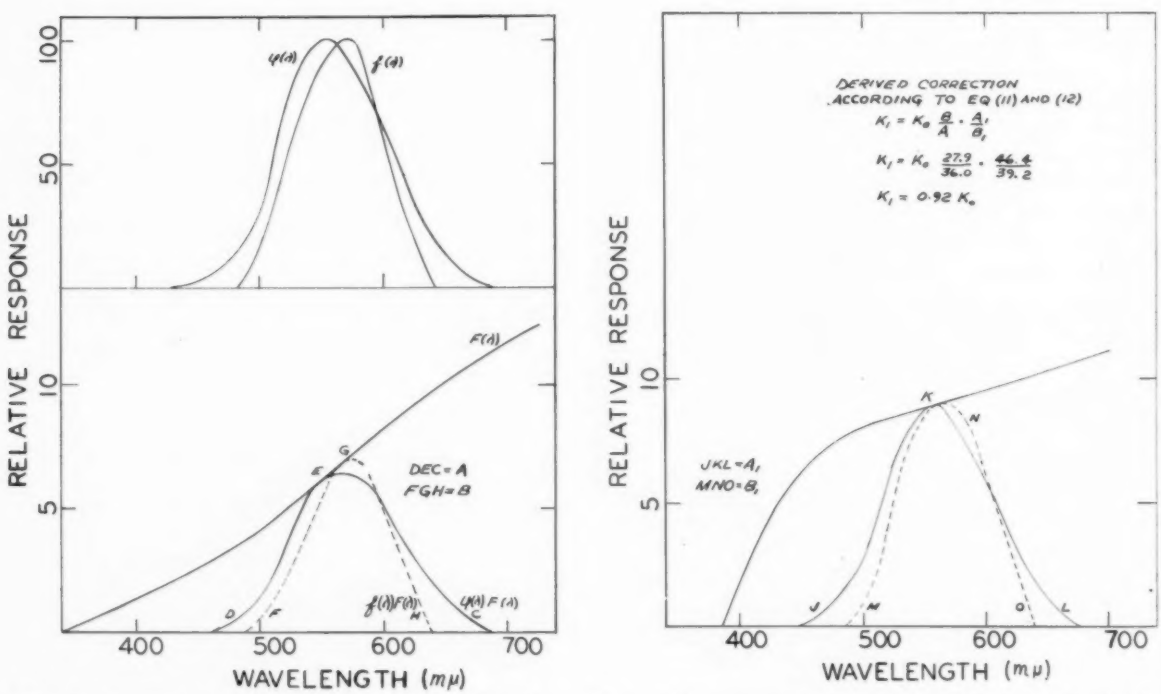

Fig. 1. Correction procedure for photometric calibrations. (Curve $\varphi(\lambda)$ represents the standard I.C.I. spectral luminosity distribution for the human eye, curve $f(\lambda)$ the relative spectral response of a filtered selenium photocell, curve $F(\lambda)$ the measured relative emission of a tungsten-filament calibration lamp, and $F_1(\lambda)$ the spectral energy distribution of the direct solar radiation corresponding to an air mass (m) value of 2.0 and an atmospheric turbidity (β) of 0.20.)

Applications

A. Calibration of Photometric Receivers

In practice, when high accuracy is aimed at in measurements of illumination, one generally tries to attain the closest possible coincidence between the relative spectral responsivity curves of the human eye and the photometer.

In many instances, this coincidence is so perfect that a correction for the spectral distribution of the source is scarcely justified, at least not in cases where the spectral emission of the source to be investigated is only approximately known. One of the authors has given[1] typical curves representing the relative spectral responsivity of two Weston selenium barrier-layer photocells specially filtered to match closely the International Commission on Illumination (I.C.I.) luminosity standard for photopic vision. If we consider the calibration of the two photocells to be undertaken with a tungsten-filament candlepower standard whose energy distribution may be regarded as corresponding to that of a blackbody at 3000°K, and that the cells shall be used afterwards for measuring natural illumination, the derived constant k_0 ought to be corrected in accordance with (11). The reference for the daylight source was an energy distribution curve based on actual measurements for specific conditions.[1] Through planimetric integration we find

(a) cell examined by manufacturer:

$$\frac{B}{A} = 0.993; \quad \frac{A_1}{B_1} = 0.989;$$

(b) cell examined by National Bureau of Standards:

$$\frac{B}{A} = 1.067; \quad \frac{A_1}{B_1} = 0.948;$$

which yields: $k_1 = k_0 \cdot 0.982$ (a) and $k_0 \cdot 1.012$ (b).

Thus, in the first instance, the calibration constant requires a correction of -2%. In the study referred to, a correction of -3% was derived for more general exposure conditions. Both values are probably within the limits of probable error, with due regard to various parameters which are incompletely known. The cases here referred to have been discussed in detail, in order to present an example of the practical application of the principles described. Other cases, however, frequently occur where the corrective factors are much larger and cannot be neglected. For instance, the case treated in detail in Fig. 1 refers to an actual, recent investigation at the Eppley Laboratory; the detector is a Leeds and Northrup illuminometer (selenium photocell sensor), the calibration source a National Bureau of Standards tungsten-filament candlepower standard, and the exposure source the sun (at air mass = 2.0, or solar height of 30°, and atmospheric turbidity $\beta = 0.20$, typical of urban conditions).

It should be noted that, in the above examples, the constant k relates the photometric flux with the instrument indication (e.g. lux/μa).

B. Relation between Natural Illumination and the Energy of Sun and Sky Radiation

Records of the natural illumination appear less frequently than is often required for satisfying biological, medical, architectural, and engineering demands. For instance, they seldom figure in routine observational programs undertaken in extended networks of meteorological and geophysical stations, such as those coordinated by the World Meteorological Organization. On the other hand, measurements of sun and sky radiation, with or without the application of filters subdividing the solar spectrum (e.g., Schott OG 1, RG 2, and RG 8 glasses),* are being introduced into national networks at a rapidly increasing rate, largely as a result of the recent International Geophysical Year. It is evident that measurements of the *energy transfer through radiation* are able to provide also a rather accurate evaluation of the *natural illumination*, if treated properly.[2]

Let us consider first the direct solar radiation. Let the energy distribution within its spectrum be expressed by $F(\lambda)$. Its luminous efficiency is then given by

$$\rho = \frac{\int_0^\infty \varphi(\lambda) F(\lambda) d\lambda}{\int_0^\infty F(\lambda) d\lambda}. \tag{13}$$

As the luminous radiation is confined to a part of the spectrum (400–700 mμ) where practically no selective absorption by the gases of the atmosphere occurs (as compared with the total radiation which is influenced by this factor) the coefficient of luminous efficiency, ρ, of the solar radiation is a function of water vapor absorption in the atmosphere, i.e., it is dependent on absolute humidity, air mass (optical path length), and height above sea level. In order to "translate" the energy radiation from the sun into units of illumination, we thus have to apply a factor which is not constant but varies from case to case. At stations near sea level the variation, however, seems, generally, to be within the limits $\pm 10\%$.

If we consider the energy of the solar spectrum which is confined to the integral $\int_0^{\lambda_m} F(\lambda) d\lambda$, where $\lambda_m < 700$ mμ, we may expect the ratio between the effective luminous radiation defined by the integral $\int_0^\infty \varphi(\lambda) F(\lambda) d\lambda$ and the former integral to be practically independ-

* Nominal center of lower cutoff at 530 (OG 1), 630 (RG 2), and 700 mμ (RG 8).

ent of the selective absorption within the atmosphere.* We denote this ratio by ρ_1 emphasizing at the same time that ρ_1 is different from ρ and defined by the equation

$$\rho_1 = \frac{\int_0^\infty \varphi(\lambda)F(\lambda)d\lambda}{\int_0^{\lambda_m} F(\lambda)d\lambda}. \qquad (14)$$

The "cutoff" filters mentioned above transmit, with a certain correction for reflection, the solar radiation totally above a given limit value, which we here may assume practically to coincide with the "center of cutoff."[3-5] If the transmitted radiation is subtracted from the total radiation (integral over-all wavelengths) measured on the same occasion, we obtain the shortwave radiation which, referred to the filters OG 1, RG 2, and RG 8, we denote by I_{o1}, I_{r2}, I_{r8} respectively.

We have:

$$I_{o1} = \int_0^{530} F(\lambda)d\lambda,$$
$$I_{r2} = \int_0^{630} F(\lambda)d\lambda, \qquad (15)$$
$$I_{r8} = \int_0^{700} F(\lambda)d\lambda.$$

Let us substitute in (14) the values of I_{o1}, I_{r2}, and I_{r8} given by (15) and investigate how ρ_1 varies with air mass and turbidity. The air mass, m, we give with the vertical air mass, at standard sea level pressure, as unit.[6] To define the turbidity we use the coefficient β.[7-9] In the following, however, our β-values are referred to the unit of air mass. Only for stations at or near sea level does β then coincide with the value β_0 referred to the vertical air mass. If the value of β_0 has been determined for a high-level station, we consequently have to multiply it by the ratio p_0/p, where p_0 and p are the air pressures at sea level and at the given station, respectively, in order to get the value of β, to which Figs. 2 and 3 refer. With these considerations in mind, the following derivations ought to be applicable within reasonable limits to all stations, independently of height above sea level.

Values of $F(\lambda)\Delta\lambda$ have now been computed by the present authors. In these computations we have started from the fundamental equation, earlier shown† to be practically valid for average cases of a clear sky, namely,

$$F(\lambda)\Delta\lambda = I_0(\lambda)\Delta\lambda \cdot p_\lambda{}^m \cdot e^{-\delta m}, \qquad (16)$$

where $\delta = \beta/\lambda^\alpha$. Here $I_0(\lambda)$ is the solar constant within the wavelength interval $\Delta\lambda$. We have used the values computed by Nicolet,[10] with the adoption of a value 1.98 cal cm^{-2} min^{-1} for the solar constant, and with $\Delta\lambda$ = 100 Å. For the transmission factor p_λ of the Rayleigh scattering, we have accepted the values of Penndorf,[11] based upon the introduction of a depolarization factor of 1.061. Penndorf gives good reasons for preferring this value to the values 1.074 and 1.042, the former applied by Möller for tabular computations, and the latter proposed by van de Hulst.

The adoption of these transmission values as a means of defining the clear dust-free atmosphere implies that the transmission as a function of wavelength is somewhat higher than that derived by Fowle.[12] Fowle ascribed the deviation from the Rayleigh scattering of the transmission values, obtained on the summit of Mt. Wilson, to scattering by water vapor. The present authors are unable to accept Fowle's view on this matter and are also of the opinion that too much weight has been placed on what is essentially a short series of measurements at Mt. Wilson. As a consequence, the values of atmospheric turbidity based upon our considerations are higher than corresponding ones derived from the tables of Hoelper and Feussner (based upon Fowle's transmission data), which are partly tabulated in the IGY Instruction Manual.[13] The difference in turbidity is practically constant at 0.015. Where, for convenience, we have used the IGY tables, a correction of +0.015 has been applied to the β-values in order that our data shall be consistent throughout. Table I gives β as a function of shortwave radiation, λ<700 mμ.

Table I. The Dependence of Sunlight Illumination (Kilolux), on a Surface Perpendicular to the Rays, on Air Mass and Turbidity, for Mean Solar Distance

β^m	0	1.00	1.25	1.50	1.75	2.0	3.0	4.0	6.0
0.000	142	119	115	112	109	106	93	84	69
0.050		105	99	93	87	83	66	54	37
0.100		93	85	78	72	66	47	35	20
0.150		83	73	66	59	53	34	23	11
0.200		73	63	55	47	41	24	15	6
h(°)		90	53	42	35	30	19	14	9

For α we have adopted the value α = 1.3, which is found to be an acceptable average value under clear-sky conditions. A variability of α, which seems probable, within the limits ±0.3, does not basically affect the following results.

We have computed the integrals $\int_0^{\lambda_m} F(\lambda)d\lambda \equiv \sum_0^{\lambda_m} F(\lambda)\Delta\lambda$, for values of λ_m equal to 530, 630, and 700 mμ, respectively. We have further computed the integrals $\int_0^\infty \varphi(\lambda)F(\lambda)d\lambda \equiv \sum_0^\infty \varphi(\lambda)F(\lambda)\Delta\lambda$, with respect to the values of air mass and turbidity. Here $\varphi(\lambda)$ is the

* A slight influence of the ozone absorption within the Chappuis band on ρ_1 is to be expected. The variations due to this effect must, in general, be below about ±2%.

† The value of the exponent α varies chiefly with the size of the scattering particles determining the extinction.

relative spectral luminosity for the human eye, according to the I.C.I. definition (see Fig. 1).

From the results of these computations, values of ρ_1 are derived. Figure 2 shows ρ_1 in its dependence on air mass and turbidity, for the radiation integrals corresponding to the three Schott filters OG 1, RG 2, and RG 8. It may be derived, from the figure, that

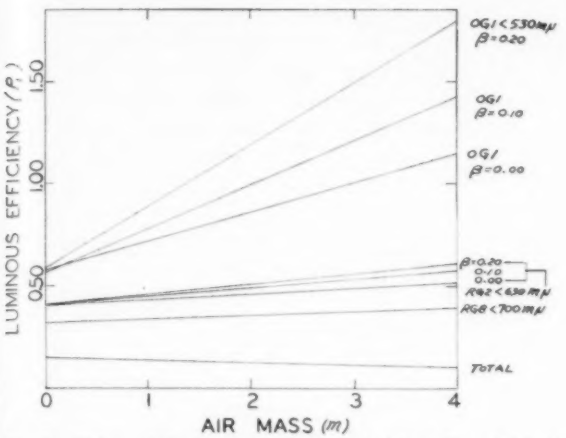

Fig. 2. Values of the luminous efficiency (ρ_1) for different Schott filters, at different air masses (m) and turbidities (β).

there is a very pronounced dependence of ρ_1 on air mass as well as on turbidity in the case of the shortwave radiation $\lambda<530$ mμ. This is naturally to be expected as the integral up to 530 mμ only covers a part of the integral $\int_0^\infty \varphi(\lambda)F(\lambda)d\lambda$. In the case of $\lambda_m<630$ mμ, corresponding to the radiation values obtained by means of the RG 2 filter, the dependence of ρ_1 on air mass and turbidity is much less pronounced but is yet clearly brought out.

The efficiency of the total radiation below λ_m = 700 mμ is considerably less than for the other wavelength integrals, but on the other hand, as is seen from the figure, ρ_1 shows here much less of a dependence on air mass and turbidity. In fact, if one observes a small dependence on air mass, no additional correction for turbidity need be applied. The values of ρ_1 for air masses 1.0 and 4.0, corresponding to solar elevations of 90° and 15°, are 0.345 and 0.380, respectively; and if a mean value of 0.36 is adopted, the variations from this value with solar height are less than ±5%, the value itself increasing slightly with decreasing height of the sun. This seems to suggest a rather important application as it implies that the differential radiation

$$\int_0^\infty F(\lambda)d\lambda - \int_{700}^\infty F(\lambda)d\lambda = \int_0^{700} F(\lambda)d\lambda \qquad (17)$$

can be taken as a measure of the illumination, and that if the proper factor is applied to the radiation values, a value ought to be obtained for the illumination, which for most practical purposes is of sufficient accuracy (±5%). For the luminous efficiency, ρ_1, of the shortwave radiation obtainable by means of the various filters, we derive:

$$\begin{aligned} &\text{OG 1: } \rho_1 = 0.58(1 + 0.235m + 1.19m\beta),\\ &\text{RG 2: } \rho_1 = 0.39(1 + 0.073m + 0.305m\beta),\\ &\text{RG 8: } \rho_1 = 0.315(1 + 0.032m). \end{aligned} \qquad (18)$$

If we multiply the energy values, W, obtained by means of the various filters, with ρ_1 we obtain a measure of the luminous flux. We have, with reference to (14),

$$\rho_1 \cdot W = \int_0^\infty \varphi(\lambda)F(\lambda)d\lambda \simeq E, \qquad (19)$$

where

$$W = \int_0^{\lambda_m} F(\lambda)d\lambda. \qquad (20)$$

If W is given in cal cm^{-2} min^{-1}, the factor K_{max} with which the integral of (19) should be multiplied in order to give the luminous flux, in kilolux, is 475 (compare *Smithsonian Meteorological Tables*, 1951, page 449). We thus have

$$E = 475 \cdot \rho_1 \cdot W. \qquad (21)$$

Introducing for W the extraterrestrial values computed from the tables of Nicolet,[10] we obtain for the luminous flux of the extraterrestrial sun radiation

$$\begin{aligned} &\text{OG 1: } E = 475 \cdot 0.58 \cdot 0.509 = 140,\\ &\text{RG 2: } E = 475 \cdot 0.39 \cdot 0.787 = 146,\\ &\text{RG 8: } E = 475 \cdot 0.315 \cdot 0.948 = 142. \end{aligned} \qquad (22)$$

The three equations thus give a mean value for the extraterrestrial luminous flux of solar radiation of 142.5 kilolux, which is in good agreement with the value 141.5 computed directly from the extraterrestrial energy distribution [$475\int_0^\infty \varphi(\lambda)F(\lambda)d\lambda = 475 \cdot 0.298 = 141.5$ at $m = 0$, $\beta = 0$]. The difference between the two values is due to the fact that, in deriving linear relationships for the dependence of ρ_1 on air mass and turbidity, some sacrifice in the accuracy at individual points had to be made in order to obtain the general relationships.

We may use these results to compute the luminous flux of the direct solar radiation corresponding to different air masses (solar heights) and turbidities. Comprehensive tables are being prepared with this object in view and will be published elsewhere. Here we limit ourselves to giving an example (Fig. 3) showing the luminous flux on a horizontal surface of the direct solar radiation at different solar heights, and for turbidities $\beta = 0.00$, 0.10, and 0.20. The values are computed from the relevant equations for RG 2 and RG 8 [(18), (21)] and from (corrected) tables giving the corresponding radiation, W.[13]

Figure 3 also gives for comparison values of the illumination at different solar elevations derived from

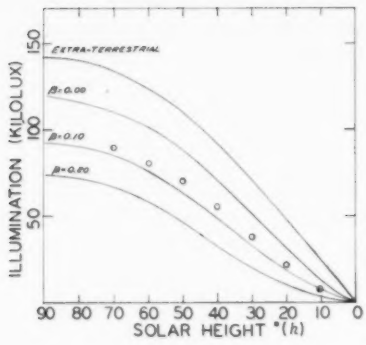

Fig. 3. Dependence of sunlight illumination of a horizontal surface at the ground, on solar height (h) and turbidity (β). (o values refer to computations, by Elvegård and Sjöstedt,[14] based on measurements mainly at Helsinki and Stockholm.)

values* given by Elvegård and Sjöstedt.[14] It is apparent that these values fall very closely along a curve of the same trend as ours. An interpolation between the β-curves suggests that the measurements correspond to a turbidity of about 0.08, with a slight rise in turbidity with increasing solar elevation.

A more extensive series of measurements of illumination has been reported from South Africa by one of the present authors.[2] The illumination due to direct solar radiation on a horizontal plane and corresponding to different seasons of the year for Pretoria (25° 45′ S, 1370 meters) have been derived from the last-named measurements. These values are plotted in Fig. 4. The highest values of the illumination by direct solar radiation occur in March (the South African fall) and December (summer); they coincide closely with the values of Elvegård and Sjöstedt, and thus correspond to a turbidity of 0.05 to 0.10. The September values are characterized by the highest turbidity. From the figure, it may be derived that the mean value of the turbidity is then close to 0.15 at noon (air mass = 1) and not less than about 0.10 at low solar elevations (air mass $\leq$ 3). It seems probable that over the South African high plateau the turbidity is subjected to a rather marked increase with increasing solar height, when the latter reaches a value between about 20 and 30°. It is reasonable to assume that the increase in turbidity is mainly due to a rapid increase in the convective transfer from the ground, caused by the pronounced heating of the lowest air layers. For convenience, computations of the direct sunlight illumination (i.e., at normal incidence) for mean solar distance, with reference to air mass and turbidity, are included in Table I. These data are the basis of the curves of Fig. 4.

* Strictly, computations on the basis of measurements by T. Aurén and H. Lunelund, mainly at Helsinki and Stockholm (about lat. 60° N).

C. Measurements of Illumination vs Radiation at Pretoria (lat. 25° 45′ S, alt. 1370 meters)

The very extensive series of observations undertaken at Pretoria provide an excellent means of assessing in detail the validity of our formulas, previously derived on the basis of general considerations. The Pretoria measurement program not only included continuous registration, on a horizontal surface, of the total daylight and, separately, the skylight photometric fluxes, but also, normal to the solar beam, of the total direct sun radiation and, simultaneously, of the spectral components defined by the Schott filters GG 7, GG 11, OG 1, RG 2, and RG 8. The specimens of RG 2 and RG 8 filters, the data for which will be discussed here, had lower cutoffs at 636 and 691 mμ, respectively.

Extracts from the mass of the Pretoria observational material, largely unpublished to date, are given in Tables II–IV. In each instance, in the several columns are tabulated (1) true solar time, (2) solar height, (3) true air mass (i.e., relative air mass corrected by the factor p/p_0, where p and p_0 are the respective mean barometric pressures at station level and M.S.L.), (4) turbidity coefficient β referred to absolute air mass 1.0 (i.e., to relative air mass 1.16 at Pretoria), (5) total daylight on a horizontal surface, (6) skylight on a horizontal surface, (7) sunlight illumination normal to the solar beam, E_0 (derived from the relationship, sunlight = (daylight − skylight)/(sin solar height), (8) solar radiation intensity within the spectral region 0–630 mμ (i.e., $I_t - I_{r2}$) normal to the solar beam, and (9) solar radiation intensity within the spectral region 0–700 mμ (i.e., $I_t - I_{r8}$) normal to the solar beam.

Columns 10 and 11 present the corresponding illumination fluxes computed from Eq. (21). They refer, respectively, to RG 8 (E_1) and RG 2 (E_2). It is evident from the tables that, as was anticipated, there is close agreement between the E_1 and E_2 sets of computations

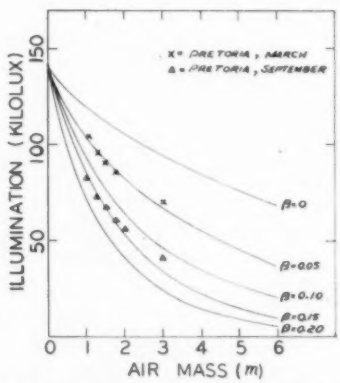

Fig. 4. Dependence of sunlight illumination of a surface perpendicular to the solar beam at the ground on air mass (m) and turbidity (β). (x and Δ values refer to the Pretoria series of measurements.)

Table II. Comparison between Measured (E_0) and Computed (E_1 and E_2) Values of Illumination at Pretoria (25° 45′ S, 1370 meters) During a Period of Relatively Low Atmospheric Turbidity at the End of the Wet Season

March 1955 Day	TST	Solar height (deg)	m	$\beta \cdot 10^3$	D	S (kilolux)	$\frac{D-S}{\sin h} = E_0$	$I_t - I_{rs}$ (mcal cm^{-2} min^{-1})	$I_t - I_{r2}$	E_1 (kilolux)	E_2	$E_1 - E_0$ (kilolux)	$E_2 - E_0$
16	7.30	21.1	2.35	72	33.8	6.9	75	443	333	72	75	−3	0
	9.30	46.6	1.18	100	82.4	10.9	98	570	446	89	91	−9	−7
	13.30	57.4	1.01	122	95.0	10.1	101	587	450	91	94	−10	−7
	15.30	34.1	1.51	90	55.3	8.0	85	530	407	84	86	−1	+1
20	7.30	20.3	2.44	112	30.9	9.7	61	355	255	58	59	−3	−2
	9.30	45.7	1.19	125	79.5	13.8	92	535	407	83	85	−9	−7
	11.30	62.6	0.95	107	105.2	12.8	104	618	475	96	98	−8	−6
	13.30	56.1	1.02	97	95.5	10.6	102	618	475	96	98	−6	−4
	15.30	33.4	1.54	83	57.2	9.1	87	545	412	86	87	−1	0
26	13.30	54.8	1.04	83	94.2	11.1	102	628	485	97	99	−5	−3
	15.30	32.1	1.59	77	53.1	8.6	84	535	406	84	86	0	+2
27	7.30	19.0	2.60	77	31.4	7.6	73	406	299	66	69	−7	−4
	9.30	44.5	1.21	80	79.3	9.8	99	597	460	93	96	−6	−3
	11.30	60.3	0.98	79	103.3	8.8	109	643	500	100	102	−9	−7
	13.30	54.6	1.05	78	91.6	8.7	102	633	490	98	100	−4	−2
	15.30	31.9	1.60	65	53.0	7.4	86	556	426	87	90	+1	+4
28	9.30	44.3	1.22	82	78.0	8.8	99	597	455	93	94	−6	−5
	11.30	60.1	0.98	85	103.8	11.1	107	639	490	99	100	−8	−7
	13.30	54.4	1.05	82	92.0	9.5	101	623	485	97	99	−4	−2
	15.30	31.7	1.63	71	53.5	8.3	86	545	412	86	87	0	+1
	Mean	43.3	1.41	88	73.4	9.6	92.6	560	428	87.7	89.7	−4.9	−2.9

Table III. Comparison between Measured (E_0) and Computed (E_1 and E_2) Values of Illumination at Pretoria (25° 45′ S, 1370 meters) During a Period of Relatively High Atmospheric Turbidity at the End of the Dry Season

September 1955 Day	TST	Solar height (deg)	m	$\beta \cdot 10^3$	D	S (kilolux)	$\frac{D-S}{\sin h} = E_0$	$I_t - I_{rs}$ (mcal cm^{-2} min^{-1})	$I_t - I_{r2}$	E_1 (kilolux)	E_2	$E_1 - E_0$ (kilolux)	$E_2 - E_0$
1	9.30	39.7	1.34	76	68.5	9.8	92	590	445	92	93	0	+1
	11.30	55.1	1.04	78	89.0	10.3	96	642	490	99	99	+3	+3
	13.30	48.9	1.13	65	79.9	9.0	94	642	495	99	100	+5	+6
7	7.30	17.1	2.88	92	25.3	9.1	55	350	240	57	57	+2	+2
	9.30	41.1	1.30	119	67.0	12.9	82	520	392	81	82	−1	0
	11.30	56.2	1.02	116	90.5	13.0	93	585	445	90	91	−3	−2
	13.30	50.6	1.10	116	79.4	13.6	85	565	431	87	89	+2	+4
12	9.30	42.6	1.26	178	66.1	19.2	69	438	328	68	70	−1	+1
	11.30	58.3	1.01	172	88.0	20.7	79	510	387	78	81	−1	+2
	13.30	52.4	1.08	167	77.3	19.5	73	488	377	74	79	+1	+6
	15.30	30.8	1.66	169	42.7	15.8	53	360	269	56	53	+3	0
20	7.30	19.4	2.55	110	27.5	9.5	54	355	240	57	56	+3	+2
	9.30	44.5	1.21	166	68.5	15.6	76	462	353	72	75	−4	−1
	11.30	61.1	0.97	165	91.6	16.5	86	540	402	83	83	−3	−3
	13.30	54.8	1.04	161	80.8	16.4	79	510	392	79	81	0	+2
	15.30	32.4	1.58	172	45.8	13.9	59	375	279	55	61	−4	+2
30	9.30	47.2	1.16	93	82.2	10.4	98	628	450	97	93	−1	−5
	11.30	64.7	0.94	120	102.5	13.4	99	637	455	98	92	−1	−7
	13.30	58.1	1.01	119	91.0	13.6	91	617	445	95	91	+4	0
	15.30	34.3	1.51	130	53.7	12.8	73	494	343	77	74	+4	+1
	Mean	45.5	1.34	129	70.9	14.2	79.3	540	383	79.7	80.0	+0.4	+0.7

and the actually observed illumination E_0. Indeed, on the basis of the means of all observations contained in the tables assembled here, $E_1/E_0 = 0.97 \pm 0.01$ and $E_2/E_0 = 0.99 \pm 0.01$. There is no evidence of the dependence of either ratio upon turbidity. The closer approximation to unity, on the whole, in the latter instance, results from the fact that the linear relationship derived from the basic computation for the dependence of the luminous efficiency on air mass fits the actual values corresponding to an air mass range of 0.9–1.5 slightly better than is the case in the equation derived for the RG 8 filter. The comparative constancy of the luminous efficiency of the shortwave radiation derived from the RG 8 filter measurements suggests, as we have already emphasized, that this filter is to be preferred to the RG 2 one for the derivation of

Table IV. Comparison between Measured (E_0) and Computed (E_1 and E_2) Values of Illumination at Pretoria (25° 45′ S, 1370 meters) During Periods of (a) Very High Atmospheric Turbidity (and Low Solar Height) and (b) Very Low Atmospheric Turbidity (and High Solar Height)

1955 Day		TST	Solar height (deg)	m	$\beta \cdot 10^3$	D	S (kilolux)	$\frac{D-S}{\sin h} = E_0$	$I_t - I_{rs}$ (mcal cm^{-2} min^{-1})	$I_t - I_{r2}$ (mcal cm^{-2} min^{-1})	E_1 (kilolux)	E_2 (kilolux)	$E_1 - E_0$ (kilolux)	$E_2 - E_0$ (kilolux)
August	17	9.30	35.9	1.45	320	46.2	23.1	40	226	152	35	35	−5	−5
		11.30	49.2	1.13	338	65.5	27.6	50	314	221	49	50	−1	0
		12.30	49.2	1.13	338	65.2	27.1	51	324	230	50	52	−1	+1
		13.30	44.5	1.21	360	57.1	26.0	45	278	196	43	45	−2	0
		14.30	35.9	1.45	347	44.2	22.7	37	231	157	36	37	−1	0
	31	9.30	39.2	1.35	271	53.5	22.0	50	340	245	53	55	+3	+5
		11.30	53.5	1.06	270	76.1	25.7	63	386	284	58	62	−5	−1
		12.30	53.5	1.06	270	76.5	25.4	63	407	304	63	66	0	+3
		13.30	48.2	1.14	283	67.4	25.0	57	350	260	55	57	−2	0
		14.30	39.2	1.35	287	53.3	23.1	48	288	218	45	49	−3	+1
	(a)	Mean	44.8	1.23	308	60.5	24.8	50.4	314	227	48.7	50.8	−1.7	+0.4
November	6	11.30	76.4	0.88	105	116.0	8.5	109	700	490	108	(100)	−1	(−9)
		12.30	76.4	0.88	101	116.2	8.9	109	689	485	106	(98)	−3	(−11)
December	2	11.30	80.9	0.86	121	118.6	10.3	110	679	480	104	(98)	−6	(−12)
		12.30	80.9	0.86	109	118.1	9.6	110	694	500	107	102	−3	−8
		13.30	69.0	0.91	117	109.0	9.5	107	663	475	102	(96)	−5	(−11)
	11	11.30	81.7	0.86	106	119.0	9.0	111	693	500	106	102	−5	−9
	(b)	Mean	77.5	0.87	110	116.1	9.3	109.3	586	488	105.5	99.3	−3.8	−10.0

Table V. Radiation Intensity of the Sun (mcal cm^{-2} min^{-1}) in Relation to Air Mass and Turbidity for the Spectral Band Isolated by the Standard RG 8 Filter ($I_t - I_{rs} = \int_0^{700} F(\lambda) d\lambda$)[a]

$\beta \cdot 10^{3\alpha m}$	0	1.0	1.25	1.50	1.75	2.0	3.0	4.0	5.0	6.0
0	948	771	742	716	698	662	569	499	436	387
25		726	688	652	619	588	479	396	333	282
50		682	638	596	559	522	404	321	256	206
75		642	592	546	505	466	342	260	196	152
100		604	549	500	455	415	290	208	148	111
125		557	510	460	413	370	246	168	114	81
150		535	475	421	371	330	200	136	90	60
175		503	445	386	337	295	180	110	68	45

[a] The results are expressed in the International Pyrheliometric Scale, 1956, in accordance with the solar spectrum derived by Nicolet.[10] From this table values of the direct solar illumination (E), in kilolux, as well as β can be obtained by application of Eqs. (18) and (21), viz., $E = 149\ (1 + 0.032m) \cdot W$ when W is given in cal cm^{-2} min^{-1}.

illumination values from absolute radiation measurements.

The excellent agreement between observation and computation (see also Fig. 5*) is particularly gratifying for values of turbidity in excess of 0.30 as the constants of (18) were originally derived from computations restricted to the range $\beta < 0.20$. It is thus clear that the linear formulas derived here can be expected to be valid, for all practical applications, over most ranges of atmospheric conditions. In Table V values of the direct solar radiation are presented, in relation to air mass and turbidity, for the spectral bands isolated by the standard RG 8 filter in accordance with Nicolet's solar spectrum.[10] From these data, generalized figures for the corresponding solar illumination may be obtained by application of Eqs. (18) and (21).

Calibration of Radiometers When Used for Photometric Measurements

It has been demonstrated that when radiometers intended, primarily, for absolute measurement of the radiation income from sun and sky are provided with a suitable filter (such as Schott RG 8), they may be used for the determination of illumination, through the application of a given factor ρ_1 to the radiation values. However, it seems appropriate to describe briefly a method for calibrating radiometers, to be used in this manner, with a known source of illumination. Such a

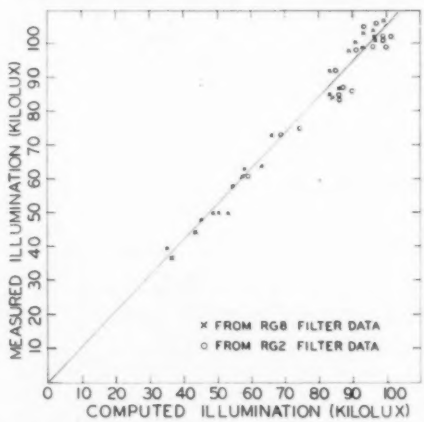
MEASURED ILLUMINATION (KILOLUX)
COMPUTED ILLUMINATION (KILOLUX)
0 10 20 30 40 50 60 70 80 90 100
× FROM RG8 FILTER DATA
○ FROM RG2 FILTER DATA

Fig. 5. Comparison between measured and computed values of illumination of a surface perpendicular to the solar beam, at Pretoria, for March and September 1955.

* On practical grounds, the data reproduced in Fig. 5 do not represent the entire mass of data treated.

calibration may serve to check data derived indirectly on the basis of established laws for atmospheric scattering.

Let the instrument be directed at a light source producing a known illumination flux through the plane of the exposure of the receiver. Let measurements be taken with and without the RG 8 filter, from which the value of $\int_0^{700} F(\lambda)d\lambda$ may be computed. For the given source, we have

$$E = k_0 \int_0^{700} F(\lambda)d\lambda. \tag{23}$$

Now, if the radiometer is to be used for determining the natural illumination, it will be necessary to apply another constant k_1 which, according to (11) given above, is related to k_0 by the equation:

$$k_1 = \frac{B}{A} \cdot \frac{A_1}{B_1} \cdot k_0. \tag{24}$$

As $f(\lambda)$ in (12) is constant and equal to unity, we therefore have

$$\begin{aligned} A &= \int_0^{\infty} \varphi(\lambda)F(\lambda)d\lambda, \\ B &= \int_0^{700} F(\lambda)d\lambda, \\ A_1 &= \int_0^{\infty} \varphi(\lambda)F_1(\lambda)d\lambda, \\ B_1 &= \int_0^{700} F_1(\lambda)d\lambda. \end{aligned} \tag{25}$$

For A_1/B_1 we have previously derived the equation [see (14)]

$$\frac{A_1}{B_1} = \rho_1 = 0.315(1 + 0.032m), \tag{26}$$

where m is the air mass value.

For the case of one of the photometric substandards (tungsten-filament lamp) maintained at the Eppley Laboratory, the relative spectral emission of which is known, we have computed

$$\frac{B}{A} = 2.88 \tag{27}$$

which gives

$$k_1 = k_0 \cdot 0.92(1 + 0.032m). \tag{28}$$

It is evident that the energy distribution of the tungsten lamp, in relation to the response curve of the human eye, is such that only a slight correction need be applied to the basic calibration constant k_0. This type of calibrating source is thus a very satisfactory one for the purpose of determining natural illumination. Where illumination measurements are restricted to a range of air mass of 1.0–4.0 (viz., to solar heights of between about 90 and 15°), the value of k_1 differs from k_0 by no more than ±5%. This implies that, for most practical purposes, we may employ the calibration constant unaltered in such determinations.

Summary

In the previous sections of the present paper the authors have attempted to set out the basic principles for calibrating photometric receivers. Methods are introduced for deriving illumination parameters from current measurements of solar radiation employing glass filters (especially the RG 2 and RG 8 types). Up to the present, the determination of illumination has been chiefly confined to measurements made with the aid of photoelectric cells, the sensitivity function of which is not always accurately known. It therefore seemed important that a technique be originated for correlating photometric values with the results of absolute measurements which are now obtainable using radiometers of high accuracy, such as the Ångström electrical compensation pyrheliometer, the Smithsonian silver disk pyrheliometer, and the Eppley (normal incidence) pyrheliometer and precision pyranometer.

In the literature, values of the natural illumination are frequently presented simply in their relation to solar height.[14] The very pronounced influence of atmospheric turbidity has either been totally neglected or taken into account only indirectly. It is clear from the results presented in this paper that, at a specific solar height, the illumination in the solar beam may vary by more than ±20%, in accordance with the turbidity. From the South African data it can also be derived that a corresponding variation of about ±10% occurs in the total illumination from sun and sky, on account of the variation in turbidity.

It now appears to be possible substantially to advance our knowledge of the illumination conditions in different locations at the earth's surface, employing the existing measurements of solar radiation evaluated within the framework of the World Meteorological Organization.

It is a pleasure to acknowledge that the observational material which has enabled the theory presented here to be adequately tested was assembled by one of the authors (A. J. D.) under the authority of the South African Weather Bureau.

References

1. A. J. Drummond, Arch. Meteorol., Geophys. u. Bioklimatol., Ser. B, **7**, 437 (1956).
2. A. J. Drummond, Arch. Meteorol., Geophys. u. Bioklimatol., Ser. B, **9**, 149 (1958).
3. A. K. Ångström and A. J. Drummond, J. Opt. Soc. Am. **49**, 1096 (1959).
4. A. K. Ångström and A. J. Drummond, J. Opt. Soc. Am. **50**, 974 (1960).
5. A. K. Ångström and A. J. Drummond, J. Meteorol. **18**, 360 (1961).

6. Robert J. List, *Smithsonian Meteorological Tables*, 6th revised ed. (Smithsonian Institution, Washington, 1951), p. 422.
7. A. K. Ångström, Geogr. Ann. **11**, 156 (1929).
8. A. K. Ångström, Geogr. Ann. **12**, 130 (1930).
9. A. K. Ångström, *Compendium of Meteorology* (American Meteorological Society, Boston, 1951), p. 50.
10. *Linke's Meteorologisches Taschenbuch* (Geest and Portig, Leipzig, 1953), Vol. 2, Table 95, p. 508.
11. R. Penndorf, J. Opt. Soc. Am. **47**, 176 (1957).
12. L. B. Aldrich and W. H. Hoover, *Annals of the Astrophysical Observatory* (Smithsonian Institution, Washington, 1954), Vol. 7 and previous volumes.
13. *IGY Instruction Manual, V, Part VI, Radiation Instruments and Measurements* (Pergamon Press, London, 1958), Table 7, p. 464.
14. E. Elvegård and G. Sjöstedt, Gerlands Beitr. z. Geophys **56**, 41 (1940).

Books Received

Reviews of some of these titles will appear in subsequent issues

Methods of Mathematical Physics, Vol. II: Partial Differential Equations, by Courant and Hilbert. Wiley, New York, 1962.

Advances in Spectroscopy, Vol. II, ed. H. W. Thompson. Wiley-Interscience, New York, 1962.

Introduction to Practical Infrared Spectroscopy, by A. D. Cross. Butterworths, London, 1960.

Polarized Light, by W. Shurcliff. Harvard U. Press, Cambridge, Mass., 1962.

Atomic Spectra, by H. G. Kuhn. Academic Press, New York, 1962.

Contents of Optics and Spectroscopy

VOL. XII, MAY 1962. *This issue will be published in complete translation by the Optical Society of America in August.*

MONTHLY—per year $15.00 **Single copies $3.00**

O. S. Pavlichenko and L. A. Dushin. Spectroscopic Study of Plasma in Phillips' Pulse Discharge

L. A. Gribov and E. M. Popov. Electro-Optical Parameters of Polyatomic Molecules and Their Calculation from the Experimental Data on Intensities and Polarization in Infrared Absorption Spectra

I. F. Kovalev. Calculation of Intensities in the Infrared Spectra of Molecules of the Type XY_3ZV_3. Methyl-Trichlorosilane

N. G. Bakhshiev. Universal Molecular Interactions and Their Effect on the Position of Electronic Spectra of Molecules in Two-Component Solutions. IV

M. N. Alentsev and L. A. Pakhomycheva. Relation between Absorption and Luminescence Spectra and the Anti-Stokes Luminescence Yield

Yu. T. Mazurenko and B. S. Neporent. On the Relation between the Electronic Absorption and Luminescence Spectra of Complex Molecules

B. Ya. Sveshnikov and V. I. Shirokov. Change in the Mean Lifetime and Yield of Luminescence in the Process of Quenching as a Function of the Law of Molecular Interaction

N. G. Bakhshiev, V. P. Klochkov, B. S. Neporent, and A. S. Cherkasov. Absorption and Fluorescence of the Vapor of Anthracene and its Derivatives

T. V. Ivanova, G. A. Mokeeva, and B. Ya. Sveshnikov. Dependence of the Fluorescence of Benzene, Toluene, and *p*-Xylene Solutions on the Concentration of Fluorescent Substance

V. L. Levshin and Kh. I. Mamedov. Fluorescence and Absorption Spectra of Stilbene in Octane at Low Temperatures

Yu. V. Morozov, Yu. I. Naberukhin, and G. V. Gursky. Effect of the Crystallization of Solvent on the Luminescence of Dyes

M. Z. Maksimov and I. M. Rozman. On the Energy Transfer in Rigid Solutions

I. S. Gorban' and S. N. Rudko. Absorption and Photoluminescence Spectra of HgJ_2 Crystals

B. P. Zakharchenya and A. I. Sibilev. Magneto-Optical Study of Crystals in Strong Magnetic Pulse Fields. I

Chjan Guan-in. Dispersion Shift of Discrete Absorption Bands in Uniaxial Crystals

M. T. Kostyshin and P. F. Romanenko. Dispersion of Certain Semiconductors in the Region of Absorption Bands

A. N. Oraevsky. Absorption and Dispersion in Molecular Crystals with the Saturation Effect Taken into Account

I. V. Krylova, A. S. Shashkov, and N. I. Kobozev. Investigation of ZnS—Cu Crystal Phosphors by the Exoelectron Emission Method

L. A. Kravtsov and A. N. Rubinov. Effect of Impurities on the Fulfilment of the Universal Relation between Absorption and Luminescence Spectra of Complex Molecules

I. S. Pominov. Absorption Spectra of Neodymium Chloride in Aqueous-Alcoholic Solutions at Low Temperatures

V. S. Zuev. Hyperfine Structure of the Inversion Line $J = 6$, $K = 6$ of $N^{14}D_3$

A. M. Gurvich. New Luminophores: Cadmium and Zinc Chlorides Activated by Sulfides

L. L. Nagornaya, L. Ya. Malkes, L. V. Shubina. Optical Study of 1,2-Diaryl-Substituted of Ethylene in Liquid Solutions

G. V. Mikhailov. Investigation of the Combination Scattering in Methane at Pressures from 15 to 250 atm

A. P. Kilimov and V. V. Voloshina. On the Photoluminescence and Absorption of Acridone in Solutions

Yu. V. Naboikin, V. K. Dobrokhotova, and V. V. Uglanova. Dependence of the Luminescence Yield of Mixed Single Crystals on Impurity Concentration

V. V. Mikho and L. V. Levkovtseva. On the Spectrum of the Near-the-Electrode Radiation of Aluminium in Electrolytic Bath

V. D. Kamenetsky. On the Collision of Slow Electrons with Hydrogen Atoms

I. K. Plyavin' and M. F. Trinkler. On the Kinetics of Intracenter Luminescence of the Region of Temperature Quenching of Activator

R. Ya. Damburg and R. K. Peterkop. On the Role of the Scattered Wave with a Moment L—1 for Is—2*p*-Transitions

D. N. Shigorin, N. V. Volkova, A. K. Piskunov, and A. I. Gurevich. Study of the Triplet States of Molecules by the Luminescence and Electron Paramagnetic Resonance Methods

D. N. Shigorin, R. N. Nurmukhametov, and Yu. I. Kozlov. Luminescence of Indigo Solutions at 77°K

The XIV Conference on Spectroscopy. *W. Koritzky and Kh. Sterin*

The Second Conference on the Spectroscopy of Lightscattering Media. *A. P. Ivanov*

The First Siberian Conference on Spectroscopy. *A. V. Korshounov*

Spectral Irradiance from Stars and Planets, above the Atmosphere, from 0.1 to 100.0 Microns

R. C. Ramsey

Using published data on star irradiances in the visible region and assuming a blackbody distribution of energy, irradiances from stars and planets are calculated over the spectral region of 0.1 to 100 microns. Results are presented in chart form for ready application in the design of viewing systems operating in space.

Introduction

The designer of optical systems which must operate against a stellar background must determine the irradiance from the stars and planets in the spectral region to which the particular system responds. In the absence of actual measurement data covering the entire spectral region, this determination ordinarily requires calculations[1] based on published measurements of visible magnitude and effective temperature.

For the convenience of these designers, pertinent data have been assembled and the necessary calculations performed for the complete spectral region from 0.1 to 100 μ. The results are presented here in the form of easy reference charts, one giving the spectral irradiance values of the brightest stars and planets, including all the "red stars" of importance in the infrared region (see Fig. 1) and the other giving the population of stars having a spectral irradiance above any given value (see Fig. 2).

The data presented here pertain to the irradiance above the atmosphere. For systems operating in the earth's atmosphere, values of spectral absorption by the atmospheric constituents can be readily applied to the chart values.

In making these calculations it was assumed that the stars behave as Planckian emitters,* and that therefore the spectral irradiance curve for any of these sources may be obtained when the visible radiance and effective temperature are known. In the case of the moon and planets, the data include both self-emission and sun-reflected energy. Self-emission values lie mainly in the longer wavelength region beyond 2.5 μ, and have been calculated as a function of known temperature, diameter, and distance from the earth.

Spectral Irradiance from Particular Stars and Planets

Figure 1 represents the spectral irradiance reaching the top of the atmosphere from the following sources:

1. *The "Brightest" Stars* (Fig. 1(a)). These include stars which exhibit the largest irradiance in the visible region as well as the more prominent red stars which predominate in the infrared spectral region by virtue of their cooler temperatures. The variable stars Betelguex, Mira, and R. Hydrae are presented at their largest value of irradiance.

2. *The Planets* (Fig. 1(b)). Only the moon and brighter planets are presented. Both the sun-reflected energy and that obtained from self-emission are given. The total irradiance is equal to the sum of the two kinds of curves.

Table I gives the visible magnitude and effective color temperature values of the stars and planets of Fig. 1. The list contains all the stars in Schlessinger's Catalogue of Bright Stars which are calculated to yield an irradiance, above the atmosphere, of at least 10^{-12} watts cm^{-2} in either the PbS region (1–3 μ) or the bolometer region (0.3–13.5 μ).

It should be noted that all the curves of Fig. 1 have the same shape on the log–log graph. This is characteristic of the Planck radiation function for a blackbody. Figure 3 shows a well-known relationship derived from the Planck function, and plotted against λT, in relative units. This function is equal to the power radiated per unit wavelength interval λ per unit area of a blackbody at temperature T, divided by the

The author is in the Infrared Department of Raytheon Company, Santa Barbara Operation, Santa Barbara, Calif.

Received October 1961.

* The validity of this assumption is discussed in Appendix A.

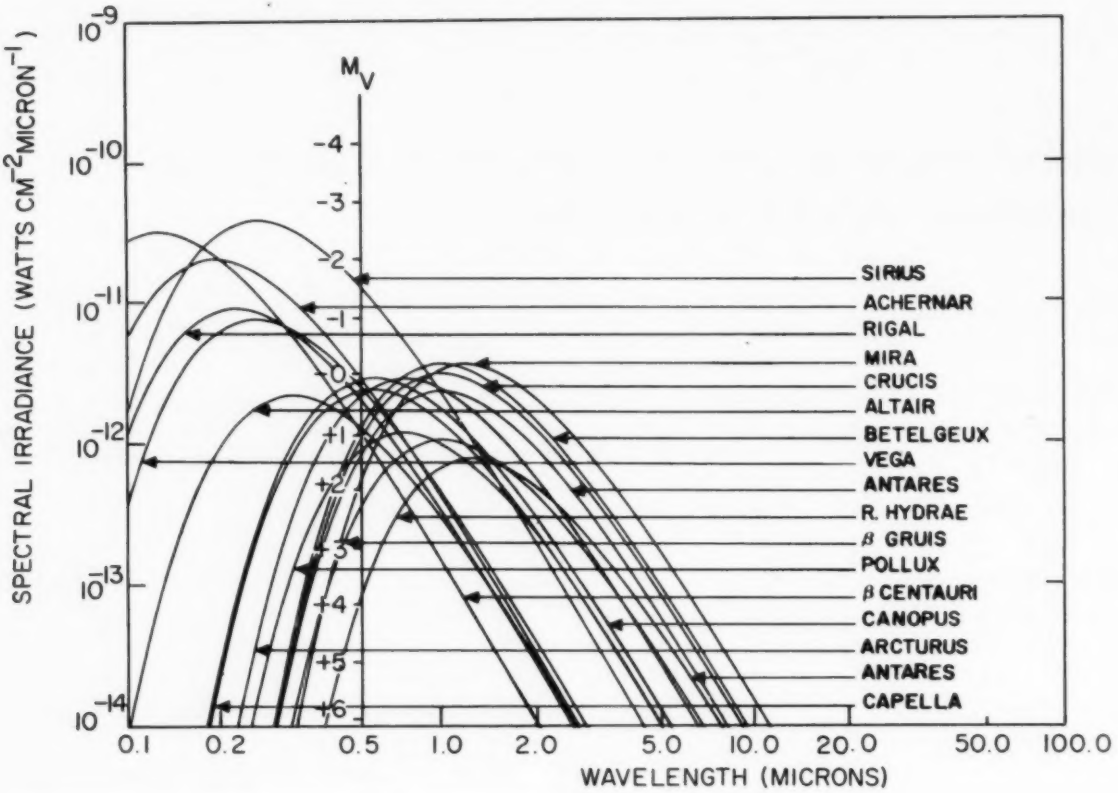

(a)

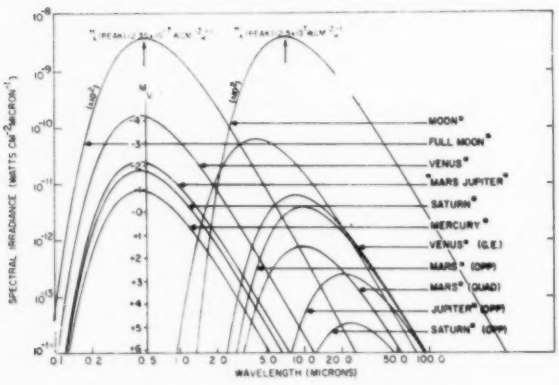

(b)

Fig. 1 (a), (b). Calculated spectral irradiance from planets and brightest stars at top of atmosphere. (b): *—calculated irradiance from planets, at brightest, due to sun reflectance only. # —calculated irradiance from planets, due to self-emission only. GE—inferior planet at greatest elongation. OPP—superior planet at opposition. QUAD—superior planet at quadrature.

maximum power radiated per unit wavelength interval. Since the stars are assumed to be radiating at one effective blackbody temperature (effective color temperature), the curve of Fig. 3 positioned along the abscissa according to appropriate values of λ will give the relative spectral irradiance for any star. The wavelength at which the peak irradiance will occur is readily obtained from Wien's Displacement Law,

$$\lambda_{max}\, T = 2898 \ (\lambda \text{ in microns};\ T \text{ in } ^\circ\text{K}). \qquad (1)$$

Now if the magnitude of irradiance at λ_{max} is known, the spectral curve for the particular star may be determined.

Determination of Peak Spectral Irradiance

The magnitude of the peak spectral irradiance is obtained by use of the quoted value of visual magnitude m_v. The visual magnitude is a function of the irradiance measured in the visible region of the spectrum from the particular star or planet. It is defined as

$$m_v = 2.5 \log_{10}(I/I_0). \qquad (2)$$

At the top of the atmosphere, zero visible magnitude corresponds to visible irradiance (I_0) of 3.1×10^{-13} watts cm^{-2} (as shown in Appendix B). Equation (2)

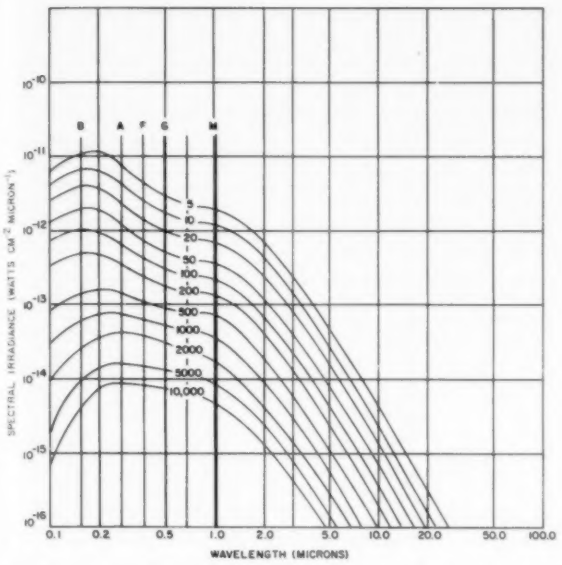

Fig. 2. Minimum spectral irradiance of stars for various population levels, above the atmosphere.

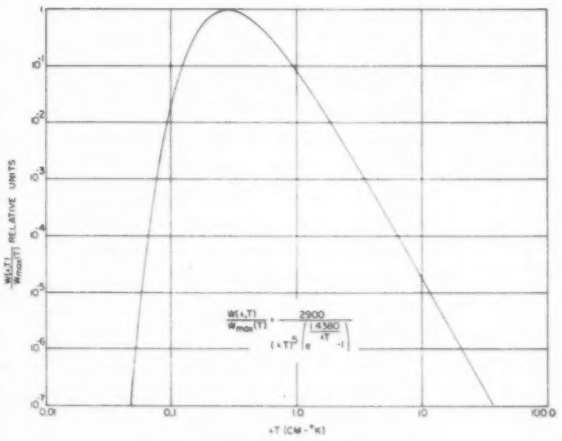

Fig. 3. Planck function.

is plotted in Fig. 4, from which the visible irradiance I, is obtained for any star or planet.

In order to obtain the peak spectral irradiance from the value of I, it is necessary to determine the blackbody visible response fraction. This is given by

$$\eta_e(T) = \frac{\int_0^\infty W_\lambda(T) S_{e\lambda} d\lambda}{\int_0^\infty W_\lambda(T) d\lambda}, \qquad (3)$$

where $W_\lambda(T)$ is the ordinate of the Planck blackbody function at wavelength λ, and $S_{e\lambda}$ is the fractional response of the eye at the same wavelength. The visible response curve (standard observer) peaks at 0.556 μ and falls to zero at approximately 0.4 and 0.7 μ. Equation (3) is plotted in Fig. 5 as a function of temperature, over the range of measured star temperatures, and was obtained by performing the numerical integration.

(Reasonably accurate values of $\eta_e(T)$ may be quickly obtained from any tables of the Planckian radiation function by assuming that S_e is flat between 0.51 and 0.61 μ, and zero everywhere else.)

The total irradiance over the complete wavelength spectrum at the top of the atmosphere is therefore the quantity $I(m_v)/\eta_e(T)$.

The peak spectral irradiance is

$$H_{\lambda peak} = \frac{I(m_v)}{\eta_e(T)} \times \frac{W_{\lambda max}(T)}{\int_0^\infty W_\lambda(T) d\lambda}. \qquad (4)$$

The second factor on the right side of Eq. (4) is the maximum value of the Planck function (equal to $1.290 \times 10^{-15} \times T^5$ watts cm^{-2} micron^{-1}) divided by the Stefan Boltzman function (equal to $5.679 \times 10^{-12} \times T^4$ watts cm^{-2}). Figure 6 shows Eq. (4) plotted for various values of the visible magnitude and effective star temperatures. The designations denoting Star Spectral Classifications are also indicated in the figure. These are explained below.

The curves of Fig. 1 were obtained from the data of Table I, Eq. (1), and Fig. 6. To facilitate the drawing

Table I. Visual Magnitudes and Effective Temperatures of Planets and the Brightest Visual and Red Stars

	Name (planets)	Visual magnitude (m_v)	Effective temperature T (°K)
1.	Moon (full)	−12.2	5900
2.	Venus (at brightest)	−4.28	5900
3.	Mars (at brightest)	−2.25	5900
4.	Jupiter (at brightest)	−2.25	5900
5.	Mercury (at brightest)	−1.8	5900
6.	Saturn (at brightest)	−0.93	5900
	Stars		
1.	Sirius	−1.60	11,200
2.	Canopus	−0.82	6200
3.	Rigel Kent (double)	0.01	4700
4.	Vega	0.14	11,200
5.	Capella	0.21	4700
6.	Arcturus	0.24	3750
7.	Rigel	0.34	13,000
8.	Procyon	0.48	5450
9.	Achernar	0.60	15,000
10.	β Centauri	0.86	23,000
11.	Altair	0.89	7500
12.	Betelguex (variable)	0.92	2810
13.	Aldebaran	1.06	3130
14.	Pollux	1.21	3750
15.	Antares	1.22	2900
16.	α Crucis	1.61	2810
17.	Mira (variable)	1.70	2390
18.	β Gruis	2.24	2810
19.	R. Hydrae (variable)	3.60	2250

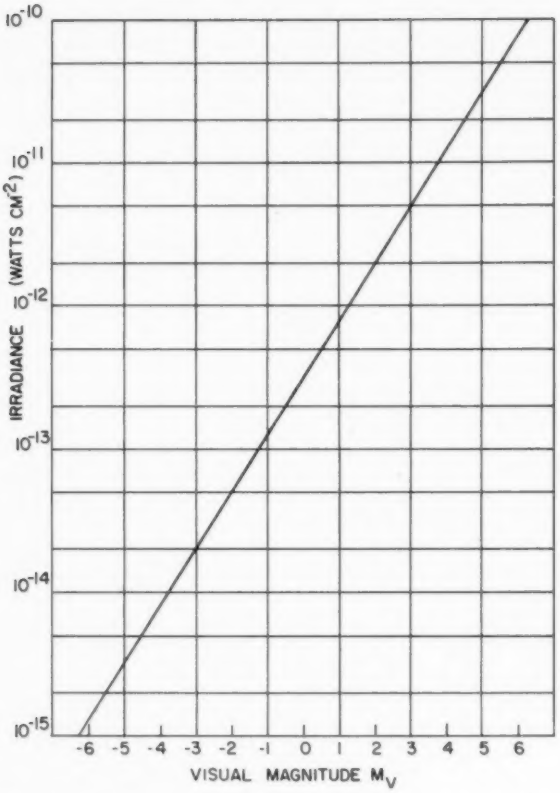

Fig. 4. Effective irradiance in the visible region (standard observer) versus visual magnitude.

of the curves, a template conforming to the curve of Fig. 3 was constructed and used. It was also found to be very useful in performing the calculations of spectral star populations.

Planetary Self-Emission

The spectral self-emission curves for the planets were also calculated, and are included in Fig. 1. The following equation was used to determine the spectral

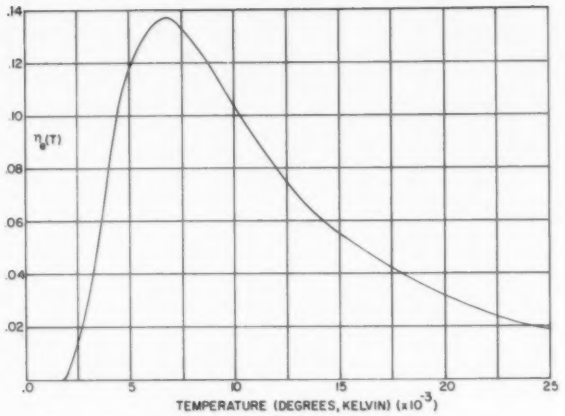

Fig. 5. Fraction of the total radiation emitted by a blackbody, at temperature, T, visible to the standard observer.

irradiance curves due to planetary self-emission.

$$H_{\lambda(\text{peak})} = \frac{W_{\lambda\max}(T)}{4\pi}(1 - A)\frac{\pi d^2}{D^2} \qquad (5)$$

where

$H_{\lambda(\text{peak})}$ = peak spectral irradiance, in watts cm^{-2} micron^{-1},

T = effective surface temperature of the planet (values taken from ref. 2, Table 832),

$(1-A)$ = assumed emissivity of the radiating body, where A is the value of the albedo in the visible region (values taken from ref. 2, Table 837); it is assumed that the planets radiate as grey bodies,

πd^2 = radiating surface area of the planet, d is the diameter (values taken from ref. 2, Table 831),

D = distance to the planet from the earth. This value is, of course, variable with the rotation of the planets around the sun. In the case of the inferior planets, Mer-

Table II. Data Used in Calculation of Planetary Self-Emission

Planet	Diameter, d (10^3 km)	Distance from earth, D (10^6 km)	Position of planet	Albedo, A	Effective temperature, T (°K)	$H_{\lambda(\text{peak})}$ (watt-cm^{-2} meter^{-1})	λ_{peak} (μ)
Mercury	4.84	137.8	Greatest	0.058	690	5.84×10^{-11}	4.20
Venus	12.32	103.3	elongation	0.76	330	6.04×10^{-12}	8.7
Mars	6.66	78.3	Opposition	0.148	285	3.75×10^{-12}	10.16
		171.8	quadrature			7.76×10^{-13}	
Jupiter	139.80	628.3		0.51	135	3.49×10^{-13}	21.46
Saturn	115.06	1277.0	Opposition	0.50	120	3.26×10^{-14}	24.14
Uranus	3.72	2720.0		0.66	90	1.96×10^{-16}	32.19
Moon	0.27	0.384		0.072	400	2.51×10^{-7}	7.24

Self-emission from Neptune or Pluto is insignificant.

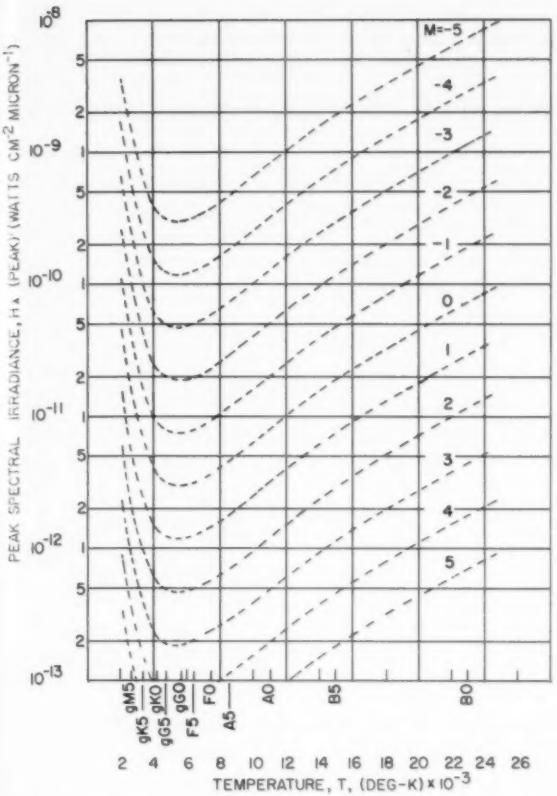

Fig. 6. Graph used to obtain peak spectral irradiance for various values of visual magnitude versus effective temperature or spectral class.

cury and Venus, the values of D were chosen corresponding to their greatest elongation. For the superior planets, values of D used correspond to their opposition. In the case of Mars, the closest superior planet, the value of D, when the planet is at quadrature, is also used. For a definition of these terms, see ref. 3, Chapter IX.

Knowing $H_{\lambda(\text{peak})}$ and the wavelength value at which this peak occurs

$$\left(\lambda_{\max} = \frac{2898}{T(°\text{K})}\right),$$

the spectral irradiance curves can be readily constructed.

Table II gives all of the values used in the calculations.

Spectral Star Populations

Figure 1 yields data for the brightest stars and planets. It is also of interest to obtain an idea of the spectral irradiance from the total star population.

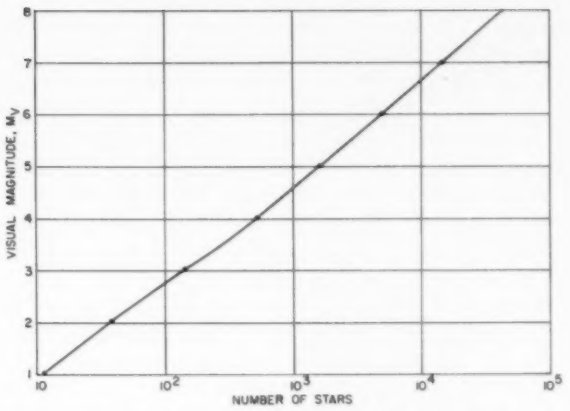

Fig. 7. Population of stars brighter than a particular visual magnitude.

As reported in ref. 3, page 604, the stars are divided into classes designated by letters, with decimal classification denoting intermediate types (Draper Classification). On page 705 it is stated that 99% of all the stars are included in six principal spectral classes, B, A, F, G, K, and M. Reference 3 also includes a table of the percentage of stars of the various spectral classes for different regions of visual magnitude and, on page 622, a list of the number of stars brighter than a given magnitude. Krasno[4] has extended this table to the small values of visual magnitude. Figure 7 shows this plot. The combination of the table of star percentages versus spectral classes and the data in Fig. 7 yields the actual number of stars brighter than a given visual magnitude for each of the six principal spectral classes. These values are listed in Table III.

The data of Table III are plotted in Fig. 8, assuming that in each spectral class, the spectral irradiance curves of the stars peak at the same wavelength value. The plot was readily obtained by use of the template corresponding to Fig. 3. For example, the data in row 1 of Table III correspond to the curves in Fig. 8 that cross the visual magnitude line at a value of 2.24, each

Table III. Number of Stars in the Principal Spectral Classes above a Given Magnitude

Magnitude limit	B (B0 to B5)	A (B8 to B5)	F (A5 to F2)	G (F5 to G0)	K (G5 to K2)	M (K5 to M8)
2.24	15	15	4	6	8	7
3.24	52	43	18	23	40	23
4.24	135	157	56	85	222	65
5.24	270	562	236	265	672	215
6.24	484	2189	792	693	1871	471
7.24	976	5879	2268	2415	5930	1332
8.24	1684	15,083	6162	8079	19,030	4164

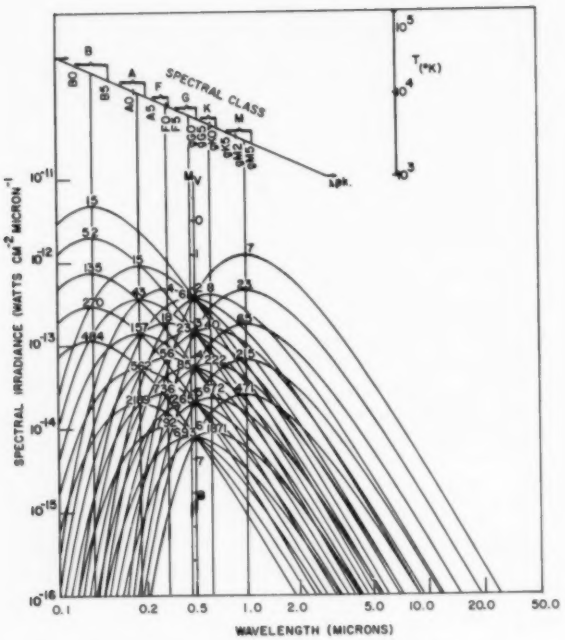

Fig. 8. Minimum spectral irradiance of stars for various population levels and spectral classes, above the atmosphere.

curve peaking at the wavelength of the corresponding spectral class. The visual magnitude line is taken from the data of Fig. 2. For example, in Fig. 4, a value of m_v equal to zero corresponds to a visible irradiance of 3.1×10^{-13} watt cm^{-2}. Now assuming that the visual spectral region peaks at 0.55 μ and extends over a 0.1 μ region, the spectral peak value of 0.55 μ equals 3.1×10^{-12} watt cm^{-2} micron^{-1}.

The information in Fig. 8 is not immediately useful in this form. Therefore, Fig. 2 was constructed. It essentially represents the drawing of contour lines of equal population values through the curves of Fig. 8. Appendix C explains the procedure used in obtaining the data of Fig. 2.

Use of Figures in System Design

It is felt that Figs. 1 and 2 yield infrared background information on the planets and stars that is immediately useful in system design. For example, assume a hypothetical infrared system operating in the wavelength region around 4 μ, with an equivalent bandwidth of 2 μ. A value of NEPD (noise equivalent power density) of the system equal to 10^{-13} watt cm^{-2} corresponds to an average spectral irradiance of 5×10^{-14} watt cm^{-2} micron^{-1} at 4 μ. From Fig. 2, one observes that there are about 12 stars that would be "seen" by the system. Most of these 12 stars can be immediately identified from Fig. 1, and the signal to noise from each calculated, as well as the signal to noise obtained from the planets.

The above assumes that the system is operating above the atmosphere. However, if below the atmosphere, absorption information may be readily applied to any data obtained from Figs. 1 or 2.

Appendix A. Blackbody Radiation from Stars

Figure 9 (taken from ref. 5) shows the measured irradiance from the sun as extrapolated to the top of the atmosphere, and compared with 5700°K and 6000°K blackbody curves. It shows that a Planckian curve gives a reasonable fit and gives some measure of the deviation or error obtained when using the blackbody assumption.

The work of Stebbins and Whitford[6] provides a good basis for assuming the star radiation to be that of a blackbody. 238 stars of all spectral types from O to M were observed in six spectral regions from 0.353 to 1.03 μ. The observed colors of the stars agree closely with the colors of a blackbody at suitable temperatures.

Measurements performed by Hall[7] cast doubt on the validity of the use of the color temperature in calculating irradiance from the cool stars (classes K and M). The calculations of Larmore (which are identical to those in this report) predict irradiance values from these stars in the PbS region that are a factor of 2 to 4 below Hall's measured values.

Appendix B. Calculation of the Effective Irradiance I_0, in watts/cm^2, in the Visible, Corresponding to a Visual Magnitude Value of Zero

In ref. 2, Table 827, page 730, it is stated that the apparent magnitude of a standard candle, at a distance of 1 meter, is -14.2.

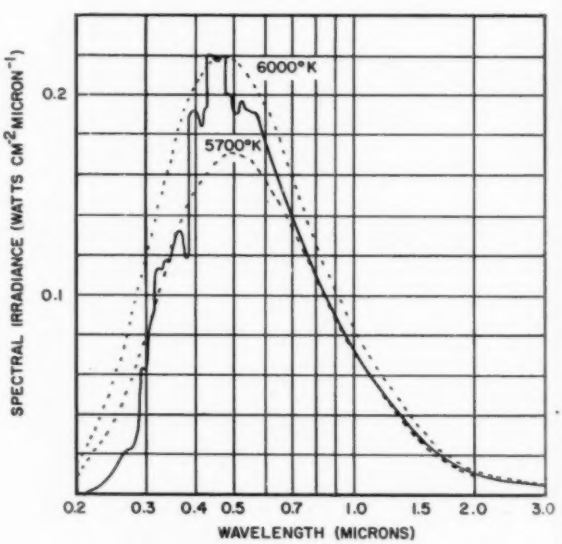

Fig. 9. Measured spectral irradiance above the atmosphere from the sun compared with blackbody curves (from ref. 5).

The relation between the visible light received from two stars and their magnitudes is expressed by the formula (see Eq. (2)):

$$\log \frac{I_1}{I_2} = 0.4(m_2 - m_1).$$

Since a unit candle source emits one lumen per steradian, when m_2 equals -14.2, I_2 equals 10^{-4} lumen/cm^2.

For

$$m_1 = 0,$$

$$I_1 = (10^{-4}\ \text{lumen/cm}^2) \times 10^{-5.68}$$

$$= 2.09 \times 10^{-10}\ \text{lumen/cm}^2.*$$

In ref. 2, Table 73, page 94, the value for the mechanical equivalent of light is given as 0.00147 watt/lumen. Therefore, for zero magnitude the effective irradiance is

$$I_0 = 0.00147 \times 2.09 \times 10^{-10}$$

$$= 3.1 \times 10^{-13}\ \text{watt/cm}^2.$$

Appendix C. Method of Obtaining Fig. 8

The contour data of Fig. 2 were obtained by use of the template corresponding to Fig. 3. The method used is as follows:

1. For example, a wavelength of 1.0 μ and a spectral irradiance value of 4×10^{-14} watt cm^{-2} micron^{-1} determines a point on the graph paper.

2. Place the template on the graph so that the peak lies along the wavelength (0.155 μ) corresponding to the B spectral class.

3. Move the template up or down so that the curve passes through the above-mentioned point.

4. Read off the value of visual magnitude determined by the position of the template and the m_v line. (For this case, m_v is +2.6.)

5. From the data in Table III, column 1, corresponding to B spectral class, which is plotted as a continuous function on a separate graph, a total of 24 stars corresponds to a value of m_v equal to 2.6.

6. This same operation is performed for all six of the spectral classes, and the total number of stars obtained for this point. (Total equals 890 stars.)

7. Steps 1 to 6 are repeated for sufficient points on the graph paper so that accurate contours of star populations may be plotted.

* Allen[8] states that this quantity is 2.43×10^{-10} lumen/cm^2. Thus I_0 would equal 3.6×10^{-13} watt/cm^2. This is larger than the value calculated above by 16%. If this new value were used in the calculations, all the curves of Figs. 1, 2, and 8 relating to the stars and the planets (sun-reflected irradiance only) would move upwards by 0.16.

References

1. L. Larmore, "Infrared Radiation from Celestial Bodies," U.S. Air Force Project, Rand Research Memorandum, 293-1 (17 March 1952).
2. *Smithsonian Physical Tables* (Smithsonian Institution, Washington, D.C., 1954), 9th revised ed.
3. H. N. Russell, R. S. Dugan, and J. Q. Stewart, *Astronomy* (Ginn, New York, 1945), Vols. I and II.
4. M. R. Krasno, private communication.
5. *Handbuch der Physik*, S. Flügge, ed. (Springer-Verlag, Berlin, 1957), Vol. 48.
6. J. Stebbins and A. E. Whitford, Astrophys. J. **102,** 318 (1945).
7. F. F. Hall, Jr., and C. V. Stanley, Appl. Opt. **1,** 97 (1962).
8. C. W. Allen, *Astrophysical Quantities* (Athlone Press, Univ. of London, 1955).

Applied Optics BOOKS

Books for review should be submitted to the Managing Editor, APPLIED OPTICS, 1155 16th St., N.W., Washington 6, D.C.

Fundamentals of Photographic Theory. Second edition. By THOMAS H. JAMES AND GEORGE C. HIGGINS. Morgan and Morgan, New York, 1960. 345 pp. $7.50.

It is a pleasure to see a new edition of *Fundamentals of Photographic Theory* published. The earlier text provided an excellent source of information useful both for classroom and reference purposes. The new edition has incorporated much recent work in photography and related fields which should prove of inspirational and practical value to the serious student of photography. However, in providing some of this additional information, the authors have been forced to use concepts and mathematics which many students who have "a basic knowledge of physics and physical chemistry" may find unusually difficult.

Throughout the 14 chapters of the book, about 20% is either new or rewritten. The book has been completely re-set, and only a few typographical errors are noticeable. For example, on page 165 a complete line in the text has been omitted, and for those of you who may wonder what it should be, the first edition gives "color change is known as fading. It is the result of a reaction be-."

Chapter 1 has been left essentially unchanged, but Chapter 2, on emulsion, includes considerably more information on emulsion preparation and the sensitizing process than was given in the former edition. Also, the added comments on special emulsions for ultraviolet, cosmic rays, and nuclear particles enhances the practical aspects of the text.

During the past ten years advances made in solid state physics have given a new impetus to an understanding of the latent image. Chapter 3 deals with these problems and presents information which should whet the appetite of physicists as well as photographic students. Even though some of the concepts may prove difficult for beginning students, sufficient background material is given to impart much useful information.

Chapter 4 remains very much the same as in the first edition but some new material on reciprocity failure draws on the solid state concepts developed in the previous chapter.

The changes in Chapter 5 stress the physical mechanisms in the development process with much of the material rewritten. In particular, the material on direct development, physical development, filament formation, and the charge effect seems to bring the

continued on next page

continued from previous page

development phase of the photographic process more nearly into the realm of physics.

Chapters 6, 7, and 8 present the information on the subjects of development, fixing, and washing in the traditional manner of most photographic texts. However, several new diagrams have been included to update the material on the effects of developer concentration, temperature, ionization, and dye-couplers. The authors freely admit that many of the chemical reactions which take place are not completely understood and that research continues toward a better understanding of these processes. The considerable progress which has been made is apparent from a comparison between the current and first editions.

The next three chapters deal with sensitometry, and three new concepts have been introduced in this edition. Color densitometry appears to have adequate treatment provided the student has some background in colorimetry. However, the discussion of vector parameters and principal components seems to require additional explanation with a few specific examples. Taken as a whole, Chapters 9, 10, and 11 provide an excellent treatise for the beginning student on the ramifications of sensitometry.

In Chapter 12 on tone reproduction the authors have clearly separated the objective from the subjective measurements. In addition, several practical suggestions are given for selection of proper photographic materials.

Chapter 13 has been considerably rewritten in order to take advantage of mathematical formulations resulting from statistical relationships. Here again, the treatment may be somewhat advanced for beginning students, but the new mathematical approaches to granularity, turbidity, resolving power, spread functions, and sine wave response serve to give the reader an appreciation of these techniques which is difficult to find elsewhere. In fact, additional material on the concept of "informational sensitivity" would also be welcome.

Mechanism of Dye Sensitizing in Chapter 14 has been completely rewritten with the stress placed on solid state physics concepts. Also of interest is the change in a statement on page 313. In the first edition the long wavelength limit of 1.4 microns for dye sensitization was attributed to water absorption while the current text refers to the instability of the dye as the limiting factor. A thorough understanding of this problem might lead to a very useful new tool in infrared radiation recording.

Progress over the past decade has certainly warranted the publishing of this new edition. Even though the binding does not appear to be as good quality as that of the previous edition, Morgan and Morgan have published a photographic text which should be valuable to everyone with a keen interest in photography.

LEWIS LARMORE

Encyclopaedic Dictionary of Physics. Volume 1: A to Compensated Bars. J. THEWLIS, Editor-in-Chief. Pergamon Press, New York, 1961. xv + 800 pp. $40.00 per vol. $298.00 per set.

This is the first volume of a set which, according to the publisher, will include six more volumes of text and a subject index volume. (The second volume was distributed to subscribers in October 1961 and completion was planned for early 1962.) The price of the eight-volume set is now $298.00, and with the complete set is supplied *gratis* a glossary of physical terms in English, French, German, Spanish, Russian, and Japanese. The glossary is for sale separately at $60.00. This 800-page first volume is apparently somewhat smaller than the average, as the eight-volume set is represented as having some 8000 pages.

To review a work such as this requires first that its purpose be clearly understood. According to the foreword of the Editor-in-Chief "The present Dictionary aims . . . at covering not only Physics proper but also to a greater or lesser extent such subjects as Mathematics, Astronomy, Aerodynamics, Hydraulics, Geophysics, Metrology, Physical Metallurgy, Radiation Chemistry, Physical Chemistry, Structural Chemistry, Crystallography, Medical Physics, Biophysics, and Photography. It should be useful not only to physicists (and would-be physicists) but to those who are concerned with any of the many branches of science mentioned or implied above, which have a physical basis." To quote the jacket, "The object of this ambitious undertaking is to put the whole of physical knowledge on the bookshelf. . . . It is intended to serve all who require easily accessible information on physical and related topics." Finally, a descriptive sheet from the publisher asserts that "Every public, technical, and school library will need this unique reference sourse" (*sic*). I may as well say here that this announced scope is such as to overwhelm any reviewer and did much to make me wonder why I ever agreed to discuss the work at all.

Inspection of the "International Board of Consulting Editors" shows that the group consists of one New Zealander, seventeen Americans (eight of whom were at Brookhaven), and fifty-one individuals from Great Britain! The sixty-seven main headings used are listed inside the cover of the volume, and some will find it puzzling that among them we find *optics, cathode rays, nuclear physics,* and *mesons* as apparent peers. Some 450 contributors to the present volume are listed, but the publisher says that in all 3609 (!) persons were involved in the writing of the work.

The book is attractive in appearance, well printed (in Leipzig), and well bound. Most of the figures are good, but a few (such as that on page 35) are poor, and the one on page 536 seems to be in need of a quarter turn. Some of the figure titles received too little attention, for we find on page 139 an illustration of a "Windowless flom counter" and on page 774 the circuit for a "Tolpitts" oscillator.

As is to be expected, the contributions vary considerably in comprehensiveness, clarity, precision, and pertinancy. In my opinion, too much space is given to purely chemical topics such as *buffer solutions, alkali, alkyl group, ammonia synthesis, cement making, etc.* Others—both colleagues and graduate students to whom the volume was shown—share this feeling.

Any technical reader will find many of the entries interesting and informative. For instance, I particularly liked the one on *combination tones.* As an example of a poorly done entry, I would propose *cathetometer.* To many of the entries are appended very helpful bibliographies, but I regret that the great majority of the references are to British books and journals. It would seem to me that as a matter of convenience to American users more American books might have been cited, even if this involved some duplication. Where library holdings are limited—at many laboratories and the smaller schools, for example—in this country, the great prevalence of British sources will make the bibliographies less helpful than they could have been. I could not but be struck also by the fact that almost no references are made to material which is not in English.

Many of the discussions include references to original discoveries, and this dash of history is to be commended. In many cases much is to be gained by consulting the original papers.

From a perusal of this single volume it cannot be determined whether a topic has been left out or whether it appears in another volume under a different heading. It would probably have been best in this connection to have reviewed the set as a whole, unless that prospect would be too dismaying—as it might

continued on page 491

Total Absorptance by Nitrous Oxide Bands in the Infrared

Darrell E. Burch and Dudley Williams

Instrumentation and experimental techniques employed for the determination of the total absorptance $\int A(\nu)d\nu$ of the bands of various atmospheric gases are described. The total absorptances of the 2563, 2461, 2224, 1285, 1167, 692, and 589 cm^{-1} bands of pure N_2O and N_2O mixed with N_2 have been determined as a function of absorber concentration w and equivalent pressure P_e which involves the partial pressures of the two gases. The results are given in graphical form. In general, it is found that in situations in which existing theory predicts absorptance proportional to the square roots of pressure and absorber concentration, the total absorptance is indeed nearly proportional to the square root of absorber concentration but not to the square root of the pressure; for the 2224 cm^{-1} band, $\int A(\nu)d\nu \propto P_e^{0.37}$. In addition to graphical presentation of results, it is possible to express $\int A(\nu)d\nu$ in terms of w and P_e by means of empirical equations applicable to certain definite ranges of the variables; the validity and the limitations of such empirical equations are discussed. For samples for which the product of the absorption coefficient $k(\nu)$ and the absorber concentration is much less than unity for all frequencies in an absorption band, it is possible to measure the band intensity or band strength $\int k(\nu)d\nu$. Values of band intensity for the 2563, 2461, 2224, 1167, and 589 cm^{-1} N_2O bands are listed and compared with values previously reported by others.

A detailed knowledge of the infrared transmission of planetary atmospheres is of importance to space physics in connection with studies of planetary heat balances and with the possible development of infrared probing and signaling systems. Laboratory studies of "synthetic atmospheres" are desirable, even in connection with telluric studies, and provide a basis for interpretation of observed absorption in the atmospheres of other planets. The major purpose of the present work is the determination of the *total absorptance* $\int A(\nu)d\nu$ of various absorption bands as a function of *absorber concentration* w and *equivalent pressure* P_e.[1] The present paper on nitrous oxide N_2O is the first in a series dealing with absorption by various telluric gases. Although N_2O is a relatively minor atmospheric constituent, a knowledge of the absorptance of N_2O bands is important in the calculation of the transmission of the "atmospheric windows" between the carbon dioxide and water vapor bands in the infrared.

Instrumentation

A double-beam single-pass Perkin-Elmer Model 21 spectrometer with an NaCl prism and thermocouple was employed for frequencies between 4000 cm^{-1} and 670 cm^{-1} and was equipped with a drive mechanism that provided a direct plot of $A(\nu)$ versus ν on the recorder chart. The spectrograph is equipped with two multiple-traversal cells, each of which has a base path of 1 meter and can be set for 40 traversals or any smaller number divisible by 4. Although the cells are equipped with heating coils capable of maintaining sample temperatures as high as 100°C, all data included in the present study were obtained at approximately 30°C. These long cells can easily be replaced by short conventional absorption cells when short absorption paths are desired.

The gas-handling manifold was equipped with packless miniature stainless steel valves, which can be connected to the sample cell, the reference cell, various pressure gauges, and various gas cylinders. Gas pressures between 1 and 50 mm Hg were measured by a Wallace and Tiernan absolute pressure gauge giving an accuracy of 1 part in 300 when properly adjusted. Pressures lower than 1 mm Hg were measured by means of a McLeod gauge, which was also used to check the

The authors are of the Laboratory of Molecular Spectroscopy and Infrared Studies, Department of Physics and Astronomy, The Ohio State University. The present address of D. E. Burch is Aeronutronic, A Division of the Ford Motor Company, Newport Beach, California. D. Williams is presently a National Science Foundation Senior Postdoctoral Fellow at the University of Liége.

Received 6 December 1961.

Supported in part by Geophysics Research Directorate, Air Force Cambridge Research Laboratories.

Wallace-Tiernan gauge at low pressures. A simple mercury manometer was employed for pressures between 50 mm Hg and 1 atm. An Ashcroft Duragauge of the Bourdon type was used to measure pressures greater than 1 atm.

Before introduction of gases into the sample cell, the entire system was first evacuated and then the reference cell was closed off. The absorbing gas was then admitted to the manifold and the sample cell at the desired pressure and then the sample cell was closed off. The manifold was then first re-evacuated and filled with nitrogen* to some selected pressure greater than that in the sample cell. Nitrogen was added to the sample cell by briefly opening the valve until the desired total pressure was obtained. By following this procedure it was possible to minimize or eliminate backward flow of the absorbing gas from the sample cell to the manifold. No data were accepted until thorough mixing of the absorbing and broadening gases had occurred in the sample cell; reproducibility of measured absorptance was the criterion for thorough mixing. At low total pressure, thorough mixing by diffusion was accomplished within a few seconds, or at most a few minutes, depending on the sample cell being used. At higher pressures it was necessary to use a fan mounted in the multiple-traversal absorption cell to ensure thorough mixing within a reasonably brief time. In order to minimize mixing time the valve was located adjacent to the cell so that nitrogen in the tubing leading to the manifold would not diffuse into the sample.

Studies of absorption at frequencies higher than 4000 cm^{-1} were made with a Perkin-Elmer Model 99 spectrometer equipped with an LiF prism and an thermocouple. A multiple traversal cell giving paths as long as 48 meters was used with this instrument; pressures employed with this cell were atmospheric or less. This spectrometer, which was mounted inside a vacuum tank, was also used with shorter absorption cells to investigate the absorption by small samples of H_2O and CO_2 in the regions of the strong absorption bands. This was found to be necessary in order to eliminate error due to absorption by the air in the optical path of the spectrometer. The larger Model 21 spectrometer could not be evacuated and could not be flushed sufficiently well that error was negligible for small samples.

The total absorptance $\int A(\nu)d\nu$ could be determined by planimetering the records obtained with the Model 21 spectrometer, since the abscissa is linear in frequency and the ordinate is linear in absorptance $A(\nu)$. In some cases slight corrections were needed to take account of scattered light, unequal attenuation in the sample and reference cells, and atmospheric absorption within the spectrograph; these effects were easily recognized and corrected so that they caused negligible errors in measured values of $\int A(\nu)d\nu$. In the case of data obtained with the Model 99, an "envelope spectrum" taken with the absorption cell evacuated was superposed on each sample spectrum. The envelope spectrum served as the zero absorption curve. Curves representing spectral absorptance as a function of frequency were then replotted and planimetered to obtain $\int A(\nu)d\nu$ as in earlier studies.[2]

Three major types of experimental error in the present work are: (1) Sampling errors, which include uncertainties in the amounts of absorbing gas and broadening gas in the sample cell, (2) errors in recording by the spectrograph due to noise, drift, and possible nonlinearity in the detection-amplification-recording system, and (3) errors in planimetering the recorded spectra. With the set of pressure gauges employed, pressures greater than 10 mm Hg could be measured to $\pm 1\%$, with somewhat greater uncertainty for smaller samples. Possible error due to incomplete mixing of gases in the sample cells was largely eliminated by use of the fan mentioned earlier. A careful study of the possible effects of adsorption of gases showed that errors due to adsorption could be minimized by certain procedures used in filling the cells; it is estimated that errors due to adsorption amount to $\pm 2\%$ to $\pm 3\%$ for larger samples and not more than $\pm 5\%$ for the smallest samples. The recording errors are estimated as $\pm 5\%$ for values of total absorptance less than 10 cm^{-1} and $\pm 2\%$ for values of total absorptance greater than 10 cm^{-1}. Repeated tests by experienced operators show that planimetering errors amount to less than $\pm 1\%$. It is estimated that the over-all error does not exceed $\pm 10\%$ for values of total absorptance less than 10 cm^{-1} and is less than $\pm 5\%$ if the total absorptance is greater than 10 cm^{-1}.

Treatment of Data

When the study of a given absorption band or region was started, a definite slit program for the spectrometer was selected and used to take all data. Although total absorptance is independent of slit width, there are occasions when it is desirable to compare spectral absorptance $A(\nu)$ at some definite frequency for different samples; such a comparison is impossible unless all data are taken with the same slit program. However, since the datum of primary interest is $\int A(\nu)d\nu$, it is not necessary to use narrow slits. It is desirable to work with slits sufficiently wide to give large signal-to-noise ratios even for the largest values of $\int A(\nu)d\nu$; wide slits are convenient from the practical standpoint of planimetering the spectral records. For nearly every band studied it would have been possible to ob-

* Although nitrogen was employed as a "broadening gas" throughout the present work, the effects of other gases can easily be computed on the basis of the relative broadening abilities given in ref. 1.

tain more detailed information concerning band shape had this been of importance to the investigation.

Once a slit program had been selected, large numbers of spectral records were made. These records provided data on $\int A(\nu)d\nu$ for wide ranges of absorber concentration w,* partial pressure p of the absorbing gas, and total pressure P—including of course pure samples of the absorbing gas for which $p = P$. The value of $\int A(\nu)d\nu$ for various cell lengths, absorber concentrations, and equivalent pressures P_e were then organized into plots to develop relationships between $\int A(\nu)d\nu$ and the variables w and P_e and to provide tests of theoretical predictions.†

One type of relationship important to nearly all current theories is the relationship between absorptance and pressure. In order to establish this relationship, a set of logarithmic plots of total absorptance as a function of equivalent pressure P_e was made for various values of absorber concentration w. From the slopes of the curves, the relation between $\int A(\nu)d\nu$ and P_e can be obtained. In general, it is found that over certain ranges of P_e and w, $\int A(\nu)d\nu \propto P_e^n$, where $n < 0.5$ even in situations where existing theories predict a square-root relationship.

Another set of logarithmic plots was then prepared giving $\int A(\nu)d\nu$ as a function of w for various values of equivalent pressure P_e. From the slopes of these curves, it is usually found that $\int A(\nu)d\nu \propto w^m$, where $m \approx 0.5$ in situations for which theory predicts a square-root dependence on absorber concentration.

The next step in attempting to establish experimental relationships between $\int A(\nu)d\nu$ and sample parameters was to make logarithmic plots of $\int A(\nu)d\nu$ as a function of wP_e^a. From the resulting plots it is frequently possible to obtain empirical equations of the form

$$\int A(\nu)d\nu = c(wP_e^a)^b, \tag{1}$$

where a, b, and c are empirical constants with $b \approx 0.5$. Such equations are valid for intermediate values of $\int A(\nu)d\nu$ and P_e for which strong but not seriously overlapping rotational lines are present throughout most of the band.

For large values of $\int A(\nu)d\nu$, the central portion of a band is a spectral region of nearly complete absorption. Further increase in w or P_e merely causes increased spectral absorptance in the wings of the band. For such a band, the total absorptance can be expressed in the form

$$\int A(\nu)d\nu = C + D \operatorname{Log}(wP_e^a), \tag{2}$$

where C, D, and a are empirical constants.

It is usually rather difficult to derive empirical equations for extremely small values of $\int A(\nu)d\nu$ and P_e. Under certain circumstances $\int A(\nu)d\nu$ is nearly independent of P_e, a result indicating that Doppler broadening is the dominant factor in determining line width; under other conditions $\int A(\nu)d\nu$ is found to vary linearly with absorber concentration, as predicted by the theory for weak lines.

It should be emphasized that, although empirical equations of the forms (1) and (2) can be useful in practical work provided they are properly applied, they are not based on any valid theory. Although they can be used to test predictions of theory, it is usually more desirable to employ interpolations between curves shown in logarithmic plots. Limitations of empirical equations will become evident in the detailed discussion of results obtained for the 2224 cm^{-1} band of N_2O.

Results for the 2224 cm^{-1} Band

The ν_3 fundamental of the $N_2{}^{14}O^{16}$ molecule has its center at 2224 cm^{-1}. However, in the same spectral region there is absorption due to the ν_3 fundamental of less abundant isotopic molecules of N_2O, and at least one weak band ($\nu_3 + \nu_2 - \nu_2$) reported by Thompson and Williams.[3] For the purposes of the present paper, all these bands will be referred to as *the* 2224 cm^{-1} N_2O band. More than 200 spectral records of this region were obtained. Cell lengths of 1.55, 6.35, 400, 800, and 1600 cm were employed. Different combinations of N_2O and N_2 were used to provide absorber concentrations from 0.00016 to 76.4 atm cm and total pressures from 1 to 3000 mm Hg. All spectra were obtained with slit widths corresponding to approximately 25 cm^{-1} and with the cell temperature near 30°C. The values of equivalent pressure were calculated from the total pressure P and the partial pressure p of N_2O by the relation

$$P_e = P + 0.12\,p$$

on the basis of earlier studies of self-broadening.[1]

Tracings of spectra of two samples having the largest absorber concentrations are shown in the left panel of Fig. 1. A slight growth of the band with increasing pressure is to be noted. The "band limits," beyond which there is negligible spectral absorptance, are indicated by the band wings in these records; these limits were used as limits of integration for total absorptance for all samples studied. The right panel

* In the present series of articles, values of absorber concentration w are expressed in atm cm and are found by $w = \frac{pl}{760} \times \frac{273}{273 + T}$, where p is partial pressure of the absorbing gas in mm Hg, l is the absorption path length in cm, and T is the sample temperature in °C. The factor including T reduces values of w to normal temperature, and a given value of w corresponds to the same number of molecules per unit area regardless of temperature.

† The term equivalent pressure is applied to the quantity $P_e = P + (B - 1)\,p$, where B is a *self-broadening coefficient* giving the ratio of the "self-broadening ability" of an absorbing gas to the line broadening ability of nitrogen. Values of B for N_2O and other absorbing gases are given in ref. 1.

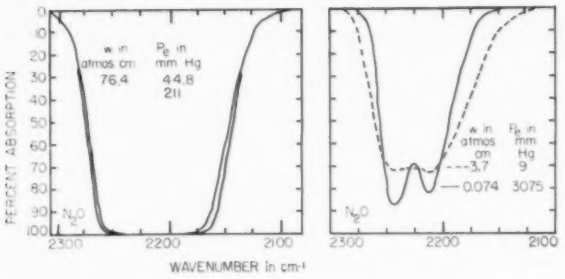

Fig. 1. Spectral absorptance, expressed as "Percent Absorption," for the 2224 cm^{-1} band. Values of P_e and w are listed for successive curves in the figure.

of Fig. 1 shows the spectra of two samples having different values of w and P_e but having approximately equal total absorptance. It will be noted that the shapes of the two bands are quite different even though the spectrometer slit widths are the same. Thus, it is apparent that different portions of the band grow differently with increasing w and P_e.

Other typical spectral records are shown in Fig. 2. Those in the upper left panel show the relatively small effects of increasing P_e when the absorber concentration is large. The curves in the upper right panel represent results obtained with pure N_2O samples; these curves illustrate the influence of simultaneous increase of w and P_e. The curves in the middle and lower panels show the effect of increasing P_e for smaller values of w. The curves in the lower left panel were obtained with the ordinate scale expanded approximately five times. It will be noted that the P- and R-branches become more clearly defined as P_e increases.

Many of the results obtained are plotted on a logarithmic scale in Fig. 3, which gives $\int A(\nu)d\nu$ as a function of P_e. Each curve corresponds to a given absorber concentration and shows the effect of increasing P_e by the addition of N_2. Path lengths indicated in the figure give the lengths of the absorption cells used for each curve. The points marked x at the lower ends of curves A through P were obtained with pure samples of N_2O; the points at the lower ends of curves Q, R, and S represent results obtained with previously mixed samples of N_2O and N_2. Parts of curves D and E are omitted from the figure for purposes of clarity; however, the upper portions actually occupy positions that can be accurately estimated by comparison with F, G, and H.

There is a general decrease in the slopes of the curves with increasing pressure, indicating a decrease in the dependence of total absorptance on equivalent pressure. This "saturation phenomenon" can be explained on the basis of the change of line shape with pressure. As the pressure increases, the half-width of a spectral line increases; the absorption coefficient $k(\nu)$ increases in the wings of the line and decreases at the line center. For pressures sufficiently high that the line half-width is equal to the spacing between the lines, the rotational fine structure diminishes, and further increases in pressure have but little effect on total absorptance. Goody and Wormell[4] have shown that the line half-width becomes essentially equal to line spacing in N_2O at a pressure of approximately 4100 mm Hg. The onset of this effect probably accounts for the saturation phenomenon in Fig. 3 at high values of P_e.

It will be noted from Fig. 3 that the value of P_e at which saturation begins is greater for large values of absorber concentration than for smaller values. In the case of large w, the decrease of $k(\nu)$ near the line centers accompanying increased P_e does not appreciably change spectral absorptance at these frequencies since $k(\nu)w$ is still sufficiently great that spectral absorptance remains essentially complete at the line centers. However, in the case of small w, a relatively small value of P_e is sufficient to reduce $k(\nu)w$ at the line centers to a value such that the *decrease* in spectral absorptance near the line centers is approximately the same as the *increase* in spectral absorptance in the wings of the lines. Therefore there is little or no increase in $\int A(\nu)d\nu$ with increasing P_e.

The small variation in total absorptance with w and P_e for large values of these parameters results in the crowding of the curves in the upper right-hand corner of Fig. 3. The observed effects are to be expected for

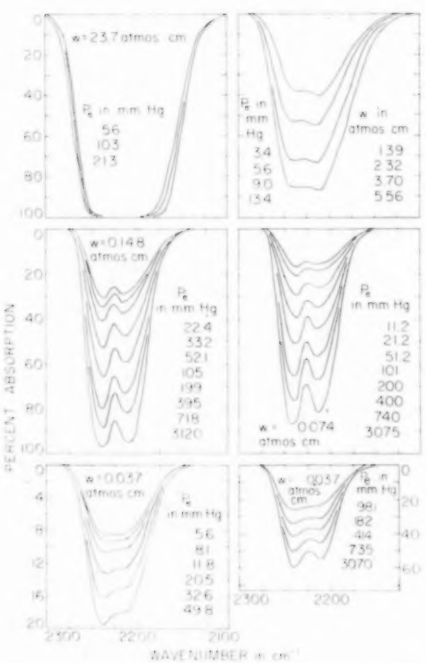

Fig. 2. Spectral absorptance of various samples in the vicinity of the 2224 cm^{-1} band.

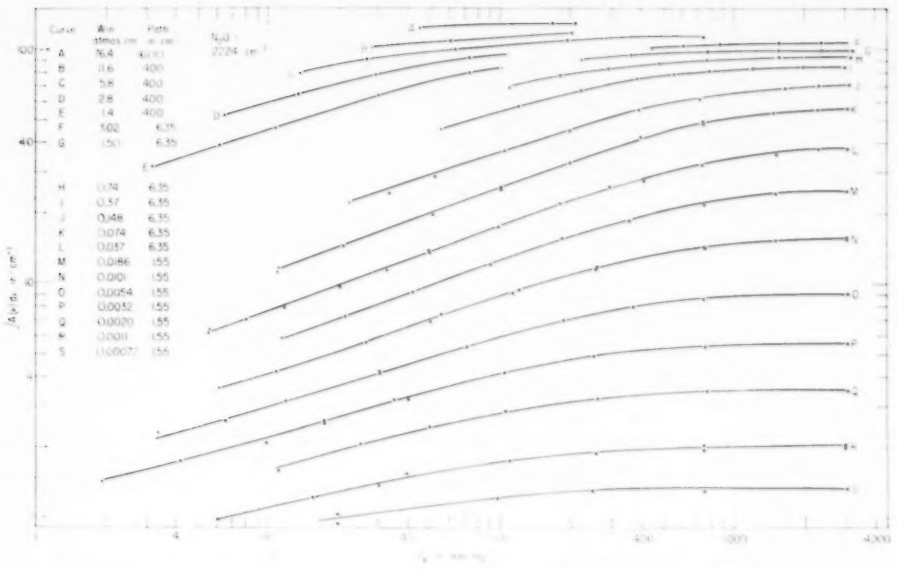

Fig. 3. Total absorptance of the 2224 cm^{-1} band versus equivalent pressure for samples having constant values of absorber concentration w, which are listed for the successive curves.

situations in which $k(\nu)w$ is large for nearly all frequencies within the band. Inspection of the spectral records corresponding to the points in the upper right-hand corner of Fig. 3 reveals that spectral absorptance is indeed complete near the band center; any band growth accompanying further increase in w or P_e is slight and occurs in the wings of the band.

Curves J through O in Fig. 3 have approximately the same slopes for pressures lower than 200 mm Hg. The average value of the slopes of these curves is 0.37. Thus, it is possible to express the total absorptance as some function of absorber concentration times $P_e^{0.37}$ for the values of w and P_e represented by these curves.

In Fig. 4 are five curves giving $\int A(\nu)d\nu$ as a function of P_e for samples in which w is directly proportional to P_e. Curves A, B, and C are for pure N_2O samples; the ratios of w to P_e for these three curves are different because of the difference in path lengths. Curve D corresponds to a mixture of one part of N_2O to nine parts of N_2 by volume; curve E gives results for a mixture of one part of N_2O to 49 parts of N_2 by volume. Therefore, for curves D and E, w is proportional to P_e as for curves A, B, and C; however, in curves D and E the ratios of w to P_e are different as a result of different dilutions with N_2. The curves in Fig. 4 are based on some data previously plotted in Fig. 3 and some additional data not previously presented. The slopes of curves A, B, and C decrease for large values of w and P_e, as in the case of the curves in Fig. 3; this saturation occurs for smaller values of P_e for long path lengths because w is greater. The maximum values of w were not sufficiently great to produce saturation in curves D and E.

It is to be noted that the curves B, C, D, and E in Fig. 4 have regions that are nearly linear over wide ranges of P_e greater than 10 mm Hg. The linear portions have slopes of 0.91, which is considerably greater than the slopes of the linear portions of the curves in Fig. 3. The greater slope of the curves in Fig. 4 is due to the fact that w increases with increasing

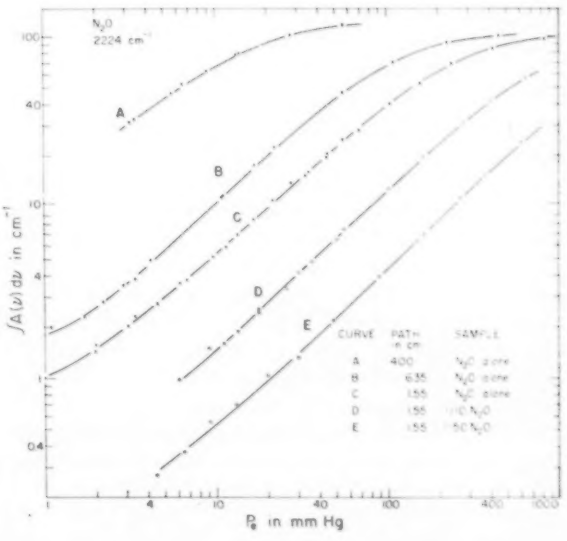

Fig. 4. Total absorptance of the 2224 cm^{-1} band versus equivalent pressure for samples in which absorber concentration is directly proportional to equivalent pressure.

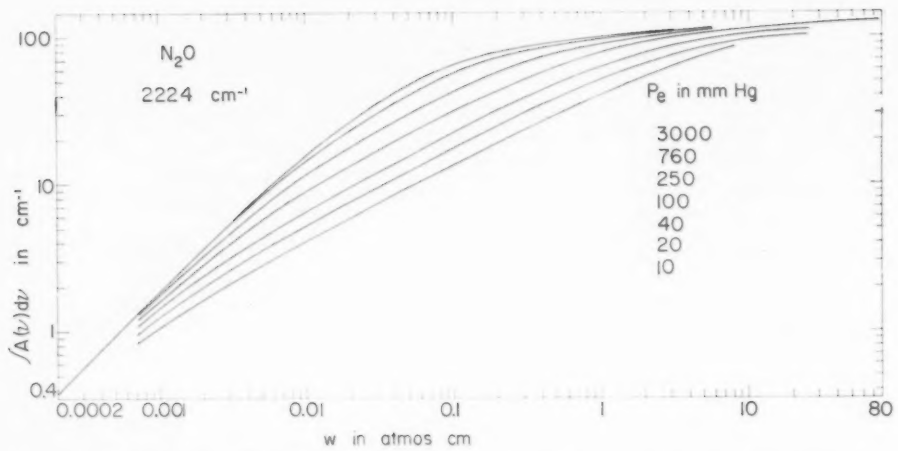

Fig. 5. Total absorptance of the 2224 cm^{-1} band versus absorber concentration for samples having the equivalent pressures listed.

P_e in Fig. 4, but w is constant for each curve in Fig. 3. The slope of 0.91 in Fig. 4 indicates that for the linear portion of the curves

$$\int A(\nu)d\nu = cw^m P_e^n, \tag{3}$$

where $m + n = 0.91$ and c is a constant for each curve. Since it was shown in Fig. 3 that $\int A(\nu)d\nu$ is proportional to $P_e^{0.37}$ over considerable ranges of w and P_e, it would appear that $n = 0.37$ and $m = 0.54$ in (3).

It will be noted that the slopes of curves B and C in Fig. 4 decrease for values of P_e less than 10 mm Hg; this decrease is general and cannot be explained on the basis of pressure-broadened lines of Lorentz shape. It is attributed to the increasing influence of Doppler broadening at low pressures; similar effects at low pressures have been reported by Goody and Wormell[4] and by Benedict *et al.*[5]

In order to show more clearly the variation of $\int A(\nu)d\nu$ with w, data from the curves of Figs. 3 and 4 were replotted in Fig. 5, in which each curve corresponds to a different value of P_e as indicated in the figure. Although the curves in Fig. 5 converge at the lowest and highest values of w, it will be noted that over considerable ranges of w the five lower curves have linear portions having slopes of 0.53 in close agreement with the value of 0.54 proposed for m in (3). The curves in Fig. 5 are quite useful in making estimates of total absorptance $\int A(\nu)d\nu$ for any value of w and P_e covered in the investigation, since interpolations for P_e between the curves shown can easily be made.

Since there is coincidence of the ranges of w and P_e for which the curves of Figs. 3 and 5 are linear, it is possible to express $\int A(\nu)d\nu$ for these ranges by

$$\int A(\nu)d\nu = cw^{0.53}P_e^{0.37} \approx c(wP_e^{0.7})^{0.53}. \tag{4}$$

In order to check the range of validity of (4) and to point out some of the dangers involved in the use of empirical equations, all the data represented in Figs. 3, 4, and 5 have been replotted in Fig. 6, which shows $\int A(\nu)d\nu$ as a function of $(wP_e^{0.7})$; each curve corresponds to a given value of P_e as indicated. If $\int A(\nu)d\nu$ were indeed a function only of $(wP_e^{0.7})$, all curves in Fig. 6 would coincide. It is not surprising that the curve corresponding to $P_e = 3000$ mm Hg falls well to the right of the other curves, since the rotational structure is nearly smoothed out at this high pressure, and the effects of increasing pressure are small. It is to be noted that the other curves diverge for low values of $(wP_e^{0.7})$; this divergence shows the extreme danger of extrapolating empirical equations like (4) to low pressures. Since some of the curves in Fig. 6 cross, one may conclude that the exponent 0.7 is too small for some values of w and P_e and too large for others.

However, it is possible from the curves of Fig. 6 to determine useful empirical relations and their ranges of validity. Thus, the nearly linear middle portions of the curve can be represented by the equation

$$\int A(\nu)d\nu = 18\,(wP_e^{0.7})^{0.53} \tag{5}$$

for the ranges 10 $cm^{-1} < \int A(\nu)d\nu < 45$ cm^{-1} and 10 mm Hg $< P_e < 250$ mm Hg. For larger values of $\int A(\nu)d\nu$, the following equation can be applied:

$$\int A(\nu)d\nu = 15 + 40 \text{ Log } (wP_e^{0.7}) \tag{6}$$

for the ranges 45 $cm^{-1} < \int A(\nu)d\nu < 120$ cm^{-1} and 10 mm Hg $< P_e < 760$ mm Hg. In (5) and (6) the absorber concentration w is expressed in atm cm. Values of total absorptance computed from these equations are believed to be accurate to $\pm 10\%$; extrapolations should be avoided.

It is desirable to compare the present results with those predicted on the basis of various theoretical band models. In view of the regularities in line spacing in the 2224 cm^{-1} N_2O band, it would appear appropriate to use an Elsasser band model,[6] for which the total

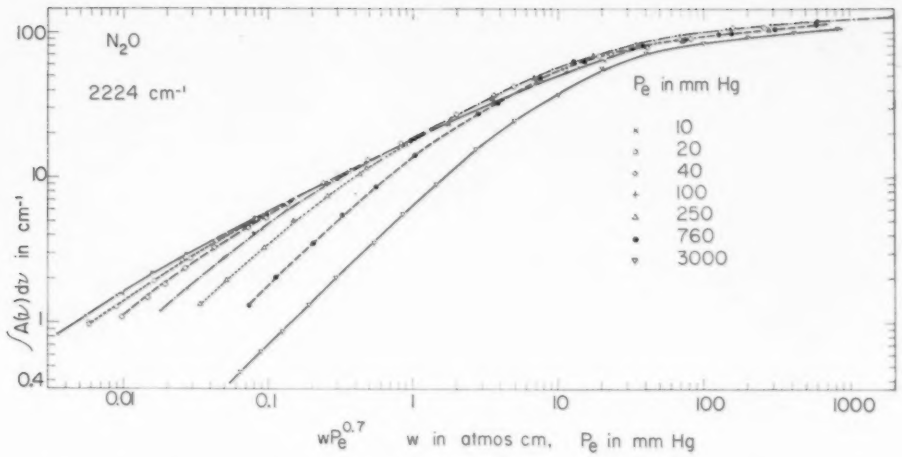

Fig. 6. Total absorptance versus $wP_e^{0.7}$. The limitations of empirical equations are illustrated.

absorptance can be expressed as a function of (wP_e) under certain conditions. In order to test the Elsasser model, the curves in Fig. 7 were plotted from the experimental data presented earlier; coincidence of the curves would indicate a function of (wP_e). It will be noted that except at the onset of saturation the various curves are separated more widely than those in Fig. 6. Use of the criteria of Plass[7] for the validity of the strong line approximation [the name given to the approximation when the total absorptance can be expressed as a function of the single variable (wP_e)], along with data of Goody and Wormell,[4] to obtain relations between w and P_e and the dimensionless parameters employed in the theoretical expressions made possible a more quantitative test of the Elsasser model. It was found that, for many values of w and P_e for which the strong line approximation would be expected to apply, agreement between theoretical predictions and experimental results was not closer than ±20%.

The experimental results show that total absorptance is less strongly dependent on P_e than on w. This weaker dependence on pressure than that required by the Elsasser model can be explained qualitatively on the basis of weak lines in the 2224 cm^{-1} region; for weak lines the effects of w are always greater than those due to P_e. It is possible that the "random Elsasser model" applied successfully by Plass[7] to the ozone spectrum might also be successfully employed in the treatment of the 2224 cm^{-1} N_2O band.

Results for Other N_2O Bands

Although the 2224 cm^{-1} band is in some respects the most important N_2O absorption band from the standpoint of telluric atmospheric transmission, other spectral regions of N_2O absorption at 2563, 2461, 1285, 1167, 692, and 589 cm^{-1} were also investigated by methods similar to those described earlier, except for the use of a KBr prism for the last two regions mentioned.

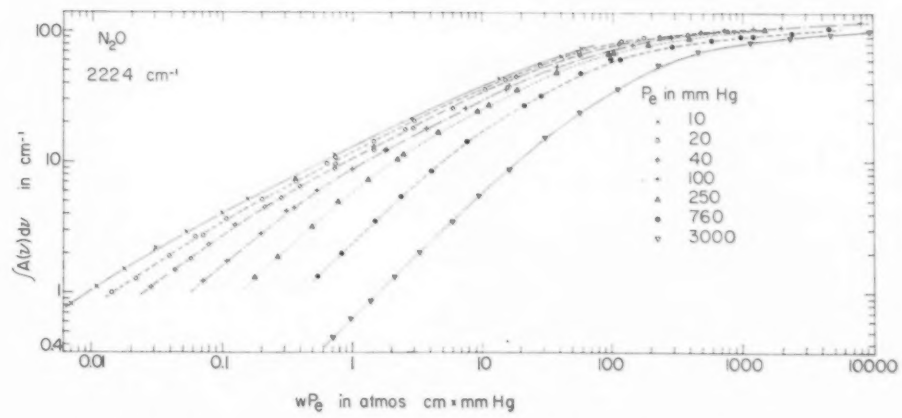

Fig. 7. Total absorptance versus wP_e. The limitations of existing theories are illustrated.

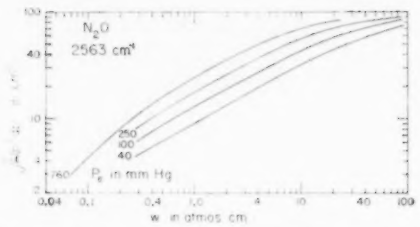

Fig. 8. Total absorptance of the 2563 cm^{-1} band versus absorber concentration for the values of equivalent pressure listed.

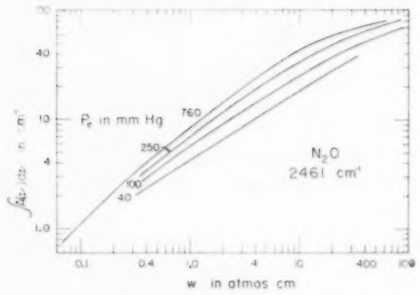

Fig. 9. Total absorptance of the 2461 cm^{-1} band versus absorber concentration for various values of P_e.

In Fig. 8 are summarized the results obtained for the 2563 cm^{-1} band. The smoothed curves shown in this figure can be used to predict values of total absorptance to $\pm 5\%$ for the range of w and P_e covered when $\int A(\nu)d\nu > 30$ cm^{-1}; somewhat greater errors may be encountered for lower values of total absorptance. Similar sets of curves for the 2461, 1285, and 1167 cm^{-1} bands are shown in Figs. 9, 10, and 11, respectively. The data presented in Fig. 10 appear to agree to within a few percent with similar data published by Goody and Wormell.[4]

Figure 12 gives a set of curves showing spectral absorptance of N_2O in the vicinity of its ν_2 fundamental at 589 cm^{-1} and at the much weaker band at 692 cm^{-1}; the spectral slit width employed was approximately 6 cm^{-1}. Absorption by the weaker band was measurable only for large values of P_e and w, and its total absorptance was not plotted as a function of w, since so few data were available. Plots of $\int A(\nu)d\nu$ versus w for the 589 cm^{-1} band are shown in Fig. 13 and may be used to estimate total absorptance for other values of w and P_e within the range covered.

The general features of the sets of curves shown for various bands in Figs. 8, 9, 10, 11, and 13 are for the most part quite similar to those discussed in detail for the 2224 cm^{-1} band.

Band Intensities

One quantity of fundamental importance in molecular spectroscopy is *band strength* or *band intensity*, defined as the integral of the absorption coefficient $k(\nu)$ over all frequencies in a band. Although the value of $\int k(\nu)d\nu$ depends on population differences between the upper and lower vibrational states and is therefore a function of temperature, basic information regarding molecular transition moments can be obtained provided $\int k(\nu)d\nu$ is known at some definite temperature. Under certain conditions band intensities can be determined from some of the data obtained in the present study.

The spectral absorptance $A'(\nu)$ obtained with a spectrometer of infinite resolving power is given by the familiar expression

$$A'(\nu) = 1 - e^{-k(\nu)w}. \tag{7}$$

However, $\int A'(\nu)d\nu = \int A(\nu)d\nu$, where $A(\nu)$ is the measured value of the spectral absorptance and the limits of integration include an entire band. Therefore, for a situation in which $k(\nu)w \ll 1$ throughout an entire band

$$\int A(\nu)d\nu = \int (1 - e^{-k(\nu)w})d\nu = w \int k(\nu)d\nu$$

and

$$\int k(\nu)d\nu = \frac{\int A(\nu)d\nu}{w}. \tag{8}$$

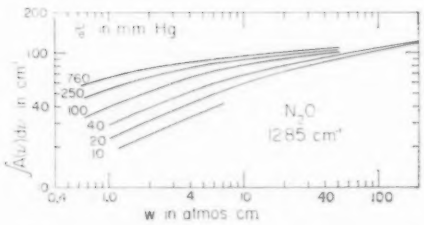

Fig. 10. Total absorptance of the 1285 cm^{-1} versus absorber concentration.

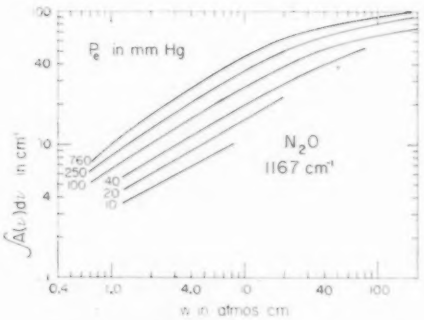

Fig. 11. Total absorptance of the 1167 cm^{-1} band versus absorber concentration.

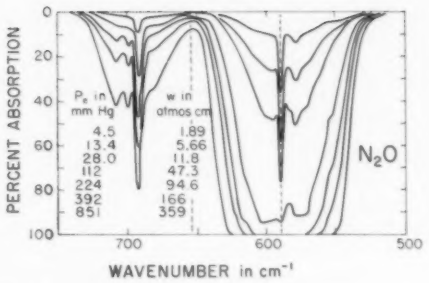

Fig. 12. Spectral absorptance of the 692 cm^{-1} and 589 cm^{-1} bands measured with a spectral slit width of 6 cm^{-1}. The bands were arbitrarily separated at 655 cm^{-1} in determining total absorptance.

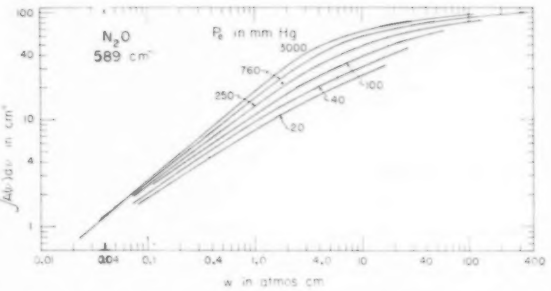

Fig. 13. Total absorptance of the 589 cm^{-1} band versus absorber concentration.

In order to obtain the band intensity from (8) by the methods used in the present study, the approximation that $k(\nu)w \ll 1$ for *all* frequencies must be valid, a requirement that is satisfied by small values of w and values of P_e sufficiently large that $k(\nu)$ is small even at the centers of rotational lines. Under these conditions, the lines are said to be "completely broadened" and the total absorptance of the band is directly proportional to w but independent of P_e.

The lower portion of the uppermost curve in Fig. 5, corresponding to a total pressure of 3000 mm Hg, is linear and has a slope of approximately unity; thus $\int A(\nu)d\nu$ is directly proportional to w. It will also be noted that the lower portions of the three upper curves of Fig. 5, which correspond to values of $P_e \geq 250$ mm Hg, converge at low values of w. Thus, it would appear that the condition $k(\nu)w \ll 1$ is satisfied under conditions applying to the lowest values of w represented in Fig. 5. Some question has been raised concerning earlier results of Thorndyke, Wells, and Wilson,[8] with regard to fulfillment of the condition that $k(\nu)w \ll 1$. However, in the present study the data are sufficient to establish the approximation involved in (8).

At the intercept of the uppermost curve in Fig. 5, $\int A(\nu)d\nu = 0.37$ cm^{-1} and $w = 2 \times 10^{-4}$ atm cm. Substitution of these values in (8) gives $\int k(\nu)d\nu = 1850$ (atm cm)$^{-1}$ cm^{-1} for the band intensity of the 2224 cm^{-1} N_2O band. It should be noted that the use of the intercept values from Fig. 5 involves the "averaging processes" used in drawing the smooth curves. Other careful measurements of $\int A(\nu)d\nu$ for samples with large P_e and small w indicate that the value stated above is accurate to $\pm 10\%$. A major source of error is the determination of w; in order to improve the accuracy of this measurement, short cells were employed to avoid the measurement of small p and in some samples N_2O was added from previously mixed samples of N_2O and N_2.

By methods similar to those described for the 2224 cm^{-1} band, it was also possible to determine band intensities for the 2563, 2461, 1167, and 589 cm^{-1} bands, but even with the smallest values of w employed it was impossible to establish the condition $k(\nu)w \ll 1$ for the 1285 cm^{-1} band. The values obtained for N_2O band intensities are listed in Table I.

The present result for the 2224 cm^{-1} band is in excellent agreement with the value of 1867 (atm cm)$^{-1}$ cm^{-1} reported by Thorndyke *et al.*[8] and possibly in fair agreement with the value 1650 reported by Eggers and Crawford,[9] provided uncertainties in both sets of data are considered; however, the present result is definitely larger than the value of 1617 reported by Calloman, McKean, and Thompson.[10] The present results for the 1167 cm^{-1} band agree within the limits of experimental error with the value of 10.9 ± 0.9 reported by Goody and Wormell[4] but are definitely larger than the value of 8.5 listed by Eggers and Crawford. Finally, the value obtained for the 589 cm^{-1} band is somewhat smaller than the value of 40 reported by Thorndyke *et al.* but is considerably greater than the value 20.9 published by Eggers and Crawford. To the knowledge of the authors no values of band intensity for the 2563 and 2461 cm^{-1} bands have previously been published. It should be noted that the "scatter" in reported values of band intensity for the various bands is rather large; further studies would seem to be in order.

Table I. N_2O Band Intensities $\int k(\nu)d\nu$

Band (cm^{-1})	Intensity (atm cm)$^{-1}$ cm^{-1}
2563	44 ± 6
2461	11.5 ± 1.5
2224	1850 ± 185
1167	12.0 ± 1.2
589	33 ± 4

The authors wish to express their appreciation to Wilbur France and E. B. Singleton who assisted in certain aspects of the present work and to Carl McWhirt and his colleagues in the Physics shop for their careful work in the construction of apparatus. Finally, one of the authors (Dudley Williams) wishes to express his appreciation to P. Swings and M. Migeotte for the use of the library and other facilities at the Institut d'Astrophysique, Universite de Liége, during the preparation of this article.

References

1. D. E. Burch, E. B. Singleton, and D. Williams, Appl. Opt. **1**, 359 (1962). The symbols and nomenclature used in the present article were introduced in this reference. In accord with the new A.I.P. glossary of optical terminology, *fractional absorption* A (ν) is called *spectral absorptance* in the present paper and the earlier term *total absorption* $\int A(\nu)d\nu$ is now called *total absorptance*.
2. J. N. Howard, D. E. Burch, and D. Williams, J. Opt. Soc. Am. **46**, 186, 237, 242, 334, 452 (1956).
3. H. W. Thompson and R. L. Williams. Proc. Roy. Soc. **A208**, 326 (1951).
4. R. M. Goody and T. W. Wormell, Proc. Roy. Soc. **A209**, 178 (1951).
5. W. Benedict, R. Herman, G. Moore, and S. Silverman, Can. J. Phys. **34**, 830, 850 (1956).
6. W. M. Elsasser, "Harvard Meteorological Studies No. 6," Harvard University, 1942.
7. G. N. Plass, J. Opt. Soc. Am. **50**, 868 (1960).
8. A. M. Thorndyke, A. J. Wells, and E. B. Wilson, J. Chem. Phys. **18**, 157 (1947).
9. D. F. Eggers and B. L. Crawford, J. Chem. Phys. **19**, 1554 (1951).
10. H. J. Calloman, D. C. McKean, and H. W. Thompson, Proc. Roy. Soc. **A208**, 332 (1951).

ANNOUNCEMENT OF PROGRAM AND REQUEST FOR CONTRIBUTED PAPERS MANGER HOTEL, ROCHESTER, NEW YORK OSA 47TH ANNUAL MEETING, OCTOBER 2 TO 5, 1962

Invited Papers. There will be six invited papers by acknowledged authorities on a wide variety of subjects, including the Purcell effect, space optics, light waves in nonlinear media, and optical glass. It is hoped that many **contributed papers** will be offered on these as well as other topics of interest to OSA members. The dinner speaker will be **Crawford Greenewalt,** President of Du Pont, who will show slides of humming birds and high-speed motion pictures of birds and insects in flight.

Rochester, New York, is the home of the Institute of Optics and of many industries of an optical and general scientific nature. October 2nd therefore has been assigned to plant and other visits. Three full days of invited and contributed paper sessions will follow. A choice of full-day and half-day trips to other points of interest will be offered on Saturday, October 3rd.

Institute of Optics will hold an open-house all day on Tuesday, October 2nd, with a lecture and program related to education in optics in the evening.

Ladies' Program. A varied and complete program is planned, including leisurely local and day trips to the Naples Wineries or the Syracuse China Works.

Hotel. Headquarters will be located in the Manger Hotel, but downtown motel and other hotel accommodation is available. Midtown Plaza, just opened with national acclaim, is adjacent to the Manger Hotel and provides unusual facilities for shopping, meals, and parking.

Applied Optics semiannual meeting of Editors, Reporters, and Patents Panelists will be held at noon on Thursday, October 4th in the Manger.

Annual Business Meeting. The Annual Business Meeting of the Society will be held on Friday, October 5th.

George Eastman House. Plan to stay Friday evening for an event at George Eastman House, including showing of early movies and viewing of the recently opened Mees Gallery.

Abstracts of Contributed Papers. An Abstract Form for submission of contributed papers is available from the Executive Secretary. Presentation time will be limited to fifteen minutes. More than one paper by the same author or coauthors on closely related topics will be accepted only if time permits; the prior choice should therefore be clearly indicated. Because blackboards are almost useless in a large auditorium, overhead projectors will be substituted. Lantern slides, infinitely preferable, should have large type and a minimum of information per slide.

Abstracts must be in the Executive Office by July 16, 1962.
NO POSTDEADLINE PAPERS CAN BE ACCEPTED FOR THIS MEETING.

Optical Society of America
Mary E. Warga, Executive Secretary

1155 Sixteenth Street, N.W. Washington 6, D.C.

Inspecting Infrared Optical Materials and Systems by Means of the Evaporograph

Gene W. McDaniel and Arthur P. DiMattia

Quality control of infrared optical elements fabricated from visually opaque materials can be accomplished either during manufacture or after completion by the use of the Evaporograph, a thermal-imaging device. The wavelength range for which the components are designed is used for this inspection. Localized variations in transmittance ranging from 100% to less than 1% are detected and typical examples are shown. The same technique can be applied to the inspection of antireflection coatings. The results obtained are enhanced by the use of suitable filters and examples are shown. Other applications include the inspection of images produced by infrared optical systems, and the determination of birefringence.

I. Introduction

Early infrared systems consisted of a simple detector and collecting mirror. In recent years, as materials such as germanium, silicon, sapphire, and others transparent to infrared radiation have become available in large sizes, these simple systems have increased in complexity. Today infrared devices incorporate intricate detector arrays and associated optical systems which may include lenses, windows, and prisms fabricated from one or more of these materials.

For proper quality control the individual elements of these systems must be inspected and their optical properties measured in the range of wavelengths in which they are intended to function. Obviously the best procedure is to inspect the unfinished blanks prior to final polish to discover any gross imperfections, such as bubbles, stria, or inclusions. This is easily done for those materials that transmit visible light by simply looking through the blank at a light source. Such is not the case for visually-opaque materials such as germanium and silicon. These materials can, however, be easily inspected with the aid of the Evaporograph, an infrared imaging device. Following a brief discussion of the Evaporograph, its application to the inspection of materials for transmittance is described and examples are shown in Section III. Next, the inspection of antireflection coatings is described and the effect of infrared filtering on the results obtained is demonstrated. Finally, the extension of this method to other inspection problems is indicated.

The authors are with Baird-Atomic, Cambridge 39, Massachusetts.

Received July 1961.

II. The Evaporograph

The principle of the Evaporograph is the oldest method of thermal imaging. It was first described in 1840 by Sir William Herschel,[1] who used it to demonstrate the existence of absorption bands in the infrared portion of the sun's spectrum. The method was forgotten until the 1920's when M. Czerny[2,3] in Germany adopted this principle to record infrared spectra and developed the device which is in use today.

In the present commercial version, the Evaporograph[4] is a thermal-imaging device which converts an infrared image into a visible image by differential evaporation or condensation of oil on a thin membrane. The variations in the oil film thickness which reproduce the image focused on the membrane by the infrared optical system can be seen by virtue of the interference between light reflected from the front surface of the oil film and from the rear surface of the membrane. For this purpose, the membrane is illuminated by a collimated beam of light from an incandescent lamp.

The Evaporograph is an integrating device which responds to total energy differences between various portions of the infrared image. In this respect its action is similar to that of a photographic emulsion. The sensitivity of current models is such that energy differences of 2% in the scene for temperatures ranging from −40°C to 500°C can be detected. This corresponds to a temperature difference of about 1°C at 20°C for materials having an emissivity of at least 0.9. With a 10°C temperature difference above 20°C and emissivities of 0.9, the resolution is ten lines per millimeter on the membrane.

III. Inspection of Materials for Transmission

Introduction

The application of the Evaporograph to the inspection of optical components for transmittance was originally conceived in an attempt to explain the low sensitivity of an infrared system employing a germanium lens. Samples of the germanium blank were obtained and polished. These were then used to develop a test method.

Description of Apparatus

A diagram of the apparatus is shown in Fig. 1. The source of infrared radiation is an aluminum plate, 2.5 cm thick which is heated from the rear by an electric heater. The front surface is painted with a flat black paint. Immediately in front of the plate is a Masonite baffle on which the sample can be mounted in front of a suitable aperture. Directly below this aperture is a sector disk which is used to provide a means of estimating the transmittance by color matching. The Evaporograph is focused on the sample, and so positioned that the sample and the sector disk fill the field of view.

As shown in the figure, the sector disk has four annular areas which have angular openings that are 75, 50, 25, and 12.5 percent of a complete circle. When this disk is rotated at a speed of approximately 600 rpm or more, the average integrated energy which the Evaporograph "sees" as originating at these annular openings is proportional to the fractional opening. Thus, these regions can be said to have transmittances of 75, 50, 25, and 12.5 percent.

Theory

Since the Evaporograph responds to long wavelength infrared radiation, it is important to consider the effects of self-emission from the baffle and the sector disk in analyzing the effect of the sector. However, one can easily show that a true transmittance scale is obtained from the sector disk. Let the source temperature be T_2 and the ambient temperature, T_1; and further assume that the sample, the baffle, and the sector disk are at ambient temperature, T_1. The infrared radiation transmitted by the sample originates at the painted aluminum plate at a temperature T_2. This can be considered to be a "grey" body with an emittance of 0.9. That is, the emittance is constant for all wavelengths. The transmittance, reflectance, and emittance of the sample are functions of the wavelength, and therefore integration over all wavelengths is required to determine the total power leaving each unit area of the sample. For the general case, this can be expressed as:

$$P_s = \int_0^\infty \tau_s(\lambda)\epsilon_1(\lambda)W_\lambda(T_2)d\lambda + \int_0^\infty \rho_s(\lambda)W_\lambda(T_1)d\lambda + \int_0^\infty \epsilon_s(\lambda)W_\lambda(T_1)d\lambda \quad (1)$$

where

P_s = radiant power leaving a unit area of the sample,
$\tau_s(\lambda)$ = spectral transmittance of sample at wavelength λ,
$\rho_s(\lambda)$ = spectral reflectance of sample at wavelength λ,
$\epsilon_s(\lambda)$ = spectral emittance of sample at wavelength λ,
$\epsilon_1(\lambda)$ = spectral emittance of source at wavelength λ,
$W_\lambda(T_1)$ = spectral radiant emittance of a black body at temperature T_1,
$W_\lambda(T_2)$ = spectral radiant emittance of a black body at temperature T_2.

Here it is assumed that the radiation incident upon the front surface of the sample from its surroundings is black body radiation at temperature T_1. The first term represents power from the source transmitted by the sample. The second term is the ambient radiant power reflected by the sample; and the third term is the power emitted by the sample due to its own temperature T_1. But

$$\tau_s(\lambda) + \rho_s(\lambda) + \epsilon_s(\lambda) = 1$$

whence

$$\rho_s(\lambda) + \epsilon_s(\lambda) = 1 - \tau_s(\lambda) \quad (2)$$

and $\epsilon_1(\lambda)$ has been assumed to be independent of wavelength. Then substituting in Eq. (1)

$$P_s = \epsilon_1 \int_0^\infty \tau_s(\lambda)W_\lambda(T_2)d\lambda + \int_0^\infty [1 - \tau_s(\lambda)]\, W_\lambda(T_1)d\lambda \quad (3)$$

Now if the transmittance of the sample, τ_s, can be considered to be constant over the wavelength range of interest, Eq. (3) can be written as

$$P_s = \epsilon_1\tau_s\sigma T_2^4 + (1 - \tau_s)\sigma T_1^4 \quad (4)$$

where σ is the Stefan-Boltzmann constant. Note that if τ_s is not essentially constant over the wavelength range, effective values must be used as defined by the equations

$$T_{s(av)}(T_1) = \frac{\int_0^\infty \tau_s(\lambda)W_\lambda(T_1)d\lambda}{\int_0^\infty W_\lambda(T_1)d\lambda} \quad (5)$$

and

$$T_{s(av)}(T_2) = \frac{\int_0^\infty T_s(\lambda)W_\lambda(T_2)d\lambda}{\int_0^\infty W_\lambda(T_2)d\lambda} \quad (6)$$

where $\tau_{s(av)}(T_1)$ is the effective transmittance for radiation from a source at temperature T_1 and $\tau_{s(av)}(T_2)$ is the effective transmittance for radiation from a source at T_2. For reasonable values of transmittance and a source temperature, T_2, appreciably higher than the ambient temperature, T_1, the first term of Eq. (3) is predominant and the second can be neglected.

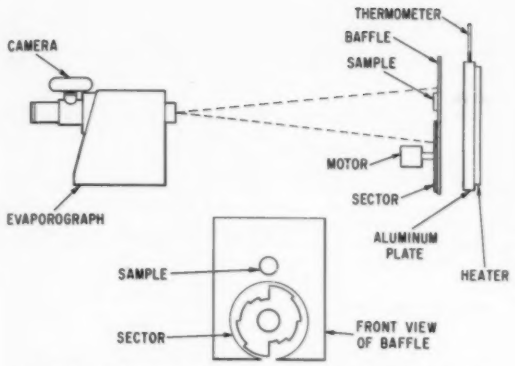

Fig. 1. Diagram of apparatus to test transmittance.

Next consider the energy which comes from one of the annular areas of the sector. During a time interval, t, which is long compared to the period of rotation of the sector, the energy originating at one of these areas is the sum of the energies emitted by and reflected from the sector while it is in place and the energy coming from the source during the time that it is visible through the open area of the sector. This can be expressed as:

$$U = (1 - k)t\left[\int_0^\infty \rho'(\lambda)W_\lambda(T_1)d\lambda + \int_0^\infty \epsilon'(\lambda)W_\lambda(T_1)d\lambda\right] + kt\int_0^\infty \epsilon_1 W_\lambda(T_2)d\lambda \quad (7)$$

where

U = total energy from a unit area,
k = fractional opening of the sector,
$\rho'(\lambda)$ = reflectance of the sector,
$\epsilon'(\lambda)$ = emittance of the sector,
t = time interval.

Since the transmittance of the sector is zero,

$$\rho'(\lambda) + \epsilon'(\lambda) = 1$$

Then Eq. (7) can be written as

$$U = kt\epsilon_1\sigma T_2^4 + (1 - k)t\sigma T_1^4$$

Dividing by t to obtain the radiant power

$$U/t = P = k\epsilon_1\sigma T_2^4 + (1 - k)\sigma T_1^4 \quad (8)$$

Comparing Eq. (8) with (4), it is obvious that the fractional opening, k, has the same effect as a transmittance of the same value.

Three major factors must be considered in transmittance measurements. These are:

1. The spectral response of the Evaporograph.
2. The spectral distribution of the radiation from the source.
3. The spectral transmittance of the sample under test.

The radiant emittance from the source is

$$W = \epsilon_1\int_0^\infty W_\lambda(T_2)d\lambda$$

This must be multiplied by the spectral response of the Evaporograph to obtain the emittance effective in forming an image.

Thus:

$$W_{eff} = \epsilon_1\int_0^\infty S_\lambda W_\lambda(T_2)d\lambda$$

where S_λ is the spectral response of the Evaporograph.

The average transmittance of the sample is the ratio of the transmitted power to the incident power, both corrected for Evaporograph response, or

$$\tau_{s(av)} = \frac{\epsilon_1\int_0^\infty \tau_s(\lambda)S_\lambda W_\lambda(T_2)d\lambda}{\int_0^\infty S_\lambda W_\lambda(T_2)d\lambda} \quad (9)$$

The spectral response of the Evaporograph is limited to the region between 3 and 19 microns, the short wavelength cutoff being determined by the infrared filter, and the long wavelength, by the salt window on the cell. The source of radiation used for these observations is an aluminum plate painted with flat black paint at a temperature of 200°C. Emissivity tests have shown that such a surface is grey and has an emissivity of approximately 0.9. In this case it is convenient to perform the integrations indicated in Eq. (9) graphically.

The several quantities concerned in a transmittance measurement are plotted as a function of wavelength in Fig. 2. Curve A is the spectral response of the Evaporograph from 2 to 16 microns. Curve B is the spectral radiant emittance of the source plotted as a fraction of the radiant emittance of a 200°C blackbody. Curve C is the spectral transmittance of a good germanium sample. Multiplying curve B by A and C yields curve D which represents the effective spectral radiant emittance as seen by the membrane, or the numerator of Eq. (9). Curve E is the effective spectral radiant emittance seen by the membrane from a 20°C blackbody, again expressed as a fraction of the radiation from a 200°C blackbody. This represents the emittance from the baffle which supports the sample under test. The difference in the areas under curves D and E is proportional to the power difference between the image of the source as seen through the germanium sample and the image of the baffle. The actual power can be obtained by applying a conversion factor. These areas were measured by a planimeter and found to be equivalent to 5.6×10^{-2} watt cm^{-2} and 1.6×10^{-2} watt cm^{-2}, respectively. Thus, the effective power difference is 4×10^{-2} watt cm^{-2}.

There is an additional contribution to the energy originating at the germanium due to energy emitted by the sample and ambient radiant energy reflected from the surface. Since the sample and the ambient temperature are assumed to be 20°C, this amounts to

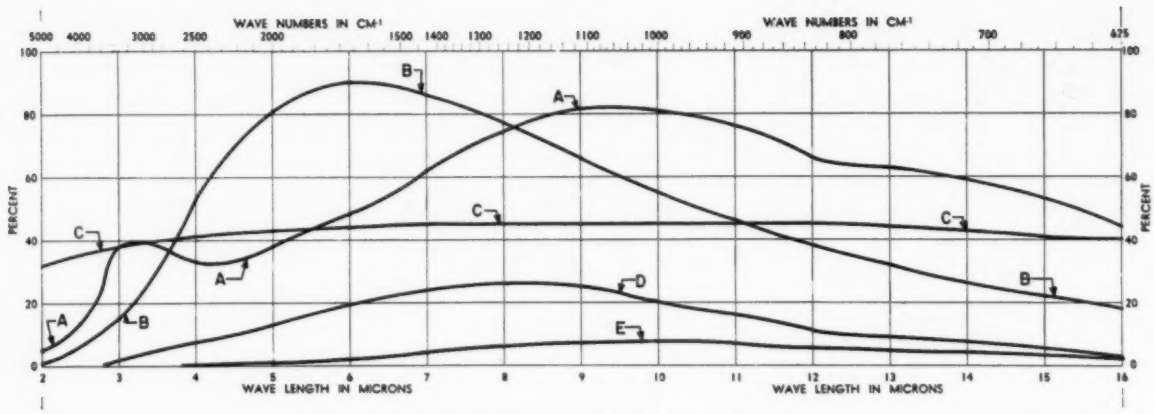

Fig. 2. Quantities concerned in transmittance measurements plotted as a function of wavelength. A—Spectral response of evaporograph. B—Spectral radiant intensity of source expressed as a fraction of the spectral radiant intensity from a 200°C black body. C—Spectral transmittance of germanium. D—Effective spectral radiant intensity from 200°C source as seen by the membrane. ' E—Effective spectral radiant intensity from a 20°C black body as seen by the membrane.

$(1 - \tau)$ times the effective energy from a 20°C source. The correction is about 15%.

It is of interest to determine the minimum transmittance of a sample that can be detected by this apparatus, using a 200°C source and a background at room temperature. The Evaporograph can detect a 2% power difference over a wide range of temperatures. Let τ_m be the minimum transmittance. Then as in Eq. (2):

$$\rho + \epsilon = 1 - \tau_m$$

Let the temperature of the sample be 20°C and consider the radiation in the room to be 20°C blackbody radiation. Then the power apparently originating at the sample will consist of a portion transmitted from the source and power reflected and emitted from the sample itself. The effective power from the 200°C source must be found by multiplying curves A and B in Fig. 2. The area under the resulting curve was found to be equivalent to 0.126 watt cm^{-2}. Then one can say,

$$0.126 \times 10^{-2}\,\tau_m + (1 - \tau_m)\,1.6 \times 10^{-2} = 1.02 \times 1.6 \times 10^{-2}$$

or

$$\tau_m = 0.003.$$

Thus, the minimum observable transmittance is less than one percent. Of course this value can be reduced by using a source having a higher temperature.

The minimum size defect that can be detected is also of interest. In practice, defects may exhibit a gradient rather than be sharply defined. In this case the maximum resolution of ten lines per millimeter may not be realized. However, if the image of such a defect covered one square millimeter, it can certainly be seen by eye. Thus, if the element under examination were imaged full size, then defects of the order of one millimeter in diameter can be detected.

Experimental Results

Figure 3 shows a photograph of the sample and the resulting Evaporograph image. This indicates that the sample transmits only in the T-shaped area designated by A and is opaque in the regions marked B. Comparing the window image with the transmittance scale indicates that the transmittance in region A is between 25 and 50 percent, while that in B is essentially zero. This is confirmed by transmissometer measurements at selected points, which indicate approximately 30 percent for A and less than one percent for B.

Next, infrared spectra of the two regions were made in a recording spectrophotometer. Figure 4 shows the results obtained. Note that there is essentially no energy transmitted through region B.

Next, both surfaces of the sample were inspected with a semiconductor resistivity test set using a four-point probe. Measurements were made at points 25 mm apart over the faces of the sample. There was no correlation between the resistivity values and the location of the opaque regions on the sample. Thus, defective components cannot be detected by this method.

The inspection technique described was also applied to finished optical components and various types of defects were discovered. Typical results obtained are displayed in Fig. 5. Evaporograph images for two convex lenses are shown. One lens has no defects while the second shows a pattern of small opaque areas. The first lens was cut from a single crystal of germanium, whereas the second was fabricated from poly-

crystalline material. Test results obtained thus far have indicated that the opaque areas usually occur in polycrystalline materials.

IV. Inspection of Antireflection Coatings

The same technique can be used to inspect antireflection coatings applied to finished optical components. To demonstrate this, a germanium and a silicon window were obtained. One-half of the germanium window was coated on both sides, and one-half of one side of the silicon window was coated.

Figure 6 is a photograph of the sample germanium window and the resulting Evaporograph images under two conditions. In the first case, the window is observed directly with no filter on the Evaporograph.

Photograph of sample

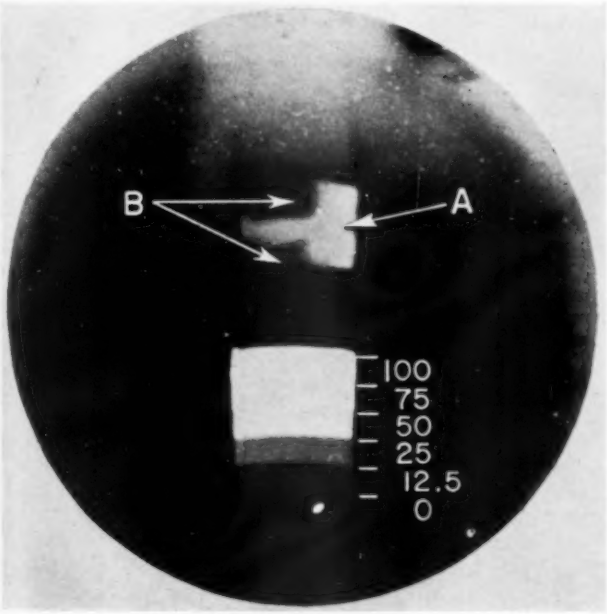

Evaporograph image

Fig. 3. Germanium sample with corresponding Evaporograph image.

In the second image, a glass filter was placed on the Evaporograph. This limits the radiation reaching the membrane to the region between 3 and 4.5 microns, the lower limit being imposed by the filter on the Evaporograph. It is obvious from the figure that the contrast between the two halves of the window is greatly enhanced by the use of the glass filter.

The effect of such filtering is explained by Fig. 7. In this figure, curve A is the transmittance of the coated half of the germanium and curve B is the transmittance of the uncoated half. Curves C and D represent the effective power from the 200°C source transmitted through the two halves of the germanium plotted as a fraction of the spectral emittance of a blackbody at 200°C. These are obtained by multiplying the spectral radiant intensity of the source by the spectral response of the Evaporograph and the transmittance of the germanium. Planimeter measurement of the areas under curves C and D gave values of 6.6×10^{-2} watt cm^{-2} and 5.7×10^{-2} watt cm^{-2}, or a difference of 15%.

Curve E is the transmittance of the glass filter, and curves F and G represent the effective energy from the two halves of the germanium corrected for the glass transmittance. The areas under these curves are equivalent to 3.2×10^{-3} watt cm^{-2} and 2×10^{-3} watt cm^{-2}, or a difference of 60%. Comparing this value with the value obtained with no filter shows that the use of the glass filter has increased the contrast four times. This demonstrates the advantages that can be obtained by filtering, or restricting the radiation reaching the Evaporograph to a definite bandwidth. The optimum wavelength interval will vary with the particular application.

Figure 8 shows a silicon window with one half coated on one side only. A glass filter was used to enhance the contrast. The difference between the coated and uncoated halves is obvious, although transmissometer measurements showed a difference of only about 10%. The Evaporograph also shows the presence of small opaque areas throughout the window.

V. Other Applications

The Evaporograph has also been applied to the inspection of detector arrays mounted behind visually opaque windows, such as germanium or silicon. The method is the same as would be used in the visible region of the spectrum. That is, the detector array is illuminated through the window with infrared radiation and the array is observed by the differences in reflectance.

Birefringence of materials such as sapphire and calcite can be detected easily. By the use of suitable filters, observations can be made at the wavelengths that will be employed in the final application. A diagram of the apparatus used is shown in Fig. 9.

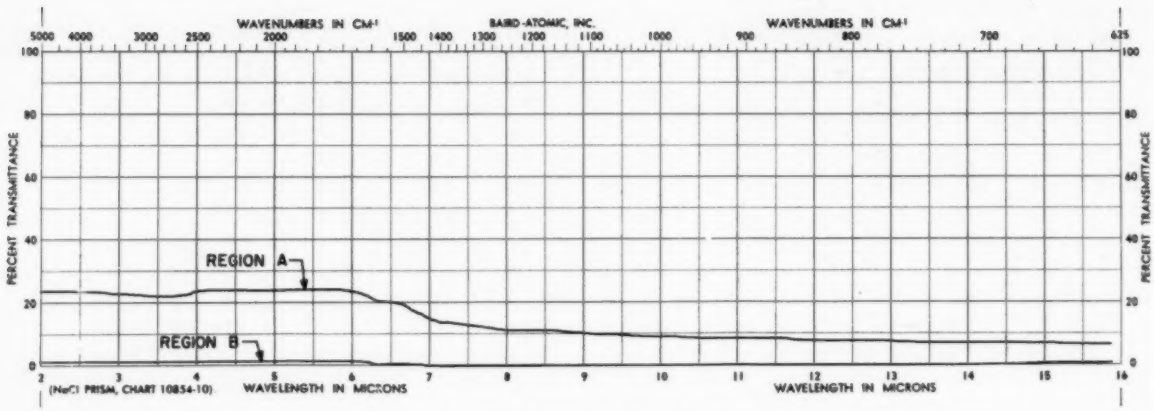

Fig. 4. Spectral transmittance of germanium sample measured by infrared spectrophotometer.

The source of radiation is a hot wire placed in back of the sample which is mounted on a suitable baffle. The Evaporograph is positioned to look through the sample at the wire and is focused on the wire. If the sample is birefringent, two images of the wire will be seen. An example of this is shown in Fig. 10, which shows the image of the wire as seen through two sapphire prisms in series, reversed so that the dispersion will cancel. Note that there are three images of the wire. This is caused by the fact that the optical axes of the two prisms are not parallel. There are actually four images produced, two of which coincide. Thus the observer sees three lines.

The images produced by infrared optical systems can be inspected for size, position, and aberrations. This may be done by focusing the image directly on the membrane, or by reimaging using the optical system of the Evaporograph. This is demonstrated in Fig. 11 which shows the image of a standard parallel-line type resolution chart. The group of lines that is resolved in this figure indicates that the system resolution is ten lines per millimeter.

VI. Conclusions

Many materials that do not transmit visible radiation are employed in infrared optical systems. Quality control of optical components fabricated from these

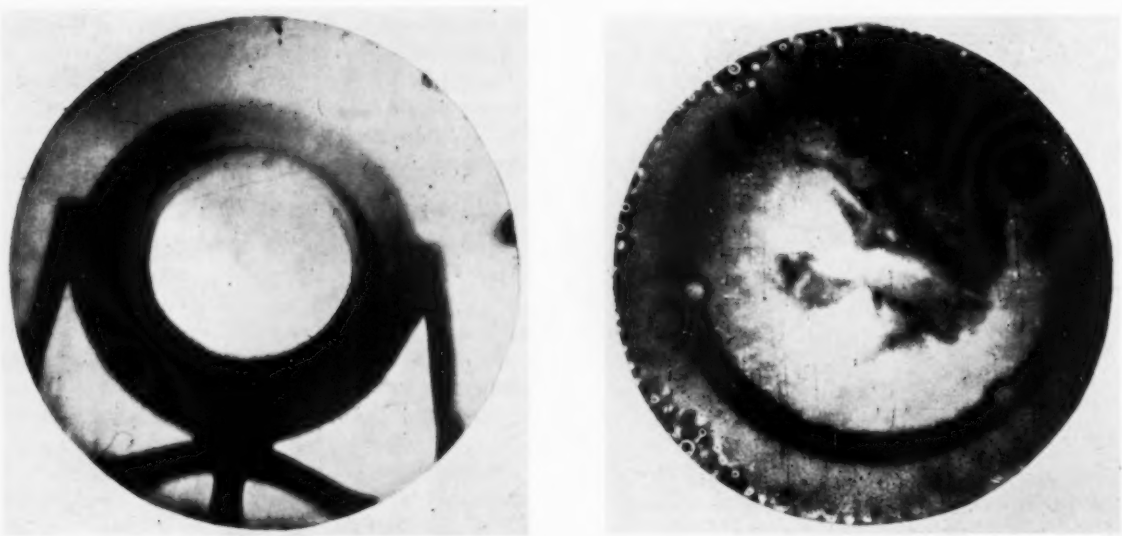

Good lens Defective lens

Fig. 5. Evaporograph images of a good and of a defective lens.

Photograph

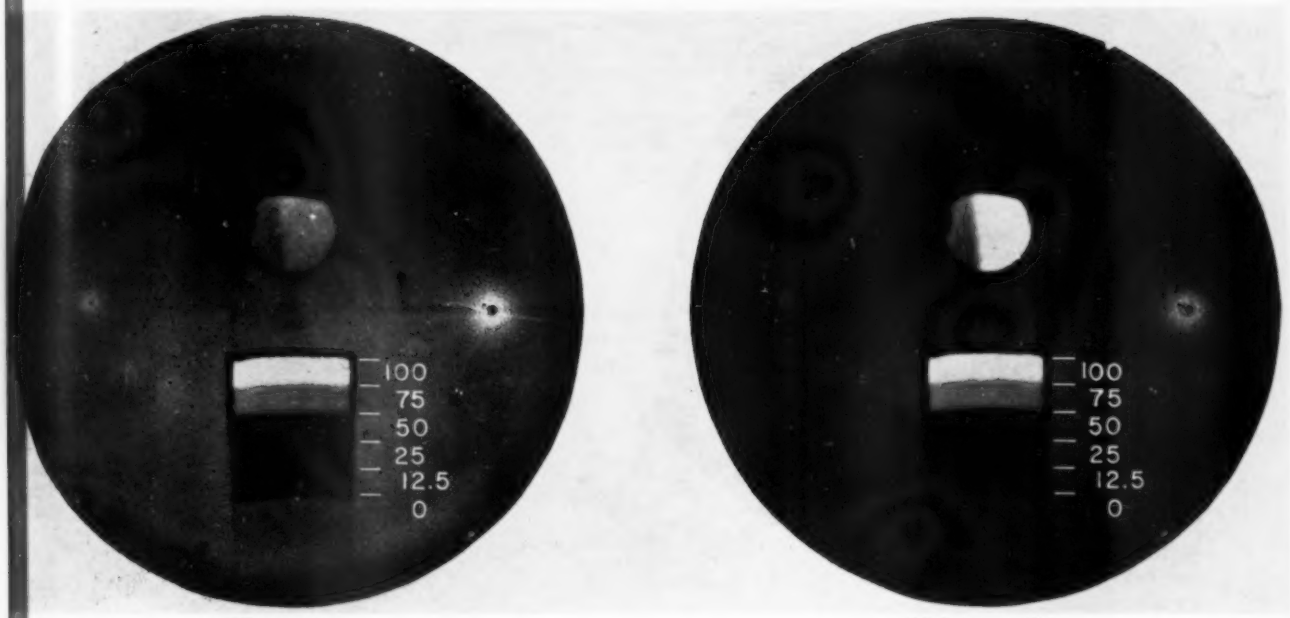

Without filter

With quartz filter

Evaporograph images

Fig. 6. Germanium window with antireflection coating on both sides of one half.

materials is therefore not possible by visual measurements or examination. It is shown that the Evaporograph can easily be applied to inspect the entire cross section of such components by a single observation for infrared transmission in the wavelength range in which they will operate. Such inspection can be made of either finished components or of partially finished blanks. Transmittances varying from 100% to less than 1% can be detected. Many optical elements made from polycrystalline materials have been found to have areas of low transmittance. The same technique can be used to inspect antireflection coatings. Examples of birefringence and inspection of image quality are shown.

The authors wish to express appreciation to Diffraction Limited of Bedford, Massachusetts, for permission to use photographs from their quality control program.

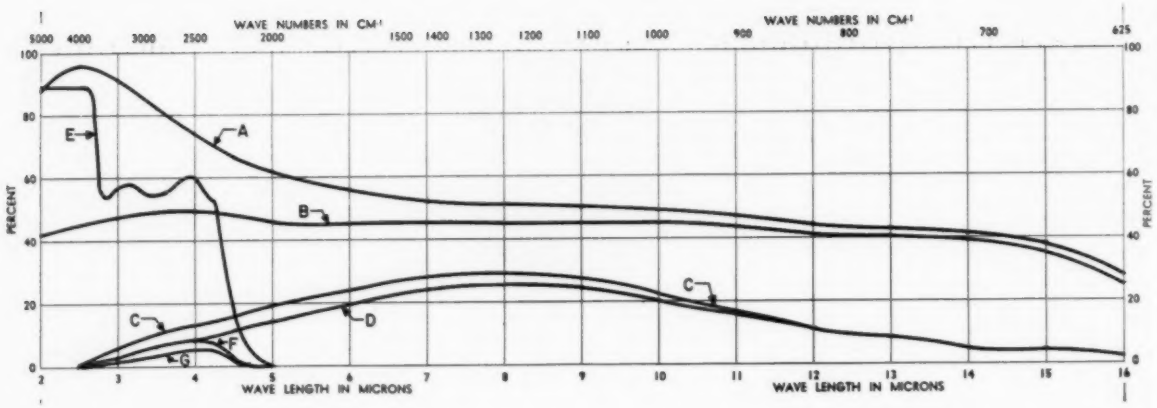

Fig. 7. Spectral transmittance of antireflection coating on germanium showing the effect of auxiliary filters. A—Measured transmittance of coated half of germanium. B—Measured transmittance of uncoated half of germanium. C—Effective radiant intensity reaching membrane through coated half of germanium expressed as a fraction of the spectral radiant intensity from a 200°C blackbody. D—Effective radiant intensity reaching membrane through uncoated half of germanium. E—Spectral transmittance of auxiliary glass filter. F—Curve C corrected for filter transmittance. G—Curve D corrected for filter transmittance.

Fig. 8. Silicon window with antireflection coating on one side of one half only, viewed through glass filter.

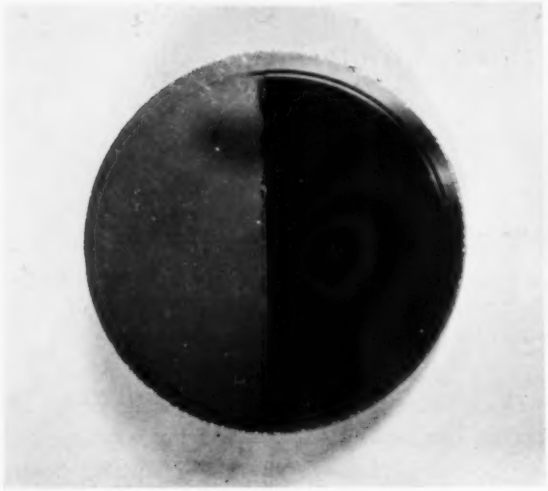

Photograph

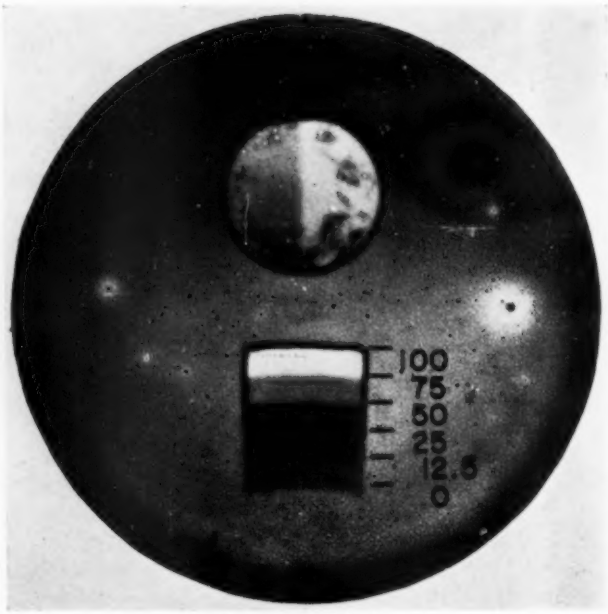

Evaporograph image

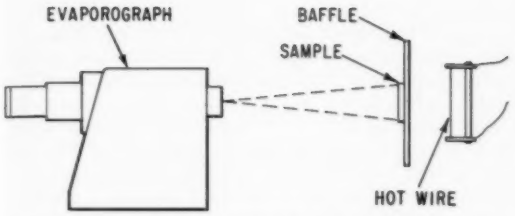

Fig. 9. Diagram of apparatus to test for birefringence.

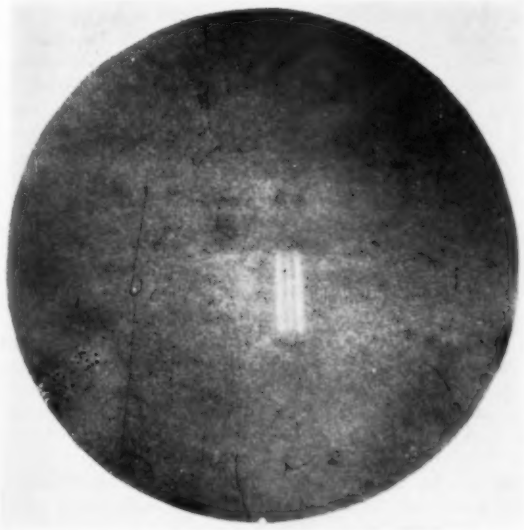

Fig. 10. Example of birefringence in sapphire.

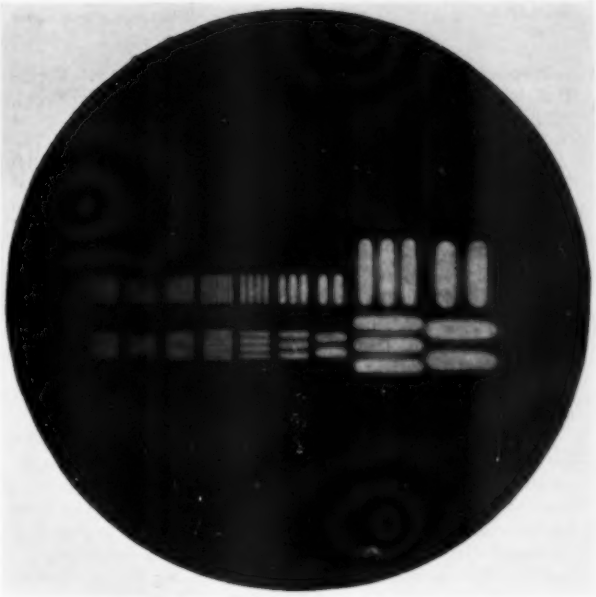

Fig. 11. Example of resolution test of optical system. Line group resolved indicates system resolution of ten lines per millimeter.

References

1. J. F. W. Herschel, Phil. Trans. Roy. Soc., London **131**, 52 (1840).
2. M. Czerny, Z. Physik **53**, 1 (1929).
3. M. Czerny and P. Mollet, Z. tech. Physik **18**, 582 (1937).
4. Gene W. McDaniel and David Z. Robinson, Appl. Optics **1**, 311 (1962).

BOOKS

Continued from page 472

well be. Some topics which were anticipated but not found are: the clock paradox, the Biot-Savart law, center of gravity, and center of mass.

A presumably unplanned yet nevertheless valuable feature of the set is that it serves to translate British terms for American readers, and *vice versa* to some extent.

To judge from carefully read random samples, the accuracy of the information presented is quite good, though there are some points on which opinions will differ. For instance, we find, "Cailletet Process. A gas expanding freely from a higher to a lower pressure does both external and internal work." Free expansion, according to most authors, involves no external work, which would make this statement contradictory. This topic, by the way, should have had fuller treatment.

As in any work of this magnitude, undetected errors persist. Some that I noted, in addition to the six on the errata slip tucked in at the back of the volume, were: "Burette. A calibrated glass tube for liquids, used vertically with a ground glass top at the bottom"—the statement that the calutron was named from its site at "California University"—page 7, "Absorption bands occur mainly in the liquid and solid phase, as well as in the infrared."—page 481, where we learn that the Bouguer-Beer (*sic*) Law is often attributed to Lambert—page 417, where we find the famous Italian optical worker Porro designated a Frenchman—and in various places the mis-accentuation of ampere (two of the six errors listed). Finally, and it really seems almost unkind to mention it, there is an error in the first word on the first page—Abbe is without an accent!

In conclusion it may be well to express an opinion as to where this work may fill a need. Its high price will as a rule preclude individual purchases, and I am doubtful whether it is the sort of thing the smaller schools should spend their money on, so we must turn to situations where price is of secondary concern. The set should be of real utility in those industrial and governmental laboratories where there is no extensive collection of technical books and journals. It may also find a place in the larger establishments where a good technical library exists, but where there are working groups located at appreciable distances from it and who could advantageously use an at-hand source of limited information. Finally, it may well merit a place in the reading room or specialized library for the other sciences and the engineering specialities. The set provides treatments which may at times be too elementary or too advanced in different cases, but in each case some immediate help can be found, frequently together with useful indications where additional information can be located.

E. Scott Barr

continued overleaf

continued from previous page

Progress in Optics, Vol. I. Edited by E. Wolf. North-Holland Publishing Co., Amsterdam (Interscience, New York), 1961. 342 pp. $12.00.

At present, a number of branches of physics are being adequately explored by serial publications presenting the latest advances in the field. To the reviewer's knowledge no adequate coverage has existed in optics. It is the main purpose of this series, entitled *Progress in Optics*, of which this is the first volume, to fulfill such a need, and Dr. Wolf has undertaken the difficult but commendable task of editing it. Judging from the standard set by this issue, we feel confident of its favorable reception by the scientific community in general and especially by the student of optics. In order to give a fair idea of the subjects covered in this volume, we shall review in some detail the main topics of each chapter.

The first chapter entitled "Modern Developments of Hamiltonian Optics" is written by Dr. Pegis. In recent years substantial progress has been made in the use of Hamiltonian methods in treating geometrical optics, but the scope of this article is more modest than the title indicates, since the analysis of geometrical aberrations is limited to the method originally developed by T. Smith. Perhaps Dr. Pegis' reason for selecting this method of approach to the geometrical theory of aberrations is to familiarize the readers with T. Smith's ideas which seem to be least known. Indeed, it is regrettable that the important and valuable contributions made by T. Smith have passed almost unnoticed by many of the principal authorities in this field and are barely mentioned in modern books on geometrical optics.

The essentials of T. Smith's method are based on the introduction of three new variables in the Hamiltonian Angular Characteristic Function (A.C.) instead of the three angular optical invariants (a.o.i.) commonly employed in treating aberrations of optical systems of rotational symmetry. The Smith variables are expressed by a linear combination of the a.o.i. with coefficients involving two parameters, identified as the optical magnification in the image and pupil planes. This special transformation of variables (symmetric in both a.o.i. and parameters) seems to have an advantage in transforming the aberration coefficients of any order from one set of parameters to another in a neat form. Dr. Pegis has described the scheme by which such a calculation may be made. Another advantage is that for a system free of aberrations the A.C. depends only on one Smith variable. An explicit expression of the A.C. in the parameters and in the Smith variable to terms of fifth degree is given for an optical system free of all image errors and of all orders of spherical aberrations of the pupil. In view of his limited knowledge of T. Smith's contributions, the reviewer wishes to recommend further study of this method for establishing a unified theory of geometrical aberrations.

In the next chapter on "Wave Optics and Geometrical Optics in Optical Design," Dr. Miyamoto's aim is to compare the results obtained for the intensity distribution of the image by using wave and geometrical theory. Following an introduction of the relationship between wave and geometrical optics, a short sketch of the diffraction theory of aberrations according to Zernike-Nijboer theory, van Kampen's treatment for large aberrations, and Herzberger's method of spot diagrams, the author formulates a procedure for calculating the response function in terms of intensity—and vice-versa—from the standpoint of wave and geometrical theory. Explicit expressions of these functions for typical aberrations have been calculated. The results show that for short wavelengths geometrical theory gives substantially the same distribution as wave theory.

The chapter on "The Intensity Distribution and Total Illumination of Aberration-Free Diffraction Images" is written by Dr. Barakat. The problem is approached using Kirchhoff's integral. The image function is evaluated according to Lommel, Nijboer, and Boivin methods. An interesting discussion on the question of the determination of the pupil function which gives an increase in resolution and maximum Stehl definition of the Fraunhofer pattern leads to the mathematical formulation of the problem in terms of an integral equation in the pupil function. The author has obtained an expression of this function (circular aperture) when the energy flow through the aperture is constant. The results show that, as the resolution is improved, the image deteriorates on account of an increase of intensity in the secondary maxima. Another important problem is to determine the pupil function which concentrates a maximum of energy within a fixed area in the image plane. To the reviewer's knowledge the mathematical formulation of this problem is lacking, except for a few simple cases which the author discusses in the text. In general, even in the absence of aberrations, the variational equations lead to a system of coupled integral equations with complicated kernels. In this connection we wish to remark that some of the calculations in Boivin's book (*Théorie et Calcul des Figures de Diffraction de Révolution*) should prove very useful in obtaining a partial solution of this difficult—and yet one of the most important—problems in image theory.

The author of the next chapter on "Light and Information" is Professor Gabor. This very important paper was a subject of a lecture delivered by him at Edinburgh University in 1951 and, although its contents were previously privately distributed, this is its first appearance in print. Its inclusion in this volume will be appreciated by a great number of scientists who have not been familiar with this interesting and, in many respects, remarkable work. After a preliminary review of how information theory is connected with optics, the author presents a critical discussion of the degree of information about the object which an optical system transmits to the image on the basis of geometrical and classical wave optics. The mathematical formulation rests on the Fourier transforms relating the amplitude distribution in the object and aperture planes for a plane wave incident normal to the object. As details of the order of less than half a wavelength are not transmitted to the image, the question is: What information can be obtained about the coarser details of the object? It is shown that the intensity pattern deteriorates as the distance of the receiving plane is further from the object, whereas the modulus of the F. T. of the object function is not affected by it. Furthermore there is less information due to the finite domain of the aperture.

These constraints imposed on the information about the object lead to an important concept, namely, the *degrees of freedom* (independent variables) which are needed to obtain the maximum possible information about the coarser part. On a geometrical optics basis, the number of degrees of freedom is, up to a constant factor, equal to the object area times the accessible Fourier area which, in general, is finite but very large. A similar formula is derived for the nonstationary case. An interesting discussion on observation without illumination leads to the statement that at least one quantum is needed to make an observation. By constructing an imaginary experiment, the author shows that classical optics fails to prove the validity of the second law of thermodynamics and one must take recourse to quantum mechanical concepts of light to rescue the second law.

Another drawback of classical optics lies in the lack of a standard measure for the intensity of light of a given frequency. In quantum theory the standard is a single photon. By pointing out this difference the author shows that, in the optical region,

continued on page 496

A Very High Temperature Infrared Cell for Pure Liquids or Solutions

E. Fishman

An infrared cell is described which extends the range of temperatures for liquids up to the critical temperature. Window materials are sapphire or calcium fluoride, sealed to the cell walls by teflon O-rings. Brass may be used for the cell body, but alloys of low thermal expansion are preferable. Thermal expansion of the cell prevents accurate determination of intensities. The cell performed well enough to yield the spectrum of liquid water and alcohol solutions up to the critical points.

Infrared spectroscopy has become an important means of studying intermolecular effects and chemical equilibria. For these purposes it is useful to vary and to control the sample temperature as well as the composition of solutions. Indeed, there is an extensive literature on temperature effects in hydrogen bonding and other equilibria involving weak complexes.[1] Hitherto most of the research using temperature variation has been concerned with low temperatures or elevated temperatures limited by the boiling point of the solution involved.

A high-pressure infrared cell previously described by the author and Harry Drickamer[2] was intended for extreme high pressures, in the 12,000 atm region, and lacked the possibility of either temperature control or window separation under 1 mm. (A device recently reported in the literature[3] tends to overcome the sample thickness problem of that cell.) Other high-pressure high-temperature optical cells recently described,[4–6] in common with the Fishman-Drickamer cell, are highly complex and difficult to build. They would hardly be adopted by one whose major research interest was not in the field of extreme conditions.

The cell described herein requires a minimum amount of precision machine work. It is described for the information of infrared spectroscopists who wish to study the temperature effect on a system but who do not wish to become involved in major instrumental problems in high-pressure research.

Liquid water presents the most severe test of such a cell because of its high critical temperature and pressure (374°C and 217 atm) and the intensity of its infrared absorption, requiring a sample thickness of the order of 2 or 3 μ. The cell illustrated in Fig. 1 has proved satisfactory for liquid water, although its high vapor pressure requires a retightening of the window guards at high temperature to compensate for the play in the threads.

The basic pressure seal is provided by O-rings made of teflon, the only satisfactory material known to the author for these extreme conditions. According to the O-ring manufacturers, their pressure range may be extended by a factor of two through the use of "backup" rings, furnished only in leather. Since the leather carbonizes at about 200°, backup rings were machined out of teflon. The geometrical arrangement of rings and windows illustrated allows a seal to be established over a range of sample thicknesses: 0 to 1 mm for the cell illustrated. The upper limit may be extended with extra center-cell sections. The rings can be used repeatedly with organic liquid samples; however, one experiment with water up to its critical point causes a severe extrusion of the rings, which must subsequently be replaced.

The sections shaded in the drawing screw into the body of the cell to form the O-ring grooves. It is nearly impossible to place teflon O-rings in a groove which does not demount in this manner.

Synthetic sapphire windows, machined by the manufacturer as illustrated in Fig. 1, suffer no deterioration with repeated use. They can be broken if they are not pressed into place or removed with evenly applied force. For this purpose a window extractor is essential. Ours consisted of a cylinder having external threads

The author is at Syracuse University, Syracuse 10, N.Y.

Received 27 October 1961.

This research was conducted while the author was a guest of the "Service de Mlle. Josien" at the Université de Bordeaux, France. It was supported in part by contract with the Air Force Office of Scientific Research and through generous aid from the French Atomic Energy Commission to the Laboratory of Infrared Spectroscopy at Bordeaux.

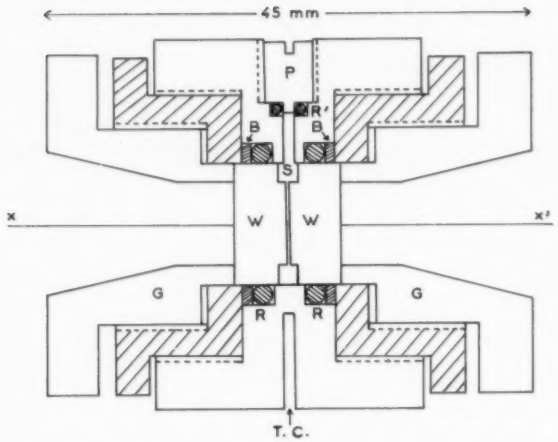

Fig. 1. High-temperature infrared cell. x–x′, light path; W—sapphire windows, diameter 12.7 mm, length 9.5 mm, shoulder, 1.6 × 1.6 mm; S—sample space; R—teflon O-rings, No. 10; R′—teflon O-rings, No. O; B—teflon backup rings; P—filling plug; G—window guards; T.C.—thermocouple well. The critical dimensions are those of the O-ring grooves, specified by the manufacturer. The choice of threads and the diameter of the cell can be left to the machinist's discretion.

which could replace either of the window guards (G in Fig. 1). A plunger was cut to fit this cylinder precisely. By pressing the plunger against the windows with a vice, an even force was applied parallel to the crystal axis. The windows were safely and easily removed. The shoulder on the windows serves two purposes: to provide a reasonable volume in the closed cell and to allow the insertion of metallic spacers when reproducible window separation is desirable. The author has tried CaF_2 windows for the investigation of the bending vibration of water at 1600 cm^{-1}. The experiment was successful, but the windows became quite plastic under these conditions and were ruined for future use. It seems that CaF_2 would be satisfactory for less drastic conditions.

One of the major problems first encountered with this cell when used with pure liquids was the thermal expansion of the sample space. Between 0°C and 300°C, the thermal expansion coefficient of sapphire is about 7×10^{-6} deg^{-1}, while that of brass is about 19×10^{-6}. Consequently, the window separation will increase by about 30 μ when the cell is heated to 300°C for the cell dimensions shown in the diagram. For a sample length of 200 μ, this is not very important. Furthermore, the increase in path length is compensated by the decrease in liquid density. This leads to a slightly diminishing amount of sample in the light path. For a pure liquid, one cannot tolerate any increase in path length. A second cell was machined from an iron–nickel alloy (48% nickel) called "Platinite" having a constant thermal expansion coefficient of 8.7×10^{-6} deg^{-1} over the temperature range 0°C to 500°C.[7] This solved the thermal expansion problem for pure alcohol, although, as mentioned above, for a water sample it was still necessary to retighten the cell at high temperatures to compensate for the mechanical dilation. Platinite has proven to be a most satisfactory material in terms of its chemical as well as its thermal stability.

This cell was used in the focal plane of an externally focusing source arrangement for the Perkin-Elmer Model 112 Spectrophotometer. In this way about 80% of the beam passed through the cell; in a converging beam, less than 50% can pass through. A second benefit of this arrangement was the possibility of complete drying of the optical path. We were able to eliminate the water vapor spectrum to less than 2% absorption for its most intense peaks.

Heating was accomplished with a cylindrical resistance furnace that fitted the cell quite snugly but left the ends of the window guards, G in Fig. 1, exposed. The window guards, having flat surfaces, were then adjusted with a pair of crescent wrenches while the cell was hot. Using a variable transformer, the temperature would be maintained manually to plus or minus 1°, because of the high heat capacity of the cell. The temperature was measured by a copper–constantan thermocouple inserted in the hole illustrated. There

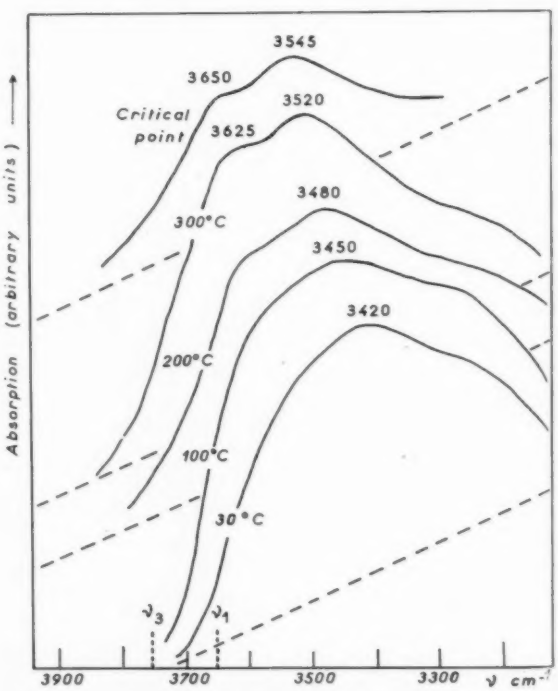

Fig. 2. Contours of the infrared-absorption band at 3 μ of liquid water from room temperature to the critical temperature. ν_1 and ν_3 of gaseous water indicated.

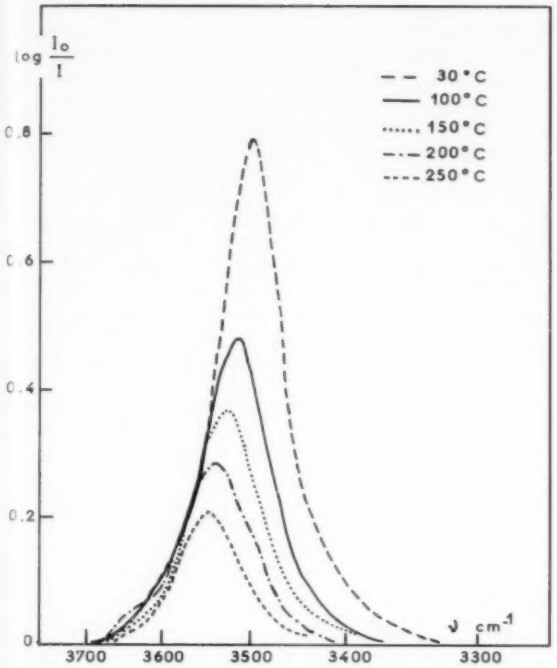

Fig. 3. Contours of the infrared absorption band at 3 μ of 2% ethanol in acetonitrile.

was approximately 1 mm of metal between the junction and the liquid in the cells. Though this could result in an error in temperature readings, the author believes that the error is quite small if a constant temperature reading is recorded for five to ten minutes before a run.

Filling the cell is not a particularly delicate operation. The critical point as such does not yield any discontinuities in the infrared spectrum. If the cell has been filled so that the average density of the contents is lower than the critical value, the meniscus may disappear a few degrees below T_c, but the temperature effects of interest spectroscopically will have been observed. If the cell is slightly overfilled (usually the case in our experiments) no discontinuities are observed at the critical temperature. Though this cell could be adapted for observation of critical opalescence in the infrared region, superior temperature control, measurement, and filling techniques would be needed.

Two of the temperature effects studied with this cell are shown in Figs. 2 and 3.

It is a pleasure to acknowledge my indebtedness to the skill and patience of M. Lauzano, machinist at the Faculty of Sciences of the University of Bordeaux.

References

1. G. C. Pimentel and A. L. McClellan, *The Hydrogen Bond* (Freeman, San Francisco and London, 1960).
2. E. Fishman and H. G. Drickamer, Anal. Chem. **28,** 804 (1956).
3. H. W. Schamp, Jr., and W. G. Maisch, Rev. Sci. Instr. **32,** 414 (1961).
4. W. C. Waggener and A. C. Tripp, Rev. Sci. Instr. **30,** 677 (1959).
5. W. C. Waggener, Rev. Sci. Instr. **30,** 788 (1959).
6. D. E. Williamson, I. A. Nichols, and B. Schurin, Rev. Sci. Instr. **31,** 528 (1960).
7. Société Metallurgique d'Imphy, 84 Rue de Lille, Paris (7e).

Future Issues

Each issue will specially feature one area of applied optics in addition to the usual contributed papers, shop and technical notes, reports of meetings, Letters to the Editor, book reviews, Meetings Calendar, and special columns. The feature subject of each issue is the responsibility of the named editor.

1962	September	**Infrared**	John N. Howard
	November	**Ultraviolet**	—
1963	January	**Astronomy**	James G. Baker
	February	**Information Theory**	F. Dow Smith
	March	**Instrumentation**	W. L. Hyde
	April	to be announced	
	May	**Interferometry**	R. A. Woodson
	June	to be announced	
	July	**Spectroscopy**	Mary E. Warga
	August	to be announced	
	September	**Lens Design and Computers**	D. P. Feder

Applied Optics Reporters

These reporters submit information from which are compiled in part the news columns of *APPLIED OPTICS*. They have a rather thankless and seldom properly recognized task, and the *APPLIED OPTICS* editors are very grateful to them.

L. H. Chasson, *San Francisco*
T. K. McCubbin, *Pennsylvania*
Stanley S. Ballard, *Florida*
E. Scott Barr, *South East*
J. L. Rood, *Rochester*
E. M. Wormser, *Connecticut*
R. A. Oetjen, *Ohio*
L. E. Bergstein, *New York City*
D. J. Lovell, *Michigan*
R. Kraushaar, *New Jersey*
Mary E. Warga, *D.C. and Baltimore*
R. K. McDonald, *North West*
M. Kent Wilson, *Boston*
David M. Gates, *Denver*
K. M. Baird, *Canada*
C. S. Williams, *Texas*
A. J. Cussen, *Los Angeles*
H. McAllister, *Hawaii*
A. Smith, *Chicago*
A. Walsh, *Australia*

continued from page 492

quantum processes must be used when dealing with the information capacity of light, thus leading to an important relation between the maximum information capacity of a light beam containing a large number of photons distributed among a large number of degrees of freedom and the definition of entropy in quantum statistics. This surprising result seems to have important implications in any study of the degree of information of the registered image about the object. In this respect information theory makes its contribution to modern optics.

In the interesting chapter by Professor Wolter, entitled "On Basic Analogies and Principal Differences Between Optical and Electronic Information," the author points out the similar mathematical formalism of wave propagation in an optical layer system and the transmission line. This, however, is not complete since, in the former, one is dealing with two polarizations and the transversality of the fields. For a closer analogy one should consider waveguides with parallel boundaries, which are illustrated by special examples. In discussing the analogy between optics and Hertzian waves, the accuracy of measuring the angular spread of a beam is limited by the uncertainty principle. However, the classical relation used in radio propagation for the angular spread may be improved by using a minimum directivity (minimum ray characteristic) rather than the maximum of the antenna diagram, which increases the accuracy of measurement. In optics this is equivalent to Zernike's method of phase contrast. With the help of spectral theory, the author formulates the basic problem of communication theory, i.e., the computation of the input function from the observable output. The optical problem is not quite so simple on account of the limitation of the aperture. Only in the case of an infinite aperture, or for an annular aperture whose angular spectrum takes the form of a rational function, is the analogy complete with the communication problem, as the time variable in communication theory does not play the same role as the space variable in the optical problem. Then follows a detailed treatment of the optical problem for a finite aperture, and here the fundamental problem is to continue the spectral function of the object beyond the angular spectrum limited by the aperture. Since the exact determination in the angular interval is not always possible, except in special cases, the Fourier transform with respect to the angular variable is not sufficient to give complete information about the object function. By imposing additional conditions on the object function, it is shown that the computed object function may be made as close to the real object function as one desires (Hilbert sense). However, this is not a convincing proof, as the calculations lead to the difficult problem of the convergence of the moment problem. To us it seems that more powerful methods, such as generalized functions, must be used in order to give a rigorous proof of this problem. Finally, the author points out the difference between the two systems: (a) the form of the transmission function (a special example is given) and (b) the image errors are not independent of position in the image plane. Only in the case of isoplanatic optical systems is the Fourier transformation significant when incoherent light is used.

In the next chapter on "Color Interference," Dr. Kubota presents an analysis of the quantitative aspects of color based on the assumption that any color may be expressed by mixing three primary colors (tristimulus) in definite amounts. These values are calculated from the spectral intensity distribution of light and the amount of primary colors given as a function of the wavelength, from which the chromatic coordinates (hue and purity) are computed. By supposing one of the luminance factors of one primary color to differ from zero, the color is completely specified by giving the tristimulus coordinates and the luminance.

The author analyzes the color of reflected light from mono- and multilayer films. Maximum purity can be achieved in two ways: (a) cos-type layers, when the reflection coefficients from the upper and lower boundaries of the layer are equal; (b) sin-type, when they have opposite signs. For oblique incidence one cannot make such a distinction, since the coefficients depend on the angle of incidence. From a detailed discussion about multilayer reflection it is found that for a certain thickness (optical) the hue is the same as in the monolayer case but the purity varies. After a discussion of color of thin films on metallic surfaces the writer considers the problem of color interference in anisotropic, especially optically active, crystals. This study is important on account of their behavior as variable band filters. Attention should be drawn to numerous color curve diagrams and the extensive table of values of chromatic coordinates and luminance factor over a large range of optical thickness for layers of types (a) and (b).

The chapter on "Dynamic Characteristics of Visual Processes" by Dr. Fiorentini gives an analysis and a review of experimental results of the capacity of information and sensitivity of the eye under various conditions of observation. The experiments show that the high visual acuity seems to be due to the unsteady movements of the eye producing time gradients of illumination in the retinal receptors. These involuntary movements are classified as *tremors* (small retinal displacements of high frequency), *flicks* (irregular rapid rotational motion of low frequency), and *drifts* (unidirectional oscillations of small amplitude occurring between consecutive flicks). By neutralizing the natural movements, vision of a steady object may be compared with vision of the object undergoing controlled motion. The main conclusions seem to be that oscillatory motion of small amplitude and long exposure time facilitate visual acuity. The natural movements of the eye aid in restoring vision of a stationary object and also visual acuity for observation times exceeding 0.2 sec, but smaller time exposures deteriorate visual acuity. Attenuation experiments show that the visual system behaves like a low-pass filter with a band spread increase at high illumination levels and a considerable amplification for high luminance at low frequencies and fast attenuation at high frequencies. Perception of visual details can be ascribed to differential brightness sensitivity and perception of contours and to the time variation of retinal illumination.

In the last chapter, on "Modern Alignment Devices", Professor van Heel presents a detailed account of several optical methods by which alignment of points and departure from flatness can be accurately set and rapidly made. One of the most accurate methods for alignment of points devised by the author and his collaborators is a double slit device (similar to Young's experiment). By observing the interference pattern one is able to align points for distances of the order of 30 meters with an accuracy of 0.01 mm. Another device is an autocollimator in conjunction with a reflecting sphere with or without a concentric cap, the latter being used when one-sided alignment is possible. If the sphere is nonreflecting, the diffraction pattern gives a good indication about the accuracy of the alignment. For alignment of surfaces a multiple reflection a sphere mounted with a collimator provides a method of testing the flatness of a surface of 20 sq meters to an accuracy of 0.1 mm. The use of solid spheres is important in two respects: the lateral displacements of the fringes are independent of the orientation of the sphere, and spherical aberration performs a useful role in observing the interference pattern. Finally, from the practical point of view, it is easier to make solid glass spheres with great accuracy than any other geometrical figures.

NICHOLAS CHAKO

(continued on page 544)

Astronomical Refraction—Some History and Theories

A. I. Mahan

Astronomical refraction has had a long and fascinating history. Cleomedes (100 A.D.) and Ptolemy (200 A.D.) were aware of its existence and understood in a qualitative way some of its properties. Alhazen (1100 A.D.) quite correctly suggested that the flattening of the sun's disk near the horizon was due to astronomical refraction. Tycho Brahe in 1587, however, was the first to make direct measurements of the magnitude of the refraction. The first theory of astronomical refraction based on Snell's law was that of Cassini, who in 1656 looked upon the earth's atmosphere as being of constant refractive index up to its upper limit at which all the refraction took place. Extensive investigations of the physical properties of the atmosphere modified these ideas and led to the "concentric spherical shell model" and the "plane parallel layer model," the latter being an approximation for the former. Attempts to evaluate the "refraction integral" for the concentric spherical shell model have led to the theories of Bessel, Bradley, Gylden, Ivory, Laplace, Mayer, Simpson, Young, and others. At the beginning of the twentieth century, investigations on the physical properties of the atmosphere extended to higher elevations, and new physical properties appeared which were not anticipated by the earlier workers. This led to the celebrated work of Harzer, who for the first time was able to compute the astronomical refraction purely from meteorological measurements. Harzer also made the first detailed investigation of the applicability of the spherical shell model, which is used almost universally by workers in this field. Harzer's work has served as a source of inspiration, but much remains to be done. This paper attempts to give a brief chronological description of some of the more significant theories of astronomical refraction for the purpose of pointing out the types of problems which have existed, how these problems were attacked, and the problems which still remain. It also gives adequate references for those wishing additional information.

I. Introduction

A continuous need for more precise information concerning star positions, for use in navigation, surveying, etc., and interest in the upper atmosphere requires us to take a more serious look at the subject of "astronomical refraction."* Several of the early theories of astronomical refraction[1,2] were developed with only a very meager knowledge of the physical properties of the earth's atmosphere. Cassini, for example, assumed that the atmosphere was of constant density out to its upper limit at which all the refraction took place, and his computed values for different "apparent zenith angles" agreed quite well with the early measurements of Brahe. As the knowledge of the atmosphere progressed outward, the "concentric spherical shell model" and the "plane parallel layer model" appeared, the latter being an approximation for the former. To obtain numerical values from the concentric spherical shell model, a "refraction integral" had to be evaluated, and this led to the older classical theories of astronomical refraction. Many of these theories were elegant examples of the use of complex mathematics, and several famous names became associated with this subject. Two of these theories (Bessel and Gylden), which by current standards were developed with still a rather meager knowledge of the physical properties of the atmosphere, are at present used for computational purposes, because as yet there has been no more complete theory developed which yields values of comparable accuracy with as much

The author is at the Applied Physics Laboratory of The Johns Hopkins University, Silver Spring, Maryland.

Received 31 August 1961.

The paper was presented at the Forty-Fifth Annual Meeting of the Optical Society of America in Boston, Massachusetts, October 12–14, 1960.

This work was supported by the Bureau of Weapons, Department of Navy.

* In this paper, astronomical refraction is a term which is reserved for those problems in which the object is at large distances above the earth compared with the radius of the earth (the detector is here assumed to be located at the surface of the earth). Astronomical refraction is one of the two subdivisions of the more general subject of "atmospheric refraction," the other being "terrestrial refraction." Terrestrial refraction is distinguished from astronomical refraction in that the object is in general close to the earth. In this paper, we shall be interested only in astronomical refraction.

ease. All these early workers were in the position of having limited information on the physical properties of the atmosphere, and it was not too difficult to develop several different types of theories which would describe these physical properties, satisfy the refraction integral, and yield computed astronomical refractions at different apparent zenith angles which would agree with Brahe's measured values.

At about the beginning of the twentieth century, new techniques were developed for sampling the atmosphere at still higher levels, and new characteristics appeared which were not anticipated by these earlier workers. As a result, it became increasingly difficult to describe these new measurements in mathematical terms, and to evaluate the refraction integral. This led to the celebrated work of Harzer, who for the first time computed the astronomical refraction from meteorological measurements, and thus was able to make a check of the validity of the concentric spherical shell model. These computations, however, were very tedious, so Harzer limited his considerations only to the atmosphere above Kiel, Germany. This work has served as an inspiration, and recent workers are using similar techniques and more modern computing facilities to make similar computations. These workers, like the earlier ones, are still in need of more information on the physical properties of the atmosphere, so that much remains to be done.

In the present paper, an attempt has been made to review very briefly some of the theories of astronomical refraction, which are characteristic of each of the periods in its history. Detailed descriptions of all the theories are impossible because of their number and complexity, and would also be somewhat presumptuous because other extended treatises,[1,2] particularly on the early theories, are already in existence. For the theories which are chosen for discussion, an attempt has been made to indicate the nature of the assumptions made and the results obtained, and the descriptions of the more recent theories are in general more detailed. By proceeding in this manner, it is hoped that the present paper will give a rather broad impression of the types of problems which have existed in this field, how these problems were attacked, and, more important still, the types of problems which remain. For those who might wish to look into certain aspects more deeply, adequate references are provided.

II. Early History of Astronomical Refraction

The subject of astronomical refraction is of course an old one and was known to the ancients. In the writings of Cleomedes[3] (1st century, A.D.), we find, "Just as a ring in a glass of water appears to be elevated toward the rim, in the same way the sun will be seen, because of refraction, when in reality it is still below the horizon." Ptolemy[4] (2nd century, A.D.) was also familiar with astronomical refraction and concluded that the polar distance of a star is always less than it appears to be. Alhazen[5] (1100 A.D.) suggested quite correctly that the flattening of the sun's disc near the horizon was due to astronomical refraction. The first person to make quantitative measurements of the magnitude of the refraction was the famous Tycho Brahe. Using divided circles which were ruled in his laboratory[6] and two slits for sighting purposes, he was able to measure the elevation and azimuth of a star to an accuracy of about ten seconds of arc. To determine the magnitude of the astronomical refraction, he had to devise a method of measurement which was independent of astronomical refraction itself. The technique used in 1587 is indicated schematically in Fig. 1, and may be of general interest, for it is still in use today. The two circles in the figure are the earth at its summer and winter solstice positions, P is its pole, and O is the position of Brahe's laboratory. Brahe first determined the polar height of his laboratory, θ, from measurements on the polar star at its extreme upper and lower positions. To determine the angle E which the earth's axis made with the normal to the plane of the ecliptic, Brahe then measured the two angles OCS which the sun formed with the normal to the earth's surface at O for both the summer and winter solstice positions. From the geometry, the average of these two angles $(90° \pm E - \theta)$ should be $(90° - \theta)$, or the complement of the polar height of his laboratory. Independent measurements on two divided circles indicated a discrepancy of four minutes between the measured and the expected values, which Brahe attributed to astronomical refraction. Brahe was therefore *the first actually to detect the presence of astronomical refraction.* With these instruments, he also measured the apparent zenith angle of the sun, moon, and stars, and compared these with the true values to be expected from trigonometric computations. In this way, he was able to obtain numerical values for the astronomical refraction for different apparent zenith angles. Table I presents some of Brahe's early measurements on the sun.[7] Brahe believed that the refraction occurred only at the

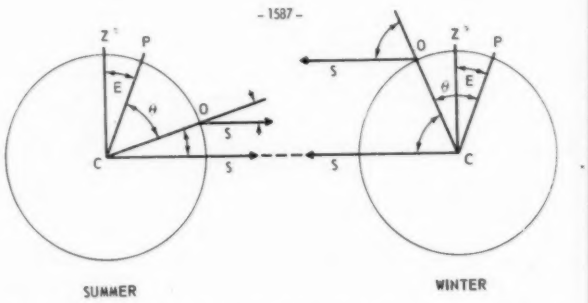

Fig. 1. Tycho Brahe's method for detecting the presence of astronomical refraction.

upper limit of the atmosphere, but we cannot be too critical of this idea, since instruments for determining the physical properties of the atmosphere were as yet unknown. These measured values for the astronomical refraction were often referred to for the next eighty years.

Table I. Brahe's Measured Astronomical Refraction on the Sun for Different Apparent Zenith Angles

Apparent zenith angle	Refraction	Apparent zenith angle	Refraction
0°	0′ 0″	70°	4′ 30″
15°	0′ 0″	75°	7′ 30″
30°	0′ 0″	80°	10′ 0″
45°	0′ 5″	85°	14′ 30″
60°	1′ 25″	90°	34′ 0″
65°	2′ 30″		

The primary difficulty in establishing theories of astronomical refraction was that the true form of the law of refraction itself had not as yet been discovered. Many attempts[8] had been made to improve on Ptolemy's earlier incorrect law stating that *the ratio of the angles of incidence and refraction was a constant*. Perhaps the most valiant of these was that of Kepler, who concluded that a correction term should be added to Ptolemy's law. Using his newly found law of refraction, Kepler then proceeded to construct the first theory of astronomical refraction in which, like Brahe, he considered the atmosphere to be uniformly dense up to its upper limit at which all the refraction took place. This theory is of little interest except historically. The most stimulating event to the study of astronomical refraction was the discovery of the true law of refraction by Snell and the expression in its final form as the ratio of the sines of the angles of incidence and refraction by Descartes in 1637.

III. The First Theory of Astronomical Refraction Based on Snell's Law

One of the first to make use of Snell's law for developing a theory of astronomical refraction[1] was the Italian astronomer, Cassini. Like Brahe and Kepler, Cassini in 1656 considered the earth (see Fig. 2) to be of radius a surrounded by an atmosphere of fixed height H and having a constant density, so that all the refraction occurred only at the upper limit of the atmosphere. Light rays proceeding from distant objects which are visible at point P on the earth will then always lie in a plane passing through the surface normal at P and the incident ray, and be incident on the earth at some apparent zenith angle Z. If then two stars are visible at point P, it is possible to write

$$\begin{aligned} \sin i_1 &= \sin(e_1 + R_1) = \mu \sin e_1, \\ \sin i_2 &= \sin(e_2 + R_2) = \mu \sin e_2, \end{aligned} \tag{1}$$

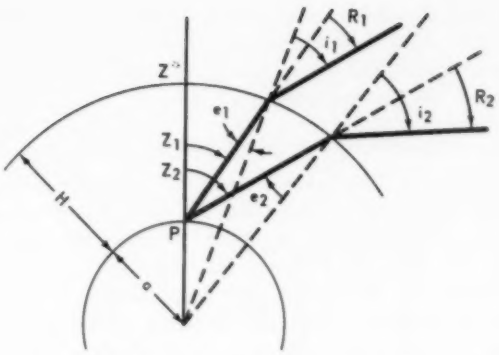

Fig. 2. Cassini's model for astronomical refraction.

where, as indicated, i is the angle of incidence, e the angle of refraction, R the astronomical refraction, and μ is the refractive index of the air layer. In each triangle formed by the refracted ray, the normal at the point of incidence on the outer surface of the air layer, and the earth's radius drawn to point P, it is possible from the law of sines to write

$$\frac{\sin e_1}{a} = \frac{\sin Z_1}{a + H}, \qquad \frac{\sin e_2}{a} = \frac{\sin Z_2}{a + H}. \tag{2}$$

The refractive index μ can be eliminated from Eqs. (1) by division. Equations (2) can then be used to substitute for e_1 and e_2 in terms of a and H, and a fourth degree equation in H is obtained. To find H, it is simply necessary to choose two stars whose values of Z_1, Z_2, R_1, and R_2 are known, and then choose the correct root of the equation. When once H is known, the corresponding values of e for any other apparent zenith angle Z are readily found from Eqs. (2), and the associated astronomical refraction R can be found from Eqs. (1). In this manner, Cassini found the height of his atmosphere to be 2000 toise = 6.82 km, and he then computed the astronomical refraction at different apparent zenith angles for an atmosphere having a refractive index $\mu = 1.000284$ when the radius of the earth was $a = 6377.36$ km. His results are indicated in Table II.

Table II. Cassini's Computed Astronomical Refraction for Different Apparent Zenith Angles

Apparent zenith angle	Refraction	Apparent zenith angle	Refraction
0°	0′ 0″	70°	2′ 39″
15°	0′ 16″	75°	3′ 38″
30°	0′ 34″	80°	5′ 28″
45°	0′ 59″	85°	10′ 32″
60°	1′ 42″	90°	32′ 20″
65°	2′ 6″		

At first, Cassini actually used different tables for spring, summer, fall, and winter, but since the values in this table agreed fairly well with the measured values of Richer, he adopted only this table.

IV. The Concentric Spherical Shell Model

Newer developments[1,8] began to appear which made a marked impression on the theories of astronomical refraction. The barometer and thermometer were discovered and used to show that both the pressure and temperature decreased with height above the earth. The Boyle-Marridotte law for gases appeared between 1660 and 1678, and Picard in 1669 established that the astronomical refraction depended upon the temperature. In 1708, Hawksbee measured the refractive indices of gases with hollow prisms, and found they were proportional to the density. Finally, Bouguer[9] in about 1725 measured the horizontal astronomical refraction in Peru and found a value of 22′ 50″, and Le-Monnier later found values in the Tornea in northern Sweden significantly larger than Brahe's value of 34′.

These developments suggested of course that Cassini's model was too simple a one, and a more appropriate model of the form, indicated in Fig. 3, came into general use. Here the earth of radius a is looked upon as being in static equilibrium with its atmosphere. For sufficiently localized regions free from pressure and temperature anomalies and for cloud free air, the atmosphere can be approximated by thin concentric spherical layers of constant refractive indices, whose refractive indices decrease in some arbitrary manner to unity in outer space. In Fig. 3, the path of a refracted ray from a distant star is indicated, which is incident upon such a concentric type atmosphere and is refracted to a point P_e on the earth at an apparent zenith angle Z. Snell's law predicts that this refracted ray will always lie in a plane determined by the incident ray and the normal to the point P_e on the earth. The true zenith angle at point P_e is then Z_0, and we shall be interested in computing the magnitude of the astronomical refraction $(Z_0 - Z)$ introduced by these concentric air layers.

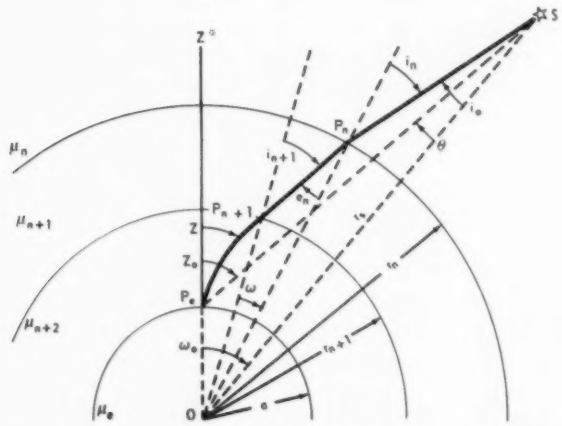

Fig. 3. The concentric spherical shell model for astronomical refraction.

For such a model, it is possible to obtain a rigorous equation for the astronomical refraction, and it is of interest to derive this equation here, for almost all the classical theories of astronomical refraction have as their function the evaluation of the integral associated with this equation. In Fig. 3, we have indicated a much magnified thick layer of air having a refractive index μ_{n+1} between the points P_n and P_{n+1}. At point P_n, it is possible from Snell's law to write

$$\mu_n \sin i_n = \mu_{n+1} \sin e_n. \tag{3}$$

In the triangle $OP_{n+1}P_n$, we see also from the law of sines that

$$\frac{\sin e_n}{r_{n+1}} = \frac{\sin i_{n+1}}{r_n}. \tag{4}$$

This equation can be used to eliminate $\sin e_n$ in the previous equation, and we obtain the important relation

$$\mu_n r_n \sin i_n = \mu_{n+1} r_{n+1} \sin i_{n+1} = \mu_e a \sin Z. \tag{5}$$

Thus, *for any system of concentric spherical refracting layers satisfying Snell's law of refraction, the product of the refractive index, the radius of curvature, and the sine of the angle of incidence is a constant at each refracting surface.* If now we simply differentiate this equation, then we find

$$di = -\tan i \frac{d\mu}{\mu} - \tan i \frac{dr}{r}. \tag{6}$$

The increase in the angle of incidence in going from one refracting surface to the next of larger r is then, from the figure, made up of a positive part due to the deviation produced by the refraction at the second surface and a negative part due to the rotation of the surface normal in going from the first surface to the second surface. If now we impose limits corresponding to the complete ray path from the earth out to the star, then we see from Fig. 3 that

$$\int_z^{i_0} di = -\int_{\mu_e}^{\mu_s} \tan i \frac{d\mu}{\mu} - \int_0^{\omega_0} d\omega, \tag{7}$$

where μ_s is the refractive index in the region of the star, i_0 the angle of incidence at the outer most refracting surface, and ω_0 the true polar angle of the star as observed at the center of the earth. Two of these integrals are easily evaluated; from Fig. 3 we see that $Z_0 = \omega_0 + \theta$, and, utilizing Eq. (5), it becomes clear that "atmospheric refraction" $(Z_0 - Z)$ at point P_e introduced by the atmosphere between the star and the observer is

$$R = (Z_0 - Z) = \int_{\mu_s}^{\mu_c} \frac{\mu_c\, a \sin Z}{\sqrt{\mu^2(a + h)^2 - \mu_c^2 a^2 \sin^2 Z}} \frac{d\mu}{\mu} - (i_0 - \theta). \quad (8)$$

This equation is now the refraction integral in its most general form[10] in which the object and observer can be at any arbitrary height above the surface of the earth. For any arbitrary apparent zenith angle Z, the atmospheric refraction R depends on the refractive index μ_c at the position of the observer, on how the refractive index changes with h along the path between the observer and object, on the refractive index μ_s at the position of the object, and on the angle $(i_0 - \theta)$. This angle represents the difference between the apparent and true directions of the point P_c on the earth as viewed from the object and hence is the atmospheric refraction at the object induced by the air between point P_c and the object.

Most of the early interest in atmospheric refraction has been devoted to the special case of astronomical refraction in which $a << r_s$ and $\mu_s = 1$, and this is quite fortunate, for it simplifies the problem. If we can assume that the object is far enough away so that both i_0 and θ are less than say 1°, then it is possible from Fig. 3 and Eq. (5) to write

$$(i_0 - \theta) = \frac{a}{r}(\mu_c \sin Z - \sin Z_0).$$

Z_0 can be replaced by $(Z + R)$, and if we assume that R is small and make the necessary expansions, then

$$(i_0 - \theta) = \frac{a}{r_s} \sin Z \left[(\mu_c - 1) - R \cos Z + \frac{R^2}{2}\right]. \quad (9)$$

Computations[11] of $(i_0 - \theta)$ on the moon (r_s = 384,389 km) with μ_c = 1.000284, a = 6377.3 km, and Z = 90° show that the atmospheric refraction on the moon is 1.2 sec of arc. This angle is small compared with the usual accuracy with which such measurements are made, so that for the special case of astronomical refraction in which r_s becomes even larger, R can be written[12,*]

$$R = \int_1^{\mu_c} \frac{\mu_c\, a \sin Z}{\sqrt{\mu^2(a + h)^2 - \mu_c^2 a^2 \sin^2 Z}} \frac{d\mu}{\mu}. \quad (10)$$

This is the famous refraction integral derived independently by Newton, Bouguer, and Simpson. This integral has served as the fundamental equation from which practically all the theories of astronomical refraction have been derived, and, in order to determine R for a given Z, one needs only to know the refractive index at the position of the observer and how it changes with h out to the upper limit of the atmosphere. The obtaining of reliable refractive index values as a function of height has been the primary difficulty which has prevented an exact evaluation of this integral. Because refractive index values have not been available, attempts have been made to evaluate this integral by indirect means in which other measured quantities are inserted. Over the years this has made it possible to develop numerous theories of astronomical refraction which are often based on rather limited physical measurements on the atmosphere and which utilize other assumptions and approximations.

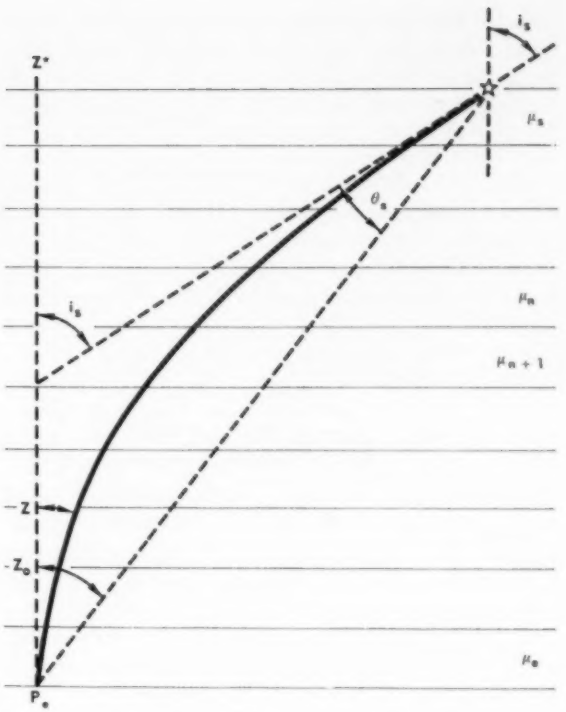

Fig. 4. The plane parallel layer model for astronomical refraction.

V. The Plane Parallel Layer Model

Before discussing the theories which have been developed from the concentric spherical shell model, it might be well to mention briefly the plane parallel layer model, for this model reappears frequently in the literature[13] and often serves as a useful approximation to the concentric spherical shell model. If the earth's atmosphere can be considered to be very thin compared with the radius of the earth and the apparent zenith angle Z is limited to sufficiently small values, then the plane parallel layer model indicated schematically in Fig. 4 can be utilized. Here, as is suggested, the earth's atmosphere is looked upon as a series of plane parallel layers whose refractive indices decrease in some arbitrary manner to μ_s in the region occupied by the

* The "trajectory integral" giving the path of the refracted ray in plane polar coordinates is also of some interest and, as already suggested by Eqs. (6) and (7), is very similar in form to the refraction integral, but has the $d\mu/\mu$ replaced by dr/r.

object. For such a model, an incident ray will always remain in a plane throughout its path, which is determined by the incident ray and the normal at the first point of incidence, and it is possible from Snell's law to write

$$\mu_0 \sin i_0 = \mu_n \sin i_n = \mu_0 \sin Z,$$

where i_0 is the angle of incidence on the layer in which the source object is imbedded. From Fig. 4, i_0 can be replaced by $(Z + R + \theta_0)$, and if this substitution is made in the previous equation and one solves for R, then

$$\sin R = \frac{\mu_0}{\mu_0} \sin Z \cos(Z + \theta_0) \times \left[1 - \sqrt{1 - \frac{\mu_0^2 \sin^2 Z - \mu_0^2 \sin^2(Z + \theta_0)}{\mu_0^2 \sin^2 Z \cos^2(Z + \theta_0)}}\right]. \quad (11)$$

This equation, like Eq. (8) for the spherical shell model, is a rigorous solution for the atmospheric refraction R, when the object and observer are at arbitrary distances above the surface of the earth. For a particularly chosen apparent zenith angle Z, the atmospheric refraction R is a function of the refractive index at the position of the observer, the refractive index in the region of the object, and the atmospheric refraction θ_0 at the position of the object, but it is independent of the manner in which the refractive index changes between the object and observer. For the special case of astronomical refraction in which the object recedes to very large distances ($\theta_0 = 0°$, and $\mu_0 = 1$), this equation reduces to the following simpler form

$$\sin R = \frac{\mu_0 \sin 2Z}{2} \left[1 - \sqrt{1 - \frac{\mu_0^2 - 1}{\mu_0^2 \cos^2 Z}}\right]. \quad (12)$$

These last two equations are not very familiar to workers in this field. For computational purposes, what is usually done is to return to the previous Snell's law equations, to assume that R is small and then make the necessary series expansions. The equation obtained in this manner with terms up to the fifth order in tan$Z$ gives identical values to the nearest second for R with those from the previous equation for apparent zenith angles up to 85° and is of the form

$$R = (\mu_0 - 1)\tan Z + \frac{(\mu_0 - 1)^2}{2} \tan^3 Z + \frac{(\mu_0 - 1)^3}{2} \tan^5 Z + \ldots \quad (12a)$$

For small apparent zenith angles, one sees now that the astronomical refraction R is proportional to the "refractivity" $(\mu_0 - 1)$ of the air at ground level and to the tangent of the apparent zenith angle Z.

To give some idea of how well the plane parallel layer model describes the refraction properties of the atmosphere, some computations have been made (see Table III) from Eq. (12a) under standard conditions (760 mm, 0°C) on the earth and compared with similar values obtained from Bessel's theory for the concentric spherical shell model to be discussed later. The refractive index under standard conditions was assumed to have the value[14] $\mu_0 = 1.0002927$. The computed values for the astronomical refraction for the plane parallel layer model are indicated under P.P.L.M., and those from Bessel's theory are indicated under C.S.S.M. One sees from this table that the plane parallel layer model gives quite good values for apparent zenith angles up to 65°. Beyond this, however, the values for the plane parallel layer model become increasingly larger (at $Z = 88° 38.03'$, $R = 81' 55.0''$) than those for the concentric spherical shell model.

VI. Early Theories of Astronomical Refraction

Some of the first attempts at evaluating the refraction integral in Eq. (10) were purely mathematical in nature. It was noticed quite early that this integral was very similar to an arc sine, which of course can be integrated directly. The suggestion therefore was to make it an arc sine by assuming that the refractive index μ decreased with r (or $(a + h)$) in the following manner,

$$\mu = \mu_0 \left(\frac{a}{a + h}\right)^{1/(m+1)}, \quad (13)$$

Table III. Comparison between Computed Astronomical Refraction at Different Apparent Zenith Angles for the Plane Parallel Layer Model and the Concentric Spherical Shell Model

Apparent zenith angle	Refraction		Apparent zenith angle	Refraction	
	P.P.L.M.	C.S.S.M.		P.P.L.M.	C.S.S.M.
0°	0′ 0″	0′ 0″	70°	2′ 46.06″	2′ 44.50″
15°	0′ 16.18″	0′ 16.18″	75°	3′ 45.78″	3′ 41.90″
30°	0′ 34.86″	0′ 34.85″	80°	5′ 44.02″	5′ 31.05″
45°	0′ 60.38″	0′ 60.32″	85°	11′ 43.80″	10′ 16.45″
60°	1′ 44.12″	1′ 44.16″	90°	—	31′ 0.12″
65°	2′ 9.55″	2′ 8.82″			

where m is an arbitrary number. If one substitutes this in Eq. (10) and integrates,* then

$$R = \frac{1}{m}\left[Z - \arcsin\left(\frac{\sin Z}{\mu_0^m}\right)\right], \tag{14}$$

which is the Bouguer-Simpson equation published in 1743. Another formula derived by Bradley in 1750 and still another by Mayer in 1781 are also derivable from the Bouguer-Simpson formula, and are therefore slightly different manifestations of the same initial assumptions in Eq. (13). The Bradley formula

$$R = (\mu_0 - 1)\tan\left(Z - \frac{mR}{2}\right), \tag{15}$$

was so simple that, although it had no sound physical basis, it was still used by astronomers[15] up to the beginning of the nineteenth century, who sought only to improve upon the numerical results by choosing different values for m and μ_0 and introducing both pressure and temperature corrections.

As instruments were developed for measuring the pressure and temperature of the atmosphere at different heights, it was only natural that the physics of the atmosphere should appear in the theories of astronomical refraction. To introduce information of this type into the refraction integral, it became necessary to make certain assumptions as to the nature of the physical properties of the atmosphere itself. For almost all these older classical theories of astronomical refraction, we find that the following equations were used:

$$\frac{\rho}{\rho_0} = \frac{P}{P_0(1 + \beta t)}, \tag{16}$$

$$\mu^2 = 1 + 2C, \tag{17}$$

$$dP = -g_0[a/(a + h)]^2\, dh. \tag{18}$$

The first equation is the Boyle–Gay-Lussac law, which suggests that the air at all heights above the earth can be approximated by an ideal gas. Nothing appears in this equation suggesting the possible appearance of water vapor. This is due to the early work of Biot and Arago† who established experimentally that the index of refraction for dry air was not "materially" different from that for wet air. The second equation is Laplace's relation between the refractive index and density, which is based on laboratory measurements. It suggests of course that the physical properties and composition of the air do not change with height above the earth. The last equation gives the pressure of an elementary column of air of density ρ and height dh in an inverse square law gravitational field, when the height of the atmosphere is assumed to be small compared with the radius of the earth. In writing this equation, we have neglected the divergence in cross section of the elementary air columns with height, the contributions of the centrifugal force, interactions between elements of the air column, their effect on the gravitational field, and gravitational anomalies. It is important to see then that, by using these equations, we have already limited the physical properties of the atmosphere. If, however, we are to substitute for the refractive index in Eq. (10) in terms of other more accessible quantities, relations of this type become necessary, and these equations have been utilized in all the older classical theories which we are about to review briefly.

In order now to fix the physical properties of the atmosphere in Eqs. (16) to (18), it is necessary to assume some particular relationship between two of the four possible variables, P, ρ, t, and h, and the types of theories which have been developed are usually distinguished by the two variables so related. Thus several theories (Baeyer, Bessel, Laplace, Svanberg) assumed particular relationships between the density and height. The theories by Bauernfeind, Euler, Gylden, Newton, and Schmidt assumed particular equations relating the temperature to the height. Other theories by Ivory, Kowalski, Oppolzer, and Radau proposed relationships between the density and temperature. Still others (Lubbock, Pizzetti) assumed particular relationships between the temperature and pressure and between the density and pressure (Young). In all these theories when once the forms of the relationships between the two chosen variables was established, it then became possible from Eqs. (16) to (18) to compute the magnitudes of P, ρ, and t as a function of h. The refraction integral in Eq. (10) was then evaluated, often utilizing many tedious steps and approximations. The criteria then used for the ultimate rejection or acceptance of a theory were: how well it continued to describe the pressure, density, and temperature as a function of height, and the astronomical refraction as a function of apparent zenith angle as these properties became better known.

Oriani was one of the early ones to attempt to evaluate the refraction integral,[16] and he came to some interesting conclusions which affected all other theories. To arrive at his equation for the astronomical refraction, Oriani made a power series development of the refraction integral in terms of $\tan Z$, assuming that the height of the atmosphere was small compared with the radius of the earth, that Eq. (18) was valid, and neglecting terms in $\tan Z$ beyond the third order. His equation was

$$R = (\mu_0 - 1)\left[\left(1 + \frac{\mu_0 - 1}{2}\right)\tan Z - \left(\frac{l_0}{a} - \frac{\mu_0 - 1}{2}\right)\tan^3 Z\right]. \tag{19}$$

l_0 is a quantity which reappears quite frequently in

* See ref. 2, p. 245.

† See ref. 1, pp. 172, 173.

astronomical refraction and is designated as the "height of the homogeneous atmosphere" of density ρ_e in a constant gravitational field g_e, which will exert the same pressure P_e as the atmosphere in question. If standard conditions prevail upon the earth (μ_e = 1.0002927, ρ_e = 0.0012926, and l_e = 7.9933 km), then R can be determined for each value of Z from

$$R = 60\,3826'' \tan Z - 57.9953'' \times 10^{-3} \tan^3 Z. \quad (19a)$$

The numerical values obtained with this equation for apparent zenith angles up to 70° will be found to agree to the nearest second with those already cited in Table III for the concentric spherical shell model. The important thing here is that in obtaining this equation no assumptions have been made as to the nature of the atmosphere and how its physical properties change with height. These considerations led Oriani to announce his law which states that *up to an apparent zenith angle of 70°, the astronomical refraction is independent of the hypothesis used for describing its properties.* This meant that all of the classical theories derived from the refraction integral should, within the previously stated assumptions, give the same numerical values up to apparent zenith angles of 70°.

At the beginning of the 19th century, there was still no satisfactory solution to the refraction integral, and Bradley's tables were used for computation purposes. Newton's idea of a constant temperature atmosphere was known to be incorrect, and his exponential decay in density had been found to be too rapid. In about 1805, Laplace sought to improve on Newton's ideas by introducing a slower density decay with height which simultaneously permitted a decrease in temperature with height. His equation for the density decay had two constants whose values were dependent upon each other and were chosen to satisfy the Gay-Lussac measurement of the temperature of −40.25°C at 6.98 km above Paris. Laplace's computed values for the astronomical refraction at different apparent zenith angles agreed quite well with the more accepted values of Bradley, but rather large discrepancies were later found between the computed and observed temperatures at different heights.* Laplace's theory, however, was the first of the old classical theories which introduced physics into the atmosphere, permitted decays in pressure, density, and temperature with height, and simultaneously gave refraction values which agreed fairly well with the accepted values.

In 1818, Bessel also sought[17] to improve on Newton's exponential decay in density by introducing an arbitrary constant in the exponent. When this form of density decay was introduced into the refraction integral, Bessel obtained an expression for R in the form of a series containing the "Kramp Function." The arbitrary constant was chosen to describe an average atmosphere at 9.13°C and at 751.5 mm pressure, and numerical values of R were computed for different apparent zenith angles. These numerical values had the property of being too small for values of Z less than 85° and too large for values of Z larger than 85°. This difficulty of obtaining correct refraction values led Bessel to adopt a semiempirical method[18] for computing the refraction, which is still in use today.[19] These tables were constructed from the well established fact that the astronomical refraction, for small apparent zenith angles, was proportional to tan$Z$ [see Eqs. (12a) and (19)]. Knowing then the form of the coefficient of this tan$Z$ term and introducing temperature corrections for the barometer (T), corrections for the pressure (B), and temperature (γ) corrections for the ambient air, Bessel then gave the following equation for the astronomical refraction, when Z was less than 85°:

$$R = \alpha(BT)^A \gamma^\lambda \tan Z. \quad (20)$$

In order to make R agree with the measured values (agreement to within 1.71″ with Argelander's measured values), α, A, and λ were made functions of Z. Beyond 85°, difficulties appeared because of the proportionality with tan$Z$, so Bessel replaced α tan$Z$ by empirically determined values based on Argelander's measured values. Bessel's tables then give logα, A, and λ as functions of Z, B as a function of the barometric pressure, T as a function of the barometer temperature, and logγ as a function of the ground level ambient air temperature. The earlier Table III gives values of R at different apparent zenith angles obtained from these tables, when the temperatures of the barometer and ambient air were both 0°C, and the pressure was 760 mm. Bessel's tables were based primarily on observations in both England and Germany. Over the years there have therefore existed differences of opinion[20] as to the degree to which they are applicable in other regions over the earth, and suggestions have appeared which indicated that the astronomical refraction ought to be a function of other variables than simply the pressure and temperature.

Another theory which should be mentioned is that of Ivory, published in 1823.[21] Ivory sought to improve on both Bessel's and Laplace's theories by assuming a relationship between the density and temperature of the form

$$\frac{1+\beta t}{1-\beta t_e} = 1 - f\left(1 - \frac{\rho}{\rho_e}\right), \quad (21)$$

where f was an arbitrary constant. Using this equa-

* See ref. 1, p. 177.

tion and Eqs. (16) to (18), Ivory could then fix the form of his atmosphere, and he was also able to evaluate the refraction integral in Eq. (10). In 1823, he published his first refraction tables for $f = 1/4$. In 1838, he extended his theory by including higher order terms in Eq. (21), but concluded that, for a value of $f = 2/9$, the horizontal refraction could be computed to an accuracy with which it was then measurable. The temperatures of Ivory's atmosphere had the property, however, of being too large below 4.8 km and then rapidly becoming too small above this height.*

In 1828, Schmidt in Göttingen published a new theory, which was particularly interesting because of its simplicity and elegance. In these early days, it was known that, in the lower regions of the atmosphere, the temperature decreased 1°C for every 170–190 meters increase in height. This difference in height was also larger in the winter and smaller in the summer. This information led Schmidt to assume a linear decay in temperature with height having the form

$$\frac{1 + \beta t}{1 - \beta t_e} = 1 - \frac{h}{H_e}, \tag{22}$$

where H_e is the upper limit of the atmosphere at which the temperature recedes to absolute zero. To determine H_e, Schmidt used the temperature measurements of Gay-Lussac referred to earlier. With this equation and Eqs. (16) to (18), it was then possible to compute the pressure, density, and temperature as a function of height. Schmidt's theory was one of the older classical theories which enjoyed considerable success in describing the temperature as a function of height throughout the region of the troposphere. In Table IV, we have again gone back to Bruhns' early computations[1] to indicate the form of Schmidt's atmosphere. The pressures, densities, and temperatures indicated in this table are understood to be those for an average quiet atmosphere reduced to standard conditions on the earth. The observed temperatures[22] are the much later results of hundreds of balloon ascensions and also

Table IV. Schmidt's Model of the Earth's Atmosphere

Height (km)	Pressure (mm Hg)	$\frac{p}{p_e}$	Temperature (°C) calc.	Temperature (°C) obs.
0	760	1.000	0	0
1.6	620	0.843	−8.7	−6.0
3.2	500	0.707	−17.4	−14.0
4.8	400	0.588	−26.1	−23.6
6.4	330	0.487	−34.8	−34.4
8.0	260	0.400	−43.5	−45.9
16.0	70	0.132	−86.9	−62.0
24.0	12	0.032	−130.3	
32.0	4	0.004	−173.8	
49.1	0	0.000	−266.7	

* See ref. 1, p. 179.

are averaged and reduced to standard conditions on the earth. Up to about 8 km in the troposphere, one finds quite good agreement between the computed and observed temperatures. Beyond this, Schmidt's theory, like all these early classical theories, encountered difficulties, because such phenomena as temperature inversions and the increase in temperature at high levels in the stratosphere[23] were unknown to these early workers.

All of these early theories attempted not only to describe the physical properties of the atmosphere as they were known at the time, but also sought to predict the magnitude of the astronomical refraction at each apparent zenith angle. To do this, the refraction integral in Eq. (10) had to be integrated, and this often proved to be a difficult and sometimes tedious task. We could not hope to describe how this integral was evaluated for all these many theories. For those who are interested in details of this type, the work of Radau[24] should be consulted. In addition to giving a critical survey of these older theories, Radau also developed some tables of his own (following Ivory's ideas) for computing the astronomical refraction as a function of both pressure and temperature. Here, in order to give some idea of the order of magnitude of the differences between the various theories, we shall simply give some of Radau's numerical results for the theories of Laplace, Ivory, and Schmidt. In Table V, the data on the left are the computed astronomical refractions for each of these theories under standard conditions on the earth. Those at the right indicate the corrections to be applied to each theory for an elevation of 10°C with no change in pressure. In each case, again, the values are understood to be average values characteristic of an average quiet atmosphere. Upon comparing Tables IV and V, one soon appreciates that it was not an easy assignment even in those early days to derive a theory which would describe the physical properties of the atmosphere as they were then known, and would simultaneously yield values for the astronomical refraction which were in agreement with the accepted measured values.

Perhaps the most successful of these early theories and the one that has made the most permanent impression on workers in this field is the Gylden theory. Gylden in 1867 was aware of the difficulties which these early theories encountered in predicting the temperature as a function of height throughout the region of the troposphere. He sought then to improve on Schmidt's theory by proposing a nonlinear temperature decay with height of the form[25]

$$\frac{1 + \beta t}{1 + \beta t_e} = \left(1 - \frac{1}{2} m \frac{h}{a + H}\right)^4, \tag{23}$$

where m was an adjustable constant. By choosing m properly, it was possible* to obtain much better agree-

* See ref. 2, p. 257.

Table V. Computed Astronomical Refractions for Different Apparent Zenith Angles, and Temperature Corrections from Theories of Laplace, Ivory, and Schmidt

Apparent zenith angle	Refraction for 0°C and 760 mm			Temperature correction for $t = 10$°C		
	Laplace	Ivory	Schmidt	Laplace	Ivory	Schmidt
45°	60.5″	60.6″	60.5″	−2.2″	−2.4″	−2.3″
70°	165.1″	165.2″	165.0″	−6.2″	−6.5″	−6.3″
75°	222.7″	222.9″	222.7″	−8.3″	−8.8″	−8.7″
80°	332.3″	332.9″	332.3″	−12.3″	−13.5″	−13.2″
85°	617.7″	619.3″	617.9″	−22.9″	−26.9″	−26.7″
86°	736.1″	738.7″	736.0″	−27.3″	−33.2″	−32.5″
87°	902.2″	906.8″	904.1″	−33.5″	−42.4″	−42.9″
88°	1145.6″	1155.6″	1152.0″	−42.5″	−57.0″	−59.0″
89°	1518.6″	1546.3″	1542.6″	−56.3″	−83.5″	−88.4″
90°	2106.0″	2200.6″	2207.8″	−78.1″	−133.8″	−148.8″

ment between the observed and computed temperatures up to elevations of 16 km than was possible by using any of the earlier classical theories. Gylden was also able to evaluate the refraction integral and thus to obtain an equation from which R itself could be computed. This equation was however too complicated for conventional use, so he went back to Bessel's Eq. (20) and introduced correction terms and adjusted the constants so as to yield correct refraction values. Gylden and Gromadski elaborated further on these ideas[26] and constructed the Pulkovo refraction tables, which are probably the most used refraction tables at the present time. In these tables, the astronomical refraction R is obtained from an equation of the form

$$R = \alpha\,(BT)^{A}\,\gamma^{\lambda}\,\tan Z\,(C{\cdot}D{\cdot}E). \tag{24}$$

C is a correction term for water vapor, D a correction for the spectral type of star, and E is the correction for altitude and latitude. This equation is then quite similar in form to Bessel's equation, but it is more attractive because it acknowledges other variables which were known to influence the astronomical refraction. To give some feeling for the versatility of these tables, we have computed the horizontal astronomical refraction for a number of positions on the earth's surface whose elevations, latitudes, average temperatures, and average pressures were known.[27] The positions chosen in each case had elevations of 10 meters or less so that elevation corrections were negligible, but no attempt was made to rule out individual positions because of geography. For these computations, the barometer was assumed to be subject to the ambient air, and no attempt was made to correct for water vapor. In Fig. 5, it can be seen that the average computed horizontal astronomical refraction reaches a minimum of about 32′ near 5°N and then rises to larger values on both sides, the rise in the northern latitudes being more rapid and reaching higher values. It should be understood both from the data on which these computations were based and from the viewpoint of the theory that these are average values, so that deviations will be expected due to time variations and abnormal local conditions. It would be interesting to know just how valid these computations are and what other possible influences might exist.

VII. More Recent Approaches to Astronomical Refraction

As our knowledge of the atmosphere progressed outward, questions were being asked about the importance of the air layers in the upper troposphere and stratosphere in the astronomical refraction process. In 1896, Bauschinger[28] made some inquiries into the importance of the first temperature inversion, which were approximate but indicative of the trend of the thinking at the time. If in Eq. (10) one argues that the effective height of the earth's atmosphere is always small compared with the radius of the earth ($\mu_e a/\mu r$ is never far from unity), then the astronomical refraction due to the air above any point in the atmosphere characterized by μ_h will be given by

$$R = \tan Z \int_1^{\mu_h} \frac{d\mu}{\mu} = \log_e \mu_h \cdot \tan Z. \tag{25}$$

Assuming that a particular barometer formula giving the pressure as a function of height was valid, that the

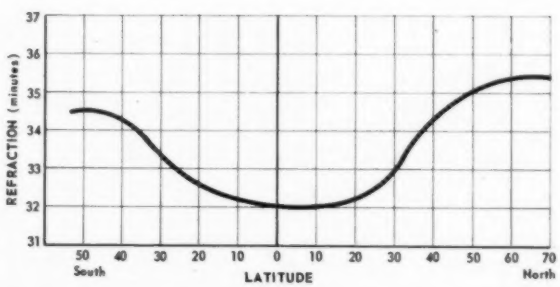

Fig. 5. Computed astronomical refraction as a function of latitude obtained from the Pulkovo tables.

temperature was known as a function of height, and that Eqs. (16) and (17) could be used, Bauschinger then computed the astronomical refraction for different apparent zenith angles for all the air above different heights h at which the refractive index was designated by μ_h. From considerations of this type, he concluded that the first temperature inversion had very little influence on the astronomical refraction for apparent zenith angles up to 80°. Beyond this, the contribution increased until, at 87° 56′, the temperature inversion increased the astronomical refraction by 16.36″.

At about the beginning of the twentieth century, new advances[29] were being made in the knowledge of the physical properties of the atmosphere up to elevations of 25 km. Harzer[30] was the first to utilize these measurements, and he developed a theory of astronomical refraction which for the first time was based on meteorological measurements. Harzer suggested that if one knew the average temperature t and the partial pressure P_γ of each of the gases (including water vapor) at all levels in the atmosphere, it should be possible from Eq. (16) and the Dale-Gladstone law* in place of Eq. (17) to write

$$(\mu - 1) = \sum_\gamma \frac{P_\gamma (\mu_{\gamma_0} - 1)}{P_0(1 + \alpha t)}, \qquad (26)$$

where the summation extends over all the individual gases present. In writing this equation, it has been assumed that each gas in the atmosphere can be approximated at all levels by an ideal gas and that the refractivities are additive. The $(\mu_{\gamma_0} - 1)$ for each gas under standard conditions was determined from laboratory measurements, and the $(\mu - 1)$ was computed at ground level knowing the partial pressures of the various gases present. For computations at different heights in the troposphere ($H = 12$ km and $t = -53.96$°C), all the gases, except for water vapor, were considered to be completely mixed, so that Eq. (26) only had two terms, one for dry air and the other for water vapor. Knowing then the partial pressures of dry air and water vapor and the temperature as a function of height, it was possible to compute the refractive index as a function of height throughout the troposphere. In the stratosphere, whose properties are not as well known, Harzer assumed first that no water vapor was present, that thermal equilibrium existed at the same temperature as at the top of the troposphere, and that each of the gases in the dry air settled out with height in proportion to their masses. With these additional assumptions, Harzer was then able to compute the refractive index in the stratosphere on out to 84 km. Similar detailed computations were made as a function of height over five other places on the earth's surface, and "optical surfaces" constructed, which were the loci of all points in the earth's atmosphere having the same refractive indices. Ray tracing was then used to follow rays from Kiel, at given initial apparent zenith angles, through sixty-one optical surfaces up to 84 km, beyond which the deviations were reduced to less than one one-thousandth of a second. The difference between the initial and final directions then gave the astronomical refraction over Kiel characteristic of each initial apparent zenith angle. This analysis showed that over Kiel there was a slight asymmetry of 28″ in the horizontal refraction when looking north and south. Harzer repeated all these tedious computations* for another quite different type of

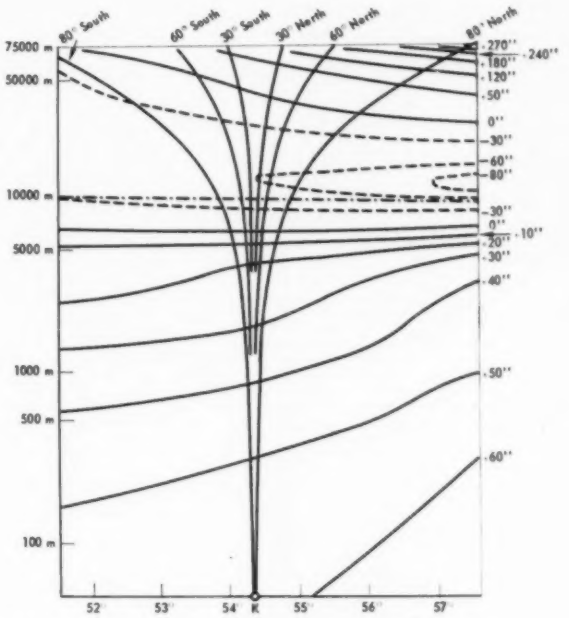

Fig. 6. Two-dimensional plot of Harzer's optical surfaces over Kiel, Germany.

stratosphere, in which the temperature increased linearly with height (1.06°C per km), and he found an increase in the horizontal refraction of 0.37″. To provide independent checks on these computations, Harzer also evaluated the refraction integral in Eq. (10) by numerical methods, assuming of course that the optical surfaces above Kiel were concentric with the center of the earth. These computations indicated that 192.7″ of a horizontal refraction of 2102.376″ could be attributed to the stratosphere, and showed a maximum deviation in the horizontal refraction of only 33″ from the previously suggested more general approach. Over a period of six years, Harzer then

* See ref. 2, p. 187.

* It took sixteen uninterrupted days to follow one ray through these sixty-one optical surfaces using five place logarithms.

Table VI. Computed Astronomical Refractions for Different Apparent Zenith Angles from the Theories of Harzer, Gylden, and Radan

Z	H_t	H_{so}	H_{no}	Gylden	Radau
30°	0′ 33.5544″	0′ 33.5475″	0′ 33.5433″	0′ 33.56″	0′ 33.56″
50°	1′ 9.176″	1′ 9.158″	1′ 9.144″	1′ 9.18″	1′ 9.17″
60°	1′ 40.349″	1′ 40.312″	1′ 40.303″	1′ 40.37″	1′ 40.36″
70°	2′ 38.390″	2′ 38.311″	2′ 38.279″	2′ 38.39″	2′ 38.39″
75°	3′ 33.661″	3′ 33.564″	3′ 33.509″	3′ 33.67″	3′ 33.68″
80°	5′ 18.952″	5′ 18.501″	5′ 18.443″	5′ 18.67″	5′ 18.70″
85°	9′ 51.246″	9′ 50.912″	9′ 50.912″	9′ 51.23″	9′ 51.59″
88°	18′ 17.712″	18′ 15.250″	18′ 18.267″	18′ 17.4″	18′ 19.85″
90°	34′ 59.840″	34′ 26.893″	34′ 55.250″	34′ 40.9″	34′ 44.45″

proceeded to carry out many detailed computations for Kiel in which he also provided first order corrections for the changes in pressure, temperature, water vapor, wind velocity, wavelength, time of year, and even time of day.

Harzer's work did much to stimulate new interest in the subject of astronomical refraction. Dnepprovski[31] and Wunschmann,[32] for example, began making comparisons between Harzer's computations and the results to be expected from other theories. In Table VI Wunschmann has given Harzer's values and the computed values from both the Gylden and Radau theories. These computations are all for Kiel, at which t = 7.48°C, P = 754.48 mm, e = 4.22 mm (partial pressure of water vapor), ϕ = 54° 21′ (latitude), and h = 52 meters (height above sea level). The H_t values are those obtained by Harzer using the concentric spherical shell model. H_{so} and H_{no} are Harzer's results using the more general approach, and the last two columns are the results obtained using Gylden's and Radau's theories. Up to 70°, in accordance with Oriani's law, the values obtained in the first column and the last two columns are all nearly the same. The Gylden and Harzer values for the concentric spherical shell model are all very close to each other except at 90°, at which Harzer's value is 19″ larger. Wunschmann also became interested in studying the forms of Harzer's optical surfaces and determining the effect of their tilt and shape on the usefulness of the concentric spherical shell model for the atmosphere over Kiel. Figure 6 shows a very interesting two-dimensional plot of Harzer's optical surfaces as a function of latitude and the logarithm of the height over Kiel, taken from Wunschmann's paper. Each horizontal curve is the locus of all points having the inclination angle with the horizontal indicated at the right; and the vertical lines indicate schematically the changes in the astronomical refraction with height for the specified apparent zenith angles. To determine the effect of the tilt and shape of each of these surfaces, Wunschmann used a method suggested by Radau.* This method consisted of constructing spherical surfaces which were of the same radius of curvature and were tangent at each point of incidence along the path of the refracted ray. The magnitude of the astronomical refraction was then computed at each point of incidence and compared with that to be expected at the same point from the concentric spherical shell model. Some of the results of these numerical integrations over specific regions of the atmosphere are indicated in Table VII. One sees from this table that the atmosphere above Kiel is of such a nature that the integrated corrections over the lower region of the troposphere are very nearly compensated for by the corrections of opposite sign introduced by the upper troposphere and stratosphere. For such an atmosphere, the concentric spherical shell model becomes quite useful. Wunschmann also discusses similar corrections for other types of atmospheres, the contributions to be expected from large temperature gradients over cities, changes in the forms of the optical surfaces with time, turbulence, wind, and seismic disturbances.

Willis[33] used a slightly different approach for evaluating the refraction integral which involved meteorological measurements and numerical integration. The refraction integral was developed into a series of $N \sec^2 Z$, where N had the value $(\mu^2 r^2/\mu_e^2 a^2) - 1$. Each of the coefficients of the powers of $\sec^2 Z$ were functions of the refractive index which had to be integrated over the complete atmosphere. These integrations were carried out numerically using values of the pressure and temperature obtained from soundings over central Europe. Two series in $\sec^2 Z$ were obtained which represented the contributions of the troposphere and stratosphere to the astronomical refraction. With this equation, Willis could compute the astronomical refraction as well as other first-order corrections for the pressure, humidity, gravity, height, wavelength, etc. The computed values were in agreement with those obtained from the Pulkovo tables.

Hagihara[34] and Sugawa[35] also have attempted to compute the astronomical refraction from meteorological measurements. The pressure, temperature, and water vapor content were determined from radiosonde measurements up to heights of 20 km over Sendai,

* See ref. 24, p. B 104.

Japan. Using the ideal gas law corrected for water vapor, it was possible to compute the density as a function of height. The density was then introduced into the refraction integral and the integration carried out with the aid of a computer. The results obtained were always smaller than the earlier more accepted values of Radau.[24] The authors could not decide whether this difference was due to the different approaches of the two theories or to the lack of data above 20 km. Computations were also made showing the changes in astronomical refraction with the time of year and other variables. Figure 7 shows the results for some of these computations on the seasonal variation in the astronomical refraction for $Z = 45°$, which may be of interest. The authors conclude that it should be possible to obtain numerical values for the astronomical refraction from meteorological measurements with the aid of a computer, but they express the hope that data on the physical properties of the atmosphere will become available up to and beyond 30 km.

It has only been possible to indicate briefly here a few of the developments which have been characteristic in each of the periods in the history of astronomical refraction. There are other interesting phases such as the diurnal and hourly variations[36,37] which are not understood and apparently do not depend on either the pressure or temperature. Corrections for these variations are introduced into Gylden's theory by simply changing the refraction constant used in computing the Pulkovo tables. The more fascinating subject of terrestrial refraction (object and observer close to each other) and its anomalies (mirages, elevation and depression of horizon, appearance of double and triple images, Fata Morgana, etc.) has been avoided completely, because it, like astronomical refraction, can be discussed extensively under the more general subject of atmospheric refraction. An introduction to this subject can be obtained from the works of Wunschmann[38] and Everdingen.[39] For those who may wish additional information about other phases of this subject or more information on the subjects discussed here, additional references are given.[40–63]

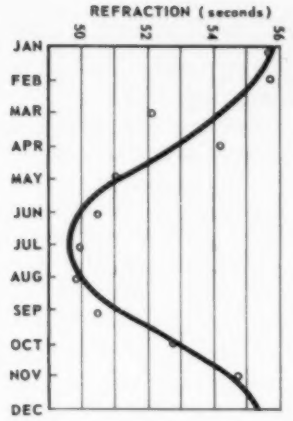

Fig. 7. Computed astronomical refraction as a function of time of year obtained from Sugawa's theory.

VIII. Conclusions

In 1906, Newcomb[20] wrote, "There is no branch of practical astronomy on which so much has been written as on astronomical refraction, and which is still in so unsatisfactory a state." This statement to a large degree is still applicable to the present state of astronomical refraction, but there have been some advances since Newcomb's time. The difficulties which have existed from Newcomb on up to the present have always been both theoretical and experimental in nature. Practically all of the theories of astronomical refraction are based on the concentric spherical shell model, but very little work has been done in establishing its usefulness in various geographic areas over the earth and under known initial conditions. This is of course a difficult and tedious task, for it suggests coordinated measurements of both the physical properties of the atmosphere as a function of height and location, and of the astronomical refraction as a function of apparent zenith angle. When once data of this type become available, extensive computations will be necessary to obtain refractive index values, to determine the forms of the optical surfaces, and to compute the astronomical

Table VII. Astronomical Refractions at Different Apparent Zenith Angles for Different Regions of the Atmosphere from Wunschmann's Computations

Region of atmosphere	30°S	60°S	80°S
Troposphere, 52–6600 meters	−0.0059″	−0.018″	−0.148″
Troposphere, 6600–13,000 meters	+0.0029″	+0.009″	+0.074″
Stratosphere, 13,000–75,000 meters	+0.0038″	+0.012″	+0.092″
Total atmosphere, 52–75,000 meters	+0.0008″	−0.003″	+0.018″
Region of atmosphere	**30°N**	**60°N**	**80°N**
Troposphere, 52–6600 meters	+0.0059″	+0.018″	+0.148″
Troposphere, 6600–13,000 meters	−0.0030″	−0.009″	−0.086″
Stratosphere, 13,000–75,000 meters	−0.0038″	−0.011″	−0.089″
Total atmosphere, 52–75,000 meters	−0.0009″	−0.002″	−0.027″

refraction by ray tracing techniques or numerical integration. Only in this way, however, will it be possible to establish the limitations involved in utilizing the concentric spherical shell model.

There is one obvious way suggested earlier for minimizing the uncertainties and the amount of computation necessary in determining the forms of the optical surfaces and evaluating the refraction integral itself. In all the previous theories, the indirect approach of measuring physical properties other than the refractive indices has been used. This was necessary simply because refractive index measurements have not as yet been possible in the atmosphere. Because of this, it then becomes necessary to utilize certain equations of state for each of the gases present in the atmosphere, refractive index–density relations, and assumptions with regard to the types of interaction between these gases. All of these can of course be checked under controlled conditions in the laboratory, but there is always the question of the importance of other possible variables such as the ionization, wind, large temperature gradients, etc. which appear in the atmosphere itself. The most direct way of avoiding this problem is that of making measurements of the refractive index in the atmosphere itself so as to eliminate the necessity for making these assumptions. This of course is not easy, for the problem of building a refractometer to obtain refractive indices which are characteristic of the unperturbed air may indeed prove to be an insurmountable one, since the difficulties of obtaining reliable refractive indices to seven decimal places or better on the earth are well known.[14] Throughout all these considerations, the importance of the stratosphere is also still an unsolved one, for the optical properties of the upper atmosphere and the limiting height which is effective in these refraction processes are simply not sufficiently well known. Measured values of the refractive index up to as high levels as is possible would also be the most direct method of determining the importance of the stratosphere. If the computed astronomical refractions obtained either by ray tracing or by numerical integration are all at apparent zenith angles less than the observed ones, then the full "effective height" of the atmosphere has not been utilized in the computations, and additional measurements of the refractive index at still higher altitudes become necessary. Obviously, the most successful theory of astronomical refraction will ultimately be that which has available sufficient data on the physical properties of the atmosphere up to its effective upper limit, and not only describes these physical properties as a function of height, but also describes the astronomical refraction as a function of apparent zenith angle. Perhaps a complete theory of this type is too much to expect because of the difficulties with the measurements, but if some sort of a positive approach is not taken, we will remain with the unpleasant prospect of obtaining our computed astronomical refractions from semitheoretical theories, which do not even follow the physical properties of the atmosphere through the first temperature inversion at the top of the troposphere (Bessel, Gylden, Radau), or from theories based on more general approaches which do not have enough data on the physical properties of the atmosphere or its refraction properties to complete the calculations or check the validity of the method (Harzer, Sugawa, Link).

The author is indebted to several people, both outside and inside the Laboratory, who have made contributions to the material presented here. The author had the advantage of having brief discussions with F. P. Scott of the Naval Observatory and J. A. Duerksen of the Coast and Geodetic Survey, both of whom were interested in this subject and were kind enough to supply some of the initial references. The Library of the Naval Observatory and its Staff were also very helpful in locating many of the references. At the Applied Physics Laboratory, Marjorie M. Clark and R. A. Lambert of the Library Staff located many additional references in other libraries in the Washington area. R. P. Illwitzer was helpful in translating some of the Russian source material and making numerous suggestions which added to the continuity and clarity of the material. Sylvia E. Ellsworth did all the numerical computations and E. W. Sultana prepared all the figures. Rosina F. Emery typed the rough drafts and final forms of the paper and made several helpful suggestions. Last, but not least, the paper had its origin in some discussions with J. T. Massey of the Laboratory Staff.

References

1. C. Bruhns, Die Astronomische Strahlenbrechung in Ihrer Historischen Entwickelung, Leipzig, 1861.
2. E. Gehrcke, *Handbuch der Physikalischen Optik* (Barth, Leipzig, 1927), Bd. I, p. 237.
3. Cleomedes, De Mundo, *Circularis Inspectionis Meteororum* (Henricum Petri, Basilae, 1585), p. 294; see ref. 1.
4. Ptolemaeus, Claudius, *Opticae* (Translated from Arabic to Latin by E. Sicile, reprinted by A. Lejeune, Lourain, 1956), Part V, p. 239.
5. Alhazen, *Opticae Thesaurus* (Translated into the Latin by Vitello and published by F. Risner, 1572), Book VII, p. 251.
6. *Tycho Brahe's Description of his Instruments and Scientific Work* (Translated by H. Raeder, E. Stromgren, B. Stromgren, Kobenhavn, 1946).
7. Tycho Brahe, *Astronomiae Instauratae Progymnasmata* (Francofurt, 1648), pp. 15, 39.
8. E. Wilde, *Geschichte der Optik* (Rücker and Püchler, Berlin, 1838), Bd. I.
9. P. Bouguer, "Sur les refractions astron. dans la zone terride," Mém. Paris, 1739.
10. W. Valentiner, *Handwörterbuch der Astronomie* (E. Trewendt, Breslau, 1901), Bd. III.
11. E. V. Oppolzer, Sitz. Ber. Kaiserlich Akad. Wiss. (Wien, 1900) Bd. CIX, Abt. IIa, p. 578.
12. This integral is often derived from Fermat's law. See for

example ref. 2, pp. 222–228; E. E. Kummer, "Uber Atmosphärische Strahlenbrechung," Monatsber. kgl. Preuss. Akad. Wiss., Berlin, p. 405 (1860).

13. Lord Rayleigh, Phil. Mag. (5) 36 (1892); L. J. Gruey, *Exercises Astronomique* (Herman, Paris, 1889), p. 119; S. Newcomb, *A Compendium on Spherical Astronomy* (Macmillan, New York, 1906), p. 190; A. Prey, *Einführung in die sphärische Astronomie* (Springer, Wien, 1949).
14. W. F. Meggers and C. G. Peters, Bull. Natl. Bur. Standards, **14,** 697 (1918).
15. J. Bradley, *Astronomical Observations at the Royal Observatory at Greenwich* (Oxford, 1798), Vol. I, p. B.1.
16. K. Koziel, *Numerikalische strenge Fassung des Laplace's Oriani's Satzes* (Cracovie Imprimerie de L'Universite, 1931); see ref. 2, p. 249.
17. F. W. Bessel, *Fundamenta Astronomiae* (Regiomonti in Commisis Apud f. Nocolovium, 1818), p. 26.
18. F. W. Bessel, *Tabulae Regiomontanae Reductionum* (Black, Young, London, 1830), pp. LIX, 538.
19. N. Bowditch, *American Practical Navigator* (U.S. Hydrographic Office, 1938), pp. 150–153; A. Court, J. Franklin Inst. **247,** 538 (1949).
20. R. T. Crawford, Lick Observatory Bull. **7** (6), 1907; S. Newcomb, *A Compendium of Spherical Astronomy* (Macmillan, New York, 1906), p. 224; C. H. Smiley, Navigation **3, 81** (1951–53); G. M. Clemence, Astron. J. **56** (5), 123 (1951); G. M. Clemence, Navigation **3,** 36 (1951–53).
21. J. Ivory, Phil. Trans. Roy. Soc., p. 437 (1823); Phil. Trans. Roy. Soc. "Bakerian Lecture," p. 169 (1838).
22. A. Wagner, "Die Temperatureverhältnisse in der freien Atmosphäre (Ergebnisse der internationalen Balloonaufstiege) Wien," Beitr. Physik freien Atmosphäre, p. 57 (1910).
23. F. J. Scrase, Nature **164,** 572 (1949); Rocket Panel, Phys. Rev. **88,** 1027 (1952); Etienne Vassy, *Physique de L'Atmosphere* (Gauthier-Villars, Paris, 1959), Tome II, Phenomenes de Refraction.
24. R. Radau, *Recherches sur la Theorie des Refract. astronom.* (Ann. de l'observ. de Paris, Mem. XVI, 1882) p. B1.
25. H. Gylden, Mem. Acad. Imp. Sci. St. Petersbourg (M. M. Eggers, H. Schmitzdorff, St. Petersbourg), **10,** 1 (1867).
26. *Refraction Tables of Pulkovo Observatory* (Acad. Sci. Press, Moscow, 1956), 4th ed.
27. F. Link, *Meteorologisches Taschenbuch* (Geest & Portig, Leipzig, 1951).
28. J. Bauschinger, "Untersuchung über die astronomische Refraktion," Verhandl. K. B. Akad. Wiss. Munich (1896).
29. Julius v. Hann, *Lehrbuch der Meteorologie* (3 Aufl. unter Mitwirkung von R. Suring, Leipzig, 1915).
30. P. Harzer, *Publikation der Sternwarte in Kiel* (C. Schaidt, Kiel, 1922–24), XIII, XIV.
31. N. Dnepprovski, "Note on Harzer's "Refraction Tables" and their comparison with those of Pulkovo and de-Ball," Byull. Akad. Nauk SSSR, Inst. Teoret. Astron., Leningrad (16), 177–186 (1927).
32. F. Wunschmann, Gerlands Beitr. Geophys. **31,** 83 (1931).
33. J. E. Willis, Trans. Am. Geophys. Union II, 324 (1941).
34. Y. Hagihara, Japan. J. Astron. Geophys. **14,** 1 (1936).
35. C. Sugawa, Astron. Soc. Japan Publ. **7,** 163 (1955).
36. W. B. Varnum, "Differential refraction in positional astronomy," Astron. Nachr. (5344) **223** (1925).
37. Gustav Land, "Anomalies in astronomical refraction," Astron. J. **59,** 19 (1954).
38. F. Wunschmann, Die terrestrische Strahlenbrechung, E. Gehrcke, *Handbuch der Physikalischen Optik* (Barth, Leipzig, 1927), Bd. I, p. 273.
39. E. van Everdingen, Anomalien der terristrischen Strahlenbrechung, E. Gehrcke, *Handbuch der Physikalischen Optik* (Barth, Leipzig, 1927), Bd. I, p. 282.
40. C. Kramp, *Analyse des Refrac. Astron. et Terres.*, Strassbourg, 1799.
41. V. Fuss, Beobachtungen und Untersuchungen über die astronomische Strahlenbrechung, St. Petersburg, 1871.
42. M. Kowalski, Recherches sur la Refraction astronomique, Imprimerie de l'Univ., Kasan, 1878.
43. M. J. Mauer, *Die Extinction des Fixsternlichtes in der Atmosphäre in ihrer Beziehung zur astronomischen Refraktion* (D. Bürkli, Zürich, 1882).
44. Maurice Loewy, *Nouvelles Methodes pour la Determination complete de la Refraction* (Gauthier-Villars, Paris, 1886, Acad. Sci. de France).
45. A. A. Rambaut, *On the Effect of Atmospheric Dispersion on the Position of a Star* (Spottiswoode, London, 1895).
46. P. H. Cowell, *Bessel's Refraction Tables arranged for Use at Royal Observatory, Greenwich* (Neill, Edinburgh, 1899).
47. A. Bemporad, "Besondere Behandlung des Einflusses der Atmosphäre," Encycloped. Math. Wiss., Leipzig **VI-2,** hft. 2, 287–334 (1907).
48. F. Nasl and J. J. Fric, "Premiere Etude sur les Anomalies de Refraction," Bull. intern. acad. sci. Boheme, Prague (1908).
49. Naval Observatory U.S., Dip and Refraction for Aerial Navigation, U.S. Naval Observatory Govt. Printing Office, 1916.
50. E. A. F. W. Grossman, Untersuchungen über astron. Refraktion, München, Verlag der Königlich Bayerischen Akad. d. Wiss. 1917.
51. H. C. Plummer, "On astronomical refraction," Monthly Notices Roy. Astron. Soc. **92,** 25 (1931).
52. Alan Fletcher, "Note on astronomical refraction," Monthly Notices Roy. Astron. Soc. **91,** 559 (1931).
53. H. Barrell and J. E. Sears, "Refraction and dispersion of air," Phil. Trans. Roy. Soc. London, Ser. A **238,** 1–14 (1939).
54. F. Link and Z. Sekera, "Dioptrische Tafeln der Erdatmosphäre," Pub. Prazske Hoezdarny, No. 14, 1–28 (1940).
55. B. Garfinkel, "An investigation in the theory of astronomical refraction," Astron. J. **50,** 169 (1942).
56. E. Esclangon, "Sur les Refractions Geodesiques," Compt. Rend., Acad. Sci. Paris, **216,** 137 (1943).
57. Axel Leijonhufvud, On Astronomic, Photographic, and Trigonometric Refraction, Dissertation, Uppsala, Stockholm, 1950.
58. C. G. Maurice, "Astronomical refraction at great zenith distances," Astron. J. **56** (5), 123 (1951).
59. M. Reis, Sobra a Teoria da Refraccao Astronomica, Tipografia da Atlantida, Coimbra (1953).
60. A. S. G. Grant, "Notes on atmospheric refractive index in Canada," Trans. Am. Geophys. Union, **35** (3), 508 (1954).
61. B. H. Dawson, "Formulas Sencillas para la Refraccion Astronomics," Rev. Astron. (Buenos Aires) **28,** II (139), 57 (1956).
62. D. H. Sadler and W. A. Scott, "Refraction at low altitudes," J. Naval Inst. London **13** (2), 139 (1960).
63. R. M. Goody, *The Physics of the Stratosphere* (Cambridge Univ. Press, 1958).

Applied Optics Patents

Reviewing panel

C. Shepard (Chairman) *Rochester*
R. Anwyl *Rochester*
G. W. Cleek *National Bureau of Standards*
A. Danti *Texas A & M*
J. Fitzmaurice *Baird-Atomic*
F. F. Hall, Jr. *ITT Federal Labs*
W. L. Hyde *Fecker*
R. Kingslake *Eastman Kodak*
D. J. Lovell *University of Michigan*
D. L. MacAdam *Eastman Kodak*
A. Mann *Spectrolab*
T. K. McCubbin *Penn. State University*
R. K. McDonald *Boeing*
J. R. Meyer-Arendt *Utah State University*
G. W. Stroke *M.I.T.*
D. E. Williamson *Cordis*

The patents reviewed below have been issued by the U.S. Patent Office on the dates quoted except where otherwise mentioned. The patent number, date of issuance, and classification number are quoted in the first line. The filing date is that of the earliest patent application. The opinions stated in the reviews are those of the reviewers and are not meant to express the thinking either of the organizations with which members of the panel are associated, of the Optical Society of America, or of this journal. Normally, statements of fact are based upon the patents and not independently verified. Printed copies of American patents may be ordered from the Commissioner of Patents, Washington 25, D.C., for 25¢ each. A weekly subscription service to any selected subclass is also available from the Patent Office.

3,022,708 February 27, 1962 (Cl. 88-57)
Correcting optical system.
J. G. Baker. (Not assigned.) Filed Dec. 16, 1957.

A highly corrected catadioptric system is described for use on a satellite tracking camera, comprising a concave spherical mirror with three aspheric corrector plates grouped closely and symmetrically about a stop situated at the center of curvature of the mirror. Two examples are given, of *f*/1 aperture covering a semifield of 15°, the image lying on a spherical surface. One example has apochromatic color correction from the near ultraviolet to the near infrared. R.K.

3,023,671 March 6, 1962 (Cl. 88-57)
Photographic objective.
Jiro Mukai. Assigned to Canon Camera Company. Filed July 31, 1957 (in Japan Oct. 9, 1956).

Two Gauss-type objectives are described, which cover a semifield of 23° at *f*/1.8, the front positive component in each being a cemented doublet with flint in front. The front negative component is a single meniscus in one example, and a meniscus-shaped cemented doublet in the second example. The rear components are conventional. R.K.

3,023,672 March 6, 1962 (Cl. 88-57)
Wide-angle objective.
I. C. Sandback. Assigned to Bell and Howell Company. Filed Oct. 9, 1958.

A 5-component reversed-telephoto system is described, which is intended to cover a wide field (±30°) at *f*/1.7 aperture. The negative front member comprises a plano-convex element followed by a negative meniscus. Behind the diaphragm there is a closely spaced member comprising a positive meniscus element concave to the front, a biconvex doublet, and a plano-convex singlet or doublet in the rear. The claims include a number of rather specific inequalities which are fulfilled by the lens in question. R.K.

3,023,673 March 6, 1962 (Cl. 88-57)
Variable-magnification afocal lens member.
A. Cox and W. R. Linke. Assigned to Bell and Howell Company. Filed Dec. 12, 1958.

A simple completely symmetrical 1:1 afocal telescopic attachment is described, for use in front of a normal projection lens. The attachment comprises two identical positive elements with a sliding negative component midway between them. The negative component consists of two identical negative elements in contact face to face, the power of each negative element being 1.1 times the power of each of the positive elements in the system. Moving the negative component along the axis gives a telescopic magnification ranging from 0.893 to 1.125× with no appreciable shift of the final focus. All four lens elements are composed of the same type of crown glass. R.K.

Brit. 888,728
Photographic or Cinematographic Telephoto lens.
M. C. Schneider. Assigned to J. Schneider & Co., Kreuznach. Filed Aug. 16, 1960 (in Germany Oct. 22, 1959).

A type of telephoto lens is described which has an aperture of *f*/4.5 and an unusually short total length from vertex to film plane (about 75% of the focal length). The diaphragm which is small in diameter is located inside the rear negative member. The front positive member comprises two components, at least one of which is compound, while the negative member contains a negative doublet ahead of the stop and a single negative meniscus element behind the stop. R.K.

3,024,697 March 13, 1962 (Cl. 88-57)
Photographic Objective for picture-taking or projection.
J. Berger. Assigned to Carl Zeiss, Heidenheim. Filed Oct. 31, 1960 (in Germany Nov. 10, 1959).

A four-component objective or projection lens is described of the plus-plus-minus-plus type, the second component of which comprises a positive lens followed by a negative lens, the two elements being preferably cemented together. By this means an aperture of *f*/1.4 can be attained covering a semifield of 12°. The first four elements are asymmetrical, the stronger surfaces being placed toward the front in the two positive elements and toward the rear in the two negative elements. The rear element is biconvex. (Corresponding British patent 892,005.) R.K.

3,024,698 March 13, 1962 (Cl. 88-57)
Optical systems in which parallax is eliminated.
G. W. Hamstead. Assigned to W. Watson and Sons, Barnet, England. Filed Jan. 20, 1958 (in England Jan. 23, 1957).

A small telescope is described which is intended for bore-sighting, comprising an objective, a prism to deflect the beam sideways, a cross-wire, and an eyepiece. The zonal spherical aberration of the objective-prism combination is balanced in such a way that the marginal focus falls at a point 8/9 of the distance from the paraxial focus to the 0.7 zonal focus. The cross-wire is placed at the marginal focus. In this way, according to a mathematical proof included in the patent, the parallax sighting error will be minimized while the definition remains within the Rayleigh quarter-wave limit. R.K.

3,027,805 April 3, 1962 (Cl. 88-57)
Zoom lens system.
Keizo Yamaji. Assigned to Canon Camera Company, Inc. Filed Oct. 22, 1958.

A high-quality mechanically compensated *f*/1.4 zoom lens is described having a 4:1 range of focal lengths. In the prior art, the front positive component is fixed, the main moving component is negative, and there is a rear positive component driven by a U-shaped cam to maintain sharp focus on the film. The cam-driven element moves forward at the ends of its motion, thus interfering with the main moving component, and at one end in particular the cam slope is very steep. To overcome these difficulties, the present invention employs a negative cam-driven component which moves rearward at the ends of its travel, and the cam is nowhere steep enough to cause trouble. A specific example of a 13-element zoom lens embodying the invention is included. R.K.

3,028,793 April 10, 1962 (Cl. 88-57)
High-edge definition lens.
S. Bousky and J. R. Miles. Assigned to Chicago Aerial Industries, Inc. Filed Nov. 15, 1957.

A thin aspheric correcting element is mounted approximately midway between an aerial camera lens and the film. The front surface of the correcting element is plane, and the rear surface is plane in the central area and has a concave toric surface in the outer area, of such a form as to improve the coma and field curvature in the outer parts of the image. A specific example of such a correcting element is given, for use behind a triplet objective of normal construction. R.K.

3,029,698 April 17, 1962 (Cl. 88-57)
High-power photographic objective.
C. Baur and C. Otzen. Assigned to Agfa A. G., Germany. Filed Oct. 21, 1958 (in Germany Oct. 26, 1957).

A six element *f*/1.9 Gauss-type objective is described, which is intended to be used in a 50-mm focal length on a 35-mm camera. In order that the lens may be used with a behind-the-lens shutter having a 22.5-mm clear aperture, the front element is made exceptionally large. The lens data are limited by some inequalities, in the usual way, and a numerical example is given. (Corresponding British patent 891,527.) R.K.

3,029,699 April 17, 1962 (Cl. 88-57)
Wide-angle lens system.
S. H. Brewer, T. I. Harris, and I. C. Sandback. Assigned to Bell and Howell Company. Filed May 25, 1959.

A distorting wide-angle lens system is described, of the reversed telephoto type, which covers a semifield of 71° at *f*/1.0. The front member comprises a strong negative meniscus element closely followed by a biconcave element and a positive cemented doublet, the air lens between the first and second elements having a biconvex form. The rear positive member, which is widely spaced from the front member, has the form of a 9-element compound Gauss objective. The whole system is limited by a series of inequalities. R.K.

continued on page 542

Continuous Optically Pumped Cs Laser

P. Rabinowitz, S. Jacobs, and G. Gould

A continuously operating 7.18-μ laser oscillator has been built using optically pumped cesium vapor as the amplifying medium. A power of 50 μw is coupled out of the confocal resonator by means of a 45° BaF_2 pickoff window. The measured intensity distribution is in good agreement with that derived from the Boyd-Gordon expression for the lowest-order mode.

Introduction

A continuously operating 7.18-μ laser oscillator has been built using optically pumped Cs vapor as the amplifying medium.[1,2] The oscillations are sustained in a resonant cavity consisting of a flat and a spherical reflector. Population inversion is achieved between the Cs $8P_{1/2}$ and $8S_{1/2}$ levels by optically pumping Cs vapor with the intense He 3888 Å line which overlaps the third resonance line of Cs (see Fig. 1).

Earlier measurements of fluorescence[3,4] and amplification[5] indicated the feasibility of obtaining oscillation at 7.18 μ or 3.20 μ. The 7.18-μ, rather than the 3.20-μ, oscillator was constructed because of the lower threshold for oscillation at the longer wavelength.

Oscillator Construction

The oscillator, shown schematically in Fig. 2, consists basically of a heated cesium cell, an rf-powered helium lamp with focusing reflectors and an optical resonator composed of a flat and spherical reflector. The optically pumped length of the cesium cell is 92 cm. Its inner diameter is 1 cm. The cesium used is triple distilled and the vapor, at a temperature of 175°C, is contained within a glass tube by means of BaF_2 windows to avoid the corrosive action of cesium on the resonator reflectors. The windows are held against the cesium cell, approximating optical contact within a few fringes, because no sealant was found sufficiently resistant to cesium attack. One window is oriented at Brewster's angle with respect to the cell's axis to eliminate the Fresnel reflection losses in one polarization. The second window is oriented at 45°, providing $^1/_2$% output coupling for the polarized beam. The cell is connected to a vacuum system to avoid quenching effects due to foreign gases liberated from the hot cesium and glass. The outer chambers, containing the resonator reflectors, are also maintained in vacuum to avoid thermal air turbulence and to insure a vacuum seal for the cell.

The rf electrodeless lamp is filled with helium at a pressure of 4 Torr and is operated at a power of 800 watts at a frequency of 15 Mc/sec, corresponding to saturation of the 3888 Å ($3^3P \rightarrow 2^3S$) line intensity (see Fig. 3). This effect is related to the saturation of the helium triplet metastable level, 2^3S, since the predominant excitation of the 3^3P is by collisions of electrons with metastable atoms. The lamp, contained within a water jacket, is covered with a silver mesh to shield the rf because it was found that direct rf excitation of the cesium occurred and was sufficient to affect the inversion.

The Optical Resonator

The optical resonator, consisting of a flat and a spherical reflector, is one variety of the confocal spherical resonator described by Boyd and Gordon.[6] The radius of curvature of the spherical reflector is 396 ± 1 cm; its separation from the flat is 193 ± 1 cm, corresponding to a deviation of 2.5% from the confocal condition. The axial mode separation, $\Delta\nu = c/2L$, is 75 mc. The separation between adjacent angular modes is $\sim$ 18 Mc.

The plane reflector is flat to better than $\lambda/30$ (visible) while the concave reflector is spherical to within $\lambda/10$ (visible). The reflecting surfaces are coated with an opaque silver film. Orientation of the flat and sphere are each controlled by means of three $^1/_4$ in.-80 adjustment screws (approx. 6 mm diam., 30 turns/cm) which provide 15 minutes of tilt per revolution.

The BaF_2 windows, located within the resonator, are of selected optical quality and are polished flat to $\lambda/10$ (visible). It should be noted that no laser power is lost

The authors are with TRG, Inc., Syosset, N.Y.

Received 16 April 1962.

This work was supported by Advanced Research Projects Agency through the Air Force Office of Scientific Research.

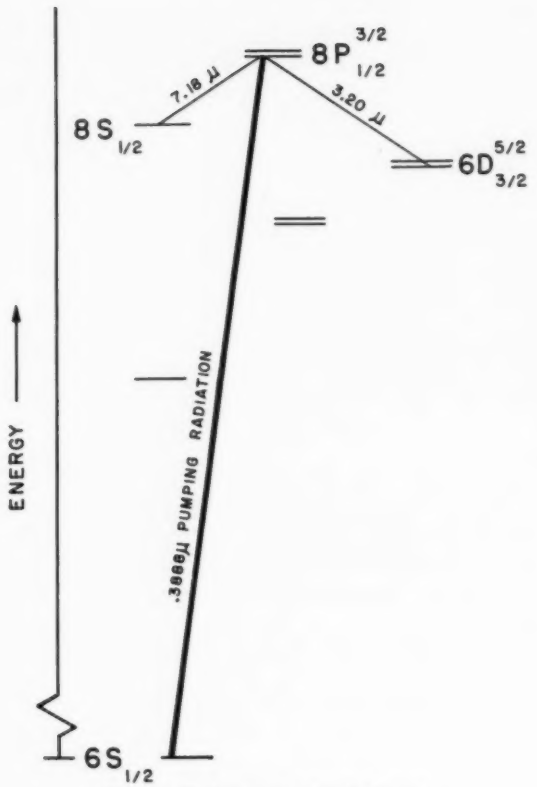

Fig. 1. Cesium energy level diagram.

by discarding one polarization. In fact, greater coherency results because of the exclusion of half the modes. The resonator simply has a high Q for one particular polarization and the population inversion, achieved by optical pumping, goes entirely into supporting these high-Q modes of oscillation.

Output Beam Characteristics

The 7.18-μ beam is detected by a gold-doped germanium photoconductor, cooled to 77°K. The power is coupled out of the resonator by reflection from the uncoated BaF_2 window oriented at 45° with respect to the cell axis. Two output beams result from the two surface reflections. The window is sufficiently thick to separate the two beams in order to avoid possible destructive interference in the near field. The beam diameters at the output window are each 3.2 ± 0.1 mm; the far field beam angular divergence is 10^{-3} radians. Rotation of a silver chloride polarizer confirms the plane polarized state of the beam.

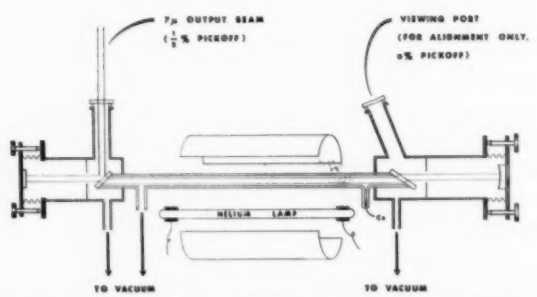

Fig. 2. Schematic view of CW optically pumped Cs laser.

The gross spectral composition of the laser output is examined by passing the beam through a Perkin-Elmer Model 98G grating monochromator located two meters from the output window of the oscillator. Oscillation is observed only at a wavelength of 7.18 μ. The beam power, measured with a thermopile, is approximately 25 μW in each beam.

Additional Properties of the Operating Oscillator

The resonator plates can be tipped by 4 min of arc before oscillation ceases. Measurements have been made of the minimum length of excited vapor which can provide sufficient gain for oscillation. This is about 4 cm, implying an effective gain of 1% per cm, assuming an estimated 4% loss per pass.

Studies of the cesium fluorescence[3] indicate that, at a temperature of 175°C, there is collision excitation of the Cs $8P_{3/2}$ level as a result of the process

$$6S_{1/2} + 8P_{1/2} + kT \rightarrow 6S_{1/2} + 8P_{3/2}.$$

The energy defect between the $8P_{1/2}$ and $8P_{3/2}$ is only 83 cm^{-1} or $kT/5$ and, therefore, it is of interest to check for possible oscillation between $8P_{3/2}$ and $8S_{1/2}$ states ($\lambda = 6.78\ \mu$). No oscillation is observed at that wavelength.*

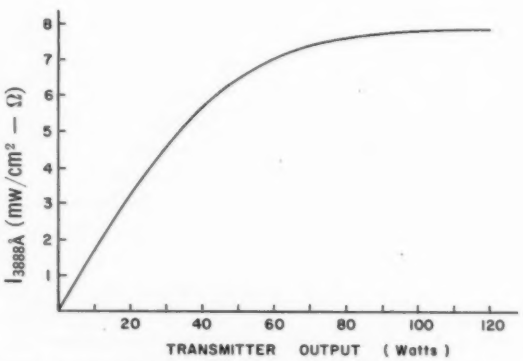

Fig. 3. Saturation of the 3888Å He-line intensity. Lamp parameters: 4 mm i.d. × 150 mm long; He pressure 4 Torr.

* Atmospheric water vapor is excluded from the optical path by flushing the path with argon, as the water vapor absorption at 6.78 μ is not small. At 7.18 μ the atmospheric absorption in our laboratory varies between 5 and 10% for a two-meter path.

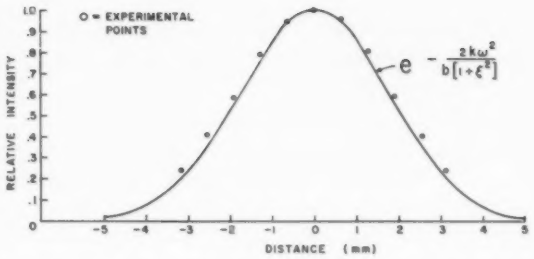

Fig. 4. Output beam intensity distribution; experimental uncertainty ±3%.

At the time of writing, the oscillator has been operated for a total of 40 hours with no noticeable deterioration. The ultimate life of the oscillator will be determined either by Cs attack on the optical elements or by exhaustion of the cesium supply.

Coherence

The spacial coherence of the oscillation has been examined by scanning the output intensity distribution with a gold-doped germanium detector and comparing this result with the expression derived by Boyd and Gordon for the lowest-order single mode output. The theoretical expression for the intensity distribution is given by

$$I(\omega) = e^{-\frac{2k\omega^2}{b(1+\xi^2)}},$$

where

$k = 2\pi/\lambda$,
b = confocal spacing,
$\xi = 2z_0/b$,

and z_0 is the distance from the center of the confocal cavity (in this case, the distance from the flat) to the region under consideration, $\omega^2 = x^2 + y^2$, where x and y are distances measured in the plane normal to the cavity axis. In the case under consideration $I(\omega) = e^{-0.159\omega^2}$ (ω expressed in millimeters) and is valid within the approximation to the angular prolate spheroidal function given by Boyd and Gordon.

Figure 4 shows the theoretical intensity distribution for the lowest-order TE_{00q} mode, and a plot of the experimental values. The experimental values closely follow the theoretical curve, indicating that only the lowest-order spatial mode is oscillating, and hence there is a high degree of spatial coherence. The fact that higher-order, nonaxial modes do not appear is due to the relatively large diffraction losses of these modes for the parameters of this cavity. The calculated losses[6] for some of the lower-order modes are:

$$TE_{00q} = 0.015\%,$$
$$TE_{01q} = 0.6\%,$$
$$TE_{02q} = 10\%.$$

Multiple slit diffraction patterns have been observed but quantitative data relating to the patterns are not presented at this time.

The temporal coherence of the oscillation can only be estimated on theoretical grounds since direct measurement of the linewidth has not been made. The beating of modes, as observed with the helium-neon oscillator[7] to obtain an upper limit of the linewidth, cannot be applied because of the relatively long response time of our detector. An estimate of the linewidth can be obtained, provided one knows the power per mode in the oscillating field, using the expression[8]

$$\Delta\nu_{osc} \cong \frac{2\pi h\nu(\Delta\nu_c)^2}{P},$$

$\Delta\nu_c$ = half-intensity width of the interferometer resonance,
$\Delta\nu_{osc}$ = half-intensity width of the oscillation,
P = power in the given mode.

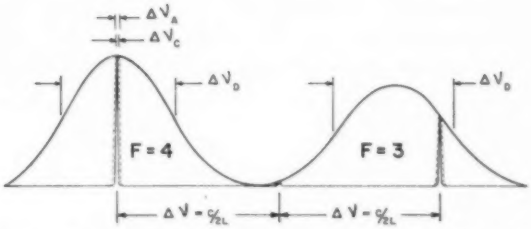

Fig. 5. 7.18 μ spectral distribution showing zero-field hyperfine components and axial modes.

Figure 5 shows the relationship of the cavity axial mode separation with respect to the spectral line. The double peak, due to the zero field hfs of the $8P_{1/2}$ level, has a separation of about 130 Mc, a value computed[9] with the known fine-structure splitting of the $8P$ doublet. The figure shows that amplification sufficient for oscillation can occur for at most 3 axial modes. This implies at least 8 μW power output in a single mode and, since the output power is only $^1/_8$ of the total power radiated by the atoms (the remaining fraction is lost mostly by absorption), the total power per mode is about 64 μw. On the basis of this total power radiated within a mode, and assuming 4% cavity losses per pass,

$$\Delta\nu_{osc} \approx 0.003 \text{ cps}.$$

Discussion

The system described above is the first gaseous laser oscillator to utilize optical pumping. It is therefore of interest to compare this laser with a system employing collisions of the second kind such as the He-Ne system.[5] The power levels are comparable, at about 1 mw, provided the cesium output coupling is increased to about 10% and the resonator is changed to a plane Fabry-Perot, capable of greater mode volume. In contrast to the helium-neon system, the optically pumped laser may be operated in short pulses, driven by an intense flashlamp. Such flashlamps have been constructed in this laboratory and yield a peak spectral intensity at $\lambda = 3888$ Å 10^3 times greater than the present continuous rf lamp. This means one can expect a peak power level of about 1 watt. The spatial and temporal coherence of both lasers are comparable.

A 3.20-μ laser oscillator of simplified design is being constructed with a sealed-off cesium cell positioned between external reflectors. Oscillation will occur at 3.20 μ, rather than at 7.18 μ, if the cavity Q at 7.18 μ is sufficiently reduced, i.e., by putting a sapphire window within the resonator. (The threshold for oscillation at 3.20 μ is $6^1/_2$ times higher than at 7.18 μ, for equal cavity losses.) Thus a single laser may be made to oscillate at either 3.20 μ or 7.18 μ.

The development of this new laser provides a valuable tool for investigations in the infrared and fills part of the gap between the optical and submillimeter region of the spectrum where there is presently a lack of bright sources of radiation.

We wish to acknowledge the valuable assistance of B. Freeman, J. Poulos, and S. Meistrich in the design and construction of the oscillator. We appreciate also the cooperation given us by the Harshaw Chemical Corporation in specially providing and selecting the high grade BaF_2 used in this work.

References

1. A. L. Schawlow and C. H. Townes, Phys. Rev. **112**, 1940 (1958).
2. G. Gould, unpublished proposal submitted to ARPA (Dec. 1958).
3. S. Jacobs, G. Gould, and P. Rabinowitz, J. Opt. Soc. Am. **51**, 477 (FA15) (1961) (paper to be published).
4. H. Z. Currins, I. Abella, O. S. Heavens, N. Knable, and C. H. Townes, *Advances in Quantum Electronics* (Columbia Univ. Press, New York, 1961), p. 12.
5. S. Jacobs, G. Gould, and P. Rabinowitz, Phys. Rev. Letters **7**, 415 (1961).
6. G. D. Boyd and J. P. Gordon, Bell System Tech. J. **40**, 489 (1961).
7. A. Javan, W. R. Bennett, Jr., and D. R. Herriott, Phys. Rev. Letters **6**, 106 (1961).
8. W. G. Wagner and G. Birnbaum, J. Appl. Phys. **32**, 1185 (1961).
9. H. Kopfermann, *Nuclear Moments* (Academic Press, New York, 1958), p. 125.

OSA—SPRING MEETING

Dr. P. Jacquinot *Paris* receiving, on behalf of Dr. Jean-Pierre Barrat *Caen*, the Adolf Lomb Medal from President D. L. MacAdam during the OSA Spring 1962 Meeting in Washington. See page 539 for Harry Hammond's report of this meeting.

ANNUAL SUBSCRIPTIONS

Per volume of six issues per year

OSA members	$ 6.00
Other AIP societies' members	$ 8.00
Non-members and libraries	$10.00
Single copies	$ 2.00

Subscriptions should be addressed to APPLIED OPTICS Subscription Handling, American Institute of Physics, 335 East 45th Street, New York, New York.

Observations Relating to the Transverse and Longitudinal Modes of a Ruby Laser

V. Evtuhov and J. K. Neeland

Observations of the light intensity variations across the partially transmitting face of a laser crystal operated near threshold are reported. The intensity variation patterns are suggestive of the modes of a cylindrical microwave cavity and are believed to be closely related to the transverse modes of the optical resonator. Preliminary polarization studies indicated that patterns with only a twofold symmetry axis are linearly polarized, whereas others are unpolarized. The pattern sizes range between approximately 170 and 850 μ. The divergence of the emerging beam (several milliradians) decreased with increasing resonator length. Fabry-Perot analysis showed only one excited longitudinal mode for a 1-cm long resonator, but the number increased with the resonator length.

Introduction

Of great importance in understanding and effectively utilizing the optical maser is the study of the mode characteristics of the optical resonator. We would like to report here some observations which could greatly facilitate such a study.

By operating a ruby laser sufficiently close to oscillation threshold ($\lesssim$1 percent above threshold) and using a high-quality crystal, we have been able to observe directly the variations of the beam intensity across the partially transmitting face of the laser crystal. Such observation provides considerable information about the field distributions inside the optical resonator. It has been found that the intensity-variation patterns are very similar to those observed in optical fibers[1] and gaseous lasers[2] and that they are suggestive of the oscillation modes of a cylindrical microwave cavity. We believe that these intensity variations are very closely related to the transverse modes of the optical resonator and that they are of the same nature as some of the patterns recently observed by Dayhoff and Kessler.[3] Transverse modes have been considered theoretically by Fox and Li[4] and by Boyd and Gordon[5] using a plane wave approximation. We have performed preliminary studies on the polarization properties of the patterns and, in some cases, have measured their size and the divergence of the emerging laser beam.

The authors are at Hughes Research Laboratories, Malibu, Calif.

Received 14 March 1962.

This work was partially supported by the Aeronautical Systems Division, Air Force Systems Command.

Along with the above experiments the frequency characteristics of the output beam were also studied using the Fabry-Perot interferometer. So far no correlation between the transverse patterns and the number of longitudinal modes excited (the only ones resolved in our experiments) has been observed. However, the number of excited longitudinal modes does seem to depend on the length of the cavity.

Experimental Results

The experiments were performed using an elliptical pumping configuration with a xenon flash lamp similar to the EGG FX-1, but with its active length reduced to 5 cm. Ruby samples having a 0.05 percent Cr^{3+} ion concentration and exhibiting an intrinsic (inhomogeneously broadened) line width of approximately 0.15 cm^{-1} were used. The samples and optical resonator configurations are summarized in Table I. In all samples the c axis was oriented along the cylinder axis within approximately 1 degree; the faces were flat and parallel within 0.25 μ.

Some of the experimental results are shown in Figs. 1–3. All the patterns shown in these figures were obtained using the 3-mm $\times$ 2.54-cm and 3-mm $\times$ 1-cm silvered samples; however, very similar patterns were obtained with the other samples and configurations listed in Table I. In some cases we have attempted a tentative identification of the modes. This was done by comparing our patterns with those obtained in optical fibers by Snitzer and Osterberg.[1] We found no simple correlation between the spiking pattern of the output and the mode patterns observed. Thus, complicated asymmetrical mode patterns apparently consisting of a superposition of several high-order modes

Table I. Ruby Samples and Optical Resonator Configurations Used in the Experiments

Sample diameter (mm)	Sample length (cm)	Type of reflector	Reflector transmission (percent)	Remarks
3	2.54	Silver on ruby faces	0 and 0.35	Two samples used
2	2.54	Silver on ruby faces	0 and 0.35	.....
3	1.00	Silver on ruby faces	0 and 0.35	.....
2	3.18	Silver on ruby faces	0 and 8.5	Sapphire cladding, 5-mm o.d.
3	2.54	Detached silvered reflectors 11.7 cm apart	5 and 5	Ruby faces antireflection coated

were sometimes observed with only a single output spike, while simple patterns were observed with quite irregular output in time. Generally, however, we found that an increase in pump power resulted in blurring of the simple pattern and, sometimes, the appearance of other seemingly uncorrelated modes.

In Fig. 2(a), we show the results of rotating the ruby in its mount. Since in the elliptical pumping configuration the pumping energy incident on the ruby is not isotropic, ruby rotation results in a change in the azimuthal pump intensity distribution. Obviously, the pump intensity distribution determines to a large extent which modes are excited. Similar but somewhat more pronounced effects have been observed by placing a 1.27-mm shielding strip along the side of the ruby. In Fig. 2(b), the effects of approximately compressional but inhomogeneous strain on the mode pattern are illustrated qualitatively. No detailed studies of the strain effects have been performed as yet. It was found, however, that straining the crystal resulted in an increase in threshold.

In order to study the mode patterns in somewhat more detail, we performed both linear and circular polarization-analysis experiments on several patterns. Knowledge of the polarization properties of simpler mode patterns should help us to understand the more complicated ones. Some of the results of these experiments are shown in Fig. 3. In general, we found that patterns with only a twofold symmetry axis are linearly polarized, while those with a higher degree of symmetry show no polarization. Figure 3(b) shows that it is possible to separate a complicated pattern into simpler components by polarization techniques.

We also performed some preliminary measurements of the output beam divergence for various resonator lengths. The approximate divergence angles are 11×10^{-3} radian for a 1-cm resonator, 4.4×10^{-3} radian for a 2.54-cm resonator, and 2.2×10^{-3} radian for a 11.7-cm resonator. This dependence is not yet clearly understood, but it may be related through diffraction to the size of the spot at the resonator plate, which increases with increasing resonator length. It is important to note that in all the cases studied the patterns seen at the face of the ruby persisted along the diverging laser beam. This seems to indicate that there is a very strong correlation between the different high-intensity spots of the pattern and thus supports the mode interpretation of the patterns. We have found the pattern sizes to range between approximately 170 and 850 μ. For the case of 3-mm $\times$ 2.54-cm silvered ruby and a single spot pattern, we have measured the spot size at approximately 200 μ. To within the present accuracy of our measurements (10 to 15 percent), we found that the spot size is independent of the radius of the resonator, but is roughly proportional to the square root of the resonator length. This result is in qualita-

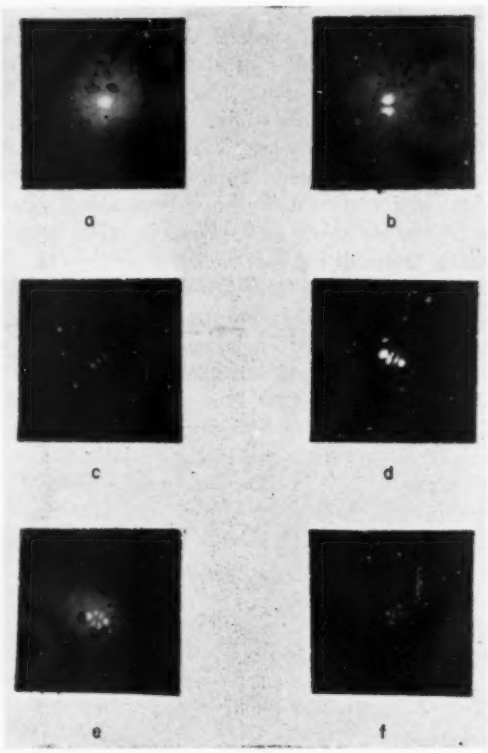

Fig. 1. Photographs of the end of a 3-mm $\times$ 2.54-cm ruby showing some of the typical transverse mode patterns. Modes are tentatively identified (Snitzer's notation) as follows: (*a*) HE_{11}; (*b*) mixture of TE_{01} or TM_{01} with HE_{21}; (*c*) mixture of EH_{11} or HE_{31} with HE_{12}; (*d*) mixture of TE_{02} or TM_{02} with HE_{22}; (*e*), (*f*), not identified.

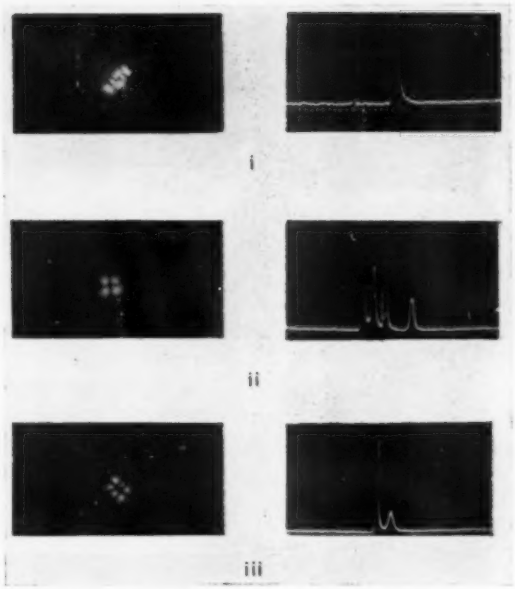

Fig. 2(a). Photographs of the end of the ruby rod (magnification ×6.3) and associated oscilloscope traces (scope sweep speed = 10 μsec/division) of the light output with time. Dependence of the patterns on angular position of the ruby about its own axis. 3-mm × 2.54-cm silvered sample. (i) Angular position ϕ = 0 degrees (reference position). (ii) ϕ = 97 degrees; tentative mode designation: mixture of EH_{11} with HE_{31}. (iii) ϕ = 125 degrees.

tive agreement with the formula for "spot size" derived by Boyd and Gordon[5] for the case of a confocal resonator. Such agreement is somewhat surprising since their analysis is not directly applicable to our case of a plane parallel resonator.

Finally, we have frequency analyzed the output of the various laser crystals by using a Fabry-Perot interferometer. It should be noted that because an optical cavity resonates in a very high-order longitudinal mode, the frequency separation between the longitudinal modes is much greater than that between the transverse modes. Assuming that the normal modes of an optical resonator are similar to those of a cylindrical microwave cavity, we estimate that for a 3-mm × 2.54-cm ruby the separation between two adjacent longitudinal modes is approximately 0.11 cm^{-1}, while that between two adjacent transverse modes is of the order of 10^{-3} cm^{-1}. Thus, with the Fabry-Perot plate separations used in our experiment, it was not possible to resolve the transverse modes.

Some of the results of the Fabry-Perot studies are shown in Fig. 4. It can be seen that three longitudinal modes appear in the case of the 2.54-cm ruby, even very close to threshold when there is only one oscillation spike in the output. On the other hand, in the case of the 1-cm ruby a single longitudinal mode appears, even for pumping power 10 percent above threshold. So far no correlation between the transverse patterns and the number of longitudinal modes excited has been observed. The reasons for the dependence of the number of longitudinal excited modes on the length of the cavity are not quite clear at present. Wagner and Birnbaum's[6] analysis of quantum oscillators in a multimode cavity implies that, for the case of thermally broadened fluorescent lines and weakly coupled modes, only one longitudinal mode should be excited. However, their analysis may not be directly applicable, since there are some indications that the observed behavior may be related to the inhomogeneous broadening of the fluorescent line. Note that in Fig. 4(c) the laser line appears to be rather wide (approximately 0.1 cm^{-1}). This may be a result of the temperature shift in both the material and the cavity resonance. Order-of-magnitude calculations indicate that such temperature shifts are not unreasonable. Moreover, quantitative estimates show that the material and cavity resonance shifts are equal, thus requiring no mode-hopping.

Discussion

It is obvious from the above that considerably more work should be done along the lines already indicated, if the mode behavior of the laser is to be well understood. In addition, it would be of interest to study the mode behavior of an optical resonator employing multilayer dielectrics, rather than silver, as reflectors. Such studies might help to explain the regular pulsations obtained with dielectric reflectors.[7] It would be of interest to analyze the frequency composition of the single longitudinal mode shown in Figs. 4(b) and (c) and attempt to correlate the results with the intensity-variation patterns. To resolve in frequency the various transverse modes which, as we have seen above, are approximately only 30 mc apart, we must use a separation between the Fabry-Perot interferometer plates of the order of 20 cm. It may be possible to use photomixing techniques[8] for these studies.

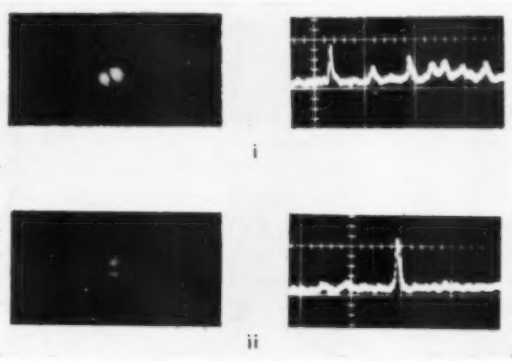

Fig. 2(b). Effect of strain on the pattern at the end of a ruby rod. Note shift and rotation of pattern relative to the ruby. 3-mm × 2.54-cm silvered sample (magnification ×7). (i) Strain applied. (ii) Strain released.

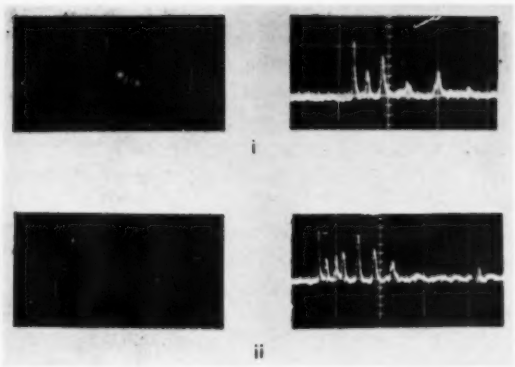

Fig. 3(a). Polarization of light in a ruby mode pattern (magnification ×7). (i) Polarizer parallel to pattern axis. (ii) Polarizer perpendicular to pattern axis.

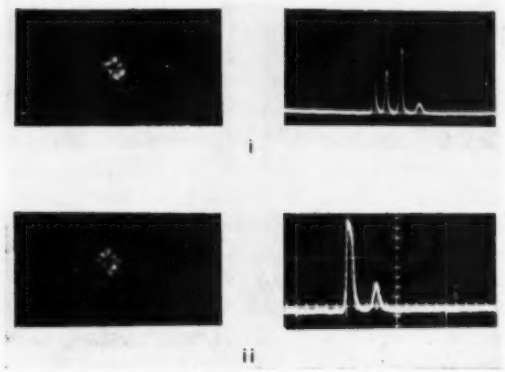

Fig. 3(b). Resolution of a complicated transverse mode pattern by means of a polarizer. 3-mm × 2.54-cm silvered sample (magnification ×6.3). (i) Polarizer parallel to pattern axis. (ii) Polarizer perpendicular to pattern axis.

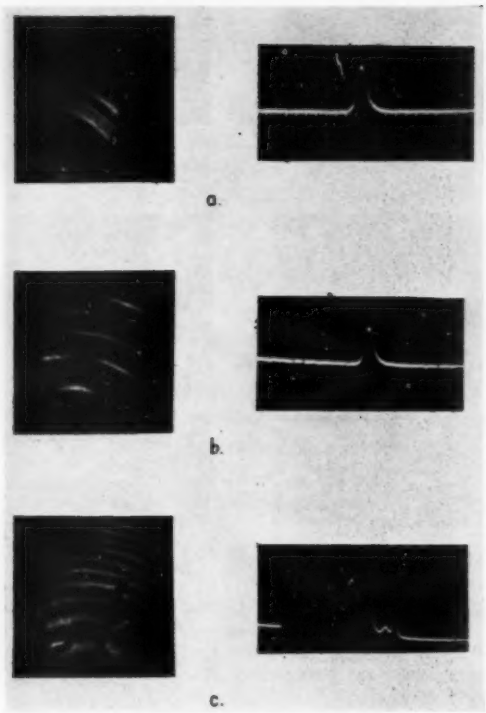

Fig. 4. Fabry-Perot analysis of the laser output at room temperature. Fabry-Perot order separation = 0.513 cm^{-1}; plate separation = 0.975 cm. (*a*) 3-mm × 2.54-cm silvered sample; optical resonator longitudinal mode separation = 0.111 cm^{-1}; scope sweep speed = 5 μsec/division. (*b*) 3-mm × 1-cm silvered sample; optical resonator longitudinal mode separation = 0.281 cm^{-1}; scope sweep speed = 5 μsec/division. (*c*) Same sample as (*b*) driven approximately 10 percent above threshold; scope sweep speed = 10 μsec/division.

We should like to thank I. J. D'Haenens, G. Birnbaum, and D. Weiner for valuable discussions. We are grateful to M. Himber and C. P. Donnelly for preparation of the samples.

References

1. E. Snitzer and H. Osterberg, J. Opt. Soc. Am. **51,** 499 (1961).
2. H. Kogelnik and W. W. Rigrod, Proc. IRE **50,** 220 (1962).
3. E. S. Dayhoff and B. Kessler, Bull. Am. Phys. Soc. Ser. II **7,** 15 (1962).
4. A. G. Fox and Tingye Li, Bell System Tech. J. **41,** 453 (1961).
5. G. D. Boyd and J. P. Gordon, Bell System Tech. J. **41,** 489 (1961).
6. W. G. Wagner and G. Birnbaum, J. Appl. Phys. **32,** 1185 (1961).
7. D. A. Buddenhagen (to be published).
8. B. J. McMurtry and A. E. Siegman, Applied Optics **1,** 51 (1962).

ICO 6 Munich Meeting Information—see page 454

Influence of Scattering on Fluorescence Spectra of Dilute Solutions Obtained with the Aminco–Bowman Spectrophotofluorometer

J. M. Price,* M. Kaihara, and H. K. Howerton

Various factors affecting the intensity of scattered radiation appearing in fluorescence and excitation spectra of molecules in dilute solution obtained with the Aminco–Bowman Spectrophotofluorometer have been investigated. The spectra can be modified and in some cases improved by the addition of colored glass filters, interference filters, and polarizing elements to the optical system. The polarizing elements permit the measurement of fluorescence polarization, and results are given for the polarization of fluorescence of some xanthydrol derivatives in glycerol at room temperature. The effects of strong sample absorption and highly intense scattered radiation on observed fluorescence spectra and quantitative assays are shown.

Introduction

The Aminco–Bowman Spectrophotofluorometer[1,2] is a useful instrument for fluorescence measurements as is attested by its wide use in research laboratories. The measurement of fluorescence and the interpretation of the results is confused by a variety of influences, namely: (1) both monochromators pass radiation in the second order of diffraction as well as the required first order, (2) the geometry of the optical system in the sample region is altered due to sample absorption and scattering of the exciting radiation, (3) Tyndall, Rayleigh, and Raman scattering together with sample fluorescence appear in the observed fluorescence and excitation spectra, and this scattered radiation leads to complicated results which are not representative of the sample fluorescence. The purpose of this paper is to point out and explain the spurious effects that can be observed when the instrument is pushed to its highest sensitivity or operated under conditions for which it was not originally designed.

J. M. Price and M. Kaihara are at the Department of Surgery, University of Wisconsin Medical School, Madison, Wisconsin. H. K. Howerton is with the American Instrument Company, Inc., Silver Spring, Maryland.

Received 11 August 1961.

Parts of this paper were presented at the Pittsburgh Conference on Analytical Chemistry and Applied Spectroscopy, Pittsburgh, Pennsylvania on March 4, 1960.

* American Cancer Society—Charles S. Hayden Foundation, Professor of Surgery in Cancer Research.

In an early description of an experimental spectrophotofluorometer, Bowman *et al.*[3] reported the presence of scattering in the excitation* spectrum in the form of a peak in the spectrum when excitation and fluorescence wavelengths were equal. The name assigned to this phenomenon by Duggan *et al.*[4] in the subsequent spectrophotofluorometric study of compounds of biological interest was *light scattering*. They pointed out that the availability of complete excitation and fluorescence spectra provided a convenient and reliable means of detecting interference due to light scattering from the blank so that appropriate corrections could be made.

During an investigation which led to the development of a fluorometric method for the determination of kynurenic acid and xanthurenic acid in human urine[5] light scattering presented a serious problem since wide slits and highly scattering solvents were used. In these studies two types of scattered radiation were observed—that appearing at the same wavelength of excitation and that appearing at a higher wavelength than the exciting radiation. That the latter was due to the Raman effect was postulated by a few observers in personal communication to one of us (H. K. H.) soon after the Aminco–Bowman Spectrophotofluorometer became commercially available in 1956. Furthermore, Parker[6] has reported the existence of Raman scattering in fluorescence spectra.

* "Activation" and "excitation" have been used synonymously in this field; less frequently used is "action."

Because scattering of light may result in practical difficulties in interpreting fluorescence spectra recorded with commercially available instruments such as the Aminco–Bowman Spectrophotofluorometer, an investigation was undertaken of the various instrumental parameters affecting scattering and the means of reducing it. The identification of Raman scattering was possible by observing the isotope effect in shifting the Raman bands and by a demonstration of the polarization of these bands.

Apparatus

General

The Aminco–Bowman Spectrophotofluorometer is a standard commercial instrument recording either excitation or fluorescence spectra. Light from the source is dispersed by the excitation monochromator into monochromatic radiation incident on the sample. Fluorescent light from the sample is dispersed by a similar monochromator into monochromatic radiation incident on the detector. There the radiation is transformed to a weak electrical signal and fed to the photometer, where it is amplified. Photometer output is coupled to the vertical (Y) axis of an oscillograph or is indicated by a meter. The gratings are oscillated by motor-driven cams to which are coupled graduated disks for visual observation and manual adjustment of the wavelength. Potentiometers, coupled to the gratings, supply wavelength information in the form of a dc signal to the horizontal (X) axis of the oscillograph. When the oscillograph X-input is connected to the scanning fluorescence monochromator, and the excitation monochromator is set at a wavelength for maximum excitation, a wavelength versus intensity diagram (fluorescence spectrum) is displayed. Similarly, when the oscillograph X-input is connected to the scanning excitation monochromator, and the fluorescence monochromator is set at a wavelength for maximum fluorescence, a wavelength versus intensity diagram (excitation spectrum) is displayed.

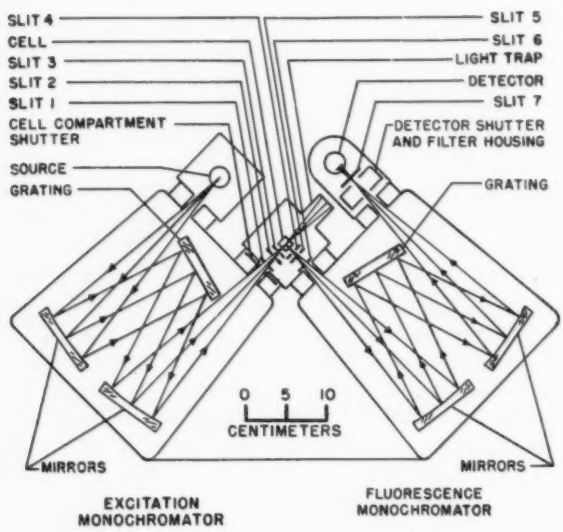

Fig. 1. Optical diagram.

Table I. Slit Arrangements (See Fig. 2 for placement)

Slit number:	1	2	3	4	5	6	7
Arrangement number:	Width (mm)						
1	0.794	0.397	3.175	3.175	0.397	0.794	0.397
2	1.588	0.794	3.175	3.175	0.794	1.588	0.794
3	3.175	1.588	3.175	3.175	1.588	3.175	1.588
4	4.762	3.175	4.762	4.762	3.175	4.762	3.175
5	None	4.762	None	None	4.762	None	4.762

Optical Unit

Monochromators

Figure 1 is a diagram of the optical system. The axes of the four spherical mirrors and the normals to both plane gratings are coplanar. The excitation monochromator focuses a monochromatic image of the xenon arc in the center of the cell. Fluorescent light from the sample is similarly monochromated and imaged on the slit in front of the detector. The plane reflectance gratings have 600 grooves/mm, 52 × 52 mm ruled area and first order blaze at 300 mμ in the excitation and 500 mμ in the fluorescence monochromator. All mirrors have a focal length of 250 mm, giving an equivalent* f/number of ~4.3 for each monochromator.

Source

Osram† XBO-162 xenon arc lamps were used in all measurements.

Slits

Seven slits are used to define the light in the vicinity of the cell and photomultiplier tube. Table I gives various arrangements which provide approximately equal resolving power for excitation and fluorescence spectra. In most of these studies one of these slit arrangements was used. Slits 1 through 6 are 4.8 mm high and the photomultiplier slit 7 is 16 mm high.

* The entire square area of both gratings is illuminated.

† Osram Gesellschaft mit beschränkter Haftung, Munich 2, Germany; available in U.S.A. from Macbeth Sales Corporation, P. O. Box 950, Newburgh, New York.

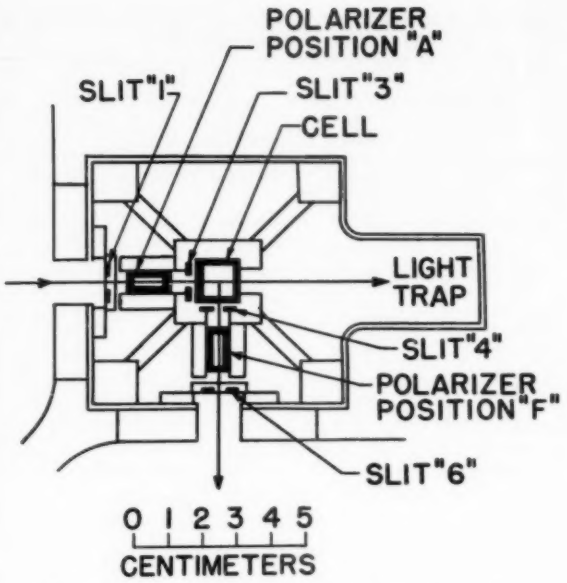

Fig. 2. Location of polarizers in cell compartment.

Cells

Fused quartz cells, 12.5 × 12.5 mm square outside, 10 × 10 mm square inside and 48 mm high were used in all measurements. Since the excitation beam is approximately 4 mm high in the cell, only 1 ml of sample is required in the cell in order to prevent radical disturbance of the excitation light by the meniscus of the liquid sample. However, the total cell volume is approximately 5 ml so 2 to 3 ml samples were usually used.

Polarizers

Table II gives the position and placement of polarizers and filters used. Figure 2 shows the geometry in the cell vicinity when using polarizers. They were Glan–Thompson prisms,* short form, having 17° aperture, 5.5 mm square in cross section and 16 mm long, permitting horizontal or vertical polarization of both excitation and fluorescence radiation. Each was mounted in a tube rotatable through 90° and attached to the cell holder after removal of appropriate slit and slit holder. We have designated E as the polarizer orientation for passing radiation whose electric vector is vertical and B the orientation for passing radiation whose electric vector is horizontal. The letters E and B are marked on the prism mount. Correspondingly, we use the symbols E_A and E_F to designate that the prisms are orientated to pass radiation whose electric vector is vertical at the exit of the excitation monochromator and at the entrance to the fluorescence monochromator, respectively. Similarly, the symbol B_F is used to specify that the prism in the fluorescence monochromator is orientated to pass radiation whose electric vector is horizontal. Figure 3 shows the unmounted polarizer assembly.

* Fabricated by Crystal Optics Co., 4318 N. Lincoln Avenue, Chicago 18, Illinois.

Table II. Position and Placement of Polarizers and Filters

Position	Placement: Polarizer (see Fig. 2)	Placement: Filter (see Fig. 4)
A	Between slit 1 and 3, repiacing slit 2	Between slit 1 and 2
F	Between slit 4 and 6, replacing slit 5	Between slit 5 and 6
P	Not used	In front of slit 7 (located in the filter housing shown in Fig. 1)

The addition of polarizers to the Aminco–Bowman Spectrophotofluorometer for fluorescence polarization measurements was suggested to one of us (H. K. H.) by Sidney F. Velick,* and they were employed by him in measurements of fluorescence polarization of complex molecules of biological importance.[7,8]

The polarization of fluorescent light emitted at right angles to the direction of excitation is defined by the intensity of two linearly polarized components, one,

* Department of Biological Chemistry, Washington University, School of Medicine, St. Louis, Missouri.

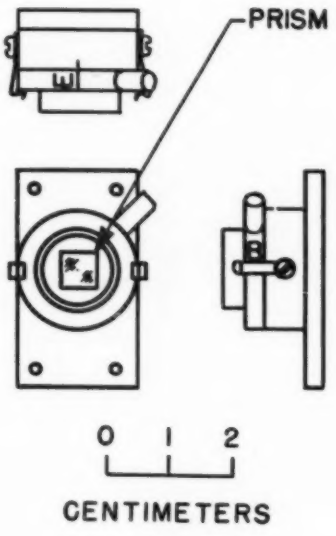

Fig. 3. Polarizer assembly.

$I_\perp$, vibrating in the direction of propagation of exciting light and the other, $I_\parallel$, vibrating normally to the plane determined by the direction of excitation and observation. The polarization of the fluorescence is then

$$p = \frac{I_\parallel - I_\perp}{I_\parallel + I_\perp}. \tag{1}$$

Rank[9] has pointed out that in order to determine $I_\parallel$ and $I_\perp$ it is necessary to measure the transmission, T, of the fluorescence monochromator for natural unpolarized radiation having the same wavelength as the fluorescence radiation, since the fluorescence monochromator does not transmit the two kinds of plane polarized light with equal facility. The transmission, T, of the fluorescence monochromator for natural unpolarized light is

$$T = \frac{S_0}{P_0} \text{ [unpolarized]} \tag{2}$$

where S_0 is the intensity measured for the parallel ($\parallel$) component, the electric vector vibrating in the vertical plane (polarizer set with orientation E_F), and P_0, the intensity measured for the perpendicular ($\perp$) component, or electric vector vibrating in the horizontal plane (polarizer set with orientation B_F). The ratio $I_\parallel/I_\perp$ for the fluorescence radiation is

$$\frac{I_\parallel}{I_\perp} = \frac{R_E}{TR_B} \tag{3}$$

where R_E is the photometer (or oscillograph or recorder) reading obtained when the polarizer is set with orientation E_F (vertical) and R_B is the photometer reading obtained when the polarizer is set with orientation B_F (horizontal). The fluorescence polarization, p, becomes

$$p = \frac{R_E - TR_B}{R_E + TR_B} \tag{4}$$

The maximum value of p is $^1/_2$ for polarized exciting radiation and $^1/_3$ for natural unpolarized exciting radiation.

Since the highly accurate fluorescence polarization measurements reported by Weber[10] serve as a basis of comparison with other methods, a comparison was made with a few of these results in order to determine whether or not any gross errors were involved in the method of measuring fluorescence polarization used here. Table III gives the polarization of fluorescence of some xanthydrol derivatives in glycerol and those reported by Weber[10] at approximately the same temperature and concentration. No attempt was made to analyze the systematic errors (resulting from faulty setting of parts, nonnegligible size of the source and stray light), since a photometer having high accuracy was not used here and since the stability of the light source was no better than 1%. The standard deviation from the mean of several measurements was ~1%

Table III. Polarization of Fluorescence of some Xanthydro Derivatives in Glycerol at 296°K[a]

Excitation wavelength (mμ)	Polarization, p			
	Rhodamine B	Rhodamine 6G	Eosin	Fluorescein
366	−0.091	−0.079	+0.278	+0.424
366	−0.0635[b]	−0.071[b]	—	—
436	0	+0.385	+0.417	+0.446
436	−0.0244[b]	+0.385[b]	—	+0.432[a]
546	+0.441	+0.439	+0.468	—
546	+0.420[b]	+0.430[b]	+0.444[b]	—

[a] Concentrations were 3.6×10^{-6} M for rhodamine B, 3.4×10^{-6} M for rhodamine 6G, 4.5×10^{-6} M for eosin, and 5.0×10^{-6} M for fluorescein. An XBO-162 lamp, 10 × 10 mm cell, and 1P21 photomultiplier tube were used. The slit arrangement was 1—4 mm, 2—polarizer with E_A, 3—1 mm, 4—1 mm, 5—polarizer with E_F and B_F alternately, 6—4 mm, and 7—1 mm.

[b] Reported by Weber[10] at 18°C with concentrations of 3.63×10^{-6} M for rhodamine B, 3.4×10^{-6} M for rhodamine 6G, 2.6×10^{-6} M for eosin, and 4.94×10^{-6} M for fluorescein.

and the agreement of the present data with those of Weber was within ±0.03, as shown in Table III. By the use of a method similar to that employed by Rank *et al.*,[11] the transmission, T, of the fluorescence monochromator was measured at the wavelengths of fluorescence maxima of the xanthydrol derivatives and was found to be 0.760 for 578 mμ (rhodamine B), 0.779 for 558 mμ (rhodamine 6G), 0.791 for 546 mμ (eosin), and 0.852 for 513 mμ (fluorescein). These values of T were used to compute the polarization from Eq. (4).

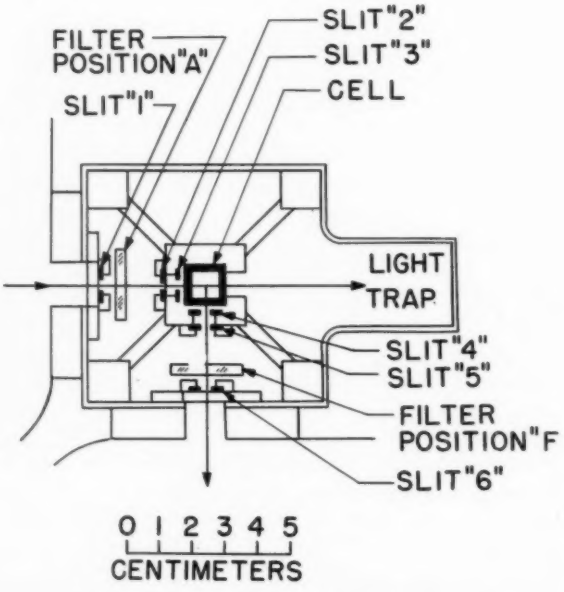

Fig. 4. Location of filters in cell compartment.

Stray light (emission from the solvent alone) was subtracted from the fluorescence intensity of the sample plus solvent. Four successive photometer readings were made, one each for the xanthydrol derivative in glycerol with E_F and B_F followed by one each for glycerol only with E_F and B_F. For maximum accuracy the fluorescence intensity for E_F or B_F, whichever was greater, was set at the maximum photometer scale reading (100) and then the lesser fluorescent intensity for either E_F or B_F was read from the scale to an accuracy of ~1%.

Yagi *et al.*[12] discuss polarization of fluorescence as influenced by wavelength of the exciting light, viscosity of the solvent, temperature, concentration, lifetime in the excited state, and isotropy of the system.

Filters

Figure 4 shows the geometry in the cell vicinity when interference or optical glass filters were used. In some cases a 5 cm square filter was cut to approximately 3.2 cm square in order to fit it into positions "A" and "F" within the cell compartment. In other cases the cell compartment mounting plates were modified to accept 5 cm × 5 cm filters which were then located in front of slits 1 and 6 outside the cell compartment. The use of one or the other of these two locations of the filters had no significant effect on the results. Position "P" (in front of slit 7) accommodates 5 cm square filters, but this position may not be satisfactory if the filter fluoresces.

Electronic Unit

Photometer

Sensitivity is controlled by a meter-multiplier switch and sensitivity potentiometer. Gross sensitivity adjustments are made with a meter-multiplier switch which reduces oscillograph and recorder output signals, together with meter readings, in fixed steps of $^1/_3$, $^1/_{10}$, $^1/_{30}$, $^1/_{100}$, $^1/_{300}$, $^1/_{1000}$. The meter-multiplier (MM) positions are numbered 1, 0.3, 0.1, 0.03, 0.01, 0.003, and 0.001 in order of increasing sensitivity. Fine sensitivity adjustments are made with a sensitivity potentiometer which continuously adjusts recorder output signal and meter readings over a range of 3.5 to 1. The angular position of the sensitivity potentiometer wiper is indicated by a graduated scale numbered from 0 to 50 in order of increasing sensitivity. A dark-current control cancels photomultiplier-tube dark current by application of an equal current of opposite polarity to the anode current. With all other instrumental parameters constant, the relative fluorescence intensity is the product of the meter multiplier setting and the meter deflection (or recorder or oscillograph deflection).

For display of some spectra, the photometer was not used; instead, a 975-volt battery pack was used to supply the photomultiplier tube voltage and the anode was connected directly to the oscilloscope *Y*-axis amplifier without intermediate amplification.

Detectors

RCA type 1P21 and 1P28 photomultiplier tubes were used having S-4 and S-5 response respectively.

Lamp Power Supplies

The Osram XBO-162 Lamp was powered by a dc supply* furnishing 7.5 amp at 19.8 volts from a constant voltage transformer and its associated capacitor supplying a step-down transformer, the output of which is rectified by diodes.

Recording Units

An E-I† Model 101 X-Y recorder and a DuMont‡ Type 304A Oscillograph were used to obtain permanent records of spectra. The recorder pen was slightly modified to accept India ink so that the spectra could be obtained on linen suitable for publication after the addition of letters, numbers, and other descriptive information. The oscillograph was modified by adding an etched Plexiglas grid with wavelength and intensity graduations to facilitate photography. Figure 5 shows the 35 mm single lens reflex camera mounted on a light-proof tube attached to a hinged device which swings into position over the oscillograph face. In preparation of slides or prints for publication, separate prints of the 35 mm film are mounted on heavy cardboard, labeled, and rephotographed. An intensity modulator, similar to that described by Kemp,[13] was used to increase the oscillograph trace intensity in proportion to its rate of vertical travel which insures adequate exposure of film when the trace moves rapidly (usually during the trace of a scatter peak). Gross *Y*-axis sensitivity adjustments are made with a multiplier switch (dc) which increases the deflection in fixed steps of ten. The positions are labeled 100, 10, 1, and 0.1 in order of increasing sensitivity in volts full scale. Fine *Y*-axis sensitivity adjustments are made with a multiplier potentiometer which continuously adjusts the sensitivity over one decade. The angular position of the multiplier potentiometer wiper is indicated by a graduated scale number from 10 to 1 in order of increasing sensitivity.

---

* Designed and constructed for The American Instrument Company Inc. by Sola Electric Company, Busse Road at Lunt, Elk Grove, Illinois.

† Electro Instruments, Inc., 3540 Aero Court, San Diego, California.

‡ Allen B. DuMont Laboratories, Inc., 760 Bloomfield Avenue, Clifton, New Jersey.

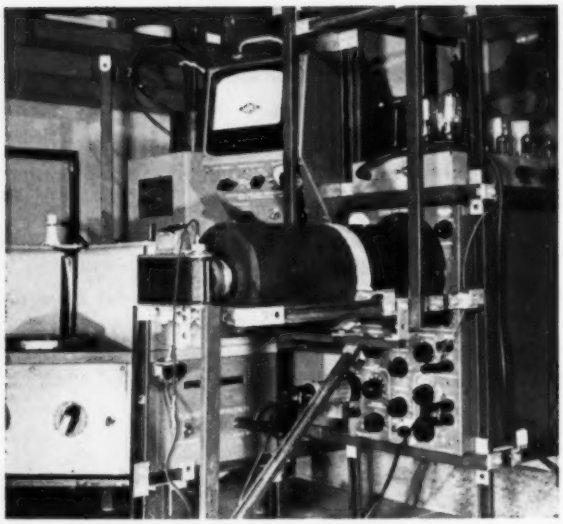

Fig. 5. Camera arrangement for photographing spectra on the oscillograph. The camera is an inexpensive single lens reflex type and is attached to the oscillograph with a light-tight cardboard tube. The camera support is attached to the oscillograph with hinges to facilitate rapid positioning of the unit when a photograph record of the observed fluorescence spectrum is desired.

Reagents

The kynurenic acid[14] and xanthurenic acid[15] were prepared as previously described. The quinine sulfate, deuterium oxide, other reagents, and the solvents were of the best available commercial grade, but were not further purified.

Scattering

Identification

In the practice of spectrofluorimetry, the proper identification of scattering avoids its confusion with excitation and fluorescence peaks. At high concentrations, the interference is slight since fluorescence intensity is usually many times greater than the intensity of the scattered radiation. At low concentrations the intensities of the scattered and fluorescence radiation are nearly equal and it may be difficult to distinguish one from the other if they have closely resembling peak height and bandwidth. At very low concentrations, scattered radiation and impurity fluorescence of the compound under examination must usually be determined by comparison with the spectra obtained from the blank.

To illustrate clearly the appearance of radiation in the second order of diffraction for both monochromators, quinine sulfate was excited at 310 mμ and at 620 mμ (Fig. 6). It is evident by inspection of the two spectra shown in Fig. 6 that when the excitation monochromator is set at 620 mμ in the first order of diffraction the 310 mμ light, also present in the second order of diffraction, (1) excites fluorescence (maximum intensity at 450 mμ), (2) appears as scattered radiation (maximum intensity at 310 mμ), (3) produces Raman scattering (maximum intensity at 350 mμ). In addition, when the excitation monochromator is set at 620 mμ, this wavelength of scattered radiation appears in the fluorescence spectrum as a minor peak due to first order diffraction of 620 mμ light and also due to second order diffraction of 310 mμ radiation.

When the excitation monochromator is set at 310 mμ, the fluorescence spectrum shown in Fig. 6 contains (1) scattered radiation peaks at 310 mμ in the first order of diffraction and at 620 mμ in the second order of diffraction, (2) Raman scattering peaks at 350 mμ in the first order of diffraction and at 700 mμ (barely perceptible) in the second order of diffraction, and (3) fluorescence (maximum intensity at 450 mμ).

The strong Stokes Raman band of water is attributed to the symmetrical vibration ν_1, producing a shift of 3600 cm^{-1}. Assuming polymeric association, the shift would be reduced to ~3300 cm^{-1} for OH stretch of intermolecular hydrogen bonds. The exact shift is of less importance for this investigation than its recognition so that it will not be confused with fluorescence or scattering produced by stray light. The scattered radiation appearing at the same wavelength as excitation (and at twice the excitation wavelength) is due almost entirely to a combination of Rayleigh scattering from water and Tyndall scattering from residual foreign particles such as dust, ground glass, or other dispersed solids which are virtually impossible to eliminate completely.

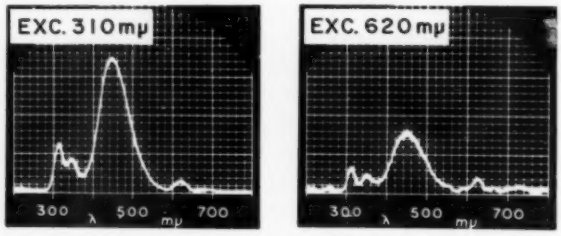

Fig. 6. Fluorescence spectra of quinine sulfate (0.0375 μg/ml) in 0.1 *N* sulfuric acid at room temperature. The 1P21 photomultiplier tube was operated with a 975 volt battery and slit arrangement No. 4 (Table I) was used. To obtain the curve with the excitation monochromator set at 310 mμ the oscillograph *Y* axis was set at 1.0 dc and the multiplier at 4. For the fluorescence spectrum with the excitation monochromator set at 620 mμ the oscillograph *Y* axis was set at 0.1 dc and the multiplier at 1.0. It should be noted that the curves have identical characteristics with peaks representing from left to right, Rayleigh and Tyndall scattering, Raman scattering, fluorescence, and scattered radiation in the second order of diffraction.

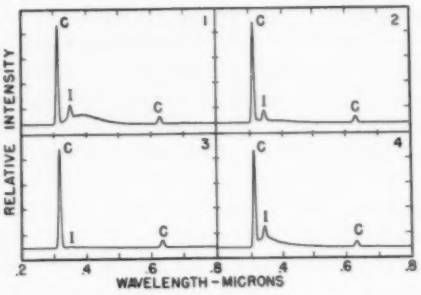

Fig. 7. Scattering from distilled water —1, ethyl alcohol —2, chloroform —3, and cyclohexane —4 at room temperature. The peaks marked (C) are due to Rayleigh and Tyndall scattering and those marked (I) are due to Raman scattering. A 1P21 photomultiplier tube and an XBO-162 lamp were used with the excitation wavelength set at 310 mμ. Slit arrangement was 1—4 mm, 2—1 mm, 3—2 mm, 4—2 mm, 5—1 mm, 6—4 mm, and 7—1 mm. The meter multiplier and sensitivity settings were respectively 0.003 and 22 for water, 0.01 and 43 for ethyl alcohol, 0.01 and 19 for chloroform, and 0.01 and 43 for cyclohexane.

Figure 7 shows scattering from distilled water, ethyl alcohol, chloroform, and cyclohexane when excited at 310 mμ. No special effort was made to purify the solvents; therefore, some impurity fluorescence is evident in all except chloroform. The minor peaks at wavelengths greater than 600 mμ appear in the second order of diffraction as explained above. The position of the Raman bands (I) is in agreement with observations by Parker[6] using a high sensitivity instrument in which the resolving power permitted more accurate measurement of Raman shifts than herein reported. The present attempts to observe Raman bands from carbon tetrachloride as reported by Parker[6] were unsuccessful due to insufficient sensitivity. The largest observed Raman shift for carbon tetrachloride[16] is ~1539 cm^{-1} and is very weak in intensity. Other very strong, strong, and medium intensity Raman shifts occur at lower frequencies; however, they appear too close to the scattering of the exciting light to be resolved by the equipment used in this study. The strong Raman band observed from ethyl alcohol is attributed to several unresolved lines due to C—H vibration at ~2900 cm^{-1} and an OH band at 3400 cm^{-1}, the former contributing mainly to the observed intensity. The strong Raman band of chloroform is without doubt due to a C—H stretching vibration with assignment ν_1^{CH} (a_1). Since cyclohexane probably has the "chair" form of a point group D_{3d}, the observed Raman band (polarized) is probably due to a C—H stretching vibration with assignment $\nu_1^{CH}(A_{1g})$. Figure 8 compares the Raman scatter from H_2O and D_2O in substance and in an equal mixture of the two. The observed shifts are in agreement with those expected on the basis of the isotope relations.

Polarization

The intensity of scattered radiation observed will depend largely on the exciting frequency, the spectral response of the receiver, and the cleanliness of the solutions. If polarizers are used, the scattered radiation usually will be much less intense when observed with the polarizer oriented to pass radiation with electric vector horizontal (B_F) in the fluorescence monochromator because even in the most anisotropic base the degree of polarization for Rayleigh scatter, ρ, will have a maximum value of $^1/_2$ for natural (unpolarized) incident light and $^1/_3$ for linearly polarized incident light. If the scattering molecule is isotropic, the Rayleigh scattering observed at right angles to the incident beam will be completely polarized in the plane at right angles to the incident beam, irrespective of whether the incident light is polarized or not.[16] If the Z axis is taken in the direction of propagation of the incident light and the direction of observation is perpendicular to the Z axis, we have

$$\rho_n = \frac{I_\perp}{I_\parallel} = \frac{TR_B}{R_E} \tag{5}$$

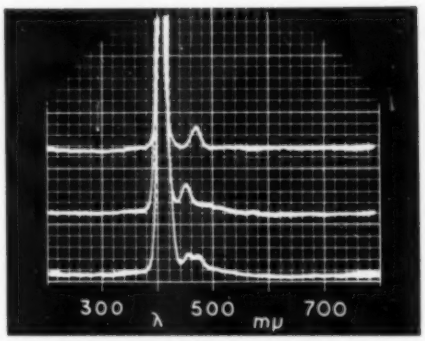

Fig. 8. Rayleigh and Tyndall scattering and Raman scattering from water (upper curve), deuterium oxide (middle curve), and an equal mixture of the two (lower curve) at room temperature. The excitation wavelength was 410 mμ (24,390 cm^{-1}). The Raman scattering due to the Stokes Raman band of water in polymeric association was expected at 24,390 cm^{-1} − 3300 cm^{-1}, or 21,090 cm^{-1}, and the observed values were 21,322 cm^{-1} (upper curve) and 21,276 cm^{-1} (lower curve). For deuterium oxide, the Raman scattering for the Stokes Raman frequency was expected at 24,390 cm^{-1} − 2300 cm^{-1}, or 22,090 cm^{-1}, and the observed values were 22,173 cm^{-1} (middle curve) and 22,075 cm^{-1} (lower curve). As has been emphasized in the text, the exact frequency of the Stokes Raman band cannot be accurately measured under these conditions, but the values observed may make it possible to identify quickly extraneous peaks in fluorescence spectra as those likely to be this type of scattering and not additional fluorescence peaks. These records were obtained using the XBO-162 Xenon lamp and the 1P21 photomultiplier tube with a 975 volt battery. Slit arrangement No. 3 (Table I) was used with the oscillograph Y-axis set at 0.1 dc and the multiplier set at 1.0.

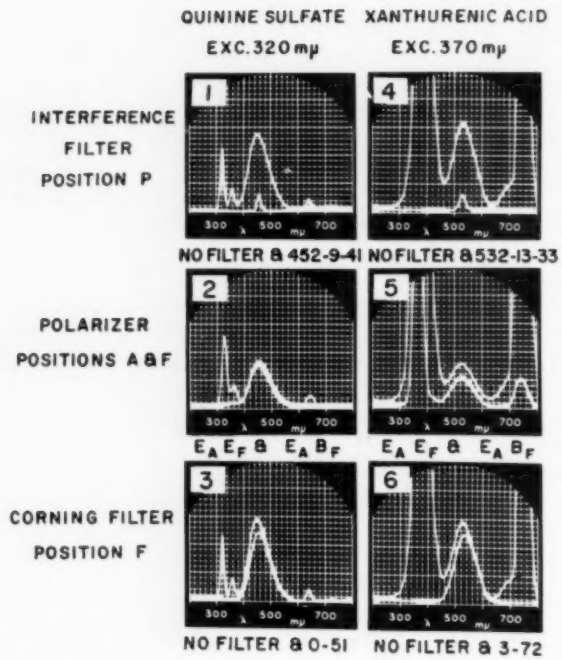

Fig. 9. The effects of certain filters on the fluorescence spectra of quinine sulfate (0.0375 μg/ml) in 0.1 *N* sulfuric acid and xanthurenic acid (0.165 μg/ml) in 9.5 *N* sodium hydroxide. Each of the six records has one curve which was photographed with the filter and one curve which was recorded without the filter. When the scattering is small (quinine sulfate) it is readily removed by any of the filters used. When the scattering is very large (xanthurenic acid) it is not possible to remove it adequately with the polarizers, but the Corning filter No. 3-72 is very satisfactory. The relatively low transmission of the interference filters renders their use unsatisfactory. These records were made with the 1P21 photomultiplier tube with a 975 volt battery. The oscillograph *Y* axis was set at 0.1 dc and the multiplier was set at 6 for quinine sulfate and at 10 for xanthurenic acid. Slit arrangement No. 3 (Table I) was used for quinine sulfate and No. 4 was used for xanthurenic acid.

where the degree o depolarization for natural (unpolarized) incident light, ρ_n, is defined as the ratio of the intensity of the scattered light polarized perpendicular to the *X*-*Y* plane, $I_\perp$, to that polarized parallel to this plane, $I_\parallel$, and R_E and R_B have the same meaning as when applied to fluorescence polarization (see Eq. (3) above); also

$$\rho_l = \frac{\rho_n}{2 - \rho_n} = \frac{TR_B}{2R_E - TR_B} \qquad (6)$$

where the degree of depolarization for linearly polarized light (at 90° to the scattered beam) is ρ_l. The maximum degree of depolarization for Rayleigh scattering is $\rho_n^{(max)} = {}^1/_2$ and consequently $\rho_l^{(max)} = {}^1/_3$. The minimum value of ρ_n and ρ_l is zero. The Rayleigh scattering of most molecules will have a smaller degree of depolarization than these maximum values.

The maximum degree of depolarization for Raman scattering is $\rho_n^{(max)} = {}^6/_7$ and consequently $\rho_l^{(max)} = {}^3/_4$. For brevity, if a Raman line shows this state of depolarization (maximum), it is said to be depolarized, whereas, if the degree of depolarization is smaller, it is said to be polarized. Since only Raman lines corresponding to totally symmetric vibrations can be polarized and since Raman lines of nonsymmetrical vibrations are expected to be weak, it was concluded that all Raman lines observed here will be polarized and therefore result from totally symmetric vibrations. The previous assignments for water, ethyl alcohol, chloroform, and cyclohexane are in agreement with this conclusion, and the Raman lines observed for these molecules were polarized. Table IV gives the depolarization factors of Raman and Rayleigh scattering from these molecules.

Reduction of Intensity

The polarization of scattering was utilized to reduce the intensity and in addition colored glass and interference filters were used for this purpose. Figure 9 compares some results obtained by these three methods. In each of the six spectra, the fluorescence spectrum was recorded with (lower curve) and without (upper curve) filters or polarizers. All scattered radiation was removed by an interference filter placed at position P (in front of slit 7) in the case of quinine sulfate (1) and xanthurenic acid (4) with a large reduction in observed fluorescence. Colored glass filters placed at position F also removed all of the scattered radiation with little effect on observed fluorescence (spectra 3 and 6). Polarizers placed at positions A and F removed practically all of the scattered radiation in the case of quinine sulfate (spectrum 2) with practically no effect on fluorescence, whereas the intensity of scattered radiation was too great to determine accurately the degree of reduction in the case of xanthurenic acid (spectrum 5). The high intensity of scattered radiation appearing at the same wavelength as excitation observed in spectra

Table IV. Depolarization Factors of Scattering from Water, Ethyl Alcohol, Chloroform, and Cyclohexane[a]

Substance	Depolarization factor, ρ_n	
	Rayleigh and Tyndall	Raman
Water	0.053	0.23
Ethyl alcohol	0.060	0.23
Chloroform	0.18	0.28
Cyclohexane	0.044	0.31

[a] The measurements were made at 296°K using a 10 × 10 mm cell, XBO-162 lamp, and a 1P21 photomultiplier tube. The excitation wavelength was set at 345 mμ except the chloroform where it was set at 300 mμ. The slit arrangement was 1—none, 2—1 mm, 3—2 mm, 4—2 mm, 5—polarizer with E_F and B_F alternately, 6—1 mm, and 7—1 mm. The accuracy is no better than 25%.

4, 5, and 6 results from particles of sodium carbonate formed from carbon dioxide (picked up from atmospheric air) reacting with the sodium hydroxide. The choice of colored glass cutoff filters for most effective reduction of the intensity of scattered radiation will depend upon the excitation and emission wavelength, and it is usually possible to choose one which cuts off in the region between the longest wavelength of scattering and shortest emission wavelength, as was done in the cases of spectra 3 and 6. If the molecule has many excitation and emission peaks, for example, anthracene, the shortest excitation wavelength (in this case ~250 mμ) usually will cause least interference due to scattering in the emission spectrum since the instrumental response will usually be low at short wavelengths, say below 300 mμ where there is rapid decrease in S-4 and S-5 response. Also, the longest emission wavelength usually will cause least interference due to scattering in the excitation spectrum due to the rapid decrease in S-4 and S-5 response at wavelengths of ~500 to 600 mμ.

The choice of interference filters for most effective reduction of scattering in the fluorescence spectrum depends mainly on the wavelength of maximum fluorescence. In the case of quinine sulfate (spectrum 1 of Fig. 9) the filter had a maximum transmission at 452 mμ (nearly the same wavelength as fluorescence maximum), and at a half bandwidth of 9 mμ it transmitted 41% of the light at this wavelength. The use of interference filters has the obvious disadvantage in eliminating other fluorescence peaks close to the maximum if the complete fluorescence spectrum is desired.

Raman scattering is less prominent (although observable) in excitation spectra than in fluorescence spectra because the detector response is usually chosen to be maximum at the wavelength of maximum fluorescence, in which case the scattering appearing when both monochromators are set at the same wavelength is usually much more intense than the Raman scattering intensity.

Table V. Stray Light (%) from Excitation Monochromator with Slit Arrangement No. 2 and XBO-162 Lamp

Excitation wavelength (mμ)	Wavelength (mμ)							
	300	350	400	450	500	550	600	650
210	0.15	1.0	0.3	0.2	1.5	1.0	1.3	0
220	0.07	0.3	0.07	0.09	0.4	0.15	0.05	0
230	0	0.08	0.02	—	0.1	0.03	0	0
240	0.02	0.03	0.02	0.02	0.01	0.01	0.01	0
250	0.05	0.03	0.02	0.02	0.01	0.01	0.01	0
260	0.08	0.03	0.02	0.008	0.02	0.009	0	0
270	0.08	0.02	0.01	0.01	0.01	—	0.02	0.008
280	0.1	0.05	0.01	0.02	0.007	—	0.03	0.05
290	—	0.03	0.007	0.007	0.005	0.007	—	0
350	0	—	0.02	0.01	0.005	0.01	0	0
450	0	0	0.02	—	0.02	0	0	0

Stray Light

Measurement by Diffuse Reflectance

Extraneous light from the excitation monochromator will appear as scattered radiation in the fluorescence spectrum when the instrumental sensitivity is high. The relative intensity of this stray light compared with observed fluorescence will depend largely on the number of scattering particles present and the wavelengths and intensity of fluorescence. The intensity of stray light compared with the intensity at peak excitation wavelength was measured using a ground glass diffusor placed in the cell compartment oriented at 45° to both excitation output and fluorescence input axes of the monochromators. Excitation wavelengths were set at a fixed value and the fluorescence monochromator was scanned. A 1P28 photomultiplier tube was used and the correction factors[17] determined by White *et al.* were applied in regions where applicable. In other regions, the S-5 response curve was used as the basis of instrumental response and in these regions the measurements may be in error by ~50%. The results are given in Table V. The entries not appearing in the table were omitted due to the fact that the measured intensities, when excitation and fluorescence wavelengths were nearly equal, were usually orders of magnitude greater than the stray light intensities, giving incorrect results at wavelengths where the bandwidths overlapped. The entries with "zero" indicated that the intensity was too small to be measured accurately by this method (usually less than $^1/_{10}$ that of the lowest value observed at any particular excitation wavelength). Since the monochromators are optically identical except for the grating blaze wavelength, the stray light in the fluorescence monochromator is expected to be of approximately the same intensity as that observed for the excitation monochromator.

Detection by Highly Scattering Media

The scattered radiation from stray light can be easily detected with Ludox* in the cell by scanning the fluorescence monochromator at various excitation wavelengths. In addition to scattered radiation from stray light, some Raman scattering will be present at excitation wavelengths of 240 through 290 mμ when using 1P21 or 1P28 photomultiplier tubes and the most favorable condition for its observation was at an excitation wavelength of 260 mμ with Raman scatter appearing at ~290 mμ. Second order effects can also be detected in this manner.

* A finely divided colloidal dispersion of silica in water which possesses high scattering, obeys the fourth-power law in the visible region, and shows no dissymmetry of scattering within experimental error. Manufactured by E. I. du Pont de Nemours and Co., Grasselli Chemicals Department, Wilmington, Delaware.

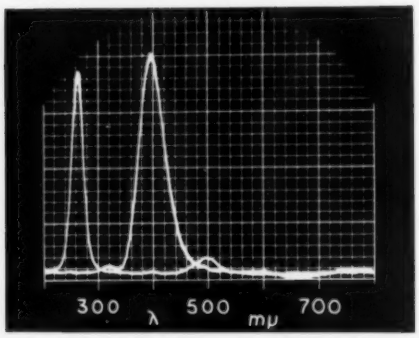

Fig. 10. Excitation spectrum (peaks at 263, 395, and 500 mμ) and emission spectrum (peaks at 320 and 395 mμ) of fused quartz at room temperature. The records were made with the XBO-162 lamp and the 1P21 photomultiplier tube with a 975 volt battery. Slit arrangement No. 3 was used with the oscillograph Y-axis set at 0.1 and the multiplier at 4.2. The excitation wavelength was set at 250 mμ for the fluorescence spectrum and the fluorescence wavelength was set at 395 mμ for the excitation spectrum.

The scattering power of Ludox in water was determined at concentrations ranging from 10^{-7}% to 100% (undiluted) and it was found that undiluted (100%) Ludox has ~3200 times greater scattering power than distilled H_2O. The measurements were made using an XBO-162 lamp, 1P21, slit arrangement No. 3 with excitation and fluorescence monochromators set at 300 mμ. Table VI lists the relative intensity of scattering observed. The difference between the intensity observed from very low Ludox concentrations and from water is attributed to pickup of scattering particles during dilution. The higher intensity at 10% than at 100% is due to absorption by the sample, thereby reducing the amount of scattering seen by the fluorescence monochromator since the most intense scattering appears in the area of greatest absorption and this area is not seen by the fluorescence monochromator.

Table VI. Relative Intensity of Scattered Radiation from Ludox in Distilled Water

Concentration (%)	Relative scattering intensity
100[a]	58
10	67
1	16
0.1	1.9
0.01	0.26
0.001	0.069
0.0001	0.056
0.00001	0.047
0.000001	0.049
0.0000001	0.045
0 (water only)	0.018

[a] Undiluted.

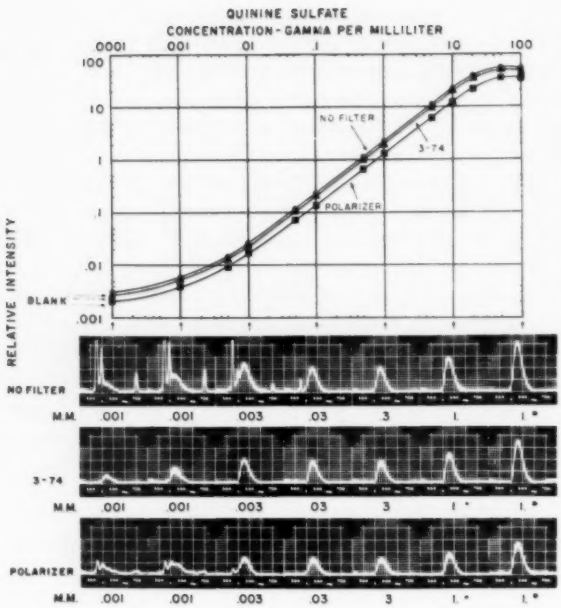

Fig. 11. Work curve and fluorescence spectra of quinine sulfate in 0.1 N sulfuric acid at room temperature. The concentration of quinine sulfate for each spectrum is indicated by the vertical arrows. The work curves and fluorescence spectra were obtained under three conditions: (1) with no filters; (2) with a Corning 3-74 glass filter in position "F" (see Fig. 4); and (3) with the polarizing filters set with the electric vector vertical at position A and the electric vector horizontal at position F (see Fig. 2). The three horizontal arrows at the left of the work curves indicate the relative intensity of the blanks for the three curves. The fluorescence spectra reveal that both Raman and Rayleigh or Tyndall scattering were present at the lowest concentrations of quinine sulfate. Raman scattering should be suspected as the cause of the second peak of these fluorescence spectra because it occurs at 25,300 cm^{-1} (395 mμ) which is shifted 3300 cm^{-1} from the excitation (28,600 cm^{-1} or 350 mμ), and thus corresponds to the strong Stokes Raman band for —OH stretch of intermolecular hydrogen bonds in water in polymeric association. The removal of this peak by the polarizing filters is further evidence that this peak represents Raman scattering. The work curve was obtained with the excitation wavelength set at 350 mμ and the fluorescence wavelength set at 450 mμ The meter multiplier settings were as shown below the fluorescence spectra. Other instrumental parameters were: lamp, XBO-162; photomultiplier tube, 1P21; slit arrangement No. 3; sensitivity, minimum; oscillograph Y axis 1 dc; oscillograph multiplier 1.0 except for a concentration of 10 μg/ml where it was set at 2 and for a concentration of 100 μg/ml where it was set at 4. (See Figs. 6, 8, 9, 10, for λ and mμ numbering.)

Emission from Quartz

A possible source of unwanted light is due to the emission from quartz used to fabricate cells. This weak violet emission usually can be observed visually from the side of the cell facing the excitation monochromator when it is set at ~250 mμ. Unsuccessful attempts were made to detect this emission under usual

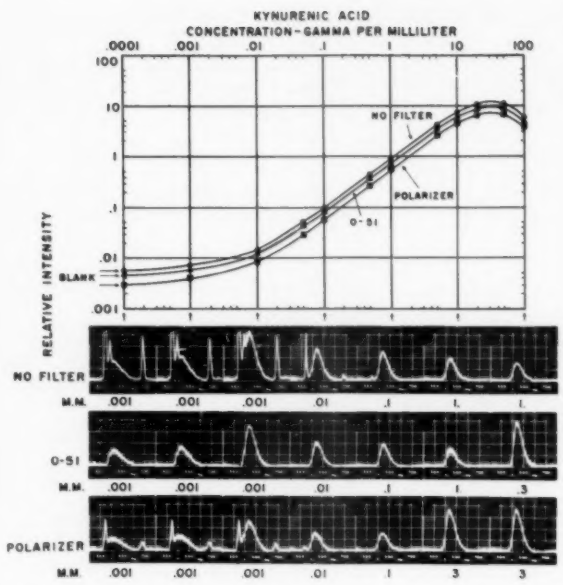

Fig. 12. Work curve and fluorescence spectra of kynurenic acid in 14.4 N sulfuric acid at room temperature. The concentration of kynurenic acid for each spectrum is indicated by the vertical arrows. The work curves and fluorescence spectra were obtained under three conditions: (1) with no filter; (2) with a Corning 0-51 glass filter in position F; and (3) with the polarizing filters set with the electric vector vertical at position A and the electric vector horizontal at position F. The horizontal arrows at the left of the work curves indicate the relative intensity of the blanks for the three curves. The excitation wavelength was set at 340 mμ and the fluorescence wavelength was set at 435 mμ for the work curve. The meter multiplier settings were as shown below the fluorescence spectra. Other instrumental parameters were: lamp, XBO-162; photomultiplier tube, 1P21; slit arrangement No. 3; sensitivity, minimum; oscillograph Y axis 1 dc; oscillograph multiplier 1.0. (See Figs. 6, 8, 9, and 10 for λ and mμ numbering.)

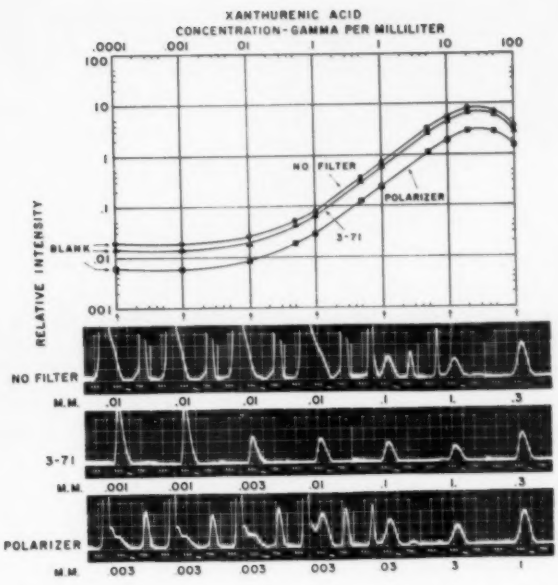

Fig. 13. Work curve and fluorescence spectra of xanthurenic acid in 9.5 N sodium hydroxide at room temperature. The concentration of xanthurenic acid for each spectrum is indicated by the vertical arrows. The work curves and fluorescence spectra were obtained under three conditions: (1) with no filter; (2) with a Corning 3-71 glass filter in position F; and (3) with the polarizing filters set with the electric vector vertical at position A and the electric vector horizontal at position F. The horizontal arrows at the left of the work curves indicate the relative intensity of the blanks for the three curves. The excitation wavelength was set at 370 mμ and the fluorescence wavelength was set at 530 mμ for the work curve. The meter multiplier settings were as shown below the fluorescence spectra. Other instrumental parameters were: lamp, XBO-162; photomultiplier tube, 1P21; slit arrangement No. 4; sensitivity, minimum; oscillograph Y axis 1 dc; oscillograph multiplier 1.0. (See Figs. 6, 8, 9, 10 for λ, mμ numbering.)

operation since the baffling in the cell vicinity prevented it from being observed by the fluorescence monochromator. Under unusual conditions (with Ludox in the cell) it was observed as an increase in scattering intensity at ~400 mμ. In order to determine the exact excitation and emission characteristics, rectangular parallelepipeds were fabricated from two grades of fused quartz* and one grade of synthetic silica.† The emission of each was measured and it was found that both grades of fused quartz were excited maximally at ~250 mμ with emission maximum at ~395 mμ and minor emission at ~320 mμ. No detectable difference was found between the two grades either by intensity or wavelength measurements; however, it is likely that a sample of fused quartz of higher purity would give less emission. Figure 10 shows the excitation and emission characteristics. The minor peak at ~500 mμ in the excitation spectrum is due to excitation by the 250 mμ radiation appearing in the second order of diffraction, and the minor peak at ~395 mμ is due to scattered radiation appearing when both monochromators are set at the same wavelength. The synthetic silica exhibited extremely weak emission at ~500 mμ.

Cells were fabricated from both grades of the fused quartz and the one grade of synthetic silica. Only under unusual conditions (Ludox in the cells) was emission from the fused quartz of the cell detectable, and no emission was detected from the synthetic silica cell with Ludox in it. Apparently the emission from Ludox was too low to be detected when undiluted. The synthetic silica cell transmitted more ultraviolet than the

* Fabricated by fusion of crystalline quartz (Optical Grades, Amersil Quartz Division of Engelhard Industries, 100 Chestnut Street, Newark, New Jersey).

† Fabricated by vaporizing a hydrolyzable compound of silicon into a high temperature flame of combustible gas combined with oxygen. U.S. Patent 2,272,342. (UV transmitting grade, fused silica, Corning Glass Works, Corning, New York.)

Table VII. Identification of Peaks of Scattered Radiation Appearing in Spectra of Figs. 11, 12, and 13

		Rayleigh and Tyndall	Raman
Fig. 11 Quinine sulfate in 0.1 *N* sulfuric acid	No filter	350 mμ first order of diffraction, 700 mμ second order of diffraction, at concentrations from 0.0001 to 0.1 gamma/ml	~395 mμ at concentrations from 0.0001 to 0.01 gamma/ml
	3–74 Filter	None	None
	Polarizer	350 mμ first order of diffraction, 700 mμ second order of diffraction, at concentrations from 0.0001 to 0.01 gamma/ml. Intensity greatly reduced	~395 mμ at concentration of 0.0001 and 0.001 gamma/ml. Intensity greatly reduced
Fig. 12 Kynurenic acid in 14.4 *N* sulfuric acid	No filter	340 mμ first order of diffraction, 680 mμ second order of diffraction, at concentrations from 0.0001 to 1 gamma/ml	~380 mμ at concentrations from 0.0001 to 0.1 gamma/ml
	0–51 Filter	None	~380 mμ at concentrations from 0.0001 to 0.01 gamma/ml. Intensity greatly reduced
	Polarizer	340 mμ first order of diffraction, 680 mμ second order of diffraction, at concentrations from 0.0001 to 0.1 gamma/ml. Intensity greatly reduced	~380 mμ at concentrations from 0.0001 to 0.01 gamma/ml. Intensity greatly reduced
Fig. 13 Xanthurenic acid in 9.5 *N* sodium hydroxide	No filter	370 mμ first order of diffraction, 740 mμ second order of diffraction, at concentrations from 0.0001 to 10 gamma/ml	Not resolved
	3–71 Filter	None	Not resolved
	Polarizer	370 mμ first order of diffraction, 740 mμ second order of diffraction, at concentrations from 0.0001 to 10 gamma/ml. Intensity greatly reduced	~420 mμ at concentrations from 0.0001 to 0.1 gamma/ml. Intensity greatly reduced

fused quartz cells; consequently, more fluorescence was observed using them at excitation wavelengths of between 230 and 270 mμ.

Quantitative Assay

The lower limit of concentration detectable in a quantitative assay is limited mainly by fluorescence of impurities in the blank, by scattering of stray light, or by Raman scattering. To demonstrate this, three assays were made using:

1. Quinine sulfate in 0.1 normal sulfuric acid excited at 350 mμ with fluorescence measured at 450 mμ (Fig. 11).

2. Kynurenic acid in 14.4 normal sulfuric acid excited at 340 mμ with fluorescence measured at 435 mμ (Fig. 12).

3. Xanthurenic acid in 9.5 normal sodium hydroxide excited at 370 mμ with fluorescence measured at 530 mμ (Fig. 13).

In all three assays, concentrations of 100 gamma/ml* were serially diluted to a level of 0.0001 gamma/ml and the fluorescence spectra recorded at various concentrations without a filter, with a cutoff filter, and with polarizers to reduce the scatter. At concentrations between 10 and 100 gamma/ml there is an "around the corner effect," due to absorption of excitation light by the sample. With increasing concentration, the fluorescence rises in intensity but retreats toward the illuminated face; consequently, the light collected by slits 4, 5, and 6 (Fig. 4) falls off, since only a fraction is able to pass through them into the fluorescence monochromator. Bowen and Wokes[18] give a pictorial representation of this effect and other factors affecting quantitative assay by fluorescence methods.

At concentrations between ~0.01 and 10 gamma/ml there is a linear relationship between concentration and fluorescence intensity.

At concentrations lower than ~0.01 gamma/ml the fluorescence of an impurity and scattering add to the apparent intensity, and at a concentration of 0.0001 gamma/ml there is no significant difference between these spectra and those of the blank. For xanthurenic acid (Fig. 13) there is no significant difference between the spectra of the blank and that at the 0.001 gamma/ml level. In all three assays, the use of a cutoff filter and polarizers gave no significant change in dynamic range.

Identification of scattering peaks appearing in spectra of Figs. 11, 12, and 13 is given in Table VII.

This work was supported in part by grants from the National Institute of Arthritis and Metabolic Diseases and the American Cancer Society.

* The term "gamma" is used synonymously with microgram.

References

1. H. K. Howerton, ISA J. **6**, 50 (1959).
2. H. K. Howerton (to American Instrument Co., Inc.), U.S. Patent 2,971,429 (Feb. 14, 1961).
3. R. L. Bowman, P. A. Caulfield, and S. Udenfriend, Science **122**, 32 (1955).
4. D. E. Duggan, R. L. Bowman, B. B. Brodie, and S. Udenfriend, Arch. Biochem. Biophys. **68**, 1 (1957).
5. K. Satoh and J. M. Price, J. Biol. Chem. **230**, 781 (1958).
6. C. A. Parker, Analyst **84**, 446 (1959).
7. S. F. Velick, J. Biol. Chem. **233**, 1455 (1958).
8. S. F. Velick, "Spectra and Structure in Enzyme Complexes of Pyridine and Flavin Nucleotides," in *Light and Life* edited by W. D. McElroy and H. Bentley Glass (Johns Hopkins Press, Baltimore, Md., 1961).
9. D. H. Rank, Anal. Chem. **19**, 766 (1947).
10. G. Weber, J. Opt. Soc. Am. **46**, 962 (1956).
11. D. H. Rank, R. J. Pfister, and H. H. Grimm, J. Opt. Soc. Am. **33**, 31 (1943).
12. K. Yagi, Z. Yoshida, and T. Tabata, *Fluorescence* (Nankodo, Tokyo, Japan, 1958), Chap. 6, p. 87. (Translated by M. Kaihara.)
13. R. E. Kemp, Rev. Sci. Instr. **26**, 1120 (1955).
14. R. R. Brown and J. M. Price, J. Biol. Chem. **219**, 985 (1956).
15. J. M. Price and L. W. Dodge, J. Biol. Chem. **223**, 699 (1956).
16. G. Herzberg, *Molecular Spectra and Molecular Structure, II. Infrared and Raman Spectra of Polyatomic Molecules* (Van Nostrand, New York, 1959).
17. C. E. White, M. Ho, and E. Q. Weimer, Anal. Chem. **32**, 438 (1960).
18. E. J. Bowen and F. Wokes, *Fluorescence of Solutions* (Longmans, Green, New York, 1953), p. 20.

Applied Optics — Letters to the Editor

Letters to the Editor should be addressed to the Editor, APPLIED OPTICS, 1155 16th St., N.W., Washington 6, D.C.

Crossed Roof Prism Interferometer*

G. Gould, S. Jacobs, P. Rabinowitz, and T. Shultz

Technical Research Group, Inc., Syosset, New York.

Received 5 December 1961.

When a medium with a negative absorption coefficient is contained within a cavity, coherent electromagnetic oscillations are possible, provided the power gained by stimulated emission from the medium exceeds the cavity losses.[1] The Fabry-Perot interferometer with plane mirrors has been used as a resonant cavity to generate plane wave oscillations in a single mode.[2] However, the oscillations may be prevented if the mirrors are not quite parallel. This letter describes a modification of the Fabry-Perot resonator with relaxed alignment tolerances.

Previously, Peck[3–5] and Murty[6,7] have used cube-corner prisms in Michelson interferometers to relax alignment tolerances. Peck[8] has shown theoretically that a Fabry-Perot interferometer with cube-corner reflectors replacing one or both flats possesses six eigenpolarizations (i.e., polarizations which are reproduced after traversing the prisms). We have observed polarized Haidinger fringes in such an interferometer.[9] These polarization properties may permit as many as six independent oscillations in a cube-corner laser cavity. In contrast, a cavity consisting of 2 crossed 90° roof reflectors, replacing the Fabry-Perot mirrors, has only 2 plane eigenpolarizations, while still maintaining relaxed alignment tolerances.[10]

The cavity in Fig. 1 has an optic axis defined by the mutual perpendicular to the roofs. A ray parallel to the optic axis remains undeviated, upon reflection, regardless of the angle between the roofs, β. When the angle β differs only slightly from 90° the condition for constructive interference is $n\lambda \cong 4L\cos\theta$, where θ is the angle between the rays and the optic axis. With $\beta = 90°$, the equality holds and the angular spacing of the Haidinger fringes and the free spectral range are the same as with plane Fabry-Perot mirrors separated by a distance $2L$. A rotation of a roof reflector through an angle ψ has no effect upon the fringes. Similarly, a rotation of the roof reflector through an angle ϕ merely tilts the optic axis and consequently reduces the aperture. These properties result in much improved alignment stability compared with the plane Fabry-Perot. In the plane Fabry-Perot, angular alignment is insensitive to rotation about only one direction, the normal to the planes, while the crossed roof interferometer has two such insensitive directions. Thus there is one extra degree of freedom in alignment of this interferometer.

Experimentally, we have observed fringes with a single roof reflector vs flat, as well as with two crossed roof reflectors. In the first case (see Fig. 2) two front-surface mirrors were mounted at a right angle, forming a roof reflector. These opposed a 95%-reflecting multilayer flat. Two sets of fringes were observed; one set polarized normal and one parallel to the plane of incidence.

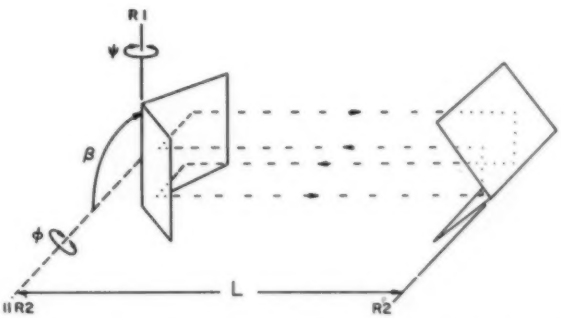

Fig. 1. Crossed roof prism interferometer, showing tip angles and ray path. R_1, R_2 are roof axes. Axis labeled $\|R_2$ is parallel to axis R_2.

* Work supported by Advanced Research Projects Agency through the Air Force Office of Scientific Research.

These were due to the different polarization phase changes upon reflection by the roof reflector. Freshly evaporated silver coatings were required on the mirror surfaces, as aluminum was found to have too low a reflectivity at $\lambda = 5461$ A. Fringes were also observed when we replaced the roof reflector with a roof prism, making use of total internal reflection.

In the second case (see Fig. 1) we replaced the flat with a second roof reflector, oriented at right angles to the first roof reflector. A single set of fringes was observed in this case. The fact that the fringes are not double as in case 1 is explained by the compensating phase shifts of the two roof reflectors: i.e., in traversing the interferometer the orientations of the two polarizations become interchanged with respect to the roof reflectors. Since, in a crossed roof interferometer, 8 reflections occur before a ray retraces itself, while only 2 occur in the plane Fabry-Perot, reflection losses in the former are correspondingly more serious. We have virtually eliminated reflection losses by employing total internal reflection in a prism; Fresnel losses were reduced by constructing the entrance faces at or near Brewster's angle (see Fig. 3). This cavity has a very low loss for one polarization. Light is conveniently coupled in and out of the cavity by orienting one entrance face at an angle slightly different from Brewster's angle.

When this cavity is used as a laser resonator, oscillation will occur in a single mode if losses in other modes are greater. Because of the reduced Q in the second polarization, oscillation is confined to the favored polarization and the laser efficiency is not reduced by the use of the Brewster angle coupling. Mode quality factors (Q) also decrease as walk-off and diffraction losses increase. These effects have been considered for the plane Fabry-Perot by Kotik and Newstein[11] and by Fox and Li.[12] Walk-off losses are the same for the crossed roof cavity as for the plane Fabry-Perot, since the ray displacement, $L \sin \theta$, is the same for both. Therefore, single-mode oscillation may be expected in the former as has been observed in the latter.[2]

In contrast to the plane Fabry-Perot resonator, rays are not reflected back upon themselves so that standing waves are not necessarily formed, and the possibility of traveling waves exists. This resonator possesses a greater advantage over the plane Fabry-Perot as a laser cavity in that there is always a single direction—the optic axis—for which rays return undeviated. This means that the resonator reflectors are always in alignment for the mode parallel to the optic axis. This property has been demonstrated experimentally and can be used to enhance the selection of single-oscillation modes.

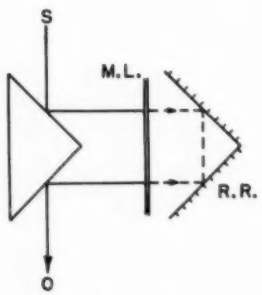

Fig. 2. Arrangement of folded Fabry-Perot interferometer. S—source, O—observer, M.L.—multilayer reflector, R.R.—roof reflector.

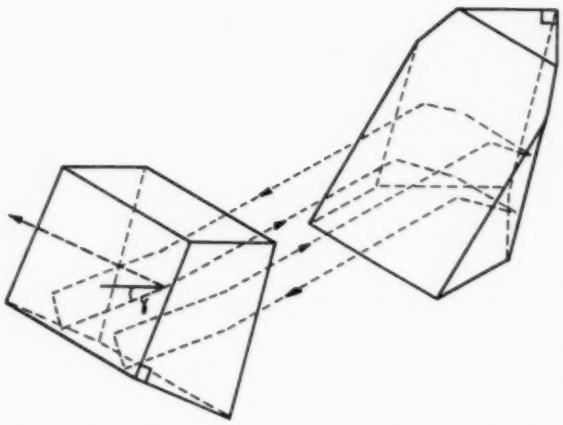

Fig. 3. Crossed roof prism optical cavity, showing pick-off angle γ.

References

1. J. P. Gordon, H. J. Zeiger, and C. H. Townes, Phys. Rev. **99,** 1264 (1955).
2. A. Javan, W. R. Bennett, Jr., and D. R. Herriott, Phys. Rev. Letters **6,** 106 (1961).
3. E. R. Peck, J. Opt. Soc. Am. **38,** 66 (1948).
4. E. R. Peck, J. Opt. Soc. Am. **38,** 1015 (1948).
5. E. R. Peck, J. Opt. Soc. Am. **47,** 250 (1957).
6. M. V. R. K. Murty, J. Opt. Soc. Am. **50,** 7 (1960).
7. M. V. R. K. Murty, J. Opt. Soc. Am. **50,** 83 (1960).
8. E. R. Peck, J. Opt. Soc. Am., in press. This work was carried out in part during the summer of 1959 at the TRG laboratory in Syosset, N.Y., with the support of ARPA.
9. G. Gould, S. Jacobs, P. Rabinowitz, and T. Shultz, J. Opt. Soc. Am., in press.
10. G. Gould, A laser cavity consisting of a crossed pair of 90° roof prisms was first described in an unpublished proposal to ARPA, December 1958.
11. J. Kotik and M. C. Newstein, J. Appl. Phys. **32,** 178 (1961).
12. A. G. Fox and Tingye Li, Bell System Tech. J. **40,** 453 (1961).

Stimulated Emission of Infrared Radiation from Ytterbium Activated Silicate Glass

H. W. Etzel, H. W. Gandy, and R. J. Ginther

U.S. Naval Research Laboratory, Washington, D.C.

Received 24 March 1962.

Since Schawlow and Townes[1] proposed the use of maser techniques to produce coherent radiation in the visible and infrared region of the spectrum, optical oscillations have been reported in various matrices containing Cr^{+3},[2] U^{+3},[3] Sm^{2},[4] and Nd^{+3}.[5,6] The purpose of this letter is to describe the stimulated emission of Yb^{+3} in a lithium-magnesium-alumino silicate glass, which has been made to oscillate optically at a wavelength of 1.015 μ at liquid nitrogen temperature and lower.

The high optical quality glass, originally developed at this Laboratory for other purposes,[7] has the following molar composition: 0.074 Li_2O, 0.296 MgO, 0.057 Al_2O_3, 0.567 SiO_2, and 0.006 Yb_2O_3. From the method of preparation it is thought that the Yb is predominantly in the trivalent state. An etalon, 4 mm

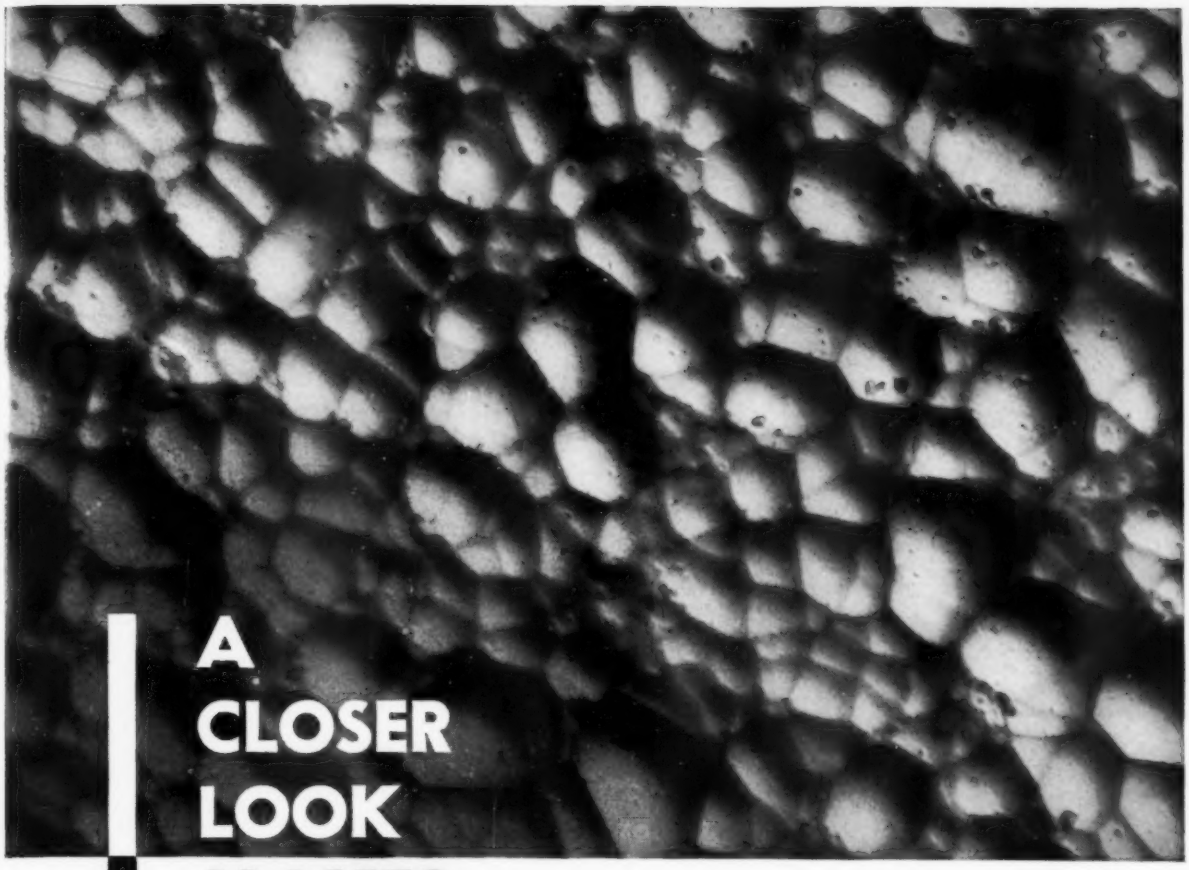

A CLOSER LOOK MAKES A DIFFERENCE*

From the outside, Itek's laboratories in Lexington may appear little different from other modern structures built to house the equipment and staff engaged in advanced research and development.

However, professional optics men, after visiting our Optics Departments — major segments in a number of interrelated activities — often comment on the unique impression they gain of strong interplay between theoretic and applied disciplines, especially the manner in which methods and techniques for improving the quality of large, ultra-precise optical systems are carried through from fundamental research to actual use.

Probably the most lasting impression our visitors receive is the manner in which exceptional professional quality, technical support and modern equipment have been combined to make a truly unique optics organization.

To arrange for a discussion write to:

Itek

Mr. Louis Rudzinsky
Technical Placement Director

10 Maguire Road
Lexington, Mass.
VOlunteer 2-6200, Ext. 581

'An equal opportunity employer'

*Scooped-out depressions, or a cobblestone road? The photomicrograph is a close-up at 1000X of a special acid-etched glass diffusing screen, which was developed at Itek to solve an illumination problem in a high-precision enlarger for aerial photographs.

It demonstrates how difficult it is for the human visual system to properly interpret the form of an unfamiliar contour. A surface of contiguous, concave depressions is rare in nature, and the eye persists in avoiding an unlikely interpretation. Inverting the photograph will not help. The light is already "normal", i.e., as if from a source above and to the right of the observer. HINT: Mask off a small area so that you may examine one concavity at a time.

B/A All-Dielectric INTERFERENCE FILTERS

Baird-Atomic announces the introduction of their radically improved Ultra-violet Filters and all-dielectric Visible Spectrum Interference Filters.

The new 'block shape' ⎍ passband in the Visible Spectrum Filters enables the user to obtain the greatest degree of spectral purity.

If the filter you require is not available in stock, normal delivery time is within thirty to thirty-five days.

Standard filter sizes are 1" x 1" and 2" x 2"; other sizes and shapes are available on special order. Write for your copy of our new filter brochure.

Engineers and scientists — investigate challenging opportunities with Baird-Atomic. Write Industrial Relations Department.

Visible Spectrum

- 4000Å - 8000Å
- New block shape ⎍ passband
- Absorption filters and/or evaporated blocking components provide for maximum blocking, reduced thickness, and improved signal-to-noise ratio
- Transmission outside of passband: under 0.1%
- Half bandwidths from 4.8 Å to 1600Å
- Total transmission from fully blocked filter: up to 70%
- Blocking — complete on low side — high side blocking to at least 8000Å (Additional blocking at extra cost)

Ultraviolet Spectrum

- 2100Å to 3400Å and 3900Å to 3999Å

BAIRD-ATOMIC, INC.

33 university road · cambridge 38, mass.

ADVANCED OPTICS AND ELECTRONICS . . . SERVING SCIENCE

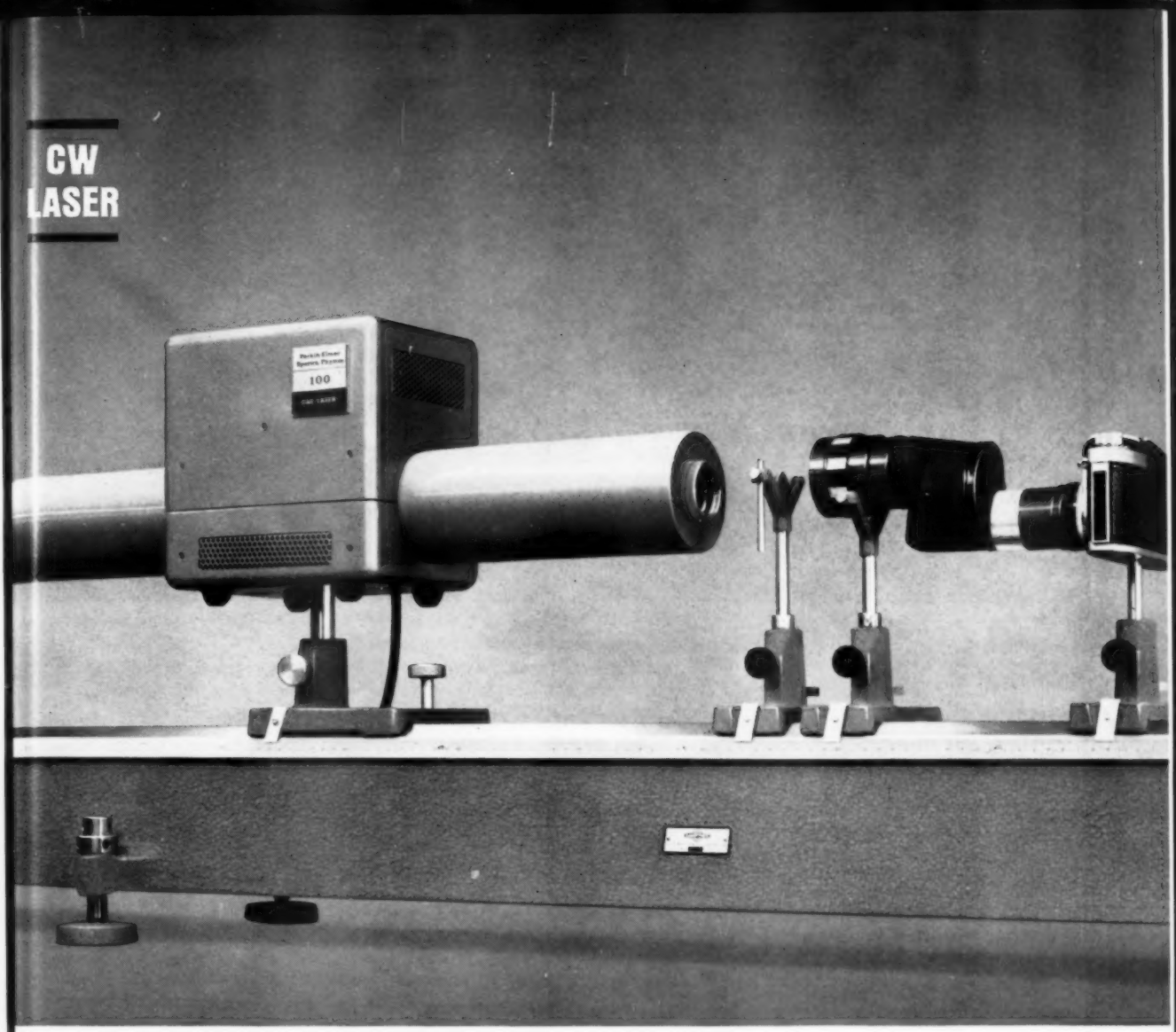

PERKIN-ELMER/ SPECTRA-PHYSICS GAS LASERS

AVAILABLE WITH
BREWSTER'S ANGLE WINDOWS.
SPHERICAL OR PLANO REFLECTORS.

The Perkin-Elmer/Spectra-Physics Gas Phase Lasers are continuous wave energy sources designed for general experimental work with coherent light.

OPERATING FEATURES

output. Continuous wave, highly coherent, monochromatic light at 11,530Å from an active medium of helium and neon gas.

input. Integral RF source with separately housed power supply operating from 115 volts AC.

portable. Lightweight, transportable unit with provision for mounting on conventional optical bench.

utility. Application of laser energy in the field as well as in the laboratory.

For complete information, contact Mr. J. H. Beardsley, Optical Maser Department, Perkin-Elmer Corporation, Main Avenue, Norwalk, Connecticut. Telephone Area code 203 Victor 7-0411.

Perkin-Elmer
Norwalk, Connecticut

Spectra-Physics Inc.
Mountain View, California

This photomicrograph is a section through a laser weld specimen made in Mo-1/2% Ti alloy 0.005 inches thick. The weld was made by imaging, at reduced magnification, the end of an experimental AO glass laser on the surface of the specimen. By pulse shaping of the pumping source to control the energy release, the highly localized melting shown was produced without significant vaporization or burning, even though done in air.

RESEARCH & DEVELOPMENT OPPORTUNITIES

Generation of coherent optical radiation and other optical maser phenomena are under intense investigation at the Research Center of American Optical Company. Advanced studies of wave propagation in small diameter optical fibers and IR and UV radiation phenomena also are being conducted. New opportunities for creative basic and applied research in these and other areas are available at both senior and junior levels.

- **SOLID STATE PHYSICISTS:**
  To investigate properties of materials for possible use in optical masers and other electro-optical devices.
- **OPTICAL PHYSICISTS:**
  To investigate the mechanics of stimulated emission and propagation of coherent radiation both within and outside the laser cavity.
- **MICROWAVE ENGINEERS:**
  To design and build equipment for investigation of modulation, propagation, and detection of coherent optical radiation.
- **OPTICAL ENGINEERS:**
  To design systems for efficient optical pumping and optimum utilization of optical maser output in both the visible and infrared.

Qualified personnel are invited to write to Dr. S. M. MacNeille, Director of Research.

RESEARCH CENTER

American Optical

COMPANY

SOUTHBRIDGE, MASSACHUSETTS

Fig. 1(a). Light output from Yb laser at 78°K, 100% over threshold. FT-503 4000 V, 300 μf, sweep time 200 μsec/div.

Fig. 1(b). Light output from Yb laser at 78°K, 100% over threshold. Same operating conditions except oscilloscope gain reduced a factor of 10.

in diameter and 24 mm long, was fabricated with ends parallel to within 30 sec of arc and plane to within a fraction of a wavelength of visible light. The etalon ends were coated with evaporated silver films, one totally reflecting and the other transmitting about two percent.

A G.E. type FT 503 xenon-filled helical flashtube was used as the optical pumping source. For the liquid nitrogen and liquid-helium experiments an evacuated system comprising the etalon, a stainless steel tube, and a sapphire window was used; the unit was then placed in a specially designed dewar in such a way that the etalon, which was in direct contact with the liquid coolant, was on the axis of the flashtube. The detector employed was an InSb photovoltaic cell operated at liquid nitrogen temperature; it had a time constant of about two μsec. A typical laser output is shown in Figs. 1(a) and 1(b), where it is seen that stimulated emission occurs approximately 750 μsec after initiating the exciting pulse and persists for about 550 μsec. As may be seen in Fig. 1(b), the stimulated emission does not occur at the peak intensity of the exciting light pulse, but commences some 300 μsec thereafter, indicating a lifetime for spontaneous luminescent emission which is of the order of, or longer than, the rise time of the exciting source. This inference was borne out by direct measurement of the spontaneous lifetime, which was found to be about 1450 μsec at a sample temperature of 78°K. The threshold lamp input energy required for laser action at liquid nitrogen temperature with this excitation scheme is about 1300 joules and decreases by about 10 percent in going to liquid helium temperature. The same general spikelike bursts of stimulated emission are also observed oscilloscopically at liquid helium temperature; but for the same excitation energy input the peak heights of the oscillations are approximately twice as high and the duration of stimulated emission is half as long at liquid helium temperature compared to liquid nitrogen temperature. The peak power density in stimulated emission in the region of 1.015 μ has been determined to be about 12 watts per cm²; by contrast, the same measurement made on ruby lasers in this Laboratory has yielded a value of several kilowatts per cm².

The glass is essentially transparent in the visible; has two absorption bands in the ultraviolet, a weak one at 310 mμ and a strong band below 220 mμ; three absorption bands in the near infrared, peaking at 914, 946, and 976 mμ, respectively. The 976 mμ absorption is the strongest of the infrared bands, with an absorption coefficient of 8 cm^{-1} and a half-width of 6 mμ; the 914 and 946 mμ bands have absorption coefficients of about 1 cm^{-1}. The peak heights, bandwidths, and spectral positions of the three infrared bands do not vary significantly with temperature. Excitation measurements show that all three infrared bands lead to spontaneous emission at 1.015 μ, the 914 and 946 mμ bands appearing relatively more prominent in the excitation spectrum than in the absorption spectrum. The measurements show that excitation into ultraviolet bands also leads to luminescence at 1.015 μ.

When a sharp-cut red filter, transmitting less than 0.01 percent of light below 600 mμ and transparent through 1.2 μ, was interposed between the flashtube and the etalon, the stimulated emission of the laser was decreased only by the small factor that one would expect because of reflection losses in the filter. From this experiment and from the excitation spectrum for spontaneous emission, it is concluded that the principal absorption bands giving laser action in the Yb-activated glass are those peaking at 914, 946, and 976 mμ. The small integrated infrared absorption may underlie the small peak power output of the Yb laser as compared to the ruby laser, for the output of the xenon flashtube is considerably less in the infrared than in the visible spectrum where ruby absorbs.

A reliable measurement of the band shape of the spontaneous emission at about 1.015 μ has not been made, but a photograph of the spectrum of the stimulated emission from the Yb-glass laser is shown in Fig. 2. The over-all bandwidth of the emission is about 6 mμ and there are at least 29 lines present. The shortest wavelength line discernible above film background is at 1.0125 μ and the longest at 1.0184 μ.

The general features of the absorption spectra and the considerable detail in the stimulated emission suggest an inner-shell transition in the $4f^{13}$ electronic configuration of Yb^{+3}. It is thought at present that the stimulated emission corresponds to electronic transitions from the $^2F_{5/2}$ excited state multiplet to the

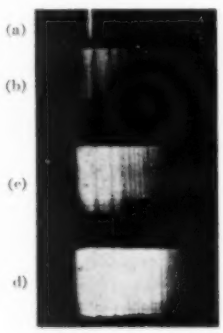

Fig. 2. Photograph of stimulated emission from Yb-activated glass at 78°K. (a) 1.0140-μ mercury reference line; (b) 2 flashes, 4000 V dc, 300 μf; (c) same, but 5 flashes; (d) same, but 10 flashes.

$^2F_{7/2}$ ground state multiplet. It would appear that if the Yb ions occupied a unique position in the glass network of less than cubic symmetry and J were a good quantum number, one would expect a maximum of 12 emission lines;[8] for sites of cubic symmetry, only 6 lines would be expected. Since many more lines are observed, this does not appear to be the case.

The authors wish to express their appreciation to J. A. Sanderson for making available the grating spectrograph and to J. A. Curcio and C. V. Acton for their invaluable cooperation in obtaining the spectrographic data.

References

1. A. L. Schawlow and C. H. Townes, Phys. Rev. **112,** 1940 (1958).
2. T. H. Maiman, Nature **187,** 493 (1960).
3. P. P. Sorokin and M. J. Stevenson, Phys. Rev. Letters **5,** 557 (1960).
4. P. P. Sorokin and M. J. Stevenson, IBM Journal of Research **5,** 56 (1961).
5. L. Johnson and K. Nassau, Optical Maser Symposium, Bell Telephone Laboratories, Murray Hill, N.J., Oct. 10, 1961.
6. E. Snitzer, Phys. Rev. Letters **7,** 444 (1961).
7. R. J. Ginther and J. H. Schulman, Symposium on Materials Research in the Navy, Philadelphia, Pa., March 1959, ONR-5, Vol. 1, p. 371 ff; R. J. Ginther, IRE Trans. on Nuclear Science, **NS 7,** 28 (1960).
8. W. A. Runciman, *Reports on Progress in Physics*, ed. A. C. Stickland (The Physical Society, London, 1958), Vol. 21, pp. 30 ff.

Measurement of Microcurrent by the Michelson Interferometer

I-Hsiun Chen

Department of Physics, Taiwain Provincial Cheng Kung University, Tainan, Taiwan, China (Formosa)

Received November 1961.

As is well known the Michelson interferometer is an instrument designed primarily to measure the wavelength of light (in air or in an optical medium) in terms of some standard of length or vice versa. Another application of this interferometer by which the sensitivity of a galvanometer can be increased is described here.

The experimental arrangement used to measure microcurrent by a Michelson interferometer is shown schematically in Fig. 1. The Michelson interferometer consists essentially of two very flat front surface mirrors M_1 and M_2 and two plane parallel glass plates G_1 and G_2. In this case M_2 is the indicator mirror of a very sensitive, critically damped D'Arsonval galvanometer. The position of the coil of the galvanometer is to be measured by the interferometer. Mirror M_2 should be perpendicular to the bed of the interferometer. The instrument is adjusted as follows:

Using conventional alignment techniques for such a galvanometer the electrical zero is made to coincide with the mechanical zero. Telescope T_2 is used to set the coil position in the center of its range of linear response. Next, the axis of the autocollimating telescope T_1 is made perpendicular to the face of mirror M_2. The Gauss eyepiece E provides for illuminating the cross hairs. The mirror M_1 is mounted on the interferometer carriage and can be moved along its well-machined track at a slow and accurately controlled rate by means of a precision drive screw and worm gear. The fine tilt adjustment screw on the support mountings of mirror M_1 permits us to adjust its angle with respect to M_2. We carefully turn the carriage drive screw until the virtual image M'_1 of mirror M_1 actually intersects M_2. When M'_1 intersects M_2, the localized fringes are perfectly straight. For the above adjustment we use monochromatic light for the source S_1. When the straight localized fringes have appeared, we replace the monochromatic light by white light. The white-light fringes are colored and symmetrical with respect to the central fringe which is dark. Then we set the movable cross hair of the filar micrometer F on the central dark fringe. Again we return to the monochromatic light and measure the 5 bright fringes on both sides of the central fringe. Let x_1 be the width of 5 bright fringes. We can adjust the tilt angle of mirror M_1 to set x_1 to a selected constant value, corresponding to the zero position of the galvanometer. When a microcurrent flows in the galvanometer circuit, the galvanometer mirror M_2 moves to an equilibrium position. Now as M_2 moves, the fringes become more widely spaced (or more slender). We use the filar micrometer eyepiece to measure the width of the 5 bright fringes on both sides of the central fringe as before, calling the new width x_2. Since the angle of deflection is very small the increment of current will be proportional to the number of fringes per unit length. We may therefore use the following approximate formula to obtain the microcurrent i:

$$i = i_0 (x_2 - x_1)/x_2,$$

where i_0 is the magnitude of the current that makes a single interference fringe fill the mirror M_2.

Galvanometer illustrated opposite

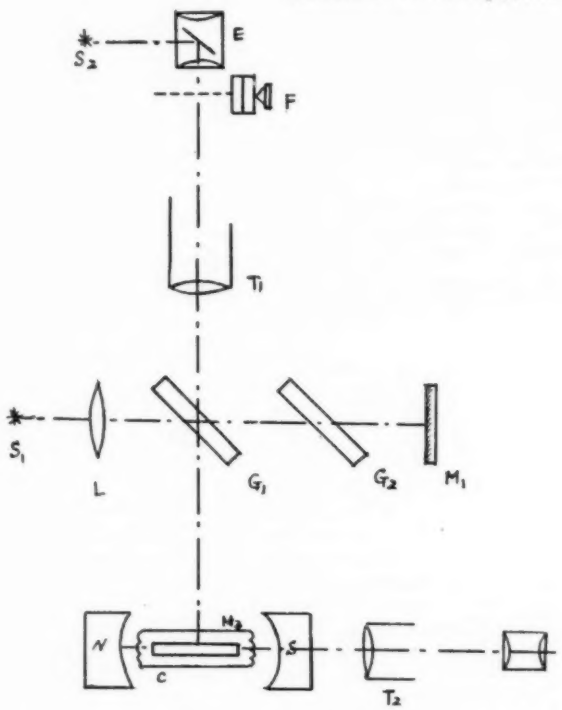

Fig. 1. Schematic diagram used to measure the microcurrent by the Michelson interferometer. C, moving coil; E, eyepiece; F, filar micrometer; G_1 and G_2, glass plates; M_1, mirror which is mounted on carriage; M_2, mirror which is fixed on the coil; T_1 and T_2, telescopes.

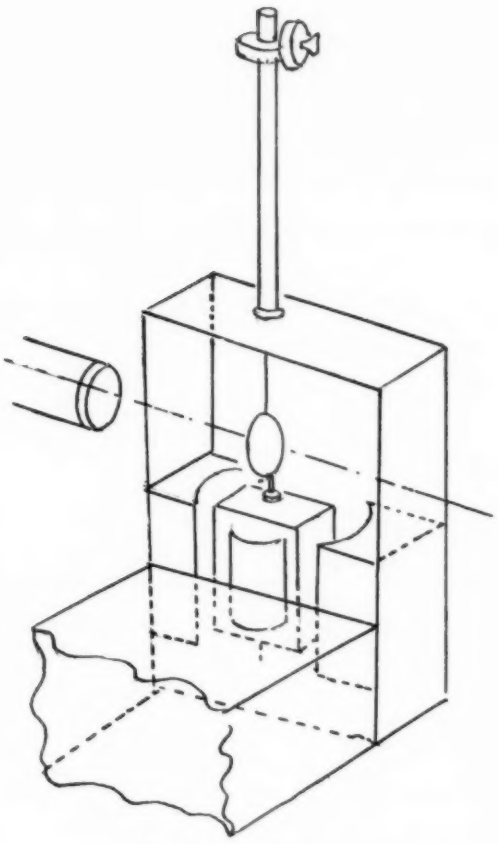

Fig. 2. Galvanometer.

Emission Pattern of Ruby Laser Output

R. L. Aagard, D. L. Hardwick, and J. F. Ready

Honeywell Research Center, Hopkins, Minnesota.
Received 26 February 1962.

Composite rod optical masers, described by Devlin *et al.*,[1] exhibit a lowered threshold for laser action because of concentration of the pumping light along the axis of the rod by refractive effects. It is the purpose of this note to point out that a similar concentration of the pumping light exists in solid ruby rods yielding an output of stimulated emission radiation that occurs preferentially from the center portion of the rod. The theoretical derivation of Devlin *et al.*[1] of the energy density of light as a function of radius is essentially unchanged for the case of a solid ruby rod except for the introduction of a factor describing absorption of the pumping light in the outer portions of the rod. The results are similar to those shown in Fig. 4 of ref. 1. Thus, for a ruby rod with a polished outer surface we expect the laser output to occur fairly uniformly within a circle of radius R/n, where R is the rod radius and n its refractive index, for operation near the threshold. For increasing pumping energies, the output should spread only slowly over the remainder of the rod end.

The derivation mentioned above assumed a two-dimensional pumping geometry, with all light incident on the rod in a plane P perpendicular to the rod axis. It can be shown simply that the same type of behavior should hold for the more realistic three-dimensional case, even though the sine of the projection of the angle of refraction on the plane P is not in general equal to $1/n$ times the sine of the projection of the angle of incidence on P. However, we have

$$\sin^2\beta' = \frac{\sin^2\beta}{1 + \cos^2\beta \tan^2\gamma},$$

where β is the angle of refraction at the rod surface, β' is the projection of β on P, and γ is the angle between P and the plane containing the incident and refracted rays and the normal to the rod surface at the point of intersection. We see that $\beta' \leq \beta$, with the equality holding only in special cases. Since β must be small enough to insure that the refracted ray passes within a circle of radius R/n, β' must have the same property for the projection of the ray on P. This argument shows that the general form of the dependence of light intensity on radius is obtained from the two-dimensional calculation.

Pictures of the output from a 9.5-mm diameter ruby rod of 0.05% Cr^{3+} concentration with polished side surfaces mounted inside the helix of an FT524 flashtube were taken with a 55-mm lens focused on the end of the ruby through sufficient neutral density filters to give good pictures. Typical results are shown in Fig. 1 for different pumping powers. The background is fluorescence and scattered light. The laser emission is not centered, because the rod did not lie along the axis of the helix. It is seen that the laser emission occurs within an area of radius approximately R/n and spreads over the surface of the rod only slowly with increasing pumping power. For a ruby with rough, diffusely refracting sides, the output occurred fairly uniformly over the rod end.

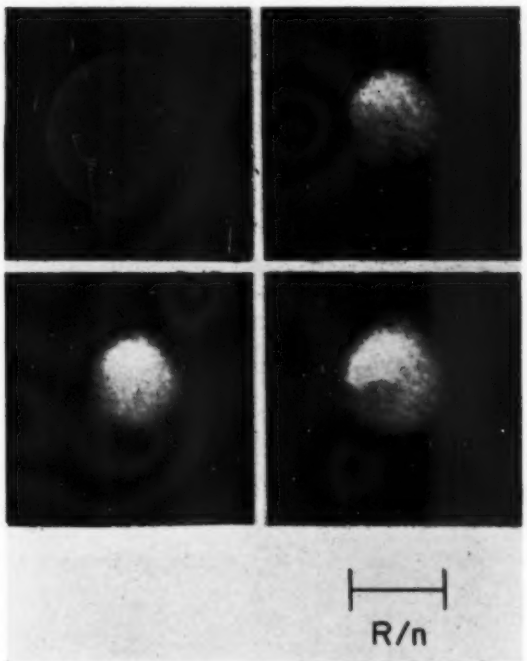

Fig. 1. Photographs of light output from end of ruby rod. Upper left: below threshold. Upper right: 1.0 times threshold. Lower left: 1.2 times threshold. Lower right: 1.3 times threshold.

These results are important for measurement of beam divergence angles of laser emission since the area of the emitting portion of the rod must be known.

Reference

1. G. E. Devlin, J. McKenna, A. D. May, and A. L. Schawlow, Applied Optics **1**, 11 (1962).

Use of an Oxyacetylene Flame to Calibrate a Prism Spectrometer in the 10–30 μ Region*

Fred P. Dickey and William H. Rogge

Department of Physics and Astronomy, The Ohio State University, Columbus 10, Ohio.
Received 6 January 1961.

A Perkin-Elmer Model 12C prism spectrometer has been used for the past few years in connection with a series of studies concerning the infrared emission spectra of flames. While there are many papers suggesting excellent ways of calibrating spectrometers using absorption lines,[1,2] it has been found most convenient to use emission lines for calibration when emission spectra are being observed. In addition, the oxyacetylene flame extends the calibration to considerably longer wavelengths.

The OH rotational emission lines provide a series of strong conveniently spaced frequency standards. These lines are shown as they appear in the spectrum of an oxyacetylene flame in Fig. 1. The flame used was that of a National 3A hand torch. The torch tip used was a National A03. The flow rates used were 4.5 liters/min for the oxygen and 1.5 liters/min for the acetylene. The primary flame was about 11 mm high. The torch tip was set at a distance of 16 mm below the center of the spectrometer slit.

The spectrum shown was obtained using a Reeder thermocouple, a Perkin-Elmer model 107 amplifier, and a Brown Electronik recorder. The slit widths were approximately 0.20 mm. The upper trace was recorded using a KBr prism and the lower trace using an NaCl prism. The line frequencies which may be obtained from the Bumblebee report[3] are given in Table I. Actually each line consists of four components and only the central frequency is tabulated.

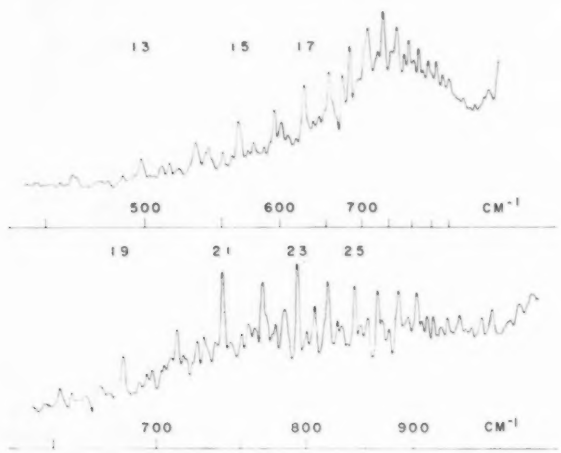

Fig. 1. Emission spectrum of OH in an oxyacetylene flame.

Table I. Frequencies of the OH Rotational Lines

Line designation K	Line frequency cm^{-1}
8	327.9
9	363.0
10	397.6
11	431.8
12	465.4
13	498.4
14	530.9
15	562.7
16	593.8
17	624.1
18	654.1
19	682.9
20	711.0
21	738.3
22	764.8
23	790.4
24	815.2
25	838.9
26	861.7
27	883.7
28	904.5

References

1. E. K. Plyler, L. R. Blaine, and M. Nowak, J. Research Natl. Bur. Standards **58**, 195 (1957).
2. E. K. Plyler, A. Danti, L. R. Blaine, and E. D. Tidwell, J. Research Natl. Bur. Standards **64**, 29 (1960).
3. G. H. Dieke and H. M. Crosswhite, Bumblebee Report No. 87, Johns Hopkins University (1948).

A Distortionless Interferometer Plate Mount

J. V. Ramsay and E. G. V. Mugridge

C.S.I.R.O. Division of Physics, National Standards Laboratory, Sydney, Australia.
Received 30 January 1962.

In a project involving the automatic control of the parallelism of the plates of a Fabry-Perot interferometer,[1] the need has arisen for a method of mounting fused silica interferometer plates of 50 mm diameter and 11 mm thickness so as to satisfy the following requirements:

1. Distortion of the surface of the plate introduced by the mount to be less than $\lambda/80$.
2. No projection in front of the reflecting surface of the plate.
3. Sufficient rigidity to enable oscillation at a frequency of 10 kc/sec with an amplitude of 10 mμ.
4. Full aperture to be clear for both front and back surfaces.

A suitable mount has been made as follows and is shown in Fig. 1. To the edge of the fused silica plate three lugs of fused silica are cemented with an epoxy resin (Araldite*), the lugs being of the same material as the plate to eliminate thermal distortions. The resin is allowed to set at room temperature (20°C) for at

* Supported in part by Geophysics Research Directorate, Air Force Cambridge Research Laboratories, Office of Aerospace Research (USAF), through a contract with The Ohio State University Research Foundation.

* Manufactured by CIBA, Ltd., Basel, Switzerland.

least 48 hr. The lugs contain a hole, slot, and plane respectively on the back surfaces to accommodate 1.5-mm-diameter balls. On the front surface three similar balls are held against plane surfaces by a spring such that the line joining each pair of balls is parallel to the axis of the plate.

Before cementing on the silica lugs, the surfaces of the plates were flat to better than $\lambda/80$ of mercury green light. After attaching the lugs, no distortion has been detected, and varying the pressure of the spring clip causes no change in the surface figure. The mount is sufficiently rigid to allow the oscillation required.

A similar form of mounting can be made from a solid piece of fused silica. However, the mount described above is much more economical in material and has the advantage that an existing interferometer plate can be mounted satisfactorily.

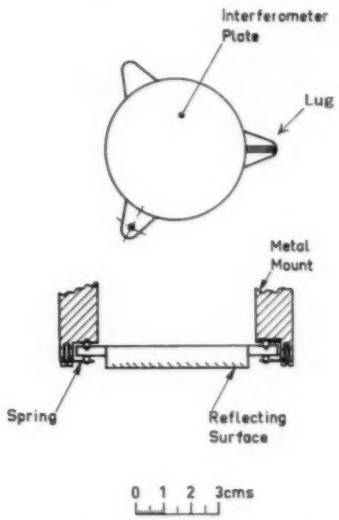

Fig. 1. Interferometer plate mount.

Meeting Reports

Fourth Annual Rocky Mountains Spectroscopy Conference, August 10–11, 1961

Reported by Edward Vejvoda, Dow Chemical

The fourth Annual Rocky Mountain Spectroscopy Conference, sponsored by the Rocky Mountain Section of the Society for Applied Spectroscopy, was held in Denver, Colorado, on August 10–11, 1961. Although regional in conception, the meeting attracted spectroscopists from 16 states, representing 44 companies, educational institutions, and governmental agencies. The Conference program was divided between individual papers and panel reviews on infrared and semiquantitative analysis by emission and x-ray spectrography.

Several instrumental reviews related to various areas of spectroscopy were also presented. Fred Brech, Jarrell-Ash Company, reviewed the progress in atomic absorption spectroscopy while H. T. Dryer, Applied Research Laboratories, discussed interrupted discharge excitation with various gaseous atmospheres. Wilbur Kaye, Beckman Instruments, suggested several analytical applications for the far ultraviolet (1600–2000 Å) spectral region and reviewed recent instrumentation designed for this region. Recent instrumental developments in the vacuum ultraviolet were summarized by Fred Walter of Ball Brothers Research Corporation.

One of the features of the Conference was an open panel discussion on infrared spectroscopy followed by a question and answer period. Panel members introduced themselves by giving a brief review on some aspect of spectroscopy. The panel members were: Chairman: R. A. Nyquist, Dow Chemical Company—*Polymers and Plastics;* G. L. Cook, U.S. Bureau of Mines—*Oil Shale and Petrochemicals;* L. D. Frederickson Jr., Spectran Laboratories—*Practical Infrared Analysis of the Unusual Sample;* G. W. Gullikson, Ohio Oil Company—*Raman vs Infrared Analysis;* and W. I. Kaye, Beckman Instruments—*Ultraviolet and Near Infrared Regions in Analysis.* Comments on the Panel Plan indicated a favorable reaction to this type of program.

The Conference program also included a Symposium on Semiquantitative Analysis, the participants being E. K. Jaycox, Bell Telephone Company, A. T. Myers, U.S. Geological Survey, A. C. Schalge, Ohio Oil Company, and M. L. Salmon of the Fluo-X-Spec Laboratory. Jaycox gave an excellent review of the status of semiquantitative analysis by optical emission spectroscopy while Myers summarized the procedure used by his emission laboratory for the semiquantitative analysis of trace elements in rocks and minerals. Schalge described a spark-in-spray emission technique and reviewed its applicability. Salmon characterized the advantages of x-ray fluorescent spectrography for routine semiquantitative analysis.

In brief, the papers presented covered the areas of fluorescence in crude oils, evaluation of synthetic lubricants by ultraviolet and infrared spectroscopy, infrared studies of the vanadium–oxygen linkage, organic reactions induced by an electron beam, geochemical applications of mass spectrometry, water analysis by direct reading techniques, and spectrographic analysis of mill products and air samples.

Abstracts of the papers presented may be obtained from the Co-Chairmen of the Conference: Dr. A. L. Schalge, Ohio Oil Company, Littleton, Colorado, and Francis S. Bonomo, Denver Research Institute, Denver University, Denver, Colorado.

OSA Spring Meeting, Washington, D.C. March 14–17 1962

Reported by Harry K. Hammond, III, National Bureau of Standards

To those of you who missed the Spring Meeting at the Mayflower Hotel in Washington, D.C., I can only say, "C'est dommage!" Many things made this meeting outstanding, of course, and it will be impossible to recount them all adequately in the space allotted to this report. In essence they were: (1) The Symposium on Physiological Optics, the first to be held in ten years; (2) The large number of invited and contributed papers on recent developments in fast-moving fields such as plasmas, masers, lasers, and space optics; (3) The provision in the program for

postdeadline papers; (4) The instrument exhibit; (5) The award of the Adolph Lomb medal and the annoucement of a new International Medal in honor of the late Dr. C. E. K. Mees, and (6) The international flavor of the meeting.

A welcome precedent was provision on the program for postdeadline papers. Several laboratories utilized this opportunity to place on the program papers that had not been released in time to meet the regular abstract deadline. This provision itself contributed to another "first" in that 3 papers in this category were presented by members of the Lebedev Physical Institute of Moscow. This meeting was truly international with papers being presented by Canadian, French, and Japanese, as well as Russian scientists, and the announcement by President MacAdam, of the establishment of an OSA International Medal in honor of the late Dr. C. E. K. Mees, English-born founder of the Eastman Kodak Research Laboratories, was most timely.

The Symposium on Physiological Optics comprised some twenty 30-minute invited papers on various phases of investigation of the visual process, describing the latest techniques that are being used by leading researchers in their attempts to uncover more information on the nature of the visual process. Our dean of retinal biochemists, George Wald, pointed out to newsmen who gathered after the first morning session that three newsworthy items had been presented: (1) Rods and cones are constructed of highly organized piles of plate-like membranes with the molecules oriented much as they are in a crystal lattice. (2) Electron micrographs of clusters of a few pigment molecules on rod and cone membranes were shown publicly for the first time. (3) A concentration of potassium inside the eye exceeding that of other parts of the human anatomy was reported as being a possible clue to the tremendous light sensitivity of the cells that constitute the photoreceptors.

Most OSA members are unaware that a number of papers are really presented twice, once formally for the membership and a second time, quite informally, for the press. A scheduled press conference was held each morning and afternoon under the able leadership of Eugene H. Kone, Public Relations Director of the American Institute of Physics. These press conferences provide an opportunity for a scientist to present a popular version of his paper, preferably preprinted, so that the press can interpret to the public the meaning and importance of his otherwise highly technical presentation.

Alan Kolb presented a most interesting paper on the "Diagnostics of High Temperature Plasmas." As he put it, first comes the problem of producing a plasma, and then of evaluating the factors that influence its production. There are many theories, but it now becomes necessary to do long hard experiments to try to prove or disprove them. One of the secrets of producing high-temperature plasmas is an intense magnetic field. Such fields require high electric currents. The apparatus at the Naval Research Laboratory is noteworthy because it is producing currents in excess of ten million amperes. Two million joules are discharged by a capacitor bank in ten microseconds, equivalent to 200,000 megawatts of power! Shortly before the March meeting the equipment was run at half energy, about 15 million amperes, the first time that currents in excess of 10 million amperes have been run anywhere. Later, perhaps by summer, the current will be stepped up to over 25 million amperes.

On Saturday morning the East Room was again filled to standing room only to hear the invited paper by Robert E. Hopkins on "Re-evaluation of the Problems in the Field of Optical Design." This presentation may not have been considered hot news by the public press, but it impressed this reporter as being worthy of more than just passing mention because it contained what appeared to be important observations by a conservative thinker. Dr. Hopkins began by pointing out that lens design some years ago was an art and that the design of lens systems was a cut and dry process. The advent of the electronic computer has provided the designer with a powerful tool, yet no "automatic design programs" have yet been formulated. The machine has not replaced the designer; instead, it permits him to calculate the performance of his design. The decision of just how to proceed with a lens design is complex. We do not yet know how to make optimal use of computing machines in the solution of lens design problems, but machines do permit much more complex designs. Dr. Hopkins painted a dark picture for the future of optical production in this country. For short production runs of as few as six lenses, the United States is holding its own, but for large production runs we are not competing effectively. There is still vigorous competition between reflecting and refracting optics, and Dr. Hopkins is a refractive man. In his view there are only two instances where refractive optics could not do as well or better than reflective optics: where the aperture is very large, as in telescopes above 50 cm, and where the transmittance of available refractive materials provides a limitation. He indicated that only three or four optical glasses are really needed, in fact just one or two made well and inexpensively would be desirable, and designers of his view should agree to reduce the number of glasses that would be used. Such reduction would effect substantial savings without adversely affecting design. Aspheric surfaces can be made, but the cost is much higher than spherical surfaces and therefore they should be avoided. The inclusion of only one aspheric surface in a design can do only a limited amount of good; when used, all surfaces should be aspheric. He pointed out that a ruby laser helps to provide a small source for test purposes, but that it is not small enough. He uses a microscope objective to focus the beam on a pinhole 0.0127 mm in diameter. Lens design today has progressed to the point where we can predict the resolution of a lens and expect to achieve within 10 lines per millimeter of the predicted resolution. This could not be done 5 years ago.

The Adolph Lomb medal was awarded to Jean-Pierre Barrat of the University of Caen, France. This is the second time in a row that this medal has been awarded to a distinguished non-American scientist. Does this mean that we no longer have distinguished young scientists in America? Or are we simply becoming aware of accomplishment worthy of international recognition? Dr. Barrat's record of achievement is fabulous.

The principal speaker at the banquet was André Maréchal, Scientific Advisor to the Prime Minister of France, Professor of the Institute of Optics in Paris, and Vice President of the International Commission of Optics. Dr. Maréchal's address on "Some Considerations about the Organization of Scientific Research in France" was of interest to many of us who were anxious to learn how things are done over there, and more information on this subject is contained in a paper in the May issue of *Applied Optics* of which Dr. Maréchal is a co-author. On the lighter side, Dr. Maréchal quoted a new definition for the word Maser: *M*eans of *A*cquiring *S*upport for *E*xpensive *R*esearch!

In spite of the length of the meeting (4 days), the program committee was obliged to schedule triple sessions of contributed papers on both Friday morning and afternoon. The large number of contributed papers caused some members to reflect on the purpose of the papers. One member commented that he would like to see a requirement that each abstract contain a statement of the *importance* and *significance* of the material presented. This reporter also heard complaints about the fact that there was practically no time, when papers were not being presented, to view the 28 exhibits or to talk with the exhibitors. Exhibitors likewise indicated that business was slow at times. This may be a point for planners of future meetings to consider. Of course, there are those who contend that OSA should not indulge in instrument exhibits, but this reporter is of the opinion that the exhibits serve a useful purpose, and he ventures to predict that we shall have them periodically in conjunction with our meetings.

International Conference on Luminescence, New York University, October 9–13, 1961

Reported by Gordon E. Gross, Midwest Research Institute

To prevent duplication of what promises to be an excellent contribution to the literature of this field (the proceedings will be published by Wiley, New York) this report will present only some observations on the meeting: it would be futile to include even the briefest discussion of the more than fifty papers presented.

Luminescence studies lead to better materials for technical applications and yield much information concerning microscopic physical properties. At this meeting the emphasis was on the latter of these consequences, although much of the information which was presented will be of value to those with practical interests. Perhaps the most important over-all feature of the conference was that it brought together many of the world's leading workers in this field without regard to the oft present forbidden gap between the disciples of chemistry and physics.

The Eisner and Lubin Auditorium of the New York University Loeb Student Center at Washington Square provided excellent facilities for the nearly 200 who attended. Hartmut Kallmann and Grace Marmor Spruch, conference chairman and secretary, respectively, and their staff deserve hearty praise for the high quality of the technical sessions and for the care with which the conference was planned and managed.

The first session of the conference was devoted to the memory of two great figures in this field, Michael Schön and Georges Destrain. The audience included many of their colleagues, students, and friends. One gathered from the technical papers that the steady improvement of experimental methods, e.g., use of spin-resonance, cryogenic temperatures, flash spectroscopy, and very fast response photometric apparatus, is leading towards a fuller understanding of the luminescence processes. Several different models must still be used for convenience in describing different materials studied. The organic phosphors, in particular, require a language of their own for most analyses. This difference is particularly apparent in the long time decay phosphorescence resulting from excited triplet states of molecules whose ground states are of singlet character. In solid inorganic crystals, on the other hand, the lattice field effects generally obliterate identification of state multiplicity to such an extent that one seldom hears states thus identified. Also, in many inorganic phosphors the excitation process involves the conduction band and some well-localized impurity level. The molecular-organic luminescence studies reported deal most often with different electronic states of a given molecule or at most with electron transitions between a very few molecules. The differences in the models used for organic and inorganic cases probably arise more from tradition than from physical requirement. The use of structural diagrams of complex molecules is an aid to visualization of events occurring there. The appreciation of these differences and of the actual underlying similarity of all the arguments used by various workers is a very important part of the contribution which Dr. Kallmann and his group have made in holding this meeting.

A break in the meeting's activities was made at a cocktail hour and banquet held the last evening the group was together. After the banquet Professor J. Franck of the University of Chicago spoke on "Reminiscences on Personalities and Problems in the Era of the Development of Modern Sciences." This was a rare opportunity to hear of the role of individual personalities and the influence of outside pressures in shaping the history of modern science; and particularly to hear such from one who has known the personalities as well as the pressures throughout much of the period.

The conference was sponsored by the Air Force Aeronautical Research Laboratory; the Army Research Office, Durham; the Office of Naval Research; and New York University.

Joint Meeting of American Congress on Surveying & Mapping and American Society of Photogrammetry, Washington, D.C. March 11–17, 1962

Reported by K. Pestrecov, Nortronics

Latest developments in the fields of ground and aerial surveying and mapping were presented to the meeting in nearly 90 papers by members of industry, educational institutions, and government agencies. A number of papers were given by representatives of foreign organizations including W. H. Dougherty (AGA Corporation of America), D. A. MacFadyen and A. F. Soutar (Hunting Survey Corporation, Canada), K. Bertil Hallert (Royal Institute of Technology, Sweden)—a well-known regular participant in these meetings—and Herbert Trager (Zeiss-Aerotopograph, Switzerland). Many papers emphasized the trend, which started several years ago, toward a greater use of electronics for photogrammetric and data handling instrumentation. The aim of some of these electronic systems is automation of the mapping procedure. In the paper presented by A. B. Jacobs (Autometric Corporation) the advantages of electronic mapping systems were discussed, and a scheme was described which may be used for the establishment of a complete mapping procedure without the aid of photography. On the other hand, it may be of interest to the readers of this journal to note that optics continues to play an important role in mapping. This was emphasized by a relatively large number of papers on new optical developments and requirements. Some representative papers in this area include G. Bormann (Wild-Heerbrugg Instruments Ltd.) Small-Scale Photogrammetric Mapping with the Super Wide-Angle System and New Lenses for Aerial Survey and Photo Interpretation; Richard F. Gettys (U.S. Navy Hydrographic Office) A Test of 70 mm Format, $1^1/_2$-Inch Focal Length Photography for Topographic Map Compilation; J. Wiley Halbrook (U.S. Army Engineer Geodesy, Intelligence and Mapping Research and Development Agency) Ultra Wide-Angle Mapping; and George F. Ziegler (Bausch & Lomb, Inc.) The Use of Zoom Systems in Photogrammetry. Requirements for new techniques, instrumentation, and maps, arise mainly from the tasks imposed by space exploration, or reconnaissance from space. What was satisfactory for surveying and mapping on the earth's surface or from airplanes flying at the altitudes from up to about 3000 to 7000 m is not good for higher altitudes. Thus in aerial photography for civil mapping from altitudes of about 3000 m, the standard lens used is of 15.25-cm focal length and the photographic resolution on the film averages 22 lines/mm. If the same detail is to be recorded with the same lens from an altitude of 322 km, the required resolution should be near 230 lines/mm on the film. No photographic systems are known as yet that would produce this resolution over the whole field of coverage. However, this approach may be somewhat misleading because the resolution on the film is not a direct measure of the detail resolved on the ground, which is of primary interest to us. A more direct approach is to use angular resolution, which depends on the aperture diameter of optics used. The angle to be resolved is determined by the target size on the ground and its distance from the lens. Going to the extreme, let us say that we are interested in resolving about 30 cm on the ground. To achieve this from an altitude of 322 km, with diffraction limited optics (and assuming a high-contrast target), the optical system should be about a meter in diameter; and this creates a substantial problem for an optical designer. For greater altitudes, the required diameter of optics may become so large that a practical solution may be impossible. Then we have to accept a

compromise with regard to the detail size of interest to us.

Practically every domestic and foreign organization active in photogrammetry and its associated fields was represented by the exhibits (there were about 90 of them).

Many other problems arise from the requirements of space exploration and also from the necessity for a better knowledge of our own planet. For example, in the past topography of the moon was primarily of purely scientific interest, but it acquires practical importance as plans are made to land a man on the moon. From this arises the problem of preparing a good topographic lunar map. As was described by A. L. Nowicki (Army Map Service) steps are being taken to prepare such a map of the visible surface of the moon at a scale of 1:5,000,000 with 1000-m contours.

A very interesting new method for aerial mapping was proposed by C. S. Draper (MIT) in his keynote address "Inertial Methods in Mapping." He outlined a system that could combine inertial guidance instrumentation, as is used in some missiles, with photography, to pinpoint accurately submarine regions, small islands in the open oceans, and remote mountain regions. A better knowledge of ocean floors has also gained in importance. G. H. Keller and C. W. Culkin (U.S. Navy Hydrographic Office) proposed the use of photogrammetry for this purpose, and outlined a stereo photographic system that would be capable of mapping underwater features in the same way as terrestrial mapping is accomplished by means of aerial photography.

The meeting provided a number of social gatherings with the aim of promoting personal contacts, but the attendance at such affairs has been growing so large over the years that it has become difficult to meet and converse with your acquaintances and make new contacts.

PATENTS

continued from page 512

3,029,700 April 17, 1962 (Cl. 88-57)
Variable magnification afocal lens converter.
W. H. Price. Assigned to Eastman Kodak Company. Filed Nov. 25, 1959.

This patent discloses an afocal zoom converter for use in front of the lens on an 8-mm motion-picture camera. The system comprises a fixed front positive cemented component with the negative element leading; an internal sliding negative cemented component with the positive element leading; and a rear positive element which is cam operated to maintain a fixed image position on the film, the whole being subject to a series of inequalities. Two numerical examples are given. R.K.

3,030,860 April 24, 1962 (Cl. 88-57)
Projection optical system.
J. D. Hayes. Assigned to Bausch & Lomb, Inc. Filed March 28, 1960.

A short-focus reversed-telephoto lens made entirely of nonbrowning glass is described, consisting essentially of a reversed Galilean telescope mounted in front of a 4-element lens similar to that shown in U.S. 3,018,688. The aperture remains at its former value of $f/2.8$, but the angular field has been increased from $\pm 17°$ to $\pm 25°$. R.K.

3,030,861 April 24, 1962 (Cl. 88-57)
Variable-power optical system for microscopes.
D. C. Mortimer and R. L. Seidenberg. Assigned to Bausch & Lomb, Inc. Filed June 29, 1959.

A 3-component approximately afocal zoom system is mounted between a microscope objective and the primary image formed by it, to give a variable magnification to the final image formed in the eyepiece of the microscope. The first of the three components of the zoom system is a fixed positive doublet, the second is a sliding negative doublet, and the third is a sliding positive doublet which is driven by a U-shaped cam to maintain a constant image position. The negative Petzval sum of the zoom system helps to reduce the field curvature of the microscope. R.K.

3,030,862 April 24, 1962 (Cl. 88-57)
Bayonet coupling for cameras.
K. Gebele. Assigned to Compur-Werk F. Deckel. Filed Oct. 19, 1959 (in Germany Dec. 23, 1958).

A bayonet mounting for attaching a lens to a camera is described, in which a screw clamp is provided to hold the mating parts together after engagement, and thus improve the support of a heavy lens. The screw clamp should be of the same size as, and mounted close to the bayonet portion itself so that both can conveniently be rotated together. R.K.

3,030,863 April 24, 1962 (Cl. 88-57)
Zoom type of variable magnification optical system for attachment to photographic objectives.
J. M. Schwartz and G. F. Ziegler. Assigned to Bausch & Lomb, Inc. Filed Dec. 28, 1959.

A highly corrected 3-component afocal zoom attachment is described for use in front of a movie camera lens, comprising two positive doublets surrounding a sliding negative component, the whole system being symmetrical. Three examples are included each yielding a 3:1 range of over-all focal lengths, the image being held stationary during a zoom by a cam which gives the front component an appropriate in-and-out motion while the middle component moves linearly. The claims give relations between the equivalent V-numbers of the various components, and a series of inequalities governing the other constructional data. R.K.

3,033,693 May 8, 1962 (Cl. 106-47)
Infrared transmitting and absorbing glasses.
E. Carnall, Jr., L. S. Ladd, D. S. Cary, and W. F. Parsons. Assigned to Eastman Kodak Co. Filed Dec. 10, 1954.

Selenium glasses, containing additives such as As, As_2S_3, As_2Se_3, As_2Te_3, Te, $TeSe_2$, P, P_2S_5, P_4Se, P_2Se, P_4Se_3, P_2Se_3, P_2Se_5, Tl_2Te_3, Tl_2Se_3, and S, are described. Some of the glasses have good infrared transmission while others are highly absorbing. The absorbing glasses are of interest because the absorption of energy in close proximity to certain infrared detectors is of importance. The refractive indices are reported to be in the range from 2.5 to 2.8 at 2 μ. The use of additives improves the thermal stability of glassy selenium. G.W.C.

3,019,693 Feb. 6, 1962 (Cl. 88-14)
Method of determining azimuthal distribution of a system of lineal elements.
H. W. Patnode. Assigned to Gulf Research and Development Co. Filed Dec. 22, 1958.

The azimuthal distribution of any system of lineal elements capable of representation by contrasting degrees of transparency of a thin sheet e.g., a photographic negative, can be determined by superimposing a pair of identical image sheets and evaluating photometrically the transmission of light through the pair as one image sheet is displaced laterally from a condition of exact registry by an amount equal to the average width of the lineal elements and, maintaining that displacement constant, varying the direction of the dislpacement. Apparatus for conveniently practicing the method is described. R.D.A.

3,020,165 Feb. 6, 1962 (Cl. 106-540)
Low-viscosity glass compositions.
E. K. Davis. Assigned to Bausch & Lomb, Inc. Filed July 5, 1960.

The compositions of glass are given that have low viscosities, low refractive indices, and coefficients of thermal expansion matching those of many optical glasses. The glasses can be worked in the temperature range from about 1700 to 1900°F (912.4 to 1023.6°C) and are used for cladding fibers made from optical glasses. The refractive indices of the glasses of this invention are about 1.520. G.W.C.

3,015,983 Jan. 9, 1962 (Cl. 88-14)
Method and flame generating apparatus for flame photometry.
J. J. J. Staunton. Assigned to Coleman Instruments, Inc. Filed Sept. 29, 1954.

A method and apparatus are described for creating a stable, concentrated, high-temperature flame capable of efficient optical focusing onto an associated photometric device. The burner embodies an atomizer for injecting into the base of the flame a mist of sample liquid which ionizes to produce radiation spectra characteristic of the elements contained in the liquid. A mechanism attached to the access door for conveying the sample container to the capillary tube of the atomizer prohibits opening the door when the container is in its working position. R.D.A.

3,018,375 Jan. 23, 1962 (Cl. 250-77)
Viewing apparatus for amplified x-ray images.
E. B. Graves and E. J. Bastin. Assigned to Picker X-ray Corp., Waite Mfg. Div. Inc. Filed Nov. 19, 1959.

This apparatus consists of a beam splitter and a mirror mounted on a movable carriage. It allows either a screen, a television camera, or a fluoroscopic cine camera to be brought into the path of the x-ray beam. The amplified x-ray image can then be monitored by any or all of these three devices. J.MA.

3,019,694 Feb. 6, 1962 (Cl. 88-14)

Refractometer.

R. J. MELTZER. Assigned to Bausch & Lomb, Inc. Filed July 3, 1959.

An improved form of the Pulfrich refractometer is described, in particular for use in measuring the amount of protein in serum samples. Initial compensation for temperature is achieved by moving the refracted light-ray image with respect to a fixed reticle, with the help of a water sample at the serum temperature. The samples are placed on top of the refracting prism, which is rigidly cemented to the refractometer housing with the help of a cylindrically shaped flat-topped, buttonlike portion used to facilitate assembly. G.W.S.

3,019,698 Feb. 6, 1962 (Cl. 88-16.6)

Photographic methods and apparatus for use in cameras and projectors.

S. L. SHELDON. Filed Apr. 20, 1953.

The object of the invention is a device to take and project still and motion pictures in three dimensions using a single camera, a single projector, and a single strip of film, which can be projected on any convenient surface and viewed without the aid of filters, and can be seen and enjoyed even by a person with one eye. The camera uses a system of prisms to expose simultaneously adjacent frames. A similar system is used in projection, with adjustable weak prisms to permit the images to be superimposed. Shutters used in projection permit the right and left eye images to be presented sequentially "in such rapid succession that the eye is not aware of the change and transmits the two pictures to the brain as one." D.E.W.

3,020,794 Feb. 13, 1962 (Cl. 88-14)

Spectrometer grating control arrangement.

A. REICHEL. Assigned to Ernst Leitz, GmbH. Filed Apr. 3, 1961 (in Germany Apr. 23, 1960).

A mechanical pulley, cable and nonlinear cam arrangement is described for rotating a recording drum in synchronism with the rotation of a diffraction grating in recording spectrometers. G.W.S.

3,023,318 Feb. 27, 1962 (Cl. 250-237)

Optical switching.

J. H. JONES. Filed Jan. 27, 1960.

A system in individually movable pairs of light-transmitting masks is operated by electromechanical relays from coded information recorded on a moving film passing under the system, and actuating a photoelectric receiver. One purpose of the optical switching system is to help in the control of computers by a saving of circuitry over comparable electrical devices. G.W.S.

3,033,080 May 8, 1962 (Cl. 88-57)

Gauss-type photographic objective consisting of five lens elements arranged in four components.

JIRO MUKAI. Assigned to Canon Camera Co. Filed Oct. 27, 1958.

A five-element Gauss-type objective of aperture $f/1.9$ covering a semifield of 24° is described, the third component (the rear negative) being a thick single element. There is a single picture claim describing the construction of the objective. R.K.

3,033,081 May 8, 1962 (Cl. 88-57)

Photographic teleobjective.

C. BAUR AND C. OTZEN. Assigned to Agfa A.G. Filed Oct. 28, 1958 (in Germany Nov. 5, 1957).

A high-aperture ($f/2$ or $f/2.8$) teleobjective covering a moderate field ($\pm 10°$ or $\pm 15°$) is described, having a front vertex to back focal distance almost equal to the focal length, the front member being a strongly telephoto form, followed by a weak positive rear member. The objective contains, in order, two single positive meniscus elements, a strong cemented negative meniscus, and, after a long airspace, a weak positive cemented meniscus component in the rear. The claims contain a number of limits which govern the construction. Three numerical examples are included. R.K.

3,033,082 May 8, 1962 (Cl. 88-57)

Inverted telephoto objectives.

P. A. MERIGOLD. Assigned to Rank Precision Industries, Ltd., trading as Taylor, Taylor and Hobson. Filed Oct. 12, 1959 (in Gt. Britain, Apr. 13, 1959).

Four inverted telephoto systems are disclosed, of high aperture ($f/1.4$ to $f/1.8$) and covering a wide angular field ($\pm 34°$ to $\pm 40°$). The front member in each case consists of two negative menisci, being a cemented doublet followed by a single element. The positive rear member is essentially a modified triplet in which each positive component has been divided into two positive elements, while the negative component is a cemented doublet. There are 10 claims, containing a large number of inequalities dominating the design. R.K.

3,035,487 May 22, 1962 (Cl. 88-57)

Variable power optical system.

J. M. SCHWARTZ. Assigned to Bausch & Lomb, Inc. Filed Feb. 15, 1960.

An optically compensated $f/1.5$ zoom projection lens for 8-mm projectors is described, covering a focal-length range from 15.6 to 26.5 mm. The system comprises a fixed rear triplet and a front zoom portion consisting of two coupled sliding positive elements with a fixed negative element between them. The various constructional data are controlled by a long series of inequalities. R.K.

3,035,490 May 22, 1962 (Cl. 88-57)

Ultraviolet lens.

T. E. TIBBETTS. Assigned to International Business Machines Corp. Filed Dec. 31, 1958.

A modified triplet lens of aperture $f/2.5$ made entirely of fused quartz and lithium fluoride is described, for use in a wavelength range from 2300 to 2700 Å, at 5:1 reduction. The semifield covered is 7°. The front and middle components of the triplet are single elements, the rear component comprising two positive elements followed by a weak negative element. R.K.

---

photo Jacqueline

Andre Maréchal *France* and N. G. Basov *USSR* during the OSA–Washington March 1962 Meeting. (See also pages 516, 539, and 544.) The paper presented by Dr. Basov to the March meeting will probably be published in the September issue of *Applied Optics*.

BOOKS

continued from page 496

Abstracts of Photographic Science and Engineering Literature (APSE). EDITED BY HENRY M. LESTER. Department of Graphics, Columbia University, New York, in cooperation with the Society of Photographic Scientists and Engineers. Monthly. Per year: $60.00 industrial, $40.00 educational, $10.00 individual.

We are happy to welcome a new abstract journal to the photographic scene. When the well-known Kodak *Monthly Abstract Bulletin* and the Ansco *Abstracts* announced that they would cease publication at the end of 1961, the Society of Photographic Scientists and Engineers decided to operate an abstract service of its own. The first issue of the new journal has now appeared, under the general editorship of Henry M. Lester, with an extensive and competent advisory board. The subjects to be covered by *APSE* are those aspects of physics and chemistry that apply to photographic processes, photographic equipment of all kinds, the many applications of still and motion-picture photography in government, science, and industry, and nonsilver processes. At the present time 250 journals and the patent files are being scanned by a team of abstractors for papers of photographic interest. A novel and valuable feature of this journal is the use of "descriptors" at the head of each abstract, enabling the reader to decide rapidly which abstracts are related to his immediate problem. For example, a typical abstract chosen at random is headed:

Descriptors: SILVER BROMIDE; CYANINE DYES; MICRO-CRYSTALS; ELECTRON SPIN RESONANCE.

The magazine will appear monthly, each issue containing about 400 abstracts. Annual indexes are planned, based on the "descriptors" appearing at the head of each abstract.

R. KINGSLAKE

---

photo Jacqueline

A. M. Prokhorov *USSR* and S. Silverman *ONR* during the OSA–Washington March 1962 Meeting. See also pages 516, 539, and 543.

Papers to appear in subsequent issues

We have had so many papers submitted for publication since *Applied Optics* was announced last year that we have already built up a backlog which is as embarrassing for a new publication as it is a demonstration of the need for this journal. We are doing our best to publish papers as quickly as we can by bringing out bigger issues than had originally been intended this year, and becoming a monthly in 1963. The Editors wish to express their sincere appreciation to all contributors who have thus demonstrated their faith in *Applied Optics*.

Luminescent Processes and Decay Laws in Crystalline Materials —*Pernick*
Durable Narrow Absorption Band Infrared Filters Utilizing Powdered Mineral Materials on Polyethylene Substrates—*Carlon*
Thermal Radiation from a Hemispherical Source in Contact with an Infinite Plane—*Kester and Minardi*
New Backscattering Computation and Tables for Dielectric and Metal Spheres—*Adler and Johnson*
Photoelectron Energy Distribution Measurements of 10 to 50 ev Photons with a Planar Analyzer and Electron Multiplier—*Heroux and Hinteregger*
Total Absorptance of CO, CH_4, in the Infrared—*Burch and Williams*
Total Absorptance of CO_2 in the Infrared—*Burch et al.*
A Microwave Powered Hydrogen Lamp for Vacuum Ultraviolet—*Warneck*
Emittance Measurements on Infrared Windows Exhibiting Wavelength Dependent Diffuse Transmittance—*Hatch*
Total Absorptance of Water Vapor in the Near Infrared—*Burch et al.*
Simulating the Solar Spectrum with a Filtered High-Pressure Xenon Lamp—*Boettner and Miedler*
Cloud Chamber for Optical Measurements of Aerosols—*Speyer*
Nine-Channel Polychromator for Observation of Time-Dependent Spectral-Line Profiles—*Spillman et al.*
Isocon Scan—A Low-Noise Wide-Dynamic-Range Camera-Tube Scanning Technique—*Cope and Borkan*
Polarization by Reflection and Some Optical Constants in the Extreme Ultraviolet—*Cole and Oppenheim*
Low Pressure Mercury Arc for Ultraviolet Calibration—*Childs*
Selected Ordinates for Solar Absorptivity Calculations—*Olson*
Design Theory for a Submersible Scattering Meter—*Tyler*
High-Speed Calculation of Diffusion Coefficients from Rayleigh Interference Fringes—*Hook et al.*
Comparison of AM and FM Reticle Systems—*Carpenter*
Effects of Telescopes on Astronomical Polarization Measurements—*Miller*
Modifications of a Beckman Spectrophotometer for Direct Measurements of Spectral Energy Distribution of Light Sources—*Grum*
A Study of the Angular Response of Lead Sulfide Photoconductors —*Schaefer*
Wedge-Immersed Thermistor Bolometer—*Dreyfus*
Quelques Resultats Nouveaux dans la Mesure des Indices de Refraction (Liquides et Solides) dans l'Infrarouge—*Geisse and Lecomte*
Production and Use of Variable-Transmittance Sinusoidal Test Objects—*Lamberts*
Analytical Radiation Model of the Earth—*McGee*
Two Light Sources for Use in the Extreme Ultraviolet—*Newburgh et al.*
Detectivity of Infrared Photodetectors—*Nudelman*
A Simple Voltage Amplifier for Photovoltaic Cells—*Paix*
Generation of Sinusoidal Light Intensity—*Julich*
Immersed Radiation Detectors—*Jones*
An Automatic Rapid-Scanning Spectrophotometer to Study Thermoluminescence Spectra—*Ghosh*
Use of a Kaleidoscope to Obtain Uniform Flux over a Large Area in a Solar or Arc Imaging Furnace—*Chen et al.*
Spatial Distribution of Light Across the End of a Ruby Laser—*Weisman*
Measurements of Second Harmonic Generation of the Ruby Laser Line in Electric Crystals—*Savage and Miller*

Applied Optics — Of Optics and Opticists

This column is compiled partly from information sent by our Reporters in various centers of optics across the continent, but the Managing Editor welcomes news from any source

> We know a subject ourselves or we know where we can find information on it.
>
> *Samuel Johnson*

"New computer programs for the automatic design of optical systems are beginning to produce spectacular results," reports **R. E. Hopkins,** director of the University of Rochester's Institute of Optics. Advanced high-speed computers are making it possible to trace rays through complete systems in the time the older computers required to deal with a single surface. A new program in use at the Institute corrects third- and fifth-order aberrations automatically. The program was tried out recently on a three-element design with the glasses picked to correct the secondary color. The machine corrected third-, fifth-, and seventh-order spherical aberration, coma, axial color, and secondary color in less than two minutes. (This work would have taken forty hours, if performed manually.) This journal will feature **Lens Design and Computers** in September 1963, with **Donald P. Feder** of Eastman Kodak as feature editor for that issue.

A medal in honor of C. E. K. Mees, founder of the Eastman Kodak Company Research Laboratories, was announced recently. Called the **C. E. K. Mees International Medal,** it bears the motto "Optics Transcends All Boundaries," and it will recognize the extension of the frontiers of optics as Dr. Mees himself extended photography. The award will be made during the OSA October 47th Annual Meeting in Rochester, N.Y. This year marks the 50th anniversary of the beginning of Dr. Mees' career in the U.S.A. . . .Another award to be made during the OSA Rochester meeting will be of the **Ives Medal** to **Max J. Herzberger** of Eastman Kodak. . . .Newly elected Fellows of the Royal Society of London include **R. W. Ditchburn** *Reading* and **R. A. Smith** *Sheffield,* both of whom have been in this country recently, and **H. L. Welsh** *Toronto.*

The **OSA Rochester Section** is considering at the present time a proposed Boy Scout or Explorer Scout Merit Badge for Optics. Rochester Section members are also taking part in the Rochester Area Educational TV Association (RAETA), which group is trying to obtain an educational TV station for Rochester. If this is achieved, a weekly half-hour program devoted to optics is proposed. . . .The **Optical Society of Northern California** is now in its second year with some sixty members holding regular bimonthly meetings. One of the recent meetings had **Herman Schepler** of **Space Technology Laboratories** speaking on "Azimuth Aiming of Ballistic Missiles." Since Dr. Schepler is also a psychologist and hypno-technician, he was able to add some sidelights to his presentation with the application of optical materials used in hypnosis.

Applied Systems Corporation is active in Palo Alto, Calif., and has recently been joined by **Herbert Berman** as its Director of Optics . . . .**Dorman E. Priest,** previously vice president for Engineering at Callidyne, has been appointed Technical Director of **Research and Control Instruments, Inc.** of Woburn, Mass . . . . **C. J. Billian** has joined the **Servo Corporation of America** as a senior materials engineer, to work on the development of new infrared transmitting materials . . . .**David Richardson,** internationally recognized authority on diffraction gratings and member of the OSA Board of Directors, has been promoted to Staff Engineer in the Scientific Instrument Division of **Bausch & Lomb, Inc.**

For Eyes to See, a new 16-mm movie in color and sound, has been released by Bausch & Lomb, Inc. Documenting optical products and scientific instruments at work, the movie illustrates typical manufacturing operations and basic optical principles. Running time is 28 minutes; black and white copies are available for TV use. . . .Readers' attention is drawn to two National Bureau of Standards Monographs: *Theory and Methods of Optical Pyrometry* by H. J. Kostkowski and R. D. Lee (No. 41) and *Thermocouple Materials* by F. R. Caldwell (No. 40). Both of these may be obtained from the U.S. Government Printing Office, Washington 25, D.C. . . .and to a new AEC Report SCR-308 *Optical Inspection Device Using Fiber Optics,* which is available from the Office of Technical Services of the Department of Commerce for **$0.75.**

The **National Bureau of Standards** announced the collaborative establishment of the **Joint Institute for Laboratory Astrophysics** (JILA) on the CU Campus at Boulder, Colo. JILA will be a unique permanent academic unit devoted to research and advanced training of students in areas of physics and astrophysics vital to the expanding U.S. space program. The Institute will also complement the growing complex of industrial, governmental, and educational space-age research and training in the Boulder area. **Lewis M. Branscomb,** Chief of the Atomic Physics Division of the NBS in Washington, and eight other NBS atomic physicists will move to Boulder this summer, and, together with two astrophysicists now at the NBS Boulder laboratories—**R. N. Thomas** and **J. T. Jefferies**—and a group of CU scientists headed by **Wesley Brittin,** Chairman of the Physics Department, will be the initial professional staff of JILA.

The **Office of Aerospace Research** recently awarded the following contracts among others: Univ. of Illinois, D. F. Holshouser *Modulation of Light by Electro-Optical Means* $49,975; Polytechnic Inst. of Brooklyn, E. Weber *et al. Research in Electromagnetic Theory and Information Processes* $175,000; Essex College of Assumption Univ. of Windsor, Ont., L. Krause *Optical Pumping of Alkali Metal Vapors* $16,894; Univ. of Chicago, F. F. Rieke *Fundamental Research on Optical Sciences* $6,976; Univ. of Illinois, P. D. Coleman *Studies in Quantum Electronics* $25,000; Purdue Research Foundation, A. K. Kamal *Investigation of the Energy Output Properties of a Ruby Laser* $8,000. . . .The AF System's Command's Rome Air Development Center at Grifiss AFB has awarded a $188,570 contract to Electro-Optical Systems, Inc., for work in optical surveillance devices and techniques using lasers.

Three of the companies now commercially producing lasers are the **Perkin-Elmer Corporation** who announced, with **Spectra-Physics** of Mountain View, Calif., the availability of a low cost, continuous-wave gas-phase laser. . . .A ruby laser modulation system using a Kerr cell shutter and associated equipment has been developed by **Electro-Optical Instruments, Inc.,** of Pasadena, Calif., designed principally for application in optical harmonic generation, optical ranging, and materials research . . . .**Hughes Aircraft** will also market ruby lasers commercially. . . . **Bausch & Lomb, Inc.,** is exhibiting an Anti-Laser Safety Eyeshield, the first announced technological development for the protection of the eyesight of workers in the laser field. . . . Two new Spectronic 20's expand **Bausch & Lomb's** colorimeter range to include electronically regulated and battery-operated models, in addition to an improved standard instrument. Design innovations include built-in power regulator, a rapid warm-up period, and constant temperature in the sample chamber. Also noteworthy is the new electronic colorimeter-spectrophotometer, containing a unique light-intensity-monitoring system for 105–125 volts, 50 or 60 cycle ac. Another new B&L instrument is their high-intensity monochromator, with a completely integrated monochromatic system offering compactness, portability, high efficiency in the ultraviolet, infrared, and visible regions, and a cost some 40% less than current comparable systems. The system incorporates three component parts, the monochromator proper, grating-cover assembly, and a choice of four illuminators with appropriate power control units. Five grating assemblies are available, each covering a specific spectral range and yielding a different dispersion. Over-all range of these five is 1800 to 32,000 Å. A set of three fixed slits is standard equipment and a variable slit assembly is offered as optional equipment. These are readily interchangeable and automatically aligned. The reciprocal dispersion in the ultraviolet range is 3.2 mμ/mm. . . . Direct chemical immersion of stable infrared sensitive lead sulfide photoconductors onto high-refractive-index optical materials, resulting in simpler electrooptical system design and increased detector sensitivity, has been announced by **Infrared Industries Photoconductor Division.** Depending on the optical material, sensitivity gains as high as 85% can be attained by replacing a conventional plate-type photoconductor with a reduced-area photoconductor immersed on a simple hemispherical lens. The reduction in sensitive area, and correspondingly enhanced signal-to-noise, is a function of the refractive index of the lens material as well as lens configuration. . . .**Itek Laboratories,** a division of Itek Corporation, has announced the availability of a wide range of resolving power test patterns based on MIL STD 150 A for use in testing and evaluating photooptical and electrooptical equipment, systems, and processes. Further information is available from their Photographic Technology Department in Lexington, Mass. . . . An ultrahigh speed Kerr cell framing camera capable of taking six frames at a rate of 100,000,000 frames per second and with exposure times as brief as five nanoseconds (μsec) was demonstrated recently by **Electro-Optical Instruments.** Built around the high optical resolution and brief exposure time Kerr cell shutter, this high-speed framing camera permits observation from one line of sight and can record on Polaroid film in instances where rapid evaluation is desired. It may also be used with high-speed fine-grain cut films offering higher optical resolution. . . . A series of small, rugged telescopes that weigh up to two-thirds less than comparable conventional instruments was announced recently by the **Perkin-Elmer Corporation.** Capable of providing a high quality image over a narrow field of view, the telescopes may be used for star tracking guidance and navigation in aircraft, satellites, and space vehicles . . . .Perkin-Elmer has established a new facility for the manufacture of crystalline $CaCO_3$ (calcite) optics to meet the increasing need for high quality polarizing optics.

At the 46th Annual Exhibition of the **Institute of Physics and the Physical Society** held in London earlier this year, masers and lasers were among the exhibits. One maser shown by the **Royal Radar Establishment** used a ruby and is cooled by liquid nitrogen. It has a gain of 20 decibels with a bandwidth of 1.5 Mcps centered on a signal frequency of 9×10^9 cps. RRE plans to use rutile (TiO_2) with iron (Fe^{+++}) doping in a maser operating at 35 gcps and expects to obtain efficient operation at a pump frequency of 70 gcps by use of a push-pull orientation of the crystal. The slow-wave structure will consist of a dielectric-filled waveguide propagating a circularly polarized TE_{11} mode. Liquid helium will be used which will enable the magnetic field to be produced by a solenoid of superconducting materials. RRE also demonstrated a ruby laser, amplifying light at a resonance radiation wavelength of 6943 Å. In addition they are working on a c.w. helium-neon gas laser, producing oscillations near 1 μ wavelength. . . .The **National Physical Laboratory** (Teddington, England) also demonstrated a laser, used as an oscillator, employing a spherical reflector designed to optimize the optical coupling between a ruby rod and a linear xenon flashtube. NPL also had on show a laser-amplifier containing two similar flashtubes inside a double-cylinder reflector. The amplifier is still in the prototype stage. NPL also has a helium-cooled $Sm^{++}CaF_2$ laser under construction, and they are developing optical devices whereby it is hoped to stabilize the frequency and power level of a laser by coupling it to an external passive resonator. . . .Readers' attention is drawn to the small report by R. A. Smith on maser and laser applications in *Nature* May 5.

Laser for plasma temperatures? The very high intensity of light from the optical maser, combined with its extremely narrow bandwidth, may make it useful as a means of measuring the electron temperature and relative density in a plasma. T. P. Hughes of AEI's Aldermaston Research Laboratory suggests in *Nature* (Vol. 194, p. 268) that it should be possible to detect the Doppler broadening of a spectral line from a laser resulting from scattering of the light by the free electrons in the plasma. The Doppler effect is directly caused by the thermal motion of the electrons and thus, by measuring the relative intensity of the scattered light for different wavelengths the temperature of the electrons can be determined. Moreover the over-all intensity of the scattered light is a function of the electron density which might conceivably be calibrated against the scattered intensity produced by a plasma of known electron density. The author suggests that it might be necessary to reflect the master light back and forth across the plasma several times to enhance the effect, which is rather a small one because the electron densities of plasmas are insufficient to produce a large amount of scattering. A photomultiplier would be used for detection of the scattered light, which would be distinguishable from the normal light emitted by a hot plasma on account of polarization accompanying the scattering process. The method should enable the temperature of a hydrogen plasma to be determined over a range of from 10,000°K to 10 million°K and should prove useful in thermonuclear research.

The Editors would like to take advantage of a few lines of space at the bottom of this column to congratulate Mr. and Mrs. Herman Friedman on the birth of their first child David Llewellyn and to use the opportunity to thank Mrs. Friedman for all she has done, in the backroom, to make *Applied Optics* what it is.

ADVERTISING

Advertising Agent | ALFRED P. OPPENHEIM
Assistant | RUTH STEGER

Advertising inquiries, orders, plates, and correspondence should be addressed to the APPLIED OPTICS Advertising Office, 55 West 16th Street, New York 11, New York. CHELSEA 2-1311

Two new stars are born: 8″ (left) and 5″. We can't tell you all about them on this small page, so write for comprehensive literature to: Tinsley Laboratories, Dept. A, 2448 Sixth Street, Berkeley 10, California.

*No price? No. What appears to be a simple 5″ scope is actually the basic component of many versatile optical systems, individually accessorized. For precise information, send letter with requirements.

Gentlemen: I am interested in applications of your new ☐ 8″ or ☐ 5″ telescope in

☐ Secondary School
☐ Research in Industry
☐ Private Observatory
☐ University or J. C.
☐ Astronomy club
Hobby: ☐ Astronomy, ☐ Photography

Name_____ Street & No._____

State_____ City_____

Company or Institution_____ Title_____

OSA Group Flight to Europe

JULY 1963

OSA is exploring the possibility of a Group Flight **next year** to tie in with the IUPAC Congress and Commission Meeting in London 11–14 July and with the possible meeting of the European Spectroscopy Group in Budapest the following week. A tentative flight schedule could be a round trip leaving New York Monday 1st July 1963 in the evening, with stopovers in Lisbon, London, Zurich, and Budapest, returning to New York on Monday 29th July. Such a round trip ticket would cost $401 plus $9 handling charge, i.e., $410. A minimum of 25 participants would be required, and this 25-minimum would have to travel as a group from stop to stop to take advantage of the reduced group fare. A possible schedule could be:

New York/Lisbon—1st July thru 5th July
Lisbon/London—5th July thru 15th July
London/Budapest—15th July thru 20th July
Budapest/Zurich—20th July thru 29th July
Zurich/New York—29th July

Alternatively, we could leave earlier and return directly from Budapest with no stopover in Zurich. (See reply form below.)

Would members who are interested in principle (there is no commitment) return the form below to OSA, so that the Assistant Secretary may gain an idea of the potential interest.

REPLY

Assistant Secretary, OSA
1155 Sixteenth Street, N.W.
Washington 6, D.C.

GROUP FLIGHT JULY 1963

( ) I am interested in principle in the OSA GROUP FLIGHT N.Y.-Libson-London-Budapest-Zurich-New York, 1st through 29th July 1963.

( ) I would prefer a 3-week trip to a 4-week trip, i.e., leave a week later . . . . return a week later . . . . .

( ) I would prefer the first stopover to be Zurich rather than Lisbon.

( ) I am a member of OSA and would be accompanied by . . . . . my wife
. . . . . children (how many?)

Name.....OSA membership No.....
Address.....
.....

FACTS FOR INFRAREDMEN ABOUT KODAK'S RUGGED POLYCRYSTALLINE OPTICS

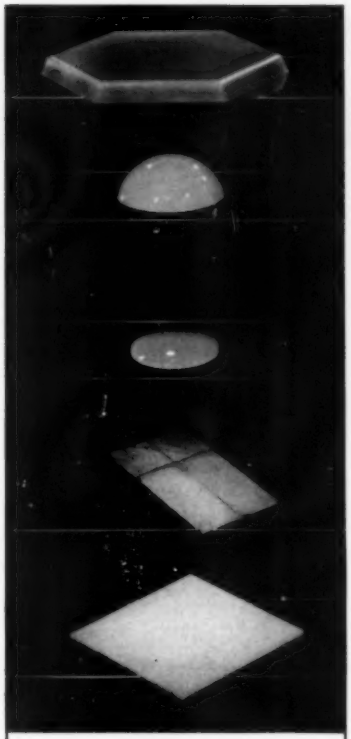

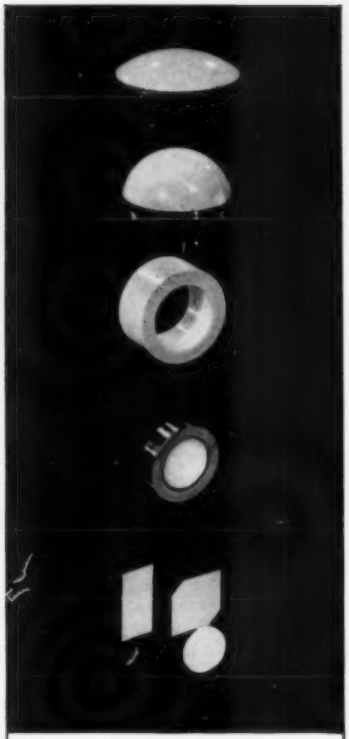

	IRTRAN-1	IRTRAN-2
RANGE:	2μ to 8μ.	1μ to 14μ.
REFRACTIVE INDEX:	1.37 to 1.31. Anti-reflection coating unnecessary and impossible. What would you use?	2.29 to 2.14. For lens power, deviation power, even a little dispersion power. Glad to coat.
MAXIMUM SIZE:	7-inch hemispheres. Other forms to 6½-inch diameter x 1 inch. Fusing extends possibilities.	6½-inch diameter x 1 inch. Stainless steel mounts can stand 600°C.
KNOOP HARDNESS:	576.	354.
ABRASION RESISTANCE:	Better than most conventional optical glasses.	Not quite as good as Irtran-1 but still better than many glasses.
THERMAL SHOCK RESISTANCE:	Survives quench from boiling water to 23°C. Good microwave characteristics.	Almost as good as Irtran-1. Resists more solvents than anything else we know for this transmittance band.

A big point of pride is the low emissivity. To achieve this relative immunity from blinding by high temperature, we have worked like galley slaves to get the absorption out. Lenses, domes, prisms, flats, filters. Some can even be shipped from stock. To get on the list of people we keep informed, write:

EASTMAN KODAK COMPANY
Apparatus and Optical Division
Rochester 4, N.Y.

Kodak
TRADE MARK

OPTICS AND SPECTROSCOPY

OPTICS AND SPECTROSCOPY publishes original experimental and theoretical studies in physical optics, atomic and molecular spectroscopy, spectroscopy of solids, luminescence, and general problems of electronic optics, photometry, applied optics, and optical instrumentation. **OPTICS AND SPECTROSCOPY** is the leading Russian journal in its field, its coverage corresponding in part to that of *J. Opt. Soc. Am.*, although the spectroscopy papers are more theoretical than analytical or instrumental. Luminescence and optical properties of materials are fully represented, instrumental optics, diffraction, and coherence problem less so.

OPTICS AND SPECTROSCOPY is published *monthly* in English translation, three months after the Russian original, e.g., the May issue appears in August.

SEND IN YOUR SUBSCRIPTION NOW

***OiS CLUB** Members of the following Societies may subscribe at the especially reduced rate of $11.00 per year: ASA, AAPT, ACS, ACA, AOCS, APS, ASTM, Ass.Tech.Phys.-Sweden, Can.Ass.Phys., Chem. Inst. Can., Coblentz Soc., Electrochemical Soc., IRDG-UK, IRIS, Inst. Chem.-India, Inst.Phys. and Phys.Soc.-UK, ISA, I-SCC, Netherlands Chem.Soc., PES Group-UK, SAS, SSP, Soc.Chem.Ind.-UK, SPSE, Soc. Anal.Chem.-UK.

---ORDER FORM

To: OPTICS AND SPECTROSCOPY
AIP Subscription Handling
335 E. 45th Street,
New York 17, N.Y.

Please enter subscription to **OPTICS AND SPECTROSCOPY** 1962 issues (Vols. XII and XIII) and continue until countermanded**

( ) **Special OSA member rate per year** $ 7.50
( ) **Special rate to members of Societies cooperating in OIS CLUB (see above)*** $11.00
( ) **Regular rate per year** $15.00
( ) **Single copy of issue** $3.00

Name of your Society.....

( ) Please send OSA membership information

OSA Membership No. .....

Name.....

Address.....

.....

.....

.....

** all subscriptions run through Jan./Dec.

CALIBRATED INTERFERENCE FILTERS

FOR PRECISE SPECTRAL ANALYIS

Optics Technology MONOPASS interference filters are designed for precise spectral analysis in the 400 millimicron to 2.7 micron region. MONOPASS filters permit highly sensitive spectral measurements since each filter passes only an extremely narrow band of wavelengths, and rejects all others from X-band to X-ray. Individual calibration curves for each filter assure pinpoint accuracy, with each curve set in laminated plastic and bound in a rugged volume for permanence. MONOPASS filters are available in complete sets, or may be ordered to specification.

VISIBLE SPECTRUM SET 10A includes ten MONOPASS filters to isolate principal lines as K, Ca, Hg, etc., from 706 millimicrons to 404 millimicrons, important in flame chemical analysis. Four neutral density filters and a linear spectral "wedge" filter are included. Price, $325.00.

VISIBLE SPECTRUM SET 12A includes ten MONOPASS filters uniformly spaced from 400 millimicrons to 700 millimicrons, as well as four neutral density filters and a linear spectral "wedge" filter. Price, $325.00.

INFRARED SET 15A includes ten MONOPASS filters spaced at every 0.1 micron between 0.8 micron and 1.75 microns. Price, $450.00.

INFRARED SET 20A includes ten interference filters on 1" diameter substrates spaced at every 0.1 micron between 1.75 microns and 2.75 microns. These filters are blocked out to 3.2 microns on the long end and to X-ray on the short end. Price, $450.00.

NEW! RUBY LASER SET 50A includes seven **all dielectric** mirrors and beam-splitters at several values of attenuation, designed to withstand high LASER powers without deterioration, plus MONOPASS Filter at 694 millimicron ruby wavelength. Price, $350.00.

OPTICS TECHNOLOGY, INC

248 Harbor Boulevard
Belmont, California
LYtell 1-0358 (Area Code 415)

SEND COUPON FOR THIS...

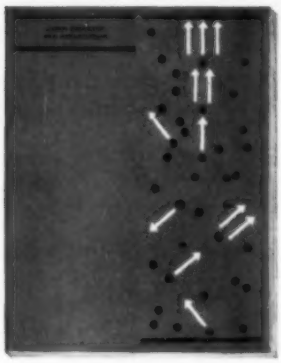

Free Laser Fact Folio

SEE RAYTHEON AD ON PAGE A3

RAYTHEON

MR. MARTIN B. CURRAN
RAYTHEON COMPANY, LEXINGTON, MASSACHUSETTS

■ Please send my copy of "Laser Research and Applications" by return mail.
I am primarily interested in:
( ) laser systems ( ) $975 laboratory head
(Specify application, if possible)

NAME _____
TITLE _____
COMPANY _____
ADDRESS _____
CITY _____ STATE _____

LASER DEVELOPMENT ENGINEERING

Raytheon's Bedford Advanced Development Lab (suburban Boston) has openings offering opportunity for unlimited professional development. Positions are immediately available for senior engineers for research and development in areas of optical and infrared masers as applicable in missile and space systems. May direct a small group of engineers currently engaged in a gas and solid-state laser program.

Applicants should have 5–6 years' experience in advanced development engineering in areas of physical optics, microwave spectroscopy, or microwave solid-state devices. M.S. required. Ph.D. in physics desired with a background in quantum mechanics, microwave spectroscopy and solid-state theory.

Interested candidates are invited to forward their resumes to Mr. Marvin Miller, Missile & Space Division, Raytheon Company, Bedford, Massachusetts. Or you may phone collect to Mr. Miller at CR 4-7100 ext 2138.

RAYTHEON

MISSILE & SPACE DIVISION

BEDFORD, MASSACHUSETTS

An Equal Opportunity Employer

DU PONT
REG U S PAT OFF

Offers A Career Opportunity In

OPTICS

A professional opening exists for an Optics Specialist in the Engineering Service Division of Du Pont's Central Engineering Department. This division's objectives are to anticipate the Company's technological needs and apply advanced engineering and scientific knowledge to improve existing and future Du Pont processes. Consultation and services are provided on problems in research, development, manufacturing, and sales.

•

The Optics Specialist will provide consultation to plants and laboratories in explaining and measuring optical behavior of unusual pigments, paints, dyes, fibers, films, and other products. He will develop and apply special optical and electro-optical devices for plant and laboratory problems in automatic measurement control and inspection. He will conceive, develop, and apply special lens, prism, and mirror systems plus related photoelectric and electronic equipment.

Location: Louviers Building-Wilmington, Delaware

Write in confidence to Mr. W. M. Redd
Engineering Department

E. I. du Pont de Nemours & Company
INCORPORATED
Wilmington 98, Delaware

An Equal Opportunity Employer

LASER OPTICS

Extend your capabilities for laser investigations by utilizing ISOMET's extensive crystal growing and precision crystal finishing facilities.

TESTED LOW THRESHOLD LASER CRYSTALS

Forms Available: Boules or fabricated rods with end polished optically flat and parallel.

Reflective Surfaces: Evaporated metallic coatings or multiple dielectric layers.

Types Stocked: CaF_2 doped with Sm^{2+}, U^{3+}, Nd^{3+}
$CaWO_4$ or $SrMoO_4$ doped with Nd^{3+},
Nd^{3+} doped glass

Custom Grown Types: CaF_2, CdF_2, BaF_2, $CaWO_4$, $SrMoO_4$, $PbMoO_4$ doped with any of the rare earths or transition elements.

UNUSUAL CAREER OPPORTUNITIES

Qualified optical physicists or engineers and optical technicians are invited to investigate the unusual growth positions now available at ISOMET. *Address resumes or telephone calls to Mr. Alan Whittaker.*

for prompt attention to your needs call Windsor 4-4100.

ISOMET
CORPORATION
434 Commercial Ave., Palisades Park, N. J.

FLASH TUBES

for LASER applications...
LARGEST VARIETY and RANGE of Sizes Available Today!

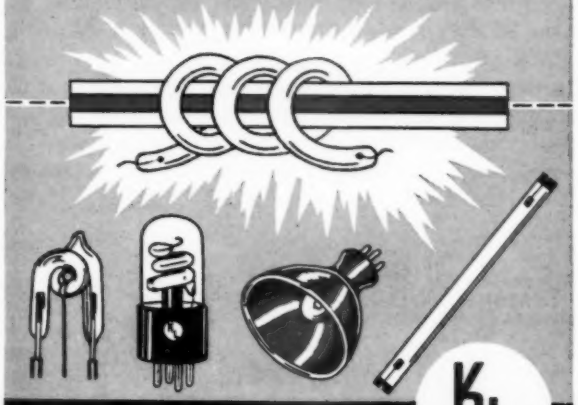

KEMLITE
LABORATORIES, INC.
1819 W. Grand Ave., Chicago 22, Ill.

THIN FILM (8μ) BEAM SPLITTERS

NO GHOSTS! NO REFRACTIVE ERRORS!

NOW!

- Flatness to 1/20 wave and parallelism to less than 1 fringe per inch; on order.
- Sizes up to 12″ diameter
- Large coating selection, including dichroics.

FOR FURTHER INFORMATION ON NPC PELLICLES, SEND FOR BROCHURE AO

NATIONAL PHOTOCOLOR CORP.
225 EAST 44TH STREET **NEW YORK 17, NEW YORK**

closed-cycle

IR COOLERS

...temperatures to 80° K
...introduce no microphonics
...need no support equipment

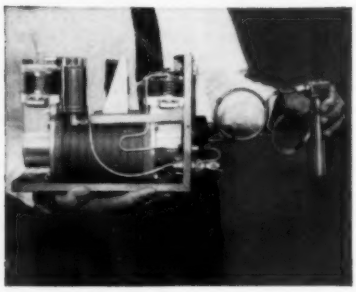

...These original systems utilize highly developed non-lubricated compressors and Joule-Thomson cryostats. Tests on both high- and low-impedance infrared detectors show that Air Products closed-cycle coolers introduce no microphonics into IR systems.

Reliable, compact Air Products cryogenic coolers include the following advanced features:

- **Dynamic balancers** counteract reciprocating motion of compressor pistons
- **Carbon-filled fluorocarbon resin piston rings** prevent gas contamination
- **Non-orificed heat exchangers** generate no measurable microphonics
- **Sound-absorbing mounts** prevent transmission of compressor-generated microphonics along gas lines

These closed-cycle cryogenic units for IR-detector cooling weigh as little as 16 pounds... measure 5" x 8" x 12" ... provide up to 5 watts of refrigeration at 80°K. Completely self-contained, they require no external liquefiers or high-pressure gas supplies.

For your IR-cooling requirements, consider using a closed-cycle refrigerator. It will enhance your system by reducing need for ground-support equipment.

ADVANCED PRODUCTS DEPARTMENT
DEFENSE AND SPACE DIVISION

Air Products and Chemicals INC.
Allentown, Pennsylvania

▶ Air Products manufactures a complete line of cryogenic electronic coolers.

INFRARED OPTICS

DOMES — LENSES — WINDOWS — PRISMS

SILICON TO 16" DIAMETER

GERMANIUM TO 24" DIAMETER

are CAST TO SHAPE by an advanced low-cost, production technique!

Many sizes in stock, including single crystal materials.

INDIUM ARSENIDE, GALLIUM ARSENIDE & INDIUM ANTIMONIDE are available in sizes up to 1" diameter.

Exotic Materials, Inc.

1534-E East Chestnut Ave. Santa Ana, California

Specialists in **LARGE** optical shapes

SUPPLEMENT ON OPTICAL PUMPING AND MASERS

An *Applied Optics* **Supplement** on Optical Pumping and Masers will be published in December 1962. This special edition will gather together all the papers in that area of activity published in *Applied Optics* during the first year of publication and include articles not previously published such as a survey of gas lasers by W. R. Bennett, Jr. In addition, a 15,000 word review will be written by O. S. Heavens, *Royal Holloway*, which will not only survey the present state of the art and give fundamental theories but will integrate all the papers published in the **Supplement.** This **Supplement** will be sold at not more than $5.00 a copy.

ORDER FORM

Optical Society of America
1155 16th Street, N.W.
Washington 6, D.C.

Please enter my/our order for the **APPLIED OPTICS FIRST SUPPLEMENT—OPTICAL MASERS,** to be published in December 1962 at a cost of not more than $5.00 a copy

Name.....
Address.....
.....
.....

COHERENT LIGHT for SYSTEMS DEVELOPMENT APPLICATIONS and RESEARCH STUDIES

NEW! *From Optics Technology...*

PRACTICAL AND VERSATILE PULSED LASER

"Zoom" telescope and transit mounting to facilitate aiming.

Adjustable Fabry-Perot multi-layer end reflectors for 6943 Å (ruby) or other LASER wavelengths.

Instrument is both coherent light source and LASER materials tester.

Peak Power: 1-2 Kilowatts (nominal) with ruby materials.

Optical System: LASER material (up to 4½" in length and ½" diameter) is positioned at one focus of an elliptical mirror, cylindrical flash lamp at other focus achieves high-efficiency optical coupling.

Pulse Width: Approximately 0.5 milliseconds.

Power Supply: Variable 0 to 1,800 volts dc; built-in Kilovolt meter; available in two capacities: Model 100A Power Supply (400 joules) or Model 100B Power Supply (800 joules).

Reflectors: Multi-layer interference reflectors with absorption and scattering <0.2% (nominal).

Price: Model 100 LASER head and cradle; with Model 100A Power Supply, $2810.00; with Model 100B Power Supply, $2965.00.

For additional information, write or call OTI or your nearest OTI representative:

New England, H. J. Schuft Co.; New York, RMC Associates; Syracuse, E. Stone & Co.; Mid-Atlantic, C. E. Snow Co.; S. California, Abbott Instrument & Engineering Co. N. California, Long & Associates

OPTICS TECHNOLOGY, INC

248 Harbor Boulevard, Belmont, California • LYtell 1-0357 (Area Code 415)

7478

THE OPTICAL PUBLISHING CO.

LENOX, MASSACHUSETTS

P.O. BOX A

ANNOUNCES THE JULY PUBLICATION OF ITS EIGHTH ANNUAL

THE 1962 OPTICAL INDUSTRY DIRECTORY

The Directory is the only compilation listing all of the American sources of technical optics—about 1000 manufacturers and suppliers are included.

Categories in the classified section number over 500 items providing the user ready access to everything from a simple lens to the most sophisticated instrument.

Contents of the book read like a complete optical glossary index.

COMPONENTS: Lenses, mirrors, prisms of all types, reticles, gratings, filters, wedges, fiber optics, light sources, shutters.

INSTRUMENTS: Spectrometers, interferometers, microscopes, photometers, benches, colorimeters, medical and optometric instruments, photoelectric controls, surveying instruments, satellite tracking equipment, optical masers, technical cameras, UV & IR instruments.

SERVICES: Consulting, designing, engineering, computing, custom manufacturing, vacuum coating, glass tempering, instrument repairing, testing.

OPTICAL TOOLING: Gages, contour projectors, collimators, alignment telescopes, internal inspection instruments, goniometers.

SENSING ELEMENTS: Photocells, thermistors, bolometers, thermoelectric and radiometric elements, radioactive detectors.

WORKING MATERIALS: Pitch, rouge, abrasives, polishing compounds, cleaning materials, cements.

RAW MATERIALS: Glass, crystals, refractories.

MANUFACTURING EQUIPMENT: Grinding, polishing, centering and edging machines, vacuum coating equipment.

CORRECTED OBJECTIVES: An appendix listing data on over 1000 "Off The Shelf" corrected lenses.

DIRECTORY PRICE—$7.50 POSTPAID

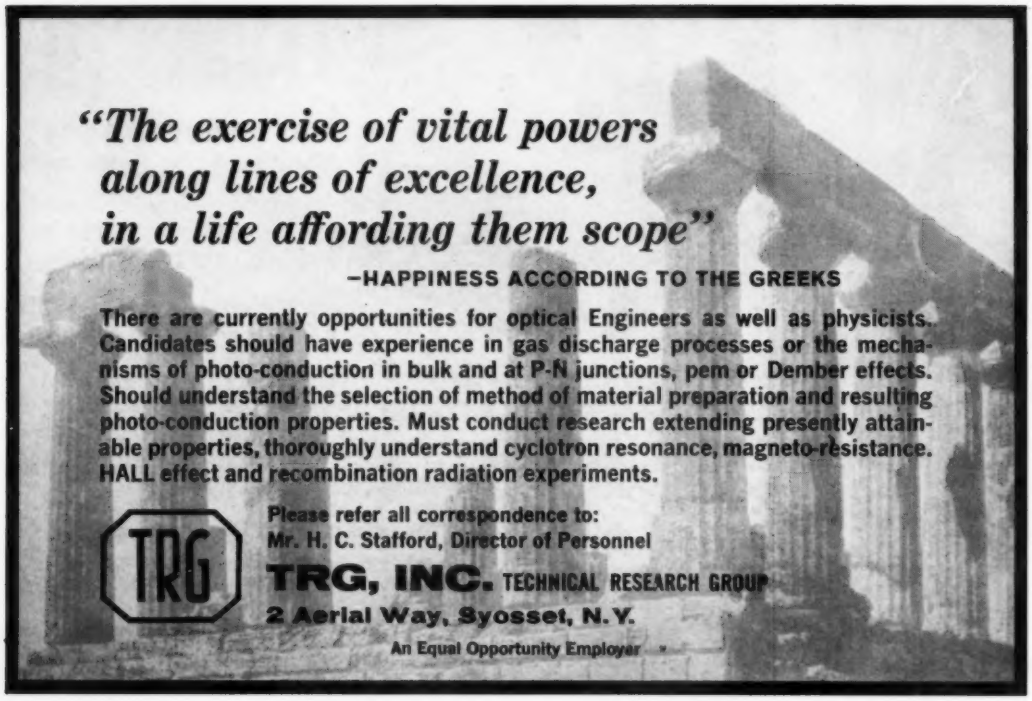
"The exercise of vital powers
along lines of excellence,
in a life affording them scope"
–HAPPINESS ACCORDING TO THE GREEKS
There are currently opportunities for optical Engineers as well as physicists. Candidates should have experience in gas discharge processes or the mechanisms of photo-conduction in bulk and at P-N junctions, pem or Dember effects. Should understand the selection of method of material preparation and resulting photo-conduction properties. Must conduct research extending presently attainable properties, thoroughly understand cyclotron resonance, magneto-resistance. HALL effect and recombination radiation experiments.
Please refer all correspondence to:
Mr. H. C. Stafford, Director of Personnel
TRG
TRG, INC. TECHNICAL RESEARCH GROUP
2 Aerial Way, Syosset, N.Y.
An Equal Opportunity Employer

PHYSICIST

Excellent opportunity for a physicist who may be the No. 2 or No. 3 in a laboratory, but who feels he is capable of moving ahead and doing much of his own planning.

Proven optical and instrument experience and accomplishments will be important in our decision. This is a technically rewarding position with a smaller company and offers immediate supervisory status. Present laboratory functions will grow rapidly under a program to be planned with the man we hire.

Our company is well-known and has demonstrated the ability to grow and prosper in the optical instrument field. Our prime customers are research labs. We are prepared to pay a high starting salary.

Please send details, including age to:

BOX AO625 % APPLIED OPTICS
55 WEST 16th ST., NEW YORK 16, N.Y.

We are an equal opportunity employer.

Advertisement

Vacuum-Deposited Coatings for Glass, Metal or Plastic

In the field of optics, Liberty Mirror Division of Libbey·Owens·Ford Glass Company has worked extensively for 20 years with laboratory and production technicians here and abroad in the development and application of vacuum-deposited coatings for a wide range of optical and scientific purposes. Three types of these coatings are treated below.

Electrically conducting coating keeps aerial-camera windows ice free, fog free

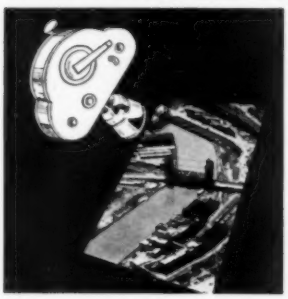

Among vacuum-deposited coatings made by Liberty Mirror is a transparent electrical conductor, *81-E*®, for defogging and deicing glass used in aerial-camera windows. Even at high altitudes at high air speed, resistance heating maintains a surface temperature that keeps the glass clear.

Applications for Liberty Mirror's *81-E* are also found in optical and instrument window surfaces, prisms, lenses and other optical elements subject to icing or fogging in service.

81-E film has a resistivity of approximately 30 ohms per square and visible light transmission of approximately 75% when applied to plate glass. These properties can be changed within limits. Power input through bus bars can be engineered according to need from 75 to 2,000 watts per square foot.

Hot and cold mirrors. They reflect or transmit infrared

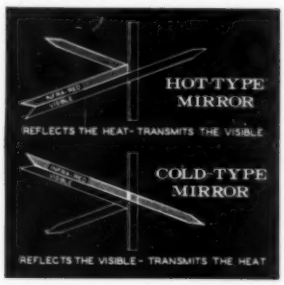

The dichroic coating on the hot-type mirror reflects at least 85% of the near infrared light at a wave length of 800 millimicrons, and its spectrophotometric reflection peaks between 770 and 820 millimicrons inclusive. The cold mirror reflects not less than 88% of the region integrated from 400 to 700 millimicrons.

Whichever serves your purposes, Liberty Mirror can supply front-surface or back-surface mirrors with Hi-Efficiency dichroic coatings applied by vacuum deposition. They are highly durable and easily cleaned with nonabrasive cleaners. The coatings themselves will withstand ambient temperatures of minus 60° F. and plus 600° F.

Transparent phosphor coating for use in electronic projection applications

This vacuum-deposited coating developed by Liberty Mirror has a light output of 15 foot/lamberts or greater, at a power-dissipation level of 25 milliwatts with peak output using a screen voltage up to 15 KV. It illuminates with extreme resolution.

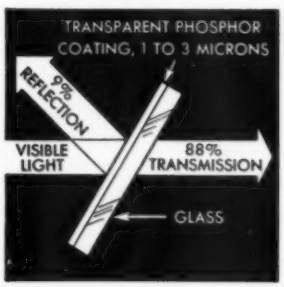

Liberty Mirror engineers will cooperate fully in design and development work on potential uses of transparent phosphor films.

★ ★ ★

Among the coatings available from Liberty Mirror are aluminum, chrome and gold front-surface mirrors, neutral filters, transparent mirrors, high-efficiency beam splitters, beam-splitting dichroic mirrors and filters. Metallic and transparent electrically conducting coatings are available for resistance heating. Static-dissipating and high-frequency shielding coatings are also available.

Liberty Mirror can apply coatings to all types of glass, plastics and highly polished metals.

Vacuum-deposited coatings are used in such varied products as scientific and optical instruments, cameras, aircraft and missiles. Free data sheets are available on all coatings. Write Liberty Mirror Division, 5572 Libbey-Owens-Ford Building, Toledo 2, Ohio.

A NEW Catalog

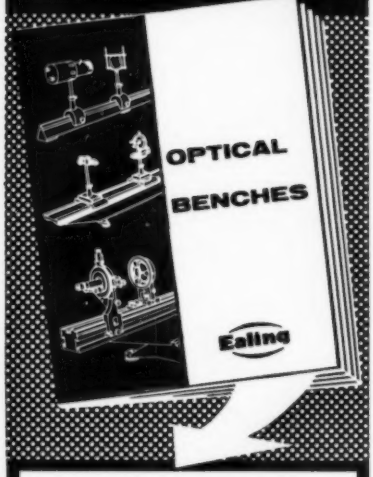

Introduction page

" This, we believe, is the most comprehensive range of Optical Benches and Accessories offered.

There are five basic benches for different applications with varying accuracies, each with its appropriate carriers. There are sixty different accessories.

This range meets every requirement from simple alignment to the precise investigation of any optical system.

A unique feature of this range of Optical Benches is its flexibility.

The first three benches all take accessories mounted on 13·5 mm. stems and therefore all 40 accessories listed — can be used interchangeably on these three benches.

The last three benches take the research accessories listed.

The middle bench, that is the Precision Lathe Bed Optical Bench — has the special advantage of taking both the standard accessories — and the research accessories listed."

WANT TO READ FURTHER?
This Catalog is FREE on request from

THE **Ealing** CORPORATION

33 University Road, Cambridge 38, Massachusetts
Telephone: 617 Kirkland 7-5760

EC.44

TO APPLIED OPTICS ADVERTISERS:

Optics and Spectroscopy, an NSF-sponsored English translation of the leading Russian journal in this field is now accepting advertising from **Applied Optics** advertisers. **OiS** coverage includes, in addition to optics, articles in solid-state physics, atomic, molecular, and applied spectroscopy, (including spectrochemistry) and apparatus and instrumentation. It has had free distribution for the past three years of some 7,000 copies per issue (1962 on is sold on subscription). Space in this journal may be purchased for $100.00 by any **Applied Optics** advertiser who wishes his **Applied Optics** ad to be picked up and run in the next issue of **Optics and Spectroscopy.**

The advertising deadline for the immediate future issues are:

May—published in English translation August
advertising closes **July 20.**

June—published in English translation September
advertising closes **August 30.**

July—published in English tanslation October
advertising closes **September 20.**

Persons interested in placing orders or desiring additional information should contact Mrs. Jacqueline Boraks, Optical Society of America, 1155 Sixteenth Street, N.W., Washington 6, D.C. Tel.: DI 7-6177 (Area Code 202).

NOW!

OPTICALLY CORRECTED SINGLE CRYSTAL LASER RODS

Adolf Meller Co. offers optically corrected laser rods in Ruby or Sapphire-clad Ruby . . .also!

$CaWO_4$ with Nd^{3+}	.5% doping
$CaWO_4$ with Nd^{3+}	.025% doping
CaF_2 with U^{3+}	.1% doping
CaF_2 with Dy^{2+}	.1% doping
SrF_2 with Sa^{2+}	.1% doping
SrF_2 with Nd^{3+}	.5 % doping

Only Meller offers this optical correction service with its outstanding guarantees:

1. *Flat End Rods:* flat to 1/20*th* wave length or better . . ends optically parallel within 2 secs. of arc.

2. *Chisels:* right angle correct within 5 secs. of arc. All faces flat to 1/20*th* wave . . and apex of angle parallel to flat end within 4 secs. of arc so that maximum TIR (total internal reflection) will be attained.

All guarantees apply to ruby rods of any length from $1^1/_2$" to 9" . . . and up to $1^1/_2$" to 2" lengths (maximum available) on other single crystals.

Meller offers round, square, triangular, and other special configurations to your specifications. Trumpet shape ruby/sapphire completely lapped and silvered available for less than $1,000.00! Also white sapphire tubes for any size ruby rod—piston fit.

Write or call ADOLF MELLER CO.,
Box 6001, Providence, Rhode Island
Phone (401) 331-3717

MELLER SAPPHIRE PRODUCTS

Synthetic Sapphires • Ruby Lasers & Masers
Alumina Powder

SCHOTT Narrow Band Interference Filters

Made by JENAer Glaswerk Schott & Gen.
WEST GERMANY

For the spectral region from 300 to 2,000 mμ.

Transmission up to 60%. Half-value width down to 5 mμ. Tolerance at peak wave length: ±1% for regular quality. $+0.5\%$ for precision quality. -0

AVAILABLE AS

Line Filters • Line Double Filters • Band Filters
Band Double Filters • Wedge Filters • Broad Band Filters

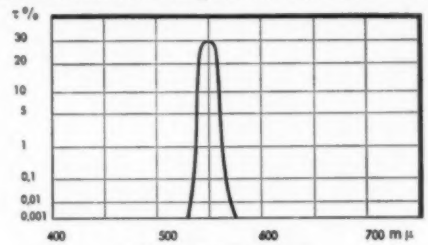

DOUBLE BAND FILTER

Tmax about 30%. Half width about 16 mμ.
Ratios: Tenth width to half width 1.5. Hundredth width to half width 2, Thousandth width to half width 3.5.

SCHOTT Colored Optical Filter Glass

Available in about 100 types for ultraviolet, visible and infrared spectral regions, including absorption filters containing neodymium for use in lasers and masers.

MULTI-LAYER INTERFERENCE FILMS

for dichroic and achromatic beam splitters and filters. High efficiency. Relatively wide band.

MULTI-LAYER HEAT DEFLECTORS

XUR-96. Reflects substantial portion of infrared spectrum while transmitting nearly all of the visible radiation.

#6143. Colorless, non-absorbing filter. Completely removes the ultra-violet and reflects the infrared. Transmits about 90% from 425 to 700 mμ reflecting longer wavelengths. Half transmission points at 412 mμ and 725 mμ.

Cold Mirror IRT-211. To reflect visible radiation from 400 to 700 mμ and transmit from 725 to 1200 mμ and longer.

COATINGS FOR LASERS and MASERS

For Ruby: #3132-N. 99% reflectivity from 694 to 760 mμ.

For Glass: #3117. 99% reflectivity from 1,000 to 1,200 mμ.

LOW REFLECTING COATING

Double and triple layer with minimum reflection of less than .1% on glass of low index.

Coatings also available to increase transmission to 9 micron on Germanium and Silicon.

FISH-SCHURMAN CORPORATION
90 Portman Road, New Rochelle, N. Y.

American Optical announces the availability of

AOLUX

its new Trivalent Neodymium Lasering Glass

Here's the latest development in maser technology—AOLUX, an optical quality lasering glass, now available from American Optical Company. The result of extensive investigations in glass compositions, this material fulfills the basic aims of producing homogenous optical quality material for laser rods.

As a glass optical maser material, AOLUX offers:

1 High-intensity output at 1.06 microns.

2 Substantially lower threshold pump power than ruby.

3 A reasonable choice of sizes and shapes.

4 The use of transparent glass cladding for rods and fibers. (These materials will be available soon.)

AOLUX glass rods, in the standard ¼″ diameter by 2½″, are now in production. Each piece is tested for laser action before shipment. Requests for other sizes will receive prompt attention.

You may obtain complete information on AOLUX rods by writing to American Optical. Address our Keene, New Hampshire, plant.

American Optical
COMPANY

K&E AUTO-COLLIMATORS

From the basic...

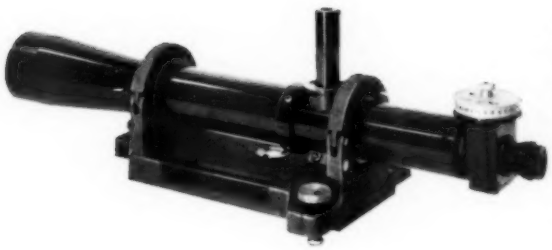

Visual Auto-Collimator

- Aperture 50 mm.
- Equivalent focal length 900 mm.
- Range 10 minutes
- Graduations to .1 second
- Working distance 0-50 ft.
- Magnification 53.5X
- Field of view 22 minutes
- Exit pupil 1 mm.

to the most sophisticated...

Two Axis, Fast Response, Electronic Auto-Collimator

- Indicating range ±125 seconds of arc
- Operating distance 0 to 5 ft.
- Linearity 2% at 5 feet distance
- Response time 25 milliseconds
- Noise 500 milliarc seconds max.

for any of these requirements

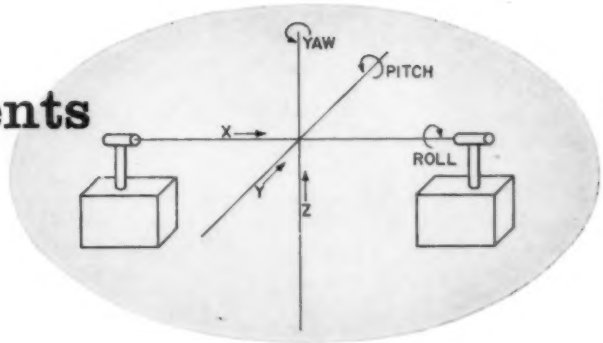

- Displacement – X, Y or Z
- Angular deviation – pitch, roll or yaw

Look to K&E for the precise visual or electro-optical equipment needed to measure, monitor, record and control the relative attitudes – in twist or displacement – of any body in relation to another. The O&M Division's capabilities also include precise distance measurement, goniometry and optical spatial-coordinate measuring systems. Write today for technical information and facilities brochure.

OPTICS AND METROLOGY DIVISION

KEUFFEL & ESSER CO.
HOBOKEN, N. J.

3838

SCIENTIFIC INSTRUMENTS

HILGER & WATTS

FOR RESEARCH, PRODUCTION, ENGINEERING SINCE 1856

- Atomic Absorption Equipment
- Auto-Collimators
- Clinometers
- Crystals, Synthetic
- Diffractometers
- Digitizers (Optical, Mechanical)
- Etalons
- Goniometers
- Hollow Cathode Lamps and other Light Sources
- Interferometers
- Measuring Microscopes
- Microwave Components
- Microphotometers
- Microptic Levels
- Monochromators
- Optics (Prisms, Lenses, Flats, Polygons)
- Photoconductive Cells
- Polarimeters
- Refractometers
- Seismometers
- Spectrographs
- Spectrometers
- Theodolites
- Thermopiles
- X-ray Equipment

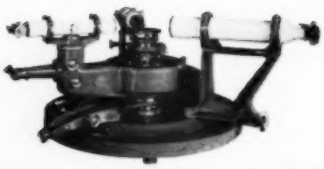

SPECTROMETER C-20 For research refractometry and highest class goniometric work. Refractive index measurement to sixth decimal can be obtained; micrometer scale divided at 0.1 second intervals.

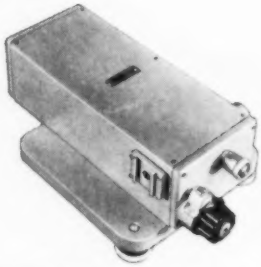

MONOCHROMATOR D-290 Small, compact, low cost; utilizes a 15,000 lines/in. plane grating with special range of 2000A to 10,000A and dispersion of 70A/mm. Easily combines with other optical systems.

PRECISION CLINOMETER TB-95 Reads angles and circular spacing direct to 1 second; by estimation to 0.5 second—through 360°. Accessories permit use in horizontal position as rotary table or dividing head for light work.

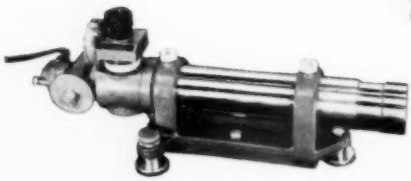

UNIVERSAL AUTO-COLLIMATOR TA-51 The master instrument for angle measurement. Reads in both planes simultaneously. Range 10 minutes of arc; direct reading to 0.1 second; straight or right angle viewing.

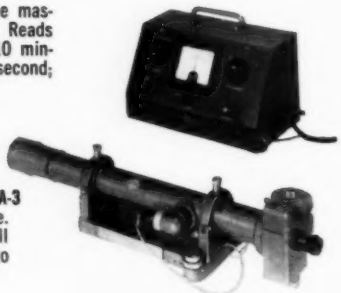

PHOTO-ELECTRIC AUTO-COLLIMATOR TA-3 Eliminates human factor — fatigue. Adjustable sensitivity and range; full visual optics. Setting accuracy to 0.05 second.

New

HILGER PRECISION OPTICAL BENCH Massive Meehanite casting holds heavy instruments with no flexing; supported at three points for precise levelling. Flat ways are hard chrome plated for long life; absolutely rust proof. Designed for convenient, universal mounting of accessories.

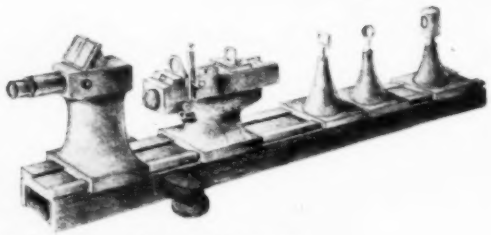

Write for complete descriptive literature of these and other Hilger & Watts instruments

HILGER & WATTS, INC.
431 SOUTH DEARBORN ST. CHICAGO 5, ILL.

Sales, Service, Parts by
ENGIS EQUIPMENT COMPANY
CHICAGO 5, ILL.